Geophysical Monograph Series

Including

IUGG Volumes

Maurice Ewing Volumes

Mineral Physics Volumes

73 Environmental Effects on Spacecraft Positioning and Trajectories (IUGG Volume 13) *A. Vallance Jones (Ed.)*

74 Evolution of the Earth and Planets (IUGG Volume 14) *E. Takahashi, Raymond Jeanloz, and David Rubie (Eds.)*

75 Interactions Between Global Climate Subsystems: The Legacy of Hann (IUGG Volume 15) *G. A. McBean and M. Hantel (Eds.)*

76 Relating Geophysical Structures and Processes: The Jeffreys Volume (IUGG Volume 16) *K. Aki and R. Dmowska (Eds.)*

77 The Mesozoic Pacific: Geology, Tectonics, and Volcanism *Malcolm S. Pringle, William W. Sager, William V. Sliter, and Seth Stein (Eds.)*

78 Climate Change in Continental Isotopic Records *P. K. Swart, K. C. Lohmann, J. McKenzie, and S. Savin (Eds.)*

79 The Tornado: Its Structure, Dynamics, Prediction, and Hazards *C. Church, D. Burgess, C. Doswell, R. Davies-Jones (Eds.)*

80 Auroral Plasma Dynamics *R. L. Lysak (Ed.)*

81 Solar Wind Sources of Magnetospheric Ultra-Low Frequency Waves *M. J. Engebretson, K. Takahashi, and M. Scholer (Eds.)*

82 Gravimetry and Space Techniques Applied to Geodynamics and Ocean Dynamics (IUGG Volume 17) *Bob E. Schutz, Allen Anderson, Claude Froidevaux, and Michael Parke (Eds.)*

83 Nonlinear Dynamics and Predictability of Geophysical Phenomena (IUGG Volume 18) *William I. Newman, Andrei Gabrielov, and Donald L. Turcotte (Eds.)*

84 Solar System Plasmas in Space and Time *J. Burch, J. H. Waite, Jr. (Eds.)*

85 The Polar Oceans and Their Role in Shaping the Global Environment *O. M. Johannessen, R. D. Muench, and J. E. Overland (Eds.)*

86 Space Plasmas: Coupling Between Small and Medium Scale Processes *Maha Ashour-Abdalla, Tom Chang, and Paul Dusenbery (Eds.)*

87 The Upper Mesosphere and Lower Thermosphere: A Review of Experiment and Theory *R. M. Johnson and T. L. Killeen (Eds.)*

88 Active Margins and Marginal Basins of the Western Pacific *Brian Taylor and James Natland (Eds.)*

89 Natural and Anthropogenic Influences in Fluvial Geomorphology *John E. Costa, Andrew J. Miller, Kenneth W. Potter, and Peter R. Wilcock (Eds.)*

90 Physics of the Magnetopause *Paul Song, B.U.Ö. Sonnerup, and M.F. Thomsen (Eds.)*

91 Seafloor Hydrothermal Systems: Physical, Chemical, Biological, and Geological Interactions *Susan E. Humphris, Robert A. Zierenberg, Lauren S. Mullineaux, and Richard E. Thomson (Eds.)*

92 Mauna Loa Revealed: Structure, Composition, History, and Hazards *J. M. Rhodes and John P. Lockwood (Eds.)*

93 Cross-Scale Coupling in Space Plasmas *James L. Horwitz, Nagendra Singh, and James L. Burch (Eds.)*

94 Double-Diffusive Convection *Alan Brandt and H.J.S. Fernando (Eds.)*

95 Earth Processes: Reading the Isotopic Code *Asish Basu and Stan Hart (Eds.)*

96 Subduction: Top to Bottom *Gray E. Bebout, David Scholl, Stephen Kirby, and John Platt (Eds.)*

97 Radiation Belts: Models and Standards *J. F. Lemaire, D. Heynderickx, and D. N. Baker (Eds.)*

98 Magnetic Storms *Bruce T. Tsurutani, Walter D. Gonzalez, Yohsuke Kamide, and John K. Arballo (Eds.)*

99 Coronal Mass Ejections *Nancy Crooker, Jo Ann Joselyn, and Joan Feynman (Eds.)*

100 Large Igneous Provinces *John J. Mahoney and Millard F. Coffin (Eds.)*

101 Properties of Earth and Planetary Materials at High Pressure and Temperature *Murli Manghnani and Takehiki Yagi (Eds.)*

102 Measurement Techniques in Space Plasmas: Particles *Robert F. Pfaff, Josesph E. Borovsky, and David T. Young (Eds.)*

103 Measurement Techniques in Space Plasmas: Fields *Robert F. Pfaff, Josesph E. Borovsky, and David T. Young (Eds.)*

104 Geospace Mass and Energy Flow: Results From the International Solar-Terrestrial Physics Program *James L. Horwitz, Dennis L. Gallagher, and William K. Peterson (Eds.)*

105 New Perspectives on the Earth's Magnetotail *A. Nishida, D.N. Baker, and S.W.H. Cowley (Eds.)*

106 Faulting and Magmatism at Mid-Ocean Ridges *W. Roger Buck, Paul T. Delaney, Jeffrey A. Karson, and Yves Lagabrielle (Eds.)*

Geophysical Monograph 107

Rivers Over Rock: Fluvial Processes in Bedrock Channels

Keith J. Tinkler
Ellen E. Wohl
Editors

American Geophysical Union
Washington, DC

Published under the aegis of the AGU Books Board

Library of Congress Cataloging-in-Publication Data

Rivers over rock : fluvial processes in Bedrock channels / Keith J. Tinkler, Ellen E. Wohl, editors.
p. cm. -- (Geophysical monograph series; 107)
Includes bibliographical references and index.
ISBN 0-87590-090-9
1. River channels. 2. Sediment transport. I. Tinkler, K. J., 1942- . II. Wohl, Ellen E., 1962- . III. Series.
GB561.R595 1998
551.441'2--dc21 98-44136
CIP

ISBN 0-87590-090-9
ISSN 0065-8448

Printed in the United States of America.

CONTENTS

CONTENTS

Methods of Studying Bedrock Channels

PREFACE

Bedrock river channels are sites of primary erosion in the landscape, fixing the baselevel for all points upstream. This volume provides for the first time an integrated view of the characteristics and operation of this important, though hitherto neglected, class of channels. Examples are provided from several continents and cover a wide range of spatial scales from the large river basins (such as the Colorado River in the United States and the Indus River in Pakistan) down to reach scales and individual sites. Likewise the geologic timescales considered range from erosion and transportation during individual flows to accumulated effects over periods of tens of millions of years.

Bedrock channels are characteristically steep and generate transcritical flow conditions. These are channels where the Froude number indicates that the fluid flow ranges from subcritical, through critical, to supercritical flow both along streamlines and in cross-sections. These flow conditions have important consequences for the distribution of shear stress and stream power on the stream bed, and for the ways in which such conditions control erosion on the boundary and the transport of coarse caliber sediment up to the size of large boulders. For these reasons, bedrock channels behave very differently than the alluvial river systems more commonly described in textbooks and journal papers.

Previous work on bedrock channels has been sporadic and frequently focused on small-scale spectacular features of worn rock surfaces such as potholes or upon the results of a single catastrophic flood, ancient or modern. In this volume we have tried to ensure a comprehensive treatment of the topic by leading experts so that bedrock channels are not treated as exotic items, but as central and important elements in the development of regional landscapes. As the first state-of-the-art survey of bedrock river channels, this book will interest hydrologists, geomorphologists, and civil and environmental engineers, as well as anyone else concerned with high-gradient fluvial channels with part of the boundary in rock. The volume was developed from a conference on the same topic held in 1996 at Pingree Park, a mountain campus of Colorado State University. In our introductory chapter, we have tried to summarize the state of knowledge as well as point out obvious lacunae and fruitful lines of attack for future work.

We are extremely grateful to all who have helped in various ways with the manuscripts, especially all the reviewers who read and commented upon the papers. Reviewers for the volume include authors of other chapters in the volume and the following individuals: A.D. Abrahams, D. J. Anthony, P. Bishop, J. E. Costa, L. L. Ely, A. Gupta, D. J. Harbor, H. Ikeda, L. A. James, R. D. Jarrett, A. Kirkbride, S. J. Kite, H. H. Mills, J. Nott, J. E. O'Connor, S. Ouchi, G. Pickup, J. E. Pizzuto, S. A. Schumm, R. L. Slingerland, and M. G. Wolman. The chapter authors have been models of helpfulness and patience during the revision stages, and of course we thank them for their manuscripts, which have very amply justified the hopeful vision that we had several years ago in preparing first the conference and later the volume. We would also like to thank Richard Pyrce for proofreading the final manuscripts.

Keith J. Tinkler
Brock University

Ellen E. Wohl
Colorado State University

Editors

A Primer on Bedrock Channels

Keith Tinkler

Department of Geography, Brock University, St Catharines, Ontario, Canada

Ellen Wohl

Department of Earth Resources, Colorado State University, Fort Collins, Colorado

In this introductory paper on bedrock channels we try to summarize the state of knowledge and point out directions for future work. Fluvial geomorphology as developed for alluvial and gravel channels does not readily transfer its results to bedrock channels, for example conventional hydraulic geometry does not seem to apply to these highly variable channels. Because bedrock channels involve changes on a resistant boundary that is usually that of the drainage basin bedrock, baselevel changes effected by channel erosion are subsequently transmitted to the rest of the basin, and therefore have an impact on all aspects of drainage basin geomorphology when viewed over geological timescales. We review existing knowledge of both morphology and process over short and long times scales, and from reach to basin scales. We point out that fundamental to an understanding of bedrock channels is the need to appreciate transcritical flow conditions in the channels, and the consequences that this may have for channel erosion and sediment transport. There are opportunities to undertake fundamental work in all aspects of the subject - from morphological description and monitoring, through the mechanics of channel bed erosion and sediment transport, to the construction of flood discharges chronologies in relation to environmental controls, and high-gradient flood hydraulics in the field, the flume and the computer.

INTRODUCTION

The intention of this chapter is to highlight roughly what is known about the modern observable dynamics of bedrock channels as a means of introducing the subjects discussed in more detail in subsequent chapters. We cannot present a definitive document, but rather hope to stimulate thinking about these little-studied channels. For the purposes of this volume, we define bedrock channels as those reaches along which a substantial proportion of the boundary ($\geq$ 50%) is exposed bedrock, or is covered by an alluvial veneer which is largely mobilised during high flows such that underlying bedrock geometry strongly influences patterns of flow hydraulics and sediment movement. This definition thus includes channels formed solely in bedrock, channels along which bedrock is exposed only in the channel bed, and channels along which bedrock may be exposed only during high flows. Broadly construed, bedrock may refer to any cohesive resistant substrate, such as cemented alluvium or gravels, or Tertiary and Quaternary clay units, which behave in a manner analogous to bedrock.

The subject of bedrock channels has a large but scattered literature dating back over a century. Figure 1 shows the world distribution of studies on bedrock channels. An increase of interest in recent years, as exemplified by the attendance at the Mountain Rivers Symposium at the

Rivers Over Rock: Fluvial Processes in Bedrock Channels
Geophysical Monograph 107

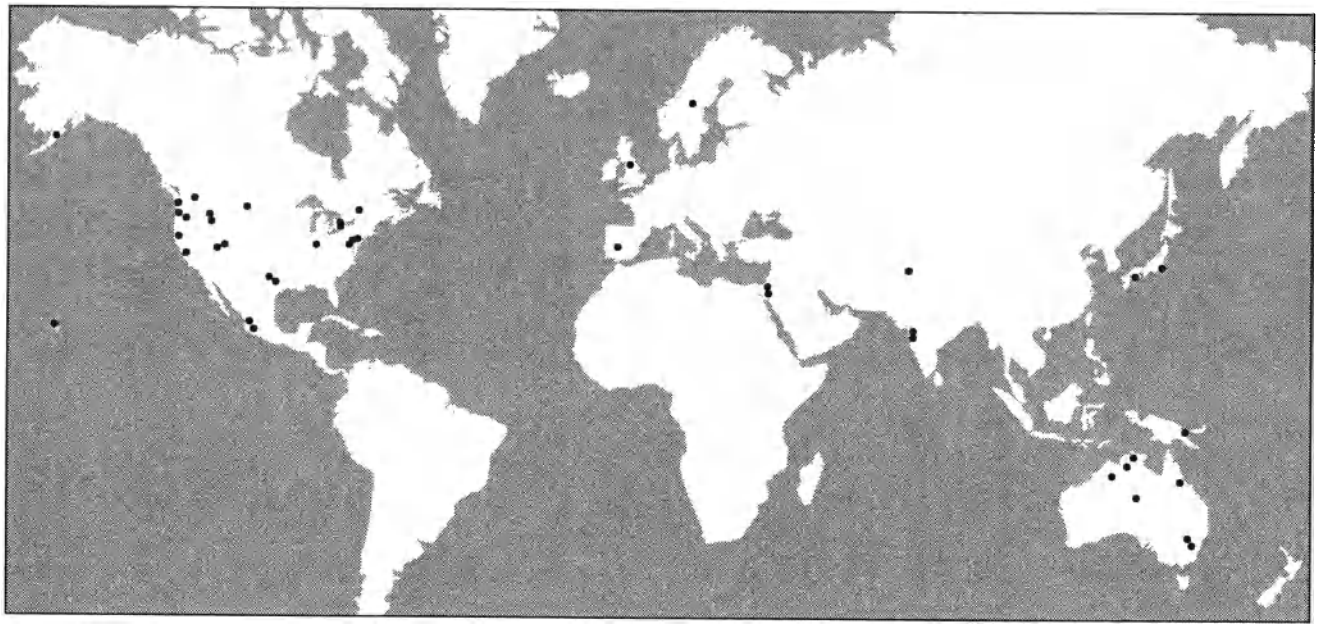

Figure 1. World distribution of bedrock channels studies.

ASCE (Hydraulics) meeting in Buffalo, NY (USA), in 1994, makes it worthwhile to review the various approaches now being taken to channels whose bed and walls are eroded in resistant material, to try to establish some of their salient characteristics. Increased pressure on uplands and more rugged terrain both for general recreational use and for urban expansion means that the hydrologic and hydraulic behaviour of these types of streams needs examination [*Jarrett*, 1984; *Carling*, 1995]. In addition there is the growing realisation that stream biota must also be allowed for in design schemes, as for example in the Green River, Utah, USA [*Harvey, Mussetter, and Wick*, 1993] which includes gravel bed reaches. Basin scale landscape evolution models [*Howard*, 1987; *Howard, Dietrich, and Seidl*, 1994] must directly model bedrock systems when significant incision is to take place into the regional landscape. Modes and rates of incision, and their variability, must be known if these models are to address the time variable effectively.

It cannot be assumed that knowledge from alluvial and gravel bed systems can be transferred directly to bedrock rivers, and indeed attempts to do this have already fallen into difficulties, especially in river engineering works [*Vaughn*, 1990] and Cooksville Creek, near Toronto [*Parish and Tinkler*, this volume]. It is probably the case that bedrock rivers are more common than is generally supposed [*Montgomery et al.*, 1996], even in low relief terrain. Alternating gravel and bedrock reaches, typical in some rivers, together with low base flow conditions and abundant summer vegetation may mask this reality. In such rivers, gravel bed reaches are usually shallow spreads over bedrock. As such, they may behave differently than standard gravel bed rivers. For example, such spreads may readily be stripped from the underlying rock when the armour is breached, and as easily rebuilt, and the hydraulics of the large flows may be controlled by the underlying bedrock geometry. Bedrock rivers are also more common than might be assumed from the percentage of papers in the fluvial literature which describes such systems.

Flows in bedrock systems, even at quite low stages, typically show greater velocities and shear stresses than those in alluvial reaches, and usually they possess highly aerated and turbulent flow structures. There is usually a noticeable water surface topography, especially as stage increases: smoothly descending water surfaces leading to hydraulic jumps, prominent standing wave trains (indicating critical flow), super-elevation at bends, topographic rises over kolks bursting on the surface, and traveling waves generated in energetic zones which cause miniature shoreline processes to operate at the stream banks. In no sense can one pretend, even as a working assumption, that the flow is steady and uniform. Substantial sections of the flow are critical (Froude number, F, close to 1) or supercritical ($F > 1$). When mixed regimes are present along a streamline, flow is said to be transcritical. A good rule of thumb is that if flow is audible in the channel, then flow is transcritical in at least part of the channel. The substantive existence of critical or upper regime flow

matter has been debated for mountain streams [*Jarrett*, 1992; *Trieste*, 1992], but some supporting evidence has been produced [*Simon and Hardison*, 1994]. In our observation critical flow is extremely common [*Grant*, 1997; *Tinkler*, 1997a; *Tinkler*, 1997b], although usually confined to part of the channel, and supercritical flow is not uncommon, although spatially restricted. As *Tinkler* [1997a] suggests, to understand channel dynamics in such streams the cross-sectional focus for calculation of cross-sectional Froude numbers must be replaced by a view along the thalweg.

REVIEW OF APPROACHES TO STUDYING BEDROCK CHANNELS TO DATE

Approaches to studying bedrock channels may be grouped into at least three categories: basin scale, reach scale, experimental. (1) Basin-scale approaches generally focus on the evolution of channel longitudinal profile at time scales of centuries or longer [*Weissel and Seidl*, this volume]. Studies may be field-based [*Merritts et al.*, 1994, *Pazzaglia et al.*, this volume] or oriented towards computer modeling of basin evolution [*Howard*, 1987; *Howard et al.*, 1994; *Seidl et al.*, 1997; *Howard*, this volume; *Sklar and Dietrich*, this volume], but the general focus is on long-term rates of profile lowering and the development of an erosion rate law. (2) Reach-scale studies are more concerned with the processes of erosion and deposition, as these affect channel morphology, at spatial scales of a few square metres to several channel widths. Such studies may focus on observable processes occurring at time scales of days to decades [e.g., *Toda*, 1994; *Tinkler and Parish*, this volume; *Tinkler and Wohl*, this volume; *Hancock et al.*, this volume] or they may take an indirect approach of inferring processes from form, with the aid of paleostage indicators and hydraulic simulation programs [*O'Connor et al.*, 1986; *Baker and Pickup*, 1987; *Wohl*, 1992a,b; *Wohl et al.*, 1993]. Finally, there is reach-scale mathematical flow modeling, some of which is now sophisticated enough to capture the transcritical character of flow in bedrock channels [*Miller and Cluer*, this volume]. (3) Experimental studies have used a variety of cohesive substrates to simulate either erosion of a specific feature, for example, potholes [*Alexander*, 1932; *Ängeby*, 1951], or knickpoints, [*Holland and Pickup*, 1976; *Gardner*, 1983], or general channel erosion under varying conditions [*Shepherd and Schumm*, 1974; *Wohl and Ikeda*, 1997].

Questions common to all these approaches include: (i) what are the actual processes and rates of bedrock channel incision? (ii) how does the presence of a cohesive substrate cause bedrock channel morphologies, flow hydraulics, and sediment transport to differ from those of alluvial channels? and, (iii) is there a consistent hydraulic geometry for "steep" channels? By this we mean, "is it possible to predict the direction and magnitude of channel response to a change in the controlling variables?"

BEDROCK CHANNEL CHARACTERISTICS

In what senses are bedrock channels different from alluvial or gravel bed systems?

Morphology

Gradient. The gradient of bedrock channels is almost certainly well in excess of those encountered in alluvial channels (see Hydraulics section below) - even though locally, when the lithology and dip are appropriate, there may be substantial sections of almost horizontal channel bed (*Miller*, 1991a, b). This 'horizontal' appearance can be misleading because as stage rises, gradient integrates over longer and longer reaches and small steps readily drown out. A relatively steep mean gradient is consistent with the typical coexistence of gravel bed and bedrock reaches and lateral or transverse bars along the channel, and the need to transport coarse clasts from the bed, walls and adjacent valley slopes.

Change. Morphological change is unidirectional - rock removed from the bed of a channel lowers the local base level for all points upstream. Importantly, local velocity fields are permanently modified. Likewise, rock removed from the walls is not replaced. In alluvial and gravel-bed channels the distinction between channel materials and bed, bar and floodplain material may be locally distinct, but sediment in transport usually contains enough clay or silt to provide coherence so that alluvial channels can aggrade, degrade, and migrate while channel morphology remains relatively constant [*Leopold et al.*, 1964]. Gravel-bed rivers, with their tendency to braid on short time periods (hours, days to months), similarly conserve channel morphology - in a statistical sense - while migrating. Bedrock channels are not immune to alluviation, but unless siliceous or carbonate precipitates are extremely common in the channel, it is in the nature of temporary "fill" and will in time be "cut" out again, speaking in terms of geological timescales. EW observed such systems in southern Utah, where aboriginal petroglyphs are partially buried by sandy alluvium in slot gorges. On a much smaller scale KT has seen fine gravel alluviation developed from mining debris with remnant 19th-century cooking pots to 1m above the present bed in the Glen Maye stream (Isle of Man, United Kingdom), but which has been subsequently mostly removed in bedrock gorges downstream from these sources. In contrast, in Texas KT has observed indurated gravel terraces (of presumed Quaternary to late Quaternary age) now partly removed which imply incision of rock to present channel bed elevations, infill with 4 to 5 metres of gravel, and subsequent removal. On small tributaries,

channel bed fragments of this fill are hard to distinguish from bedrock and may be smoothed and shaped by present channel processes.

In contrast to alluvial and gravel-bed systems then, bedrock channels are not self-repairing, and do not conserve morphology because, in effect, they are more intimately connected with the hillslope systems, and a lateral increase in channel size is also an increase in valley size. The exceptions again prove the rule here because slot gorges, which imply virtually no valley wall erosion, usually contain spectacular sculpted forms [*Engeln*, 1961; *Baker and Pickup*, 1987; *Maxson*, 1940; *Maxson and Campbell*, 1935] as evidence of their longevity, together with high-water slackwater deposits in overhangs and caves [*Ely*, 1985; *Enzel et al.*, 1993].

Variability. Large spatial variability in channel morphology (even within reaches) both reflects and controls spatial variability in hydraulic forces.

The commonly observed spatial variability in hydraulics along bedrock channels may be reflecting variability in the lithology or structure of the channel substrate [*Wohl and Ikeda*, 1997; *Miller* 1991b], tributary inputs of coarse sediment [*Kieffer*, 1988; 1989], minimum variance of downstream energy expenditure between bedrock and alluvial reaches [*Wohl et al.*, 1994], or even a different hydraulic geometry centered on critical flow.

Despite generally slow rates of morphological change [*Schumm and Chorley*, 1983], bedrock systems nevertheless do act to accumulate change, and the rock form reflects a time integration of change through time, up to centuries and probably millennia. The rock acts as a medium and high pass filter by essentially ignoring the effects of low magnitude high frequency events. Low magnitude events may effect limited wear and polish but not large morphological change. Regularities of morphology may be studied as a guide to the locus of effective forces in streams, be this on the scale of meanders [*Miller*, 1935; *Blank*, 1970], or gravel bars [*O'Connor et al.*, 1986] or of sculpted forms at the scale of pin head rattails [*Baker and Pickup*, 1987]. For this reason, the existence of inner channels in streams - real and experimental [*Shepherd*, 1972; *Shepherd and Schumm*, 1974; *Wohl and Ikeda*, 1997] - should be taken to reflect a zone of persistent power expended on the bed, and to be a persistent characteristic of the flow dynamics. For example, KT has recently found a short reach of Cooksville Creek containing a longitudinal groove several tens of metres long, 1 to 1.5 m wide in a channel 15 m wide. It has an undulating thalweg and is occupied by a thread of water with critical wave systems (F = 1, standing waves) of similar wavelength to the bed undulations. From the installed engineering works in the reach [*Tinkler and Parish*, this volume], it is known that the feature has developed during the last twenty years as the entire bed has incised 30 to 40 cm. Between August 1997 and June 1998, 2 to 3 mm deep slots cut across the trough bed have been worn away entirely. It thus expresses very localised, but persistent forces expended on the bed.

One cause of spatial variability in morphology is separated flow, in which circulating cells of water are virtually cut off from the main flow. Wear, accumulating over long periods within these cells, produces potholes and scour holes marginal to the main flow. In essence, all separated flow features should be placed in the same category of sculpted forms. At low flow the channel has a fantastic baroque appearance, but during high flows water in the separation cells is driven by two factors: the divergence of some flow into them when a jet impinges on a resistant surface at a large angle to flow direction (e.g. the distal lip of a pothole), and shearing and vorticity along the fluid boundary between the two water bodies, including the point where re-circulating water in the cell returns to the shear zone. Some of the sediment entrained in the main flow as wash load is diverted into the separation cells and effects the wear. The entire complex of forms may be seen as a spatially specific sink for energy dissipation and turbulence at high flows.

Resistance. The rock resistance to flow dynamics obviously varies according to lithological considerations - and the morphology is a compromise between fluvial forces applied and bedrock resistance offered. *Miller,* [1991a,b], describes channels in almost horizontally bedded calci- and siliclastics, and gives precedence to lithological controls on rock channels, but it seems likely that this issue has to been to some extent over-stressed. There are some variations in morphology which may be attributed to lithological control, as in the Katherine Gorge of Australia [*Baker and Pickup*, 1987]. *King* [1927] and *Blank* [1958] describe longitudinal grooves on the stream bed which begin at joint-delimited edges facing upstream in rocks which dip slightly downstream. Horizontally and well-bedded rocks typically erode by the removal of individual slabs delimited by bedding planes and joints [*King*, 1927; *Blank*, 1958; *Tinkler*, 1993; *Hancock et al.*, this volume]. Because of the characteristics of dynamic flow conditions over level beds (see below), metre dimension slabs - provided the c axis is no larger than about 30 centimetres - can usually be moved by flows close to the Mean Annual Flood (MAF) even in small channels. If the rock on the other hand is very coarsely and evenly jointed in all directions, then the channel may have a 'chunkier' appearance - as for example happens on the igneous and metamorphic terrain of the Canadian Shield. To a large extent the thickness of lithological units (susceptible bedding or cleavage planes) controls the c axis of entrained clasts.

In contrast, *Wohl* [1993] describes longitudinal grooves and other incisional bedforms which bear no apparent relation to lithologic controls. Similar features have been formed in massive homogeneous substrates during flume runs [*Shepherd*, 1972; *Schumm and Shepherd*, 1973; *Wohl and Ikeda*, 1997] and have been observed in substrates

varying from glacial ice through cohesive sediment to sandstone, limestone, and granite.

Lithology. There appear to be substantial differences in morphology between channels in quasi-horizontal well-bedded sediments, and those in 'chunky' lithologies which may require larger shear stresses to remove rock from the channel. In the former lithology channels tend to be flat in most of the cross section with a subdued parabolic channel boundary and little sign of an inner channel. At downsteps in the profile the water jet is rectangular (wide and shallow) and lacks penetration power with the result that plunge pools may be quite shallow (for small headwater streams they are often less than a metre deep, occasionally they are non-existent). In the 'chunkier" lithologies, inner channels commonly exist and concentrate the flow into a circular jet at down steps. This jet excavates deep plunge pools and separation cells (with upward and upstream flow) develop at the margins of the jet where it re-enters downstream channel flow. Scour from entrained sediment creates spectacular sculpted forms.

Evidence of morphological change.

Seidl and Dietrich [1993] have raised the question as to how erosion is accomplished in bedrock channels in the presence of river bed gravels. Of course this raises the question more generally because much is based upon inferential evidence, there are few direct records of erosion processes.

Monitoring. KT has been monitoring two streams (Swayze Creek, 6 km^2 and Twenty Mile Creek 300 km^2) intensively for several years, and keeps an eye on several others. Repeat photography and careful postflood (falling limb and low flow) inspection reveals a variety of mechanisms whereby erosion is accomplished. At the largest scale, blocks delimited by joints and bedding planes are removed during flows which, so far, have not exceeded the MAF, but which are close to it (see Figure 2a,b, top and bottom, of a small knickzone with plates removed in MAF January flood). On the smaller stream, whose bed is composed of thinly-bedded (a few cm maximum) dolostones, he has never failed to find the removal of some plates from the bed after a moderate flood flow, or larger. Removed plates are easily identified by their fresh buff colour compared to the oxidized and algae-rich surface after several months of exposure. In a few instances it has been possible to locate and "refit" detached plates (for a huge example see Figure 3), including a small one which had been lifted and partly displaced from its "scar" during an small winter flood on Swayze Creek - suggesting it was lifted by means of anchor ice adhering to the bed. On the larger system, flows must be very close to the MAF to accomplish change in terms of the quarrying of blocks because the bed units are substantially thicker (to several tens of centimeters).

It is not always clear that pure hydraulic quarrying (plucking, lifting) is involved in the removal of rock from the bed. In the smaller stream it is nearly always the case that one of the bounding joints shows signs of fresh fracture. On the dry bed, tapping the bed usually reveals that plates are already parted and do not always cohere to the bed. In association with these observations, on both systems it is normally possible to see tracks of clast bang marks on the bed and from this KT deduces that clast impacts probably play a significant role in detaching plates (after which measured velocities of several meters/second are well able to entrain the clasts).

Waterfall recession. Recessive waterfalls and gorges with their knickpoints and their associated plunge pools are frequent and scenic features of bedrock systems. The energy gained from the head as the water drops over the knickpoint is dissipated in the plunge pool. The lithology of bedrock systems usually means that the long profile is stepped, and thus repetitive energy gain and dissipation is an intrinsic feature. There are suggestions [*Howard*, this volume; *Weissel and Seidl*, this volume] that knickpoints can stream from non-linear stream dynamics independently of base level change. Although rock downsteps may migrate upstream, and even laterally in a channel (as a knickzone enlarges), they are typically not easily effaced entirely. Virtually nothing is known about recession rates on major waterfalls - although there is *Derricourt* [1976] on the Victoria Falls (mm to cm/year, but over millions of years), *Tinkler et al.,* [1994] on Niagara Falls (mean 1m/yr, but 10 cm/yr during low flow phase), and *Nott et al.,* [1996] on the Shoalhaven Catchment in southeastern Australia. In the Shoalhaven catchment headwater recession has been 15 times faster than main escarpment wall recession. The now-regulated St. Anthony Falls on the Missouri River probably receded at about the same rate as Niagara Falls through the Holocene - about 1m year [*Winchell*, 1888; *Sardeson*, 1908]. In many recently glaciated terrains there is the possibility of assessing post-glacial rates of recession provided that there has been no re-occupation of ancestral gorges [*Engeln*, 1961; *Flint and Lolcama*, 1985; *Tinkler*, 1994], and provided some allowance can be made for the existence of different climatic conditions in the early post glacial period.

The mechanisms of retreat for major or minor knickpoints are not well documented. For Niagara, *Philbrick* [1970, 1974] has documented stages in the historic retreat of the crestline which are probably associated with major rockfalls from the crestline, and with the development of a series of plunge pools in the "Maid of the Mist" pool below the Falls, and which are separated by rock bars thought to represent former quasi-stationary positions of the crestline. *Tinkler et al.* [1994] report similar features at Niagara Glen, a remnant of the Niagara Gorge formed during lower average discharges.

Sculpted forms. Sculpted forms are expressions of persistence and localized turbulence which, because of the

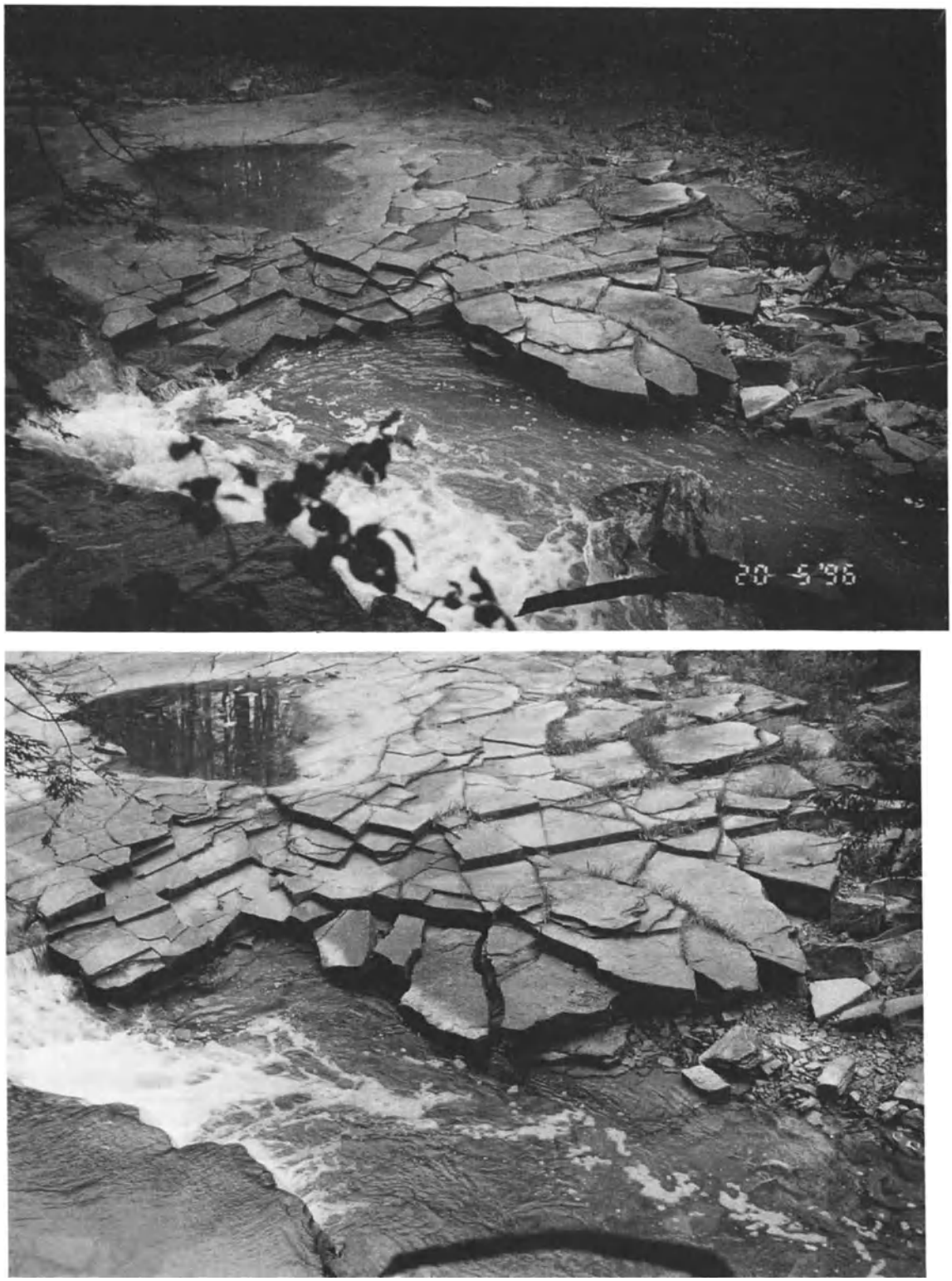

Figure 2. Twenty Mile Creek, Niagara Peninsula, Ontario. Evidence of block quarrying at a small knickzone on Twenty Mile Creek. Over a period of six years the zone has widened by about a meter over a length of 5 meters to a depth of about 70 cm [see Figure 2, *Tinkler and Wohl*, this volume, for reach map.) In the top photograph note that slabs have been parted along joints and slightly shifted by flows the previous years. In the bottom photograph, notice the arrival of a large limestone block located in the position occupied in flood flows by a large standing wave, generated by the knickpoint. In February 1997, this boulder moved further downstream during an ice drive [*Tinkler and Wohl*, this volume; *Carling and Tinkler*, this volume].

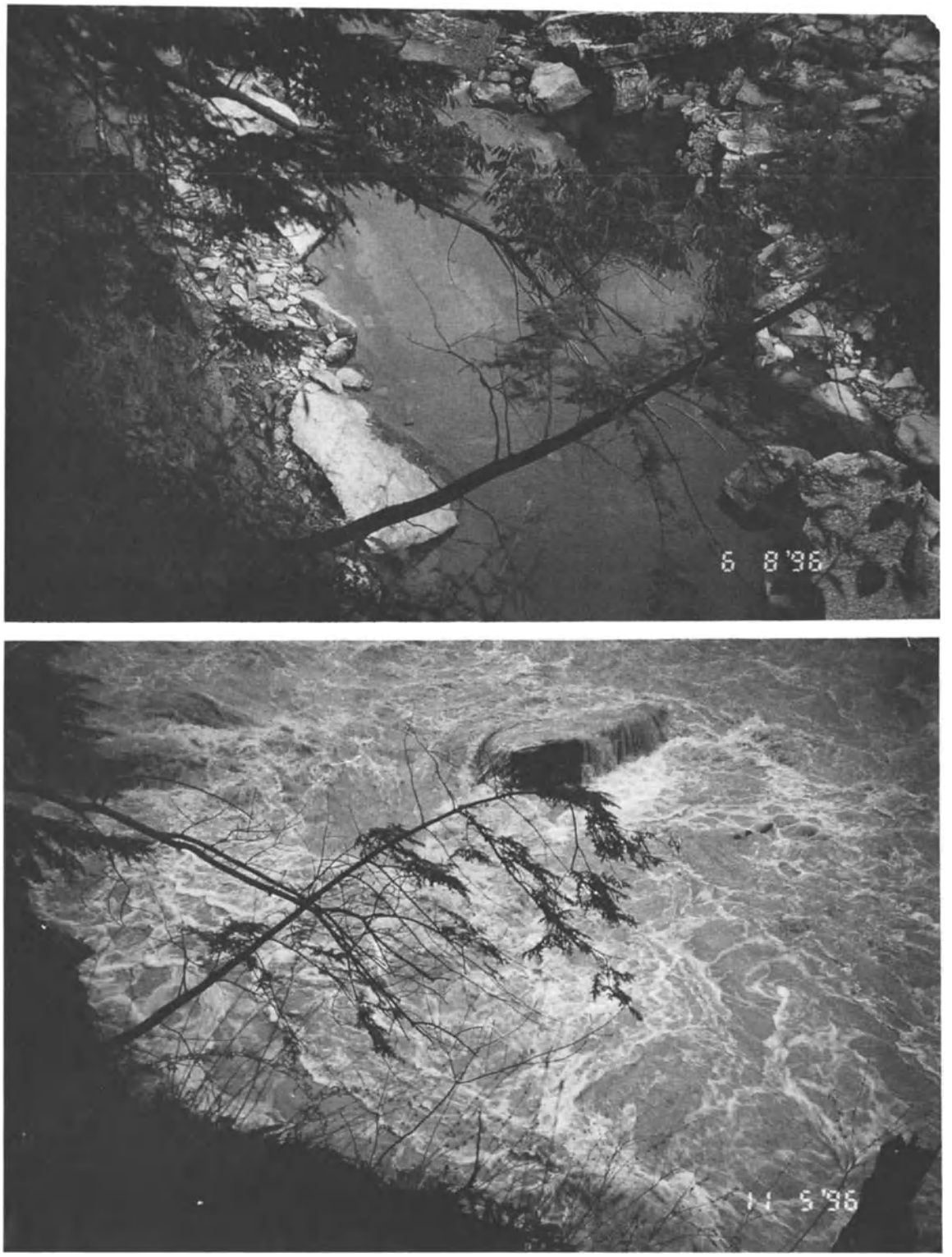

Figure 3. Seventy metres upstream of the last figure. Top photograph: the pale scar indicates a slab (seen bottom left), quarried from the bed during a flood (stage 130 cm) close to a Mean Annual Flood magnitude, and augmented by ice effects, in January 1996. The slab is four meters long, 2 meters wide, and about 25 cm thick. Several other comparable slabs were quarried from the stream bed a few tens of meters upstream during the same flow. Bottom photograph: flow conditions during a subsequent flood in May 1996, stage 105 cm. A hydraulic jump forms downstream of the boulder constriction (top left), and its locus moves downstream as stage rises. Downstream of the jump is a series of standing waves. [This photograph continues the bottom photograph in Figure 4.]

resistant nature of the rock, are able to persist as distinct morphologies through low flows [*Wohl,* this volume; *Hancock et al.*, this volume]. *King* [1927] describes forms which have degraded under the influence of limestone corrosion because they are now abandoned on a marginal channel ledge due to lowering of the central channel and which are now affected primarily by atmospheric forces.

Despite the spectacular character of potholes, grooves, and similar features [*Ängeby*, 1951; *Baker and Pickup* 1987; *Wohl*, 1992a, b; *Wohl*, 1993], smoothed rock surfaces are probably the most common and overlooked features. According to *Foley's* results [1980] using an abrasion model of rock incision, if a fluid is supplied with sufficient sediment, it can effect substantial erosion very quickly. *Sharpe and Shaw* [1989] and *Kor et al.*, [1991] in discussion of sub-glacially formed sculpted features attributed by them to meltwater, claim that the features formed within the timeframe of a single subglacial flood - something which may last at most a few days to a week or two. However, very little is known about true production rates, and it can probably be said with some safety that most of the time such features spend on actual stream beds is "downtime." Such forms are primarily evidence of slow morphological change, probably punctuated by periods of rapid change during large floods, as is implied by the model in *Foley* [1980], and by the need to submerge the forms below water with sufficient sediment, shear stress and power. They are best seen as expressions of turbulence which are able to persist through low flows, and on occasion for many years [*Tinkler*, 1997c].

Mechanisms. But the question posed as to how channel erosion is accomplished remains largely unanswered. With the exception of *Chapell's* [1974] work on carbonate terrains in New Guinea, no one has tried to estimate the relative proportions of channel erosion effected by different erosional propcesses, and there are almost no event-based measurements of channel erosion. In some systems very large clasts may form bed steps and may never move in present flow regimes. In such circumstances no erosion may take place, although sub-surface weathering may weaken the resisting rock so that when exposed it is more vulnerable to erosion. Alternatively the very large clasts may move in exceptional flows [*Grant et al.*, 1990].

Investigations of extreme flows along natural channels have indicated that cavitation may be an important process under conditions of turbulent, sediment-impoverished flow [*Baker* 1973; *O'Connor*, 1993]. Measurements of cavitation-induced erosion along engineered structures such as concrete-lined dam spillways support this idea. During the 1983 flood flows along the Colorado River, Arizona (USA), discharges of up to 900 m^3/s were released into the spillways of the Glen Canyon Dam for several days. Cavitation during these flows eroded pools up to 6 m long and 10 m deep in a staircase configuration down the face of the spillway [*Eckley and Hinchliff*, 1986].

Flow dynamics and hydraulics

Steepness. Of the controls on fluvial dynamics in bedrock channels, steepness is probably the most important. *Howard and Kerby* [1983] show that in a badlands system "bedrock" channels were systematically steeper than other channels. *Tinkler* [1997a] shows that by equating the critical flow equation to the Manning equation and solving for slope, an expression is obtained in which Manning's "n" and flow depth along the streamline determine the slope, s_{crit}, required for critical flow (revealed as standing waves):

$$s_{crit} = gn^2d^{-0.333}, \text{ where } g \text{ is } 9.81.$$

This criterion defines a "steep" fluvial system in the conventional hydraulic sense [*Chow*, 1959] as one in which flow is just critical, and in which discharge is at maximum efficiency for the energy available, and related aspects of velocity, stream power and shear stress are maximised. In consequence, sediment is readily entrained and the likelihood of a bedrock channel being revealed is at its greatest.

Critical flow. There are strong implications for channel morphology if critical flow dominates the channel [*Grant*, 1997; *Tinkler*, 1997a,b] because velocity, v, is determined entirely by depth via the equation $v = \sqrt{(gd)}$. Other features of channel morphology scale with this expression because the wavelength (λ) of standing waves controls the spatial distribution of shear stress on the bed, which in turn controls clast deposition both transverse and marginal to flow. Because critical flow is independent of roughness, slope and channel width, attempts to find consistent relationships of conventional hydraulic geometry such as characterize alluvial and subcritical systems will be doomed to failure.

The most obvious feature of a bedrock river in flood is the existence of quasi-stationary topography on the water surface, although at pronounced downsteps aerated flow and spray may disguise this fact. Standing wave trains (figure 4), zones of supercritical 'slick' flow, more placid zones of subcritical flow (typically at channel margins, or between critically flowing tongues of water), marginal zones of slack water and reversed flow cells, pronounced hydraulic jumps, and stable zones of intense vortices and upwelling and spreading 'bubbles' of water all characterize the flow surface. Observations in some wide and shallow bedrock rivers reveal that there is a central section of critical flow which is contained in what can be loosely thought of as a fluid 'floodplain' of slack or backwater whose depth increases as the discharge rises. At the same time, the central tube of critical flow increases in depth and speed [indexed by the increased distance between the standing waves *Tinkler* 1997b] but remains critical (figure 4a,b).

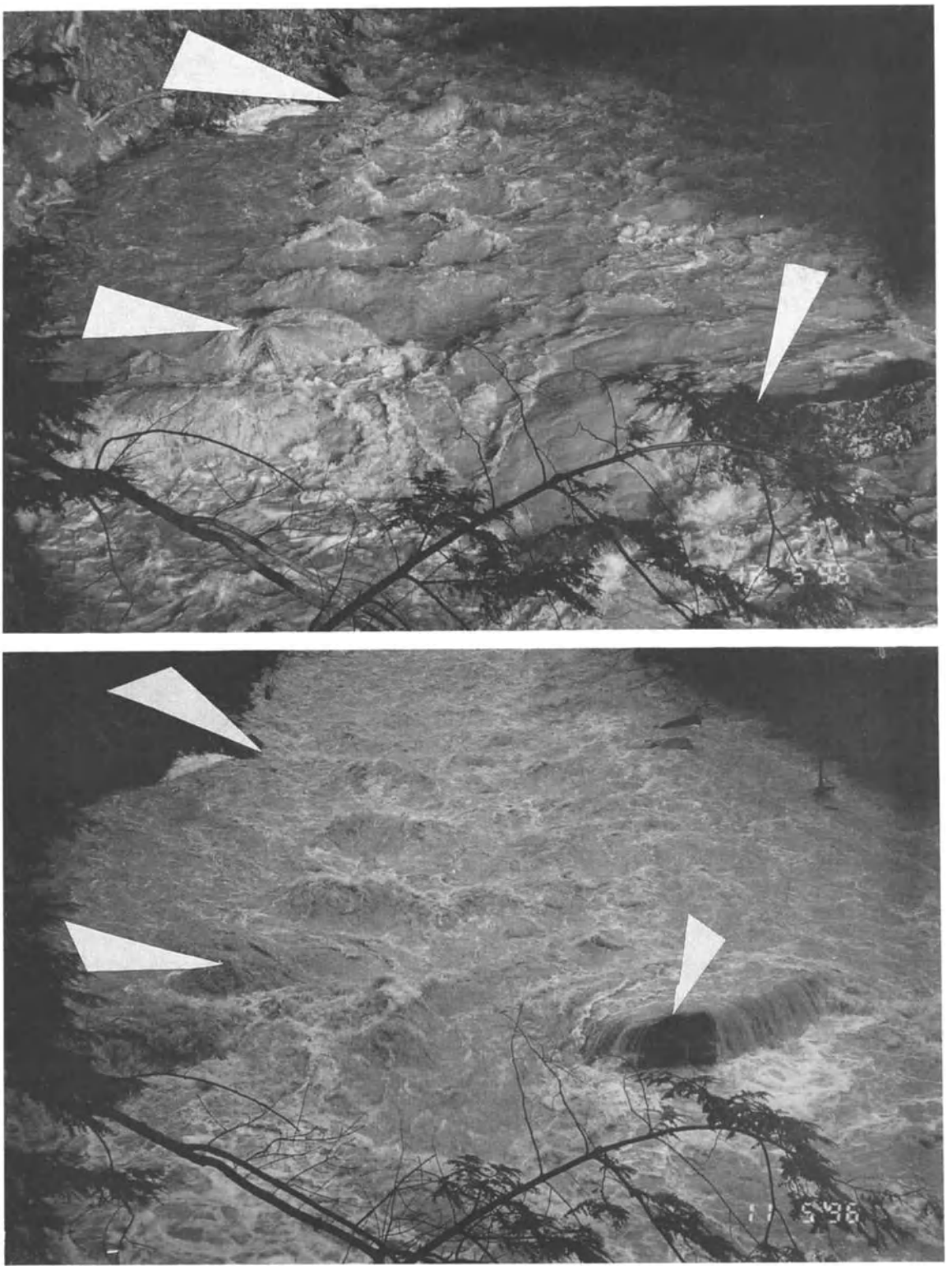

Figure 4. Standing wave trains at two different stages (for location see Figure 2 in *Tinkler and Wohl* [this volume]. Stage is 80 cm with wavelengths of 3.5 m (velocity 2.3 m/s) in the upper photograph; stage is 105 cm, wavelengths of 7 m (velocity 3.3 m/s) in the lower picture. Notice area of pooled water at upper left margin of photograph, with separated flow and water flowing upstream at both stages. At highest stage so far observed in this reach (153 cm, March 1998), wavelengths were about 10 m (velocity 3.95 m/s).

Standing wave systems are amazing to see - a winding line of strong stable wave hummocks (figure 5a). KT has innumerable photographs in a variety of situations, sometimes becoming oblique wave systems at bends when criticality extends across the channel. (KT saw evidence of critical flow on news videos of the Quebec floods in the summer of 1996). The wave systems are certainly related to normally clast-free zones and prominent zones of clast tracks, revealed on the stream bed when the flow drops (figure 5b).

A related factor to the standing wave trains is that kolks, or macro-turbulent structures originating near the bed [*Matthes*, 1947], are seen to emerge in stable locations alongside the wave trains, usually disturbing the surface of the marginal sub-critical water bodies.

An advantage of critical flow for modeling is that almost all the required characteristics of the flow can be computed directly. Because of the steeply sloping wave surfaces, basal shear stress, otherwise computed in the normal fashion, produces extraordinarily high values typical of catastrophic flood systems [about 25 times the reach mean value, *Tinkler*, 1997a].

Critical flow appears to be common in bedrock streams, although confined to a restricted spatial zone, because of the smooth boundary and the tendency to steep gradients. Because supercritical or critical flow is shallower, but faster, than subcritical flow, it follows that sediment transport of large clasts is enhanced, in view of the sensitivity of large clasts to roughly the sixth power of ambient velocity [*Hopkins*, 1844]. However, as depths increase in the bedrock channel the flow may remain critical, become supercritical, or revert to subcritical as downsteps and smaller knickpoints begin to 'drown out.' Field evidence [*Tinkler*, 1997a,b] suggests that flow may remain critical with increasing stage. On the other hand, velocities may stabilise without increasing as energy is dissipated across the entire channel width [*Tinkler*, 1997a; *Tinkler*, 1997b]. This is especially likely to happen if the channel bounds at high stages (water levels) are strongly confined or are especially rough. Gradients may simply be insufficient to maintain the required velocity, especially if roughness increases noticeably towards the channel boundary and reduced depths and marginal gravel are encountered. The latter is probable because of marginal gravel beaches, imbricate clast clusters, expansion bars, and the roughness of channel walls (which are sometimes gravel terraces), once the central, but expanding zone of critical flow encounters them. This suggests a sudden increase in friction from vorticity, possibly not matched by an equal decrease in boundary friction, and a reversion to subcritical flow. A possible corollary is a rapid increase in depth, and a reduction, or stabilisation of velocity as the regime transition - commonly termed 'drown-out' - takes place in a vertical sense within the channel.

On the other hand the integration of gradient along the channel may permit a transition to supercritical flow and indeed on a plane bedrock channel, as the wavelength of the standing waves of critical flow increases, substantial sections between the waves are, in effect, in a state of supercritical flow.

Supercritical flow. Despite controversy over the substantive existence of supercritical flow in natural channels, there has been the recent suggestion that on occasion both supercritical flow and the appearance of roll waves which surge down the channel, may be an overlooked factor in some reconstructions. *Hjalmarson and Phillips*, (1997) reviewed a flood analysis of 1971 for Bronco Creek, Arizona, and found that eye-witness evidence of traveling waves in the channel was ignored in subsequent analysis. Calculations showed that roll waves could have developed and persisted, and would have seriously affected discharge estimates. Such waves (of similar dimensions to those of standing waves appropriate to the channel depth) of water surging downstream, can, in extreme cases, store so much water that the channel between waves is almost dry [*Holmes*, 1936; *Foley and Vanoni*, 1977]. There are implications for palaeohydraulic estimates of peak flows, because the transient wave may emplace marginal debris mistakenly taken to evidence steady peak flow conditions so that discharge estimates may be substantially in error. Likewise, the velocities associated with the apparent depths may be seriously underestimated when large boulder transport is being considered. Roll waves appear to be likely whenever the Froude number is in excess of 1.6 [*Hjalmarson and Phillips*, 1997) and are more likely to be initiated on wide, shallow, steep systems, and over gravel surfaces (which may give rise downstream to rock bed channels). The waves generated then travel downstream, and they may persist for periods of hours during peak flow. Eye witnesses have often reported "walls of water" appearing in channels and these are almost certainly roll waves.

Balance of form and process, time and grade. There are two additional considerations. First, the balance between process and form is expressed over much longer time scales than is the case in alluvial systems because in many (but not all) instances the time scales of recurrent events effective in changing the form may be exceptionally long [*Baker and Kale*, this volume; *Tinkler and Wohl*, this volume]. This can mean, however, that properly interpreted morphology can be used to index flow dynamics. Second, there is extreme longitudinal variability in morphology, hydraulics and sediment transport, which may not scale with normal hydraulic geometry. As explained above, this may arise from the fact that critical or supercritical flow regimes dominate at channel-shaping discharges. The vexed issue of stream grade highlights this point. *Snow and Slingerland* [1987], and *Mackin* [1948 - see the famous "cream cheese" quote] show that highly irregular profiles may be substantially graded, even though substantial incision into bedrock remains to be effected.

In the much longer term, the hydrological flow series controls the very large-scale floods (documented in some

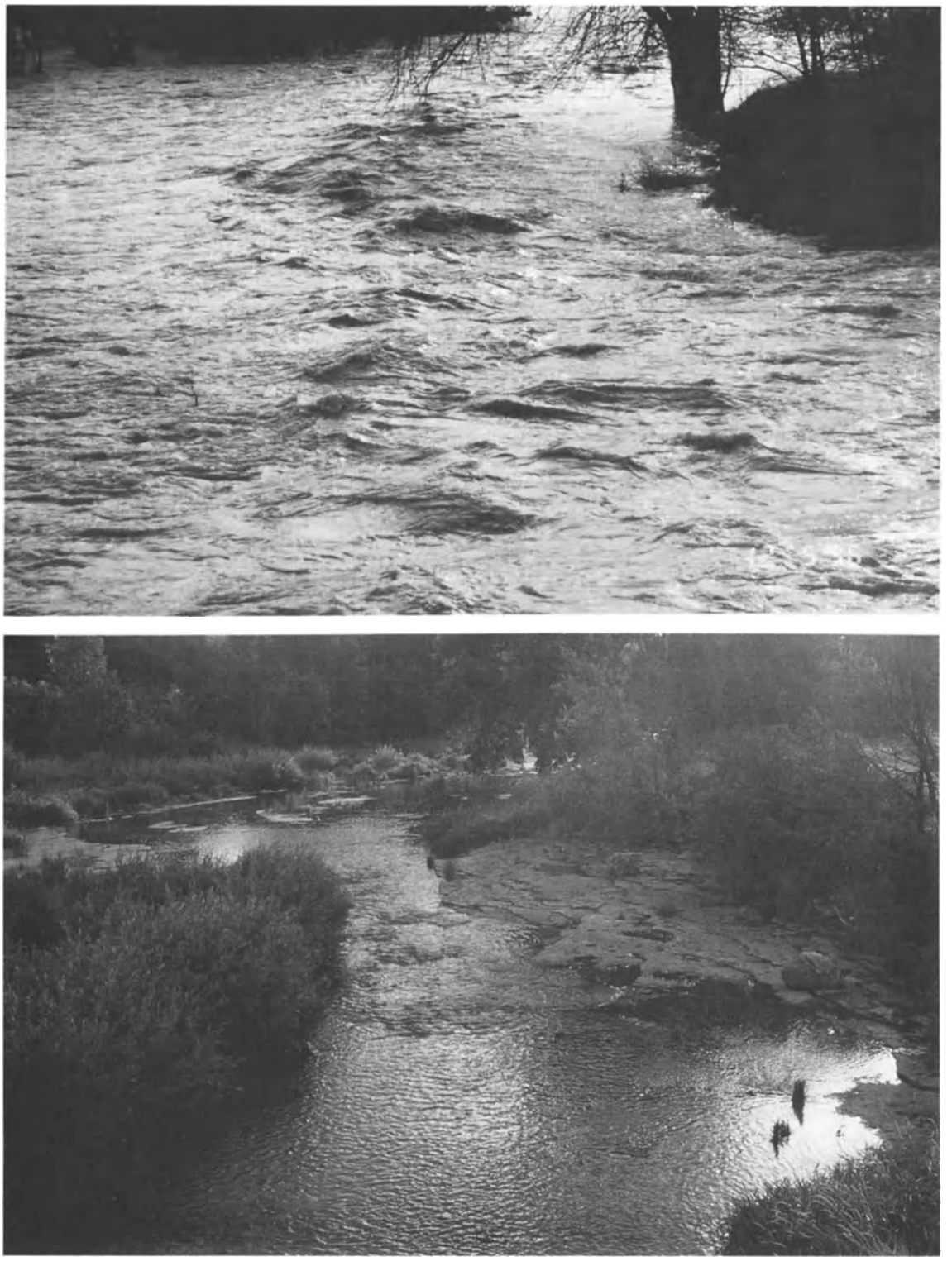

Figure 5. Twenty Mile Creek, Niagara Peninsula, Ontario. Top photograph: a system of critical flow standing waves generated by a gradually steepening gradient in a bedrock channel, viewed from the bridge on Victoria Avenue, looking downstream. The train is over one hundred meters long, and about 4 to 5 meters wide. Flow depth is about 1 meter (stage 105 cm), wavelength 6 to 7 meters. Bottom photograph: the same reach two months later. Notice the clear rock bed followed by the low flow, and the tiny rock downsteps (a few centimetres, each revealed by water ripples) which act to keep the gradient sufficient to maintain critical flow. Standing wave sets exist in this reach from at least stage 55 cm to stage 153.

systems by flood slackwater deposits) which affect river systems. Of course, these systems must be viewed as non-stationary over centuries and millennia; time scales which begin to be equivalent to postglacial time and major climatic anomalies (The Little Ice Age, Younger Dryas, etc.). The relative importance of such "catastrophic", long recurrence interval floods to bedrock systems can only be evaluated against the effects of smaller floods in the flood series [*Baker and Kale*, this volume].

Exceptions and catastrophic discharges. These criteria may have been violated during some exceptional catastrophic discharges such as the Missoula Flood [*Bretz*, 1923; *Bretz et al.*, 1956; *Baker*, 1973; *Baker*, 1978], the Bonneville Flood [*Jarrett and Malde*, 1987; *O'Connor*, 1993], and the Big Lost River Flood [*Rathburn*, 1993] but insofar as these discharges are exogenous to the normal flow regimes, they may be the exceptions that prove the rule. On the other hand there is little or no evidence that a particular canyon or scabland - in its entirety - is the result of a single flow, however tumultuous. If, for example, the Bonneville Flood cut the Snake Gorge in a single event, an account would have to be made of the progress of such incision during the flood. There is abundant evidence that gorge filling flows need not be gorge cutting flows - *Rashleigh* [1935] reports that the Guayra Falls (in Brazil) entirely drowned out during exceptional floods in 1905 and 1935 as a water level rise of 43 m in the lower gorge submerged the 40 m knickzone. Similarly the Falls on the Iguazu River were drowned out on two occasions by backed-up water from a 43 m rise on the Parana river to which the Iguazu is tributary, and in extreme floods the 58 m Paulo Affonso Falls lose at least half their height due to the water level rise in the lower gorge [*Rashleigh*, 1935]. But this is not to deny that unimaginable forces on Scabland scales may be in operation on the wetted perimeters of these systems. However, as will be highlighted later, very similar values of shear stress, shear velocity and power may exist in quite ordinary rivers during quite ordinary highflows, although admittedly in very restricted spatial zones such as under the distal faces of standing wave trains in critical flow, and in similar positions under any steep water surfaces.

Because of the relative resistance of bedrock channels to transient deformation, the caricatured image of bedrock systems is of an immobile, very resistant channel. However, even in resistant channels, rates of change may vary by several orders of magnitude along channels and among channels [Table 1, *Schumm and Chorley*, 1983] and noticeable change within a few decades is recorded (Table 2). Cooksville Creek, near Toronto (Canada) has a 'weak' shale bed and a recently urbanized basin, and provides an example of short term change [*Parish and Tinkler*, this volume]. There is abundant evidence of lowering rates on the order of 1 to 3 centimeters per year for the entire bed width of up to 10 meters along reaches of hundreds of meters, as a consequence of the standard (urbanized) flow regime. In knickzones below downsteps the rate has been several times higher. This is about ten times the rate that can be deduced for incisions since the early post-glacial in immediately adjacent streams in identical bedrock.

Methods of flow measurement. For all these reasons quite different and indirect methods have had to be developed to gauge flow, and some of these depend on sedimentological structures developed by the flow itself [*Baker*, 1973; *Foley and Vanoni*, 1977; *Shaw and Kellerhals*, 1977; *Carling*, 1989; *O'Connor*, 1993; *Carling*, 1995]. Others depend on characteristics of the water surface itself - for example, the size and height of waves, the spacing of standing wave trains [*Tinkler*, 1997a,b] or the vertical dimensions and planimetric angles of hydraulic jumps [*Carling*, 1995]

However, there is some chance that critical standing waves remain the primary form in the channel thalweg even at higher stages. Calculations on catastrophic flows (Missoula Flood, Bonneville Flood, Big Lost River) using the idea of critical flow show that they give good estimates of flow parameters obtained on the basis of HEC-2 modeling.

Sediment transport

It is well to bear in mind that the velocity and turbulence structures of rock-bound rivers are not well-known, and least of all as they bear upon sediment transport. In particular the role of macroturbulence. Macroturbulence is probably responsible for the suspension of substantial blocks and cobbles [*Leighly*, 1932, 1934; *Matthes*, 1947, and see discussion by *F. Matthes* in this paper with reference to the Potomac]. It must also be a factor in the development of lateral potholes [*Putzer*, 1971; *Zen and Prestegaard*, 1994] on steep rock faces, and fossil examples of which are known in the Niagara Gorge at Niagara Glen [*Tinkler et al.*, 1994]. Macroturbulence likely also is partly responsible for the emplacement of marginal clast clustering which in KT's streams seem to be spaced at similar intervals to the standing waves and which may be related to the outward sloping flanks of the critical waves.

It has sometimes been asserted that rocky rivers carry no fine sediments, but of course it depends entirely on the sediment available within the catchment; Niagara Peninsula rivers coat surfaces with up to 0.5 cm of fine silt and clay as the stage recedes. Typically this fine sediment then dries, contracts and curls, and washes away during intense rainfall which may not be long or extensive enough to affect river stage.

In general though, what characterizes bedrock rivers is coarse sediment from sand size upwards, but often and usually including coarse gravel upwards to boulders of metre or several metre dimensions. Large boulders clearly move in floods of catastrophic dimensions, but there is evidence that they also move in floods lying within the normal flood range. *Vaughn* [1990] records the quarrying and transport of

Table 1. Published long-term average rates of bedrock channel incision (after Schumm and Chorley, 1983, Table 3-5, and Wohl et al., 1994b, Table 1).

Rate (cm/kyr)	Lithology	Location	Drainage Area (km^2)	Climate, tectonics	Time range of incision	Source
9	granite, andesite	Sierra Nevada, California, USA	35 000	arid, uplift	Pliocene-Quaternary	Huber, 1981
30	sedimentary	Colorado, USA	11 800	semiarid, uplift	Miocene-Quaternary	Larson et al., 1975
7	metamorphic	Colorado, USA	----	semiarid, uplift	Pliocene-Quaternary	Scott, 1975
45-130	sedimentary	Nahal Zin, Israel	1 540	hyperarid, uplift	Quaternary	Goldberg, 1976 Schwarcz et al., 1979 Yair et al., 1982
10	sedimentary	Nahal Paran, Israel	3 600	hyperarid, uplift	Quaternary	Wohl et al., 1994b
30	basalt, limestone	Utah, USA	9 900	semiarid, uplift	Quaternary	Hamblin et al., 1981
9.5	sedimentary	Arizona, USA	68 500	semiarid, uplift	Quaternary	Rice, 1980
23-25	basalt	Jalisco, w. Mexico	----	arid, uplift	Pliocene-Quaternary	Righter, 1997
15	suggested average rate of bedrock channel incision in the middle latitudes					Pitty, 1971
25-47	sedimentary	Utah, USA	115 000	semiarid, uplift	Quaternary	Harden and Coleman, 1989
1 000	igneous and metamorphic	Pakistan	260 000	semiarid, uplift	Quaternary	Leland et al., 1995
70-180	sedimentary	n. California, USA	655	Mediterranean, uplift	Holocene	Merritts et al., 1994
<25	sedimentary, intrusive igneous	Central California, USA	10-20	Mediterranean, uplift	Quaternary	Rosenbloom and Anderson, 1994
0.5-8	basalt	Kauai, USA	0.1-90	seasonal tropical to semiarid, uplift	Pliocene-Quaternary	Seidl et al., 1994
*40-100	basalt	Kauai, USA	0.1-90	seasonal tropical to semiarid, uplift	Pliocene-Quaternary	Seidl et al., 1997
50-690	sedimentary	Montana, USA	1 420	humid temperate, uplift	Quaternary	Foley, 1980b
≤1000	mudstone	s. Japan	0.15-0.4	humid temperate, uplift	Quaternary	Mizutani, 1996
5.7	limestone	New Guinea	0.02	humid tropical, uplift	Quaternary	Chappell, 1974
*$\leq 1.57 \times 10^5$	sedimentary	Ontario, Canada	686 000	humid temperate, passive	Quaternary	Tinkler et al., 1994
0.5-3	basalt, metamorphic	southeastern Australia	20-400	humid temperate, passive	Miocene-Quaternary	Young and McDougall, 1993
300	basalt, sedimentary	Svalbard, Norway	----	subpolar, passive	Quaternary	Büdel, 1982
2.7	Carbonates, Crystalline rocks	Virginia, USA	----	humid temperate, passive	Quaternary	Granger et al., 1997

* knickpoint migration upstream

Table 2. Published short-term rates of bedrock channel incision based on direct measurements.

Rate (cm/yr)	Lithology	Location	Drainage Area (km^2)	Climate, tectonics	Time range of incision	Source
6-38	sedimentary	Virginia, USA	$9.2x10^{-6}$ to $9.2x10^{-2}$	humid temperate, passive	2 years	Howard and Kerby, 1983
2	sedimentary	Ontario, Canada	34	humid temperate, passive	Variable	Parish and Tinkler, 1996, in this volume
2-3	sedimentary	Boso Peninsula, Japan	10	humid temperate, uplift	300 years	Wohl and Ikeda, in press, 1998
4-10	sedimentary	Ukak River, Alaska	n/a	sub-arctic	~80 years	Dollenmayer and Whipple, 1997
≤0.4	igneous	Indus, India	10^5	tropical	1 year	Dick et al., 1997, Hancock et al., this volume

concrete blocks in an urban channel in Kansas City. This is likely because of the critical flow conditions, and correspondingly high velocities, which seem to characterize bedrock channels. There are few formal records of sediment transport in bedrock channels, although to the extent that in some rivers bedrock alternates with gravel bed one would expect a partial carry over from the documented behaviour of gravel bed streams. From our experience, step-lengths for coarse sediment in rock channels are long (tens to hundreds of meters, even for big blocks), mainly reflecting (i) high ambient velocities and (ii) the limited opportunities for trapping sediment in transit within niches offered by larger debris - as for example may happen with gravel-bed streams. Depositional characteristics of sand and gravel sediments have been used to infer discharge and hydraulic variables along bedrock canyons [*Baker*, 1973, 1987; *Baker and Pickup*, 1987; *O'Connor et al.*, 1986; *Wohl*, 1992a; *Cluer* 1997]. Boulder bars and boulder berms may also reflect cross-channel and longitudinal patterns of hydraulics [*Carling*, 1989, 1995; *Cenderelli and Wohl*, in press; *Cenderelli and Cluer*, this volume].

Suspended sediment - on the experience of alluvial streams [*Stone and Saunderson*, 1992] - is rarely regarded as being coarser than sand-sized, but there is abundant evidence from Niagara Peninsula streams that it may be as coarse as -6 phi, or even larger - and this as a matter of course in flows approaching the MAF. Because it is suspended sediment - or as *Martin and Church* [1995] has redefined it "wash load" - it is capable of generating wear on channel surfaces of both *in situ* rock, and large boulders. Because the sources and quantities of this sediment may be limited, and the flood long enough to remove most of it from channel bed locales, the fine sediment (wash load) is not immediately apparent in the channel after floods. From (mainly solutional, but also partly worn) potholes 25 cm deep and about 10-15 cm in diameter KT has collected several hundred grams of sediment after a single flood. These potholes are perched above the rock bed in positions in which the only feasible entry is as suspended sediment in the body of the fluid. The proximal faces of these boulders display wear from the impact of clasts.

Clearly the suspension of such coarse sediment facilitates wear on rock surfaces. However, fine sculpted detail must owe more to more normally fine-grained sediment in suspension *[Hancock et al.*, this volume], but certainly there is much to be discovered in this area.

QUESTIONS NEEDING ANSWERS

Given the dearth of recent work on modern processes acting along bedrock channels the field is wide open, and indeed one essential aspect is the description of bedrock systems in a wide variety of environments. Under the headings discussed above we will try to indicate some major vacuums. In the effort to understand long-term landscape change, bedrock systems are important because they are, for the most part, the locus of the most rapid change in the basin, and in continental scale systems they control the delivery of base level change to the interior.

We need to know the distribution in specific regions of bedrock channels, proportions relative to other channel types, and their relationship to position in the standard stream-ordering schemes. The relationship of bedrock exposure to basin and reach slope and its relationship to gravel bed systems needs exploring.

A working definition

Is the working definition given earlier adequate? or are other proportions more appropriate? Also, should we use "bedrock" or "rockbed"; KT and EW disagree on this point. Bedrock is the term entrenched in the geological literature, although with much wider use than channels. Rockbed is more specific to channels, and is consistent with the terms "sand bed" and "gravel bed."

Bedrock channel characteristics

Evidence of morphological change. Much, though sporadic, emphasis has already been placed on the description of sculpted forms: perhaps now we need more formal studies of these forms in relation to rates of wear, controlling flow conditions, distribution in the channel, AND, a recognition that erosion may be proceeding faster (and may be easier to track) in systems which do not display dramatic sculpted forms. In addition, good descriptions of bedrock channel morphologies are required and their relation to transitional forms of gravel and alluvial bed systems both laterally in the channel, and longitudinally along reaches. Under what conditions do substrate discontinuities (joints, bedding, lithologic change) dominate bedrock channel morphology, and under what conditions do bedrock channels approximate *Allen's* (1969) passive-bed that records flow-structure? What are the relative importances of the primary erosional processes of cavitation, corrasion, and corrosion in bedrock channels? The process of channel bed and wall weathering, and the preparation time for block removal - which makes possible morphological change - are also major lacunae. Complementary needs are to assess the instruments and find the best methods to quantify the form, state of weathering and general resistance of the 'hard' channel boundary.

There is a good chance that careful fieldwork together with the range of modern geochronologic techniques will refine our present understanding of rates of incision (and their relation to individual flows, or long term control by the hydrological 'climate') and knickpoint retreat (including major knickpoints such as waterfalls).

Flow dynamics and hydraulics

There is a huge range of questions here. A primary one is the confirmation, or otherwise, of the existence, distribution and characteristics of critical and supercritical flow during highflows and floods: aerial or elevated view photographs should enable the identification of standing wave trains and the oblique waves characteristic of supercritical flow. Close observation and measurement of high flood flows will remain a priority for many years to come. Whatever the outcome, considerable attention must be paid to the gamut of transcritical flow structures that develop within the complex morphologies of natural channels as stage changes.

As a corollary, the cross-sectional character of highflows must be carefully established, especially when flow is transcritical. Water-surface topography with particular attention to slope (and its short-term variability) over small areas is a very important area to explore because of its impact on basal shear stress. The vertical profile of velocity, and the near-bed velocities experienced over smooth beds in deep flows are open problems with obvious impacts on sediment entrainment and transport and bed erosion (hydraulic lifting, plucking or quarrying). In extension, a better three-dimensional understanding of flow structure and turbulence is clearly required. Some of these questions are well-suited to laboratory work, and the hard bed forms (and their impact on flow structures) perhaps offer less difficulty to modeling and measurement than soft bed systems.

The interaction of these factors with sediment production and transport and morphological change (erosion of the channel) is the driving purpose behind such investigations. The development of a series of remote, reliable, non-invasive measurement techniques is paramount, because the velocities encountered in such systems make nonsense of the usual methods. This should be an area where techniques tested and experience gained in the flume may in time be transferred to selected natural channels.

As a corollary, numerical modelling needs to address more completely transcritical flow in the cross-section and three dimensional structures within the water body. The nature of flow dynamics in highly turbulent high gradient zones - stepdowns and knickpoints up to the scale of major waterfalls - has to be tackled.

Sediment transport

Although bedrock systems are sediment sparse, they are typically extremely efficient. However, this understanding needs refining in the light of better information on sediment budgets. The common relationship of bedrock reaches to gravel bed systems suggests that complementary approaches may be possible. The probability of the existence of extremely coarse suspended sediment needs to be borne in mind, and attention needs to be paid to the modes of entrainment and transport of large clasts [*Graf*, 1979; *Carling and Tinkler*, this volume]. The measurement of clast velocities, and their method of motion, during entrainment would clarify their energetics. Methods of estimating the resistance of these large clasts need further attention; present methods (of estimating size and weight) are probably all too "rough and ready" for the accuracy that is really needed.

Other factors

These include the effect of winter ice (anchor ice) and meltout effects, and large woody debris dams. Both these factors in their separate ways have material effects on flow dynamics and sediment entrainment, and both are treated too

often as exotica; they need to be seen as intrinsic, not extrinsic, factors, especially in light of the natural woodland vegetation prevailing in many regions until recently.

The effects of flow regulation associated with large dams on erosional and depositional patterns along bedrock canyons need much attention. Much the same can be said for urban bedrock systems. Changes in such patterns may affect flood hazard, aquatic and riparian communities, and human recreational use of these canyons. A substantial body of research has been conducted in the Grand Canyon of the Colorado River (USA), but this is an exception worldwide, despite the increasing prevalence of large dams on canyon rivers.

Acknowledgments. We thank Stanley Schumm for his helpful remarks on an earlier version of this paper. Keith Tinkler wishes to thank Brock University for research support over many years, and NSERC (Canada) for a Research Grant to work on bedrock fluvial systems.

REFERENCES

Alexander, H. S., Pothole erosion, *J. Geol.*, 40, 305-337, 1932.

Allen, J. R. L., Erosional current marks of weakly cohesive mud beds, *J. Sed. Pet.*, 39, 607-623, 1969.

Ängeby, O., Pothole erosion in recent waterfalls, *Lund Studies in Geography, Series A, Physical Geography*, 2, 1951.

Baker, V., *Paleohydrology and sedimentology of Lake Missoula flooding in eastern Washington*, 79p, Geological Society of America, 1973.

Baker, V. R., Paleohydraulics and hydrodynamics of Scabland Floods, in *The Channeled Scabland*, edited by V. R. Baker and D. Nummedal, pp. 59-80, NASA, Washington, D.C., 1978.

Baker, V. R., The Spokane Flood Debate and its legacy, in *Geomorphic Systems of North America*, edited by W. L. Graf, pp. 416-423, Vol, Centennial Special Volume 2, Geological Society of America, Boulder, 1987.

Baker, V. R. and G. Pickup, Flood geomorphology of the Katherine Gorge, Northern Territory, Australia, *Geol. Soc. Amer. Bull.*, 98, 635-646, 1987.

Blank, H. R., Pothole grooves in the bed of the James River, Mason County, Texas, *Texas J. Sci.*, 10, 293-301, 1958.

Blank, H. R., Incised meanders in Mason County, Texas, *Geol. Soc. Amer. Bull.*, 81, 3134-3140, 1970.

Büdel, J., *Climatic Geomorphology*, Princeton University Press, Princeton, New Jersey, 1982.

Bretz, J. H., The Channeled Scabland of the Columbia Plateau, *J. Geol.*, 31, 617-649, 1923.

Bretz, J. H., H. T. U. Smith and G. E. Neff, Channeled Scablands of eastern Washington: new data and interpretations, *Geol. Soc. Amer. Bull.*, 67, 957-1049, 1956.

Carling, P., Hydrodynamic models of boulder berm deposition, *Geomorphology*, 2, 319-340, 1989.

Carling, P. A., Flow-separation berms downstream of a hydraulic jump in a bedrock channel, *Geomorphology*, 11, 245-253, 1995.

Chappell, J., The geomorphology and evolution of small valleys in dated coral terraces, New Guinea, *J. Geol.*, 82, 795-812, 1974.

Chow, V. T., *Open Channel Hydraulics*, 680p, McGraw-Hill, New York, 1959.

Cluer, B.L., Eddy bar responses to sediment dynamics of pool-riffle environments, PhD thesis, Colorado State University: Fort Collins, 1997.

Derricourt, R. M., Retrogression rate of the Victoria Falls and the Batoka Gorge, *Nature*, 264, 23-25, 1976.

Dick, G.S., R.S. Anderson, and K.X Whipple, Fluvial bedrock erosion measurements, Indus River, Pakistan, reveal control by local flow conditions, *EOS, Transactions, American Geophysical Union, 78* (46), F299, 1997.

Dollenmayer, K., K.X Whipple, and N.P. Snyder, Rates and processes of bedrock channel incision along the upper Ukak River, Valley of Ten Thousand Smokes, AK, *EOS, Transactions of the American Geophysical Union, 78* (46), F299, 1997.

Eckley, M. S. and D. L. Hinchliff, Glen Canyon Dam's quick fix, *ASCE Civil Engineering*, 56, 46-48, 1986.

Ely, L. L., Y. Enzel, V. R. Baker and D. R. Cayan, A 5000-year record of extreme floods and climate change in the southwestern United States, *Science*, 262, 410-412, 1993.

Engeln, O.D. von, *The Finger Lakes Region: its origin and nature*, 156p, Cornell University Press, Ithaca: New York, 1961.

Enzel, Y., L.L. Ely, P.K. House, V.R. Baker, and R.H. Webb, Paleoflood evidence for a natural upper bound to flood magnitudes in the Colorado River Basin, *Water Resourc. Res., 29* (7), 2287-2297, 1993.

Flint, J. J. and J. Lolcama, Buried ancestral drainage between Lakes Erie and Ontario, *Geol. Soc. Amer. Bull.*, 97, 75-84, 1985.

Foley, M. G., Bed-rock incision by streams, *Geol. Soc. Amer. Bull.*, 91, Part II (2189-2213), 1980.

Foley, M. G. and V. A. Vanoni, Pulsing flow in steep alluvial streams, *J. Hyd. Eng.*, 103(8), 843-850, 1977.

Gardner, T. W., Experimental study of knickpoint and longitudinal profile evolution in cohesive, homogeneous material, *Geol. Soc. Amer. Bull.*, 94, 664-672, 1983.

Goldberg, P., Upper Pleistocene Geology of the Avdat/Aqev area, in *Prehistory and Paleoenvironments in the Central Negev, Israel*, edited by A.E. Marks, pp. 25-55, Southern Methodist University Press, Dallas, 1976.

Graf, W. L., Rapids in canyon rivers, *J. Geol.*, 87, 533-551, 1979.

Granger, D.E., and J.W. Kurchner, Quaternary downcutting rate of the New River, Virginia, measured from ^{26}AL and ^{10}Be, *Journal of Geology, 25* (2), 107-110, 1997.

Grant, G.E., Critical flow constrains flow hydraulics in mobile-bed streams: A new hypothesis, *Water Resourc. Res.*, 33, 349-358, 1997.

Grant, G.E., Swanson , F.J. and M.G. Wolman, Pattern and origin of stepped-bed morphology in high-gradient streams, Western Cascades, Oregon, *Geol. Soc. Amer. Bull., 102*, 340-352, 1990.

Hamblin, W.K., P.E. Damon, and W.B. Bull, Estimates of vertical strain rates along the western margins of the Colorado Plateau, *Geology, 9*, 293-298, 1981.

Harden, D.R., and S.M. Colman, Geomorphic and Quaternary History of Canyonlands, southeastern Utah, in *Geological SOciety of America field trip Guidebook Professional*

Contributions of the Colorado School of Mines, edited by G.S. Hoden, pp. 336-369, Geological Society of America, Boulder, Colorado, 1988.

Harvey, M. D., R. A. Mussetter and E. J. Wick, A physical process-biological response model for spawning habitat formation for the endangered Colorado squawfish, *Rivers*, 4, 114-131, 1993.

Hjalmarson, H. W. and J. V. Phillips, Potential effect of translatory waves on estimation of peak flow, *J. Hyd. Eng.*, 123(6), 571-575, 1997.

Holland, W. N. and G. Pickup, Flume study of knickpoint development in stratified sediment, *Geol. Soc. Amer. Bull.*, 87, 76-82., 1976.

Holmes, W. H., Travelling waves in steep channels, *Civil Eng.*, 6(7), 467-468, 1936.

Hopkins, W., On the transport of erratic blocks, *Trans. Cambridge Phil. Soc.*, 8(2), 220-240, 1844.

Howard, A. D., Modelling fluvial systems: rock-, gravel- and sand-bed channels, in *River channels: environment and process*, edited by K. Richards, pp. 69-94, Basil Blackwell, Oxford, 1987.

Howard, A. D., W. E. Dietrich and M. A. Seidl, Modelling fluvial erosion on regional to continental scales, *J. Geophys. Res.*, 88(13), 971-986, 1994.

Howard, A. D. and G. Kerby, Channel changes in badlands, *Geol. Soc. Amer. Bull.*, 94, 739-752, 1983.

Huber, N.K., Amount and timing of late Cenozoic uplift and tilt of the central Sierra Nevada, California - evidence from the upper San Joaquin River Basin, *United States Geological Survey Professional Paper, 1197*, 1-28, 1981.

Jarrett, R. D., Hydraulics of high-gradient streams, *J. Hyd. Eng.*, 110, 1519-1539, 1984.

Jarrett, R. D., Hydraulics of mountain rivers, in *Channel Flow Resistance: centennial of Manning's formula*, edited by B. C. Yen, pp. 287-298, Water Resources Publications, Littleton, Colorado, 1992.

Jarrett, R. D. and R. E. Malde, Paleodischarge of the late Pleistocene Bonneville Flood, Snake River, Idaho, computed from new evidence, *Geol. Soc. Amer. Bull.*, 99, 127-134, 1987.

Kieffer, S.W., Hydraulic maps of Major Rapids, Grand Canyon, Arizona, *United States Geological Survey Miscellaneous Investigations* (Map Series I-1897- A-J), 1988.

Kieffer, S.W., Geologic nozzles, *Rev. Geophys., 27*, 3-38, 1989.

King, P. B., Corrosion and corrasion on Barton Creek, Austin, Texas, *J. Geol.*, 35, 631-638, 1927.

Kor, P. S. G., J. Shaw and D. R. Sharpe, Erosion of bedrock by subglacial meltwater, Georgian Bay, Ontario: a regional view, *Can. J. Earth. Sci.*, 28, 623-642, 1991.

Larsen, E.E., M. Ozima, and W.C. Bradley, Late Cenozoic basin volcanism in northwestern Colorado and its implications concerning tectonism and the origin of the Colorado River system, in *Cenozoic History of the Southern Rocky Mountains*, edited by B.F. Curtis, pp. 155-178, Geological Society of America, Boulder: Colorado, 1975.

Leighly, J.B., Towards a theory of the morphologic importance of turbulence in the flow of water in streams, *University of California Publications in Geography, 6* (1), 1-22, 1932.

Leighly, J. B., Turbulence and the transportation of rock debris by streams, *Geographical Review*, 24, 453-464, 1934.

Leland, J., D.W. Burbank, and M.R. Reid, Differential bedrock incision rates along the Indus River in northern Pakistan determined by cosmogenic dating of straths, *EOS Trans AGU., 75*, 288, 1994.

Leopold, L. B., M. G. Wolman and J. P. Miller, *Fluvial processes in Geomorphology*, 522p, W.H. Freeman, San Francisco, 1964.

Mackin, J. H., Concept of the graded river, *Geological Society of America, Bulletin*, 59, 632-636, 1948.

Matthes, G. H., Macroturbulence in natural stream flows, *EOS Trans. AGU.,*, 28, 255-265, 1947.

Martin, Y., and M. Church, Bed-material transport estimated from channel surveys: Vedder River, British Columbia, *Earth Surf. Proc. Landf., 20*, 347-361, 1995.

Maxson, J. H., Fluting and faceting of rock fragments, *J. Geol.*, 48, 717-751, 1940.

Maxson, J. H. and I. Campbell, Stream fluting and stream erosion, *J. Geol.*, 43, 729-744, 1935.

Merritts, D. J., K. R. Vincent and E. E. Wohl, Long river profiles, tectonism, and eustasy: a guide to interpreting fluvial terraces., *J. Geophys. Res. (Special Issue on Tectonics and Topography)*, 99(B7), 14031-14050, 1994.

Miller, A. A., Entrenched meanders of the Hertfordshire Wye, *Geographical Journal*, 85, 160-78, 1935.

Miller, J. R., Controls on channel form along bedrock-influenced alluvial streams in south-central Indiana, *Physical Geography*, 12, 167-186, 1991a.

Miller, J. R., The influence of bedrock geology on knickpoint development and channel-bed degradation along downcutting streams in south-central Indiana, *J. Geol.*, 99, 591-605, 1991b.

Mizutani, T., Longitudinal profile evolution of valleys on coastal terraces under the compound influences of uestasy, tectonism and marine erosion, *Geomorphology, 17*, 317-322, 1996.

Montgomery, D. R., T. B. Abbe, J. M. Buffington, N. P. Peterson, K. M. Schmidt and J. D. Stock, Distribution of bedrock and alluvial channels in forested mountain drainage areas, *Nature*, 381(June 13th), 1996.

Nott, J., R. Young and I. McDougall, Wearing down, wearing back, and gorge extension in the long-term denudation of a highland mass: quantitative evidence from the Shoalhaven catchment, southeast Australia, *J. Geol.*, 104, 224-232, 1996.

O'Connor, J. E., Hydrology, Hydraulics, and Geomorphology of the Bonneville Flood, *Geol. Soc. Amer. Special Paper*, 274, 83, 1993.

O'Connor, J. E., R. H. Webb and V. R. Baker, Paleohydrology of pool-riffle pattern development: Boulder Creek, Utah, *Geol. Soc. Amer. Bull.*, 97, 410-420, 1986.

Philbrick, S. S., Horizontal configuration and the rate of erosion of Niagara Falls, *Geol. Soc. Amer. Bull.*, 81, 3723-3732, 1970.

Philbrick, S. S., What future for Niagara Falls?, *Geol. Soc. Amer. Bull.*, 85, 91-98, 1974.

Pitty, A.F., *Introduction to Geomorphology*, 526 pp., Methuen, London, 1971.

Putzer, H., Kolke im Cabora-Bassa Canyon des mittleren Sambesi, *Zeit. Geomorph.*, 15, 330-338, 1971.

Rashleigh, E. C., *Among the waterfalls of the world*, 288p, Jarrolds, London, 1935.

Rathburn, S. L., Pleistocene cataclysmic flooding along the

Big Lost River, east central Idaho, *Geomorphology*, 8, 305-319, 1993.

Rosenbloom, N.A., and R.S. Anderson, Hillslope and channel evolution in a marine terraced landscape, Santa Cruz, California, *Journal of Geophysical Research, 99* (B7), 14,013-14,029, 1994.

Rice, R.J., Rates of erosion in the Little Colorado valley, Arizona, in *Timescales in geomorphology*, edited by R.A. Cullingford, D.A. Davidson, and J. Lewin, pp. 317-331, Chichester, John Wiley and Sons, 1980.

Righter, K., High bedrock incision rates in the Atenguillo River Valley, Jalisco, Western Mexico, *Earth Surf. Proc. Landf.*, *22*, 337-343, 1997.

Sardeson, F. W., Beginning and recession of Saint Anthony Falls, *Bull.Geol.Soc. Amer.*, 19, 29-52, 1908.

Schumm, S. A. and R. J. Chorley, Geomorphic controls on the Management of Nuclear Waste, US Regulatory Commission, Washington, DC, NUREG/CR-3276, 1983.

Schwarcz, H.P., B. Blackwell, P. Goldberg, and A.E. Marks, Uranium series dating of travertine from archeological sites, Nahal Zin, Israel, *Nature, 277*, 558-560, 1979.

Scott, G.R., Cenozoic surfaces and deposits in the southern Rocky Mountains, in *Cenozoic History of the Southern Rocky Mountains*, edited by B.F. Curtis, pp. 227-248, Geological Society of America, Boulder: Colorado, 1975.

Seidl, M. A. and W. E. Dietrich, The problem of channel erosion into bedrock, in *Functional Geomorphology*, edited by K.-H. Schmidt and J. d. Ploey, pp. 101-124, Vol, Catena Supplement 23, 1993.

Seidl, M.A., W.E. Dietrich, and J.W. Kirchner, Longitudinal profile development into bedrock: an analysis of Hawaiian channels, *Journal of Geology, 102*, 457-474, 1994.

Seidl, M. A., R. C. Finkel, M. W. Caffee, G. B. Hudson and W. E. Dietrich, Cosmogenic istope analyses applied to longitudinal profile evolution: problems and interpretations, *Earth Surf. Proc. Landf.*, 22, 195-209, 1997.

Sharpe, D. R. and J. Shaw, Erosion of bedrock by subglacial meltwater, Cantley, Quebec, *Geol. Soc. Amer. Bull.*, 101, 1011-1020, 1989.

Shaw, J. and R. Kellerhals, Paleohydraulic interpretation of antidune bedforms with applications to antidunes in gravel, *J. Sed. Pet.*, 47(1), 257-266, 1977.

Shepherd, R. G., Incised River Meanders: evolution in simulated bedrock, *Science*, 178, 409-411, 1972.

Shepherd, R. G. and S. A. Schumm, Experimental study of river incision, *Geol. Soc. Amer. Bull.*, 85, 257-268, 1974.

Simon, A. and J. H. Hardison, Critical and supercritical flow in two unstable mountain rivers, Toutle River system, Washington, paper presented at *Hydraulic Engineering, Buffalo*, edited by G. V. Cotroneo and R. R. Rumer, American Society of Civil Engineers, 732-736, 1994.

Snow, R. S. and R. L. Slingerland, Mathematical modeling of graded river profiles, *J. Geol.*, 95, 15-33, 1987.

Stone, M. and H. Saunderson, Particle size characteristics of suspended sediment in southern Ontario rivers tributary to the Great Lakes, *Hydrological Processes*, 6, 189-198, 1992.

Tinkler, K. J., Fluvially sculpted rock bedforms in Twenty Mile Creek, Niagara Peninsula, Ontario, *Can. J. Earth. Sci.*, 30, 945-953, 1993.

Tinkler, K. J., Déja vu: the downfall of Niagara as a chronometer 1845-1941, in *Niagara's Changing Landscapes*, edited by H. J. Gayler, pp. 81-109, Carleton University Press, Ottawa-Canada, 1994.

Tinkler, K. J., Critical flow in rockbed streams with estimated values for Manning's *n*, *Geomorphology*, 20, 147-164, 1997a.

Tinkler, K. J., Indirect velocity measurement from standing waves in rockbed streams, *J. Hyd. Eng.*, 123(10), 918-921, 1997b.

Tinkler, K. J., Rockbed wear at a flow convergence zone in Fifteen Mile Creek, Niagara Peninsula, Ontario, *J. Geol.*, 105(2), 263-274, 1997c.

Tinkler, K. J., J. W. Pengelly, W. G. Parkins and G. Asselin, Postglacial recession of Niagara Falls in relation to the Great Lakes, *Quaternary Research*, 42, 20-29, 1994.

Toda, M., Bedrock channel erosion on the upper Obitsu, Boso Peninsula. A field experiment on the influence of a fissure on erosion, *Geographical Review of Japan*, 67A(1), 14-25, 1994.

Trieste, D. J., Evaluation of supercritical/subcritical flows in high-gradient channels, *J. Hyd. Eng.*, 118, 1107-1118, 1992.

Vaughn, D. M., Flood dynamics of a concrete-lined, urban stream in Kansas City, Missouri, *Earth Surf. Proc. Landf.*, 15, 525-537, 1990.

Winchell, N. H., The recession of the Falls of St Anthony, *Geological Survey of Minnesota, Final Report*, II, 313, 1888.

Wohl, E. and H. Ikeda, Experimental simulation of channel incision into a substrate of varying gradients, *Geology*, 25, 295-298, 1997.

Wohl, E. E., Bedrock benches and boulder bars: Floods in the Burdekin Gorge of Australia, *Geol. Soc. Amer. Bull.*, 104, 770-778, 1992a.

Wohl, E. E., Gradient irregularity in the Herbert Gorge of northeastern Australia, *Earth Surf. Proc. Landf.*, 17, 69-84, 1992b.

Wohl, E. E., Bedrock channel incision along Picanniny Creek, Australia, *J. Geol.*, 101, 749-761, 1993.

Wohl, E.E., and H. Ikeda, Patterns of bedrock channel erosion in the Bozo Peninsula, Japan, *J. Geol.*, 1998 in press.

Wohl, E. E., N. Greenbaum, A. P. Schick and V. R. Baker, Controls on bedrock channel incision along Nahal Paran, Israel, *Earth Surf. Proc. Landf.*, 19, 1-13, 1994.

Wohl, E. E., K. R. Vincent and D. J. Merritts, Pool and riffle characteristics in relation to channel gradient, *Geomorphology*, 6, 69-84, 1993.

Yair, A., P. Goldberg, and B. Brimer, Long term denudation rates in the Zin-Havarim badlands, northern Negev, Israel, in *Badland Geomorphology and Piping*, edited by R. Bryan, and A. Yair, pp. 279-291, Geo Books, Norwich, 1982.

Young, R.W., and I. McDougall, Long-term landscape evolution: Early Miocene and modern rivers in southern New South Wales, Australia, *J. Geol.*, *101*, 35-49, 1993.

Zen, E.-a. and K. L. Prestegaard, Possible hydraulic significance of two kinds of potholes: examples from the paleo-Potomac River, *Geology*, 22, 47-50, 1994.

K. J. Tinkler, Department of Geography, Brock University, St Catharines, Ontario L2S 3A1, Canada, ktinkler@spartan.ac.brockU.ca

E. Wohl, Department of Earth Resources, Colorado State University, Fort Collins, Colorado 80523, United States.

Conditions for the Entrainment of Cuboid Boulders in Bedrock Streams: An Historical Review of Literature with Respect to Recent Investigations

Paul Carling
Institute of Environmental and Natural Sciences, Lancaster University, United Kingdom

Keith Tinkler
Department of Geography, Brock University, St. Catharines, Canada

We present an historical perspective on the development of force-balance equations for initial motion of large boulders or cuboid blocks by sliding as well as by pivoting, although we concentrate on sliding motion. Particular attention is given to theoretical and experimental work which has relevance to the initial motion criteria of large rounded boulders or cuboid boulders in bedrock channels. Published, and some new, data concerning the friction coefficient and particle drag coefficient for sliding and rolling are reviewed. We consider the case of ice-encrusted boulders, and also present data and analysis of clasts in motion in a steep flume-like natural channel. Recent study has indicated that incipient motion of large boulders on bedrock surfaces is associated with Froude numbers near 1 when flow depth may be of similar order to the boulder height such that flow regime transitions and ventilation may occur around and over the boulder. Consequently, the particular entrainment conditions associated with critical, unsteady, and non-uniform flow are discussed. Both isolated and grouped boulders are considered. Recommendations are made for further investigation.

INTRODUCTION

Large stationary boulders or cuboid blocks in bedrock streams play a significant role in flow resistance and influence the large-scale flow structure and patterns of turbulence. Large boulders may be of similar magnitude in the vertical dimension to the depths of 'normal' floods with recurrence intervals (RI) in the range of 1 to 5 years. In those instances when boulders are especially large relative to channel width and depth, it is questionable if the flow magnitudes experienced over decades or centuries are competent to move them [*Fearnsides and Wilcockson*, 1928; *Carling*, 1986]. Generally, if channels are to be kept clear, large boulders supplied to the channel from the valley walls must be entrained, if only for re-deposition elsewhere in the channel In the case of smaller channels, the largest rocks may be the same magnitude as channel width, and may in some cases act as chock stones blocking the channel. In steep boulder-strewn channels the largest clasts may be grouped to form transverse ribs [*Allen*, 1983] or the bed steps of a step-pool system [*Grant*, 1997]. These are the two groups of bedforms in bedrock channels which are most well researched. In each case the bedforms appear to be related to the development of standing waves associated with local transitions from subcritical to supercritical flow, returning to subcritical flow immediately downstream of the sedimentary structure [*Grant and Mizuyama*, 1991]. However, standing waves also develop over isolated rocks [*Zgheib and Urroz-Aguirre*, 1990]. A related and fundamental problem therefore is to determine the initial motion criteria for large boulders in shallow, nonuniform, and unsteady flow, together with information on the mechanics of movement and typical locii of deposition with respect to reach-scale flow structures [*e.g. Carling*, 1995]. This is not a trivial issue because rocks derived locally from the bedrock may be blocky in shape, angular and only is sub-rounded if derived for example, from a glacial deposit rich in rounded boulders. In gravel-bed streams it is usual to

Rivers Over Rock: Fluvial Processes in Bedrock Channels
Geophysical Monograph 107

apply pivoting entrainment models in uniform deep flow. In bedrock systems, however, not only the flow is frequently nonuniform [*Tinkler*, 1997] but the mode of boulder motion may be by sliding as well as rolling. The orthogonal axes of large boulders may not be of comparable size and consequently the attitude of boulders may have a major influence on resistance to flow entrainment. In addition, boulders may protrude from the water surface such that air is entrained in the area of the leeside, a situation called ventilation, further complicating the flow structure and entrainment process. The relevance of ventilation is the localized reduction in pressure associated with the entrainment of air, or indeed the total removal of water if the bed becomes exposed in the lee of the boulder in supercritical flow with Froude numbers in a certain range. This obviously affects the balance of forces on the boulder. Consequently, the attitude of isolated boulders and the 'fabric' of grouped boulders in relation to surrounding water depth needs measuring and recording in a consistent manner. A tentative scheme is detailed in the *Appendix.*

The processes competent to move large rocks - the erratic boulders of the older natural sciences literature - has been a problem for more than three centuries. Although many processes (floods, earthquakes, vulcanism, glacial ice] were proposed for moving boulders, perhaps the earliest serious attempt to address the process problem from physical principles was by *William Hopkins* [1844], who examined the balance of forces on boulders of various shapes and obtained threshold conditions for their entrainment. Hopkins' results are reviewed later.

Although the mechanics of movement of boulders may appear to be relatively simple, almost all existing work considers only the theoretical condition of a boulder resting alone on a plane rock surface in uniform flow. Experimental or field data are rare, as are adequate descriptions of the boulders themselves - their dimensions, shape, weight and specific weight. Basic parameter values such as the friction coefficient, the relative importance of drag and lift coefficients, and measures of particle 'embeddedness' or protrusion from the bed, and subsequently from the water body; all are generally assumed from limited data bases derived from engineering experience with the stability of concrete boulders. In our experience these data are of limited utility. Firstly, the engineering literature typically is concerned with the stability of multiple boulders piled pell-mell to form steep stable slopes such as river revetment or embankments. Consequently, many detailed design functions are not readily applicable to bedrock systems. Secondly, the modern engineering literature still draws largely from a small data base (of some antiquity) for the critical parameters. Another factor of general importance in natural rivers is that of large woody debris impacting on large rocks, or acting as fulcra for levering boulders from rest by the fluid drag acting on the mass of debris. In addition, the effects of various types of channel ice [*Drake and McCann*, 1982; *Beltaos*, 1996] perhaps should not be underrated. Woody debris is difficult to account for [*Abbe and Montgomery* 1996], but it will have had general importance to fluvial systems before forest clearance. Woody debris may cause dams and clast accumulation, until the wood acting as a dam rots, and clasts are released. Ice, however, can be more readily incorporated into entrainment models, as we shall briefly indicate, and large areas of the circumpolar northern continents are annually affected by channel ice [*Beltaos*, 1996].

Consequently, in this chapter we review the most useful historical studies of the entrainment of boulders with a view to stimulating more detailed studies especially pertinent to bedrock systems. In addition we evalute some experimental data we have collected to illustrate parts of the discussion.

PERSPECTIVE

Empirical and theoretical relationships between the entrainment force and the force resisting motion commonly involve coefficients which are substitutes for the imperfect knowledge of critical parameter values in the force balance. For example, the variation in the coefficients relating critical entrainment velocity to clast size for either rolling or sliding from a number of studies firstly may merely reflect the different groupings of pertinent parameters adopted by different investigators. Secondly, variation between coefficients may represent the inclusion of adjustment factors. For example, different investigators may use depth-averaged mean velocity, surface velocity or the velocity impinging on a clast as the critical entrainment velocity. Linear, parabolic, and logarithmic functions have all been applied to convert a velocity at one elevation to another reference level. This is despite the fact that little is known about the nature of the vertical velocity profile and the distribution of turbulence in bedrock rivers [*Wohl and Ikeda* 1998]. In some studies the effect of inertia [*Denny*, 1988], or of ventilation in the flow [*Hoerner*, 1965] is considered, but this is rare. More pertinent is the uncertainty surrounding the correct values to assign to the drag effect of irregularly shaped clasts in the flow, and the appropriate coefficients of friction for different clast and bedrock surfaces. The result may be that a single coefficient subsumes various physically distinct effects. Consequently, it is useful to review firstly the basic approach to developing a force balance.

According to *Leliavsky* [1955], all approaches may be traced to considerations of moments which derive from the equation developed independently by Brahms in 1753 and Airy in 1834;

$$V_O = kW^{1/6} \tag{1}$$

where V_C is the critical entrainment velocity of a clast of weight W and k is a coefficient. Equation 1 is functionally

equivalent to the sixth power law [a modern derivation is given by *Carson*, 1971], derived by *Hopkins* [1844];

$$W \propto V^6 \quad (2)$$

It is significant that Brahms, Airy, and Hopkins all derived equations 1 and 2 theoretically as the case for sliding, reducing other factors associated with drag and the friction force to equal the coefficient k. It can be shown [*Komar and Li*, 1988] that the coefficient k in equation 1 is equal to;

$$k = \sqrt{(\mu / C_d)} \quad (3)$$

where μ is the coefficient of static friction between clast and bedrock and C_d is the coefficient of drag associated with a clast in flowing water. Historically, values for the angle of static friction, μ (tan the angle in degrees), have usually been estimates based on the angles of rest for similar boulders on nearby hillsides, and the general knowledge that very few hillslopes with substantial clasts resting on them are steeper than 35° to 40° (μ = 0.70 to 0.84). Thus, the upper limit is close to 45° (μ = 1). Laboratory tests can be conducted on suitable materials, and a later section reports some data for a collection of moderate-sized clasts.

If for near-spherical boulders the characteristic length is taken as the radius *(r)* to represent the mass of a clast then Equation 1 may also be written [*Leliavsky*, 1955] as;

$$V_c = \zeta\sqrt{(2r)} \quad (4)$$

where ζ is a coefficient.

In a detailed work, *Hopkins* [1844], derived equation 4 from a consideration of moments and obtained theoretical values of the product $\varsigma\sqrt{2}$ for different geometric shapes (see below). Subsequent studies in the late 19th and early 20th centuries adopted a similar approach, but very few studies have included empirical data obtained from field or flume to compare with theory. An important exception was *Sternberg* [1875] who derived equation 3 and reported experimental data which showed the coefficient ς varied between 3.5 and 4.75, averaging 4.0. However, usually the details of the experiments are not known with certainty and thus are difficult to evaluate.

The relationship between the parameters k, ζ, μ, ρ and C_d can be readily shown as follows for the particular case of spherical particles, with the lift force neglected, [*Leliavsky*, 1955]:

$$V_o = \sqrt{\frac{\mu}{Cd}}\sqrt{\frac{(\rho_s - \rho)}{\rho}\frac{4gd}{3}} \quad (5),$$

therefore substituting 2r for d:

$$V_o = \sqrt{\frac{\mu}{Cd}}\sqrt{\frac{(\rho_s - \rho)}{\rho}\frac{4g}{3}}\sqrt{2r} \quad (6),$$

therefore comparing (4) and (6):

$$\zeta = \sqrt{\frac{\mu}{Cd}}\sqrt{\frac{(\rho_s - \rho)}{\rho}\frac{4g}{3}} \quad (7).$$

If other clast shapes are of interest then the coefficients change but the basic form of the equations remains constant. For a given boulder it usually possible to estimate ρ_s either from the boulder type, or by direct measurement of a chip, or of a smaller clast of identical lithology. Tabulated values of rock densities range from about 1.8 g/cm^3 (for some shales) through to about 2.7 for metamorphic rocks, and 3 for basalt, with values nearer to 2.4 to 2.5 being usual for porous grainstones, and 2.65 for denser sedimentary rocks. Using ρ_s = 2.65, then if ς typically ranges between 3.5 and 4.75 averaging 4 as reported by Sternberg, then;

$$\zeta = 4.65k \quad (8),$$

and k should vary between 0.75 and 1.02, averaging 0.86. With k in this range and taking μ = 0.82 (as we do hereafter) we obtain a range for the drag coefficient between 0.68 and 1.27.

Subsequent studies have produced modifications to these basic relationships or have suggested limits to the range of parameter values. For example, *Chick* [1929] re-analysed the field and experimental data of *Groat* [1920; see also *Grimm and Leupold*, 1939], providing a theoretical analysis and tentatively suggested functions for sliding and rolling. Groat's study involved observation of the movement of large irregular concrete boulders tipped in the St. Lawrence River to form a weir, as well as scaled model studies for sliding. Unfortunately, the exact nature of Groat's experiments are not known and so Chick's results are not readily applicable to other systems. Latterly, *Torpen* [1956] commented on the meager data base for initial motion of large boulders and reported simple empirical curves for sliding and overturning based on the work of *Groat* [1920] and *Isbach* [1935] amongst others. Sparse data were available from model tests for velocities up to 5 m s^{-1} and up to boulder weights of 455 kg. In a similar vein, over subsequent years a number of theoretical analyses producing broadly similar results have been published for the stability of boulders dumped for river training works. For example,

Chee [1975] included parameters for the lift force and for the effect of clast interlocking but provided no data to support his theoretical analysis. *Stephenson* [1979] summarized basic equations for sliding and rolling which effectively are similar to those developed by *Leliavsky* [1955] and *Chee* [1975]. Stephenson did note that these analyses assume the drag coefficient is independent of Reynolds number but he did not comment on any Froude number dependency.

The dependency on Froude number can be deduced from the drag studies of *Hoerner* [1965] but has been given scant attention in the engineering literature as it has little practical relevance in alluvial river engineering, where typically Froude numbers are << 1. Although we find some engineering studies extremely useful [*e.g. Izbash and Khaldre*, 1970; *Naylor*, 1976], often in the engineering literature, interest and emphasis is placed on theoretical calculations usually applied to rip-rap stability and the dumping of stone for closure of training works. The state-of-the-art for riprap design is reported in *Thorne et al.* [1995]. However, the many stability criterion for pell-mell boulders forming steep angle-of-repose slopes in deep waters of relatively low Froude number cannot be transfered readily to bedrock channels with near-critical flow because natural channel boulders are rarely if ever piled pell-mell. Some of these methods remain relatively simple, but typically the coefficients subsume unknown parameter values such as *inter alia* the degree of particle 'embeddedness'. For example, the Californian Division of Highways approach [see *Maynord*, 1995] published in 1970, is based on the method of *Isbach* [1938]. Isbach developed guidelines for the stability of isolated rocks against the impinging critical velocity (V_c), whereas latter studies modified this for the depth-averaged velocity. Isbach's function is:

$$D_C = C_1(\rho/(\rho_S - \rho))(V_c^2/2g) \quad (9),$$

where D_c is a characteristic boulder size in meters, C_1 is a coefficient equal to 1.35 for isolated stones and 0.69 for 'embedded' stones, ρ and ρ_S are unit weights of water and stone respectively (in g/cm^3) and g is the acceleration owing to gravity.

PREVIOUS STUDIES

Hopkins

Hopkins [1844] attempted to establish velocities and competence for large oceanic waves of translation created during hypothetical localised uplifts of the seabed. He refers to earlier theoretical and experimental work on fluid forces acting on geometric bodies, but provides only one incomplete citation for experimental work by D'Alembert. Through a consideration of moments, Hopkins equated the fluid force exerted on a boulder to the resistance offered, and obtained the critical boulder dimension along the streamwise axis, which he labelled (a), for five different shapes and for the cases of rotating and sliding initial motion (Table 1). As far as we are aware these are the most comprehensive, though theoretical, calculations conducted for the case of large boulders until the work of *Allen* [1947] provided detailed experimental results. Hopkins made no allowance for the potential velocity profile of the flow - perhaps on account of the assumed large size of the boulders considered, and the imagined great depth of the floods he envisioned.

Hopkins noted that the solutions for both pentagonal and hexagonal forms converge for both rolling and sliding so that in the end the spheroidal form is only given as the rolling solution. Using these equations he estimated critical dimensions and weights (with rock density as 2.5 g/cm^3) for his geometric shapes. He then attempted to calculate the distance which an entrained boulder will travel under the influence of a wave of translation and found it to be extremely short. He took the velocity of the entrained boulder (the transport velocity) as equal to that of the water velocity minus the critical entrainment velocity and related the transport to the wave's length. He found that the boulder would move only a small fraction of the wavelength as the wave passed, and that to transport the boulder a great distance (as was the case for the glacial erratics he considered), it was necessary for there to be a large series of waves of similar dimensions. It is an interesting question whether a similar approach could be extended and used to estimate travel distance for large boulders beneath unsteady flows. Hopkins is often remembered for his demonstration that the entrainment function is extremely sensitive - to the sixth power of velocity, but his specific calculation of entrainment functions has gone unremarked.

Butcher and Atkinson

Butcher and Atkinson [1934] developed a simple theory which they supported by field experiments and scaled laboratory study. They argued that the weight of water and therefore the inertia, of a cube of side length D, and specific weight $\gamma_S = g\rho_S$, is effectively equal to the submerged relative density multiplied by the boulder volume. Consequently, the inertia is proportional to $(\rho_S - \rho)D^3$. If the entraining force is proportional to the projected area (D^2) then the resistance of the boulder to motion is given by the quantity $I = (\rho_S - \rho)D$. However, in order to justify this approach it is also necessary to assume the fluid force is not only proportional to the projected area of the cube but also to the velocity squared [*Allen*, 1947]. Nevertheless, I is termed the 'immovability' number. The notation I_n was then employed to denote a boulder for which $(\rho_S - \rho)D = n$, where parameters were measured in consistent units. Thus, different sized cuboids with different densities can have the

Table 1. Equations to yield entrainment threshold a-axis for boulders [from *Hopkins*, 1844]

boulder cross section parallel to flow	equation from *Hopkins*[@]	equation reduced[$] solved for v
terms		
a = streamwise axis of the boulder		
a' = (spheroidal case) the average radius calculated as = $\sqrt{(0.5(a^2+c^2))}$ see note below		
b = axis transverse or perpendicular to flow (all results are independent of this axis)		
c = vertical axis		
v = mean fluid velocity at threshold		
μ = coefficient of friction, 1 = tan 45°		
g = acceleration due to gravity		
f = internal angle of the boulder		
g = specific gravity of boulder - Hopkins used 2.5 when missing from equation below		
g' = specific gravity of water (or the fluid in question), taken as 1		
n = c/a, except for the spheroidal case when n = (a/(a-c)), where a>c		
(note: Hopkins uses a and b for the two axes of the spheroid in cross section, but to allow for the b axis transverse to flow we have changed his b to c for consistency with the above.		
triangle	$a = (1-(\mu/\sqrt{3}))(v^2/g)$	$v = 4.82\sqrt{a}$
for the equilateral - inside angle f = 60		
when f represents the internal angle of the boulder, then he shows that for sliding to take place that it is required that tan $f > \mu$. He shows that no triangular section boulder can roll continuously.		
cube	$a = (0.667n)(v^2/g)$	$v = 3.84\sqrt{a}$ - sliding [also found in analysis of *Graf*, 1979]
where n = c/a, and n = 1 represents a cubical section.		
For c=na the boulder rolls for m >1/n, and when c=a it rolls if m > 1.		
for rolling	$a = (0.667/\mu))(v^2/g)$	$v = 0.78\sqrt{a}$ - rolling
pentagon	$a = 0.568(v^2/g)$	$v = 4.24\sqrt{a}$
almost identical equations for either sliding and rolling		
hexagon	$a= 0.57(v^2/g)$	$v = 4.24\sqrt{a}$
almost identical equations for either sliding and rolling		
spheroids[*]	$a = (n/6)(v^2/g)$ rolling	$v = 4.43\sqrt{a'}$ taking n = 3

[@] we have organised the terms from *Hopkins* [1844]in a more consistent manner
[$] we have taken g as 9.81m s^{-2} and submerged specific gravity as 1.6 t m^3 rather than 1.5.
[*] for spheroids it is assumed that the *a* axis is not equal to the *b* axis, and the ratio n = (a/(a-c)) acts as an index of shape relative to a sphere.

same 'immovability'. For example, a boulder with a density of 2 g/cm^3 and length of 1 m, has the same I_n value as a boulder with a density of 3 g/cm^3 and 0.5 m length. Interestingly, Butcher and Atkinson dismissed the importance of the coefficient of friction for sliding. They argued instead, that boulders are either stationary, or in unsteady motion owing to turbulence so that true sliding does not effectively occur.

For experimental verification of the theory, different sized boulders with the characteristic length measured in cm and with densities in the range 1.5 g/cm^3 to 4.0 g/cm^3 such that $I_{0.5}$, I_1 etc., were employed in flow models at three different scales to represent entrainment conditions on a full-scale concrete apron. Model results were consistent, demonstrating for example that for the field conditions the full scale value of *I* needed to be greater than 2, when units

of meters and tonnes are employed. The smallest stable boulders selected for use in the engineering scheme could be either 1 m cubes of density 3 g/cm^3 or 2 m cubes of density 2 g/cm^3.

Allen

In an important study, *Allen* [1942; 1947] provided detailed experimental data on the sliding and overturning of solitary regular boulders which were submerged in a unidirectional current which varied from sub-critical to near-critical. In the latter case the relative submergence of the particle (D_c) to the water depth (d) was about 1 (Table 2). Three particle densities were tested (2.41 g/cm^3, 2.09 g/cm^3, 1.73 g/cm^3), and the results recorded in imperial units. However, in the examples given in Table 2, Allen's results are recalculated assuming a cubic rock of 1 m sides, a particle density of 2.65 g/cm^3 and a water density of 1.0 g/cm^3.

Allen reported the variation in critical surface flow velocities for entrainment of scaled 1 m cubic boulders for a variety of relative depths (Table 2) above a flat concrete bed. He assumed firstly that a linear function described the vertical velocity distribution and secondly that a parabolic velocity defect law applied such that the surface velocity is somewhat depressed compared to velocity at depth. For the defect distribution, it is possible to reduce Allen's analysis to the following function for overturning;

$$V_s = \alpha\sqrt{((\rho_s-\rho)/\rho)D_c)} \quad (10),$$

and for sliding;

$$V_s = \beta\sqrt{(\mu(\rho_s-\rho)/\rho)D_c)} \quad (11),$$

where V_s is the critical surface velocity, D_c is the vertical dimension of the cube, α and β are coefficients, ρ_s is the density of the boulders and ρ is the density of water in g/cm^3. Comparing equations 10 and 11 using data in Table 2, it is evident that cubes slide at a lesser critical velocity compared to overturning and that for sliding cubes there is an important dependency on the coefficient of friction (μ). Allen measured this latter factor by dragging boulders using a spring balance and obtained an average value of $\mu = 0.62$, a value somewhat less than that obtained by other investigators (*i.e.*~ 0.82). Allen noted that the mode of initial motion depended on the location of the boulder on the bed and which side was in contact with the bed. Sometimes the boulder would slide intermittently and then overturn. These observations indicate considerable variation in the coefficient of friction (probably owing to the use of rough-cast concrete). It is probable that Allen's reported coefficient of friction is not equal to μ but is equal to μ/C_d.

Table2. Data from *Allen* [1947]

ß	$Vs_{(cal)}$	Fr	C_d/D	m/s
6.15	3.44	1.09	2.26	1
6.21	3.47	0.78	2.22	2
6.55	3.66	0.52	2.00	5
6.96	3.89	0.39	1.77	10
7.30	4.08	0.34	1.61	5

NB: Froude number calculated using surface velocities. If the entraining velocity directly impinging on the boulder is used as a characteristic velocity, then in the shallowest flow, Fr = 1.25.

(following (3)). Therefore, the value of $\mu = 0.82$ is used in subsequent calculations below because it appears that C_d (the drag coefficient) is subsumed within Allen's μ and β coefficients.

From Allen's analysis of parabolic curves, a multiplication factor can be derived correcting surface velocity to provide the velocity impinging on the cube at a height c above the bed equal to $c/2$. As one would expect, because the critical entrainment value for a certain boulder should be constant, even as relative depth is varied, a constant value for V_c equal to about 3.92 m s^{-1} is obtained for initial motion of a 1 m cube. For shallow flow (i.e d/D_c in the range 1 to 2), the critical velocity is about 1.14 times the surface velocity. For deep flows ($d/D_c > 10$) the multiplier (*circa* 0.98) indicates the critical impinging velocity is only slightly less than the surface value. Note also that Allen gives a function indicating the maximum velocity which will occur between the top of the boulder and the water surface.

From the work of *Leliavsky* [1955], it may be shown that the variation in Allen's coefficients α and β depend mainly on the apparent drag coefficient (C_d) of the clasts. For example, in the case of rolling of a sphere;

$$\alpha = \sqrt{\frac{8g}{3C_d}} \quad (12),$$

and for sliding of a cube;

$$\beta = \sqrt{\frac{2g}{C_d}} \quad (13).$$

Given a critical velocity of 3.92 m s^{-1}, ρ_s = 2.65 g/cm^3, ρ = 1 g/cm^3, and a coefficient of friction of 0.82, it can readily be calculated that the drag coefficient of Allen's cubes was equal to 1.72. This is higher than the typical value for a free-falling cube [C_d = 1.05; *Hoerner*, 1966;

Denny, 1988] and reflects the enhanced energy dissipation effect of a cube adjacent to the boundary in shallow flow. This drag coefficient reaches a maximum of around 2.0 for near critical flow conditions [*Hoerner*, 1965] as is explained below.

As the flow shallows and becomes critical, a standing wave develops upstream of the boulder with a depressed water surface over the top of the boulder. Once the boulder breaks the surface, ventilation will occur on the downstream side. Ventilation progressively extends downwards to the base of the obstruction as the Froude number is increased until the bed is exposed at a Froude number of between 1.4 and 1.8, depending on obstacle shape [*Hoerner*, 1965]. Wave drag reduces for fully ventilated flow conditions and although an additional spray-drag component can become important, the total drag reduces in supercritical flow (i.e. Fr > about 1.4) to a constant value. The Froude number of the flow when Allen's boulders became emergent is about 1.25, so ventilation would have occurred over a significant proportion of the height of the boulder. At this stage, Hoerner's analysis for boulders protruding from flow indicates that the relationship

$$C_d = C_d' + (C_d'/Fr^2) + 0.3D_b/d \qquad (14)$$

yields the effective drag coefficient C_d, where C_d' is the free-fall drag coefficient for a cube and D_b is the width of the boulder normal to the stream flow. The second term on the right reflects the enhanced drag owing to ventilation and the third term represents the spray drag. Excluding spray drag, the solution of Equation 14 gives C_d of about 1.72, equivalent to that calculated from Allen's flow data.

In subsequent analyses Allen lengthened the boulder in a downstream direction by a factor of two and indicated from the result that C_d increases in proportion; *i.e.* double the length and you double C_d. Allen also considered boulders in small flow-transverse arrangements stacked either two boulders high, or rows of two boulders or more placed transverse to the flow to give contiguous flow parallel boulder lines with no gaps. The thin gaps between boulders were filled with plasticine. Several interesting results were found pertinent to the group entrainment of packed boulders on a concrete bed surface. Given a relative depth $d/D_c = 5$, one or two contiguous rows of boulders had essentially the same entrainment threshold as a solitary boulder. The same result pertained for three rows if the relative depth $d/D_c > 5$. Successive rows of cubes stacked two high gave the following result. The entrainment threshold for two rows was equivalent to a single cube whereas for three rows the threshold increased by 25% and for 4 rows by only an additional 5%. Allen noted the importance of relative depth. Relative depth became unimportant in all test cases when $d/D_c > 10$. Consequently, depending on the stacking geometry of multiple rows, and variation water depth, the critical entrainment threshold for grouped particles could be either less than or greater than that for a solitary cube; the variability being as much as - 59% and + 35% (Fig. 1). The significance of this important series of results has yet to be fully considered. Nevertheless, the complexity in the variability of threshold conditions for simple boulder geometries reflects the importance of a combination of factors. Chiefly these are: variable flow blocking, different degrees of inter-boulder friction for given row and stack geometries, and finally, the development of critical and subcritical flow conditions as relative depth is varied.

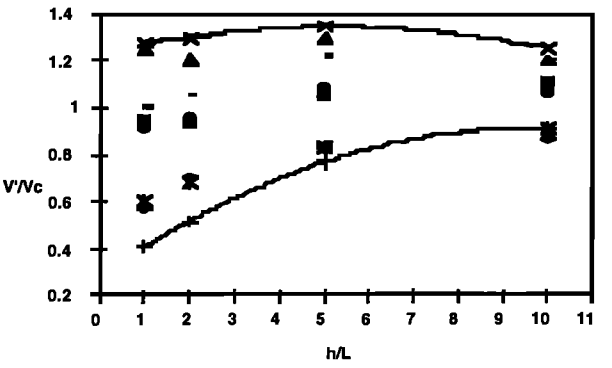

Figure 1. Grouped boulder data of Allen [1942]. Entrainment velocity (V') normalized by the entrainment velocity for a single boulder (Vc), as a function of relative depth (h/L) for various boulder groupings. ◊ single row of boulders; ■ double row; ▲ triple row; x quadruple row; * double row with one additional row centrally placed on top. ● triple row with two rows centrally placed on top; + pyramid of three, two and one row; – pyramid of four and three rows. The data range is shown by the pecked lines.

Graf

Graf [1979] considered a theoretical balance of forces for both fully and partially submerged boulders. Here we only consider the case of fully submerged rocks because a consideration of his equation for the case of critical flow (see the end of the section) indicates that flow depths for most normal parameter choices must be about equal to or larger than the streamwise axis of the boulder (D_a) for initial motion. Consequently, because critical flow maximizes discharge and velocity for the available energy [*Henderson* 1970], and because the streamwise boulder axis is almost always larger than the vertical axis (D_c), the boulder will not likely move in subcritical flow unless submerged.

The Graf model in the fully submerged case at threshold of motion reduces to:

$$1 = \frac{\gamma D_b D_c V_c^2}{\mu(y_s - \gamma) D_a D_b D_c g(\cos S)} \qquad (15).$$

The numerator represents the force exerted on the upstream face of the boulder by the flow, and the denominator represents the resistance to motion of the boulder on the bed. Compared with the previous analyses, the only additional element to the terms is dimensionless stream bed slope S, entering the equation as cos(S). For most practical cases this term may be taken to be 1 unless the slope is greater than 10% (~6°), as may γ (the specific weight of water). In his assessment of boulder stability in the Grand Canyon, Graf uses a relatively low friction coefficient of 0.65 (~ 33°). No consideration is given to a drag coefficient (which would enter as C_d in the numerator), nor is any allowance made for the lift force once the boulder is well submerged.

Solving for V_c:

$$V_c = \sqrt{\mu(\gamma_s - \gamma)gD_a} \qquad (16).$$

Taking g = 9.81 m/s^2 we obtain:

$$V_c = 3.13\sqrt{(\mu(\gamma_S-\gamma)D_a)} \qquad (17).$$

When γ_S is 2.5 g/cm^3 and μ is 1, values used by Hopkins, the coefficient is equal to 3.84, the value he gives for the cubic case (see Table 1). When the Froude number is 1, mean velocity is described by $\sqrt{(gd)}$, where d is the flow depth. Substituting this expression into equation 16, we obtain the velocity for initial motion in terms of depth (in any system of consistent units):

$$d = \mu(\gamma_S-\gamma)D_a \qquad (18).$$

For example, with typical values of $\mu = 0.82$ and $(\gamma_S-\gamma) = 1.65$, the equation reduces to $d = 1.35D_a$. It should be noted that, if calibrated by actual data (see SMALL CLAST EXPERIMENT section below), the coefficient estimated as $\mu(\gamma_S-\gamma)$ would include an unknown factor due to the drag coefficient. Note too that D_a is the streamwise axis of the boulder, and thus for a perfect cube (with $D_c = D_a$), it predicts the required flow depth relative to the vertical axis of the boulder. With this in mind, as μ ranges from 0.36 to 2.14 (see NEW DATA section below), probably with a highly positively skewed distribution peaking near 0.85, the required depth of flow d (to yield a velocity V_c for initial motion) goes from 0.60 to 3.53 (using extremes of the data set collected below). Because the required depth is defined by the downstream axis of the boulder as it rests in the channel, the required depth for initial motion in critical flow can be different for the same boulder, depending on its orientation. Because μ is much less well defined in the field than the term $(\gamma_S-\gamma)$, it points up the need for a better knowledge of that coefficient, together with the factors which bear upon it - surface roughness, percentage contact with the bed and the number of points of contact relative to other surfaces.

Bacon, Cahill and Tombrello

Bacon et al. [1996] analyzed the forces involved in moving the "sailing" stones of Racetrack Playa in Death Valley, but they focus on estimating the coefficient of static friction μ for which experimental data was available on some of their roughly cubical clasts. Their equation in our notation is:

$$\mu = (C_d V_c^2 \gamma)/(2g\gamma_S\sqrt{(D_a D_b)}) \qquad (19)$$

where C_d is the drag coefficient (taken by Bacon et al. as between 0.8 and 1.0, although in their case it was relevant to air), and γ_S is rock density in g/cm^3. Application to water would require the addition of an extra term in the denominator (converting γ_S to $(\gamma_S- \gamma)$) to allow for submergence in the fluid. The combined term under the square root sign estimates the flowwise length of the boulder and allows for the fact that the wind may affect the boulder from different directions. It is equivalent to the situation in a stream where a boulder may have either of its plan axes transverse to the current at a moment of rest on the bed. To allow for the vertical velocity profile in the wind, they use V_c as 80% of the upper wind speed in a way similar to the correction often applied to surface water velocity to obtain mean velocity in streams [*Matthes*, 1956]. It is implicit (but not proven) that the registered wind velocity they used is a threshold velocity - one which was just able to move the rocks on the playa. It may, however, have exceeded the required threshold velocity by an unknown amount. Applying Equation (19) to their data shows, however, the effect of another hidden factor which must be considered in field studies of natural boulders - that of shape. The listed dimensions of their boulders and an assumed cubical shape lead to some serious overestimates relative to the mass they tabulate. In reality this is a difficult problem to handle for large boulders in natrual settings and one which calls for further attention.

Komar and Li

Komar and Li [1988] introduced a coefficient (Ω) into a force balance equation to allow for uncertainty with respect to turbulence fluctuations in the flow. However, they did not suggest any value for this coefficient. Within flows close to and either side of the critical transition Fr = 1, macroturbulence may play an important role in dislodging boulders from rest [*Breusers and Raudkivi*, 1991; *Fiorotto and Rinaldo*, 1992]. The average velocity, however, needs

to be sustained to transport boulders or motion will be erratic or will cease. In a similar manner, stability when boulders are deposited can only be assured if the positive excursions from the mean are below the threshold for motion. *Rajaratnam* [1967] and *Razvan* [1989] measured turbulence in the transition through hydraulic jumps where Froude numbers ranged from 2 to 10. The flow appeared well-mixed in the vertical such that the velocity at any depth is similar to the mean value. *Razvan* [1989] noted that macroturbulence was approximately normally distributed around the mean value and provided a simple function to describe the range of velocity fluctuations around this mean value. Given that the shear stress acting on a boulder varies as the square of the velocity, it is possible to derive similar functions to describe the anticipated range of shear stress values [*Leliavsky*, 1955; *Termes*, 1988; *Farhoudi and Narayanan*, 1991]. To our knowledge only *Carling and Grodek* [1994] have tried to incorporate these distributions in force balance considerations.

NEW DATA ON THE ANGLE OF SLIDING FRICTION

In order to get a better understanding of the values of μ, 40 platy clasts (mean dimensions of the axes are 0.15 m, 0.09 m, 0.03 m) collected in the process of another project, were used with a simple adjustable slope ramp apparatus to determine the angle at which sliding began for each side of each clast, and with each side started in three or four different orientations (depending on particle shape), and on four different grades of sand paper from very fine (grit 240 - fine siltstone equivalent) to very coarse (grit 36, rough granite or very coarse sandstone equivalent). Insofar as boulders in bedrock channels often rest on smoothed surfaces these may be quite appropriate surfaces.

It can be seen (Table 3) that the global mean value is 41.5° or μ = 0.88, although the three standard deviation (sd) range for the full data set is from 26° to 57° (μ = 0.49 to 1.54). As expected, the mean friction angle decreases, and with reduced variability, as the sandpaper grade becomes finer. Extreme values collected in the data set indicate a range of 20° to 65° (0.36 to 2.14), values lying beyond a ±4 standard deviation range. Thus, caution should be applied in using a single value form of equations involving this term. Strictly speaking the angle measured is the one at which initial motion began, the angle of static friction would be slightly less.

Data were also collected on the surface relief of the clasts and the percentage contact each clast had with the plane. The marks left by the sand paper on the base of the clast were the basis for the determination of the area of contact, and the number of points of contact. The data were also checked by placing a stiff transparent sheet on the rock surface to find the points of contact. From this data it was found (n = 80) that the percentage of contact was 3.83% ± 5.69 (standard error (se) 0.64, range 0.5% to 44%) - with a highly skewed distribution. The number of distinct points of contact the clasts made with a plane surface was found to be 3.80, with strong modal values for 3 and 4 (77% of the total sample). This too is highly skewed because a plane requires three points (of contact) to define it mathematically, and therefore 3 is a lower limit for the number of contacts. However, in some instances extensive areas of plane surface caused only one or two contact points to be recorded - in these cases the actual percent area in contact was significantly higher than for larger numbers of contact points. Surface relief on the clasts was estimated as 5.3 mm ± 4 mm (se 0.04). Admittedly the data is for a natural rock surface matched against a plane surface (roughly simulating grainstones), rather than a natural one. The additional variation of a basal natural rock surface can be expected to introduce additional variance to the data, but may not greatly affect the mean values. Studies of the latter situation are in progress at Lancaster University.

Table 3. Experimental data on angle of sliding friction

Grit >	36 (coarse)	80	120	240 (fine)	All data
mean	45.8	43.2	39.5	37.4	41.5
sd	5.6	4.2	3.6	3.0	5.3
se	0.33	0.25	0.21	0.18	0.16
max	65	55	50	47	65
min	21	21	20	21	20
n	279	279	279	279	1116

The preliminary conclusion that may be drawn from this data is that boulders resting on rock surfaces usually have few and spatially-limited points of actual contact, although obviously, cases of effective interlocking will exist and cause substantial excursions from the mean values. Submerged in the flow, a strong velocity and pressure differential can exist between the top and bottom of a boulder (*cf Allen*, 1947), which will enhance the operation of the lift force as a factor in entraining the boulder. The lift force will only operate once there is substantial flow depth over the boulder. Equally, when channel ice develops, the limited basal contact enables the boulder to be effectively encased by ice. Other processes which may be effective when the base of the boulder is not flush with the bed are hydraulic wedging of clasts into open spaces as described by *Hancock et al.* [this volume], and leverage by organic debris. KJT has seen a 20 cm diameter log wedged under the front of a fallen armour stone from a protective wall in Cooksville Creek [*Tinkler and Parish*, this volume]. In motion, boulders sometimes leave striae on the bed [*Tinkler and Parish*, this volume], which constitute only a tiny percentage (a few centimeters) of a meter wide boulder in motion sliding over the bed.

Using this data with the Graf model and the coefficient mix in Equation (18), it is possible to estimate (by

combining the means and 3 standard deviation ranges for the various values of μ and likely ranges of γ_s from 1.8 to 3.0 g/cm^3, and assuming γ=1) that the term $\mu(\gamma_s - 1)$ varies from 0.39 to 3.08, with the lower values occurring for rather unlikely combinations. For equation 17 and combined with g, it varies from 1.96 to 5.50. Therefore:

$$V_C = (\text{range of } 1.96{:}5.50)\sqrt{D_a} \qquad (20).$$

Note that the coefficient reduced from $\sqrt{(g)}$ in an earlier step includes the dimensions $\sqrt{(m)/s}$ which ensures that (20) is dimensionally homogenous.

If data are available on threshold velocity, V_C, then in combination with a boulder dimension representing the downstream axis, D_a, an estimate may be made of μ, whenever γ_s can be easily established, by re-arranging equation 16:

$$\mu = V_c^2/gD_a(\gamma_s - \gamma) \qquad (21).$$

The estimate will contain an unknown quantity representing the drag coefficent which will enter in the numerator on the right hand side. It may be noted that the term γ_s may also be used with ice-encased boulders - in which case the ice shell may significantly reduce the effective mean "boulder" (rock + ice shell) density in g/cm^3.

We now examine how much variation can be expected from the development of an ice shell around a boulder, and how it affects, however temporarily, a boulder's physical characteristics.

ESTIMATES ON EFFECTIVE DENSITY OF ICE ENCASED BOULDERS

In this section we show how effective a modest sheet of ice is in reducing effective rock density following *Drake and McCann* (1982) who considered isolated boulders on coastal flats. Simple analysis shows that a volume of ice equal to or greater than $(\gamma_s - \gamma)/(\gamma_i - \gamma)$ times the volume of the clast is required to "float" an ice-encased boulder, if ice, γ_i, is assumed to have a specific weight of 0.9 g/cm^3, water, γ, has a value of 1 g/cm^3, and the clast has a specific weight of 2.65 g/cm^3. Small clasts frozen into river ice in rivers will often satisfy this condition (bottom line, Figure 2). We use a cubical form for the boulder and assume the development of an ice shell of even thickness around it, apart from the basal surface.

Figure 2 shows the effective density of a boulder encased in ice for three selected boulders similar, but not identical, to those reported below. Such shells develop when receding flood stages of winter meltouts splash water onto boulders in sub-zero temperatures. In addition, anchor ice (sticky and

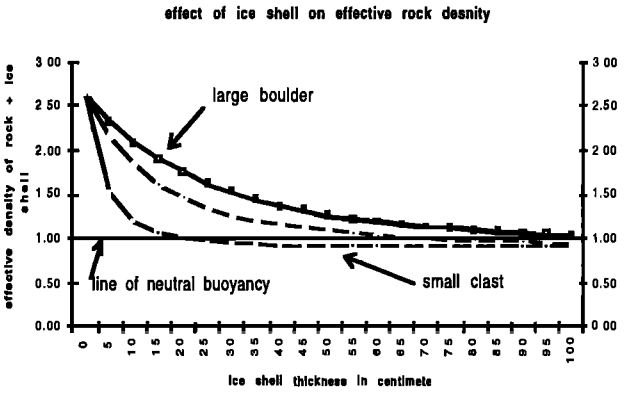

Figure 2. The highest line is for the largest boulder: 2.00 x 1.25 x 0.65 m; the middle line is for a boulder: 100 x 0.75 x 0.45 m; the lowest is for the smallest boulder: 40 x 25 x 8 cm.

slushy under water and liable to collect in separation zones) freezes solid as it is exposed. Thus, in much of northern North America this is an annual event. Elsewhere in the world it may be less frequent (with RI up to 100 years in mid-latitudes) or non-existent (low latitudes) as a bed process, but it may be extremely effective in mobilizing sediment when it does occur.

In the Fall and Winter of 1996/7 in Twenty Mile Creek, a high flow (21 October 1996) with a peak stage of about 0.95 meters failed to move a boulder (❑1.50 x 0.80 x 0.60 m, for notation, see Appendix) left stranded the previous year in the center of the channel (figure 3a,b). Yet it moved twice during January and March when it had developed an ice shell of 0.10 to 0.15 meters and an ice "skirt" developed in fringing flow separation zones. The first time (Jan 23rd 1997) it moved 22 metres when the motion was sliding, which is known because semi-continuous striae connecting its two locations were observed on the bed during subsequent low flow. The open water stage was 0.62 m, but a meltout ice drive (figure 4) raised water levels to about 1.00 to 1.10 m for a few minutes, the evidence for the duration is data from a water pressure gauge in a stream bed trough in the same reach [see *Tinkler and Wohl*, this volume, figs 6, 7, 8)]. The second time it moved (22 February 1997) over 100 meters, and may have done so in both sliding and rolling motion as no tracks were seen subsequently on the stream bed. On the other hand, conditions for inspecting the bed immediately after the flood were less favorable on the second occasion. The flood peaked at about 1.15 m without any evidence of higher levels due to ice drives. In the same two flows, another boulder (Δ 1.30 m, 0.80 m, 0.75 m) moved 6m (and 2 to 3 m to the left of a main streamline), and then 15 m, with an ice shell of similar thickness. It moved over an uneven rock and large gravel strewn bed, and there was no opportunity to inspect the bed between successive locations. During the

a

b

Figure 3. (a) Boulder in center stream (flow is left to right) in Twenty Mile Creek, 16th January 1996 (date of photograph is erroneous), with developing ice shell and skirt. The field pole is 1.8 meters long, the left scale of scale card is centimeters, water depth is about 25 centimeters. The boulder (60 cm high) did not move in ice-free Fall floods with flow depth of 95 centimetres. It moved 22 m by sliding in an ice drive 23rd January 1997 when flow levels reached 100 to 110 centimetres for a few minutes. (b) The boulder on 15 February 1997 in its subsequent position downstream with a developing ice shell and ice skirt. Two days later the ice skirt was connected to the far bank. The boulder subsequently moved over 100 m in a flow with stage 115 centimeters on February 22nd.

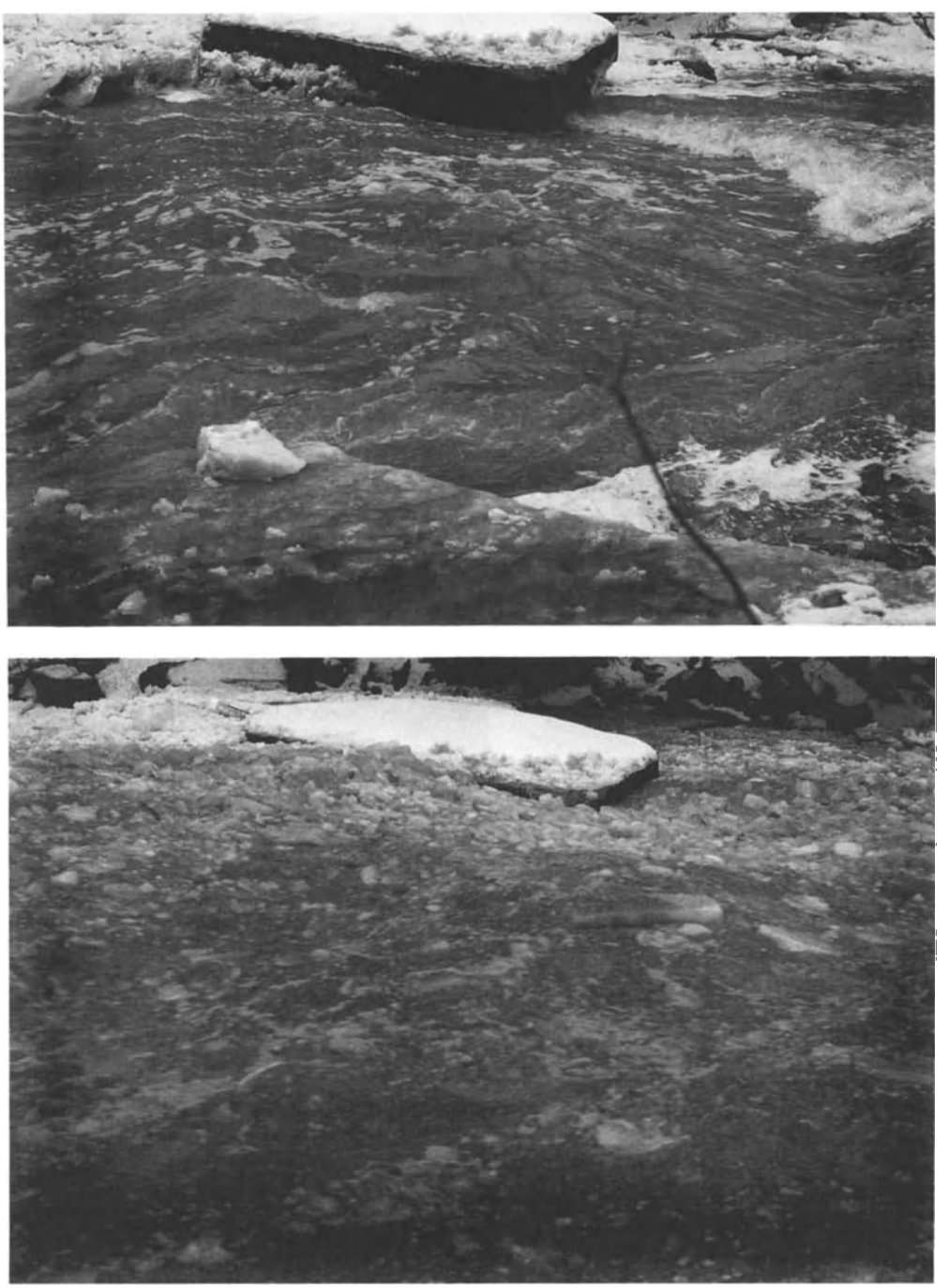

Figure 4. Photographs of an ice drive observed in January 1996, the year before the illustrations in Figure 3. (a) The top photograph shows a low but rising stage. The rucked-up snow and ice on the large boulder on the far side of the stream attests to an ice drive recorded on the pressure gauge and observed two hours before by a student of KJT. Notice imbricate ice floes on upstream (left) side of the large boulder. (b) The top photograph shows the same site a few minutes later with abundant ice in the water. This ice drive did not quite attain the elevation of the previous one (see height of rucked-up ice and snow on the boulder, right lower corner). The entire ice drive, caused by burst out from a collapsing ice dome over a plunge pool upstream, lasted less than five minutes, by which time the river returned to the state in the top photograph.

February 22nd 1997 peak stage, another smaller boulder (ΔΔ 1.00 m, 0.80 m, 0.50 m) moved off a bar to a position on the transverse outlet bar of the plunge pool immediately downstream (about 20 meters of movement). All three boulders moved to their initial positions during a peak stage of 1.45 m the previous year, when an ice drive reached that stage for a few minutes, and was followed by an open water stage at the same level. Thus it seems that the existence of an ice shell and associated ice skirts on large boulders faciliated their movement during flow stages at which they would have otherwise remained stationary. A subsequent stage of 1.08 m a few days later did not move any of the boulders.

A conservative analysis of the conditions for the first boulder discussed is obtained by assuming a 10 cm ice shell on all exposed surfaces. An extensive ice skirt also observed is neglected here on the grounds it may have broken off with rising stage. A 10 cm shell increased the volume of the clast 65% from 0.72 m^3 to 1.19 m^3. The associated specific weight changed from an assumed value of 2.65 g/cm^3 for sandstone, to 1.95 g/cm^3 with the associated ice shell. A similar analysis for the second boulder showed a volume increase of 63% and a concomitant reduction in specific weight to 1.97 g/cm^3. The smallest boulder showed an estimated volume increase of 80%, and a reduction in specific weight from 2.65 to 1.87 g/cm^3. These are dramatic changes, and illustrate how effective such a common process can be (Figure 2). Even if the ice shell is partly lost in subsequent motion, it can be highly effective in initiating motion.

SMALL CLAST EXPERIMENT

Our review of initial boulder movement has been through force balance considerations applied to a stationary boulder. An alternative view, which parallels post-hoc flood estimates of the stream velocities in relation to boulders known to have moved in the flood, is to measure boulders in motion in a water body with similar flow and bed condition and to estimate the initiation of motion velocity, V_c, by subtracting the clast transport velocity from the mean water velocity. It can be expected that the estimate may be too low, since the shear stress needed to keep a particle in motion is about half that needed to initiate transport [*Bacon et al.*, 1996]. In addition, it will include a factor due to the drag coefficient which is not easily analyzed separately.

To assess the velocity of initial motion for some small clasts we make use of equation (21) and the experimental assessment of μ. An experiment was conducted with natural clasts under natural conditions in a steep rock channel that was 30 mm deep and 230 mm wide. Water was flowing supercritically over a moss or algal surface adhering to the rock. Surface water velocity was measured using leaves as floats timed over a 1.5 m reach. Velocities were checked at the start and end of each session which lasted about an hour. Over several days mean velocity (taken as 80% surface velocity) ranged from 1.16 to 1.5 m/s, with corresponding Froude numbers of 2.14 to 2.76. Flow was visibly unsteady and somewhat aereated and the Froude numbers lie in the range where roll waves may be expected to develop [*Hjalmarson and Phillips*, 1997], and which would contribute to unsteady flow conditions. The channel gradient was 18^o or about 0.32, and from the estimated mean velocities, Manning's roughness was calculated to lie within the range 0.036 to 0.047. Clasts of quartzite and Manx slate (both with specific weights of 2.65 g/cm^3, measured from field samples) were collected with masses ranging from 5 g to 1090 g. The velocity was sufficient to ensure that clasts were entrained after being released, and all clasts were covered in water during motion, although sometimes this was because of waves they generated around themselves. In general the vertical axis of each clast was of the order of the water depth. Each clast was released from an identical start position, eleven times, and the particle velocity through a measured reach of 1.5 metres was timed with a stopwatch. A mean clast velocity was computed.

The data obtained are given in Table 4. Used in practice, Graf's equation subsumes a drag coefficient of unknown magnitude. Following Hoerner [1965], we calculated a drag coefficient for each clast using an average Froude number of 2.45, and known particle dimensions, for which it was assumed that the longest axis lay transverse to the channel, and that the intermediate axis lay along the channel. A mean drag coefficient (including the spray term) was computed for the 29 clasts as 1.72 (sd. 0.46).

In order to estimate initial motion velocity we subtracted the observed mean clast velocity from the observed surface velocity. The other terms in equation (21) are all known, and from the data we computed μ for each particle. Because in the observed velocity data must already include the drag coefficient, we divided our estimate of μ from equation (21) by this value for each particle. We averaged the results to obtain $\mu = 0.68$ (sd 0.28), equivalent to 34°. This is a very reasonable assessment of μ in the circumstances. However, *Bacon et al.* [1996] state that the shear stress needed to keep a particle in motion is significantly lower than (perhaps only half as much) that needed to entrain it. Therefore, the initial motion velocity (stream velocity minus clast velocity), estimated in the manner described from the experimental data, may be much lower than that needed to actually initiate transport. On the other hand, as all clasts entrained upon release, then we surmise that mean surface water velocity easily exceeded the value required to initiate transport. To refine the estimate of initial motion velocity we experimented with a multiplier to determine how much larger the initial motion velocity would be need to be, relative to our estimate from the field data, in order that the estimate of μ be brought to the experimental mean value (0.88) that we reported earlier. This multiplier was found to be 1.15, whereas mean water surface velocity averaged 2.02 (sd 0.77) times our first estimate of initial motion velocity.

Table 4. Experimental data for small clast experiment

clast grams	water velocity m/s	clast velocity m/s	Entrain velocity m/s	a axis cm	b axis cm	c axis cm
73	1.50	0.57	0.93	8.2	5.6	1.6
38	1.50	0.73	0.77	3.2	3.1	1.5
23	1.50	0.87	0.63	6.7	2.8	1.2
253	1.45	0.50	0.95	10.0	7.0	3.9
232	1.45	0.59	0.86	10.0	4.5	3.2
230	1.46	0.63	0.83	9.9	7.0	2.2
186	1.45	0.42	1.03	11.0	7.3	1.4
29	1.45	0.87	0.58	4.5	3.9	0.8
10	1.45	1.10	0.35	3.0	3.0	0.5
8	1.45	1.02	0.43	2.5	1.5	1.3
4	1.45	1.14	0.31	2.2	1.5	0.4
1090	1.76	0.36	1.40	13.5	9.5	4.2
167	1.76	0.64	1.12	6.5	5.0	2.5
147	1.76	0.66	1.10	7.0	6.0	1.6
122	1.76	0.76	1.00	8.0	4.0	1.8
88	1.88	1.12	0.76	3.8	3.5	2.7
152	1.88	0.99	0.89	6.1	3.9	3.0
130	1.88	0.86	1.02	6.0	5.7	2.4
357	1.88	0.56	1.32	10.8	7.8	2.5
605	1.88	0.86	1.02	10.8	7.4	3.9
759	1.88	0.57	1.31	12.5	8.6	3.4
590	1.88	0.80	1.08	11.8	8.3	3.6
119	1.88	0.93	0.95	7.6	4.5	2.5
185	1.70	0.71	0.99	7.4	4.8	3.8
103	1.70	0.66	1.04	6.3	3.8	2.7
158	1.70	0.85	0.85	7.0	4.8	3.7
236	1.70	0.59	1.11	7.3	4.7	4.9
76	1.70	0.78	0.92	6.8	2.9	2.9
289	1.70	0.76	0.94	10.3	6.5	4.5

Thus there is abundant energy left to provide the clast with its own velocity. Notice that to stay close to our data we did not adjust the mean water surface velocity to a supposed mean velocity. Clearly this would be easier to do in a laboratory setting and would give more refined results.

DISCUSSION

Recent investigations have indicated that in bedrock channels with bed gradients greater than about 0.5%, flow may be close to critical (Fr ~ 1) during flows which may be competent to move coarser bed elements [*Tinkler*, 1997; *Grant*, 1997]. For example during field studies by *Inbar and Schick* [1979] the largest boulders present were entrained by Froude numbers estimated to range between 1.0 and 1.1. Supercritical flow over extended reaches occurs mainly in hydraulically smooth channels such as concrete spillways [*Vaughn*, 1990], and can occur over distances of 10's of meters in bedrock channels where the river bed may be parallel to very flat bedding planes in the bedrock, even at low stage. Examples observed by the authors include streams in Yellowstone National Park, U.S.A., and in the River Dee in Dentdale, U.K.. How the Froude number changes with a rise in stage in such systems is scarcely known at present, but it seems to follow that the initial motion of large boulders in such systems will occur beneath standing waves at low relative submergence. It may be observed in flumes that moving particles, with low relative submergence, can carry the standing waves they generate along with them as they move. Under these conditions the assumption of uniform flow is violated, such that traditional entrainment functions require modification. Equally importantly, the development of standing waves upstream of nearly emergent boulders reflects enhanced drag coefficents owing to flow blocking and air entrainment which tend to be maximized at flows close to critical with Froude numbers ranging between 0.8 and 1.4. At higher Froude numbers, the drag reduces such that large boulders may be less susceptible to entrainment in supercritical flow than at critical flow conditions. However, macroturbulence probably increases at high Froude numbers [*Carling and Grodek*, 1994]. In this case the importance of large turbulent excursions in flow velocity probably become more important for entrainment of exceptionally large 'erratic' boulders than variation in the drag coefficient. Other factors of importance in appropriate field localities is the presence of winter ice in rivers, and the leverage effects of large pieces of vegetation.

Although we have records of large boulder movement in natural streams we are still far from understanding the precise channel conditions affecting them at the time they are entrained, or when they are in transit. Frequently the entrainment conditions can only be estimated from high water marks, and in many instances the original location of boulders known to have moved may not be known. In the field we require careful stage calibration and observation of flow conditions in reaches with well-documented large boulders, and from low through high stages, together with the best possible information on boulder characteristics and movement.

Although our focus has been on initial conditions, a full understanding will require better knowledge of large boulder motion during transport. It seems likely that some of this understanding will come from controlled experiments in flumes.

Acknowledgements. Keith Tinkler thanks Hiroshi Kwamura for collecting the experimental data on sliding friction and related matters, NSERC (Canada) for a Research Grant, and Brock University for general research support over many years. We thank Steve Kite and Dan Cenderelli for incisive remarks on an earlier version of the paper.

APPENDIX ON BOULDER NOTATION

An arbitrary boulder resting on a plane bed may be recorded as follows. The D_a, D_b, D_c axes are given in order of decreasing size. They are preceded by a shape factor

which lies between 0 and 1 and which adjusts the computed cuboid volume $D_a*D_b*D_c$ towards a more accurate assessment of the actual volume. A cuboid (❑) as value 1, and pyramid (ΔΔ) has value 0.17. A form triangular in one the axes projections (Δ) has value 0.5 (normally in the plan form, though exceptions do occur). A spheroid (O) has value 0.52. The field worker makes the judgment as to the form, which may be modified upwards or downwards for transitional forms.

In assessing shape one of us (KT) has found it useful to adopt the triangular notation for many rhomboidal boulders, even when not strictly triangular. The same boulder carefully measured as a cuboid (although along slightly different axes in plan) should yield the same volume.

The D_a, D_b, D_c values are marked as follows. Underline the two axes seen in plan view (i.e. from above), and double underline the axis which is parallel to the stream axis in the immediate reach. If the boulder is oblique to the flow, both plan axes may be underlined and l or r added at the end to indicate whether the boulder faces obliquely the left or right banks. A final number may be added to indicate an angle of imbrication (a positive value is assumed to dip upstream, a negative angle indicating reverse imbrication, dipping downstream).

As examples:

Δ 130 x 80 x 40 - 35 -- long axis along river, 35° imbrication

O 80 x 70 x 30 - 0 -- short axis along river, resting flat on the bed

❑ 110 x 80 x 44 - L - 25 -- oblique to flow, facing left bank, 25° imbrication, with this clast the sign indicates a cuboid form.

❑ 130 x 80 x 40 90 -- cuboid clast resting on edge transverse to flow (perhaps between others)

Shape factor signs, if omitted, can indicate the cuboid form, but it is safer to write them in explicitly to show that shape was considered.

REFERENCES

Abbe, T.B. and Montgomery, D.R., 1996. Large woody debris jams, channel hydraulics and habitat formation in large rivers. *Regulated Rivers: Resource Management*, 12: 201-221.

Allen, J. R. L., A simplified cascade model for transverse stone ribs in gravelly rivers, *Proceedings of the Royal Society of London*, A 385, 253-266, 1983.

Allen, J., An investigation of the stability of bed materials in a stream of water, *Journal of the Institute of Civil Engineers*, 5, 1-4, 1942.

Allen, J., *Scale Models in Hydraulic Engineering*, 407p, Longmans, Green and Co., London, 1947.

Bacon, D., T. Cahill and T. A. Tombrello, Sailing Stones on Racetrack Playa, *J. Geol.*, 104, 121-125, 1996.

Beltaos, S., Editor, *River Ice Jams*, 390p, Highlands Ranch, Colorado, Water Resources Publications, LLC, 1996.

Breusers, H. N. C. and A. J. Raudviki, *Scouring*, 143p, Balkema, Rotterdam, 1991.

Butcher, A. D. D. and J. D. Atkinson, The cause and prevention of bed erosion, with specific reference to the protection of structures controlling rivers and canals, *Minutes of the Proceedings of the Institute of Civil Engineers*, 235, 175-222, 1934.

Carling, P. A., Flow-separation berms downstream of a hydraulic jump in a bedrock channel, *Geomorphology*, 11, 245-253, 1995.

Carling, P. and T. Grodek, Indirect estimation of ungauged peak discharges in a bedrock channel with reference to design discharge criteria, *Hydrological Processes*, 8, 497-511, 1994.

Carson, M. A., *The mechanics of erosion*, 174p, Pion, London, 1971.

Chee, S. P., Resistance of rocks to movement, paper presented at International Congress for Hydraulic Research, 16th Congress, Sao Paulo, Brazil, IAHR, 450-452, 1975.

Chick, A. C., The principle of similitude, in *Hydraulic Laboratory Practice*, edited by J. R. Freeman, pp. 796-799, American Society of Mechanical Engineers, New York, 1929.

Denny, M. W., *Biology of the wave-swept environment*, Princetown University Press, Princetown, 1988.

Drake, J. J. and S. B. McCann, The movement of isolated boulders on tidal flats by ice floes, *Can. J. Earth Sci.*, 19, 748-754, 1982.

Farhoudi, J. and R. Narayanan, Force on slab beneath hydraulic jump, *J. Hyd. Eng.*, 117, 578-596, 1991.

Fearnsides, W. G. and W. H. Wilcockson, A topographical study of the floodswept course of the Porth Llwyd above Dolgarrog, *Geographical Journal*, 72, 401-419, 1928.

Fiorotto, V. and A. Rinaldo, Fluctuating lift and lining design in spillway stilling basins, *J. Hyd. Eng.*, 11, 578-596, 1992.

Graf, W. L., Rapids in canyon rivers, *J. Geol.*, 87, 533-551, 1979.

Grant, G. E. and T. Mizuyama, Orign of step-pool sequences in high-gradient streams: A flume experiment, paper presented at Japan-U.S. Symposium on Snow Avalanche, Landslide, and Debris Flow prediction and Control, Tsukuba, Japan, edited by M. Tominga, Science and Technology Agency of the Japanese Government, 523-532, 1991.

Grant, G.E., Critical flow constrains flow hydraulics in mobile-bed streams: A new hypothesis, *Water Resources Research, 33* (2), 349-358, 1997.

Grass, A. J., Structural features of turbulent flow over smooth and rough boundaries, *Journal of Fluid Mechanics*, 50, 233-255, 1971.

Grimm, C. I. and N. Leupold, Hydraulic data pertaining to the design of rock revetment, U.S. Engineering Office, North Pacific Division, Portland, Oregon, 23pp, 1939.

Groat, B. F., Ice diversion for the St. Lawrence River Power Company, *Canadian Engineer*, 39, 545-552, 1920.

Henderson, F. M., *Open channel flow*, 522p, MacMillan, New York, 1970.

Hjalmarson, H. W. and J. V. Phillips, Potential effect of translatory waves on estimation of peak flow, *J. Hyd. Eng.*, 123(6), 571-575, 1997.

Hoerner, S. F., *Fluid Dynamic Drag*, Hoerner Fluid Dynamics, Bricktown, New Jersey, 1965.

Hopkins, W., On the transport of erratic boulders, *Trans. Camb. Phil. Soc.*, 8(2), 220-240, 1844.

Inbar, M., and A.P. Schick, Bedload transport associated with high stream power, Jordan River, *Proceedings of the National Academy of Science, 76*, 2515, 1979.

Isbach, A., Construction of dams by depositing rock in running water, paper presented at Second Congress on Large Dams, 135-140, 1938.

Izbach, S. V. and K. Y. Khaldre, *Hydraulics of River Channel Closure*, 174p, Butterworth, London, 1970.

Komar, P. D. and Z. Li, Applications of grain-pivoting and sliding analysis to selective entrainment and to flow-competence evaluations, *Sedimentology*, 35, 258-266, 1988.

Leliavsky, S., *An Introduction to Fluid Mechanics*, 257p, Constable, London, 1955.

Maynord, S. T., Corps riprap design guidance for channel protection, in *Rivers, Coastal and Shoreline Protection*, edited by C. R. Thorne, S. R. Abt, F. B. J. Baends, S. T. Maynord, and K. W. Pilarczyk, pp. 41-52, Wiley, Chichester, 1995.

Matthes, G. H., River surveys in unmapped territory, *American Society of Civil Engineers*, 121, 739-758, 1956.

Naylor, A. H., A method for calculation the size of stone needed for end-tipping rubble banks in rivers, CIRIA, 60 56pp, 1976.

Rajaratnam, N., Hydraulic Jumps, in *Advances in Hydrosciene*, edited by V. T. Chow, pp. 197-280, Vol, 4, Academic Press, New York, 1976.

Razvan, E., *River Intakes and Diversion Dams*, 508p, Elsevier, Amsterdam, 1989.

Stephenson, D., *Rockfill in Hydraulic Engineering*, 215p, Elsevier, Amsterdam, 1979.

Sternberg, H., Untersuchungen uber langen - und querprofil geschiebfuhrender, *Zeitschrift für Baüswen*, , 483-506, 1875.

Termes, A. P. P., *Rivers: application of mathematical models for turbulent flow field above artificial bedforms*. Report on computations, Delft Hydraulics, Q 787, 1988.

Thorne, C. R., S. R. Abt, F. B. J. Baends, S. T. Maynord and K. W. Pilarczyk, *Rivers, Coastal and Shoreline Protection*, 766p, Wiley, Chichester, 1995.

Tinkler, K. J., Indirect velocity measurement from standing waves in rockbed streams, *J. Hyd. Eng.*, 123(10), 918-921, 1997.

Torpen, B. E., Large rocks in river works, *Civil Engineering*, 26(9), 56-61, 1956.

Vaughn, D. M., Flood dynamics of a concrete-lined, urban stream in Kansas City, Missouri, *Earth Surface Processes and Landforms*, 15, 525-537, 1990.

Wohl, E.E. and Ikeda, H., 1998. The effect of roughness configurations on velocity profiles in an artificial channel. *Earth Surface Processes and Landforms*, 23: 159-169.

Zgheib, P. W. and G. E. Urroz-Aguirre, Flow transitions around single large bed element, paper presented at *National Conference*, edited by H. H. Chang and J. C. Hill, ASCE, 1036-1041, 1990.

Paul A. Carling, Institute of Environmental and Natural Sciences, Lancaster University, Lancaster LA4 4YB, United Kingdom, p.carling@lancaster.ac.uk

Keith J. Tinkler, Department of Geography, Brock University, St Catharines, Ontario L2S 3A1, Canada, ktinkler@spartan.ac.BrockU.ca

Beyond Power: Bedrock River Incision Process and Form

Gregory S. Hancock and Robert S. Anderson

Department of Earth Sciences, University of California, Santa Cruz, California

Kelin X Whipple

Department of Earth, Atmospheric, and Planetary Sciences, MIT, Cambridge, Massachusetts

We present a quantitative discussion of the processes active in bedrock-floored river channels, drawn from field observations, erosion rate measurements, and simple scaling rules. Quantitative documentation of process is needed to improve our understanding of bedrock river channels and aid in the formulation of erosion rules to be used in landscape evolution simulations. Our observations in a channel with "hard" rock (Indus River, Pakistan) suggest quarrying and abrasion are the primary erosion processes. It appears that block quarrying is the most efficient process when joints and bedding planes are sufficiently close. The block thickness a river is capable of quarrying goes as the square of the local flow velocity, v. Quarrying requires block "preparation", during which subaerial weathering, bedload bashing, and/or hydraulic wedging, a previously undocumented process, act to free a block for quarrying. The Indus River is capable of quarrying blocks of up to ~0.7 m during annual peak flows. Rock abrasion should go as $\sim v^5$. Abrasion is most effective in regions of separated flow, generating a suite of sculpted rock bedforms that includes flutes, and this suggests abrasion occurs primarily by suspended sediment. Cavitation is unlikely to be a major process, as it requires unusually high velocity, and is suppressed by flow aeration. Abrasion measured on the Indus over 1 year using drill holes is ≤4 mm, with maximum rates within flutes, and in locally steep, narrow channel segments. Cosmogenic radionuclides from the same bed locations reveal average erosion rates over ~1.5-2.0 ka that are an order of magnitude lower than the maximum 1 year rates. We reconcile these measurements by appealing to the passage of bedforms such as flutes. Our Indus River rate measurements are many times lower than longer-term rates, possibly implying substantial hydrologic variation induced by climate change. Incision rates in bedrock channels are controlled by very local hydraulic conditions well below the resolution of reach-based erosion rules. Incorporation of this geometric complexity represents a significant challenge to the landscape evolution modeling community.

1. INTRODUCTION

1.1 *Why Study Bedrock River Channels?*

Bedrock channels and the erosional forms found in them are some of the most glorious features on Earth. They provide the primary non-glacial mechanism of incision into

Rivers Over Rock: Fluvial Processes in Bedrock Channels
Geophysical Monograph 107

the bedrock of tectonically active regions. This incision steepens bounding hillslopes and produces relief between the mountain tops and the channel bottom, and removes mass from mountain ranges, leading to flexural isostatic response that can drive the uplift of peaks [e.g., *Small and Anderson*, 1995; *England and Molnar*, 1990]. Bedrock channel incision provides the essential link between tectonics and landscape evolution, through communication of base level changes through the landscape. The rate at which channels incise into bedrock sets the rate at which the rest of the landscape surface evolves, and hence controls the response time of such landscapes to tectonic and/or climatic forcing.

That the role of bedrock rivers in landscape evolution is central requires that we be able to predict properly bedrock channel incision and profile development in models attempting to simulate landscape evolution [*Howard et al.*, 1994]. "Rivers" in such models must be able to respond to changes induced climatically (e.g., stream discharge, hillslope sediment production) or tectonically (e.g., changes in gradient due to tilting, baselevel changes), and to variations in substrate (e.g., rock hardness) that in turn dictate the available erosion processes. A complete model for bedrock channel evolution should be flexible enough to incorporate these variables in a meaningful way.

However, bedrock rivers remain a poorly understood part of the geomorphic system. In an attempt to understand these features more fully, we have undertaken a field study to assess quantitatively the processes that are active in bedrock rivers. In this paper, we start by discussing the existing models for predicting erosion rates in bedrock channels. Much of the recent research interest in bedrock rivers stems from the need for model development, and by discussing these models we highlight the necessity of reconsidering field evidence to understand these systems. We then discuss our field observations of processes (abrasion, quarrying/hydraulic wedging, and cavitation) that are potentially important in the bedrock rivers in which we have worked. For each process, we attempt to develop a quantitative expression that allows us to discuss how process efficiency might vary with hydraulic and channel characteristics. We then discuss how these processes potentially interact in these systems and influence channel shape and profile evolution. Finally, we discuss our direct, short-term measurements of abrasion on the Indus River, northern Pakistan, and the implications these rates have for erosion in this and other channels is accomplished.

1.2. *Modeling Bedrock Channel Erosion*

The effort to understand how bedrock channels work is motivated in part from interest in treating these features in landscape evolution models [e.g., *Howard et al.*, 1994]. Physical "rules" developed to predict rock channel erosion rates build on either an erosion process, which we term "process rules", or reach-averaged expressions of erosive capacity, which we term "reach-scale rules". Process rules are attractive because they 1) develop a physically-based understanding of individual processes; and 2) allow direct estimation of how erosion by that process might vary with changing hydraulic and sediment load conditions. However, if the goal is to use a physical rule in a numerical simulation of channel profile development or landscape evolution, the typical time and length scales of such simulations will likely preclude direct calculation of the parameters (e.g., flow velocity, sediment concentration) required for prediction of erosion rates with a process rule. As an alternative, reach-scale rules employ surrogates for erosive capacity, like shear stress and stream power, coupled with a parameter that relates these functions to channel erosion rates. The parameters necessary for calculating erosion rates with these rules, like drainage area and slope, are measured at a map scale, rather than the microphysical scale, making them more computationally efficient than process rules. However, in abstracting the incision processes, we may lose the ability to predict accurately how incision rates might vary in space and time in response to changing conditions, and, hence, the ability to predict accurately the evolution of the profile. We now discuss in detail the "process" and "reach-scale" rules.

1.2.1. *Process rules. Foley* [1980a] outlines the only published, well-developed "process rule" for predicting erosion rates in bedrock channels. *Foley* [1980a] develops his model for cutting and deformation abrasion of bedrock by bedload impact, and tests this model using measured (e.g., grain size) and estimated (e.g., discharge, rock susceptibility) parameters against field-determined incision rates. He builds on *Allen* [1971] by using the engineering wear literature for prediction of volume loss from a rock surface as a function of kinetic energy delivery by impacts. The removal of material of a rock surface (i.e., erosion, or wear), *dz/dt*, produced by this kinetic energy delivery is expressed as

$$\frac{dz}{dt} = \frac{1}{2}\frac{C_{sed}}{\lambda}\left(\frac{v_g - v_0}{S_a}\right)^2 \qquad (1)$$

where C_{sed} is the bedload sediment concentration, l is the saltation hop length for the bedload, v_g is the particle velocity perpendicular to the bed, v_0 is the threshold particle velocity necessary for initiation of erosion, and S_a is the "susceptibility" of the rock relating kinetic energy delivered to mass of rock removed [*Foley*, 1980a].

Abrasion rates predicted by this model are highly sensitive to the flow hydrograph. *Foley* [1980a] estimates that flows representing only a small fraction (<0.05%) of the annual hydrograph could account for all of the long-term average incision at his field site (Dearborn River, Montana). He emphasizes the importance of hydrograph changes produced by climate cycling (here,

interglacial/glacial cycles) on erosion rates. Two critical implications of the nonlinearity of Eq. 1 and the quantitative field analysis by *Foley* [1980a] are 1) while there is a tradeoff of flow frequency and magnitude, the highest flows are likely the most important in accomplishing erosional wear of the bed by abrasion, and 2) long term changes in the details of the stream hydrograph and in sediment concentration can strongly influence bedrock incision rates.

This equation is very limited in application to quite specific channel types, as *Foley* [1980a] very clearly describes, precluding broad use of this rule. This arises from the need to know the local C_{sed}, v_g, and v_0 in order to predict *dz/dt*. Such quantities cannot be predicted efficiently or confidently in a long-term model simulating drainage basin evolution, because information about these quantities is difficult to extract from the geologic record. In addition, abrasion by bedload impacts as outlined in Eq. 1 is not the predominant process in all places or even in one place at all times, requiring that rules be developed for other processes, and that we understand how to predict which process dominates at a particular time or place.

1.2.2. *Reach-scale rules.* The "reach-scale rules" move away from explicitly addressing a process, and instead rely on relationships between map-scale (100's m to many km) measurable quantities and erosion rate. These rules start with either shear stress, τ,

$$\tau = \rho g S_e H \tag{2}$$

as in *Howard and Kerby* [1983], or "specific" stream power, ω,

$$\omega = \frac{\rho_w g S_e Q}{w} \tag{3}$$

where ρ_w is the density of water, g is gravitational acceleration, Q is water discharge, w is channel flow width, S_e is energy slope, and H is flow depth (equal to hydraulic radius for wide, shallow streams). Erosion rules that utilize these as a starting point explicitly assume, in the case of shear stress, $dz/dt \sim t$, or, in the case of stream power, $dz/dt \sim w$, where dz/dt is the average erosion rate at a point. With these assumptions, we can develop an erosion rate law that is a function of discharge, Q. We use the Darcy-Weisbach equation for mean flow velocity, $\bar{v}$,

$$\bar{v} = \left(\frac{8 g S_e H}{f} \right)^{1/2} \tag{4}$$

where f is the Darcy-Weisbach friction factor, and the continuity equation, $Q = \bar{v} H w$, to relate Q to S_e and H. Combining these with Eq. 2, we obtain a shear stress-based rule,

$$\frac{dz}{dt} = K_1 \frac{Q^{1/3} S_e^{2/3}}{w^{2/3}} \tag{5}$$

where K_1 is a constant. Combining these with Eq. 3, we obtain a stream power-based rule,

$$\frac{dz}{dt} = K_2 \frac{Q S_e}{w} \tag{6}$$

where K_2 is a constant.

In landscape evolution models, addressing the specifics of discharge and channel width are difficult at large spatial and temporal scales, particularly given the stochastic variation of Q over long time scales. A solution is suggested by *Howard and Kerby* [1983], and reviewed by *Howard et al.* [1994], who argue that the long term average incision rate is proportional to the shear stress exerted by the "dominant discharge" in the channel [*Costa and O'Connor*, 1995; *Wolman and Miller*, 1960]. *Howard and Kerby* [1983] suggest drainage area, A_D, as a surrogate for this dominant discharge, and develop an equation for estimating channel erosion rates,

$$\frac{dz}{dt} = K A_D^m S^n \tag{7}$$

where K is a constant, S is channel bottom slope (replacing S_e), and m and n are exponents that depend on the choice of shear stress or stream power as the erosion surrogate. Although K is frequently referred to as a channel resistance term, this is not strictly correct; K folds in many factors, including but not limited to rock resistance, that are sensitive to the erosional process and setting [e.g., *Stock and Montgomery*, in press; Figure 1].

Several studies have attempted to calibrate the parameters m, n, and K in Eq. 7 with field data. *Howard et al.* [1994] suggest using the empirical relationships $Q_b \sim A_D^b$, where Q_b is the bankfull discharge and b ranges from ~0.65 to ~0.80, and $w \sim Q^{(0.5)}$, both determined from drainage basins with primarily alluvial channels [*Leopold et al.*, 1964; *Knighton*, 1984]. It is an important and often unstated assumption that bedrock channels have similar relationships between Q and w and A_D; these relationships have not been empirically determined for any bedrock river system, and defining a "bankfull" discharge in most bedrock rivers is inherently impossible. Using these empirical relationships, one obtains m=0.2 to 0.3 and n=2/3 for a shear stress rule, and m=0.3 to 0.4 and n=1 for a stream power rule. In both formulations, the final erosion

rate is not as strongly dependent on Q as channel slope, S. This results from the dependence of both w and Q on A_D. Using measurements of erosion rates, and of channel slopes and drainage area for badland channels, *Howard and Kerby* [1983] find the best-fitting values, m=0.45 and n=0.70, similar to what is expected by following a shear stress development. Several studies have attempted to calibrate K, m, and n in the field [e.g., *Rosenbloom and Anderson*, 1994; *Seidl and Dietrich*, 1992; *Seidl et al.*, 1994; *Stock and Montgomery*, in press], with highly variable results.

Rate laws similar to Eq. 7 are used extensively in landscape and stream profile evolution models to study how landscapes respond to tectonics and climate change [e.g., *Howard*, 1994; *Tucker and Slingerland*, 1997]. A major drawback in this rate law, however, is that most factors that are relevant to the variability of incision rates in a particular setting are folded into the K parameter, which is not readily estimated because it subsumes such a large number of variables (Figure 1). It is also possible that channel erosion rates change with changing hydrologic forcing through time (e.g., through changing climate), or with changes in dominant processes along a channel reach. As written, a rate law like Eq. 7 cannot explicitly incorporate such variability in either time or space, unless K is allowed to vary in some meaningful way, because A_D is fixed for a particular channel location.

We also note that Eq. 6, the origin of the stream power erosion rule, implies no dependence of erosion rates on the shape of the hydrograph. For an annual hydrograph passing a point in the channel, the integrated stream power (effectively, the total potential energy loss of the water) is always equal regardless of the details of the flow hydrograph. Unlike microphysical rules, like Eq. 1, this implies erosion rates are insensitive to the hydrograph shape, unless a threshold stream power for erosion exists.

1.3. *Stepping Back: Field Investigation of Bedrock Rivers*

We think that improving our understanding of bedrock channels requires more direct field observations of the processes that actually operate in these channels. Attempts to develop and calibrate reach-scale rules have motivated much of the recent quantitative research related to bedrock channels [e.g., *Howard*, 1987; *Howard et al.*, 1994; *Howard and Kerby*, 1983; *Seidl and Dietrich*, 1992; *Seidl et al.*, 1994; *Sklar and Dietrich*, 1997; *Slingerland et al.*, 1997; *Stock and Montgomery*, in press]. In contrast, recent field studies tend to focus either on individual processes or bedforms [e.g., *Foley*, 1980a; *Miller*, 1991; *Nemec et al.*, 1986; *Tinkler*, 1993; *Zen and Prestegaard*, 1994] or on reach-scale energy expenditure in bedrock channels and related channel form [e.g., *Ashley et al.*, 1988; *Wohl*, 1992; *Wohl*, 1993; *Wohl et al.*, 1994]. These process studies have not been directed towards model development (with the exception of *Foley* [1980a]), and have not provided estimates of process rates.

We have gone to the field, with simulation models in mind but understanding processes a priority, in a quantitative investigation of which processes are active, what scales the rates of these processes, how these processes interact, and how fast these processes act. Our observations of sculpted rock bedforms and channel morphology demonstrate that incision into bedrock is not accomplished by any single process, but through a linked and interconnected set of physical processes that vary in their efficacy from place to place and from time to time. In this paper, we present an overview of the incision processes we observe to be most critical (abrasion, quarrying) or potentially important (cavitation) in eroding "hard" bedrock channels. For each, we attempt to develop a simple, conceptual process model, and a mathematical expression that allows scaling of process rates and discussion of where each may be most important. While we do not attempt to develop new "rate laws", we discuss whether existing reach-scale rate laws are appropriate for particular processes. One of the greatest limiting factors in understanding process in these settings is the lack of rate measurements, given the slow rates at which bedrock channels typically erode. We have directly measured erosion by abrasion on the Indus River, and discuss the results and their relevance to how such a river erodes.

We draw insight from a variety of rivers with different character: 1) the Indus River Middle Gorge, Pakistan, a steep, bedrock-floored river with huge annual swings in discharge, that crosses "hard" igneous and metamorphic rocks amongst some of the most rapidly uplifting topography in the world [*Burbank et al.*, 1996]; 2) the Wind River, which is forced by glacial/interglacial cycling and incises through weak, early Tertiary continental deposits [*Chadwick et al.*, 1997; *Hancock et al.*, 1998]; and 3) several rivers draining the Sierra Nevada, California, which are primarily snow-melt streams running on mixed bedrock ("hard" igneous and metamorphic rocks) and alluvium-mantled beds. We use the Indus River as a test case for estimating process rates, because it is a large river in a tectonically active setting, and we have made measurements of erosion rates on this river.

2. BEDROCK EROSION PROCESSES

We consider in detail abrasion, quarrying/hydraulic wedging, and cavitation. These processes either appear to be very active in the channels we have observed (abrasion and quarrying), or are potentially important (cavitation). While other processes are certainly active in some bedrock river channels (e.g., chemical dissolution), they appear to be less significant in the "hard" rocks that floor the rivers we have considered. We will address the physics and scaling of each process initially, and then discuss where each process is likely most effective. We then consider the interaction among these processes in a conceptual model of bedrock channels.

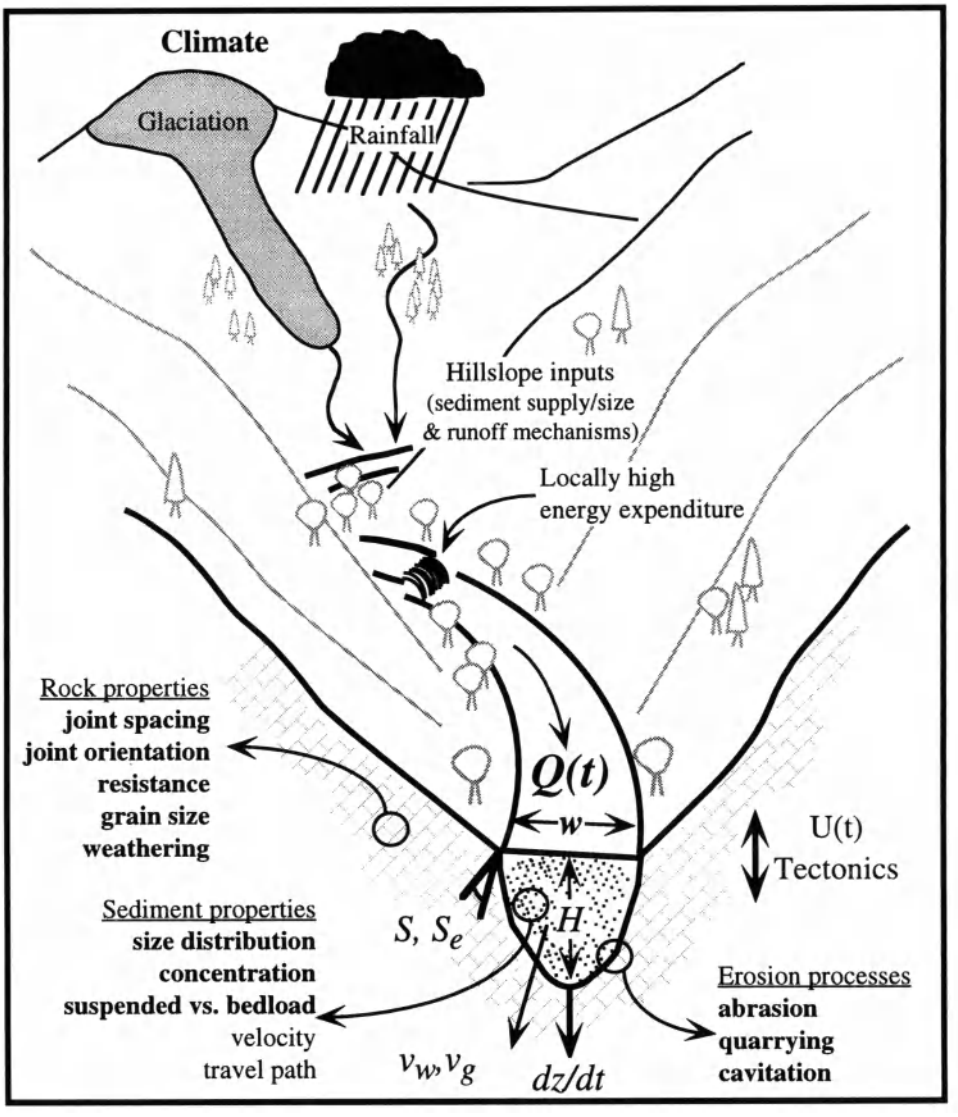

Figure 1. A schematic of a bedrock channel system, showing important variables that act to set the erosion rate, dz/dt, of the channel and terms used in the text. Channel variables are: $Q(t)$: discharge as a function of time; w: channel width; H: flow depth; v_w: water velocity; v_g: sediment velocity; A_D: drainage area; and S and S_e: channel and energy slope, respectively. Variables that are at least partially subsumed within the parameter, K, found in all reach-scale erosion rules, are shown in bold.

2.1. *Abrasion*

2.1.1. *Theory*. Rock erosion by abrasion is accomplished by removal of material from a rock surface through forcible impact by entrained sediment. The rate at which material is removed depends upon the kinetic energy flux to the surface, delivered by impacting grains, and the "susceptibility" of the rock surface to abrasion [e.g., *Anderson*, 1986; *Foley*, 1980a]. The impacts produce fractures within minerals, dislodge individual grains, or break off flakes from the rock surface. Experimental studies of abrasion by aeolian sediment transport reveal that the mass of material removed is roughly proportional to the to the kinetic energy delivered by the impact [e.g., *Greeley and Iversen*, 1985; *Suzuki and Takahashi*, 1981]. At the grain scale, the grain velocity, v_g, diameter, D, and density, ρ_g, set its kinetic energy, and the delivery of this kinetic energy increases as grain impact angle, a, relative to the bed, increases toward vertical (90 degrees). The "susceptibility", S_a, relates kinetic energy delivery to mass of rock material removed, and is dependent primarily on the density, hardness, and fracture-mechanical properties of the

target and impacting grains. In a development analogous to aeolian abrasion presented by *Anderson* [1986], we can express, in simple terms, an abrasion erosion rate as

$$\frac{dz}{dt} \sim \frac{S_a C_{sed} v_g^2 v_w}{2\rho_r} \quad (8)$$

where C_{sed} is the mass concentration of a particular grain size, v_w is water flow velocity, and ρ_r is the target rock density, and we have assumed impact by spherical grains. Assuming $v_g \sim v_w$, and a C_{sed} proportional to shear stress ($C_{sed} \sim t \sim v_w^2$), Eq. 8 suggests that $dz/dt \sim v_w^5$. This argues that abrasion rates are very sensitive to local flow conditions and the details of the flow hydrograph, with high local stream velocities and the largest, rare flow events producing the greatest instantaneous erosion rates.

Abrasion rates are sensitive to the grain scale microphysics. The most relevant velocity is the particle velocity, v_g, relative to the channel bed, rather than simply the water flow velocity. For a particle to impact the channel floor, sediment must decouple from the flow, because flow velocity vanishes at the bed. The entrained sediment must possess enough momentum to decouple from the flow, punching through the near-surface flow boundary layer and forcibly impacting the bed. The sediment concentration, C_{sed}, is not sufficient for predicting erosion as presented in Eq. 8. Analogous to aeolian abrasion by suspended sediment *Anderson* [1986], particle trajectories are influenced by the response of water flowlines to the microtopography of the bed. A particle may be steered by the water around obstacles, or be forced to impact the obstacle obliquely if its inertia is sufficiently low. Increased sediment in the flow may actually decrease the rate of erosion as sediment supply begins to choke off access to the bed [*Sklar and Dietrich*, 1997].

Exceedence of a threshold may also be required to initiate erosion by abrasion. A threshold kinetic energy is explicitly included in several abrasion rules, requiring grains exceed either a threshold velocity, v_0, or diameter, D_0 [*Anderson*, 1986; *Foley*, 1980a]. Burial of the bed by sediment at low flow conditions is commonly observed in bedrock channels [e.g., *Howard*, 1987]; sufficient sediment transport and local bed scour is therefore required to remove sediment mantles on the bed before abrasion can take place. Both of these thresholds presumably require surpassing a threshold discharge and/or flow duration. The long-term abrasion rate of a channel will therefore be influenced by climatic changes that change the frequency of exceeding these thresholds.

2.1.2. *Insights from abrasion-related bedforms.* Sculpted rock bedforms like flutes (or "troughs") and potholes represent the most actively abrading portions of a rock bed. Our observations indicate that such forms originate where sharp flow expansions on the downstream edges of bed protrusions allow flow separation with an associated flow recirculation zone. Flow separation occurs where the boundary layer of a stream of viscous fluid detaches itself from the boundary in response to abrupt expansions or adverse pressure gradients, generating a free shear layer with a region of separated flow. These flow separation regions, which are characterized by high water flowline curvature, allow entrained sediment to decouple from the flow and impact the bed. We establish several lines of evidence that argue that the primary tools in accomplishing this abrasion are the suspended grains. The erosional "bedforms" that adorn rock surfaces require that the grains be capable of delivering significant kinetic energy to the back sides of flow obstacles and expansions. Below we illustrate several forms that support this notion that the abrasional "attack is from the back".

We take as a first example the ripple-like bedforms shown in Figure 2, which are many times smaller in amplitude than the flow depth. These are presumably similar to the "hummocky" bed topography described by *Wohl* [1992]. We find these forms are often well developed on the tops of bedrock protrusions, and on the crests of large boulders in the flow. They are especially well developed in fine-grained rocks. We propose that these forms evolve from incipient, low amplitude, long wavelength sinuous ridges in the surface to more sharply crested forms. Once sharp crested, the ridges become ornamented on their downstream sides by subsidiary flutes with near bilateral symmetry in planview (Figure 3) similar to those discussed by *Allen* [1971] in cohesive mud beds, but without a central axial rise [Figure 1d, *Allen*, 1968]. The flutes are often overhanging on the upstream side (Figure 3). The symmetry and overhang argue that the flutes reflect the vortices generated in the zone of flow separation developed at the crest, as suggested for similar features by *Maxson and Campbell* [1940]. We suggest that the high angular acceleration of the flow is capable of flinging high momentum suspended grains energetically out of the vortex and against the bed, causing efficient imprinting of the flow field into the rock form (Figure 3). These flow separation vortices are also spawned by joints, fractures and small bed irregularities, and flutes and potholes are often formed in association with these features. Once growth of these forms is initiated, their presence tends to enhance the flow separation region. The flutes migrate in an upstream direction, like miniature knickpoints, as erosion rates are highest on the upstream, overhanging end of the form (Figure 4), where recirculating flow is focused [*Allen*, 1968]. Flutes appear to occasionally "stall" in their upstream march and develop a more rounded rather than elongated shape (Figure 4). The "stall" may result from changes in the feature or the surrounding bed which diminish the strength of flow separation. Once reaching this morphology, the flute may behave more like a pothole, with erosion focused downward rather than headward as vertical vortices act to selectively erode the flute bottom [*Alexander*, 1932].

A.

B.

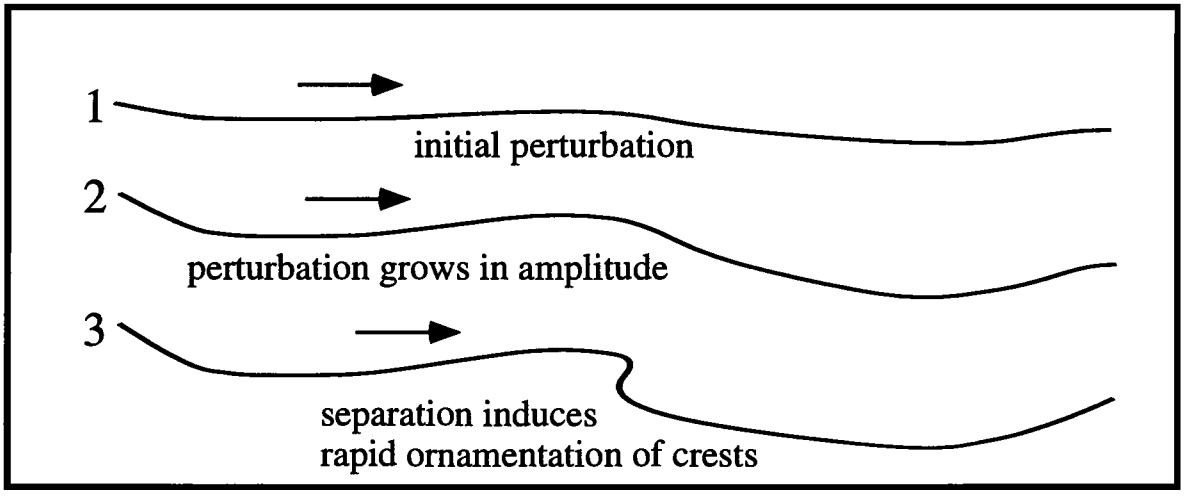

Figure 2. A) Active channel bed on the Indus River (Site H, Figure 10) showing ripple-like bedforms developed in bedrock. Flow direction is from lower left to upper right, and flow covers this bed by many meters during high flow (this is many times the ripple amplitude; note backpack for scale). Note how ripple forms are fairly regularly spaced, grow in amplitude and become more sharp-crested as a drop in the bed (upper limit of visible bed) is approached. Ripples at upper right have grown sufficiently to spawn flutes on their crest, which are effectively incising downward and headward into the rock surface. B) Schematic ripple cross-section, showing initial bed perturbation (1), growth of perturbation through differential bed erosion (2), and ornamentation of the ripple crest by flutes once crest begins to generate flow separation vortices on the downstream side.

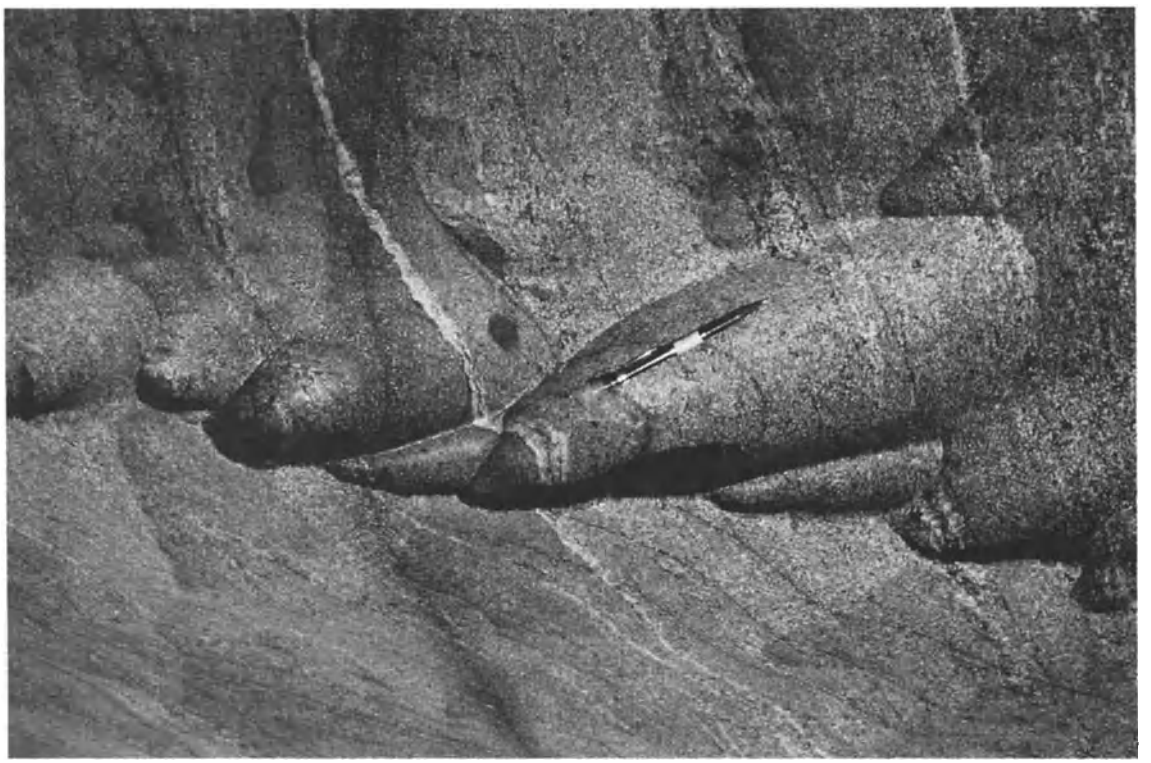

Figure 3. Flutes developed in bedrock on the Indus River (Site C, Figure 10). Flow direction is from top to bottom, in line with pencil (pencil length is ~15 cm). The flutes are nearly symmetrical in planview (note flute containing pencil), and several are overhanging. These flutes are presumably spawned by flow separation vortices generated by an edge on the rock face; these vortices allow effective decoupling of suspended sediment from the flow, and imprinting of the flow field on the rock. Note subordinate flute (small flute to left of flute containing pencil), presumably resulting from vortices shed from the edge of the large flute [*Allen*, 1971], and now eating into the head of the next flute downstream.

We often find that bedrock or boulders that protrude into the flow have a smooth, polished upstream side, a highly etched, fluted flow parallel side, and a heavily fluted, and potholed downstream side (Figure 5; see figures in *Maxson and Campbell* [1940]). We argue that the smooth front surface results from abrasion by suspended sediment, but that the rate of abrasion must be lower than on the flow-parallel and downstream sides, where rock is more rapidly removed in the abrasional bedforms. Because the flow can "feel" an upcoming obstacle at some distance upstream, on the order of several obstacle diameters, the flow field is able to diverge gradually as the obstacle is approached (Figure 6). Flow lines diverge slowly, resulting in low flow curvature and lateral acceleration. The suspended load remains coupled with the flow as it approaches the obstacle. In contrast, in the flow expansion downstream of the obstacle, in bed downdrops, or in fractures, the flow separates if the pressure increase associated with the decelerating flow is sufficient, producing recirculating eddies with extreme flow line curvature. Suspended sediment of sufficient momentum cannot be steered by the flow in such eddies, and may be flung against the bed, generating the "attack from the back". We expect that the larger grain sizes (fine to medium sand in the case of the Indus River) within the suspended load will be most effectively decoupled.

2.2. Bed Quarrying and Hydraulic Wedging

2.2.1. Quarrying of blocks. Quarrying, or plucking, of bedrock blocks from the bed is accomplished by lifting or sliding of blocks defined by an existing set of discontinuities in the rock (e.g., joints, fractures, bedding planes). Quarrying is a common and efficient mechanism for lowering bedrock river channels where joint and bedding plane spacing and their dip relative to stream flow direction allow it to be active [e.g., *Miller*, 1991]. Our field observations suggest that quarrying of blocks is the most rapid means of eroding a bedrock channel floor where the

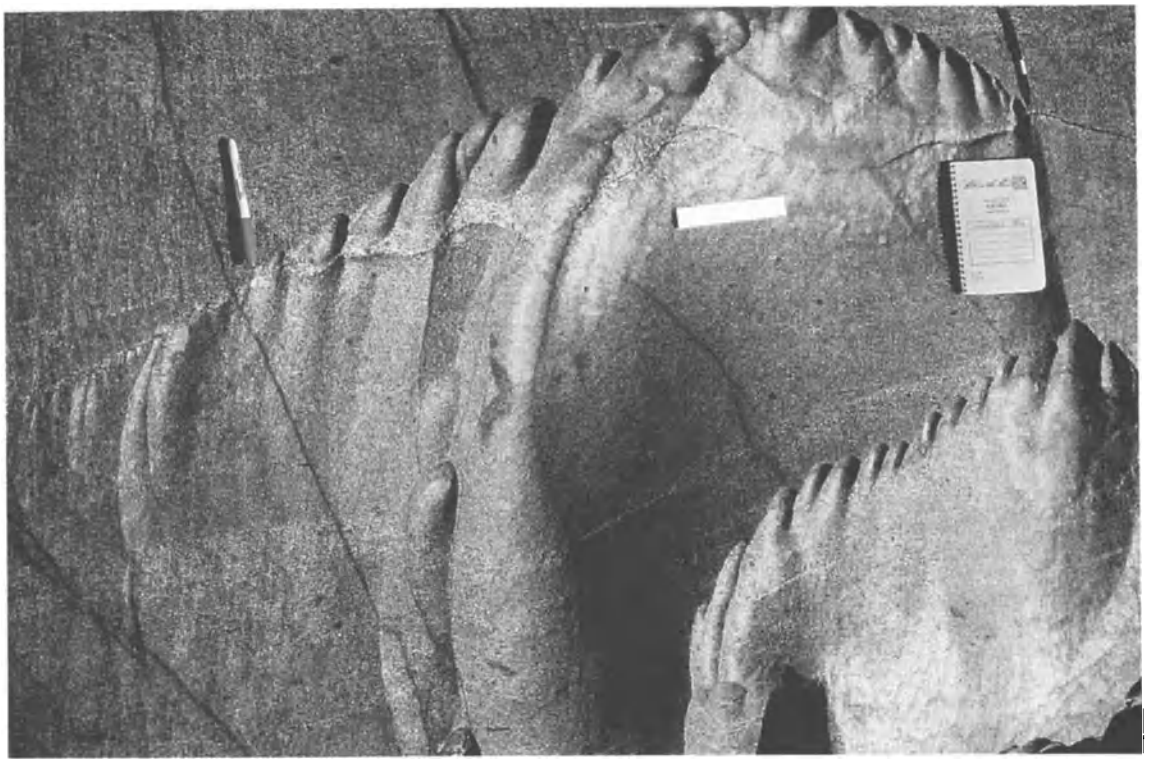

Figure 4. Upstream migrating flutes on horizontal surface on top of a boulder (focus of Figure 5, Indus River, Site C, Figure 10). Flow direction is from left to right, and flow covers this site by up to ~5 m in high flows. Ruler length is ~15 cm. These flutes are spawned by separation along a joint in the rock, which can be seen running from top to bottom, parallel and left of the ruler, and passing the tips of the pen and pencil. Below the lower pen, incipient flutes are currently developing along the joint. Between the pen and pencil, the flutes have migrated upstream (left) and away from the joint surface by up to ~20 cm. Note several flutes directly left of the ruler have become rounded, rather than elongate; these "flutes" may be stalled in their upstream march, evolving into incipient potholes.

joint spacing is sufficiently close to allow blocks to be moved by river flow. We base this hypothesis on observations that 1) in channels where joint or bedding plane spacing allows quarrying, the bed morphology is blocky and is defined by joint or bedding planes, reflecting the removal of blocks; and 2) abrasional flutes and potholes etch only shallowly into the bedrock touching up the corners of the joint blocks, and do not appear to evolve quickly enough to mute the blocky topography.

We develop two simple physical models of bed quarrying to place constraints on the type of flows adequate to quarry blocks. Blocks defined by joint edges or bedding planes may be lifted or slid out of their intact positions by the flow. This is likely preceded by some "preconditioning period" during which the joint surfaces are weathered, wedged apart (e.g., by hydraulic wedging, discussed below), and/or weakened by bashing with bedload. Assuming block removal following this preconditioning proceeds without the need for breaking chemical bonds, the block may be removed by 1) lift generated by pressure differences in the flow, or 2) sliding or rotating in response to the shear stress exerted on the upper block surface.

We first consider a simple hydraulic "lifting" of the block in the case where only the upper surface is exposed to flow. By assuming hydraulic connection between water in the joints and the free flowing water above the bed, we can use the Bernoulli equation to estimate the threshold velocity necessary to lift the block (Figure 7). Joints are assumed to be perfectly horizontal and vertical. The water in the joints will exert a pressure, P_1, on the joint faces, while the free-flowing water above the block will be have pressure, P_2, dictated by the flow velocity, v. To initiate lift of the block, the force difference associated with pressure differences, $(P_1\text{-}P_2)xy$, must be sufficient to overcome the buoyant weight of the joint block, $g(\rho_r\text{-}\rho_w)xyz$, where ρ_r and ρ_w are the density of the bedrock and water, respectively, and x, y, and z are the dimensions of the joint block (Figure 7). Rearranging this equation, we can estimate the threshold velocity, v_t, required to initiate lift of the block,

Figure 5. Boulder illustrating variation in bed erosion with orientation relative to the flow, Indus River. Flow direction is from left to right, and flow covers this site by up to ~5 m in high flows (low-flow stage river is seen in background). Note large boulder left of person is smoothly polished on the upstream side, fluted on the top, flow parallel side (see Figure 4 for detail), and heavily potholed on the downstream side. We argue the smooth front reflects abrasion, but erosion here is at a slower rate than within the flutes and potholes, where flow separation, resulting in high flowline curvature and angular acceleration, allows decoupling of suspended sediment from the flow.

$$v_t \sim \left[\frac{2gz}{\rho_w}(\rho_r - \rho_w)\right]^{1/2} \tag{9}$$

This will be a minimum threshold, as we have ignored the friction against the bounding blocks. The bed-parallel block dimensions, x and y, do not play a role in determining whether a block will be lifted.

An alternate formulation considers that a block is slid out of its intact position by the shear stress acting on the block surface. This scenario is analogous to the degradation of knickpoints described by *Miller* [1991] in carbonate rock-floored streams in southern Indiana. Again, it is likely that the block must be "prepared" by weathering or wedging for some period of time before this process can be activated. In this case, we consider the shear forces, exerted by the shear stress acting at the top of the block in opposition to the frictional forces acting to hold the block in place (Figure 7). Again the joints are assumed to be perfectly horizontal and vertical. In order for a block to slide, the shear force, F_S, must exceed the frictional force, F_F, $\rho_w g S H x y > \mu_s g(\rho_r - \rho_w) x y z$, where μ_s is the coefficient of static friction, and H is the water depth above the block. We again rearrange to derive the dependence of block thickness, z, that can moved on the flow conditions, HS_e,

$$HS_e \sim \frac{z\mu_s}{\rho_w}(\rho_r - \rho_w) \tag{10}$$

The mean flow velocity, v, in a channel goes as $(HS_e)^{1/2}$ (Eq. 4), indicating that for this process $v_t \sim z^{(1/2)}$, or $z \sim v_t^2$ or as in Eq. 9.

We now estimate the potential for maximum block thicknesses quarried under field conditions. In the Indus River, with maximum $S \sim 0.01$ (we substitute S for S_e), $H \sim 10$ m, and shear velocities $(u^*) \sim 1$ m/sec, we estimate velocities of ~5 m/sec at ~1 m above the bed during high flows. Assuming $\rho_r = 2.7$ g/cm^3 and $\rho_w = 1.0$ g/cm^3, these conditions are sufficient to initiate lift of a block with $z \sim 0.7$ m (Eq. 9), or, assuming dry rock-to-rock contact ($m_s = \sim 0.4$), to initiate sliding of a block with $z \sim 0.15$ m (Eq.

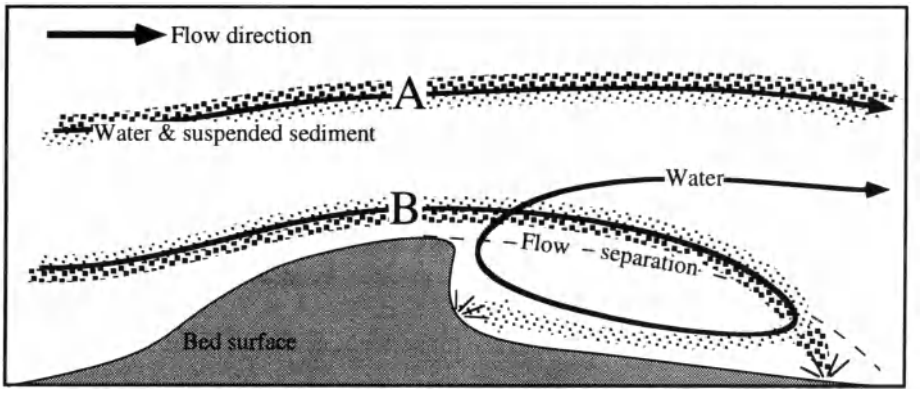

Figure 6. Schematic of flow around a bed obstacle. Flow is from left to right, and two flow lines are shown, A and B. On flowline A, the water and the suspended sediment remain coupled although flow adjusts to passing over the bed obstacle. Following flowline B, sediment and water remain coupled on upstream side of the obstacle, as flowline curvature is relatively slow as the flow approaches the obstacle. However, downstream of the obstacle, flow separation is initiated in response to the flow expansion and adverse pressure gradient. Water recirculates in this region before escaping downstream, but because the flowlines in this region are highly curved, the water flow cannot steer the sediment. The sediment is flung out of the flow and against the bed, with the location of sediment decoupling within the separation region dependent upon the grain size.

10). This estimate for block sliding does not consider possible water lubrication of the joints or assistance by block lift (both effectively lower m_s), both of which will increase potential size of the block which may be moved under these conditions. For both, the dip of the joint planes relative to the horizontal will also enhance or reduce the potential for block motion [*Miller*, 1991].

These expressions suggest that the ability of a river to erode its bed by quarrying increases as the square of velocity, which is expected because both $(P_1\text{-}P_2)$ and t go as v^2. This implies that the largest flows are capable of removing substantially thicker blocks than low flows. We note that in this case the local joint spacing of a channel therefore sets a threshold velocity and, hence, a threshold discharge, Q_t, below which no quarrying can take place. If $Q_t > Q_{max}$, abrasion will be the dominant process. According to Eqs. 9 and 10, with a given discharge through a river reach, quarrying will be enhanced locally where water surface slopes and flow velocities are high, like channel constrictions and steep drops. While not considered in Eqs. 9 and 10, the distribution of joint dip and strike relative to flow direction also controls quarrying rates [*Miller*, 1991]. We have neglected as well the needed "preparation time" of the joint blocks, which introduces a waiting-time threshold to the quarrying process.

2.2.2. Hydraulic wedging. We report here another process, previously undocumented, that loosens and prepares blocks for quarrying by wedging clasts into fractures and joints. We have termed this process "hydraulic wedging". We have noted in nearly every setting where joints are found in the bedrock that transported clasts, ranging in size from fine sand to boulders, are wedged very tightly into the joints (Figure 8). Removal of the clasts requires significant force, like a hammer blow, that often shatters the clast before it comes loose. This implies that the clasts are either emplaced forcefully, or are passively inserted as a joint temporarily widens. Forceful emplacement might be accomplished either by very high flow velocities and forceful injection by water, or if clasts possess sufficient momentum to slam into the joints. Both seem unlikely, because flow velocities should be relatively low in joints and even the finest (cm) scale fractures contain wedged grains. Another possibility is bashing of the clasts into joints by larger, saltating bedload particles. Deposited sediment is often not found on the bed outside of the filled joints (Figure 8), implying that sediment is trapped in the joints as it is being transported efficiently across the surface, rather than being "sieved" into the joints as a layer of sediments rests on the bedrock surface. A more likely scenario for clast emplacement may be slight widening of joint faces by pressure fluctuations exerted by the turbulent water flow, temporarily creating space for clasts with dimensions nearly equal to the static joint width. The clasts, if trapped during this temporally widening, act to "ratchet" the joint open through time by preventing the joint relaxation following expansion, or to weaken the joint face as it closes back down on the clast. Opening and widening of the joint will enhance subaerial weathering during low flow conditions, and promote hydraulic communication between the flow above the bed and the joint waters. In this way, hydraulic wedging likely plays an important role in setting the "preparation time" required before blocks can be quarried from the bed. The mechanics of this process are far from understood.

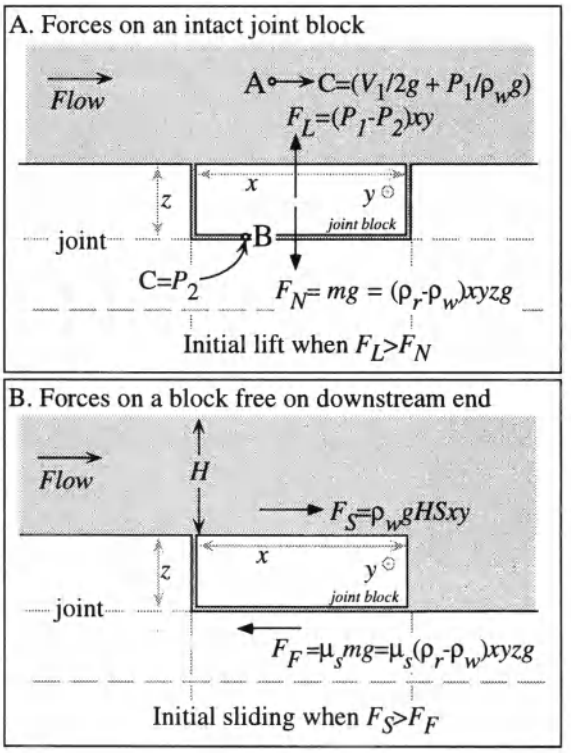

Figure 7. A) Sketch of forces acting on a joint block bounded on all sides except the top, and with dimensions x, y, and z. The total hydraulic head, C, at the two points, A and B, is equal, assuming hydraulic communication between the joint waters and the free-flowing stream, and negligible elevation difference between the points. Lift of the block will be initiated when the lift force, $F_L=(P_2-P_1)xy$, exceeds the buoyant weight of the block, $F_N= g(\rho_r-\rho_w)xyz$. Threshold velocity for initiation of lift for a given block thickness, z, is given in Eq. 9. B) Sketch of forces acting on a joint block bounded on all sides except the top and rear, and with dimensions x, y, and z. Initiation of block motion will occur when the tractive force, $F_S=\rho_w gSHxy$, exceeds the force of frictional resistance, $F_F=\mu g(\rho_r-\rho_w)xyz$. Threshold velocity for initiation of lift for a given block thickness, z, is given in Eq. 10.

2.3 *Cavitation*

Cavitation in water occurs when local flow velocities are sufficiently high to produce small regions in the flow in which pressure falls temporarily below the water vapor pressure. This may occur where flow is constricted and obstructed locally, resulting in increased water velocities [*Barnes*, 1956]. In such regions, water-vapor filled cavities, or bubbles, then form within the flow. As these cavities are advected into regions of higher pressure associated with lower flow velocity, they collapse. During collapse, a powerful microjet of water threads through the bubble [see figure 4-18 in *Hammitt*, 1980]. Although small in size (<mm), these microjets act as miniature water hammers of remarkable strength if they impact a solid surface, and can lead to surface pitting and cracking [see figures in *Barnes*, 1956; *Bourne and Field*, 1995].

While cavitation is clearly a concern in engineered structures (e.g., turbines), it remains unclear whether it plays a role in natural river channels. We attempt herein to determine if conditions necessary for cavitation are likely in a natural bedrock channel. *Barnes* [1956] developed an equation for predicting cavitation in natural channels based on the Bernoulli energy balance equation expressed in terms of hydraulic head,

$$\frac{v_m^2}{2g}+\frac{p_a}{\rho_w g}+z_s=\frac{v_c^2}{2g}+\frac{p_v}{\rho_w g}+z_b \qquad (11)$$

This assumes a constant (mean) velocity, v_m, across the "normal channel cross section" and a local velocity at the point of cavitation, v_c, which is k times higher than the mean flow velocity. The terms p_a and p_v are the atmospheric pressure and the vapor pressure of water, respectively, and z_s and z_b are the elevation at the stream surface and bottom, respectively. Following *Barnes* [1956] and *Wohl* [1992], we make the assumption that $v_c=kv_m$, $z_b=0$, and $z_s=H$ (stream depth), and solve for the mean flow velocity required for cavitation to occur,

$$v_m=\left[\frac{2(p_a-p_v)}{(k-1)\rho_w}+\frac{2gH}{(k-1)}\right]^{1/2} \qquad (12)$$

While probably oversimplified, this equation illustrates that the threshold velocity needed for cavitation initiation in a channel decreases (hence, cavitation likelihood increases) with increasing H, p_v, and ρ_w, and with decreasing p_a.

We now estimate the likelihood of cavitation in a natural channel. With estimates of threshold velocities given by Eq. 12, and assuming near steady and uniform flow conditions to allow substitution of S_e with S, we can predict the channel slope, S, needed to generate cavitation for a given flow depth H by rearranging Eq. 4,

$$S=\left(\frac{f}{8Hg}\right)v_m^2 \qquad (13)$$

where we substitute S for S_e. Figure 9 shows threshold v_m and S values for given flow H assuming a range of 2 to 3 for k, and a range of typical values for S and H found in the Middle Gorge Indus River. The mean stream velocities and slopes for cavitation are quite high relative to typical stream values, even a steep, high discharge river such as the Indus. The v_m and S thresholds are likely exceeded only

Figure 8. Example of clast-filled joints, resulting from hydraulic wedging of clasts. Flow direction is left to right, and reach ~10 m maximum depth at high flow.

in locally steep or narrow reaches along a stream (Figure 9). However, we note that these locally steep reaches are often locations where rapids aerate the flow. Entrained air impedes cavitation by increasing the compressibility of the water. Very little air entrainment is required (roughly 0.3% by volume (*Rasmussen* [1949], cited in *Barnes* [1956]) before cavitation is reduced to a minor or negligible process.

We therefore suspect erosion of rock by cavitation in natural bedrock channels is not significant. We have not observed the pitting or cracking of rock surfaces, which are expected to result from cavitation damage and would tend to roughen the bed surface [*Barnes*, 1956; *Bourne and Field*, 1995]. In addition, the extreme velocities necessary for cavitation are rare, even in a steep river. Unlike many engineered structures, roughness in rivers, like rapids, may substantially aerate the flow, inhibiting cavitation.

2.4. *Processes, Channel Evolution, and Simulations*

The bedrock channels we have investigated erode through the interaction of the processes described above. The most efficient process in any given location depends on the flow conditions (e.g., channel hydraulics, sediment size and load)

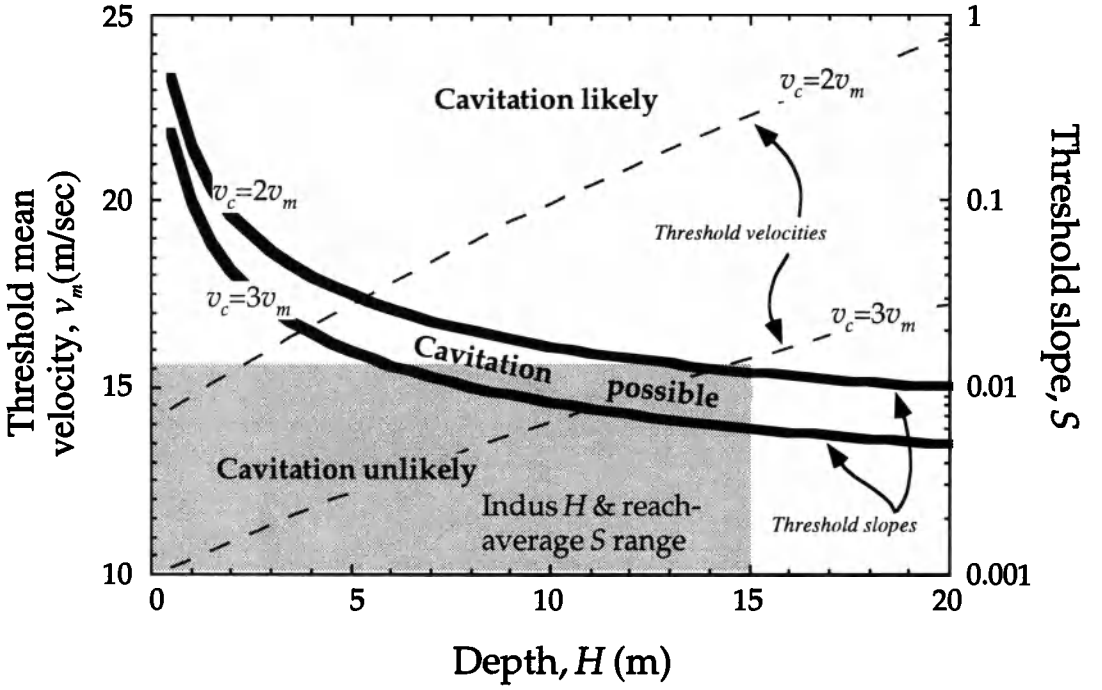

Figure 9. Estimated likelihood of cavitation in the Indus River using Eqs. 12 and 13, and assuming local bottom flow velocities range from 2 to 3 times higher than mean velocities ($3v_m \geq v_c \geq 2v_m$, k=2-3, see Eq. 12). We use the values p_a=101 kPa (sea-level), p_v=1.23 kPa (10°C value for water), ρ_w=1.0 g/cm^3, g=9.8 m/sec^2, and a value for f corresponding to a Manning's n=0.03. Thin dashed lines show threshold mean velocities, v_m, required to produce local bottom velocities, v_c, sufficient to initiate cavitation, with one line for $3v_m=v_c$ and one for $2v_m=v_c$ calculated with Eq. 12. Thick black lines show channel slopes required to generate these mean velocities, calculated using Eq. 13. Below the lower thick black line, slope is insufficient to generate the velocities necessary to produce cavitation at the specified depth; between the thick black lines, slopes and depths are potentially sufficient to drive cavitation; and above the upper thick line, cavitation is likely. The gray box shows the range of typical flow depths and reach-average slopes (over 100's of meters) for the Indus. Cavitation is possible only at the highest flows in the Indus according to the criteria we have selected.

and rock characteristics (e.g., joint spacing, "susceptibility", grain size). Quarrying is most effective where joint blocks are closely spaced enough to allow the available channel flow to quarry them regularly (implied by *Tinkler* [1993]), or for rare events to accomplish substantial quarrying in a short time. The efficiency of this process is not dependent on entrained sediment. The need to prepare the blocks for removal by subaerial weathering and/or hydraulic wedging of joints results in a block "preparation time". Once rocks too massive to be quarried are encountered, abrasion becomes the tool of choice. In a river with generally similar rock susceptibility but variability in joint spacing, we suggest reaches where abrasion is the predominant process must become steeper and narrower relative to the quarried reaches. This provides the additional energy expenditure required by abrasion to keep pace with quarried reaches. If a channel erodes into a massive rock unit that can only be eroded by abrasion, this reach will exert a rate-limiting control on the profile evolution upstream until this reach can steepen and narrow sufficiently, or until the massive rock is sawed through. In these settings, the potential rate-limiting nature of abrasion makes it a critical process to understand.

In all rivers, access to the rock bed is required before rock erosion can take place. Channel incision occurs only when the supply of sediment to the channel cannot keep it constantly mantled. In many bedrock stream systems, bedrock is covered at least partially by sediment [*Howard et al.*, 1994; *Sklar and Dietrich*, 1997]. The flow must therefore be sufficient to allow removal of the sediment cover before erosion can take place. Sediment transport therefore plays a role not only in setting rates of abrasion, but also in clearing the way for erosion to take place. Places where channels narrow and are steeper, with an accompanying increase in flow velocities relative to up- and downstream, may be better able to remain "cleaned" of sediment, allowing enhancement of bed erosion. Differential erosion of such sections may lead to steepening of upstream sections, enhancing sediment capacity and potential for bedrock erosion [*Howard et al.*, 1994].

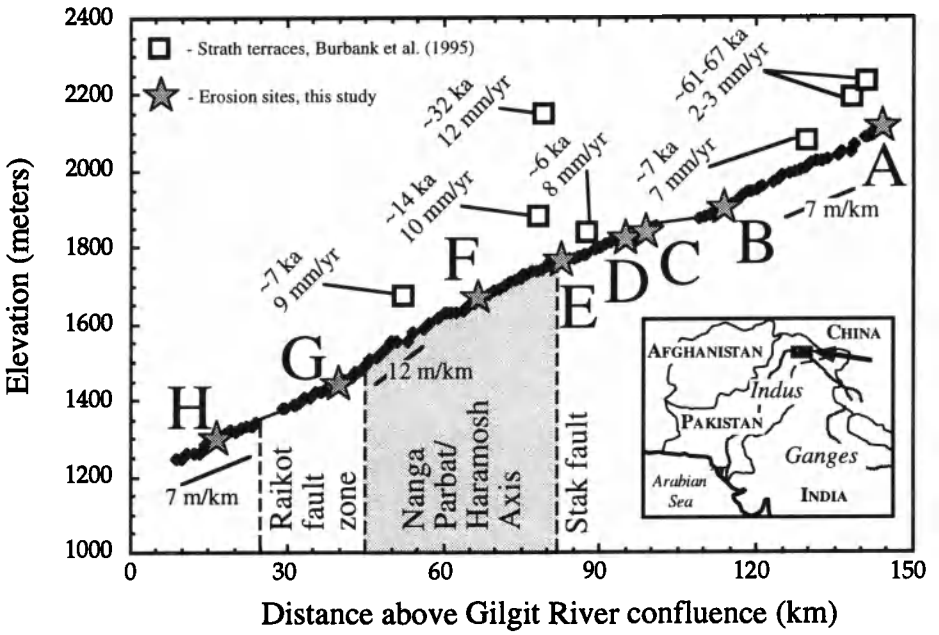

Figure 10. Profile of the Indus River through its Middle Gorge, with inset showing position of Middle Gorge in southern Asia. Each diamond in the profile reflects a survey point along the river. Reach-averaged slopes within the Middle Gorge range from 7 to 12 m/km, and are steepest as the river crosses the Nanga Parbat - Haramosh axis. Open boxes show position, CRN exposure ages (i.e., dates) and mean incision rates since terrace abandonment for strath terraces documented by *Burbank et al.*, 1996. Stars and accompanying letters show the position of the 7 erosion monitoring sites used in this study. The arrow marks the position of the Kachura gauging station at the upper end of the gorge.

Sediment transport needs to be treated in simulations of channel evolution to incorporate realistically the commonly observed bed protection by sediment cover.

The effectiveness of each process is sensitively dependent on flow conditions, and needs consideration in reach-scale models. In all of the expressions above, the process effectiveness scales nonlinearly with flow velocity. This points out the potential importance of large, rare flow events, and the details of the flow hydrograph in a river system [e.g., *Wohl*, 1992]. The "dominant discharge" may be different for each process, and therefore may not be well-characterized by a single choice for discharge surrogate. These are not captured explicitly in erosion rules relying on drainage area as a discharge surrogate. In addition, this sensitivity to velocity, coupled with our observations and measurements (discussed below), strongly suggest reach to sub-reach scale variations in channel width, slope and morphology are critical in setting channel bed erosion rates for each process. Abrupt topographic breaks in the channel long profile ("knickpoints") are examples of such places [e.g., *Howard et al.*, 1994; *Miller*, 1991; *Wohl et al.*, 1994]. A two-fold increase in mean flow velocity, induced by local channel narrowing and/or steepening, can lead to a ~2 to 10 fold increase in erosion rates, following the developments done for each process outlined above. Erosion rules relying on channel slopes calculated over reaches of 100's to 1000's of meters, which are typical length scales in simulation modeling, cannot account for the importance of sub-reach scale variations. Simulation models need to incorporate meaningfully variation of slope and width at scales below the reach scale, or predicted profile evolution may not be realistic.

3.0 FIELD MEASUREMENTS OF ROCK ABRASION RATES, INDUS RIVER

To measure short-term, local incision rates in a very active bedrock channel, we selected seven sites to monitor erosion along a ~150 km stretch of the Middle Gorge of the Indus River (sites A through H, Figure 10; Table 1). This river crosses "hard" metamorphic and igneous rocks throughout the Middle Gorge, and is steep, with reach-averaged slopes up to ~12 m/km (Figure 1). The Indus here has a drainage area of ~100,000 km^2, and has a large average annual swing in discharge from ~300 to >4000 m^3/sec. Maximum discharges during the period of gauging record (1970-1986) are >7500 m^3/sec. *Burbank et al.* [1996] estimated river bed erosion rates of ~1-10 mm/yr over the last ~6 to 70 ka by dating abandoned fluvial strath terraces now tens to hundreds of meters above the river (NPHA,

Table 1. Erosion monitoring site information.

Site	Local village name	Distance above confluence (km)[a]	Rock type	Schmidt hammer test[b]	Slope[c]	Estimated maximum stream power (W/m^2)[d]
A	Kachura	144	schist	65±2.9	0.0073	3800
B	Baghicha	118	granite	60±4.8	0.012	4500
C	Mendi	100	granite	69±1.5	0.0022	850
D	Triku	99	granite	66±1.1	0.0074	1500
E	Stak	83	mica schist	56±2.6	0.0017	800
F	Subsar	68	gneiss	64±2.7	0.02	17000
G	Burumdoir	39	gneiss	60±3.0	0.0076	3800
H	Hanochal	17	schist	64±4.4	0.023	3200

[a] Distance above confluence with Gilgit River
[b] Units are arbitrary - 100 is maximum for Schmidt hammer reading
[c] Measured locally (elevation change over ~250-500 m along river)
[d] Estimated for the mean annual peak discharge measured at Kachura gaging station (~146 km above Gilgit confluence)

Figure 10). These erosion rates are unusually rapid for a large bedrock river, and are thought to reflect rapid rock uplift, particularly along the Nanga Parbat - Haramosh Axis (Figure 10). Apatite and zircon fission track ages suggest denudation rates of this region up to ~cm/yr, with maximum rates located within the NPHA [Figure 8; *Burbank et al.*, 1996; *Zeitler*, 1985]. These apparently rapid river incision rates suggest this is an ideal site to study the processes of bedrock river incision, and to monitor erosion over a short time scale.

Our aim was to obtain first-order estimates of the 1) spatial and temporal variation of bed erosion rates, both at a site and over a ~150 km reach of the river; 2) erosion of the bed during "typical" flow conditions; and 3) variation in erosion rates through time, using erosion rates estimated over three timescales differing by several orders of magnitude. We measured erosion rates using two methods: 1) by drilling holes in the channel bedrock whose depth could be measured repeatedly to estimate the lowering of the surrounding rock surface over one year; and 2) by measuring cosmogenic radionuclide concentrations in rock collected from the bed of the river, providing an estimate of mean erosion rates over 1000's of years. To make these measurements, we selected accessible channel locations on the Indus 1) where substantial exposed bedrock extends from the low-flow river level to many meters above, allowing installation of drill holes and collection of cosmogenic radionuclide samples where maximum annual water depths reach up to ~10 m; 2) with a variety of bed morphologies, ranging from smooth rock to heavily ornamented surfaces etched by flutes and potholes; and 3) where sediment cover has likely been minimal through the recent past. Most of the seven sites chosen appear to be eroding primarily through abrasion, as joint spacing is sufficiently large to prevent quarrying. However, at sites C, D, and H, there is some evidence for at least occasional quarrying of blocks.

We documented the rock resistance, and the local channel geometry necessary to infer the stage history. At each site we measured channel cross sections and local (~0.5 km) river slope, noting the position and height of significant channel elevation drops and the elevation of a reddish stain line we infer reflects the mean high flow water level. Rock hardness was measured by using a Schmidt hammer test at each site [*Selby*, 1980], which measures rock compressive strength, a good surrogate for erosional resistance of rock [e.g., *Wohl et al.*, 1994]. Ten repeat measurements were made at each site, taking care to keep the hammer in a vertical orientation and to test spots away from discontinuities such as joints, fractures, and edges. These granites, schists, and gneisses are relatively resistant. Mean hammer test results from each site range from 56 to 69, and the hardness varies by only 10% among the seven sites (Table 1).

To estimate the typical hydrographic forcing and water coverage, we surveyed flow cross sections and slope at each site, and use flow records collected at the head of the Middle Gorge. Flow data were obtained from daily average flow records at the Kachura Bridge gauging station, collected from 1970 to 1986, which is near the upstream end of the Middle Gorge (~150 km upstream of the Gilgit River confluence, Figure 8). As the Indus River drainage area at

Figure 11. Example of drill hole placement (Site C, Figure 10). Flow is left to right, and reaches ~10 m depth during maximum flows. Note hole placement on smooth upstream faces (left of leftmost pen), and within flutes (between pencil and vernier caliper).

Kachura is ~100,000 km^2, and only relatively small tributaries enter the river within the Middle Gorge, it is likely that typical flows at each erosion site are well-represented by the measurements made at the Kachura station, despite the ~150 km length of the gorge We calculated the specific stream power (Eq. 3) using the average maximum daily discharge for an average year, and slopes measured using an inclinometer and laser rangefinder to measure elevation change over 100's of meters at each site (Table 1). We now discuss the specifics of the drill hole and cosmogenic radionuclide methods for measuring erosion rates.

3.1. Drill Hole Method

In Spring 1996, during low flow conditions, we drilled 3-9 holes in the channel floor in a variety of bed positions (Figure 11) at each of the seven sites. We selected the hole sites to capture the variation of erosion rates over short (meter) distances, where mean flow conditions, such as flow depth, sediment concentration, and total period of flow submersion, are likely similar, but local flow dynamics, such as streamline curvature, vary significantly. We drilled holes in local groups, located on the walls of flutes and potholes, as well as on the bed outside of such features (Figure 11). We used a hand held rock drill and rock hammer; holes were ~1.5-2.0 cm deep and ~0.5 cm wide, and ~1 to 6 m above the low flow river stage. We carefully cleaned sediment from each drill hole after installation, and then measured hole depth with a vernier caliper (Scienceware Type 6914) with a precision of ±0.05 mm. The depth was measured at the deepest portion of the hole, which was easily located because the drill bit produces a conical depression at the hole bottom. At least five repeat measurements were taken of each hole, with the micrometer consistently in the same orientation. Each hole was marked with the measurement orientation and a number, and then photographed.

During the peak flows in summer 1996, Indus River levels in the Middle Gorge reached roughly average maximum stage, based on anecdotal and photographic evidence (*D. Burbank*, pers. comm.; Figure 12). There is no evidence for unusually high or low flow conditions during this year. Given these flow conditions, the drill holes at the seven sites were under ~2-10 m of water at maximum discharges (~4250 m^3/sec). We reoccupied the drill hole sites in Spring 1997, and remeasured the hole depths following the procedure outlined above. We assume any decrease in hole depth reflects lowering of the bed around the hole by abrasion. We collected a sample from a

A.

B.

Figure 12. High and low flow photographs on the Indus River at Site H (Figure 10). Flow is toward the viewer. A) Site H shown at low flow conditions in April 1997. Discharge is ~300 m^3/sec. The drill hole and cosmogenic sample site is located on the platform near the center of the photo which juts into and constricts the flow. Flow width directly right of the platform is ~10 m. B) Site H shown at near mean annual flood in July 1996. Discharge is ~4200 m^3/sec, assuming flow is near mean annual maximum, which typically occurs at this time of year. At this stage, the platform on which the drill holes are located is buried by ~10-15 m of water.

slackwater deposit likely laid down during high flows in Summer 1996. Mean grain size from this deposit is ~1.9 ϕ (~0.27 mm, fine sand), and 80% of the grain size distribution falling between 2.5 ϕ to 1 ϕ (0.18 to 0.50 mm, fine to medium sand). This material is in suspension at high flows, and is likely the tool with which abrasion is accomplished. The hole depth changes are shown in Figure 13.

3.2. Cosmogenic Radionuclide Method

In order to estimate erosion rates on longer time scales, we utilize the newly evolved methods employing cosmogenic radionuclides (CRN). The concentration of radionuclides in a surface sample is used to infer the time the sample has taken to be exhumed through a production rate boundary layer of ~1-2 m. The erosion rates will therefore be average rates over this depth interval, assuming erosion is nearly steady. For example, if the true erosion rate is 1 mm/year, the measured rate will be averaged over ~1-2 ka. At several of the erosion sites, we collected samples to determine the concentration of the cosmogenic radionuclides (CRN) ^{10}Be and ^{26}Al in quartz within exposed bedrock. CRNs accumulate in a target mineral, such as quartz, through bombardment by secondary cosmic ray particles [see reviews in *Bierman*, 1994; *Nishiizumi et al.*, 1993], with the production rate P falling off exponentially below the surface. The concentration of CRNs, N, contained in a mineral now exposed at a surface which has been steadily eroding through time at a rate $\dot{\varepsilon}$ can be expressed as:

$$N = \frac{P_0 z^*}{\dot{\varepsilon} + \lambda z^*} \tag{14}$$

where P_0 is the CRN production rate at the rock surface, and z^* is the length scale for production attenuation as a function of depth ($z^*=\Lambda/\rho_r$, where Λ is the mean free path for the secondary cosmic ray particles, ~150 g/cm^2, and ρ_r is the rock density, ~2.7 g/cm^3). For rapid erosion rates (≥0.01 mm/yr), one may safely ignore radioactive decay. The above equation can then be rearranged to estimate the erosion rate, $\dot{\varepsilon}$,

$$\dot{\varepsilon} = \frac{P_0 z^*}{N} \tag{15}$$

where N is the measured CRN concentration.

We collected samples from bed locations that were well-exposed (i.e., no horizon blockage by local bed topography), near horizontal, and were adjacent to drill holes at all seven sites. Unfortunately, only three samples from these sites provided sufficient quartz for the CRN analysis. Maximum water depths over these sites range from ~2 to 10 m during a typical flow year. We estimated cosmic ray shielding from horizon blockage by measuring the angle to the skyline in 8 radial directions spaced by 45°, and using the equation of *Nishiizumi et al.* [1993]. We then calculate P_0 at each site by correcting the sea level, high latitude spallogenic production rate value of 21.29 atoms ^{27}Al/(g quartz - year) [*Clark et al.*, 1995] for the sample latitude and altitude using the production correction factors given in Table 2 of *Lal* [1991]. We neglect production of ^{27}Al by muon interactions, which should introduce negligible error at our sample elevation and latitude [*Brown et al.*, 1995].

At each site, we collected ~1 kg of rock, crushed the rock and extracted quartz. Typical quartz yields were ~50 g (Table 2), and ~1 g of ^{9}Be and ^{27}Al carrier was added to each sample. The quartz was purified and prepared for CRN isolation following the method of *Kohl and Nishiizumi* [1992]. Samples were analyzed for ^{10}Be/^{9}Be and ^{26}Al/^{27}Al ratios by accelerator mass spectrometry (AMS; *Elmore and Phillips*, 1987) at the Lawrence Livermore National Laboratory. Stable ^{27}Al concentrations in each sample were measured by ICP-MS at University of California - Santa Cruz. We were unable to obtain ^{10}Be/^{9}Be ratios, presumably due to very low concentrations in the quartz samples. However, we did obtain ^{26}Al/^{27}Al ratios, and used the measured ^{27}Al concentration in each sample to determine the concentration of the cosmogenic ^{26}Al (Table 2).

While CRNs have been used for inferring long term erosion rates in a number of geomorphic settings, as far as we know, this has never been attempted on an actively eroding river bed. There are several complexities to consider when interpreting the CRN concentrations obtained from samples collected from an active river bed. The surface production rate, P_0, could vary with time by: 1) variation in blockage of CRN production (lowering of P_0) during the year by water coverage; 2) variation in shielding produced by differential lowering of local bed topography surrounding the sample site; and 3) periodic burial of the bed by sediment. In addition, the steady state erosion assumption of Eq. 15 could be violated by non-steady

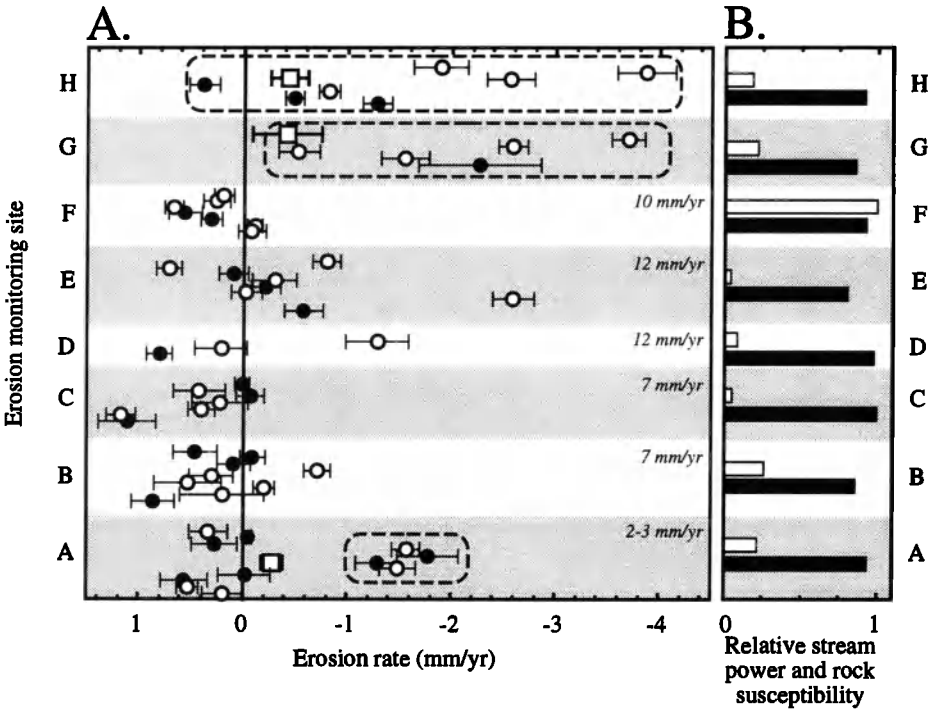

Figure 13. A) Erosion measurement results. On graph, open circles show depth changes for drill holes installed within flutes and potholes, and solid circles for drill holes placed outside of such forms (see Figure 11). The drill hole depth changes are obtained by subtracting the mean hole depth obtained from 5 measurements in 1997 by the results of the same measurements made in 1996, and error bars on drill hole measurements correspond to propagation of 1s errors obtained from these measurements. The open boxes are the erosion rates estimated using the concentration of ^{26}Al in rock collected from the bed surface at each site, using Eq. 15, and 1s error bars reflect propagation of all analytical and CRN production rate errors. The dashed circles enclose drill holes installed in locally narrow and steep (i.e., high energy expenditure) channel segments. Numbers on right side of graph correspond to long-term erosion rates estimated from the strath terraces dated by ***Burbank et al.***, 1996 nearest to each site. B) Relative stream power (hollow bars) and rock susceptibility (solid bars - inferred from Schmidt hammer tests) for each site.

erosion of the bed. Of these potential complicating factors, only the sample site coverage by water can be constrained quantitatively with available data. We have chosen our sampling sites to minimize the problems associated with the other complexities.

We calculate CRN production shielding by water coverage using measured flow data to estimate flow depths over each site. As CRN production decays exponentially with depth, z, in material, $P=P_0e^{(-z/z^*)}$ (z^*=~1.6 m for water), we require a history of water depth above each sample site. First, we establish a rating curve (flow depth vs. discharge) for each river cross section at which a sample was collected. To do so, we use the surveyed cross section and local slope, and input these into the Manning equation to calculate mean flow velocity at each flow depth (Figure 14). We compiled the minimum, average, and maximum daily flow for each day of the year from the data collected at the Kachura gauging station. We take the red stain line to reflect the average high flow, which is supported by high flow observations in summer 1996 [*D. Burbank*, pers. comm., 1996]. Second, using the rating curve, we estimate the discharge at which the CRN sample site first becomes covered. We use the rating curve and daily flows to yield a graph of flow depth above the sample site through the year (Figure 14). We then integrate the daily production rate over a year, and obtain the annual production rate in the face of water shielding. Annual production rates calculated by this method tend to be 75-95% of the uncovered production rates (Figure 14), despite burial of these sampling sites by up to ~10 m of water during high flows. The small magnitude of the correction reflects the small portion of the year during which high flows occur on the Indus.

The variation in shielding associated with local bed topography evolution, and with possible temporary burial by sediment, are more difficult to constrain. The effect of shielding would tend to lower the average production rate experienced by the sample. As with water shielding,

Table 2. Cosmogenic radionuclide results.

Site	Altitude (m)	Latitude	Sample thickness (cm)	Horizon shielding correction[a]	Water shielding correction[b]	Total quartz extracted (g)	^{26}Al concentration (atoms/mg)[c]	Exposure age (yr)[d]	Erosion rate (mm/yr)[d]
A	2099	35.3	5	0.92	0.95	56.5408	2.84±1.0	2560±1000	0.230±0.086
G	1440	35.8	5	0.88	0.75	51.4326	1.80±1.4	1700±1400	0.347±0.28
H	1300	35.8	5	0.90	0.75	50.3467	1.33±0.5	1640±710	0.375±0.16

[a] Calculated according to procedure of Nishiizumi et al. (1993)
[b] Calculated using average annual hydrograph to estimate sample site coverage (see text)
[c] ^{10}Be samples yielded no measurable values for these locations
[d] Calculated using a latitude and altitude corrected production rate of 29.21 atoms ^{26}Al/(g quartz - yr) (Lal, 1991, Table 2; Clark et al., 1995)

neglect of past topographic shielding therefore results in an overestimate of the average erosion rate, $\dot{\varepsilon}$. In an effort to avoid periodic burial by sediment, we collected from sites that are currently devoid of sediment and are not in topographic depressions on the bed. The collection sites are in narrow, bedrock reaches that we feel are not likely to be covered with sediment often. We therefore assume that errors introduced by periodic sediment burial are insignificant.

Non-steady erosion effects should also introduce negligible error into the estimated erosion rates. The steady erosion assumption underlying Eq. 15 could be tested by using the ratio of ^{26}Al/^{10}Be and the "banana" diagram [Fig. 5, *Lal*, 1991; Fig. 3, *Nishiizumi et al.*, 1993]. Unfortunately, in this study, ^{10}Be results were below detection limits, precluding the use of this test. However, we first consider a non-steady scenario where erosion is periodic, with each erosion episode nearly instantaneously (relative to 1000's of years) removing an equal thickness from the bed, and no bed lowering otherwise, as carefully considered by *Small et al.* [1997]. If these erosional episodes are very frequent, instantaneous rates must be only slightly greater than the long term erosion rate; this scenario effectively collapses to the steady assumption of Eq. 15 [*Small et al.*, 1997]. However, even for low frequency events, we can constrain the error. For example, a ~1 m block quarried once every ~1000 years with negligible erosion otherwise ($\dot{\varepsilon}$=~1 mm/yr), the analysis of *Small et al.* [1997] suggests an erosion rate estimated using CRNs off by at most ±~50% from the true mean erosion rate for that spot. While bed erosion in a river is likely episodic, erosional episodes may not be equal. However, if erosion in these episodes varies over a range of approximately of the order of the long term erosion rate, erosion rates estimated with CRNs using Eq. 15 should again approximate well the long-term average rate. The erosion rates estimated with CRNs, using Eq. 15, are shown with the drill hole results in Figure 13. Error bars represent primarily analytical and production rate errors; no attempt is made to correct for possible non-steady erosion.

3.3. Discussion of Erosion Measurements

We first discuss the changes in the drill hole depth between 1996 and 1997, shown on Figure 13. There were several holes (at sites A and H) that spawned small flutes trailing off of their downstream side (Figure 15). These flutes had widths of about the hole diameter, maximum depths of up to ~1 cm, and lengths of ~2 cm. The generation of these small flutes clearly demonstrates that the holes influenced local flow conditions, and illustrates the critical role of local bed perturbations in focusing erosion. We took care not to include the spawned flutes in the measurements of bed lowering around the holes. Many of the holes were partially to fully filled with fine to coarse sand, with some grains nearly equal in size to the hole diameter tightly lodged in the hole. None of the bed surfaces around the drill holes were covered by more than ~1 cm of sand. In most cases, our measurements of drill hole depth changes reflect the lowering of the bed around the drill hole, rather than lowering of the hole opening only. We realize that several of the holes actually appeared to deepen (depth changes are positive, Figure 13). This likely results either from deepening of the holes accidentally while we attempted to clean them of sediment in 1997, or from an improvement in our hole cleaning technique in 1997. It seems unlikely that the hole bottoms were lowered selectively, given their high aspect ratio and narrow diameter. At worst, all of the bed lowering measurements may be considered underestimates of the actual bed lowering, by ~0.5 mm. We believe that the measured bed lowering is the direct result of abrasion, which we infer because 1) chatter marks and chips made in the rock during drill hole installation have been significantly smoothed, suggesting polishing by abrasion (rather than cavitation); 2) quarrying appears to operate on larger scales; and 3) the highest erosion rates are found in abrasional forms, like flutes.

The drill-hole bed lowering measurements reveal that erosion rates are highly variable both between and within sites (Figure 13). In several locations (sites B, C, and F),

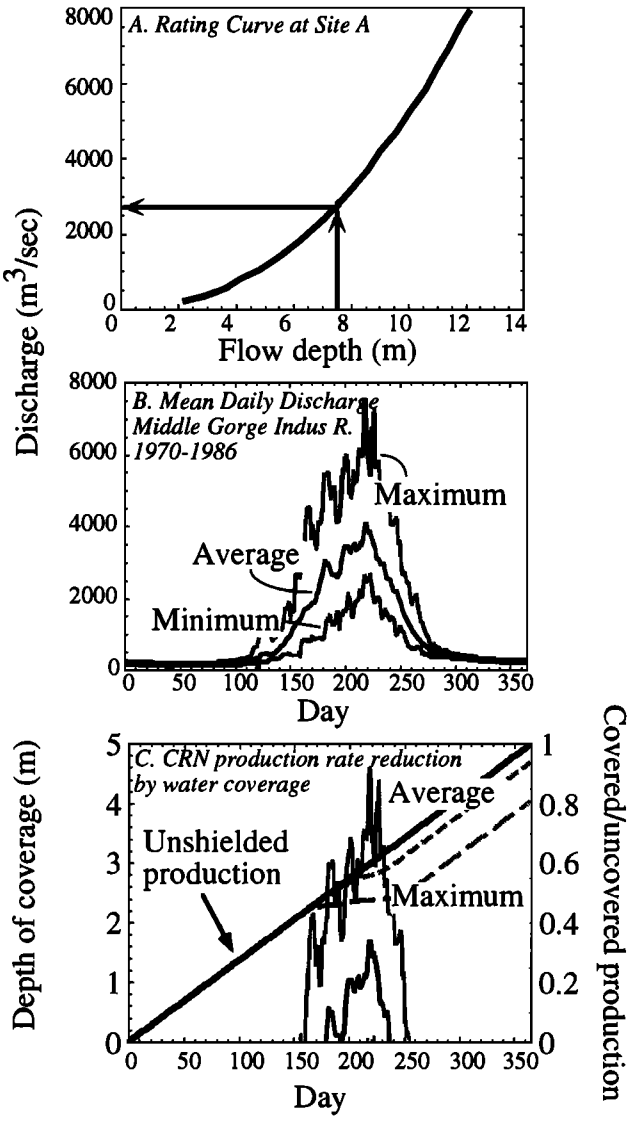

Figure 14. Example of correction of CRN erosion rate for water shielding, performed for Site A (Figure 10). We seek a history of water depth above the site to estimate the shielding. A) Rating curve for the site, relating flow depth to discharge. B) The maximum, average, and minimum historical mean daily flows for each Julian day recorded at Kachura gauging station, 1970 and 1986. C) Daily water depth above CRN sample site obtained from historical daily average flows (thin black line) and maximum flows (thin gray line) obtained by using the discharge data presented in B to determine flow depth with rating curve in A. Mean minimum daily flows are insufficient to cover site. The thick line tracks the relative accumulation of CRNs on the bed assuming no water shielding; the slope of this line is the relative unshielded production rate, $P_0/[P_0(365$ days$)]$. The dashed lines track CRN accumulation in the face of water shielding by the average and maximum flows; the slopes of these lines are the instantaneous relative production rate, $P_0e^{(-H/z^*)}/[P_0(365$ days$)]$, where H is the flow depth. The slopes of the dashed are lower than the solid, unshielded line when the site is covered by water, reflecting lowered production rates. The right axis shows the relative annual production rate, with a value of 1 equivalent to the unshielded rate. The production rates on the bed surface are lowered by ~5-20% relative to the unshielded production rate.

there appears to be no appreciable bed lowering over the Spring 1996 to Spring 1997 interval. At the remaining sites, maximum bed lowering rates range from ~1 to 4 mm; the maxima are typically within flutes (open circles, Figure 13). The maximum bed lowering rates of ~4 mm/yr was measured in a flute of ~10 cm maximum depth. Remarkably, at these rates, flutes like those in Figure 3 may require only a few 10's of years to evolve, particularly if erosion rates increase nonlinearly with discharge. Importantly, erosion rate variations do not appear to reflect rock hardness variations. While erosion rates vary by about an order of magnitude, the Schmidt hammer tests vary by only ~10%, suggesting that the abrasional resistance of these rocks at each site are comparable (Table 1; Figure 13). Abrasional wear therefore must reflect instead variations in the local flow field.

The measured rates are highest where channel width decreases and/or slope increases to produce channel segments of locally high energy expenditure. The holes with the highest erosion rates are within short reaches of steep elevation drops and channel narrowing (holes at sites A, G, and H, enclosed by dashed circles, Figure 13). We infer from this that erosion rates are greatest where stream power (Eq. 3) is locally high. In contrast, reach-averaged stream power estimates for each site, calculated using slopes averaged over 100's of meters comparable to those one would obtain from maps and similar to the length scales used in channel erosion rules (Eq. 7), fail to predict well the locations of most rapid bed lowering (Figure 13). For example, site F, with the highest reach-averaged stream power, showed no abrasion during our monitoring. This points out a significant problem with trying to apply reach-averaged slopes to predict bedrock erosion rates, as in Eq. 7, particularly given the strong erosion rate dependence on channel slope in the rate-predicting rules discussed in section 2.

The CRN estimated erosion rates of ~0.25-0.50 mm/yr at sites A, G, and H are several times lower than the maximum bed lowering rates obtained from the drill holes (Figure 12, squares). We report as well one other CRN measurement on the bed at site F, which yields a similar rate [*J. Leland*, pers. comm., 1997]. These rates are very low compared to the drill hole measurements at each site (except site F). Comparison of the CRN rates, which effectively average bed lowering rates over ~1.5 to 2 ka, to the annual rates obtained from the drill holes implies that bed erosion rates at a point on the bed must vary

Figure 15. Drill holes in a flute at Site H, showing small flutes generated on the downstream edge of both holes. Flow is from left to right. The flute on hole 6 is the more visible. The drill hole is located just above the "6", with two black lines on either side. Hole diameter is ~0.5 cm. The flute extends upward and to the right for ~5 cm, and is ~0.5 cm deep, and shallows away from the hole.

significantly through time. If bed erosion is accomplished by abrasion, the loci of bed erosion may move as active flutes migrate across the bed surface, and as potholes are born and die, as outlined in Section 2.1.3 above. This implies erosion by abrasion is episodic at any single point on the bed, with much of the erosion accomplished within flutes and potholes, where suspended sediment efficiently delivers kinetic energy through impact.

Reconciliation of our measurements with the rates of *Burbank et al.* [1996] is also needed. The much higher long-term rates obtained from the strath terraces may reflect hydrologic and/or sediment supply changes in the Indus River system during the ~6 to 70 ka since terrace abandonment that allowed incision rates to be at times much higher than present. Glacial/interglacial climate cycling provides one possible explanation. In this scenario, changes in the frequency or magnitude of discharge and/or of the sediment supply alter erosion rates. Our lower annual (drill hole) and millennial (CRNs) erosion rates may reflect modern and recent (last ~2 ka) flow and sediment supply conditions that are unlike those that accomplished much of the bed lowering since abandonment of the straths. We hypothesize that during glacial or glacial/interglacial transitions, the magnitude and/or frequency of discharge and sediment conditions favorable for bed erosion were greater, resulting in bed erosion rates higher than at present. This scenario has been suggested for other river systems [e.g., *Foley*, 1980b], and requires that incision rates on the Indus during these periods are even higher than the remarkably high long-term average rates obtained by *Burbank et al.* [1996].

Another alternative explanation is that we have measured rates of the wrong process. Perhaps quarrying of the bed is the primary mechanism by which the river is incising, over the long term. As outlined in Section 2.2, quarrying is likely to be a more efficient erosional process where it can be active. To account for the long-term average erosion rates, quarrying must currently act in locations within the channel we have not measured, or was active prior to the time period covered by our mean erosion rates (~1 to 2 ka). Both seem unlikely at our sites, because joint spacing seems sufficiently large to prevent quarrying. We can, however, also consider the possibility that quarrying is active in the very sites we have measured. To do so, we interpret our CRN concentrations as exposure ages ($t=N/P_0$) of ~1.5 to 2 ka, assuming essentially no surface erosion;

these "ages" are interpreted to reflect the period of time elapsed since the last quarrying episode. Reconciliation of the "waiting times" with the long-term erosion rates of ~2 to 10 mm/yr *Burbank et al.* [1996] requires blocks or many blocks totaling ~3 to 20 m were quarried during the last quarrying episode. While we see no evidence of this, it is nonetheless difficult to rule out.

4. SYNTHESIS

Bedrock channels erode and evolve through an interconnected set of erosion processes. Our observations indicate that the primary mechanisms in hard bedrock are abrasion by suspended load and quarrying of blocks from the bed. Quarrying is the more efficient of these processes, and, where joint spacing allows, accomplishes much of the incision in a bedrock river channel. However, more massive rocks require cutting by abrasion. As this process is less efficient, in order to maintain a steady profile, a river must become steeper and/or narrower relative to quarried reaches, providing sufficient energy to allow abrasion to keep pace. Such reaches often appear to form local base-level for the upstream reach, which may have the potential to erode more rapidly through plucking; if true, reaches where abrasion is the primary tool may limit the rate at which a river slices through underlying bedrock.

Abrasion rates are very sensitive to the local flow velocity, and our bedform observations and measurements suggest it is most effectively accomplished by the suspended load. A simple scaling rule, developed following *Foley* [1980a] and *Anderson* [1986], implies $dz/dt \propto v_w^5$. Abrasion is most effective where sediment can be "flung" forcefully from the flow, and we argue this occurs in regions of separated flow, which generate high flow curvature. Flutes and potholes, which our measurements show are places of most active abrasion, are formed in and enhance flow separation. Since sediment must be entrained and carried into these forms, and the surfaces of these features are typically smooth rather than chipped and chatter marked, the effective abrasive impacts are delivered by the suspended load.

Quarrying appears to be the most efficient process where it is active. The process removes material from the bed by removing joint-defined blocks, either by lift or sliding. Our scaling rules imply the capacity of a flow to quarry blocks goes as $\sim v_w^2$; again, a nonlinear process. Typical flows on the Indus River are capable of generating lift to quarry blocks of ~0.7 m thickness, and of sliding blocks up to ~0.15 m, given the assumptions in our calculations. However, erosion by the quarrying process likely requires a "waiting period" to allow blocks to be loosened by subaerial weathering, bashing by bedload, or widening by a previously undocumented process, hydraulic wedging. Hydraulic wedging refers to the forcible emplacement of rocks into a joint, possibly during slight joint widening in response to turbulent pressure fluctuations within the flow. In this way, hydraulic wedging acts to ratchet open the joint, assisting in preparing the block to be quarried, both directly and by enhancing weathering rates in the widened crack.

Cavitation is not a significant erosive mechanism in natural bedrock channels we have investigated. Evidence for cavitation, such as small-scale surface pitting, has not been confidently identified on the bed of these channels. The flow conditions necessary for cavitation to occur require very high velocities for a given flow depth, and, hence, the water surface slope must be quite high to exceed the threshold for cavitation. Even on the Indus, a high discharge and steep channel, cavitation appears possible only at the most extreme high flows. Locally steep segments of bedrock river channels with water slopes high enough to generate the velocities necessary for cavitation are also typically locations where flow aeration is greatest. Introduction of even relatively small amounts of entrained air into the flow can reduce cavitation to a negligible or nonexistent process.

Through development of simple scaling rules for each of the major channel eroding processes (abrasion, quarrying, and cavitation), we find a strong dependence of process rate on local flow conditions. Each of the scaling rules indicate a nonlinear dependence of process rate on velocity, with powers of ~2 to 5. Our measurements of abrasion on the bed of the Indus quantitatively support the importance of local flow conditions for setting erosion rates.

Erosion rates measured with drill hole depth changes on the bed of the Indus River are remarkably variable in space, and reflect local variations in both flow dynamics and energy expenditure. Our annual (drill hole) bed lowering rates vary from ~0 to ~4 mm/yr, with these rates varying both within and between the seven monitoring sites. Miniature flutes with depths up to ~1 cm and similar in form to those shown in Figure 3, were spawned on several holes, confirming the ability of bed perturbations to enhance dramatically local bed erosion through alteration of the water flowlines. Consistent with this idea, the highest drill hole erosion rates are typically within flutes and potholes. Nearly all of the most rapid measured bed lowering took place within channel segments of a few 10's of meters length that were narrower and steeper, and with correspondingly greater energy expenditure, than was typical for the reach. Taken together, these results imply local variations in flow dynamics and energy expenditure are perhaps the most critical factors in setting erosion rates, at least by abrasion, and that these variables must be considered meaningfully when constructing reach-scale rules for bedrock erosion.

The differences in mean erosion rates obtained from drill holes (annual), CRN bed measurements (~1.5 to 2 ka), and long-term strath terrace dates (~6-70 ka) are up to ~2 orders of magnitude. The CRN bed measurements are several times lower at 3 sites (A, G, and H) than the maximum drill hole measurements. This is consistent with our

conceptual idea that flutes, which with potholes are the locations of the most rapid bed abrasion, migrate across the bed, and are separated by more slowly eroding to non-eroding bed surfaces. These "dead" surfaces wait until the next flute is generated or migrates past, and long-term erosion rates measured with CRNs integrate this "waiting time" between form passage, and are therefore necessarily lower than the maximum drill hole rates. The typical spacing between forms is consistent with the ten-fold difference between drill holes measurements and the CRN bed erosion measurements. All of our measured erosion rates, however, are substantially lower than the rates estimated from strath terraces [*Burbank et al.*, 1996] near these locations. These higher long-term rates require erosion to have been higher in the past, possibly during glacial times or glacial/interglacial transitions, when larger and/or more frequent high discharges coupled with more available erosive tools likely provided the river with more capacity for bed erosion. An alternative is that we have missed the relevant process by focusing on abrasion. Quarrying of blocks may be the more efficient process. If so, it must be currently active elsewhere in the channel if quarrying is presently eroding the bed at the rates of *Burbank et al.* [1996]. If quarrying were to be the dominant process at our CRN measurement sites, interpreting the CRN concentrations as "waiting times" since the last quarrying event requires that ~3 to 20 m of total lowering by block removal took place at ~1.5 to 2 ka to produce erosion rates comparable to *Burbank et al.* [1996]. We would argue that this is less likely, and that the discrepancy instead reflects true variation in erosion rates, associated with hydrologic changes, in the reaches on which we have focused.

Acknowledgments. Funding for this project has been provided by National Science Foundation grant EAR-9417798 (to RSA and KXW), and an IGPP Award from Lawrence Livermore National Labs (to RSA). We thank J. Khan, A. Khan, D. Burbank, G. Pratt, A. Felton, and E. Small for help in lab, field and writing, and to E. Wohl and K. Tinkler for organizing the conference leading to this volume. We greatly appreciate the insightful comments on the manuscript provided by G. Pickup and J. Costa. Many thanks are also given to the wonderful people of the Indus River Middle Gorge - their curiosity and kindness are unforgettable.

REFERENCES

Alexander, H.S., Pothole erosion, *.l Geol., 40*, 335-347, 1932.

Allen, J.R.L., Flute marks and flow separation, *Nature, 219*, 602-604, 1968.

Allen, J.R.L., Transverse erosional marks of mud and rock: their physical basis and geological significance, *Sed. Geol., 5* (3/4), 167-370, 1971.

Anderson, R.S., Erosion profiles due to particles entrained by wind: Application of an eolian sediment transport, *Geol. Soc. Amer. Bull., 97*, 1270-1278, 1986.

Ashley, G.M., W.H. Renwick, and G.H. Haag, Channel form and processes in bedrock and alluvial reaches of the Raritan River, New Jersey, *Geology, 16*, 635-646, 1988.

Barnes, H.L., Cavitation as a geological agent, *Amer. J.Sci., 254*, 493-505, 1956.

Bierman, P.R., Using in situ produced cosmogenic isotopes to estimate rates of landscape evolution: A review from the geomorphic perspective, *J. Geophys. Res., 99* (B7), 13885-13896, 1994.

Bourne, N.K., and J.E. Field, A high-speed photographic study of cavitation damage, *J. Appl. Phys., 78* (7), 4423-4427, 1995.

Brown, E.T., D.L. Bourles, F. Colin, G.M. Raisbeck, F. Yiou, and S. Desgarceaux, Evidence for muon-induced production of 10Be in near-surface rocks from the Congo, *Geophys. Res. Lett., 22* (6), 703-706, 1995.

Burbank, D.W., J. Leland, E. Fielding, R.S. Anderson, N. Brozovic, M.R. Reid, and C. Duncan, Bedrock incision, rock uplift and threshold hillslopes in the northwestern Himalayas, *Nature, 379*, 505-510, 1996.

Chadwick, O.A., R.D. Hall, and F.M. Phillips, Chronology of Pleistocene glacial advances in the Central Rocky Mountains, *Geol. Soc. Amer. Bull., 109* (11), 1443-1452, 1997.

Clark, D.H., P.R. Bierman, and P. Larsen, Improving in situ cosmogenic chronometers, *Quat. Res. (New York), 44* (3), 367-377, 1995.

Costa, J.E., and J.E. O'Connor, Geomorphically effective floods, in *Natural and anthropogenic influences in fluvial geomorphology: The Wolman volume: Geophysical Monograph 89*, edited by J.E. Costa, A.J. Miller, K.W. Potter, and P.R. Wilcock, pp. 45-56, American Geophysical Union, Washington, D.C., 1995.

Elmore, D., and F. Phillips, Accelerator mass spectrometry for measurement of long-lived radioisotopes, *Science, 236*, 543-550, 1987.

England, P.C., and P. Molnar, Surface uplift, uplift of rocks, and exhumation of rocks, *Geology, 18* (12), 1173-1177, 1990.

Foley, M.G., Bed-rock incision by streams, *Geol. Soc. Am., Bull., 91* (10), I 577-I 578, II 2189-II 2213, 1980a.

Foley, M.G., Quaternary diversion and incision, Dearborn River, Montana, *Geol. Soc. Am., Bull., 91* (10), I 576-I 577, II 2152-II 2188, 1980b.

Greeley, R., and J.D. Iversen, Wind as a geological process on Earth, Mars, Venus and Titan, *Cambridge Planetary Science Series*, 333, 1985.

Hammitt, F.G., *Cavitation and Multiphase Flow Phenomena*, 423 pp., McGraw-Hill, Inc., New York, 1980.

Hancock, G.S., R.S. Anderson, O.A. Chadwick, and R.C. Finkel, Dating fluvial terraces with ^{10}Be and ^{26}Al profiles: Application to the Wind River, Wyoming, *Geomorphology*, in press, 1998.

Howard, A.D., Modelling fluvial systems; rock-, gravel- and sand-bed channels, *Special Publication Inst. Brit. Geogr., 18*, 69-94, 1987.

Howard, A.D., A detachment-limited model of drainage basin evolution, *Water Resour. Res., 30* (7), 2261-2285, 1994.

Howard, A.D., W.E. Dietrich, and M.A. Seidl, Modeling fluvial erosion on regional to continental scales, *J. Geophys. Res., B, Solid Earth and Planets, 99* (7), 13,971-13,986, 1994.

Howard, A.D., and G. Kerby, Channel changes in badlands, *Geol. Soc. Amer. Bull., 94* (6), 739-752, 1983.

Knighton, D., *Fluvial forms and processes*, 218 pp., Edward Arnold, London, 1984.

Kohl, C.P., and K. Nishiizumi, Chemical isolation of quartz for measurement of *in-situ* -produced cosmogenic nuclides, *Geochim. Cosmochim. Acta, 56*, 3583-3587, 1992.

Lal, D., Cosmic ray labeling of erosion surfaces: in situ nuclide production rates and erosion models, *Earth Planet. Sci. Lett., 104*, 424-439, 1991.

Leopold, L.B., M.G. Wolman, and J.P. Miller, Fluvial processes in geomorphology, W.H.Freeman, San Frncisco, 1964.

Maxson, J.H., and I. Campbell, Fluting and facetting of rock surfaces, *J. Geol., 48*, 717-751, 1940.

Miller, J.R., The influence of bedrock geology on knickpoint development and channel-bed degradation along downcutting stream in south-central Indiana, *J. Geol., 99*, 591-605, 1991.

Nemec, W., M.N. Lorenc, and J. Saavedra, Potholed granite terrace in the Rio Salor Valley, western Spain: a study of bedrock erosion by floods, *Techniterrae*, 6-21, 1986.

Nishiizumi, K., C.P. Kohl, J.R. Arnold, R.I. Dorn, J. Klein, D. Fink, R. Middleton, and D. Lal, Role of in situ cosmogenic nuclides ^{10}Be and ^{26}Al in the study of diverse geomorphic processes, *Earth Surf. Proc. Land., 18*, 407-425, 1993.

Rosenbloom, N.A., and R.S. Anderson, Hillslope and channel evolution in a marine terraced landscape, Santa Cruz, *J. Geophys. Res., 99* (B7), 14013-14029, 1994.

Seidl, M.A., and W.E. Dietrich, The problem of channel erosion into bedrock, *Catena Supplement, 23*, 101-124, 1992.

Seidl, M.A., W.E. Dietrich, and J.W. Kirchner, Longitudinal profile development into bedrock; an analysis of Hawaiian channels, *J. Geol., 102* (4), 457-474, 1994.

Selby, M.J., A rock mass strength classification for geomorphic purposes: with tests from Antartica and New Zealand, *Zeit. Geomorph. N.F. Band 24*, 31-51, 1980.

Sklar, L., and W.E. Dietrich, The influence of downstream variations in sediment supply and transport capacity on bedrock channel longitudinal profiles, *Eos, Trans. AGU, 78*, F229, 1997.

Slingerland, R., S.D. Willet, and H.L. Hennessey, A new fluvial bedrock erosion model based on the work-energy principle, *EOS Supplement, 78*, F299-F300, 1997.

Small, E.E., and R.S. Anderson, Geomorphically driven late Cenozoic rock uplift in the Sierra Nevada, California, *Science, 270* (5234), 277-280, 1995.

Small, E.E., R.S. Anderson, J.L. Repka, and R. Finkel, Erosion rates of alpine bedrock summit surfaces deduced from in situ 10Be and 26Al, *Earth Planet. Sci. Lett., 150* (3-4), 413-425, 1997.

Stock, J.D., and D.R. Montgomery, Can we predict the rate of bedrock river incision (using the stream power law)?, *J. Geophys. Res.*, in press.

Suzuki, T., and K. Takahashi, An experimental study of wind abrasion, *J. Geol., 89* (1), 23-36, 1981.

Tinkler, K.J., Fluvially sculpted bedforms in Twenty Mile Creek, Niagara Peninsula, Ontario, *Can. J. Earth Sci., 30*, 945-953, 1993.

Tucker, G.E., and R. Slingerland, Drainage basin responses to climate change, *Water Resour. Res., 33* (8), 2031-2047, 1997.

Wohl, E.E., Bedrock benches and boulder bars; floods in the Burdekin Gorge of Australia [with Suppl. Data 92-14], *Geol. Soc. Amer. Bull., 104* (6), 770-778, 1992.

Wohl, E.E., Bedrock channel incision along Piccaninny Creek, Australia, *J. Geol., 101* (6), 749-761, 1993.

Wohl, E.E., N. Greenbaum, A.P. Schick, and V.R. Baker, Controls on bedrock channel incision along Nahal Paran, Israel, *Earth Surf. Proc. Land., 19* (1), 1-13, 1994.

Wolman, M.G., and J.P. Miller, Magnitude and frequency of forces in geomorphic processes, *J. Geol., 68* (1), 54-74, 1960.

Zeitler, P.K., Cooling history of the NW Himalaya, Pakistan, *Tectonics, 4* (1), 127-151, 1985.

Zen, E.A., and K.L. Prestegaard, Possible hydraulic significance of two kinds of potholes; examples from the paleo-Potomac River, *Geology, 22* (1), 47-50, 1994.

Gregory S. Hancock, Dept. of Earth Sciences and Institute of Tectonics, University of California, Santa Cruz, CA, 95064, ghancock@bagnold.ucsc.edu.

Robert S. Anderson, Dept. of Earth Sciences and Institute of Tectonics, University of California, Santa Cruz, CA, 95064, rsand@bagnold.ucsc.edu.

Kelin X Whipple, Dept. of Earth, Atmospheric, and Planetary Sciences, Massachusetts Instiute of Technology, Cambridge, MA, 02138, kxw@mit.edu.

Modeling Considerations for Simulation of Flow in Bedrock Channels

Andrew J. Miller

Department of Geography and Environmental Systems,
University of Maryland Baltimore County, Baltimore, Maryland

Brian L. Cluer

National Park Service, Fort Collins, Colorado

Numerical models have become popular tools for exploring flow patterns in rivers. These include step-backwater models based on the one-dimensional energy equation, but two- and three-dimensional models based on the Reynolds-averaged Navier-Stokes equations are also becoming more widely available with advances in computer technology and in software design. Bedrock channels are often characterized by unsteady, turbulent flow conditions that pose a serious challenge for modeling; this paper provides a short introduction to the different classes of flow models that are available, and identifies some of the questions that need to be addressed in applying these models in bedrock channels. Case studies using both one- and two-dimensional flow models are provided to illustrate how the models perform in different geomorphic settings and to suggest how the models may be applied both for reconstruction of past flows and for predicting selected aspects of the flow field.

1. INTRODUCTION

Bedrock channels are characterized by boundaries that are for the most part more rigid and less adjustable than those of alluvial channels. Nevertheless they are dynamic environments with enormous spatial and temporal diversity of flow hydraulics. Numerical models provide us with a useful tool for exploring the interaction between boundary conditions and flow patterns.

The number of published modeling studies treating bedrock-controlled systems is still quite small by comparison with the volume of literature on flow modeling in alluvial channels or in estuarine and tidal environments. Among the studies that do treat bedrock systems, the majority have focused on the application of one type of model, the one-dimensional step-backwater model for computation of water-surface profiles. Many of the research studies published to date have pursued the goal of estimating paleoflood discharge peaks, although some have been concerned with reconstruction of the longitudinal distribution of hydraulic variables such as velocity, depth, slope, shear stress or stream power. As the amount of attention devoted to the morphology and dynamics of bedrock channels increases, it is inevitable that a wider variety of hydraulic models will be applied to a more diverse set of questions.

The purpose of this paper is to provide an introduction to the types of models that are currently in use, with specific reference to potential applications in bedrock channels, and to identify some of the issues that require consideration. For general guidelines on the various classes of flow models, their governing equations, simplifying assumptions, and numerical solution techniques, the reader is referred to

Rivers Over Rock: Fluvial Processes in Bedrock Channels
Geophysical Monograph 107

open-channel hydraulics texts including *Chow* [1959], *French* [1986], and *Chaudhry* [1993]; reviews by *Fread* [1993] and *Yen* [1996]; and selected contributions to the computational fluid dynamics (CFD) literature, including *Rodi* [1984], *ASCE Task Committee on Turbulence Models in Hydraulic Computations* [1988], *Abbott* [1992, 1997], *Anderson* [1995], *Wendt* [1996], and *Olsen* [1997].

Most bedrock-controlled channels have alternating reaches of exposed bedrock and sediment cover, and the sediment may include coarse blocks, pebble clusters, and an array of depositional features composed of gravel or sand and associated with flow separation, recirculation, and reattachment (for details refer to *Cenderelli and Cluer*, this volume). For the purposes of this paper, the term "bedrock channels" will be used to refer to the range of channels whose gross morphology is constrained by bedrock, rather than to the more limited class of channels where the bed and the banks are entirely composed of bedrock.

Flow in bedrock channels obeys the same physical laws that govern flow in alluvial channels. There are no published flow models that are uniquely designed for use in bedrock channels, nor are there particular solution techniques devised specifically for bedrock channels. However there are several important characteristics that distinguish typical bedrock channels from alluvial channels. Bedrock channels generally have higher gradients and frequently are incised as a result of regional uplift or base-level lowering. They often occupy narrow valleys bounded by steep walls; in extreme cases they may be slot canyons with vertical or even overhanging walls. Irregular boundaries are common and may include abrupt constrictions and expansions or periodic undulations in plan form, as well as stepped-bed profiles, potholes, and other scour features such as longitudinal grooves and inner channels. Flow patterns may be complex and flow fields are often difficult to measure directly, especially at high flows when conditions are hazardous and accessibility is limited. Thus, paradoxically, flow models become more important in efforts to understand channel behavior, even as the availability of data for model verification decreases. *Tinkler and Wohl* [1996] observe that:

> Flows in rockbed systems, even at quite low stages, typically show greater velocities than those in alluvial reaches, frequent knickpoints and highly aerated and turbulent flow structures, and there is usually a noticeable water surface topography, and especially as stage increases: smoothly descending water surfaces leading to hydraulic jumps, prominent standing wave trains (=> critical flow), super-elevation at bends, topographic rises over kolks bursting on the surface, and traveling waves generated in energetic zones... In no sense can one pretend, even as a working assumption, that the flow is steady and uniform... In our observation critical flow is extremely common, although usually confined to part of the channel, and supercritical is not uncommon, although spatially restricted.

The importance of flow transitions between subcritical and supercritical conditions has attracted the attention of several authors [*Jarrett*, 1984; *Kieffer*, 1985, 1989; *Trieste and Jarrett*, 1987; *Trieste*, 1992, 1994; *Hubbard and Thorne*, 1994; *Simon and Hardison*, 1994; *Carling*, 1995; *Grant*, 1997; *Tinkler*, 1997a, b]. The irregular and discontinuous shape of the water surface and velocity field in the presence of transcritical flow poses a challenge for modeling and therefore any consideration of model applications in bedrock channels needs to address this issue. However, not all modeling studies require comparable levels of detail in simulating flow patterns.

2. TYPES OF PROBLEMS

The problems addressed with the help of numerical modeling generally fall into one of the following classes:

1. Reconstruction of discharge values associated with flood peaks;
2. Reconstruction of the longitudinal distribution of hydraulic variables such as velocity, depth, shear stress or stream power;
3. Detailed simulation of local interaction between flow pattern and boundary conditions;
4. Simulation of the dynamics of flood-wave transmission.

Although there is a body of literature involving the coupling of flow and sediment transport models, most of the studies in question are concerned with alluvial rivers rather than with bedrock or mixed systems. There are studies that consider supply-limited sediment transport [e.g.*Wiele* et al., 1996; *Topping*, 1997; *Rubin et al.* 1998], but none that treat the dynamics of sediment transport together with the range of processes causing bedrock erosion. There is also an important class of models that treat landscape evolution, including channel incision and formation of valley networks, as the cumulative result of flow and sediment transport processes [*Howard and Kerby*, 1983; *Howard*, 1987, 1994, this volume; *Willgoose et al.*, 1991 a,b; *Rodriguez-Iturbe et al.*, 1994; *Howard et al.*, 1994; *Ellis et al.*, 1997; *Sklar and Dietrich*, 1997], but these are based on long-term time-averaged relationships and are not equally concerned with the local dynamics of transient flow events. Studies of this type lie outside the scope of the current paper. The scope of this paper is limited to the use of models that treat flow only, and that are confined to the context of either steady flow or event-based unsteady flow simulation within a limited channel reach under specified boundary conditions.

3. TYPES OF MODELS

There are several different types of models that are applied to the problems identified above. These models are

distinguished by the set of governing equations and simplifying assumptions used, which in turn affect (1) whether they are limited to modeling of steady flow or can also model unsteady flow, (2) whether or not they are capable of handling rapidly varied and transcritical flow conditions, and (3) whether they are one-, two- or three-dimensional. All of the models discussed here are numerical models that rely on dividing the flow domain into discrete increments and on the use of iterative approximation techniques to approach a convergent solution. Therefore the results are also affected by the type of spatial discretization of the flow domain, and by the solution techniques used. A detailed review of numerical solution techniques is beyond the scope of this paper; interested readers may consult the references cited for additional information.

All of the relevant models, other than those relying on the standard step method, are based on a combination of the continuity and momentum equations for incompressible flow. These equations can be expressed either in conservation form or in nonconservation form. Derivatives of the flow variables in the nonconservation form are expressed in terms of velocity and water depth, whereas the derivatives in the conservation form are expressed in terms of discharge and cross-sectional area.

The distinction is significant in the present context because velocity changes abruptly in the presence of a hydraulic shock such as a supercritical-subcritical flow transition, whereas discharge is more likely to remain constant or at least to follow a trend that is smooth and continuous. *Samuels* [1989] notes that "it is a common feature of most numerical methods that discontinuities of a primary variable are difficult to capture without special action within the code" (p.415). Other authors have pointed out that numerical codes based on the nonconservation form of the flow equations tend to have stability problems in the presence of shocks associated with hydraulic jumps [*Whitlow and Knight*, 1992; *Hicks and Steffler*, 1995; *Berger and Stockstill*, 1995; *Jin and Fread*, 1997]. The two strategies that are available for handling these shocks are characterized, on the one hand, as "shock fitting" or "shock tracking" or, on the other hand, as "shock capturing" [*Anderson*, 1996; *Berger and Stockstill*, 1995]. The first of these techniques may be utilized in conjunction with the nonconservation form of the flow equations by explicitly introducing an internal boundary within the flow domain, whereas the second requires no explicit adjustments but is much more stable when the conservation form of the equations is adopted. According to *Anderson* [1996],

> the shock-capturing method is ideal for complex flow problems involving shock waves for which we do not know either the location or number of shocks. Here, the shocks simply form within the computational domain as nature would have it. Moreover, this takes place without requiring any special treatment of the shock within the algorithm, and hence simplifies the computer programming. However, a disadvantage of this approach is that the shocks are generally smeared over a number of grid points in the computational mesh, and hence the numerically obtained shock thickness bears no relation what-so-ever to the actual physical shock thickness, and the precise location of the shock discontinuity is uncertain within a few mesh sizes. In contrast, the advantage of the shock-fitting method is that the shock is always treated as a discontinuity, and its location is well-defined numerically. However, for a given problem you have to know in advance approximately where to put the shock waves, and how many there are. (p.49)

It is to be expected that most users will prefer the convenience of the shock-capturing option, and that the availability of numerical models based on the conservation form of the flow equations will provide advantages for modeling of flow in bedrock channels. This advantage must be weighed against other characteristics in deciding which model to apply in a particular study.

3.1 One-Dimensional Models

3.1.1 One-dimensional energy equation and the standard step method. The simplest and most widely used hydraulic models are those based on the one-dimensional energy equation with an iterative solution technique known as the standard step or step-backwater method [*Chow*, 1959]. These are steady-flow models in which the channel system is characterized by a series of cross-sections, with information provided about distance between cross-sections for the purpose of specifying longitudinal gradients.

The energy equation is coupled with a second equation specifying head loss between successive cross-sections, and the most important adjustable parameter is the roughness coefficient (typically Manning's n or Chezy's C), which in practice includes the effects of multiple forms of energy loss. Among these are bed roughness, vegetative roughness, and irregularities in cross-section and plan form that may cause additional dissipation of energy [*Chow*, 1959]. Contraction and expansion coefficients incorporated in the head-loss equation also account for some of the changes caused by longitudinal variations in channel width.

Although the cross-sections may be subdivided, the models essentially predict longitudinal water-surface profiles for specified discharge, with single values of water-surface elevation derived at each cross-section. Other hydraulic variables are calculated either as cross-section averages or as averages pertaining to a specified portion of the cross-section (e.g. channel, left overbank, right overbank), but the actual dynamics of flow within the cross-section are not completely specified in the solution.

The models in this category that are the most widely distributed and that have been most frequently used are HEC-2 [*Hydrologic Engineering Center*, 1982] and WSPRO

[*Shearman*, 1990]. Although both HEC-2 and WSPRO can generate profiles for subcritical, supercritical or critical flow, the shocks associated with hydraulic jumps are not modeled. Where the locations of hydraulic jumps are well-defined (e.g. controlled by local contractions and expansions with fixed positions), the standard procedure is to run supercritical profiles from upstream to downstream and subcritical profiles from downstream to upstream, matching profiles at locations where the flow becomes critical in either direction.

However for channels that are close to critical flow along some considerable longitudinal distance, modeling with the standard one-dimensional energy equation is problematic. Alternative approaches that utilize the momentum equation are preferred under these circumstances [*Samuels and Chawdhary*, 1990; *Beffa*, 1996]. The HEC-RAS model (Hydrologic Engineering Center - River Analysis System) was released in 1996 as a replacement for HEC-2 with a superior user interface and extended capabilities for analysis of transcritical flow profiles [*Hydrologic Engineering Center*, 1995, 1997]. A modified form of the 1-d standard step model incorporates the momentum equation for use in situations where flow passes through critical depth. The model requires the assumption of a hydrostatic pressure distribution and is applicable to slopes less than 10%. In most other respects, the current version of the model is computationally similar to HEC-2.

One-dimensional step-backwater models have been more frequently applied in bedrock systems than any other type of model. Most of the research studies have involved reconstruction of paleoflood discharge. Bedrock canyons and their tributaries are particularly opportune locations for the preservation of paleo-stage indicators, and the most common examples are fine-grained slackwater deposits in tributary valleys or bedrock alcoves [*Patton, Baker, and Kochel*, 1979; *Kochel and Baker*, 1982, 1988]. Paleoflood reconstruction most often involves use of hydraulic models to produce longitudinal flood profiles that match elevations of local paleo-stage indicators [*Kochel et al.*, 1982; *O'Connor and Webb*, 1988]. There are numerous studies utilizing such reconstructed flood peaks to extend flood frequency records as far back as the early-middle Holocene [e.g. *Kochel and Baker*, 1982; *Partridge and Baker*, 1987; *Ely et al.*, 1993; *Enzel et al.*, 1993; *O'Connor et al.*, 1994; *Kale et al.*, 1993; *Zawada*, 1997]. The method has also been used to reconstruct discharge values for catastrophic late-Pleistocene meltwater floods [*Jarrett and Malde*, 1987; *O'Connor and Baker*, 1992; *Baker et al.*, 1993].

Other applications have used longitudinal profiles of modeled cross-sectional-average depth and velocity to calculate the longitudinal distribution of bed shear stress and unit stream power, and to relate these trends to the distribution of boulder deposits or to the probability of achieving hydraulic thresholds for causing major changes in channel morphology [*O'Connor, Webb, and Baker*, 1986; *Magilligan*, 1992; *O'Connor*, 1993; *Wohl et al.*, 1994; *Benito*, 1997]. *Kieffer* [1985] also utilized the energy equation (but without application of a step-backwater model) to draw conclusions about hydraulic conditions affecting the evolution of debris-fan constrictions in the Grand Canyon.

3.1.2. Roughness coefficients and critical flow in high-gradient streams Because the roughness coefficient plays such an important role in determining the characteristics of the modeled flow, a digression is necessary at this point in order to highlight a significant unresolved question. The literature on determination of roughness coefficients is voluminous. Most studies provide empirical equations that are applicable to a limited range of channels. Roughness in high-gradient streams and mountain rivers is positively correlated with slope and inversely correlated with hydraulic radius, flow depth, or relative submergence [e.g. *Jarrett*, 1984].

Although roughness is expected to decrease with increasing depth of flow, there is considerable uncertainty about the choice of appropriate roughness coefficients at flood flows exceeding the range of the empirical data. *Trieste* [1994] suggests that "flow resistance increases to the level needed for predominately subcritical flow to occur. As channel gradient increases, and thus energy of flow, so do the effects of the factors contributing to flow resistance thereby checking velocity and maintaining flows in the subcritical range" (p. 733). The factors cited include "debris, obstructions, effects of unsteady flow, turbulence, sediment and bedload, floodplain-main channel interface, bedforms, hydraulic jumps, etc." (p. 734).

On the other hand, *Glancy and Williams* [1994] describe an example of an indirect discharge measurement on a steep (3.2%) ephemeral wash that yielded an apparent mean velocity of 5.2 m/s and a Froude number of 1.5: "When six U.S. Geological Survey hydrologists, with a cumulative 150 years experience, examined the flood site, they found no major errors with the field survey or calculations, but were unable to agree regarding the results. The major point of concern to some was the high apparent velocity and resultant supercritical Froude number" (p. 637). The same paper cites another discharge measurement collected using a current meter and yielding a Froude number of 2.5, and comments that "the apparent state of supercritical flow may not in itself be a disqualifying factor in the assessment of the hydraulic acceptability of indirect flow-measurement results" (p.638).

Wahl [1994] points out that "many of the applications of the Manning equation for high-gradient mountain streams are for large floods. Yet, the data are presently not available to define and test such equations against floods greater than about the median annual peak discharge. This is a serious

limitation and emphasizes the need for additional data collection to define the hydraulic processes for large discharges on high-gradient streams" (p. 731).

Both *Grant* [1997] and *Tinkler* [1997b] point out that critical flow is probably much more common in high-gradient channels than is generally recognized in the literature. *Tinkler* [1997b] observes that critical flow "typically exists as a train of standing waves within the main channel, the margins of which reveal subcritical flow (F<<1), sometimes for a substantial proportion of the total width" (p.148). He notes further that "cross-sectional averaging of channel characteristics can be expected to predict subcritical Froude numbers, even if threads of critical flow are present" (p.148). *Tinkler* [1997b] then develops an equation that solves for Manning's n as a function of slope and depth at critical flow. After analyzing several examples from the literature on catastrophic floods, he suggests that it may be reasonable to use roughness values associated with critical flow when modeling catastrophic floods or flows in hydraulically steep systems. Whether or not this approach is adopted, it is prudent when modeling flood flows in high-gradient bedrock channels to include a sensitivity analysis indicating how the flow field responds to a range of roughness-coefficient values.

3.1.3 One-dimensional dynamic models for hydraulic routing of flood waves. The models described above are used in analyzing steady-flow conditions rather than the time history of flow during a flood or the transmission of a flood wave. Another class of one-dimensional models, designed specifically for application to unsteady flow conditions, are described collectively as routing models. The most complete and accurate among these, according to *Fread* [1993] and *Yen* [1996], are the dynamic routing or dynamic wave models. These models rely on numerical techniques for solving the complete St. Venant equations. The one-dimensional St. Venant equations, like the governing equations for the two- and three-dimensional models discussed below, include a continuity or conservation of mass equation and a momentum equation, both written in unsteady form with temporal and spatial derivatives and with energy-loss coefficients accounting for channel friction and for contractions and expansions.

The equations generally are solved using finite-difference schemes (see *Yen*, 1996 for examples). Some dam-break models have been applied to mountain valleys with steep valley walls and irregular topography, and are therefore appropriate for discussion with reference to bedrock channels. *Wurbs* [1987], for example, describes case studies applying several models to simulate the flood waves resulting from the failure of the Teton Dam in Idaho in 1976 and the failure of a dam on Laurel Run near Johnstown, Pennsylvania in 1977. The dynamic routing models were the most accurate but were also subject to computational instabilities "associated primarily with abruptly changing valley geometry and supercritical flow" (p. 36). The preferred model, DAMBRK [*Fread*, 1988] was able to handle entirely supercritical or entirely subcritical flow, but ran into difficulty with mixed-flow regimes.

The need for models capable of simulating sharp discontinuities in the flow field led to development of a class of numerical solution techniques known as upwind difference or upwinding schemes [*Anderson*, 1995, p. 497-500]. One version of this approach was introduced by *Brooks and Hughes* [1982] as the Streamline Upwind Petrov Galerkin (SUPG) Finite Element technique. This technique was adapted by *Hicks and Steffler* [1992], under the name "Characteristic-Dissipative-Galerkin" (CDG) Finite Element Method, for use in solving the one-dimensional St. Venant equations in conservation form. *Hicks and Steffler* [1997] compared the CDG method with a model based on the non-conservation form of the St. Venant equations and solved by the four-point implicit finite difference method, the same method used in DAMBRK. They concluded that the CDG method performed better in simulating the mixed subcritical/supercritical flow regime associated with a flood wave generated by an experimental dam break, and that any conservative, shock-capturing one-dimensional model should produce equally good results.

Jin and Fread [1997] also noted that the four-point implicit finite difference method utilized in DAMBRK had numerical stability problems with mixed or transcritical flow regimes. Methods designed to work around this difficulty were still problematic in channels where flow was near critical along much of the reach or where large dam-break-induced flood waves were characterized by a moving supercritical-subcritical mixed-flow interface. The generalized one-dimensional channel flood-routing model, FLDWAV [*Fread*, 1993; *Jin and Fread*, 1997] is designed to replace the National Weather Service DAMBRK and DWOPER models and contains an algorithm for handling these problems in channels with irregular shapes and internal boundaries. This model includes both the original implicit finite-difference solution technique as well as a characteristics-based, upwind, explicit scheme for the conservation form of the complete St. Venant equations. The upwind explicit scheme is more computationally intensive, requires shorter time and distance steps, and is numerically less accurate in many common situations other than those where the implicit scheme breaks down. Therefore a mixed implicit-explicit capability is considered desirable and is also implemented in the model.

Although there has been a considerable amount of attention in the engineering literature to dynamic routing models with specific emphasis on simulation of dam breaks, there are relatively few published studies with geomorphic implications or with applications to bedrock channels. One example

among these is the study by *Jarrett and Costa* [1986], documenting the use of DAMBRK to model travel times and stages of the 1982 Lawn Lake flood in Colorado, which resulted from two dam failures. Despite the extremely high discharge in this flood, flow along bedrock reaches of the channel system evidently remained subcritical [*R. Jarrett*, U.S. Geological Survey, personal communication, 1998]. *Costa* [1997] also used DAMBRK to simulate behavior of lahars from Cascade Range volcanoes. The model was calibrated to recorded flow depths and results were compared to flow characteristics including time-of-travel and inundation area. Although lahars and debris flows clearly do not behave as Newtonian fluids, the calibration studies were successful in providing approximate or order-of-magnitude predictions of flood-wave behavior that might be useful in planning for public safety.

3.2 Two- and Three-Dimensional Models

Two- and three-dimensional numerical models are all, like the 1-d dynamic routing models, based on equations for conservation of mass and conservation of momentum. The full 3-d form of the equations of motion are the Navier-Stokes equations. These are applied to a diverse range of problems throughout the field of computational fluid dynamics. Applications in river hydraulics generally assume that flow is incompressible and that the mean effects of turbulence can be handled through Reynolds averaging, yielding the Reynolds-averaged Navier-Stokes equations, sometimes referred to as the RANS or Reynolds equations.

3.2.1 Turbulence closure. The Reynolds stress terms that result from the averaging process must be resolved using some form of turbulence closure, and there are several choices that have been widely applied [*Rodi*, 1984; *ASCE Task Committee on Turbulence Models in Hydraulic Computations*, 1988]. One turbulence closure approach uses the Boussinesq eddy viscosity, which is based on the assumption that the turbulent stresses are analogous to viscous stresses and can be estimated as proportional to the gradient of the mean velocity. Some models employ a constant eddy viscosity parameter, whereas others calculate eddy viscosity as a function of local velocity gradients and grid scale. Unlike molecular viscosity, eddy viscosity is not truly a property of the fluid but is instead a property of the flow field and of the grid scale and solution technique used in the numerical model.

More sophisticated turbulence models employ one or more differential transport equations to calculate the turbulence parameters. These include one-equation models, relating the eddy viscosity to the turbulent kinetic energy k; and two-equation k-ε models, which relate eddy viscosity to a function of turbulent kinetic energy k and dissipation rate ε [*ASCE Task Committee*, 1988; *Rodi*, 1984]. More complex models that are not based on a single common velocity scale are also available and lead to separate transport equations for each of the components of the Reynolds stresses [*ASCE Task Committee*, 1988; *Olsen*, 1997]. Simplifying assumptions reducing these differential equations to algebraic equations have also been developed and lead to a class of turbulence closure known as algebraic stress/flux models [*Rodi*,1976; *ASCE Task Committee*, 1988]. More advanced approaches, including Large Eddy Simulation (LES) and Direct Numerical Simulation (DNS), are important areas of research in the field of CFD [*Peyret and Taylor*, 1983; *Libby*, 1996] but have not been developed for practical applications in hydraulic engineering [*Olsen*, 1997].

3.2.2. Discretization. All of these models require discretization of the flow domain and adoption of a specific set of algorithms to solve the discretized forms of the flow equations. The discretization options generally fall into the categories of finite difference, finite element, and finite volume methods [*ASCE Task Committee*, 1988].

Finite difference methods involve the creation of a rectilinear grid with uniformly spaced nodes, and approximation of the differential equations by algebraic terms - the finite difference approximations - based on Taylor series expansions applied to each grid point in the flow domain. Finite element methods subdivide the flow domain into a series of discrete elements, generally triangular or quadrilateral, which may be irregular in shape and size and allow great flexibility in defining the shape of the boundary and the internal geometry of the flow field. An interpolation or shape function is used to approximate the values of the flow variables within each element. Any one of several alternative approaches may be used to derive and to solve algebraic equations for the unknowns that satisfy continuity requirements at element boundaries and that minimize the error or residual terms. (It is also not uncommon for a model to be expressed in terms of finite elements in the spatial domain while utilizing a finite-difference approach to model changes from one time step to the next.) Finite volume methods divide the computational domain into elementary volumes and apply an integral form of the conservation laws to a typical control volume [*Peyret and Taylor*, 1983; *Olsen*, 1997].

3.2.3. Two-Dimensional Models. Two-dimensional numerical models based on depth-averaged forms of the RANS or Reynolds equations (commonly referred to as the "shallow-water equations") are becoming increasingly popular for use in hydraulic engineering and in geomorphology. Virtually all of the available 2-d models assume a hydrostatic pressure distribution and are therefore incapable of handling substantial vertical accelerations or bed gradients larger than about 10 percent [e.g. *Waterways Experiment Station*, 1997]. Most have the ability to simulate both unsteady flow and steady flow.

There are advantages in using two-dimensional models as compared with one-dimensional models, but there are also associated costs and additional questions that require careful consideration. Clearly open-channel flow, particularly in high-gradient, high-velocity channels, is characterized by irregularities in the water surface that are not simulated by one-dimensional models. For example, in the Teton Dam flood, there was a 6-m difference in measured high-water elevations between the right and left sides of the valley just below the canyon mouth [*Wurbs*, 1987]. Lateral variations in velocity also are important to understanding of channel dynamics. Flow separation and recirculating eddies may be significant components of the flow field, particularly in bedrock channels with irregular boundaries. Where supercritical flow does occur, it generally does not occupy the entire channel cross-section and flow transitions are not necessarily oriented parallel to the channel boundaries [e.g. *Tinkler*, 1997b]. The ability to model and to visualize any of these aspects of the flow field may lead to valuable insights.

Two-dimensional models are also computationally more demanding, although the computational resources needed are rapidly becoming available in the average desktop personal computer. There are additional requirements with regard to the input data needed, the construction of the grid, the selection of appropriate model parameters, and the method used to attain a convergent solution. There are also differences among the capabilities of different two-dimensional models, and therefore the choice of which model to use and which modeling options to select may affect the success of the study. Even if it is possible to run the model successfully, in many cases the data available for verification are sparse or even nonexistent, and the level of detail provided in the model output - particularly if displayed with sophisticated graphics routines - may create a seductive illusion of reality. Finally there are limits to the length of channel reach that may be practical for two-dimensional modeling, primarily related to the number of elements or grid cells required and the associated computation time for achieving a convergent solution. Therefore it is important for the researcher to consider the scale of the problem under study in deciding whether to employ a two-dimensional approach.

3.2.4. Conservation and nonconservation forms of the governing equations. In considering whether a particular 2-d model is suitable for application in bedrock channels, several features of the model need to be reviewed.

The importance of knowing whether the governing equations are written in conservation or nonconservation form has already been addressed. Because the conservation form of the governing equations is considered more stable under conditions where hydraulic jumps may occur, many 2-d models are written in conservation form. These include widely-available public domain models such as FESWMS [*Froehlich*, 1989] and HIVEL2D [*Berger and Stockstill*, 1995], commercial models such as AQUADYN [*Gidas et al.*, 1996] and TELEMAC-2D [*Galland et al.*, 1991; *Hervouet*, 1991], and research models that are reported in the literature but may not be widely available for distribution [e.g.,*Younus and Chaudhry*, 1994; *Molls and Chaudhry*, 1995; *Fraccarollo and Toro*, 1995; *Ghanem et al.*, 1995; *Steffler*, 1997; *Ye and McCorquodale*, 1997; *Stockstill et al.*, 1997].

It is worth noting that even a model written in nonconservation form may be capable of achieving a convergent solution that includes small regions of supercritical flow, and that such regions may be realistic in their overall shape and position even if the local distribution of velocity and depth is not considered reliable in the vicinity of the supercritical flow region and associated hydraulic jump [*Miller*, 1994]. The documentation for RMA2, the model used in *Miller* [1994], explicitly cautions users that the model is designed for analysis of subcritical flow problems [*Donnell et al.*, 1997]. However we have found in practice that in some situations where supercritical flow and hydraulic jumps are predicted by a conservation model such as HIVEL2D [*Berger and Stockstill*, 1995], RMA2 predicts a flow field that closely resembles the HIVEL2D output for the same boundary conditions. For example, most of the the flow fields illustrated in *Miller* [1995] were simulated first using RMA2 before HIVEL2D was used to produce the final published results. These RMA2 model runs were intended merely to set up initial-condition files for use with HIVEL2D and no quantitative comparison of the results was performed. However RMA2 did produce convergent solutions, and the gross features of the flow fields were similar using both models. Furthermore the velocity vectors and water-surface elevations were virtually identical at distances on the order of one channel width or more from the locations where supercritical flow was predicted.

All other things being equal, it is preferable when simulating flow through bedrock channels to use a model based on the conservation form of the governing equations. However there may be circumstances where a model based on the nonconservation form is chosen because of other capabilities that are lacking in the conservation models that are available.

3.2.5. Turbulence closure. The importance of the choice of turbulence closure model is emphasized in much of the CFD literature. In studies where model output is compared with the results of well-constrained experiments, the k-ε model tends to perform better than the simpler turbulence models. However it is also more computationally demanding, and there is some uncertainty as to how much accuracy is gained with increasing complexity of the turbulence closure when applied to field situations with irregular boundary conditions. The models that are most readily available and easiest

to use tend to have relatively simple turbulence models. Even where the turbulence closure is simple, it is advisable to explore the sensitivity of the flow field to different values of the parameters affecting eddy viscosity. Higher values of eddy viscosity tend to damp out lateral variations in velocity and shear stress across the channel, whereas lower values lead to more pronounced variations [*Vreugdenhil and Wijbenga*, 1982, Figure 4; *Miller*, 1994]. Eddy viscosity coefficients that are set too high may also suppress the formation of flow separation and recirculating eddies, whereas values that are too low may lead to numerical instability and periodic oscillations in the flow field.

The literature provides some guidance in choosing eddy-viscosity values. *Rodi* [1984] suggests that in open-channel flow, the depth-averaged eddy viscosity or diffusivity is "reasonably well correlated" (p.16) with the product of u_* (shear velocity) and h (water depth), and that an empirical constant C is estimated as 0.135 for wide laboratory channels but may vary with width/depth ratio. (The product of shear velocity and depth yields an eddy viscosity expressed in SI notation with units of m^2s^{-1}, equivalent to the units of kinematic viscosity.) *Froehlich* [1989] recommends a value on the order of $0.6u_*h$. *Olsen* [1997], after *Keefer* [1971], suggests that a value of $0.11u_*h$ may be appropriate for use in rivers. *Jenkins* [1993] cites studies by *Rastogi and Rodi* [1978] and *Fischer et al.* [1979] indicating that a similar relationship with a coefficient of 0.3+/-50% (i.e. 0.15 to 0.45) is suitable for use in natural channels with irregular boundaries. *Ghanem et al.* [1995] and *Ghanem et al.* [1996] also cite *Fischer et al.* [1979] in support of a coefficient in the range 0.14+/-0.07 u_*h. They point out that it is fairly common for model developers to recommend excessively high values of the eddy viscosity or turbulent diffusion coefficients as a means of damping out spurious oscillations in the flow field and stabilizing model behavior.

3.2.6. Wetting and drying. Many research models have sophisticated turbulence closures but make no provision for changes in the wetted area of the computational domain as water level rises and falls. Some of the models written in conservation form, for example HIVEL2D [*Berger and Stockstill*, 1995] and AQUADYN [*Gidas et al.*, 1996], are able to solve transcritical flow problems but cannot solve problems associated with wetting and drying along the boundary of the flow field. (According to M.Carreau, one of the model developers, a forthcoming version of AQUADYN will include a wetting and drying algorithm [personal communication, 1998].)

The implications are twofold: first, in the absence of a wet-dry boundary it is common to assume vertical sidewalls with a slip condition (i.e. nonzero velocity parallel to the boundary), neglecting sidewall friction with potential impacts on the validity of the modeled distribution of velocity and water-surface elevation [*Molls et al.*, 1998]. Second, many field situations involve irregular topography where the elevation and shape of the wetted perimeter are unknown and where solution of these aspects of the flow field is one of the primary modeling objectives. Models that do not allow some adjustment in the location of the water's edge may be useful but are less universally applicable for the range of boundary conditions occurring in natural channels.

Among models that do allow for wetting and drying, the algorithm that is used may have considerable impact on the stability of the model and the probability of achieving a convergent and physically realistic solution. One approach is to develop a moving grid finite element method, which adjusts the boundary elements and regenerates the grid to account for changes in water level. This approach was taken by *Akanbi and Katopodes* [1988], but their model was restricted to use on flat surfaces and the efficiency of the model was limited by the number of cycles required for mutual adjustment of the grid and the flow field. In addressing the problem of wetting and drying on sloping sidewalls in supercritical channels, *Stockstill et al.* [1997] also employed a moving-boundary approach. In order to avoid serious distortions of element shapes, the coordinates of the moving boundary nodes were updated with each iteration and the side slopes were regridded with each time step, and then the flow variables were computed by interpolation from the previous version of the grid. The model was tested against a flume experiment with a trapezoidal channel and a horizontal curve, and against a straight channel with multiple flow obstructions. Superelevation and wave oscillations in the curved channel were modeled successfully, as was a choke in the straight channel upstream of a set of bridge piers. Although the authors express some confidence in the capabilities of the model, the moving-boundary method has not been incorporated in any version available for general distribution.

Another approach is simply to remove an element from the computational domain whenever the water depth at any one of its nodes approaches zero; this is referred to as the element elimination approach. This may create a jagged, irregular boundary that changes shape from one iteration to another. There is also the potential to create isolated areas or "ponds" that are no longer connected with the main body of flow, thereby causing problems with conservation of mass as well as oscillations in velocity and water level from one iteration to the next [*Donnell et al.*, 1997].

The problem becomes particularly acute in simulation of flow through bedrock channels with steep walls where there are constrictions and expansions. The example illustrated in *Miller* [1994] provides a case in point: flow approaching a debris-fan constriction is ponded upstream of the constriction and drops steeply as it cascades around the front of the fan. Initial runs using RMA2 with the element elimination algorithm (not illustrated in the paper) caused elements at

the toe of the fan to be removed from the finite-element mesh; this tended to exaggerate the constriction of the flow, causing further acceleration and further lowering of the water surface, in turn causing additional elements to be eliminated from the mesh. As the constriction became narrower, the upstream water level rose, and in several instances this resulted in wetting of elements on the hillside above the constriction and in "stranding" of water in a position that was not physically realistic. A similar algorithm, subject to the same kind of instability, is responsible for wetting and drying in the two-dimensional FESWMS code [*Froehlich*, 1989].

An alternative algorithm, available with RMA2, is described as the "marsh porosity" approach [*Roig*, 1995; *Donnell et al.*, 1997]. This approach allows for a gradual transition between wet and dry conditions by retaining partially wet elements in the mesh until all nodes are dry. An effective porosity coefficient is used to estimate the percentage of the element carrying flow as the water level changes. Although the algorithm was designed for use in wetlands with broad, flat areas that are subject to wetting and drying with modest changes in stage, it also promotes smoother transitions toward convergent solutions when used in bedrock systems with steep sidewalls and irregular boundaries [*Miller*, 1994]. A similar solution is incorporated into the two-dimensional finite-element code CDG2D [*Steffler*, 1997; *Ghanem et al.* 1995]. In this model groundwater flow equations are invoked when elements are partially dry, with transmissibility coefficients set low enough to reduce the flow rate drastically without actually eliminating elements from the mesh. This model, unlike RMA2, is based on the conservation form of the shallow-water equations and is capable of handling supercritical as well as subcritical flow. *Ghanem et al.* [1995] also provide a useful review of the literature on wetting and drying algorithms.

TELEMAC-2D is a commercially available model that includes another approach designed to adjust the computed water-surface elevation within an element where at least one node is dry [*Hervouet and Janin*, 1994; *Bates et al.* 1997]. The model applies a correction to the water slope terms in the momentum equation on partially dry elements. This approach is also designed for use in situations where there is shallow flow over a low-gradient surface, but has been applied successfully to dam break studies on steep slopes [*Paul Bates*, personal communication, 1998]. In addition *Bates* [personal communication, 1998] has recently added a marsh porosity-type algorithm within the TELEMAC-2D code and compared it successfully with the other existing algorithms. It is not known whether this algorithm will be added to the version of the software that is commercially available.

3.2.7. Boundary roughness. Parameterization of boundary roughness is another issue of importance. This is often accomplished using Manning's n or Chezy's C; the resultant vector of bed shear stress (e.g. the vector sum of x- and y-components) is usually modeled as shown below:

$$\tau_b = \frac{\rho g\left(u^2 + v^2\right)}{C^2} \tag{1}$$

or

$$\tau_b = \frac{\rho g n^2\left(u^2 + v^2\right)}{h^{1/3}} \tag{2}$$

assuming that SI units are used, where u and v are velocity components, ρg is the unit weight of water, and h is water depth.

In some models, a characteristic length scale related to grain size on the bed is used as the basis for determining the roughness coefficient using a Nikuradse-type relationship. For example, the CDG2D model [*Steffler*, 1997] calculates a non-dimensional Chezy coefficient as

$$C_* = 5.75 \log\left(12 \frac{h}{k_s}\right) \tag{3}$$

where h is flow depth and k_s is an effective roughness height. According to *Steffler* [personal communication, 1998], good results are generally obtained from gravel-bed rivers using a roughness height equal to about twice D_{84}.

The Manning and Chezy coefficients were originally developed for use in one-dimensional models, where they account not only for boundary roughness but also for energy losses associated with irregular boundary geometry. As the boundary geometry should already be accounted for in the two-dimensional form of the governing equations, a lower value of the roughness coefficient should suffice to account for boundary resistance alone. Several authors report that the results are typically much less sensitive to the choice of roughness coefficients than in one-dimensional modeling [e.g. *Molls and Chaudhry*, 1995; *Ghanem et al.*, 1996]. *Ghanem et al.* [1996] report on a CDG2D simulation compared with a field data set, where a 100% increase in roughness parameter over the optimal value resulted in an 8% increase in calculated water depths.

The major exception to the preceding statements suggesting the use of lower values for roughness coefficients occurs in the situation where a flow model lacking a wetting and drying algorithm assumes that the lateral flow boundaries have vertical sidewalls with free-slip conditions or non-zero velocities along the boundary. *Molls et al.* [1998] point out that it may be necessary in such cases to correct the friction slope calculations to account for frictional resistance along the sidewalls. Some models that assume vertical walls [e.g., HIVEL2D; *Berger and Stockstill*, 1995] do apply the resistance coefficient along the walls as well as the bed. However if this is not the case, or if velocities along the wall are

otherwise unrealistically high, the modeler can add frictional resistance along the walls by creating a narrow row of elements along the walls with high enough roughness coefficients to retard flow [*Miller*, 1995; *Donnell et al.*, 1997]. Clearly this is a situation where modeling draws on art as well as science.

3.2.8. Vorticity correction for flow around a bend. A common feature of some two-dimensional depth-averaged numerical models is a tendency for the maximum velocity in a bend to stay close to the inner wall. This demonstrates a tendency for irrotational motion that runs counter to common experience, wherein the main thread of flow tends to cross over toward the outer bank. This modeling problem is more noticeable in curved channels with trapezoidal cross-sections (a form that is most often encountered in laboratory experiments) than in most natural channels, where asymmetric cross-sections are common near channel bends and where topographic steering often diverts the maximum thread of velocity toward the deeper water along the outer bank.

One modeling approach seeks to improve the solution through introduction of a bendway vorticity correction [*Donnell et al.*, 1997]. The fundamental problem cannot be resolved in two dimensions, as it results from the three-dimensional, helical nature of the flow field. The correction involves introducing a transport equation for streamwise vorticity in the vertical plane perpendicular to the flow. The utility of this correction for application in bedrock channels has not yet been investigated in detail, but it is not expected to make a substantial difference in channels where sinuosity is relatively low.

3.2.9 Mesh generation. The two-dimensional models that are most readily applicable for simulation of flow through bedrock channels with irregular boundaries are generally finite-element models. According to *Ghanem et al.* [1995],

> The FE [finite element] method is attractive for simulating flow of water in natural streams and water bodies having irregular boundaries and complex topography. The flexibility of the method allows the choice from a wide array of linear and higher order elements which can be combined to give the best representation of complex domains using an unstructured mesh. It is possible to concentrate nodes in regions of complex geometry and/or interesting flow features and have a more sparse layout in areas which are more uniform. Further, the FE method, through integration by parts of the governing equations, facilitates a natural implementation of boundary conditions. This, together with the overall consistency and accuracy of the method results in requiring usually less nodes than FD [finite difference] and FV [finite volume] methods to achieve similar accuracy. (p.4)

The unstructured nature of the finite-element mesh imposes a greater degree of responsibility on the model user to design the layout of elements to facilitate rather than hinder the smooth operation of the model. By far the greatest amount of time and effort involved in any two- or three-dimensional modeling study is that required to generate the grid or mesh. Field data on topography and roughness are almost always sparse by comparison with the level of detail that needs to be specified. Therefore a good mesh-generation program, together with a strong intuitive feel for the physical characteristics of the system being modeled, is a virtual necessity for effective modeling. Most of the widely available models either come packaged with mesh-generating software or are compatible with commercially available software packages. All such packages are capable of triangulating a set of elements from a set of input nodes with specified coordinates, and most have routines that provide a range of additional options. In all cases, however, it is important to obey some basic rules with respect to the geometry of individual elements, the spatial pattern of element shape and size, and the relation of element shape, size, and orientation to the underlying topography and primary flow direction. It is also necessary to provide sufficient resolution to simulate the details of the flow field in areas of particular interest.

3.2.10. Geomorphic applications of two-dimensional models. Most of the geomorphic applications of two-dimensional models have involved studies of compound channel flow and floodplain hydraulics. According to *Bates et al.* [1997], "the fundamental analytic problem for hydraulic models of such environments is ... a simulation of the covering and uncovering of floodplain areas caused by the downstream propagation of a low amplitude flood wave" (p.3). Thus in this series of studies, most of which apply RMA2 or, in the last case, TELEMAC-2D to river reaches on the order of 10-30 km in length [*Gee et al.*, 1990; *Bates et al.*, 1992; *Feldhaus et al.*, 1992; *Bates and Anderson*, 1993; *Anderson and Bates*, 1994; *Bates et al.*, 1994; *Bates et al.*, 1997], the two-dimensional models are used to investigate unsteady flow and to resolve the temporal history of floodplain inundation during a high-flow event. Although some issues that are of concern in bedrock channels may be less important in lowland floodplain rivers, some of the lessons learned may provide guidance for application in bedrock channels.

First, the choice of roughness or boundary resistance parameters may be less important as a determinant of the flow field than the specification of topographic detail and the resolution and spatial layout of the model grid. (Note, however, that in the examples discussed later in this paper, roughness coefficients still had an important effect on the flow field.) Although it is possible to calibrate the models in order to select optimal values of the roughness coefficients, the calibration is not necessarily independent of the rest of the spatial discretization scheme. If we recognize that a turbulent flow field dissipates energy at many different spatial

scales, it is obvious that discretization of the flow field limits the ability of any model to represent the detailed physics of flow at sub-grid scales, and therefore the effects of roughness coefficients, grid scale, and eddy viscosity coefficients (in models with simple turbulence closures) may be difficult to separate. *Rodi* [1984] states that "the solution often depends on the numerical grid chosen because, owing to computer limitations, the grid cannot be made so fine as to obtain grid-independent solutions... all convective motions within the mesh, such as in small recirculation zones, cannot be resolved and their contribution to the transport must be accounted for by the diffusivity...." He also points out that "the approximation of the differential equations by difference equations introduces errors which act to smooth out variations of the dependent variables and thus effectively increase the diffusivity. This numerical or false diffusion is of course larger for coarser grids" (p.16).

Second, there is a clear tradeoff between the extent of topographic detail incorporated in the model grid or mesh and the computation time needed to achieve a solution. User's manuals typically suggest refining the mesh (i.e. subdividing grid cells or elements to provide finer resolution) in order to resolve convergence problems or to improve the accuracy of the results in flow regions with complex topography and steep velocity gradients, but computation time tends to increase exponentially with the number of elements. In addition it is not always the case that additional topographic detail leads to improved accuracy in the results. In some cases a more detailed representation of complex topography may generate numerical instability in modeling the flow [*Bates et al.*, 1992], and smoothing of the topography may enhance stability. In cases where additional topographic detail is advisable, some parts of the flow field are much more sensitive than others with respect to the amount of detail provided; *Bates et al.* [1997] suggest that further investigation of the spatial pattern of sensitivity may be useful in guiding field data collection efforts for future studies.

In addition the choice of numerical solution techniques may affect the predicted extent of floodplain inundation and shape of the outflow hydrograph. Although there is not one clearly superior option that is preferable to others in all respects, it is important for researchers to be cognizant that some of their results may be model-dependent, and to attempt to determine whether the extent of that dependence is likely to affect interpretation of the results in answering a particular research question. This issue is of particular concern because the level of spatial detail in the output from a two-dimensional model is often greater than any data set available for verifying the flow field. More comparative studies are needed in order to assess the utility of available models for application to particular types of flow problems.

3.2.10. Applications in bedrock channels. Miller [1994, 1995] used RMA2 and HIVEL2D to investigate spatial patterns of velocity and water-surface elevation associated with peak discharges. These were routed through finite-element meshes designed to represent major topographic features - including constrictions, expansions and channel bends - characteristic of bedrock-bound valleys that have been studied in the field. The examples had highly idealized topography, and no attempt was made to simulate flood-wave transmission. Model results were used to investigate (1) sensitivity of the flow field to boundary geometry, and (2) relevance of the resulting flow field to the spatial pattern of geomorphic impacts in a catastrophic flood. Simplifying assumptions were made in order to avoid computational problems, e.g. in *Miller* [1995] it was necessary to assume vertical sidewalls rather than realistic side slopes in order to use the HIVEL2D model, which has no wetting and drying algorithm.

Two-dimensional models have also been used to simulate flow patterns in the Grand Canyon, with particular attention to the mechanics of flow separation and recirculating eddies. These have been identified as characteristic features tied directly to patterns of channel constriction and expansion in canyon rivers, and they function as critical sediment-storage zones [*Schmidt*, 1990]. Modeling efforts have included specialized investigations focusing in detail on the eddies themselves [*Nelson*, 1991; *Nelson et al.* 1994] as well as application of RMA2 for simulation of general characteristics of the flow field along a study reach of the order of 1km in length [*Cluer*, 1997; also see the next section of this paper].

Wiele et al. [1996] used coupled flow and sediment transport models, together with a bed-evolution model, to simulate the effects along a section of the Grand Canyon of a flood emanating from the Little Colorado River. The flow model was a finite-difference discretization of the shallow-water equations, with a friction coefficient based on a logarithmic velocity profile scaled by a characteristic roughness length. Eddy viscosity was calculated as the product of shear velocity multiplied by a linear function of flow depth, and sand transport in suspension was modeled by an advection-diffusion equation. The model was used to simulate changes in the channel over a 6-day period of steady flow, and the predicted flow fields also include depictions of major recirculating eddies. Although no locally measured velocity or stage data were available for comparison with model results, measured and computed cross-section changes were compared. Results show a cumulative difference of 6% between the sums of measured and computed cross-sectional areas, with local differences as large as several meters along some individual cross-sections. The authors point out that "in regions with ledges and pools, substantial vertical velocity

components, hence nonhydrostatic pressure gradients, may be produced by accelerations or decelerations that vary with depth as a consequence of the obstructions and topographic contractions or expansions." (p.3585) However they note that the primary concern of the modeling effort is to predict bed evolution along sand-covered sections of the channel. At these locations, the hydrostatic approximation generally is satisfied and rapid deposition damps out topographic irregularities that are associated with nonhydrostatic pressure fields.

3.3. Three-Dimensional Models

As the quote from *Wiele et al.* [1996] above indicates, there are aspects of flow in bedrock-dominated systems that cannot be resolved by the shallow-water equations. Although two-dimensional models may be capable of simulating horizontal eddies, secondary flows in natural channels are often three-dimensional and may involve vertical accelerations that violate the assumption of hydrostatic pressure. Many of the 3-d models reported in the literature are designed for use over large areas in estuarine and coastal environments and incorporate a hydrostatic assumption, which simplifies the model [*Abbott*, 1997]. However in our opinion the effort of applying a 3-d model in a bedrock system is probably not justified unless the model is capable of handling the full range of flow phenomena that involve vertical accelerations. Therefore the treatment of 3-d models in this paper is limited to a small number of examples where the model in question appears to meet this criterion. We have not used these models and therefore the interested reader will need to investigate further for a more authoritative treatment of this topic.

Olsen and Stokseth [1995] apply SSIIM (Sediment Simulation In Intakes with Multiblock option), a 3-d finite volume model with a k-ε turbulence closure, to a short (about 80 m long), relatively straight reach of a mountain river with coarse bed material up to 2-3 m in diameter. Comparative plots of measured and calculated velocity profiles show agreement to within 10 or 15% for almost all measurements, and most of the measurements achieve a much closer match. Larger discrepancies are observed only at low flow where roughness elements cause pronounced distortion of the flow profile. The primary objective of the study was to develop a porosity model for the effects of the large bed roughness elements. Despite the complex bottom topography of the study reach, there is no discussion of three-dimensional flow structures.

Sinha et al. [1998] review the literature on 3-d models applied to natural rivers and conclude "Although most of these studies have thoroughly addressed issues regarding the effects of stress anisotropy and bed roughness in straight open-channel flows, none of them is suitable for simulating arbitrarily shaped natural geometries." (p. 14) They propose a finite-difference model with a k-ε turbulence closure, designed for simulating three-dimensional flows through river reaches with complex bathymetry and irregular boundaries. The model is applied to a 4-km reach of the Columbia River. Comparison of measured and calculated velocities is generally within 5-10% when optimized roughness distributions are used. The water surface is treated as a fixed or rigid lid rather than a free surface, thus requiring empirical data (or a solution derived separately from a free-surface model) to specify the shape of the water surface before running the model. Clearly this is not the most practical approach for the general case where the shape of the water surface is one of the unknowns to be solved for, but further improvements in the model should make it possible to incorporate an algorithm that can predict the shape of the free surface.

There are several other commercial programs that may also be applicable for flow through natural rivers; one example, FLUENT, has recently been used to simulate flow through a river bend [*Hodskinson*, 1996]. Although the version of FLUENT used in the simulation was also a fixed lid model, newer editions of the program do incorporate algorithms for predicting the shape of the free surface without such an assumption. Other three-dimensional models have been developed for application in irregular channels [e.g. *Banihasemi*, 1994]; however, despite active research and development, most 3-d models capable of simulating rapid flow with a contorted water surface require massive supercomputer resources and are not generally accessible [*R. Stockstill*, Waterways Experiment Station, personal communication, 1998]. We have not found any published studies applying such models to the kinds of rivers discussed here.

4. SELECTED CASE STUDIES

The remainder of this paper provides information from several examples that further illustrate some capabilities of flow models applied in bedrock valleys and some of the issues that require consideration. Three examples are described:

(1) a comparison of 2-d modeling results with a high-resolution field data set describing the water surface and velocity field along an 800-m reach of the Colorado River in Grand Canyon;
(2) a comparison of 1-d and 2-d model results for matching water-surface profiles to surveyed elevations of silt lines, preserved along the walls of a slot canyon formed by an ephemeral tributary of the Escalante River on the Colorado Plateau;
(3) a comparison of 1-d and 2-d model results for simulating peak flow associated with a preserved slackwater

terrace along the Cache la Poudre River, a tributary of the South Platte River in north-central Colorado.

All three examples assume steady flow, i.e. they represent "snapshots" of the flow field associated with specific discharge values. A dominant theme throughout these examples is the importance of understanding the interaction between the boundary conditions and the flow field, and of recognizing potential causes of uncertainty that may affect the conclusions of the modeling study.

4.1 *"Mohawk" Site, Grand Canyon*

The "Mohawk" site is located in the Grand Canyon of the Colorado River, 303 kilometers downstream from Glen Canyon Dam [*Cluer*, 1997]. Mean channel width at the site is approximately 90 meters and Cambrian Bright Angel Shale is exposed at river level. Adjacent talus slopes are covered primarily by blocks from the overlying Cambrian Muav Limestone. The site is a typical example of a channel geomorphic unit described in detail by *Schmidt* [1990] and given the name "fan-eddy complex" by *Schmidt and Rubin* [1995]. The main features of the fan-eddy complex include a channel constriction at the upstream end, created by a tributary debris fan; a channel expansion and deep pool downstream of the constriction, with a flow separation zone along the channel margin occupied by a recirculating eddy; and sand bars located at the separation and reattachment points of the eddy. Eddy bars sometimes form in the center of the recirculation zone and are susceptible to episodes of rapid erosion [*Cluer*, 1995]. The downstream end of the pool grades into a shallow riffle.

Detailed bathymetric and velocity-field surveys were conducted at the site in the summer of 1993 [*Cluer*, 1997]. Survey data reported here were collected at a constant discharge of 440 m^3s^{-1}. Along an 800-m reach of the channel, 32 cross-sections were surveyed at 25-m intervals, together with three parallel longitudinal profiles, one oriented along the thalweg and the other two at lateral distances of 25 m from the thalweg. Channel topography and water-surface-elevation data were collected using a system consisting of a power-boat-mounted depth sounder, a manually operated tracking theodolite, a laser distance meter, and a radio modem data link between the boat and land equipment. The velocity field was recorded simultaneously with a broadband acoustic Doppler current profiler, which can measure velocity in three dimensions at multiple depths from a moving boat. Velocity was determined in 0.5 m increments from 0.8 m depth to approximately 85% of the total water depth. Separate data files for velocity and for channel bottom depth and position were combined in post-processing to assign geographic positions to the velocity measurements. The three-dimensional velocity data were processed to derive a depth-averaged two-dimensional velocity field for comparison with results obtained from two-dimensional flow modeling.

Each subsystem has design and operation limitations that ultimately dictate the accuracy and reliability of the field data. The boat tracking system was designed and built for this project specifically to measure the water surface in addition to the channel bottom. The channel topography data are generally of good quality, with individual channel bed measurements repeatable within approximately 10 cm vertical and 20 cm horizontal. However the water surface along most of the study reach was virtually flat (see Figure 2 below), and therefore measured variations in water-surface elevation were of the same order of magnitude as the measurement errors. Although the velocity data were not compared with any other direct measurements at the site, velocity transects also were measured under three gage cableways at other locations in the Grand Canyon and the acoustic Doppler profiler yielded discharge values that were identical to the gaged discharges.

The bathymetry of the study site is illustrated in Figure 1, together with the locations of four cross-sections and a longitudinal transect along the thalweg. Among the four cross-sections, the one farthest upstream (section 1) is located at the constriction, and section 2 intersects the channel expansion and the deepest part of the pool, as well as the recirculating eddy along the channel margin. Section 3 is at an intermediate location between the pool and the downstream riffle, and section 4 is located at the approach to the riffle. The longitudinal profile (Figure 2) shows that the water surface at a discharge of 440 m^3s^{-1} is almost perfectly flat through the pool, and a measurable gradient is detectable only toward the downstream end in the approach to the riffle. The cross-sections are illustrated in Figure 3.

4.1.1 Flow modeling. The two-dimensional finite-element flow model RMA2 [*Donnell et al.*, 1997] was used to simulate flow conditions at the "Mohawk" site. Like the other two-dimensional models mentioned above, RMA2 computes water-surface elevations and depth-averaged horizontal velocity components for free-surface turbulent flow. The original model was developed by *Norton et al.* [1973]. Further development was carried out by King and Roig at the University of California, Davis, by King and Norton of Resource Management Associates, and by the Waterways Experiment Station (WES) Hydraulics Laboratory, which supports the current version 4.35. Friction is calculated as shown in equations (1) and (2) above, and eddy viscosity coefficients are used to characterize turbulence.

Construction of the finite-element mesh and visualization of model results for all of the two-dimensional modeling examples described in this paper were accomplished using the

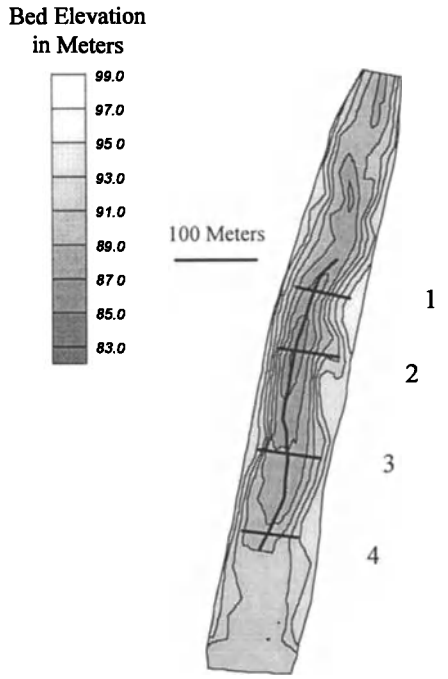

Figure 1. Bathymetry of the "Mohawk" site along the Colorado River in Grand Canyon, including thalweg profile and cross-section locations.

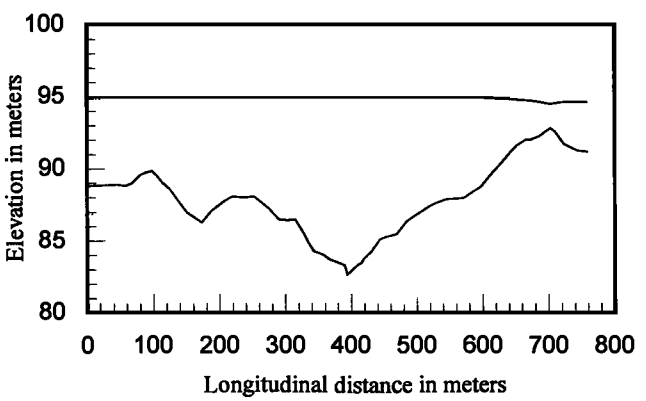

Figure 2. Thalweg profile of "Mohawk" site at discharge of 440 m^3s^{-1}. Locations are shown in figure 1. Elevation above arbitrary datum.

Surface Water Modeling System (SMS), an integrated pre- and post-processing software package [*Brigham Young University*, 1997] that supports several public-domain hydrodynamic models including RMA2, HIVEL2D [*Berger and Stockstill*, 1995], and FESWMS [*Froehlich*, 1989]. The finite-element mesh developed for the "Mohawk" site contains 876 elements and 2493 nodes (Figure 4). All modeling results reported for this site are based on a discharge of 440 m^3s^{-1}.

Roughness coefficients were specified for three types of elements: bank roughness, consisting of large angular and subangular rocks with interstitial sand (Manning's n=0.035), the partially sand-covered gravel-bedded main channel (n=0.025), and channel-margin sand bars (n=0.020). Sensitivity analysis indicates that a uniform increase of 0.01 for all three element types, amounting to a 40% increase in roughness coefficient for most of the channel, causes the model water-surface elevation to increase by 0.09 to 0.11 m. The same increase in roughness causes a 4 to 9% decrease

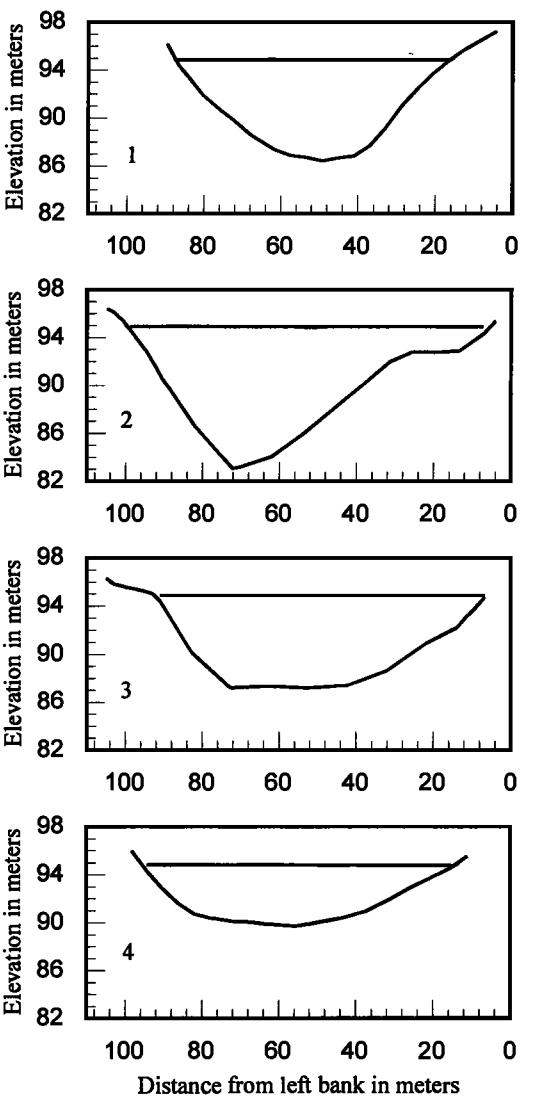

Figure 3. Cross-sections of Colorado River at "Mohawk" site at discharge 440 m^3s^{-1}. Elevation measured with respect to arbitrary datum. Locations are shown in figure 1.

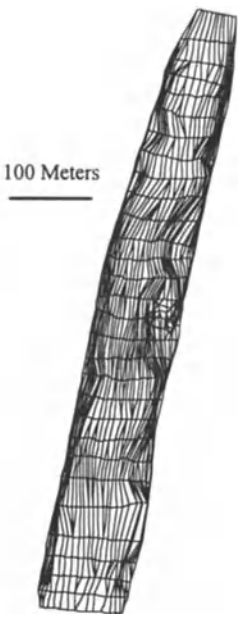

Figure 4. Finite-element mesh used for RMA2 modeling of flow at the "Mohawk" site, Grand Canyon.

in model peak velocities near the center of the channel, but also smears out the velocity distribution, in some cases causing a slight increase in velocities closer to the channel margin.

The influence of eddy viscosity coefficients on the modeled flow field was investigated in some detail. Although the constant coefficients used in RMA2 are specified in units equivalent to those of dynamic viscosity (Nsm^{-2}), all values reported here are expressed in units equivalent to kinematic viscosity (m^2s^{-1}) in order to maintain consistency with the recommendations cited earlier, where eddy viscosity was correlated with the product of shear velocity and depth and recommended coefficients ranged between 0.11 and 0.6.

Several model runs were completed using constant coefficient values ranging from 0.15 to 1.2 m^2s^{-1}, and the resulting flow patterns were compared with the two-dimensional distribution of depth-averaged velocity as derived from field measurements for the study site (Figure 5). Close examination shows that the highest eddy viscosity value is associated with suppression of flow separation and recirculation zones (Figure 5b), and is also associated with lower velocities in the vicinity of the thalweg and with smaller cross-channel velocity gradients as compared with model runs based on lower eddy viscosity coefficients. At the opposite end of the spectrum, the lowest value generates flow separation at locations consistent with field observations, but is also associated with formation of flow separation zones that are not evident in the field data set, as well as some evidence of instability in the vector pattern (Figure 5d). As a first approximation the optimal choice for eddy viscosity in this particular example appears to be a value between 0.15 and 0.5 m^2s^{-1}. A more detailed comparison may be seen using the thalweg transect and cross sections whose locations are indicated in figs. 2 and 5.

As the thalweg profile shows, there are slight undulations in the measured water surface, with amplitude 5 to 10 cm (center panel of Figure 6). These undulations are of the same order of magnitude as the measurement errors cited above, but it is noteworthy (particularly between 450 and 550 m on the horizontal axis) that the anomalies in the water surface appear to coincide with local increases in velocity, which are not affected by the same sources of error. The undulations are not simulated by the model, but the model profiles do reproduce the average trend - e.g., the generally flat water surface - through the pool. The model profiles also begin to slope downward approaching the riffle, although in all cases the model water surface is slightly steeper than the measured water surface. (This discrepancy is noticeable primarily because of the exaggerated vertical scale in the center panel of Figure 6.) The profile with the lowest eddy viscosity provides the best match to the measured water surface, but the intermediate eddy viscosity value raises the water level by no more than 5 to 10 cm. The highest eddy viscosity value raises the water surface by 25 to 30 cm.

Field measurements of velocity show a general deceleration from the upstream constriction to the pool, followed by a downstream acceleration approaching the riffle. The model results mimic this pattern but do not replicate all of the local undulations in the velocity profile. The profile with the lowest eddy viscosity is most successful at reproducing some of these undulations, but overpredicts the velocity by an average of 20%, or about 0.2 to 0.3 ms^{-1}. The intermediate eddy viscosity provides the closest match in terms of average velocity, and the highest eddy viscosity value leads to a smoother profile with underprediction of velocity along most of its length.

Examination of the cross-section trends supports these observations and provides some additional information. The model water surface profiles are generally parallel to the measured profiles but small-scale local undulations are not reproduced (Figure 7). Even the lowest eddy viscosity value is associated with a slight overprediction of water-surface elevation, but otherwise the sensitivity of the model water surface to the choice of eddy viscosity coefficient follows the same pattern described previously.

Cross-section velocity profiles (Figure 8) confirm the trends observed in Figure 5: the lowest eddy viscosity value is generally associated with the highest velocity near the

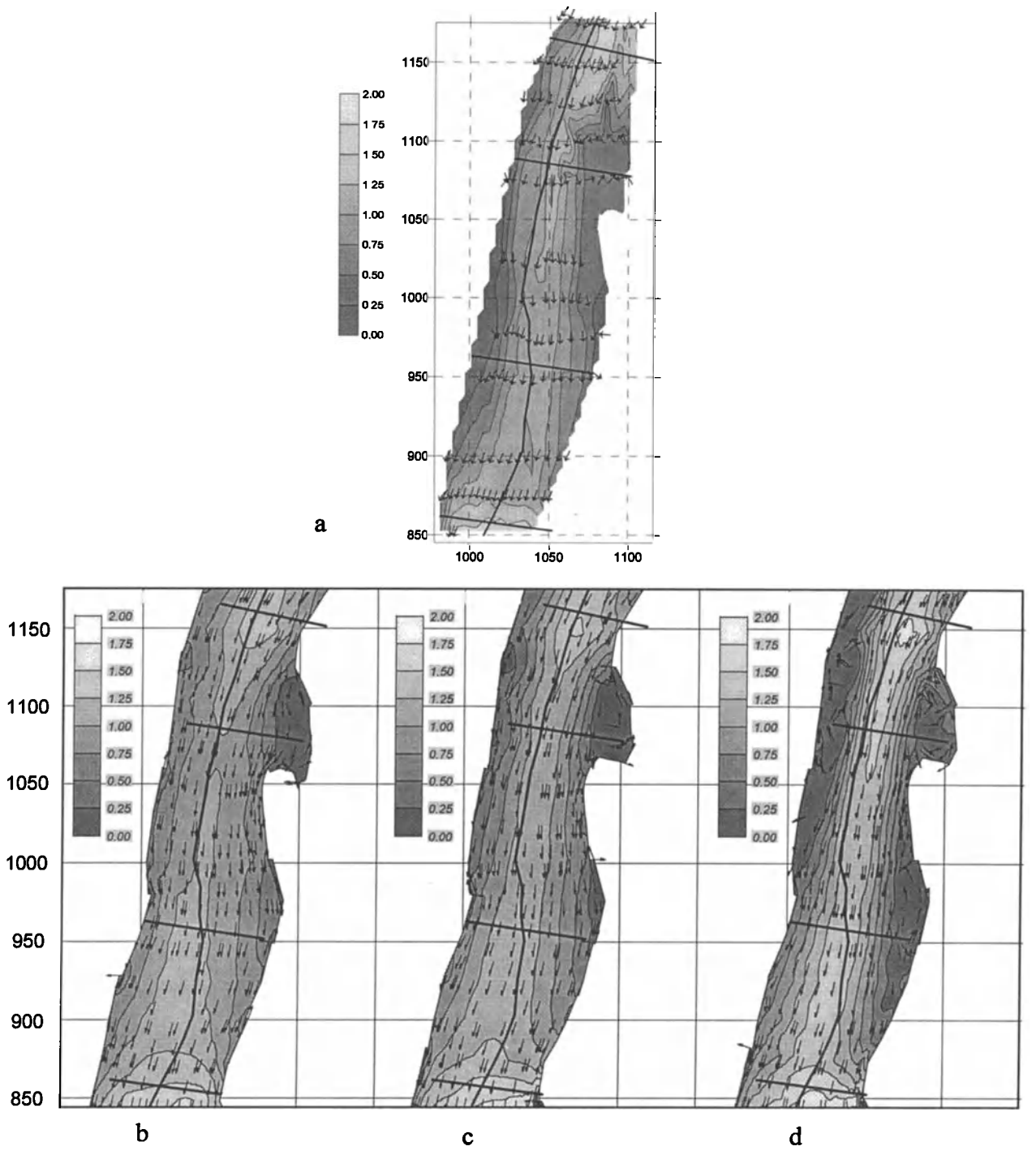

Figure 5. Comparison of vector plots showing influence of eddy-viscosity coefficients on modeled velocity field. Contour values represent velocity in ms^{-1}. Grid scale is in meters. Heavy lines indicate thalweg transect and cross-section locations. a: Depth-averaged velocity for field measurements at a discharge of 440 m^3s^{-1}. b, c, d: Modeled velocity fields for kinematic eddy viscosity coefficients of 1.2, 0.5, and 0.15 m^2s^{-1}, respectively.

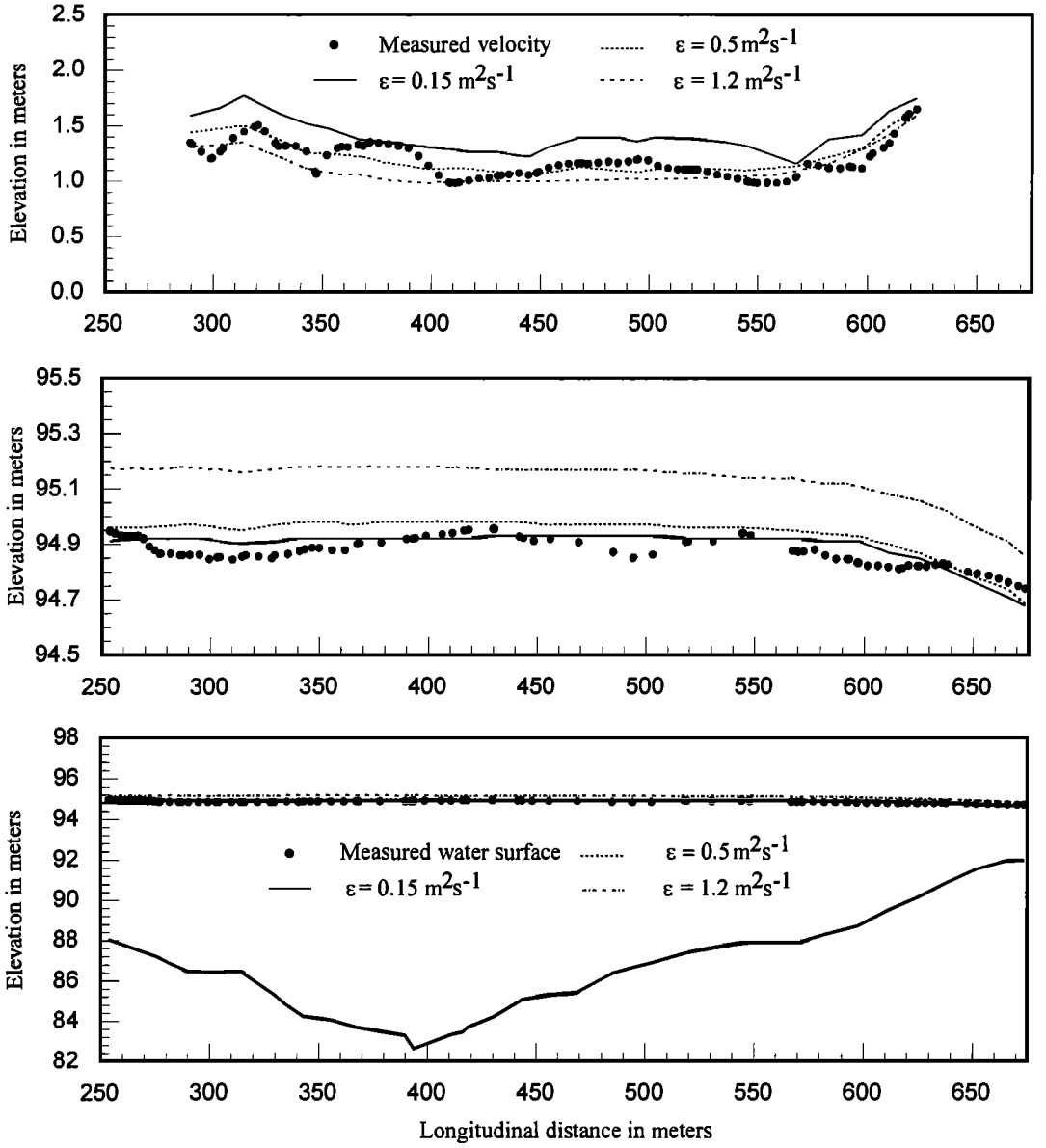

Figure 6. Thalweg profile of "Mohawk" site comparing model results with field measurements. Location of this transect is shown on figure 5. Center panel shows water-surface profiles with exaggerated vertical scale.

center of the channel and the steepest cross-channel velocity gradients. This leads to a modest overprediction of the maximum measured velocity on all four cross-sections, and in several instances leads to underprediction of velocity closer to the channel margins. Higher eddy-viscosity values smear out the velocity distribution, yielding lower velocities in the center and higher velocities along some of the channel-margin areas. The intermediate profile (ε = 0.5 m^2s^{-1}) underpredicts the maximum velocity on sections 1 and 2 by about 10-20% and provides a fairly close match for maximum velocity on sections 3 and 4. Closer to the channel margins, the higher eddy viscosities sometimes provide a better match to the field data than the lowest eddy viscosity, but there are several notable discrepancies. All three profiles underpredict velocities at the left margin of section 1 and in the vicinity of the recirculating eddy along the left

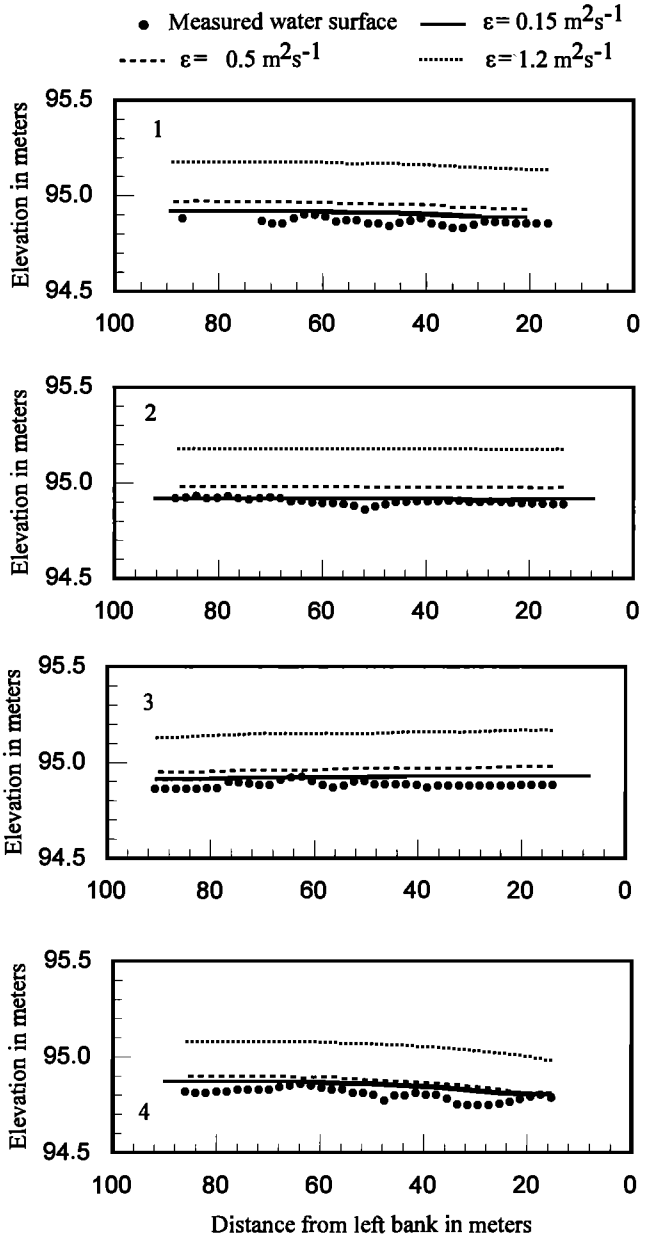

Figure 7. Cross-sections of "Mohawk" site comparing model results with field measurements of water surface elevation. Locations are shown on figure 5.

side of section 2, and all three overpredict velocities along the right channel margin on sections 3 and 4 (note the reversed orientation of the x-axis). The lowest eddy viscosity provides the closest match to the field observations along the right side of section 1.

In an effort to determine whether model performance can readily be improved, several additional model runs were completed. In one of these another intermediate eddy-viscosity value of 0.3 m^2s^{-1} was used. In another, a variable eddy viscosity was assigned using an option in RMA2 that determines eddy viscosity for each element as a function of the dimensionless Peclet number. The Peclet number in this usage is defined as follows:

$$P = \frac{udx}{\varepsilon} \tag{4}$$

where u is average velocity for the element, dx is maximum element dimension, and ε is the kinematic eddy viscosity. By choosing a constant Peclet number for the model run, the user specifies that the eddy viscosity will be assigned as a function of element size and velocity; the larger the Peclet number, the lower the eddy viscosity. The RMA2 user's manual recommends the use of this option with Peclet numbers between 15 and 40, and the best results in the present study were obtained with a Peclet number of 30. Other options were used in additional model runs, including the bendway vorticity correction [*Donnell*, 1997]. The closest matches to the measured velocity profiles were obtained in model runs using constant eddy viscosities of 0.3 and 0.5 m^2s^{-1} and using a Peclet number of 30 (Figure 9). The Peclet number option generated a range of eddy viscosity values between 0.1 and 0.5 m^2s^{-1}; calculated values of 0.3 u_*h, based on model output, generally ranged between 0.05 and 0.24 m^2s^{-1}. The bendway correction generated profiles that differed slightly from those shown, but without improving the results. None of the profiles illustrated in Figure 9 is clearly superior to the others, and all provide good results along a substantial portion of each of the four cross-sections shown. However it is evident that even the best choice of model parameters provides an imperfect simulation of the lateral velocity distribution.

4.1.2. Discussion. The results are more than adequate for general visualization of flow patterns. Clearly the major features of the velocity field are reproduced by the model, and the errors chiefly involve either modest shifts in the location of maximum velocity, in the breadth of the main thread of flow, or in the mean velocity of flow within the recirculating eddy. Thus the results shown here would be useful for predicting general spatial patterns of scour and deposition at this discharge, as Cluer (1997) has done. Whether they are good enough for other applications is in large part a question of the initial goals of the modeling project. For example, if the model results are to be used for calculating local sediment transport rates and simulating bed evolution over time, it is important to note that most bedload transport formulae are proportional to velocity raised to an exponent between 3 and 4 [*Graf*, 1971]. Thus the predicted local bedload transport rate based on model results for the left side of section 2 in Figure 9 might be lower than the transport rate based on measured velocity by a factor of 20

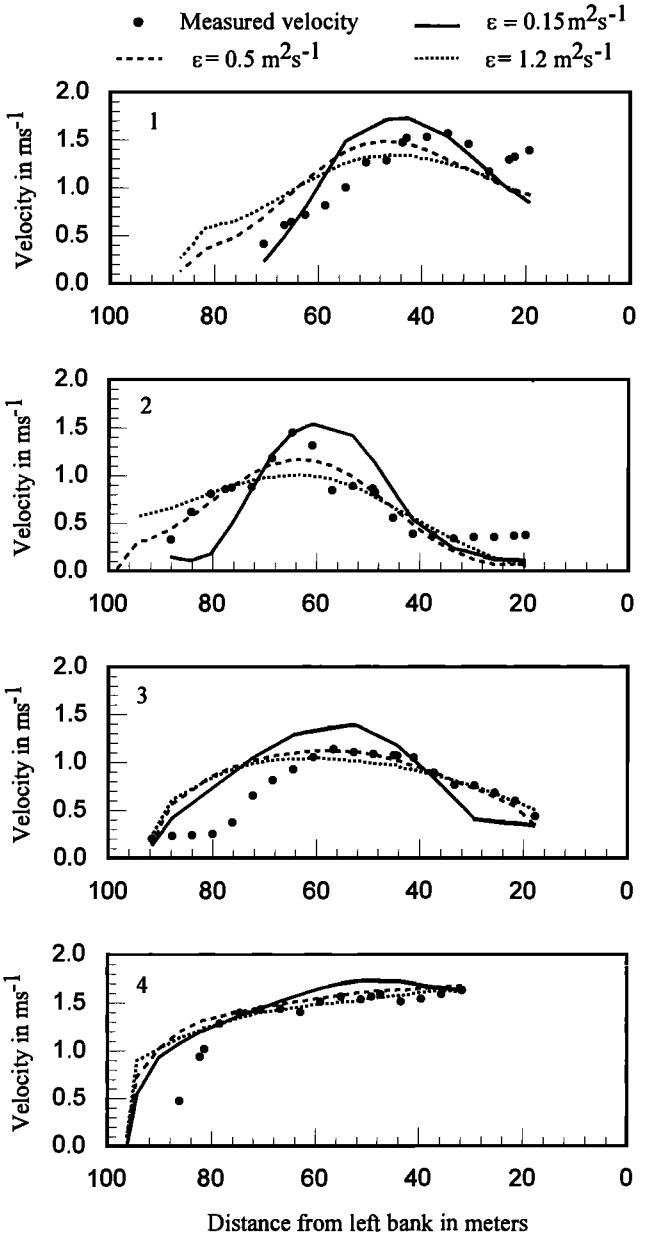

Figure 8. Cross-sections of "Mohawk" site comparing model results with field measurements of depth-averaged velocity. Comparisons illustrate sensitivity to value of eddy viscosity coefficient ε. Locations are shown on figures 1 and 5.

to 100. Conversely, transport rates based on model results might overpredict those based on measured velocity by a comparable factor along the right side of section 3. It is therefore not surprising to see significant local discrepancies between model results and field measurements in verifying a bed evolution model such as the one used by *Wiele et al.* [1996] along a comparable reach of the Colorado River.

It remains to be seen whether other two-dimensional models can match or improve on the results shown here. There is also an open question as to how well the model will perform with the same initial parameters applied to a much higher flow or a more turbulent set of conditions along a different part of the river. As the next two examples indicate, potential applications of flow models fall well outside the range

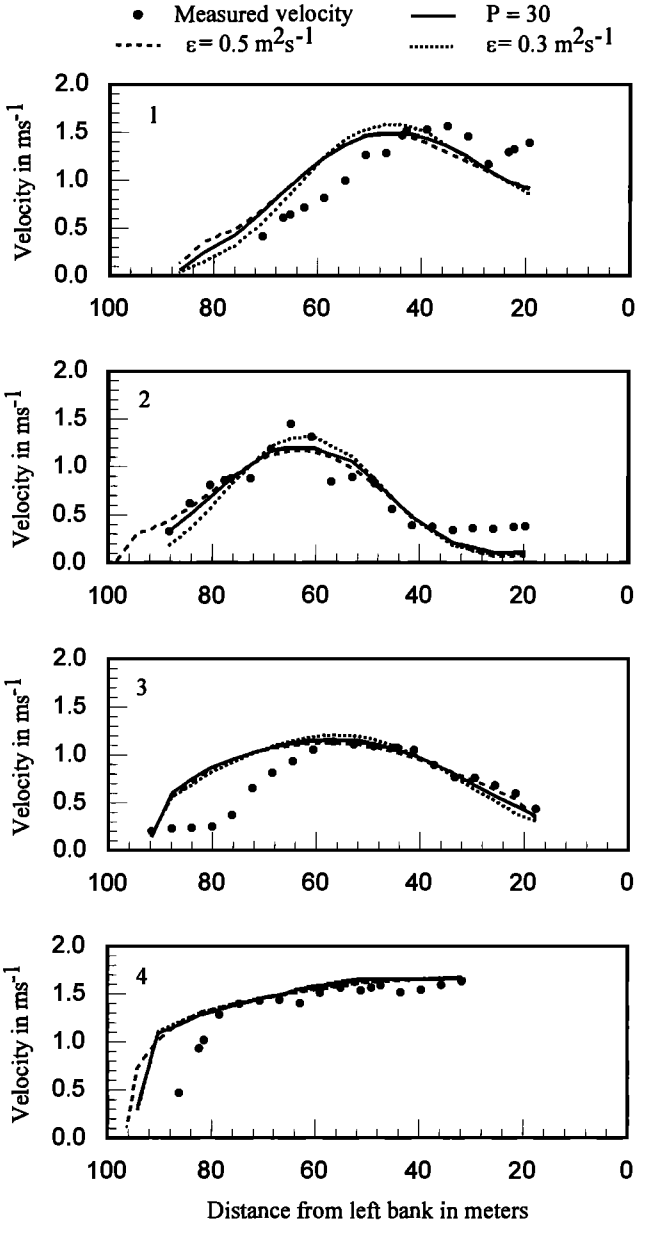

Figure 9. Cross-sections of "Mohawk" site comparing model results with field measurements of depth-averaged velocity. Results shown here illustrate the best match between model and field data. P is the dimensionless Peclet number (see text for discussion). Locations are shown on figures 1 and 5.

of conditions under which most high-resolution field data are collected. Clearly there is a need for additional testing of this and other similar models against a range of flows in different geomorphic settings.

4.2 Dry Fork Coyote Narrows

Dry Fork Coyote Narrows (referred to below simply as Coyote Narrows) is a slot canyon formed by an ephemeral tributary of the Escalante River in the arid Colorado Plateau of south-central Utah. Mean annual rainfall is estimated to be 20 mm and the drainage area is 65 km^2; the stream has no gage and no discharge record. The channel is incised in the Triassic-Jurassic Navajo Sandstone and has vertical or, in some cases, overhanging sidewalls. Field surveys were completed by Ellen Wohl in 1994 and included a series of 252 cross-sections along a channel reach about 500 m long that were collected using hand level and tape. The channel bed is flat and sandy and the walls of the canyon are narrow, with measured widths in the study reach ranging from a minimum of 1 m to a maximum of 5.5 m. Channel gradient along the study reach is about 0.01; the uppermost 125 m are irregular and are broken by several knickpoints, but the remaining section of the reach has a fairly smooth, almost linear bed profile (Figure 10).

Although there are no gage records for this stream, there are paleostage indicators in the form of silt lines that are locally continuous along the channel walls. At some locations two separate silt lines were visible. A set of flood marks included in the field survey (Figure 10) were based on locations and elevations where the heights of the silt lines were recorded at channel cross-sections. The lines typically are smeared out over a vertical distance of several centimeters. These, together with the surveyed channel geometry and estimated values of roughness parameter (Manning's n), provide the input data for hydraulic modeling to reconstruct flows that have passed through this channel. There are no dates associated with the flood marks. The ensuing discussion compares 1-d and 2-d modeling efforts.

A single value of Manning's n (0.03) was chosen during field investigations to represent the smooth, sandy bed and the rock walls of Navajo sandstone, which were relatively homogeneous along the length of the survey reach. The model runs assume that roughness is homogeneous in the longitudinal direction, but include an analysis of profile sensitivity to the choice of roughness coefficient.

4.2.1 Model input. The survey data were used to compile a data set for one-dimensional modeling using HEC-RAS. Although the channel walls were often vertical or even overhanging, the one-dimensional hydraulic model requires walls that slope (even very slightly) away from the channel. The HEC-RAS cross-sections therefore assume that the channel walls are nearly vertical, with a rise of 5 m over a lateral distance of 0.1 m. The model can be run in subcritical, supercritical, or mixed-flow mode. In the present study the mixed-flow mode was selected because it was anticipated that the flow would be mostly subcritical with several short intervals of supercritical flow. In subcritical or mixed-flow mode the model requires that the user specify discharge at the upstream boundary, roughness, expansion and contraction coefficients, and a downstream water-surface elevation. The default values of the expansion and contraction coefficients were used in the HEC-RAS model runs.

In addition the locations of cross-section endpoints were identified and were used to reconstruct the plan form of the channel bed along the study reach. This in turn was used to produce a finite-element mesh for two-dimensional flow modeling. The walls were assumed to be vertical and were not explicitly incorporated in the mesh. This made it possible to use HIVEL2D [*Stockstill and Berger*, 1994; *Berger and Stockstill*, 1995], which cannot simulate wetting and drying but can model hydraulic jumps and shock waves associated with high-velocity flow through abrupt channel transitions. The typical application of this model is for use in wide, shallow concrete-lined flood channels. However there is no reason in principle why it cannot be applied to channels with irregular boundaries, so long as the basic principles of finite-element mesh design and the limitations of the model (e.g. no wetting and drying algorithm, bed gradients less than 10%) are observed. Successful verification tests reported by *Stockstill and Berger* [1994] and *Berger and Stockstill* [1995] include a high-velocity channel with an abrupt expansion and another channel with two abrupt changes in bed gradient immediately upstream of a pair of channel bends.

Shear stress is calculated in HIVEL2D using the same relationships described by equations (1) and (2) above. Eddy viscosity is calculated as the product of shear velocity and flow depth multiplied by a constant coefficient. The default value of the coefficient is approximately equal to 0.3 and is automatically increased to 1.5 in the vicinity of a shock. The base value is within the range cited earlier from published sources.

The finite-element mesh required in order to run HIVEL2D consists of a mixture of quadrilateral and triangular elements with nodes at the corners. The mesh constructed for Coyote Narrows consists simply of a series of rows of five elements spaced across the channel, and was based on the layout of the cross-sections surveyed in the field (Figure 11). (Length/width ratios of the narrow elements along the channel margins are greater than the optimal value of 3 recommended by the model developers, but these rows of elements made it possible to specify greater flow resistance along the walls as compared to the channel.) Water-surface

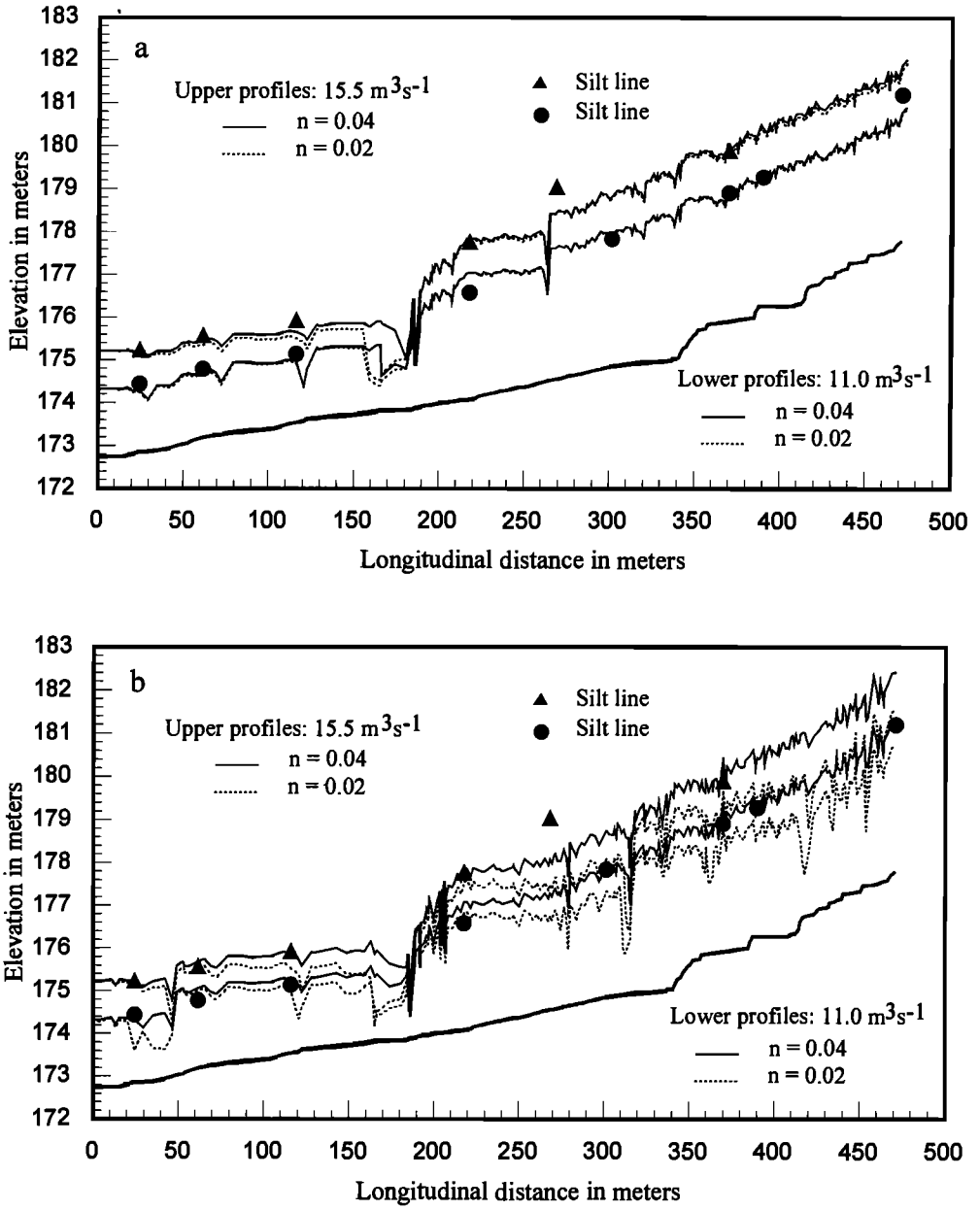

Figure 10. Longitudinal profiles of Coyote Narrows site, including a comparison of surveyed silt-line elevations with model water-surface profiles. Results illustrate sensitivity of each model to choice of roughness coefficients. a: HEC-RAS results, b: HIVEL2D results.

elevation is specified at the downstream boundary, and unit discharge is specified for the nodes along the inflow boundary at the upstream end of the mesh. The mesh constructed for this reach contains 1848 nodes and 1553 elements. In cases where it is important to resolve the details of the cross-channel distribution of velocity or local zones of flow separation and reattachment, further refinement of the mesh is necessary. In the present case, however, the primary objective was to fit model water-surface profiles to the surveyed flood marks and to compare the profiles generated by 1-d and 2-d models for the same initial boundary conditions. Although some aspects of the lateral variability of flow can be seen in the model results (e.g., Figure 13), they are not of primary concern here.

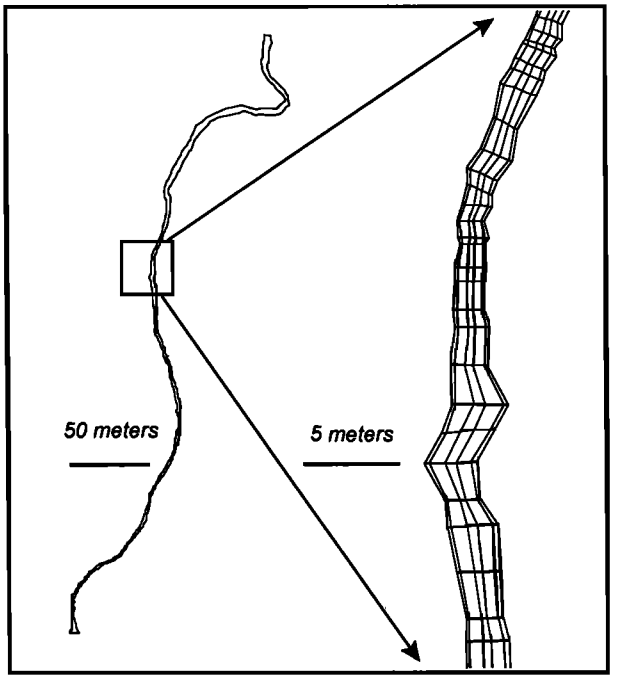

Figure 11. Plan view of Coyote Narrows field site (left) with a larger-scale view of part of the finite-element mesh used in HIVEL2D modeling (right).

At five out of nine locations with surveyed flood marks, two discrete silt lines were observed separated by vertical distances of 0.8 to 1.2 m. Therefore the modeling effort for both HEC-RAS and HIVEL2D required simulation of at least two different high-water profiles. The outflow boundary condition for each of the profiles was set at an elevation close to that of the mark farthest downstream (174.30 m for the lower set and 175.21 m for the higher set), and a series of flow values were used in trying to match the elevations of each set of high-water marks along the length of the reach.

Before determining which profiles provided the best match to the flood marks, it was necessary to investigate first whether the profiles were sensitive to the choice of roughness coefficient. Constant Manning's n values of 0.02 and 0.04 were used with both HEC-RAS and HIVEL2D to bracket the field estimate (0.03) and to investigate the sensitivity of the results to a 100% variation in the parameter value. Although HIVEL2D does not allow for sloping walls, it does assume that Manning's n values specified for the bed will also apply to the vertical sidewalls. However, based on the possibility that the rock walls might exert greater frictional resistance than the smooth channel bed, an additional option used with HIVEL2D was to increase the roughness parameter to 0.05 along a narrow row of elements bordering the channel walls, and to reduce Manning's n to 0.025 for the remainder of the channel floor. The default values of the turbulence coefficients and of the Petrov-Galerkin weighting coefficients for the numerical solution were used in the HIVEL2D model runs.

4.2.2 Modeling results. It is generally recognized that 1-d models like HEC-2 and HEC-RAS are highly sensitive to the choice of roughness coefficient. Sources cited earlier in this paper suggest that 2-d models are less sensitive than 1-d models. However, in this case sensitivity analysis using alternative values of Manning's n yielded unexpected results for both HEC-RAS and HIVEL2D.

Modeling results using HEC-RAS for two different discharge values (11 m^3s^{-1} and 15.5 m^3s^{-1}) indicate that varying Manning's n over a 100% range yields profiles that are almost indistinguishable (Figure 10a). The only prominent exception is in the vicinity of a sharp drop in the water surface, marking a region of supercritical flow followed by a hydraulic jump, at a longitudinal position between 160 and 180 m from the downstream end of the reach. At this location the profiles with n = 0.02 are lower in elevation and remain in the supercritical range over a longer distance than the profiles with n = 0.04. The intermediate profile (n = 0.03) is not illustrated in order to preserve legibility.

The HIVEL2D profiles are much more sensitive to the choice of roughness coefficient. The profiles with specified Manning's n = 0.02 are more irregular in shape than those with n = 0.04, and they are also significantly lower, in some cases by more than 1 meter (Figure 10b). Along a 100-m section at the upstream end of the study reach, the elevation of the model water surface for a discharge of 15.5 m^3s^{-1} with n = 0.02 is so low that it occupies the same range as the model water surface for a discharge of 11 m^3s^{-1} with n = 0.04. Given this degree of variability, any application of HIVEL2D for this particular finite-element mesh requires some confidence in the correct choice of roughness coefficient.

Guidelines for selection of Manning's n were originally derived for use with cross-sectional averages and one-dimensional analysis, and there are no published sources with specific recommendations as to how it should be chosen for use with two-dimensional models or whether the criteria should be any different. Moreover the evidence in Figure 10 appears to contradict the observations of other authors that were cited earlier, which otherwise would suggest that a lower value of Manning's n might be appropriate for two-dimensional modeling. Therefore the best guidance available is the degree of success in matching the available profiles. It is evident, for example, that the lower roughness coefficient yields profiles that are a poor match for either set of high-water marks, whereas the higher roughness coefficient provides a much better match. Subsequent application of HIVEL2D involved selection of those combinations of

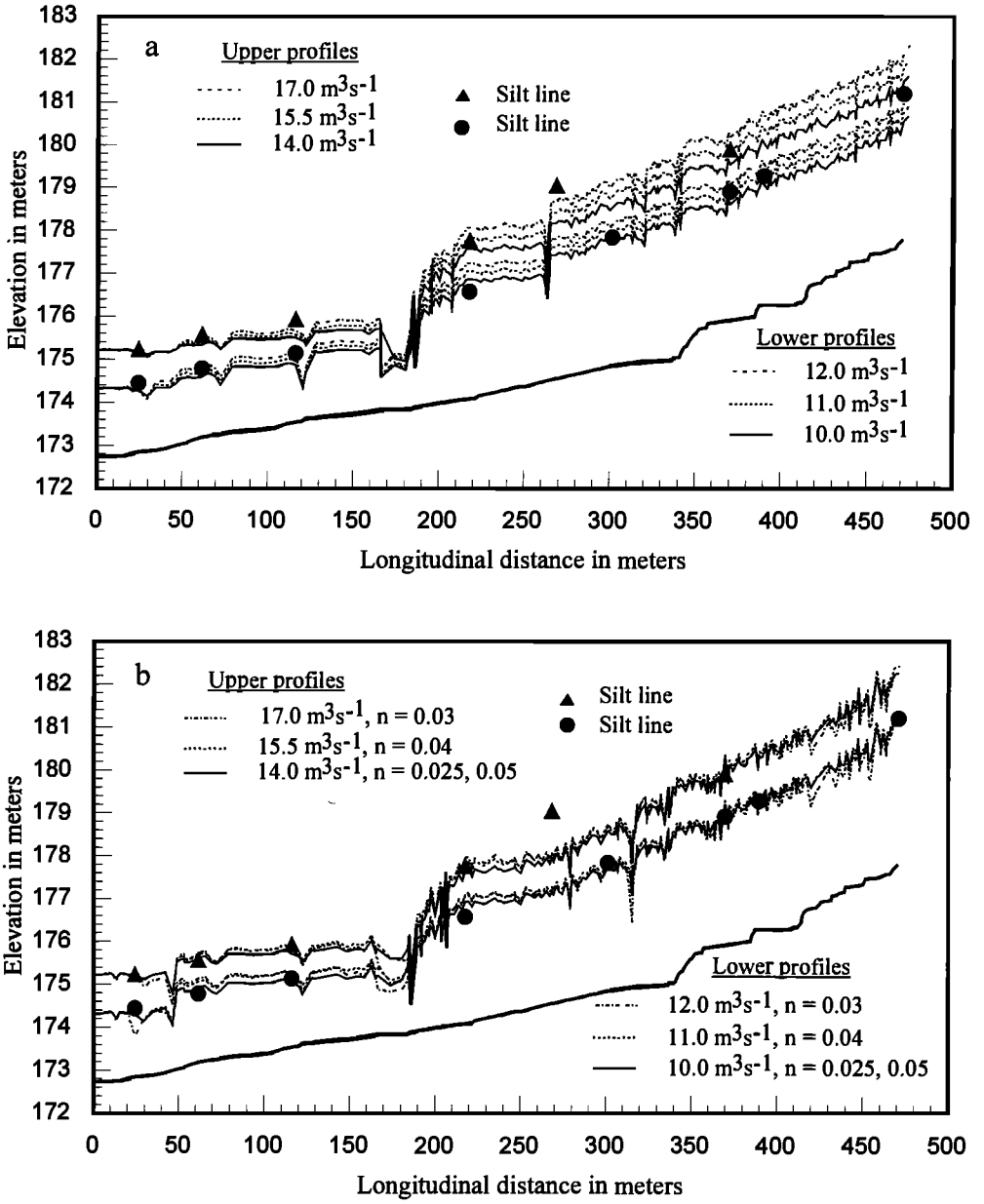

Figure 12. Comparison of model water-surface profiles for alternative discharge values at Coyote Narrows site. a: HEC-RAS results. All profiles assume Manning's n = 0.03. b: HIVEL2D results. Profiles illustrated are those that come closest to matching the surveyed silt-line elevations.

discharge and roughness coefficient that were most successful in matching each of the two sets of surveyed marks. Because HEC-RAS was relatively insensitive to the choice of roughness coefficient, all HEC-RAS profiles used a Manning's n value of 0.03 and only the discharge was varied between model runs.

Comparison of several HEC-RAS model runs for each set of high-water marks indicates that water stage is sensitive to modest variations in discharge, probably owing to the narrow, deep flow in this slot canyon (Figure 12a). Neither set of flood marks is matched perfectly by a single profile, but in both cases a set of discharge values varying over a total

Table 1. RMS error for Coyote Narrows profiles

Discharge (m^3s^{-1})	HEC-RAS (m)	HIVEL2D (m)
Lower profile (n=8)		
10.0	0.27	0.17
11.0	0.23	0.25
12.0	0.31	0.35
Upper profile, excluding outlier (n=5)		
14.0	0.29	0.17
15.5	0.23	0.22
17.0	0.30	0.22

RMS errors represent root-mean-square difference between predicted water surface profile and surveyed elevations along silt line. Profiles are illustrated in Figure 12 and roughness coefficients are indicated in legend.

range of about 20% comes fairly close to bracketing all of the marks associated with the set. The only prominent exception is a mark located at about 270 m along the horizontal axis. This mark is higher than all of the profiles that fit the other marks, regardless of which model is used, and appears to be an outlier. It may be associated with a higher flow or with some local obstruction or perturbation that is not otherwise identifiable from the survey data.

HIVEL2D profiles are about as sensitive to modest variations in discharge as HEC-RAS profiles if roughness coefficients are held constant. As was indicated above, however, the profiles chosen for illustration in Figure 12b are those produced by the combinations of discharge and roughness coefficient that provided the best match for the surveyed marks. As in Figure 12a, the range of discharge values applied to each set of marks varies by about 20% and in both cases the match appears reasonable with the exception of the single outlier identified above.

A comparison of the root-mean-square (RMS) error for all of the model profiles illustrated in Figure 12 indicates that a discharge of 11.0 m^3s^{-1} provides the best match to the lower set of marks when using HEC-RAS, whereas the optimal discharge for HIVEL2D is 10.0 m^3s^{-1} (Table 1). The optimal choices for the upper set of marks (excluding the outlier) are 15.5 m^3s^{-1} and 14.0 m^3s^{-1} for HEC-RAS and HIVEL2D, respectively. It is entirely possible that further fine-tuning would yield intermediate values that would fit well for both models, but in each case the agreement is already within about 10%. For HIVEL2D the profile with the mixed roughness coefficient (n=0.05 along the margins and 0.025 in the center) appears to provide the best match for both sets of marks, and the RMS error in both cases is lower than the RMS error for the best of the HEC-RAS profiles (0.17 m vs. 0.23 m).

4.2.3 Discussion. Although it was possible, by calibrating the roughness coefficients, to achieve a slightly better match to the surveyed marks using HIVEL2D, a more rigorous test would be needed before drawing definitive conclusions in comparing the relative merits of the models for this particular application. What is most striking about the comparison, given the amount of noise in both profiles, is that the two models produce such similar results. Although they differ in detail - RMS differences between the best-fit HEC-RAS and HIVEL2D profiles are 0.11 m and 0.26 m for the lower and upper profiles respectively - both capture the same major flow features, and therefore it is reasonable to conclude that these features are not model-dependent. This is particularly true in the vicinity of the most singular hydraulic feature along the length of the study reach - the steep transition from subcritical to supercritical flow that begins shortly upstream of 200 m on the longitudinal axis. Both models predict the occurrence of a hydraulic jump in a similar location at the end of this stretch of supercritical flow. Although it is possible that both models may be predicting the shape and length of the hydraulic jump incorrectly (as noted by *Stockstill et al.* [1997], 2-d models based on the hydrostatic assumption have difficulty with undular jumps), they both appear to be responding to a physical feature of some significance. It is interesting to note that this transition does not coincide with any of the major breaks in the longitudinal profile of the stream bed. This topic will be addressed in another forum.

The results indicate that a one-dimensional treatment performs reasonably well, by comparison with a two-dimensional treatment, in modeling flow through a slot canyon such as this one. Although the HIVEL2D results produced a somewhat better fit to the surveyed flood marks, the discharge estimates are not demonstrably more precise. The two models yield the same range of discharge values for both sets of survey marks.

On the other hand it is also true that there are aspects of the flow field that may be important and that cannot be resolved by one-dimensional modeling. Although Coyote Narrows is narrow and deep, some parts of the flow field predicted by HIVEL2D show substantial cross-channel variations in both water-surface elevation and velocity (Figure 13). In some cases the water surface on one side of the channel is predicted to be 0.4 to 0.6 m higher than on the other side, where the channel in question may be between 1 and 2 m wide. Lateral and longitudinal variations in velocity also appear to be quite large. In observing this pattern it is important to keep in mind that in this channel, where flow events

are rare and direct measurement of the velocity field during a flash flood would be both technically difficult and dangerous, we are unlikely to have the kind of data needed to verify its details. Furthermore it is likely that the hydrostatic assumption of no vertical acceleration is violated in some parts of the flow field. Thus when viewed at reach scale, the one-dimensional model may be adequate to illustrate major trends. When viewed at the scale of an individual channel cross-section, a full three-dimensional model may be required in order to produce an accurate simulation of the flow field.

4.3 Cache la Poudre River

The Cache la Poudre River (henceforth referred to simply as the Poudre River) is a tributary to the South Platte River in north-central Colorado, and it flows east from its headwaters in the Front Range of the Rocky Mountains. The river is incised in a canyon formed of Precambrian igneous and metamorphic bedrock along much of its descent to the Piedmont zone. Along the canyon, bedrock walls alternate with reaches where glacial outwash deposits are present. The climatic regime is semiarid, with mean annual precipitation ranging from 1000 mm at the higher elevations to 350 mm at the base of the mountains. The study site is located a short distance upstream of the mouth of the canyon, near the city of Fort Collins. The width of the valley floor at the site varies between 70 m and 250 m, and the thalweg gradient varies between 0.003 and 0.03. A gage just downstream of the site has been in operation since the early 1880's and has a drainage area of 2735 km^2 and a mean annual flood peak of 92 m^3s^{-1}. The flood of record at the gage is estimated to have been 595 m^3s^{-1}.

Topographic data consisting of a set of 26 surveyed cross-sections were collected by Ellen Wohl and colleagues in 1990-91 along a 1.8-km-long reach of the valley. This data set was used to compile a HEC-2 input data set, which was converted to a HEC-RAS data set for the present study. Additional interpolated cross-sections along the steeper parts of the channel brought the total number of cross-sections in the HEC-RAS data set to 58.

Wohl's field data were also used to construct a finite-element mesh for use with RMA2, and a series of model runs were completed in order to compare the performance of the one-dimensional and two-dimensional models. In addition both models were tested for sensitivity to the choice of boundary roughness and eddy viscosity coefficients.

A perspective view of the site is illustrated in figure 14. The site consists of three topographically distinct sections: an upstream, straight section of moderate gradient flanked by a narrow-but well-defined valley flat; a narrow, steep middle section with a channel bend at its upstream end and another bend downstream; and a more open downstream section where the channel traverses a broad meander while running along one valley wall and then crosses over to run along the opposite valley wall. The valley becomes narrower again approaching the downstream end of the surveyed reach.

This topographic information has been incorporated in a finite-element mesh containing 7648 nodes and 2661 elements. Figure 15 illustrates the layout of the mesh, together with a location map showing several features that are referenced in the ensuing discussion. Dashed lines on the figure indicate the boundaries between upstream, middle, and downstream sections as determined on the basis of flow modeling. Because the flow pattern established in the steep, narrow middle section affects the water surface and velocity distribution through the meander immediately downstream, the hydraulic boundary of the middle section is located downstream of the topographic boundary. Other features shown on the location map include left and right channel-margin profiles and a thalweg profile, as well as two cross-sections used in subsequent analysis.

A series of fine-grained sediment deposits have been identified at the study site [*Ellen Wohl*, personal communication,

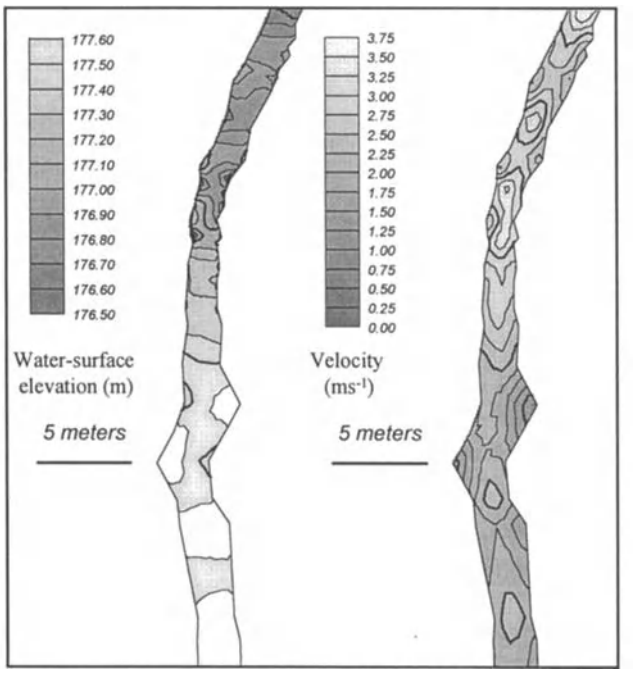

Figure 13. Shaded contour maps showing spatial patterns of water-surface elevation and depth-averaged velocity from HIVEL2D model results along a section of the Coyote Narrows site. Discharge = 14 m^3s^{-1}, n = 0.025, 0.05.

1995-1998] and have been interpreted as indicators of paleoflood stage. Similar deposits have been observed elsewhere along the canyon upstream of the study site, but no systematic study has been completed to date. However one particular feature along the left valley wall (Figure 16) has been interpreted on the basis of geomorphic and sedimentological evidence as a slackwater terrace, and a sample of charcoal embedded within the upper layer of sediment on this surface has been radiocarbon dated with an age of 690 +/- 105 BP. Most of the other deposits along the study reach are difficult to link together and identify as the products of any single, clearly defined flood event. Therefore the analysis reported here focuses partly on model runs to determine whether it is possible to constrain the magnitude of a prehistoric flood or floods that might have attained an elevation high enough to deposit sediment on this surface. As the present investigation is intended primarily to compare performance of 1-d and 2-d models with respect to different assumptions about boundary conditions, no attempt will be made here to provide a detailed interpretation of the deposits or to construct a paleoflood chronology.

4.3.1 Model input. In order to include the widest possible range of paleoflood discharge estimates that might be appropriate to the site, model runs were completed for discharge values ranging between 1000 and 5000 m^3s^{-1}. As no high-water marks were available at the downstream boundary, a downstream boundary condition of normal depth for each discharge was estimated by trial and error until a depth was found that was slightly greater than critical depth and that had little or no backwater or drawdown effect along the remainder of the profile. This procedure generates an M2 profile [*Chow*, 1959], with the intention of approaching as close to the "true" normal depth as possible for each discharge.

Three sets of assumptions about the roughness coefficients were used in alternate runs for each model at each discharge. Wohl's field estimates of Manning's *n* were 0.03 for the channel and 0.045 for the adjacent valley floor and walls and were assumed to remain constant along the length of the study reach. Two other alternatives were investigated in order to test the sensitivity of both models to a range of values: 0.040 (channel) and 0.055 (adjacent valley floor and walls), and 0.05 (channel) and 0.08 (valley floor and walls). An additional model run was performed using RMA2 to determine sensitivity of the results to possible changes in the elevation of the river bed.

RMA2 was selected for two-dimensional modeling of this site because the sloping valley walls forming much of the boundary under flood conditions precluded use of a model such as HIVEL2D, which can handle subcritical/ supercritical flow transitions but cannot handle wetting and drying. The marsh porosity algorithm was selected in order to facilitate smoother transitions as the water level changed elevation during successive iterations of the model. In most of the model runs described below, the constant eddy viscosity coefficient was reduced to the lowest value for which a convergent solution was possible, typically $\varepsilon = 0.3$ to 0.6 m^2s^{-1}. A limited sensitivity analysis was also carried out in order to determine whether the value chosen for ε had a significant influence on the results. Except where noted otherwise, the RMA2 results shown in the comparative longitudinal profiles represent a series of nodes along the channel thalweg (profile c in Figure 15).

4.3.2 Modeling results. Figure 17 compares longitudinal profiles produced for all three sets of roughness coefficients by both models at two different discharge values. The profiles confirm the presence of three hydraulically distinct sections, an upstream and a downstream section of relatively smooth flow and a middle section that is hydraulically steep and characterized by an unstable, irregular profile. The boundaries between these distinct sections (located at about 520 m and 1160 m along the horizontal axis in Figure 17) coincide with the locations of the dashed lines in Figure15.

Both models are sensitive to the choice of roughness coefficients. The largest discrepancies between the two models and between alternative runs of each individual model arise along the hydraulically steep middle section. These discrepancies increase in magnitude with increasing discharge and with lower values of Manning's *n*. As was observed in the Coyote Narrows example, lower roughness coefficients tend to produce longer excursions of supercritical flow and a lower water surface in the supercritical region. This effect is particularly noticeable in looking at the HEC-RAS profiles. The pattern of flow along this middle section, together with selected aspects of the two-dimensional flow field, will be discussed in greater detail below.

Along the upstream and downstream sections, the agreement between the two models appears to be fairly close at the lowest discharge of 1000 m^3s^{-1}. (Bear in mind that this "low" discharge is almost twice the size of the maximum flood of record, and that all of the modeled discharges are far above the range for which observations are available.) The differences between the low- and high-roughness profiles and between the RMA2 and HEC-RAS profiles tend to increase with discharge, and the difference between the RMA2 and HEC-RAS profiles also increases with decreasing roughness.

In order to quantify these trends, water-surface elevations were compared for different model runs along the upstream section, beginning at a distance of 1163 m along the horizontal axis in Figure 17. Results are presented in Tables 2 and 3. This section was selected for analysis because it is

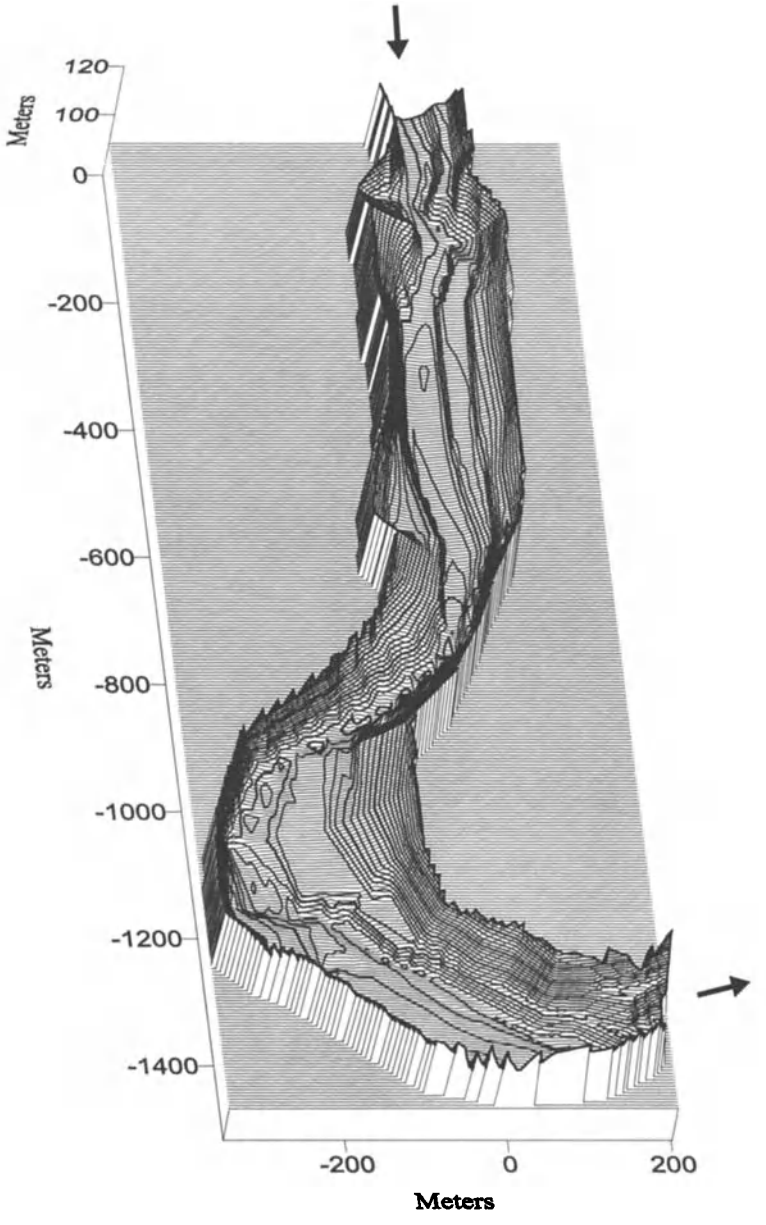

Figure 14. Perspective view looking upstream along the Poudre River study site. Arrows indicate flow direction.

not influenced by boundary conditions at the downstream end or by the rapidly varying pattern of flow in the middle section of the study reach. All values reported in Table 2 represent the root-mean-square difference in water-surface elevation between the profiles with the lowest (n = 0.03, 0.045) and highest (n = 0.05, 0.08) roughness coefficients, and the table therefore provides some indication of the sensitivity of the water-surface profile to a 67% variation in channel roughness and a 77% variation in roughness along the channel margin and valley walls. The absolute magnitude of the RMS difference ranges between about 0.8 and 1.8 m and generally increases with discharge. This effect is more pronounced in the RMA2 results than in the HEC-RAS results. As was observed in the Coyote Narrows example, this contradicts the suggestion made by previous authors that the 2-d model should be less sensitive to the

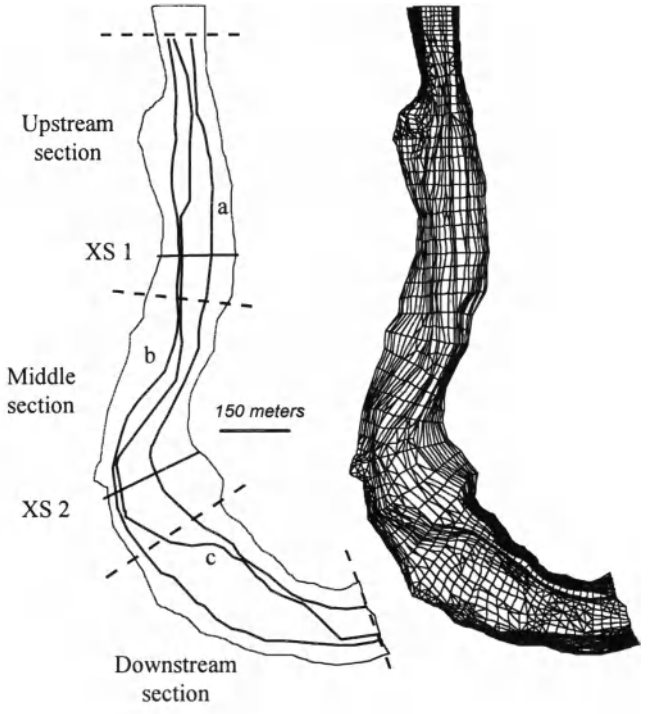

Figure 15. Location map (left) showing longitudinal profiles, cross-sections, and boundaries between hydraulically distinct sections of the Poudre River study site; the finite-element mesh used in RMA2 modeling is shown at right.

value of the roughness coefficient than the 1-d model. When the RMS differences are normalized and expressed as percent of water depth, all of the differences are within a range between about 10 and 15% of water depth. The normalized value of the RMS difference decreases with increasing discharge for the HEC-RAS runs, whereas it increases somewhat with discharge for the RMA2 runs.

RMS differences between water-surface profiles along the upstream section based on comparison of RMA2 and HEC-RAS model runs are presented in Table 3. Differences for model runs based on the same boundary conditions and roughness coefficients range between 0.25 m and 1.95 m, increasing with discharge, and at higher discharge there is also better agreement between profiles with higher roughness values than between profiles with lower roughness values. Note, for example, that at a discharge of 4000 m^3s^{-1}, the RMS difference for Manning's n = 0.05, 0.08 is half of the RMS difference calculated for Manning's n = 0.03, 0.045. At the highest discharges the closest match is found between the HEC-RAS profiles with n = 0.04, 0.055 and the RMA2 profiles with n = 0.05, 0.08. Visual inspection of Figure 17 clearly shows that the closest match along the downstream section occurs where both models specify n = 0.05, 0.08.

RMS differences were also calculated between water-surface elevations along thalweg profiles from different RMA2 model runs in order to test sensitivity to the choice of eddy viscosity coefficient. The water surface was much

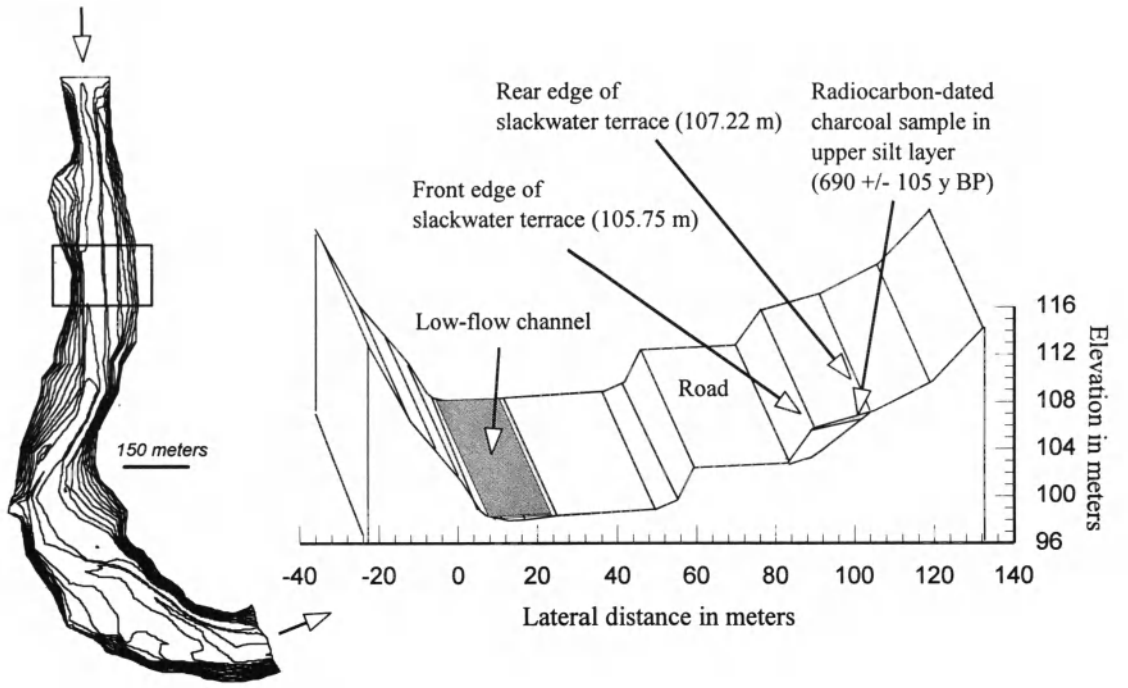

Figure 16. Location map and cartoon illustrating the feature interpreted as a slackwater terrace on the left side of the Poudre River valley along the upstream section of the study site.

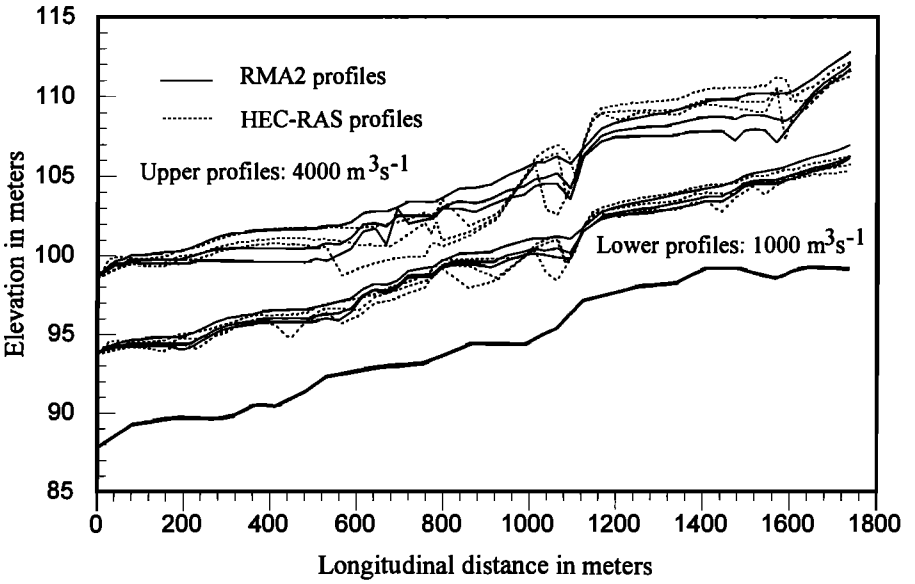

Figure 17. Comparison of water-surface profiles predicted by RMA2 and HEC-RAS at the Poudre River site for two discharge values and three alternative sets of roughness coefficients (n = 0.03, 0.045; n = 0.04, 0.055; n = 0.05, 0.08). For each set of three profiles the lowest elevation is associated with the lowest value of Manning's n.

Table 2. RMS differences between longitudinal profiles produced by models using different roughness coefficients along upstream section of Poudre River site

n = 0.03, 0.045 vs. n = 0.05, 0.08				
Discharge	HEC-RAS		RMA2	
(m^3s^{-1}) (m)	(% depth)		(m)	(% depth)
1000	0.91	13.3	0.80	11.7
2000	1.26	13.9	1.25	14.1
3000	1.16	10.6	1.50	14.6
4000	1.30	10.7	1.76	15.1
5000	1.42	10.4	1.62	12.8

Table indicates relative sensitivity of each flow model to the value of roughness coefficient with increasing discharge.

less sensitive to eddy viscosity than to the choice of roughness coefficient. RMS differences of 0.06 to 0.1 m were observed in comparing profiles with ε = 1.2 $m^2s^{-1}$and profiles with ε = 0.6 m^2s^{-1}, and RMS differences of 0.03 to 0.04 m were observed in comparing profiles with ε = 0.6 $m^2s^{-1}$and with ε = 0.3 m^2s^{-1} (Table 4). However it was not always possible to achieve convergent solutions with the lower eddy viscosity coefficient. High values of roughness and eddy viscosity have a stabilizing or damping effect on the flow field; conversely, numerical problems tend to develop when low values of eddy viscosity are combined with low values of Manning's n.

4.3.3. Discharge associated with slackwater deposits/paleostage indicators. Given the lack of stratigraphic information linking the deposits on the slackwater terrace (Figure16) to other paleostage indicators further downstream along the surveyed reach, it appears that the problem of selecting a best-fit flood profile matching the elevation of the slackwater deposits is not very well constrained. With the evidence currently available this is not an ideal site for a paleoflood hydrology study, but it does provide an opportunity to highlight some of the sources of uncertainty associated with the application of flow models in such studies.

Flood profiles for five discharges ranging between 1000 and 5000 m^3s^{-1} are illustrated in Figure 18. Superimposed on these profiles are two sets of symbols representing surveyed elevations and longitudinal positions of the front and rear edges of the slackwater terrace. The location where the radiocarbon-dated charcoal sample was excavated coincides with the cross-section identified in Figure 15 as XS1, and RMA2 results showing the cross-channel pattern of predicted velocity and water-surface elevation at XS1 for discharges of 1000 m^3s^{-1} and 4000 m^3s^{-1} are shown in Figure 19.

Several points are worth noting. First, the slackwater terrace is located along a hydraulically mild and relatively flat section of the valley where there is a greater likelihood of

Table 3. RMS difference between RMA2 and HEC-RAS longitudinal profiles along upstream section of Poudre River site

Discharge (m^3s^{-1})	n = 0.03, 0.045 (m)	(% depth)	n = 0.04, 0.055 (m)	(% depth)	n = 0.05, 0.08 (m)	(% depth)	"best-fit" comparison (m)	(% depth)
1000	0.35	5.1	0.25	3.6	0.28	4.1	0.25[a]	3.6
2000	0.74	18.4	0.35	4.0	0.39	4.4	0.35[a]	4.0
3000	1.09	15.9	0.95	13.9	0.57	8.4	0.57[b]	8.4
4000	1.52	13.1	1.13	9.7	0.76	6.5	0.61[c]	5.2
5000	1.95	15.4	1.46	11.5	1.28	10.1	0.73[c]	5.6

Table indicates variation of RMS differences with roughness coefficients. Best-fit comparison is the minimum RMS difference for any pairwise comparison of RMA2 and HEC-RAS model runs at the specified discharge. [a] n = 0.04, 0.055 for both models [b] n = 0.05, 0.08 for both models [c] n = 0.04, 0.055 for HEC-RAS, n = 0.05, 0.08 for RMA2

depositing fine-grained sediments during high flow than along the section immediately downstream. RMA2 predicts velocities over this surface ranging from 1 to 2 ms^{-1} at a discharge of 4000 m^3s^{-1} and velocities less than 1 ms^{-1} at a discharge of 3000 m^3s^{-1}. Although these values are somewhat higher than would be consistent with deposition of silt, they are considerably lower than velocities closer to the center of the channel. Results from a similar cross-section at the Mohawk site (section 2 in Figure 9) suggest that actual velocities along the left channel margin could be lower than those predicted by the model.

Second, the surface of the terrace is not flat (note the elevations of the surveyed points on Figure 18), nor is it parallel to the water-surface profiles; moreover, the elevation difference between the front and rear boundaries is fairly large. This leaves an open question as to what elevation or elevations should be set as index values to be matched by hydraulic modeling. The highest point on the surface of the terrace is 2.3 m higher than the point where the charcoal sample was found, and the lowest surveyed point along the front edge of the terrace is almost 4 m lower than the highest point along the rear edge. Comparison of these survey points with the model profiles in Figure 18 shows that the uncertainty between these two extremes is approximately equivalent to a 100% range of discharge values, regardless of whether RMA2 or HEC-RAS model runs are being considered.

Clearly the quality and consistency of the field evidence is the first and most important factor affecting the relative accuracy of the results. However our concern here is to assess the extent to which those results are also affected by modeling assumptions. The procedure followed here is to examine the relationship between stage and discharge predicted by each model in the vicinity of a particular paleostage indicator or high-water mark, and to determine the extent to which the predicted discharge matching that stage may vary with the model chosen or the model parameters selected. Model results were examined for sensitivity to both roughness coefficient and eddy viscosity coefficient. The two locations selected for this purpose are the location of the charcoal sample at XS 1 and the location where the maximum elevation of the slackwater terrace was surveyed (Figure 18).

Figure 19c illustrates the variation in RMA2 predictions of water-surface elevation at XS 1 for different values of Manning's *n*. Varying the eddy viscosity coefficient over the range between ε = 0.3 m^2s^{-1} and ε = 1.2 m^2s^{-1} produced cross-section water-surface profiles that were indistinguishable from each other at this scale; therefore these are not shown and they are not considered further in analyzing the variability of model results. Although the sensitivity of the velocity profile to the choice of model parameters is not directly germane to this part of the discussion, it is illustrated in Figure 19 in order to see whether the patterns are similar to those observed at the Mohawk site in the Grand Canyon. The cross-sectional distribution of velocity was slightly more sensitive than the water-surface profile to the choice of eddy viscosity coefficient (Figure 19a), but the differences along this cross-section were less significant than those at the Mohawk site (Figure 8). The choice of roughness coefficient had a much stronger influence on the velocity profile (Figure 19b).

A series of rating curves (e.g. stage-discharge relationships in graphical form) were constructed for each of the two locations selected for analysis. Discharge values corresponding to the intersections of surveyed elevations with the rating curves were estimated for both models and for each set

Table 4. RMS differences between longitudinal profiles produced by RMA2 using different eddy viscosity coefficients along upstream section of Poudre River site

Discharge (m^3s^{-1})	$\varepsilon = 0.3$ m^2s^{-1} vs. $\varepsilon = 0.6$ m^2s^{-1} (m)	$\varepsilon = 0.6$ m^2s^{-1} vs. $\varepsilon = 1.2$ m^2s^{-1} (m)
1000	0.04	0.10
4000	0.03	0.06

of roughness coefficients. Rating curves for XS1 are illustrated in Figure 20; elevations corresponding to the front edge (105.75 m) and the rear edge (107.22 m) of the slackwater terrace are used to identify the corresponding discharge value on each rating curve. Rating curves compiled from RMA2 model runs with different roughness coefficients are shown in Figure 20a, and a similar set of curves based on results from HEC-RAS are shown in Figure 20b. The range of variation between the two models using the same choices for roughness coefficient can also be determined by comparing results derived from these plots.

Results from the rating curves at XS1 and at the upstream cross-section were combined to estimate the percent differences in predicted discharge associated with each comparison (Table 5). As indicated in the table, differences attributable to the choice of roughness coefficients range from 13 to 47%, and the differences are greater when using RMA2 than when using HEC-RAS. Differences between the discharges predicted by the two models range from 12 to 36%, and these differences increase as roughness decreases. On the other hand, the comparison between the two models when using the "best-fit" profiles identified for the higher discharges in Table 3 (i.e. $n = 0.04, 0.055$ for HEC-RAS and $n = 0.05, 0.08$ for RMA2) is much closer, with differences of 1.0 to 5.8%. These results represent too small a data set to have any statistical validity or general predictive power; they serve rather to indicate the types of comparisons that may be useful to readers in thinking about how to assess the uncertainty of modeling predictions.

An additional source of error may be attributed to uncertainty in the long-term stability of the boundary conditions. Matching a flood profile to a paleostage indicator or high-water mark requires some confidence that the channel and valley floor have not changed significantly over the time interval since the flood whose magnitude is being investigated, yet there is often no way to prove that this is the case. Bedrock-controlled valleys may have significant accumulations of debris derived from flash floods or debris flows emanating from tributary valleys, and these can cause rapid alteration of channel form. Alternatively, debris deposits that may have formed fans and channel bars at a site in the past could have been removed by an intervening flood, and present boundary conditions may be significantly different from the conditions that existed prior to that flood. (See *Miller*, 1994 for photographs.) Alluvial deposits within a bedrock-controlled valley also may be subject to rapid change even in the absence of extreme flow events, and the resulting change in boundary conditions can have important implications for the modeled flow pattern [*Cluer*, 1997].

Miller [1994] used a hypothetical example in order to estimate the potential influence on discharge estimates of a change in boundary conditions caused by erosion of a debris fan. This was a local perturbation whose influence decayed rapidly with distance from the site of the fan. In the present example a very simple alternative assumption was made. For modeling purposes the bed of the Poudre channel was raised by 2 m along the entire length of the finite-element mesh, leaving the floodplain and valley walls unchanged. Comparative RMA2 runs were made in order to test the influence of this change on the predicted water surface and on the rating curves and discharge estimates at the site of the slackwater terrace. The choice of a 2-m change was somewhat arbitrary and was intended to serve as an estimate of the maximum possible change that might affect the water-surface profile at the site over a time scale of several hundred to several thousand years.

A plot comparing the longitudinal profiles for discharges of 1000 and 4000 m^3s^{-1} is shown in Figure 21, and a comparison between rating curves at XS 1 for alternative bed profiles is shown in Figure 20c. The influence of the change in bed elevation on the local flood stage is greatest at the lowest discharge and decreases with increasing flow, ranging from a maximum difference of about 1.5 m to a minimum of about 0.7 m in the vicinity of the slackwater terrace. This is evident both in Figure 21 and in the way the rating curves tend to converge toward the right side of Figure 20c. Comparison of results from the same two locations described previously in Table 5 indicates that the increase in bed elevation reduces the discharge required to match the elevation of the slackwater terrace by 15 to 27%.

The cumulative result of all of these comparisons is to suggest that the uncertainty attributable to any one of the factors cited above may fall in the range of 10 to 50% when estimating the peak discharge of a paleoflood. The cumulative error associated with modeling decisions may be on the order of 40 to 60%, and in some cases more, before we even take into account the uncertainty involved in estimating the elevation of peak flood stage. Nevertheless it is still important to note that, at least in the present instance, ambiguities in correctly identifying flood peak stage are associated with

the greatest potential for error. In practice the uncertainty due to modeling assumptions may be reduced if a more extensive set of reliable paleostage indicators are available; as was seen in the Coyote Narrows example, this may be helpful in eliminating some modeling options as clearly unrealistic choices, thereby narrowing the final range of predicted discharge values.

4.3.4 Rapidly varying flow and two-dimensional aspects of the flow field. As indicated by the previous discussion of the longitudinal profiles in Figure 17, the middle section of the Poudre study site is a hydraulically steep part of the channel where both models, and HEC-RAS in particular, predict an irregular water surface that appears to be marked by transitions between subcritical and supercritical flow. The regions of supercritical flow are indicated on the profile by a sharp drop in the water surface upstream and by a hydraulic jump downstream. For both models the higher values of roughness coefficient tend to damp out this effect, as was also observed in the Coyote Narrows example; in fact the uppermost of the 4000 m^3s^{-1} profiles derived from RMA2 modeling and shown in Figure17 does not intercept any of the small areas of supercritical flow predicted by this particular model run.

Although the developers of RMA2 state that the model is intended for use with subcritical flow, in most cases it does produce convergent flow fields for the problem illustrated here. Previous experience, described above, has indicated that when supercritical flow is limited to a small part of the flow field, the flow patterns themselves are not radically different from those produced by models that are based on the conservation form of the shallow-water equations. The results from the RMA2 model runs along the middle section of this study reach are used in order to illustrate the patterns of two-dimensional flow and water-surface topography that may be predicted along a steep, irregular channel reach. The validity of these patterns remains to be tested by conducting detailed measurements in steep channels with rapid flow transitions.

All of the RMA2 longitudinal profiles presented for the Poudre up to this point were aligned along the thalweg for comparison with the HEC-RAS results. However along this middle section the model water surface exhibits strong cross-channel gradients. Therefore paired profiles of the water surface along the left and right margins of the channel are shown in Figure 22 and are compared with HEC-RAS profiles for discharges of 1000 and 4000 m^3s^{-1}. Because the two models showed the best agreement when using the higher roughness coefficients, and because the steep profile and turbulent flow of the middle section suggested that higher roughness coefficients might be particularly appropriate here, the 4000 m^3s^{-1} RMA2 profiles in Figure 22a are derived from model runs using n values of 0.05 for the channel and 0.08 for the valley margins. The 4000 m^3s^{-1} HEC-RAS profile shown in the figure has a mixed set of n-values, using n = 0.04, 0.055 along the upper section and n = 0.05, 0.08 along the middle and lower sections, thus combining the parameter choices that provided the best match between RMA2 and HEC-RAS along different parts of the longitudinal profile in Figure 17 and Table 3. In Figure 22b, the 4000 m^3s^{-1} profiles for both RMA2 and HEC-RAS use n = 0.04, 0.055. The 1000 m^3s^{-1} profiles assume n = 0.04, 0.055 for both models in figs. 22a and b.

Several trends are apparent. At 1000 m^3s^{-1} the left and right RMA2 profiles do exhibit some out-of-phase undulations, but for the most part they track each other quite closely and the cross-channel difference in water-surface elevation rarely exceeds 0.5 m. Furthermore the HEC-RAS profile is in fairly close agreement with both of the RMA2 profiles, with the exception of a couple of short supercritical excursions along the middle section (between 800 m and 1000 m on the horizontal axis).

At 4000 m^3s^{-1} the left and right RMA2 profiles are in close agreement along the upper section and are generally within 0.2 to 0.5 m of each other along the lower section, but they are strongly out of phase along the middle section, with a maximum difference of about 1.5 m when roughness is high (Figure 22a); the maximum difference increases to just under 2.5 m if roughness coefficients of 0.04 and 0.055 are used instead (Figure 22b). In both figs. 22a and 22b the HEC-RAS profile tracks the left RMA2 profile fairly closely as it traverses a dip, a rise, and another dip just downstream from the 1000-m mark on the x-axis. Subsequently, the left RMA2 profile adopts a steep but relatively smooth gradient for the next 200 m, whereas the HEC-RAS profile drops more abruptly into supercritical flow followed by a hydraulic jump before rejoining the RMA2 profile further downstream. Neither of the RMA2 channel-margin profiles in Figure 22a actually intercepts the small area of supercritical flow that developed along the center of the channel in this model run (Figure 23); the left channel-margin RMA2 profile in Figure 22b does intercept the somewhat larger area of supercritical flow that developed in the model run with lower roughness coefficients (Figure 24).

The major features of the two-dimensional pattern can be visualized using contour and vector plots based on RMA2 results. Examination of figs. 23 and 24 indicates that the primary differences between the left and right profiles in Figure 22 are attributable to superelevation of the water surface on opposite sides of the channel in two successive bends, and that there is an irregularly shaped filament of higher-elevation and high-velocity flow that stays along the right bank some distance beyond the downstream bend. This filament is the site of the undulations along the right-channel-margin profile between 600 and 800 m in Figure

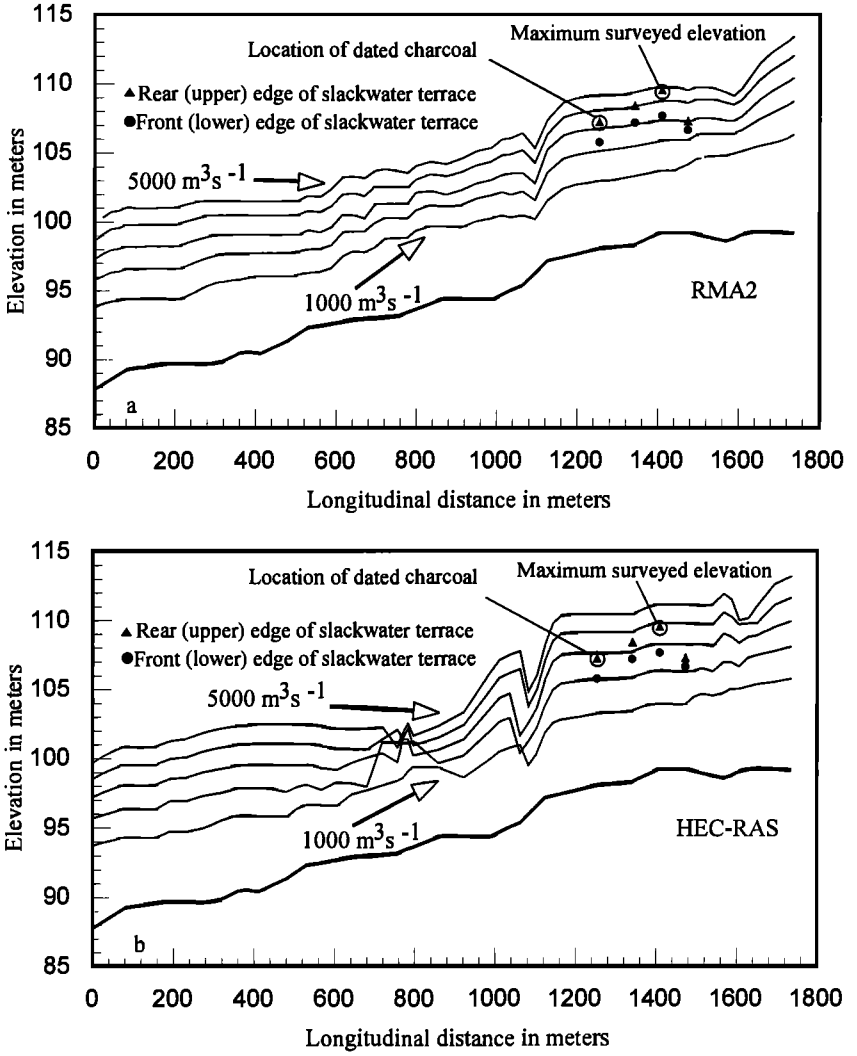

Figure 18. Comparison of water-surface profiles along the Poudre River site for discharges of 1000, 2000, 3000, 4000, and 5000 m^3s^{-1}. Elevations of surveyed points from the slackwater terrace along the upsream section are also shown. a: Profiles based on RMA2 results for n = 0.04, 0.055. b: Profiles based on HEC-RAS results for n = 0.04, 0.055.

22, which in turn are marked by indentations in the water-surface contours in the left panels of figs. 23 and 24. The contour map of Froude numbers in the panel on the far right in Figure 23 depicts a thread of nearly critical (i.e. Froude number greater than 0.75) flow that coincides fairly closely with the thread of maximum velocity along the length of the steep middle section. There are only a few small, isolated regions of critical or supercritical flow predicted by the model at this discharge for n = 0.05, 0.08, most prominently at the downstream bend where the maximum velocity coincides with a steep drop in the water surface. The amplitudes of superelevation and of the undulations in the water surface clearly are greater for model runs utilizing lower values of Manning's n (Figure 24), the predicted velocities are higher, and there are also several additional, somewhat more extensive regions of supercritical flow that appear in the model flow field under these circumstances.

A direct comparison of these patterns is more easily visualized using a cross-section; Figure 25 compares RMA2 results at discharges of 1000 m^3s^{-1} and 4000 m^3s^{-1} for water-surface elevation and velocity along XS2. The bottom panel (Figure 25c) illustrates the stark differences in cross-channel water-surface gradient that are predicted by the model as the roughness coefficients vary from n = 0.03, 0.045 to n =

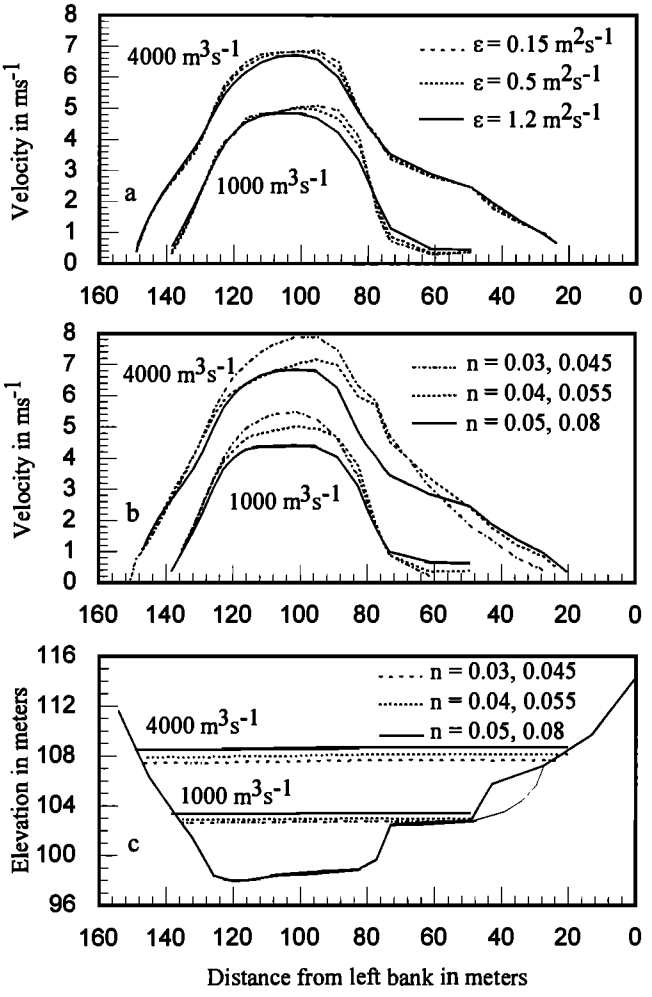

Figure 19. Distribution of velocity and water-surface elevation at section XS1, based on RMA2 results for two discharge values. a: Comparison of velocity profiles for three alternative eddy-viscosity coefficients. b: Comparison of velocity profiles for three alternative sets of roughness coefficients. c: Comparison of water-surface profiles for three alternative sets of roughness coefficients.

0.05, 0.08. As was the case for XS1 (Figure 19), predicted water-surface elevations were insensitive to the choice of eddy-viscosity coefficient, with maximum differences of only a few centimeters, and therefore the differences attributable to varying eddy viscosity are not shown. Tinkler [personal communication 1998] reports for the James River, Texas, super-elevation of 1.8 m across a bend for a flood of roughly 3000 m^3s^{-1}, with a mean depth of 6.4 m, a total water surface width of 165 m, and a bottom width of 31 m. These figures are similar in magnitude to those in figure 25c. Cross-channel trends in velocity were only slightly sensitive to variations in eddy viscosity (Figure 25a), as was also observed at XS1. By contrast the sensitivity of the velocity pattern to the choice of roughness coefficient is striking, particularly at the higher discharge (Figure 25b).

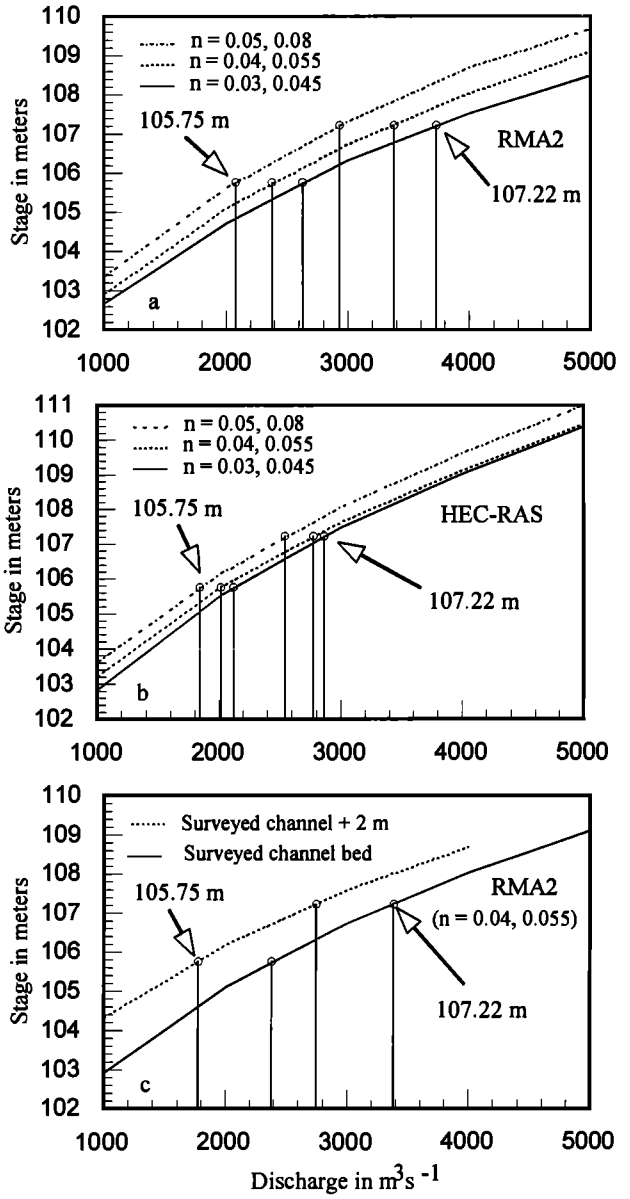

Figure 20. Rating curves derived from modeling results and discharge values corresponding to surveyed elevations of the front and rear edge of the slackwater terrace at XS1. a: Rating curves derived from RMA2 results using three alternative sets of roughness coefficients. b: Rating curves derived from HEC-RAS results using three alternative sets of roughness coefficients. c: Rating curves derived from RMA2 results based on two alternative bed profiles (as shown in figure 21).

Table 5. Comparison of predicted discharge values matching slackwater terrace elevation at two locations along the Poudre River study site

Roughness values	Predicted discharge, front edge of terrace (m^3s^{-1})			Predicted discharge, rear edge of terrace (m^3s^{-1})		
	RMA2	HEC-RAS	$\frac{Q_{RMA2}}{Q_{HEC-RAS}}$	RMA2	HEC-RAS	$\frac{Q_{RMA2}}{Q_{HEC-RAS}}$
			Results for XS1			
0.03, 0.045	2622	2120	1.24	3722	2864	1.30
0.04, 0.055	2372	2015	1.18	3352	2768	1.21
0.05, 0.08	2079	1832	1.13	2929	2540	1.15
$\frac{Q_{0.03,0.045}}{Q_{0.05,0.08}}$	1.26	1.16		1.27	1.13	
"Best fit" ratio[a]			1.03			1.06
			Results for upstream section			
0.03, 0.045	3822	2803	1.36	>5000	3993	>1.25
0.04, 0.055	3242	2632	1.23	4728	3806	1.24
0.05, 0.08	2606	2331	1.12	3872	3370	1.15
$\frac{Q_{0.03,0.045}}{Q_{0.05,0.08}}$	1.47	1.20		>1.29	1.18	
"Best fit" ratio[a]			0.99			1.02

[a] Ratio of Q_{RMA2} for n = 0.05, 0.08 to $Q_{HEC-RAS}$ for n = 0.04, 0.055

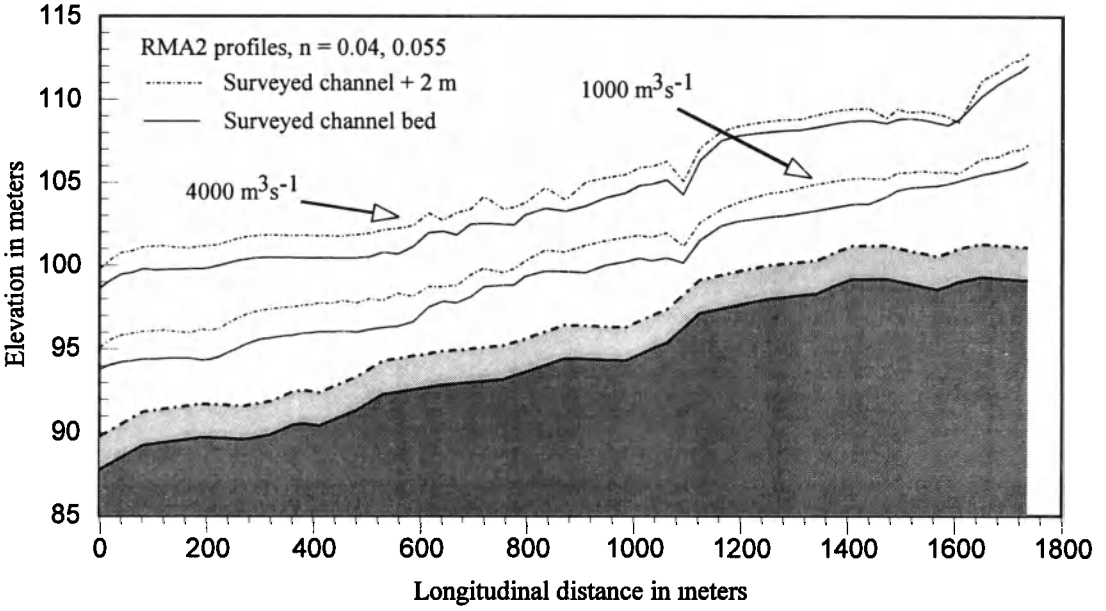

Figure 21. Comparison of RMA2 water-surface profiles along the Poudre River site for alternative scenarios involving a 2-m change in channel-bed elevation.

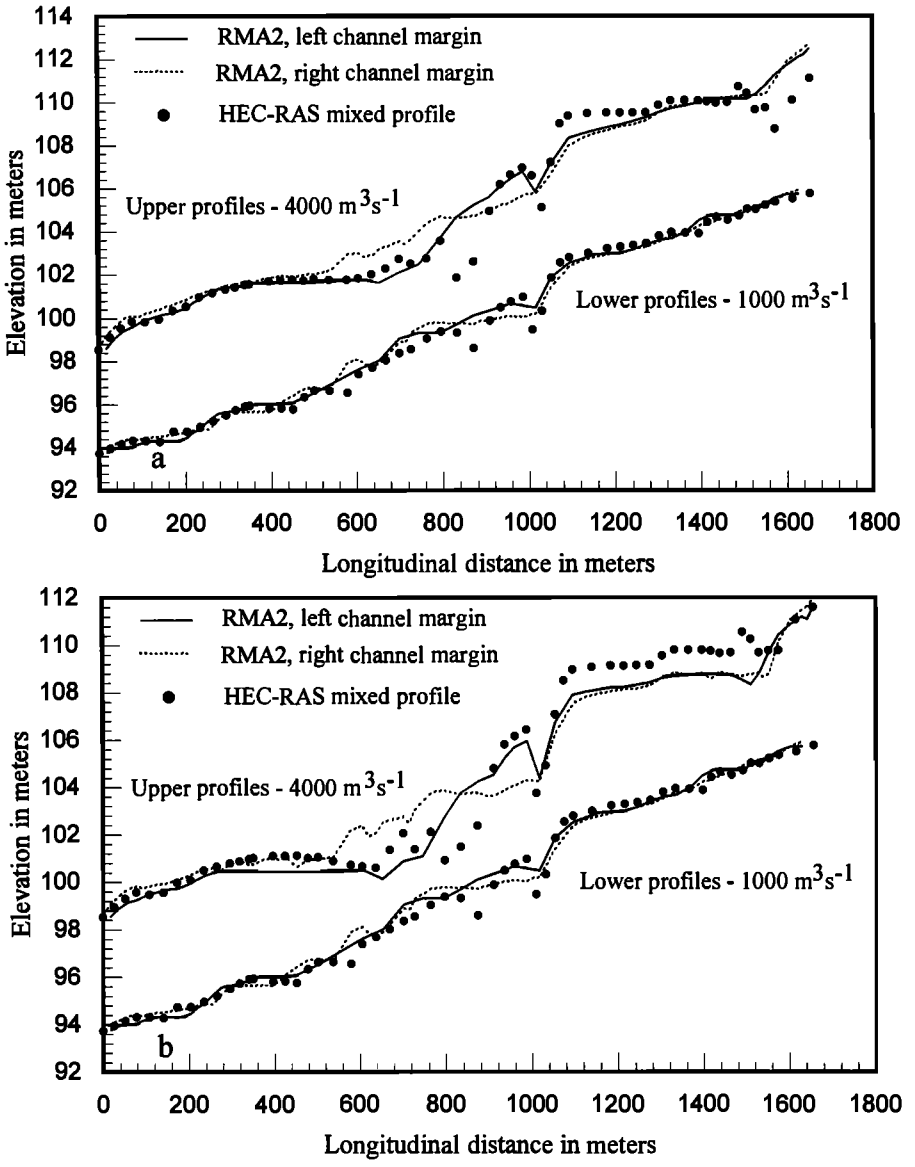

Figure 22. Comparison of left and right channel-margin RMA2 profiles with longitudinal HEC-RAS profiles for two different discharges. a: 4000 m^3s^{-1} profiles use $n = 0.05, 0.08$ for RMA2 and mixed n (see text) for HEC-RAS; 1000 m^3s^{-1} profiles use $n = 0.04, 0.055$ for both models. b: $n = 0.04, 0.055$ for both models at both discharges.

The contour maps serve to highlight one of the phenomena described by *Tinkler* [1997b]: namely, that critical and supercritical flow regions in natural channels are almost always flanked by areas of subcritical flow. The trains of standing waves that are also typical of the conditions described by *Tinkler* are beyond the capabilities of RMA2 and are not modeled here, although the undulations along the right channel-margin profile in Figure 22 are reminiscent of standing waves.

4.3.5 Discussion. Several points emerge from the application of flow models at the Poudre site:

1. In the case of Coyote Narrows, it was possible to estimate the discharge from a series of paleostage indicators with a precision of about 20%; whereas along the Poudre there is a range of variation in predicted discharge for any one flood mark of about 40 to 60%, and a total range on the order of 100% or more when we consider the uncertainty about which flood mark to use. This reflects not only the

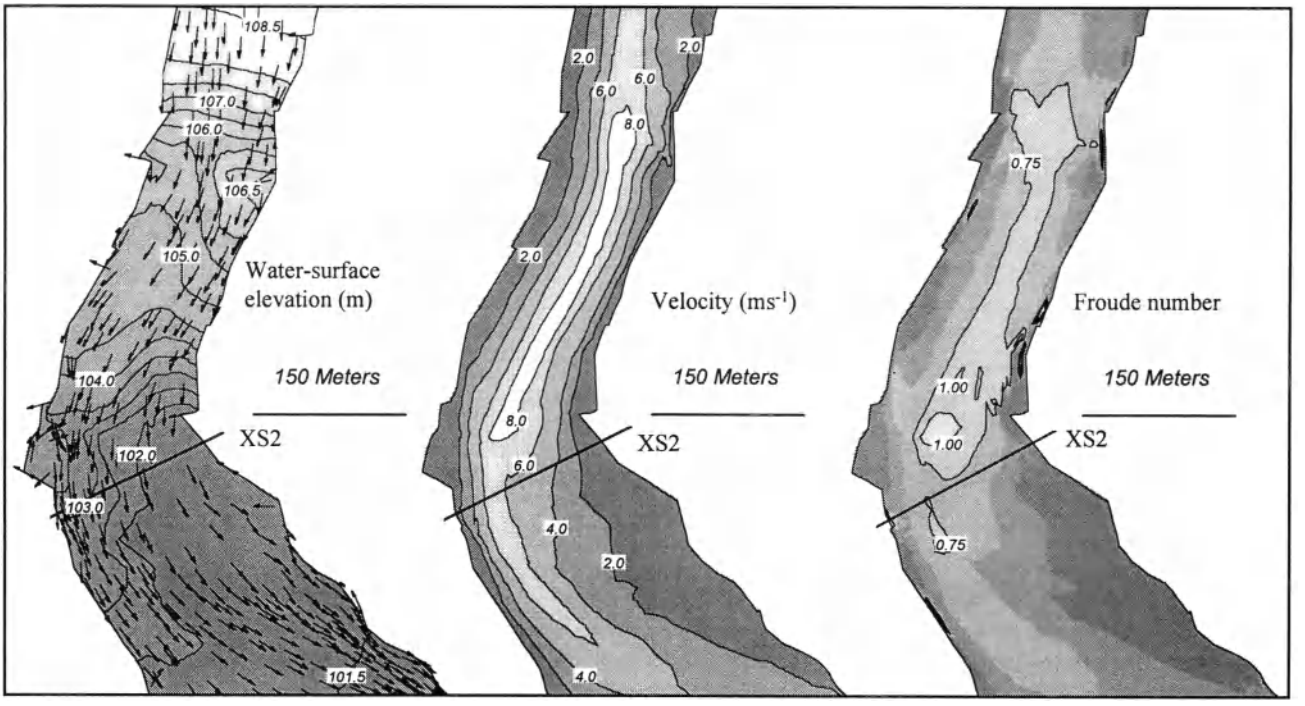

Figure 23. Contour and vector plots illustrating the 2-d pattern of flow hydraulics along the middle section of the Poudre River site. Patterns are based on RMA2 results for a discharge of 4000 m^3s^{-1} with $n = 0.05, 0.08$.

limitations of the models but also the relative quality of the available evidence and the difference in geologic and geomorphic environment at the two sites. Reliable field information about boundary conditions is essential if models are to be used for reconstructing flood peaks. In the absence of such information, it is important to have some sense of the potential range of answers that might be produced under reasonable alternative boundary conditions.

2. Both the 1-d and the 2-d model exhibit strong sensitivity to the choice of roughness coefficients. This was expected in the 1-d case but runs counter to the experience of previous authors in the case of the 2-d model. In fact the 2-d model as applied here appears to be even more sensitive to roughness than the 1-d model. The results from the Poudre example are in agreement with the results from the Coyote Narrows example on this point. However it would be premature to generalize based only on the examples presented here. Considering that the observed sensitivity is more pronounced as discharge increases, and that even the smallest discharge value used with this example is nearly twice the size of the flood of record, it is possible that the effect in question arises primarily under hydraulic conditions that are extreme by comparison with most common model applications. The results do suggest that anyone applying a flow model under comparable circumstances should perform a sensitivity analysis to determine how alternative sets of roughness coefficients affect the results.

3. The 2-d model, RMA2, showed little sensitivity to the choice of eddy viscosity coefficients. This was true particularly for water-surface elevation, but it was also observed that velocity profiles were less sensitive to eddy viscosity than to the choice of roughness coefficient. This runs counter to the results obtained using RMA2 at the Mohawk site in the Grand Canyon.

4. Matching of profiles between HEC-RAS and RMA2 was most successful at the lower discharges, but simple adjustments in the roughness parameters led to significant improvements in the match at higher discharges. If the closeness of the fit is regarded as an index of the quality of the results, then the highest roughness coefficients are to be recommended when modeling extremely high discharge, and slightly higher roughness for the 2-d model than for the 1-d model produces the best fit. Because the higher roughness suppresses and reduces the extent of supercritical flow, it is possible that both models are simply better behaved in the sense that they generate smoother profiles when roughness is higher, without necessarily providing an accurate simulation. But the results from the Coyote Narrows example suggest that the choice of higher roughness coefficients does lead not only to a better match between 1-d and 2-d models,

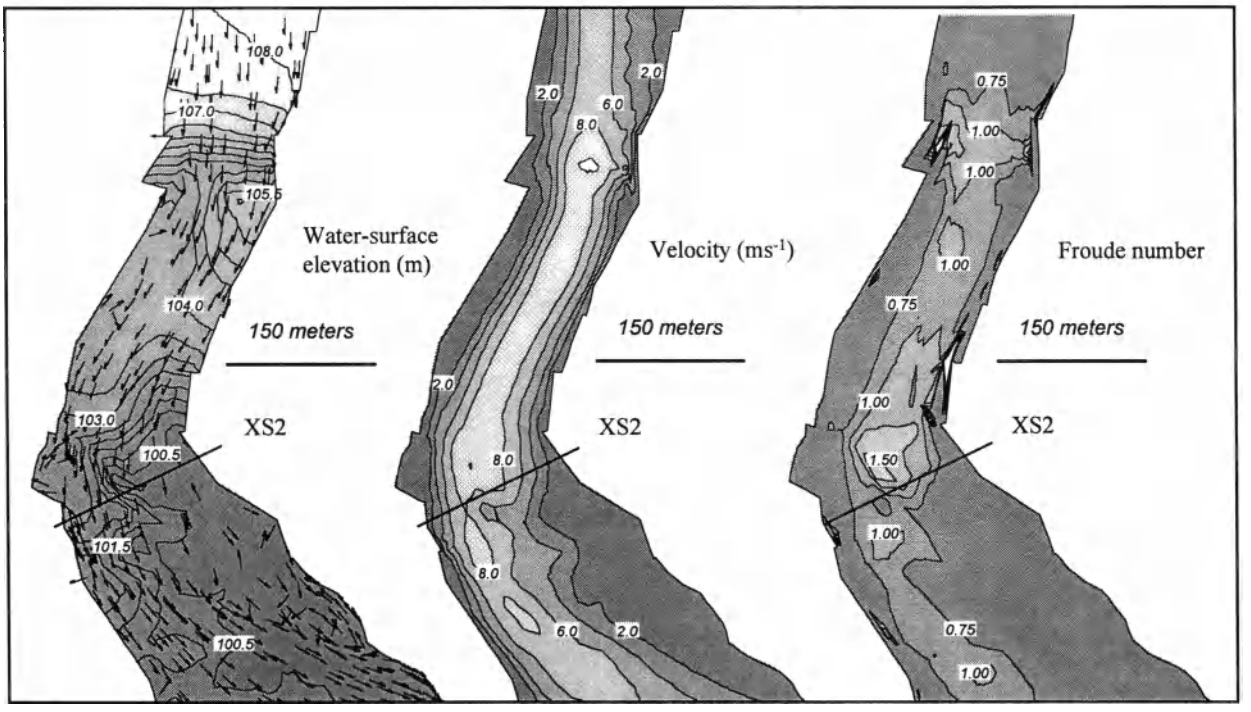

Figure 24. Contour plots illustrating the 2-d pattern of flow hydraulics along the middle section of the Poudre River site. Patterns are based on RMA2 results for a discharge of 4000 m^3s^{-1} with n = 0.04, 0.055. Although the vector pattern is not illustrated in order to improve legibility, it is similar to the pattern shown in fig. 23a.

but also to a closer fit between the models and the high-water marks. This subject is open to further study and requires comparison with field measurements.

5. The Poudre results do not allow us to determine the relative accuracy and reliability of the two models, but they do illustrate the potential of the 2-d model in situations where detailed visualization of the flow field is desirable. Although the topography of the water surface varies with the choice of roughness coefficient, superelevation clearly does occur at channel bends and there are other local perturbations within cross-sections that are not simulated by 1-d models, including closed depressions or "holes" in the water surface, periodic undulations that do not extend all the way across the channel, zones of recirculating flow, and flow transitions that are not oriented perpendicular to the channel thalweg.

6. It may be argued that a detailed comparison of RMA2 and HEC-RAS results along the steep middle section of the Poudre River site is not worth pursuing because the model results are simply outside the range of hydraulic conditions where useful conclusions can be drawn. Some of the RMA2 model runs do contain significant areas of supercritical flow; and although HEC-RAS is designed to handle transcritical flow, there is some question about how to interpret the 1-d longitudinal profile given the inability of 1-d models to simulate the existence of subcritical and supercritical flow in the same cross-section. However the model results are not simply chaotic but instead display features that in general form are consistent with what we might expect to see. Although some modest calibration of the roughness coefficients was involved in producing the comparisons shown in Figure 22, and despite some obvious discrepancies, the fit between the two models along the more turbulent 4000 m^3s^{-1} profile is closer than might have been anticipated. This does not prove that either model provides an accurate prediction of what would happen during a flood of this magnitude. But the persistence of some features of the flow field, even when different models are used over a range of parameter values and are applied to conditions far outside the realm of empirical measurement, leads to the suggestion that response of the water surface to the input boundary conditions is at least partly model-independent. The trends illustrated in figs. 22 and 25 suggest that the most important issue to be resolved in applying these two models is the characterization of

boundary roughness, and that the sensitivity of the flow pattern to this parameter is particularly acute in regions of the flow field where there is a possibility of critical flow.

5. CONCLUSIONS

The three examples discussed in this paper encompass a wide range of flow conditions, beginning with a study in the Grand Canyon where a detailed verification data set was available owing to an intensive program of flow measurements under conditions of steady flow. Moving from the Mohawk site to the Coyote Narrows and Poudre sites, we move further toward the extreme end of the spectrum with regard to flow regime, and there is a corresponding decline in the availability of baseline data for validating model results. At the Mohawk site we can identify the extent to which the model water surface and velocity distributions depart from measured values. At Coyote Narrows we are modeling discharges caused by flash floods in an ephemeral system that are not readily accessible for measurement, but we have a set of high-water marks that helps to constrain the choice of model parameters. At the Poudre site we are trying to reconstruct paleoflood flow based on limited stratigraphic evidence, and the range of discharges modeled falls well above the range of flows experienced in the historic record. Although some readers may regard this progression as moving from the concrete to the purely hypothetical, in fact one of the ultimate advantages of modeling lies precisely in its ability to cross this threshold and provide useful predictions for situations that occur rarely and for which detailed field measurements are difficult or impossible to obtain.

The examples illustrate that there is considerable uncertainty in predicting the velocity field even for the low-flow situation in the first example, and by extension the reader may be forgiven a much larger degree of skepticisim with regard to the flow fields in the third example.

Even in the Poudre example, however, there are major and persistent features in the flow field that are predicted by two different models across a range of parameter values, because both models are responding to the influence of the boundary conditions imposed by this bedrock-controlled system. There are also major differences that are sensitive to the parameter values specified, and these differences serve to point out where more attention needs to be focused. Although we cannot assess the accuracy of the flow field in all of its details, the types of hydraulic features illustrated may also be observed at lower flows in some steep bedrock channels. One objective of future research will be to identify both existing field data sets and new field sites for data collection where analogous flow structures can be explored in a controlled study and used for more rigorous calibration and testing of a variety of models.

The results presented here may also be used to provide limited guidance in deciding which class of model to apply in a particular study. The decision to use a 2-d model instead of a 1-d model should be based on a need for the kind of information that only the 2-d model can provide. In the Coyote Narrows example, the questions being asked did not require a 2-d approach, and the primary utility of that example is to see whether the two modeling approaches produce comparable results. Although there are undoubtedly some very complex flow structures that develop at high flow in this slot canyon, an understanding of those structures is not essential for purposes of matching a series of high-water marks distributed at various locations along the channel. The 2-d model did achieve a slightly better fit to the high-water marks than the 1-d model, but the main features of the longitudinal profile were predicted by both models and the improvement may not justify the additional effort involved. On the other hand a detailed investigation of geomorphic or sedimentological features associated with local constrictions, expansions, or undulations in the walls or bed of the channel might well benefit from a 2-d, or even a 3-d modeling approach. A case in point is the example described by *Dick et al.* [1997], where bedrock erosion rates along the Middle Gorge Indus River "are highly sensitive to very localized flow conditions... local flow turbulence strongly controls abrasion and block plucking. Given a particular discharge and sediment concentration, incision rates will be very sensitive to local slope and width variations over distances comparable to channel width." A more sophisticated modeling approach can be helpful in predicting these very localized flow conditions.

In the Poudre example, the longitudinal profile produced by 1-d modeling may be reasonable for the upstream and downstream sections, where there are only modest cross-channel gradients in the water-surface profile. Discrepancies between the 1-d and 2-d profiles along these less turbulent portions of the flow field leave some uncertainty as to which provides a better discharge estimate for matching a flood profile, but this can only be resolved with additional field evidence and there is no inherent reason why a 2-d analysis would be required. However the response of the 2-d flow pattern to boundary conditions along the middle section is more complex, and a single longitudinal profile representing cross-section average conditions cannot capture the major elements of this pattern. The best choice for this site would be a 2-d model capable of simulating both transcritical flow and wetting and drying. Modeling runs illustrated here were completed before such a model was available to the authors, but several are now becoming available and should be tested in comparable situations.

The analyses performed to evaluate model sensitivity to roughness and eddy viscosity coefficients are themselves

based on simplifying assumptions: for the most part, both roughness and eddy viscosity coefficients were assumed in each example to be uniform along the entire length of the study reach, with roughness taking on only two or three values linked to different surface types, while eddy viscosity was assigned a constant value for the entire flow field. The introduction of more complex distributions of these constant coefficients might have altered model performance. In defense of the choices made, additional permutations of the input variables would have made the study considerably longer and the comparisons more difficult to interpret; furthermore it is not clear whether anything fundamentally different would have been learned about model behavior. Assignment of eddy viscosity by Peclet number at the Mohawk site, for example, did not cause major changes in the modeled flow pattern. Future studies with detailed verification data may benefit from the the introduction of more sophisticated modeling options, such as calculating Manning's n as a function of depth or introducing a more sophisticated turbulence closure such as the k-ε model.

The case studies provided here cover only a limited subset of the available flow models or of the potential applications of flow models in bedrock channels. It is anticipated that the number of applications documented in the literature will grow as different classes of models become more widely available, as the software becomes easier to use, and as the detailed information about surface topography needed for modeling becomes increasingly accessible from a wide variety of sources. This trend will be assisted by technological improvements in field data collection, in remote sensing of surface characteristics at finer resolutions, and in the quality of digital topographic data available for large parts of the earth's surface. It is inevitable that, as flow models of increasing complexity become more popular and easier to use, it will also become easier to confuse simulation with reality. In some cases the models will actually be good enough to provide accurate answers, but the increasing sophistication of visualization tools will ensure that even inaccurate results can be made to look convincing. It is for this reason that we need a better understanding of model behavior in the particular geomorphic environments where the models are to be applied. Bedrock channels provide particular challenges that test the capabilities of many of the available models, and often the field data needed for verification are not available. The application of flow models will be most useful when carried out in tandem with the kinds of detailed field studies that are yielding important new information about rates and processes of bedrock channel evolution.

Acknowledgement. This paper was significantly improved with the help of comments from Deb Anthony and Bob Jarrett. We are grateful to Ellen Wohl for graciously providing her field data for use in this study.

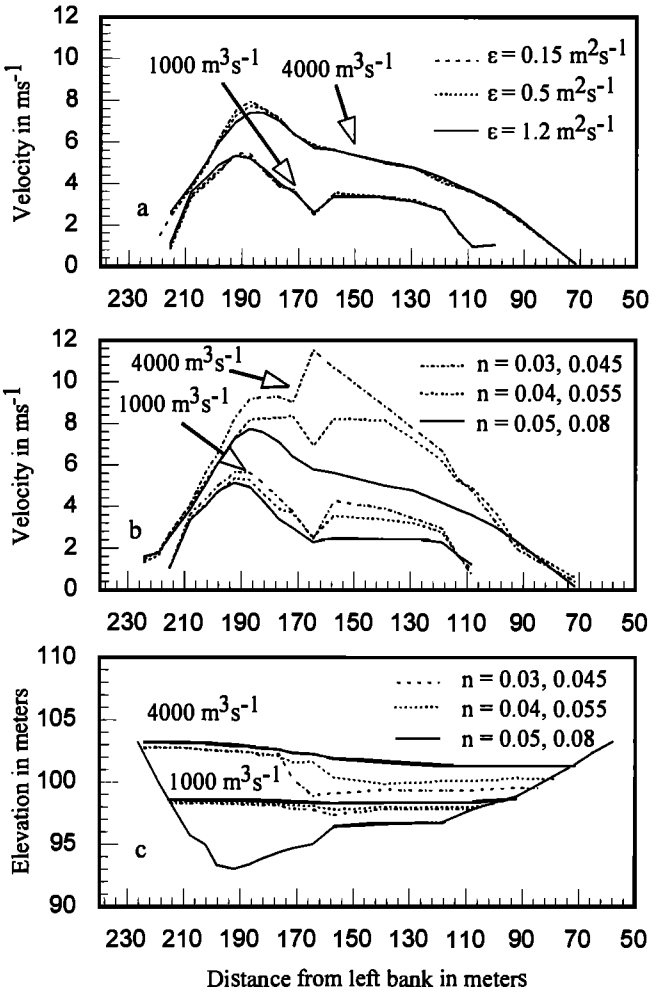

Figure 25. Distribution of velocity and water-surface elevation based on RMA2 results for two discharge values at XS2. a: Comparison of velocity profiles for three alternative eddy-viscosity coefficients. b: Comparison of velocity profiles for three alternative sets of roughness coefficients. c: Comparison of water-surface profiles for three alternative sets of roughness coefficients.

REFERENCES

Abbott, M.B., *Computational Hydraulics: Elements of the Theory of Free Surface Flows*, Ashgate, Aldershot, England, 1992.

Abbott, M.B., Range of tidal flow modeling, *J. Hydr. Eng.*, 123(4), 257-277, 1997.

Akanbi, A.A. and N.D. Katapodes, Model for flood propagation on initially dry land, *J. Hydr. Eng.*, 114, 689-706, 1988.

Anderson, J.D., Jr., *Computational Fluid Dynamics: the Basics With Applications*, McGraw-Hill, New York, 1995.

Anderson, J.D., Jr., Governing equations of fluid dynamics, in *Computational Fluid Dynamics: an Introduction*, edited by J.F. Wendt, pp.15-51, Springer-Verlag, Heidelberg, 1996.

Anderson, M.G. and P.D. Bates, Evaluating data constraints on two dimensional finite element models of floodplain flow, *Catena*, 22, 1-15, 1994.

ASCE Task Committee on Turbulence Models in Hydraulic Computations, Turbulence modeling of surface water flow and transport, Parts I-V, *J. Hydr. Eng.*, 114(9), 970-1073, 1988.

Baker, V.R., G. Benito, and A.N. Rudoy, Paleohydrology of late Pleistocene superflooding, Altay Mountains, Siberia; *Science*, 259, pp. 348-350, 1993.

Banihasemi, M.A., *Computation of Turbulent Flows in Irregular Open Channels*, Ph.D. dissertation, University of Queensland, Brisbane, Australia, 1994.

Bates, P.D., M.G. Anderson and J.-M. Hervouet, Computation of a flood event using a two-dimensional finite element model and its comparison to field data, *in Modelling Flood Propagation Over Initially Dry Areas*, edited by Molinaro, P. and L. Natale, American Society of Civil Engineers, New York, pp. 243-256, 1994

Bates, P.D., M.G. Anderson, L. Baird, D.E. Walling and D. Simm, Modelling floodplain flows using a two-dimensional finite element model, *Earth Surf. Proc. Landf.*, 17, 575-588, 1992.

Bates, P.D., M.G. Anderson, J.-M. Hervouet and J.C. Hawkes, Investigating the behaviour of two-dimensional element models of compound channel flow, *Earth Surf. Proc. Landf.*, 22, 3-17, 1997.

Bates, P.D. and M.G. Anderson, A two-dimensional finite element model for river flow inundation, *Proc. Roy. Soc. Lon. Series A*, 440, 481-491, 1993.

Beffa, C., Backwater computation for transcritical river flows, *J. Hydr. Eng*, 122(12), 745-748, 1996.

Benito, G., Energy expenditure and geomorphic work of the cataclysmic Missoula flooding in the Columbia River Gorge, USA, *Earth Surf. Proc. Landf.*, 22, 457-472, 1997.

Berger, R.C. and R.L. Stockstill, Finite-element model for high-velocity channels, *J. Hydr. Eng.*, 121(10), 710-716, 1995.

Brigham Young University, *Surface Water Modelling System v. 5.0 Reference Manual and Tutorials*, Engineering Computer Graphics Laboratory, Provo, Utah, 1997.

Brooks, A.N. and T.J.R. Hughes, Streamline Upwind Petrov Galerkin formulations for convection dominated flows with particular emphasis on the incompressible Navier-Stokes equations, *Computer Methods in Applied Mechanics and Engineering*, 32, 199-259, 1982.

Carling, P.A., Flow-separation berms downstream of a hydraulic jump in a bedrock channel, *Geomorphology*, 11, 245-253, 1995.

Cenderelli, D. and B.L. Cluer, , this volume, 1998.

Chaudhry, M.H., *Open-Channel Flow*, Prentice-Hall, Englewood Cliffs, N.J., 1993.

Chow, V.T., *Open-Channel Hydraulics*, McGraw-Hill, New York, 1959.

Cluer, B.L., Cyclic fluvial processes and bias in environmental monitoring, Colorado River in Grand Canyon, *J. Geol.*, 103, 411-421, 1995.

Cluer, B.L., *Eddy Bar Responses to the Sediment Dynamics of Pool-Riffle Environments*, Ph.D. dissertation, Colorado State University, Ft. Collins, 1997.

Costa, J.E., 1997, Hydraulic modeling for lahar hazards at Cascades volcanoes. *Environmental and Engineering Geoscience*, 3 (1), 21-30, 1997.

Dick, G.S., R.S. Anderson and K.X. Whipple, Fluvial bedrock erosion measurements, Indus River, Pakistan, reveal control by local flow conditions [abs.], *EOS Trans. AGU*, 78(44), Fall Meeting Supplement, 299, 1997.

Donnell, B.D., Finnie, J.L., Letter, J.V. Jr., McAnally, W.H.Jr., Roig, L.C. and Thomas, W.A., *Users Guide to RMA2 WES Version 4.3*, U.S. Army Corps of Engineers, Waterways Experiment Station Hydraulics Laboratory, 1997.

Ellis, M., X. Cai and R.S. Anderson, Graded longitudinal river profiles by coupled bedrock incision and bedload sediment transport [abs.], *EOS Trans. AGU*, 78(44), Fall Meeting Supplement, 299, 1997.

Ely, L.L., Y. Enzel, V.R. Baker, and D.R. Cayan, A 5000-year record of extreme floods and climate change in the southwestern United States, *Science*, 262, 410-412, 1993.

Enzel, Y., L.L. Ely, P.K. House, and V.R. Baker, Paleoflood evidence for a natural upper bound to flood magnitudes int he Colorado River Basin, *Water Resour. Res.*, 29(7), 2287-2297, 1993.

Feldhaus, R., J. Hottges, T. Brockhau, and G. Rouve, Finite element simulation of flow and pollution transport applied to a part of the River Rhine, in *Hydraulic and Environmental Modelling: Estuarine and River Waters*, edited by Falconer, R.A., K. Shiono, and R.G.S. Matthews, pp. 323-33, Ashgate Publishing, Aldershot, 1992.

Fischer, H.B., E.J. List, R.C.Y. Koh, J. Imberger, and N.H. Brooks, *Mixing in Inland and Coastal Waters*, Academic Press, New York, 1979.

Fraccarollo, L. and E.F. Toro, Experimental and numerical assessment of the shallow water model for two-dimensional dambreak type problems, *J. Hydr. Res.*, 33, 843-864, 1995.

Fread, D.L., *The NWS DAMBRK model: theoretical background/user documentation, HRL-256*, Hydrologic Research Laboratory, National Weather Service, Silver Spring, Md., 1988.

Fread, D.L., *Flow routing, in Handbook of Hydrology*, edited by D.R. Maidment, pp. 10.1-10.36, McGraw-Hill, New York, 1993

French, R.H., *Open Channel Hydraulics*, McGraw-Hill, New York, 1986.

Froehlich, D.C., *Finite Element Surface-Water Modeling System: Two-Dimensional Flow in a Horizontal Plane--Users Manual*: Federal Highway Administration Report FHWA-RD-88-177, 285 p., 1989.

Galland, J.-C., N. Goutal, and J.-M. Hervouet, TELEMAC. A new numerical model for solving shallow water equations, *Advances in Water Resources*, 14, 138-148, 1991.

Gee, D.M., M.G. Anderson and L. Baird, Large-scale floodplain modelling, *Earth Surf. Proc. Landf.*, 15, 513-523, 1990.

Ghanem, A., P. Steffler, F. Hicks and C. Katopodis, *Two-dimensional finite element modeling of flow in aquatic habitats*, Water Resources Engineering Report 95-S1, Department of Civil Engineering, University of Alberta, Edmonton, Alberta, 122 pp., 1995.

Ghanem, A., P. Steffler, F. Hicks and C. Katopodis, Two-dimensional hydraulic simulation of physical habitat conditions in flowing streams, *Regulated Rivers Research & Management*, 12, 185-200, 1996.

Gidas, N.K., M. Carreau, J.-C. Tessier, and V. Sapin, AquaDyn software of the 2DH hydrodynamic model, in Computational

Methods in Surface Flow and Transport Problems, *Proceedings of the 1996 11th International Conference on Computational Methods in Water Resources*, Cancun, Mexico, v.2, 199-206, Computational Mechanics Publishers, Southampton England, 1996.

Glancy, P.A. and R.P. Williams, Problems with indirect determination of peak streamflows in steep, desert stream channels, in *Hydraulic Engineering* '94, edited by G.V. Cotroneo and R.R. Rumer, v.1, 635-639, American Society of Civil Engineers, New York, 1994.

Graf, W.H., *Hydraulics of Sediment Transport*, McGraw-Hill, New York, 1971.

Grant, G.E., Critical flow constrains flow hydraulics in mobile-bed streams: A new hypothesis, *Water Resour. Res.*, 33(2), 1997.

Hervouet, J.M., TELEMAC, a fully vectorised finite element software for shallow water equations, in *Computer Methods in Water Resources II, Proceedings of the 2nd International Conference on Computer Methods in Water Resources*, Feb 20-22 1991, Marrakesh, Morocco, 147-158, Computational Mechanics Publishers, Southampton, England, 1991.

Hervouet, J.-M. And J.-M. Janin, Finite element algorithms for modelling flood propagation, in *Proceedings of the Specialty Conference on Modelling of Flood Propagation Over Initially Dry Areas*, Jun 29-Jul 1 1994, Milan, Italy, 102-108, American Society of Civil Engineers, New York, 1994.

Hicks, F.E. and P.M. Steffler, Characteristic Dissipative Galerkin scheme for open-channel flow, *J. Hydr. Eng.*, 118(2), 337-352, 1992.

Hicks, F.E. and P.M. Steffler, Comparison of finite element methods for the St. Venant equations, *Int. J. Num. Meth. Fluids*, 20, 99-113, 1995.

Hicks, F.E. and P.M. Steffler, One-dimensional dam-break solutions for variable width channels, *J. Hydr. Eng.*, 123(5), 464-468, 1997.

Hodskinson, A., Computational fluid dynamics as a tool for investigating separated flow in river bends, *Earth Surf. Proc. Landf.*, 21, 993-1000, 1996.

Howard, A.D., Modeling fluvial systems: rock-, gravel- and sand-bed channels, in *River channels: environment and process*, edited by K. Richards, pp. 69-94, Oxford, Basil Blackwell, 1987.

Howard, A.D., A detachment-limited model of drainage basin evolution, *Water Resour. Res.*, 30(7), 2261-2285, 1994.

Howard, A.D. and G. Kerby, Channel changes in badlands, *Geological Society of America Bulletin*, 94, 739-752., 1983.

Howard, A.D., W.E. Dietrich and M.A. Seidl, Modeling fluvial erosion on regional to continental scales, *J. Geophys. Res.*, 99(7), 971-986, 1994.

Hubbard, L.C. and C.R.Thorne, Flow patterns in a mountain stream, in *Hydraulic Engineering* '94, edited by G.V. Cotroneo and R.R. Rumer, v.2, 737-741, American Society of Civil Engineers, NewYork, 1994.

Hydrologic Engineering Center, *HEC-2 Water Surface Profiles: User's Manual*, U.S. Army Corps of Engineers, Davis, California, 1982.

Hydrologic Engineering Center, *HEC-RAS River Analysis System version 1.0*, Hydraulic Reference Manual, U.S. Army Corps of Engineers, Davis, California, 1995.

Hydrologic Engineering Center, *HEC-RAS River Analysis System v. 2.0 User's Manual*, U.S. Army Corps of Engineers, Davis, California, 1997.

Jarrett, R.D., Hydraulics of high-gradient streams, *J. Hydr. Eng.*, 110(11), 1519-1539, 1984.

Jarrett, R.D. and Costa, J.E., Hydrology, geomorphology, and dam-break modeling of the July 15, 1982 Lawn Lake Dam and Cascade Lake Dam failures, Larimer County , *U.S. Geological Survey Professional Paper* 1369, 78 p., 1986.

Jarrett, R.D. and R.E. Malde, Paleodischarge of the late Pleistocene Bonneville flood, Snake River, Idaho, computed from new evidence, *Geol. Soc. Amer. Bull.*, 99, 127-134, 1987.

Jenkins, G., Estimating eddy kinematic viscosity in compound channels, in *Advances in Hydro-Science and Engineering*, edited by Sam S.Y. Wang, Center for Computational Hydroscience and Engineering, University of Mississippi, volume I, part B, 1277-1282, 1993.

Jin, M. and D.L. Fread, Dynamic flood routing with explicit and implicit numerical solution schemes, *J. Hydr. Eng.*, 123(3), 166-173, 1997.

Kale, V.W., S. Mishra, V.R. Baker, S.N. Rajaguru, Y. Enzel, and L.Ely, Prehistoric flood deposits on the Choral River, Central Narmada Basin, India, *Current Science*, 65(11), 877-878, 1993.

Keefer, T.N., *The Relation of Turbulence to Diffusion in Open-Channel Flow*, Ph.D. dissertation, Colorado State University, Ft. Collins, 1971.

Kieffer, S.W., The 1983 hydraulic jump in Crystal Rapid - implications for river-running and geomorphic evolution in the Grand Canyon, *J. Geol.*, 93, 385-406, 1985.

Kieffer, S.W., Geological nozzles, *Rev. Geophys.*, 27, 3-38, 1989.

Kochel, R.C. and V.R. Baker, Paleoflood hydrology, *Science* 215, 353-361, 1982.

Kochel, R.C., V.R. Baker and P.C. Patton, Paleohydrology of southwestern Texas, *Water Resour. Res.*, 18, 1165-1193, 1982.

Libby, P.A., *Introduction to Turbulence*, Taylor and Francis, Washington, D.C., 1996.

Magilligan, F.J., 1992, Thresholds and the spatial variability of flood power during extreme floods, *Geomorphology*, 5, 373-390, 1992.

Miller, A.J., Debris-fan constrictions and flood hydraulics in river canyons: some implications from two-dimensional flow modelling, *Earth Surf. Proc. Landf.*, 19, 681-697, 1994.

Miller, A.J., Valley morphology and boundary conditions influencing spatial patterns of flood flow, in *Natural and Anthropogenic Influences in Fluvial Geomorphology*, Geophysical Monograph 89, edited by J.E. Costa, A.J. Miller, K.M. Potter and P.E. Wilcock, AGU, 57-81, 1995.

Molls, T. and M.H. Chaudhry, Depth-averaged open-channel flow model, *J. Hydr. Eng.*, 121(6), 453-465, 1995.

Molls, T., G. Zhao and F. Molls, Friction slope in depth-averaged flow, *J. Hydr. Eng.*, 124(1), 81-85, 1998.

Nelson, J.M., Experimental and theoretical investigation of lateral separation eddies [abs.], *EOS Trans. AGU*, 72(44), Fall Meeting Supplement, 219, 1991.

Nelson, J.M., R.R. McDonald, and D.M. Rubin, Computational prediction of flow and sediment transport patterns in lateral separation eddies, *EOS Trans. AGU*, 75(44), Fall Meeting Supplement, 268, 1994.

Norton, W.R., I.P. King, and G.T. Orlob, *A finite element model*

for lower Granite Reservoir, Water Resources Engineers, Inc., Walnut Creek, California, 1973.

O'Connor, J.E., *Hydrology, hydraulics, and geomorphology of the Bonneville flood*, Geological Society of America Special Paper 274, 1993.

O'Connor, J.E. and V.R. Baker, Magnitudes and implications of peak discharges from glacial Lake Missoula, *Geol. Soc. Amer. Bull.*, 104, 267-279, 1992.

O'Connor, J.E., L.L. Ely, E.E. Wohl, L.E. Stevens, T.S. Melis, V.S. Kale and V.R. Baker, A 4500-year record of large floods on the Colorado Riiver in the Grand Canyon, Arizona, *J. Geol.*, 102, 1-9, 1994.

O'Connor, J.E., and R.H. Webb, Hydraulic modeling for paleoflood analysis, in *Flood Geomorphology*, edited by V.R. Baker, R.C. Kochel, and P.C. Patton, pp. 393-418, Wiley, New York, 1988.

O'Connor, J.E., R.H. Webb, and V.R. Baker, Paleohydrology of pool and riffle development, Boulder Creek, Utah, *Geol. Soc. Amer. Bull.*, 97, 410-420, 1986.

Olsen, N.R.B., *Computational Fluid Dynamics in Hydraulic and Sedimentation Engineering*, Division of Hydraulic and Environmental Engineering, Norwegian University of Science and Technology, Trondheim, 1997.

Olsen, N.R.B. and S. Stokseth, Three-dimensional numerical modelling of water flow in a river with large bed roughness, *J. Hydr. Res.*, 33, 571-581, 1995.

Partridge, J.B. and V.R. Baker, Paleoflood hydrology of the Salt River, central Arizona, *Earth Surf. Proc. Landf.*, 12, 109-125, 1987.

Patton, P.C., V.R. Baker and R.C. Kochel, Slackwater deposits: a geomorphic technique for the interpretation of fluvial paleohydrology, in *Adjustments of the fluvial system*, edited by D.D. Rhodes and G.P. Williams, pp.225-253, Kendall/Hunt, Dubuque, Iowa, 1979.

Peyret, R. and T.D. Taylor, *Computational Methods for Fluid Flow*, Springer-Verlag, New York, 1983.

Rastogi, A.K. and W. Rodi, Predictions of heat and mass transfer in open channels, *Journal of the Hydraulics Division, ASCE*, 104(HY3), 397-420, 1978.

Rodi,W., A new algebraic relation of calculating the Reynolds stresses, *Zeitschrift fur Angewandte Mathematische Mechanik*, 56, 1219-1221, 1976.

Rodi, W., *Turbulence Models and Their Application in Hydraulics*, State-of-the-Art Paper, International Association for Hydraulic Research, Delft, The Netherlands, 1984.

Rodriguez-Iturbe, I., M. Marani, R. Rigon, and A. Rinaldo, Self-organized river basin landscape: fractal and multifractal characteristics, *Water Resour. Res.*, 30(12), 35331-3539, 1994.

Roig, L.C., Mathematical theory and numerical methods for the modeling of wetland hydraulics, in *Water Resources Engineering: Proceedings of the First International Conference*, Aug 14-18 1995, San Antonio, TX, USA, edited by W.H. Espey, Jr. and P.G. Combs, v. 1 pp.249-253, American Society of Civil Engineers, New York, 1995.

Rubin, D. M., J.M. Nelson and D.J. Topping, Relation of inversely graded deposits to suspended-sediment grain-size evolution during the 1996 flood experiment in Grand Canyon, *Geology*, 26(2), 99-103, 1998.

Samuels, P.G., Some analytical aspects of depth average flow models, in *Hydraulic and environmental modelling of coastal, estuarine and river waters*: Proceedings of the International Conference held at the University of Bradford, 19-21 September 1989, edited by R.A. Falconer, P. Goodwin and R.G.S. Matthew, pp. 411-418, Gower Technical, Aldershot, England, 1989.

Samuels, P.G. and K.S. Chawdhary, A backwater method for transcritical flows, in *Proceedings, Conference on River Flood Hydraulics*, edited by W.R. White, pp.79-89, Wiley, Chichester, 1990.

Schmidt, J.C., Recirculating flow and sedimentation in the Colorado River in Grand Canyon, Arizona, *J. Geol.*, 98, 709-724, 1990.

Schmidt, J.C. and D.M. Rubin, Regulated streamflow, fine-grained deposits, and effective discharge in canyons with abundant debris fans, in *Natural and Anthropogenic Influences in Fluvial Geomorphology*, edited by J.E. Costa, A.J. Miller, K.W. Potter, and P.R. Wilcock, AGU Monograph 89, 177-195, 1995.

Shearman, J.O., HY-7 - *User's Manual for WSPRO - a Computer Model for Water Surface Profile Computations*, U.S.Federal Highway Administration Report FHWA-IP-89-027, 1990

Simon, A. and J.H. Hardison III, Critical and supercritical flow in two unstable mountain rivers, Toutle River system, Washington, in *Hydraulic Engineering* '94, edited by G.V. Cotroneo and R.R. Rumer, v.2, 737-741, American Society of Civil Engineers, New York, 1994.

Sinha, S.K., F. Sotiropoulos, and A.J. Odgaard, Three-dimensional numerical model for flow through natural rivers, *J. Hydr. Eng.*, 124(1), 13-24, 1998.

Sklar, L. and W.E. Dietrich, The influence of downstream variations in sediment supply and transport capacity on bedrock channel longitudinal profiles [abs.], *EOS Trans. AGU*, 78, 299, 1997.

Steffler, P.M., *CDG2D Depth Averaged Hydrodynamic Model Reference Model*, University of Alberta, Edmonton, 1997.

Stockstill, R.L. and R.C. Berger, *HIVEL2D: a two-dimensional flow model for high-velocity channels*, Technical Report REMR-HY-12, U.S. Army Engineer Waterways Experiment Station, Vicksburg, 1994.

Stockstill, R.L., R.C. Berger, and R.E. Nece, Two-dimensional flood model for trapezoidal high-velocity channels, *J. Hydr. Eng.*, 123(10), 844-852, 1997.

Tinkler, K.J., Indirect velocity measurement from standing waves in rockbed rivers, *J. Hydr. Eng.*, 123 (10), 1997a.

Tinkler, K.J., Critical flow in rockbed streams with estimated values for Manning's *n*, *Geomorphology*, 20, 147-164, 1997b.

Tinkler, K.J. and Wohl, E.E., A primer on rock bed channels, *Bedrock channels conference: abstracts and field trip guidebook*, Colorado State University, Fort Collins, 1996.

Topping, D.J., *Physics of flow, sediment transport, hydraulic geometry, and channel geomorphic adjustment during flash floods in an ephemeral river, the Paria River, Utah and Arizona*, unpublished Ph.D. dissertation, University of Washington, Seattle, 1997.

Trieste, D.T., Evaluation of supercritical/subcritical flows in a high-gradient channel, *J. Hydr. Eng.*, 118(8), 1107-1118, 1992.

Trieste, D.T., 1994, Supercritical flows versus subcritical flows in natural channels, *in Hydraulic Engineering* '94, edited by G.V.

Cotroneo and R.R. Rumer, v.2, 732-736, American Society of Civil Engineers, New York, 1994.

Trieste, D.T. and Jarrett, R.D., Roughness coefficients of large floods, in *Irrigation Systems for the 21st Century*, Proceedings of the 1987 Irrigation and Drainage Division Specialty Conference, Portland, OR, 32-40, American Society of Civil Engineers, New York, 1987.

Vreugdenhil, C.B. and J.H.A. Wijbenga, Computation of flow patterns in rivers, *J. Hydr. Eng.*, 108, 1296-1310, 1982.

Wahl, K. L., Variation of Froude number with discharge for large-gradient streams, in *Proceedings of the National Conference on Hydraulic Engineering*, July 25-30, 1993, v.2, 1517-1522, American Society of Civil Engineers, New York, 1993.

Wahl, K.L., Bias in regression estimates of Manning's *n*, in *Hydraulic Engineering '94*, edited by G.V. Cotroneo and R.R. Rumer, v.2, 727-731, American Society of Civil Engineers, New York, 1994.

Waterways Experiment Station, *HIVEL2D v2.0 Users Manual*, Coastal and Hydraulics Laboratory, Waterways Experiment Station, U.S. Army Corps of Engineers, Vicksburg, 1997.

Wendt, J.F.(ed.), *Computational Fluid Dynamics: an Introduction*, Springer-Verlag, Heidelberg, 1996.

Whitlow, C.D. and D.W. Knight, An investigation of the effect of different discretizations in river models and a comparison of non-conservative and conservative formulation of the St. Venant equations, in *Hydraulic and Environmental Modelling: Estuarine and River Waters*: Proceedings of the Second International Conference, v.2, edited by R.A. Falconer, K. Shiono and R.G.S. Matthew, pp. 115-126, Ashgate, Aldershot, 1992.

Wiele, S.M., J.B. Graf, and J.D. Smith, Sand deposition in the Colorado River in the Grand Canyon from flooding of the Little Colorado River, *Water Resour. Res.*, 32(12), 3579-3596, 1996.

Willgoose, G., R.L. Bras, and I. Rodriguez-Iturbe, A coupled channel network growth and hillslope evolution model, 1, Theory, *Water Resour. Res.*, 27(7), 1671-1684, 1991a.

Willgoose, G., R.L. Bras, and I. Rodriguez-Iturbe, A coupled channel network growth and hillslope evolution model, 2, Applications, *Water Resour. Res.*, 27(7), 1685-1696, 1991b.

Wohl, E.E., N. Greenbaum, A.P. Schick, and V.R. Baker, Controls on bedrock channel incision along Nahal Paran, Israel, *Earth Surf. Proc. Landf.*, 19, 1-13, 1994.

Wurbs, R. A., Dam-breach flood wave models, *J. Hydr. Eng.*, 113(1), 29-46, 1987.

Ye, J. and J.A. McCorquodale, Depth-averaged hydrodynamic model in curvilinear collocated grid, *J. Hydr. Eng.*, 123(5), 380-388, 1997.

Yen, B.C., Hydraulics for excess water management, in *Water Resources* Handbook, edited by L.W. Mays, pp. 25.1-25.55, McGraw-Hill, New York, 1996.

Younus, M, and M.H. Chaudhry, A depth-averaged k-ε turbulence model for the computation of free-surface flow, *J. Hydr. Res.*, 32, 415-444, 1994.

Zawada, P.K., Paleoflood hydrology in South Africa, *Geotimes,* 42 (6), 24-28, 1997.

A.J. Miller, Department of Geography and Environmental Systems, University of Maryland Baltimore County, Baltimore, Maryland 21209 (e-mail: miller@umbc.edu)

B. L. Cluer, National Park Service, Water Resources Division, Suite 250, Fort Collins, Colorado 80525

Depositional Processes and Sediment Supply in Resistant-Boundary Channels: Examples from Two Case Studies

Daniel A. Cenderelli

Department of Geology, University of Alabama, Tuscaloosa, Alabama

Brian L. Cluer

U.S. National Park Service, Water Resources Division, Ft. Collins, Colorado

Coarse-grained deposits produced by a rare, extreme flood in the Mt. Everest region of Nepal and fine-grained deposits produced by frequent, moderate floods along the Colorado River in and near the Grand Canyon, U.S.A. illustrate a wide range of depositional patterns, processes, and mechanics along resistant-boundary channels. Deposition processes in each of these case studies were strongly influenced by sediment supply. The availability of sediment was an important factor in both case studies in determining the occurrence, location, stability, and sedimentologic characteristics of deposits produced by their respective floods. A glacial-lake outburst flood in the Mt. Everest region of Nepal eroded, transported, and deposited large quantities of boulders, cobbles, pebbles, and sand along the outburst-flood route. Depositional macroforms produced by this flood include: (1) expansion bars at abrupt expansions immediately downstream of constricted reaches, (2) longitudinal bars at local flow expansions along valley margins, (3) point bars along the inner margins of valley bends, (4) pendant bars immediately downstream of obstructions, and (5) imbricate clusters of cobbles and boulders immediately upstream of obstructions. Along the upper 16 km of the outburst-flood route, deposition is more extensive and deposits are thicker, are more poorly sorted, have more finely-skewed distributions, and have a higher percentage of fine-grained sediment than deposits below 16 km. Additionally, deposits along the upper 16 km of the flood route are reverse graded and coarsen in the downstream direction, whereas deposits below 16 km lack grading or are normally graded. These deposit characteristics suggest that the flood waters along the upper 16 km had higher sediment concentrations and were closer to their transport capacity than the flood waters below 16 km. Most resistant-boundary channels are supply limited with respect to entrainment and transport of cobble- and boulder-sized particles during frequent, low to moderate flows. However, superimposed on this supply limited coarse-grained system is a dynamic fine-grained system in which eddy bars along the channel margins are eroded and redeposited during the rising limb of a given

1. INTRODUCTION

Interactions between valley and channel geometry, flow hydraulics, flow magnitude and frequency, sediment size, and sediment supply are important controls for determining the

Rivers Over Rock: Fluvial Processes in Bedrock Channels
Geophysical Monograph 107

flood. Eddy sand bar deposits along the Colorado River in and near the Grand Canyon are an excellent example of this dynamic erosional and depositional cycle that occurs during frequent, moderate floods. The erosional and depositional cycle of eddy bars during a given flood is strongly controlled by sediment delivered to the plunge pool adjacent to the eddy bar. Sediment delivered to the plunge pool on the rising limb of the flood alters the flow patterns and hydraulics in the pool and causes the eddy bar to scour. As discharge increases, plunge pools are scoured and deposition resumes in the recirculating eddies. If fine-grained sediment supply is reduced along a river because of flow regulation structures, this dynamic cycle of erosion and deposition associated with pools and eddy sand bars no longer occurs and the eddy bars become stable.

spatial distribution, morphologic and sedimentologic characteristics, and preservation of deposits in channels and valley bottoms. Fluvial deposits in resistant-boundary channels and valleys have similar morphologic and sedimentologic characteristics as those in alluvial channels. However, the fluvial processes responsible for the formation of deposits in resistant-boundary channels and valleys can be markedly different from those in alluvial environments.

Alluvial channels are those that have formed their channel in bed and bank sediment that the stream can readily entrain and transport for a wide range of flows [*Leopold and Maddock*, 1953; *Schumm*, 1977; *Schumm and Winkley*, 1994]. As a result, alluvial channels adjust their geometry, pattern, and gradient to flows that transport the most sediment, which are typically frequent, low to moderate flows that are close to bankfull conditions [*Leopold and Maddock*, 1953; *Hey*, 1982]. During these flows, deposits in alluvial systems can be destroyed, modified, and redeposited in a relatively short time period as flow conditions change [e.g. *Leopold and Maddock*, 1953; *Fahnestock*, 1963; *Smith*, 1974; *Hein and Walker*, 1977; *Davoren and Mosley*, 1986; *Ferguson et al.*, 1992]. For the most part, alluvial channels are not supply limited systems because of the availability of sediment along the channel bottom and banks, and the ability of the stream to readily entrain and transport this sediment for a wide range of flows.

In contrast, coarse-grained (primarily cobbles and boulders) and fine-grained (primarily sand and fine pebbles) deposition in resistant-boundary channels and valleys is typically associated with infrequent, extreme floods. Infrequent, extreme floods in resistant-boundary valleys generate flows that are "out-of-bank" and extend across the entire valley bottom. Such flows cause extensive erosion and deposition along the course of the flow [e.g. *Krumbein*, 1942; *Stewart and LaMarche*, 1967; *Scott and Gravlee*, 1968; *Baker*, 1977; *Martini*, 1977; *Shroba et al.*, 1979; *Iseya et al.*, 1990; *Miller*, 1990; *Miller and Parkinson*, 1993]. Erosion occurs primarily in constricted reaches where valley side slopes are comprised of coarse, unconsolidated sediment. The erosion that occurs in constricted reaches increases the amount of sediment transported and deposited by the flood. Much of this sediment is conveyed through the constricted reaches because flow energy and competence are high. Deposition of coarse and fine sediment occurs where flow diverges or separates causing a reduction in flow energy such that the competence of the flow drops below the critical thresholds needed to maintain sediment transport. Coarse-grained deposition typically occurs at locations where the channel and/or valley widen, upstream and downstream of obstructions, and along the margins of channel bends [*Martini*, 1977; *Baker*, 1978, 1984; *Church and Jones*, 1982; *Carling*, 1987, 1989, 1995; *Wohl*, 1992, *O'Connor*, 1993]. Fine-grained sediment (slackwater deposits) is typically deposited in areas upstream of constrictions where ponding occurs, along channel margins downstream of protrusions where eddying occurs, and at the mouth of tributaries that are back-flooded [*Kochel et al.*, 1982; *Ely and Baker*, 1985; *O'Connor et al.*, 1986; *Baker and Kochel*, 1988; *O'Connor*, 1993].

Resistant-boundary channels and valleys generally consist of a combination of bedrock, coarse colluvium, and coarse alluvium that are not readily entrained during frequent, low to moderate flows. Thus, resistant-boundary channels are supply limited, with respect to coarse sediment, during frequent, low to moderate flows. Only during infrequent, extreme flows may the sediment supply become abundant in resistant-boundary channels [*Baker*, 1988]. The sediment source is typically from constricted reaches in which valley side slopes comprised of coarse, unconsolidated sediment are eroded by flood waters. However, the supply of coarse-sediment is spatially discontinuous [*Baker*, 1988] and strongly controlled by the availability of sediment in constricted reaches, the ability of the flow to entrain and transport the sediment, and the number and proximity of depositional areas to the sediment source.

Resistant-boundary channels are generally covered by a veneer of cobbles and boulders that are not readily entrained during frequent, low to moderate flows, and thus are supply limited with respect to coarse sediment. However, in some environments, quantities of fine-grained sediment are entrained, transported, and deposited during frequent, low to

moderate flows. Fine-grained deposits typically occur in zones where flow recirculates along channel margins and immediately upstream and downstream of constrictions [*Schmidt*, 1990; *Cluer*, 1995]. The dynamics of fine-grained sedimentation during frequent, low to moderate flows in a resistant-boundary channel have been documented along the Colorado River below Glen Canyon Dam to assess the effects of damming and flow regulation [*Howard and Dolan*, 1981; *Schmidt*, 1990; *Cluer*, 1995]. *Howard and Dolan* [1981] documented that reduced supply of fine-grained sediment and reduced discharges by the dam have decreased the areal extent of fine-grained deposits downstream of the dam because of scour and vegetation encroachment. However, as shown by *Cluer* [1995], annual time-scale evaluations are misleading because they do not account for the cyclic erosional and depositional processes that substantially effect many eddy sand bars on shorter time scales of a few days to several weeks.

Depositional patterns in resistant-boundary channels can be evaluated at various spatial and temporal scales, for different flow magnitudes and frequencies, and for a wide range of sediment sizes. In this paper, we will examine coarse-grained deposition that occurred during an infrequent, extreme flood in the Mt. Everest Region of Nepal and fine-grained deposition that occurred during frequent, low to moderate floods along the Colorado River in and near the Grand Canyon, U.S.A. Each case study is unique in that it evaluates the importance of sediment supply in affecting coarse- and fine-grained deposition in resistant-boundary channels.

2. COARSE-GRAINED DEPOSITS

2.1. *Physical Setting and Flood Hydrology*

The Mt. Everest region in eastern Nepal (Figure 1) is situated in the High Himalayas, primarily underlain by Precambrian crystalline rocks [*Vuichard*, 1986], and characterized by high relief. The three principle drainages in the area, Bhoti Kosi, Dudh Kosi, and Imja Khola, are deeply incised and have valley floors that are 4000 to 5000 m lower in elevation than the surrounding mountains. Valleys at elevations higher than 3600 m were glaciated during the Pleistocene, are distinctly U-shaped, and are bounded by a combination of bedrock, coarse-grained colluvium, and coarse-grained glacio-fluvial sediment. Currently, alpine glaciers are positioned at elevations above 5000 m. Most of these glaciers have receded from their Little Ice Age maximum positions, resulting in the formation of numerous moraine-dammed lakes [*Mayewski and Jeschke*, 1979; *Fushimi et al.*, 1985]. Below 3600 m, valleys are V-shaped and bounded primarily by bedrock and secondarily by terraces comprised of coarse-grained sediment.

Runoff in the study area generally consists of low flows from late fall to early spring and high flows from late spring to early fall produced by monsoonal precipitation and snowmelt. The annual peak discharge of floods from snowmelt and monsoonal precipitation along the Dudh Kosi at an elevation of 2700 m was estimated to be 205 m^3/s [*Cenderelli and Wohl*, 1997]. In the past 20 years, two large-magnitude floods have occurred in the Mount Everest region as the result of the failure of moraine-dammed lakes. The erosional and depositional effects of each of these floods have been described by *Fushimi et al.*, [1985], *Zimmermann et al.* [1986], *Vuichard and Zimmermann* [1986, 1987], *Ives* [1986], and *Cenderelli and Wohl* [1998].

The most recent outburst flood occurred on 4 August 1985 when a moraine-dammed lake located below the Langmoche Glacier failed and released approximately 5,000,000 m^3 of water into the Langmoche Khola, Bhoti Kosi, and Dudh Kosi [*Ives*, 1986; *Vuichard and Zimmermann*, 1986, 1987](Figure 1). Along the upper 16 km of the flood route, the outburst flood caused extensive erosion and deposition. Below 16 km, erosion and deposition were minor to moderate when compared to the upper 16 km. Using the one-dimensional step-backwater model HEC-RAS [*Hydrologic Engineering Center*, 1995], *Cenderelli and Wohl* [1997] estimated the peak discharge of the outburst flood at eight reaches along the course of the flow. Along the upper 16 km of the outburst flood route, the peak discharge of the outburst flood ranged from 2250 to 2400 m^3/s and was 25 to 60 times greater than the peak discharges of seasonal snowmelt and monsoonal precipitation floods (Figure 2). By 27 km downstream from the breached moraine, the peak discharge attenuated to 1375 m^3/s and was about seven times greater than the typical peak discharges of seasonal snowmelt and monsoonal floods (Figure 2).

2.2. *Erosional and Depositional Patterns*

Two representative reaches along the 1985 glacial-lake outburst flood route were selected to illustrate the spatial distribution of erosional and depositional features produced by this outburst flood. Reach A is located on the Bhoti Kosi approximately eleven km downstream from the breached moraine (Figure 1). Reach A has an average gradient of 0.059, a valley width ranging from 46 to 222 m, and valley boundaries consisting primarily of coarse-grained glacio-fluvial terraces or coarse-grained colluvium (Figure 3; Table 1). The peak discharge of the glacial-lake outburst flood at reach A was estimated at 2250 m^3/s and the flood waters extended across the entire valley bottom. Reach B is located on the Dudh Kosi approximately 27 km downstream from the breached moraine (Figure 1). Reach B has valley boundaries of bedrock or coarse-grained glacio-fluvial terraces, an

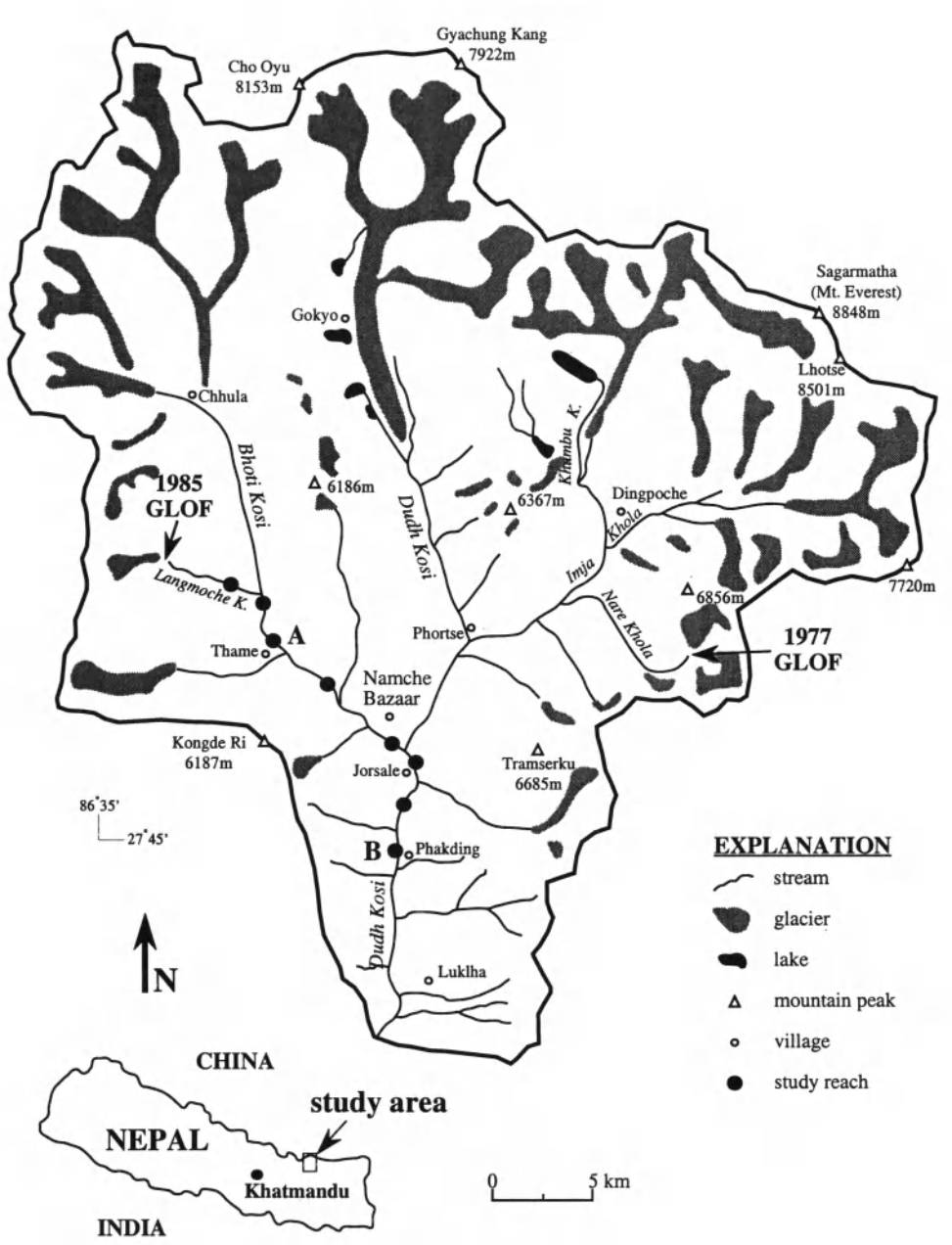

Figure 1. Map of the study area showing the locations of reaches studied along the 1985 glacial-lake outburst floods. Reach A and reach B are the primary reaches discussed in this paper.

average gradient of 0.029, and a valley width ranging from 41 to 87 m (Figure 4; Table 1). At reach B, the peak discharge of the glacial-lake outburst flood was estimated at 1375 m^3/s.

Along reach A, erosional features are most apparent where the valley is steep, narrow, and bounded by unconsolidated sediment (Figure 5). At these locations, the lower margins of the valley side slopes were undercut, which destabilized the upper portions of the slopes. As a result, sediment has fallen from the upper slopes, accumulated along the base of the valley walls, and influenced post-flood valley bottom morphology (Figures 3 and 5).

In contrast, there was much less erosion of valley side slopes from the outburst flood in reach B (compare Figure 3 to Figure 4), probably due to the downstream attenuation of

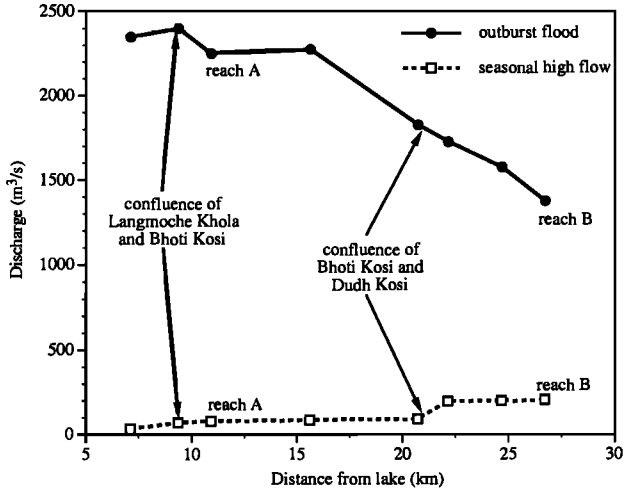

Figure 2. Peak discharges of the the 1985 glacial-lake outburst flood and seasonal high flow floods along eight reaches of the outburst-flood route.

the outburst flood combined with more resistant valley walls. Nevertheless, portions of lower glacio-fluvial terrace surfaces were eroded by as much as three meters, and the flow formed a distinct channel of cobbles and boulders (Figures 4 and 6). Substantial erosion of valley bottom surfaces is commonly associated with extreme floods in resistant-boundary valleys [*Nanson*, 1986; *Miller*, 1995]. *Miller* [1995] showed that catastrophic erosion of valley bottom surfaces occurred along the North Fork South Branch of the Potomac River when the valley walls directed a substantial portion of the flow onto the pre-flood surfaces because the main channel was oblique to the valley orientation. Similarly, erosion of valley bottom surfaces along reach B occurred where the main channel was oblique to the dominant valley trend (Figure 6).

The deposits at reach A and reach B are depositional macroforms [*Baker*, 1978, 1984; *Church and Jones*, 1982] and consist primarily of expansion bars and longitudinal bars and secondarily of point bars, pendant bars, and imbricate clusters (Figures 5 and 6). This classification is similar to those used by *Martini* [1977], *Baker* [1977, 1984], and *Church and Jones* [1982] and is based on deposit form and the position of the deposit in the flow field during deposit formation. The deposits at reach A and reach B are composed primarily of cobbles and boulders with varying amounts of sand and pebbles. The majority of the deposits have plan forms that are parallel or subparallel to valley alignment (Figures 5 and 6). Deposition is more extensive and deposits are thicker along reach A than along reach B. Deposits at both reaches overlie older pre-outburst flood glacio-fluvial surfaces that are three to five meters above the present-day channel.

2.2.1. *Expansion bars.* *Baker* [1978, 1984], *Elfström* [1987], and *O'Connor* [1993] have used the term expansion bar or boulder delta to describe massive depositional features located at abrupt expansions immediately downstream of constricted reaches. Descriptions of these deposits indicate that the surfaces of expansion bars consist of multiple linear and lenticular bars separated by shallow channels. A well-developed expansion bar formed along reach A where the valley widened by a factor of two (Figure 5). This abrupt expansion resulted in a rapid reduction of flow energy and flow competence which, in turn, caused rapid, extensive deposition. The expansion-bar deposit consists of multiple, linear boulder bars separated by parallel swales that are two to three meters lower than the adjacent bar crests (Figure 3). The thickest accumulations of sediment along the outburst-flood route are associated with the expansion bars, where deposits are up to three meters thick. The irregular surface of the expansion bar may reflect the topography of the underlying pre-flood surface (see XS-15, XS-11, and XS-10 in Figure 5). Flow energy during deposition was probably higher in the swales than the adjacent bar crests because of greater flow depths in the swales. Thus, as the expansion bar aggraded, the higher portions of the bar caused flow to converge into the swales forming secondary channels. As a result, these low areas of the expansion bars have a weakly developed step-pool channel morphology that formed when the secondary channels incised into and reworked sediment (Figure 7).

2.2.2. *Longitudinal bars.* Longitudinal bars are narrow, linear to curvilinear features that formed at local flow expansions along valley margins (Figures 5, 6, and 8). Flow was considerably slower along the channel margins when compared to the main concentration of flow and possibly recirculating. Longitudinal bars commonly form at local expansions because secondary cross-valley currents transport cobbles and boulders from the main concentration of flow into a shear zone that separates the main concentration of flow from the reduced flow region [*Carling*, 1987]. Longitudinal bars along reach A and reach B are at least five times longer than they are wide, are 0.3 to 1.5 meters thick, and have steep fronts and flanks indicating deposition along or aligned with a longitudinal shear zone (Figures 5, 6, and 8). Multiple longitudinal bars adjacent to each other probably indicate deposition at different flood stages of the outburst flood; the outer bars formed at a higher stage of the flood and the inner bars formed at lower stages (Figures 5 and 6).

2.2.3. *Point bars, pendant bars, and imbricate clusters.* Rarer depositional forms include point bars, pendant bars, and imbricate clusters along reach A and reach B (Figures 5 and 6). Point bars form along the inner margins of valley bends where flow energy is reduced and secondary cross currents transport sediment from the main channel to this

Figure 3. Downstream view of reach A along the 1985 glacial-lake outburst flood which is located 11 km from the breached moraine. In the foreground, the valley width ranges from 150 to 225 m. Up to three meters of primarily cobbles and boulders were deposited across the entire valley bottom. The deposit is an expansion bar consisting of multiple linear bars separated by chute channels. In the background, note the eroded glacio-fluvial terrace along the left bank where the valley is less than 100 m wide.

reduced flow region [*Knighton*, 1984; *Dietrich and Smith*, 1984; *de Jong and Ergenzinger*, 1995]. The well-developed point bars along reach A (Figure 5) may have formed when some of the sediment eroded from the outer valley terrace by the flood was transported across the channel to the inner valley margin by transverse currents. Pendant bars along reach A and reach B form immediately downstream from large rock fall obstructions (Figures 5 and 6). These obstructions cause flow separation, and recirculating flow that moves particles into the area downstream from the obstruction where flow velocities are considerably less than those in the main concentration of flow (*Baker*, 1978, 1984; *O'Connor*, 1993; *de Jong and Ergenzinger*, 1995]. Small, imbricate clusters of cobbles and boulders were deposited immediately upstream from large rock fall obstructions in the main channel along reach A and reach B (Figures 5 and 6).

2.2.4. *Fine-grained deposits*. There were few fine-grained deposits in areas where they would typically be found such as areas upstream of constrictions, downstream of constrictions, or along channel margins where ponding or eddying were likely. The absence of fine deposits indicates that sand and gravel was limited and deposition of these sediments occurred in conjunction with cobble and boulder deposition.

Immediately below the maximum stage of seasonal high flow floods that occur from snowmelt and monsoonal precipitation in the study area, there are abundant sand and pebble deposits along the channel margins immediately upstream from local constrictions and downstream from obstructions. These fine-grained deposits were not studied and simply noted during the investigation of the coarse-grained deposits produced by the 1985 outburst flood. At a given depositional site, the sand and pebble deposits are probably destroyed, modified, and redeposited during the duration of flooding from seasonal snowmelt and monsoonal precipitation. The dynamic erosional and depositional processes associated with fine-grained deposits for frequent, moderate flows were not the focus of the study in Nepal, however, we will discuss these processes along the Colorado River in and near the Grand Canyon later in this chapter.

2.3. *Sedimentology, Flow Processes, and Depositional Mechanics*

The reach averaged sedimentologic characteristics of deposits sampled along reach A and reach B are summarized

Table 1. Physical and hydrologic characteristics for two reaches along the 1985 glacial-lake outburst flood route.

Reach variables	Drainage area (km^2)	Distance from breached moraine (km)	Length (m)	Valley width (m)	Bed slope	Energy slope	Discharge outburst flood (m^3/s)	Discharge seasonal high flow (m^3/s)	Unit stream power, outburst flood (W/m^2)	Unit stream power, seasonal high flow (W/m^2)
Reach A										
ave.	295	11	1565	113	0.059	0.056	2250	80	12246	1647
std. dev.				41	0.014	0.012			7431	564
max.				222	0.100	0.075			39512	2653
min.				46	0.029	0.035			6171	738
Reach B										
ave.	1151	27	745	66	0.029	0.027	1375	205	5233	1813
std. dev.				13	0.011	0.009			1890	905
max.				87	0.057	0.040			8978	3232
min.				41	0.014	0.013			2130	663

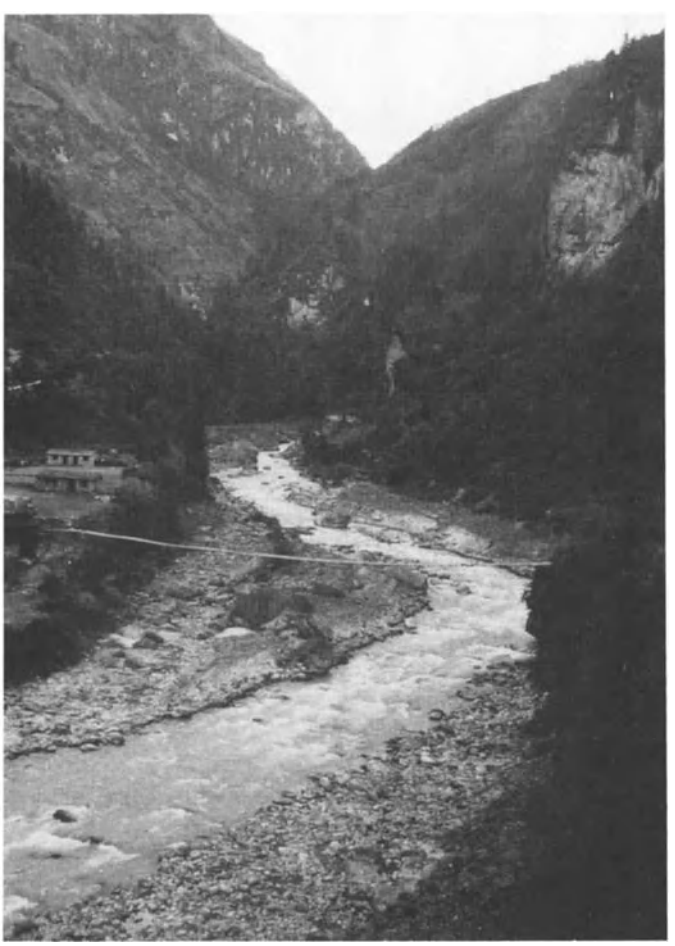

in Table 2. The deposits at reach A and reach B are clast-supported and composed primarily of cobbles and boulders, but also contain considerable amounts of sand and pebbles, particularly at reach A. A total of 19 sites were sampled at reach A; thirteen sites on the expansion bar, three sites on a point bar, and three sites along the channel margin. The expansion bar at reach A is coarser than the point bar and channel deposits. The longitudinal bars that make up the expansion bar at reach A are typically reverse graded and coarsen in the downstream direction (Figure 7). The point bars at reach A lack grading, but fine in the downstream direction. Fourteen of the seventeen sites sampled along reach B were on longitudinal bars and the other three sites were along the channel margin. The longitudinal bars at reach A lack grading, appear massive, and show no trends with respect to particle size in the downstream direction.

Deposits along the upper 16 km of the outburst-flood route are more poorly sorted, finely skewed, and have a higher percentage of fine-grained sediment (less than 64 mm) than deposits below 16 km (Figure 9). Deposits along the upper 16

Figure 4. Upstream view of reach B along the 1985 glacial-lake outburst flood route which is located 27 km from the breached moraine. The footbridge that extends across the valley bottom has a length of appoximately 70 m. Deposition consists primarily of longitudinal bars that were deposited on the surfaces of lower glacio-fluvial terraces along the valley margins. Along the right bank in the vicinity of the footbridge, the lower glacio-fluvial terrrace was eroded when the flood waters overtopped this surface. The overflow channel is approximately 12 to 15 m wide and up to 3.5 m deep.

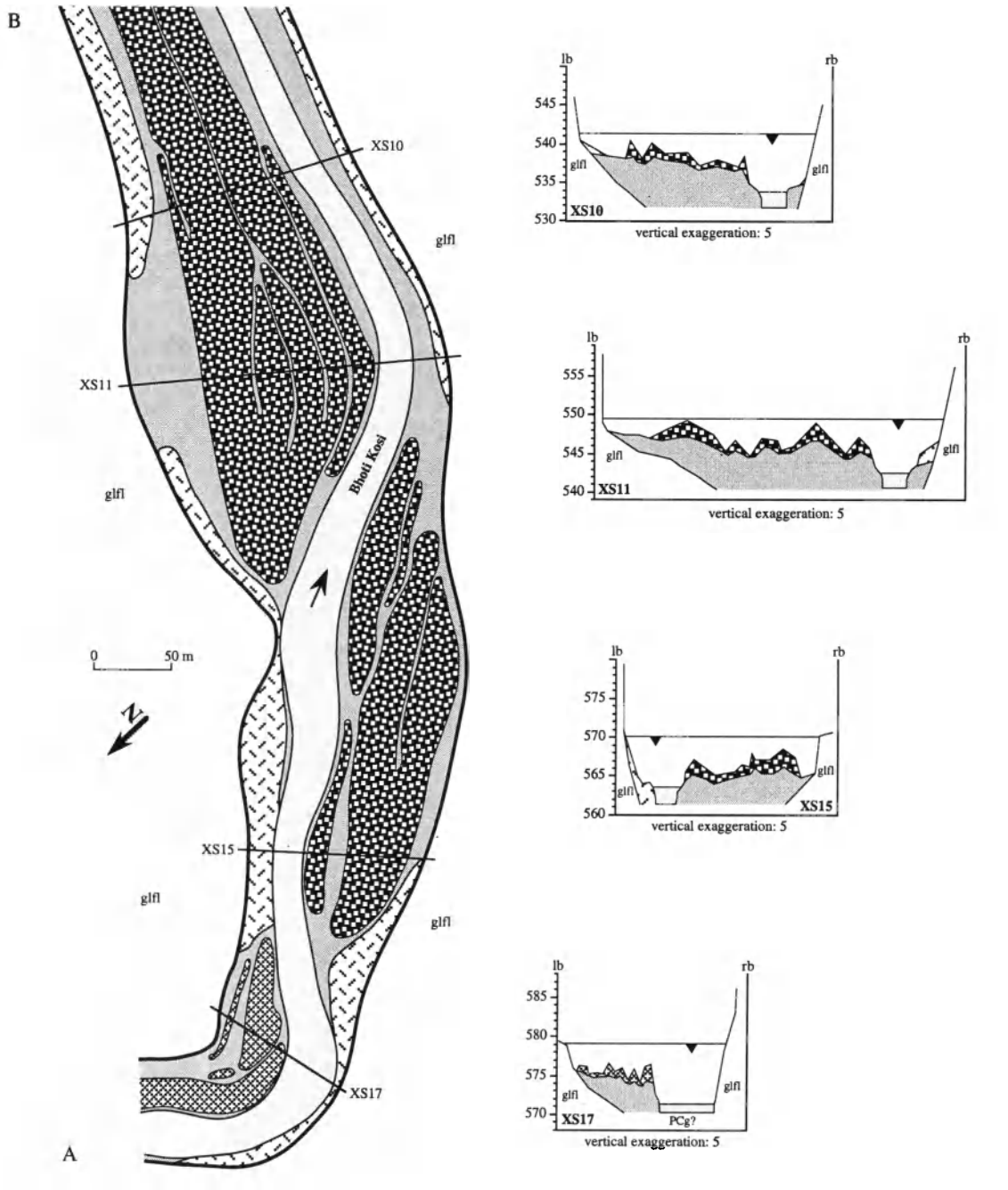

Figure 5. Geomorphic map of reach A illustrating the distribution of erosional and depositional features produced by the 1985 glacial-lake outburst flood. Reach A is located approximately 11 km from the breached moraine.

km of the flood route are reverse graded and coarsen in the downstream direction (Figure 7), whereas deposits below 16 km lack grading or are normally graded. Additionally, deposition is more extensive and the deposits are thicker along the upper 16 km of the outburst-flood route than below 16 km (compare Figures 3 and 5 to Figures 4 and 6). These sedimentologic and morphologic differences suggest that the flood waters that produced the deposits along the upper 16 km of the outburst-flood route had a higher sediment concentration than below 16 km. The inferred higher

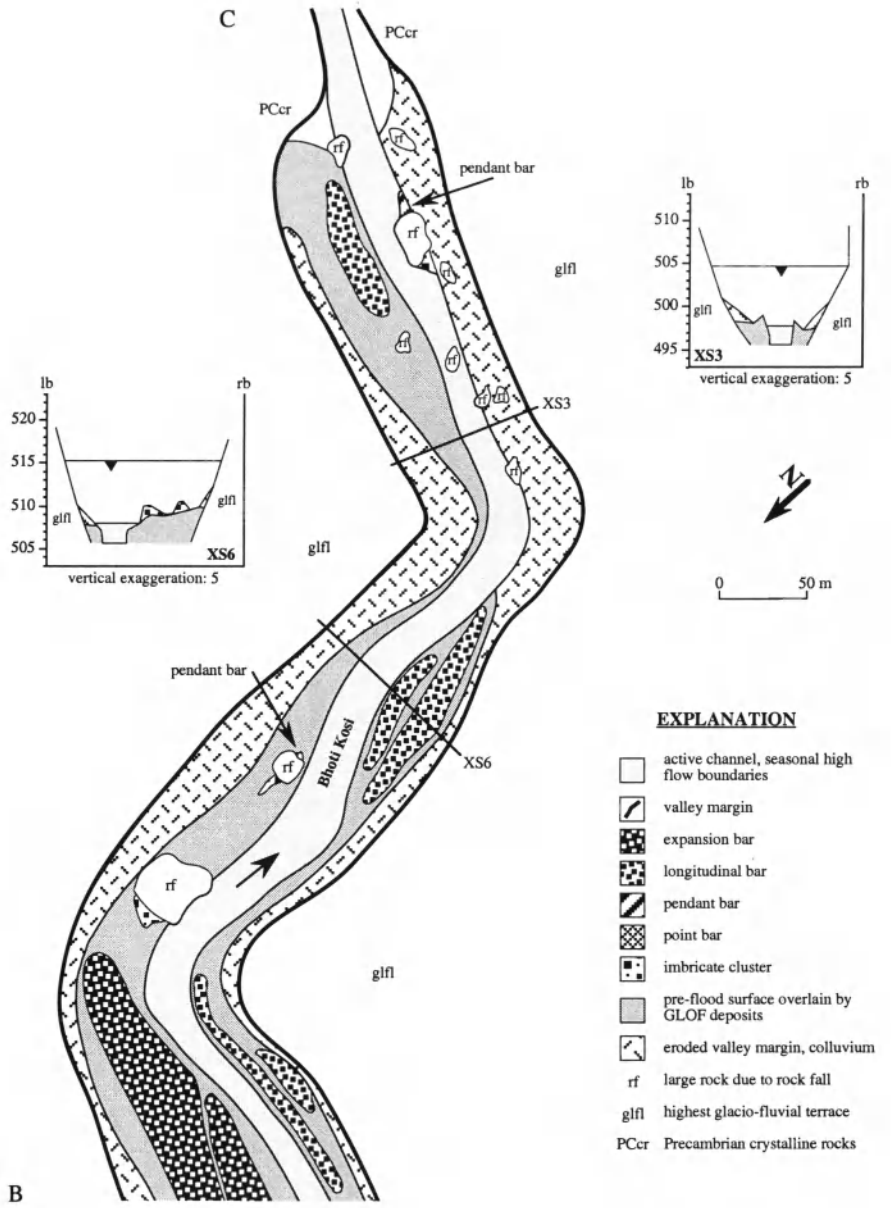

Figure 5. Continued.

sediment concentration of the flood waters along the upper 16 km of the outburst-flood route may have approached hyperconcentrated-flow conditions. *Cenderelli and Wohl* [1998] used the term transitional flow to describe the flow conditions of the outburst flood along the upper 16 km of the flood route because the sedimentologic and morphologic features of the deposits produced by the outburst flood were not distinctly water flood (especially when compared to the deposits below 16 km from the breached moraine) or hyperconcentrated flow.

In their report on the depositional features produced by the 1964 flood on the Rubicon River, California, U.S.A, *Scott and Gravlee* [1968] described clast-supported, reverse graded berms. These berms were deposited on pre-flood surfaces and *Scott and Gravlee* [1968] suggested that the berms represented deposition of bedload gravel waves. *Iseya et al.*

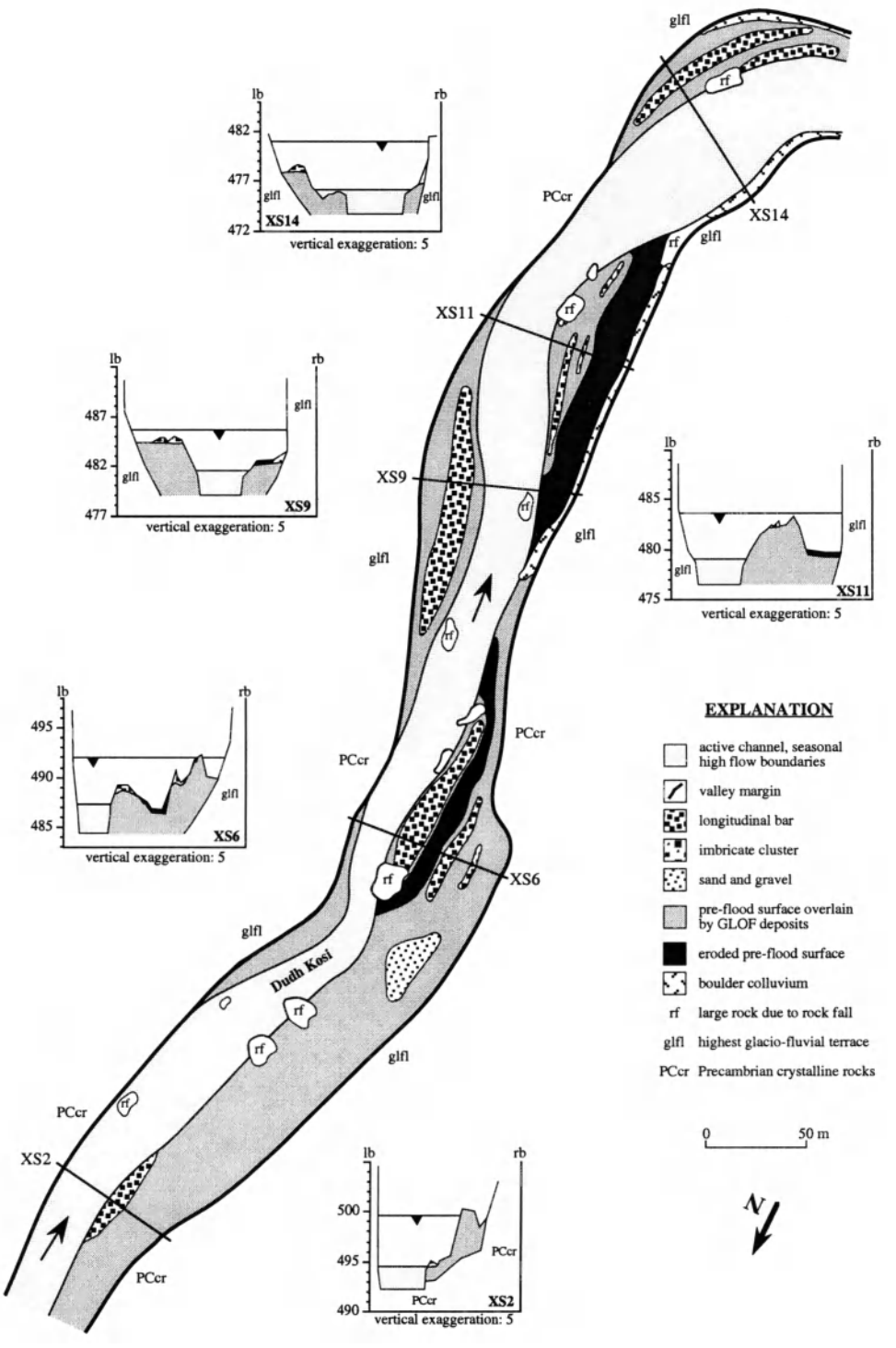

Figure 6. Geomorphic map of reach B illustrating the distribution of erosional and depositional features produced by the 1985 glacial-lake outburst flood. Reach B is located approximately 27 km from the breached moraine.

Figure 7. Side view of a linear bar that is part of a larger expansion bar. The bar is composed primarily of cobbles and boulders, is clast-supported, is reverse graded, and coarsens in the downstream direction. The pre-outburst flood surface is just above the head of the person. The low area adjacent to the linear bar is a chute channel with weakly developed, step-pool morphology. The chute channel probably formed during the peak stages of the outburst flood.

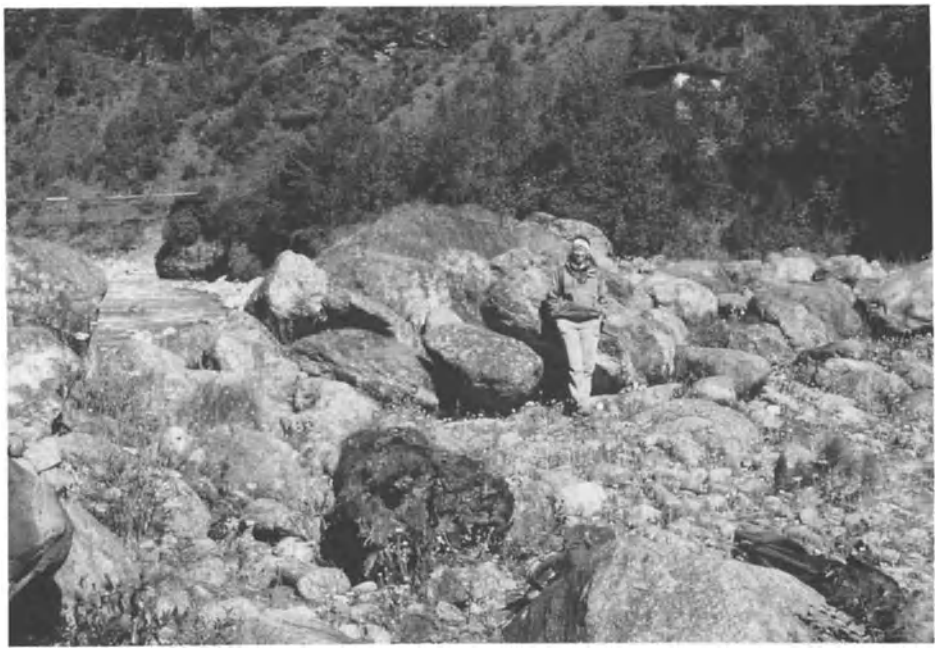

Figure 8. A longitudinal bar deposited on a pre-outburst flood surface that is four to five meters higher than the channel bottom.

Table 2. Summary of sedimentologic characteristics at two reaches along the 1985 glacial-lake outburst flood route.

Reach, variables	Number of sampling sites	Percent finer than 64 mm	d_{50} (mm)	d_{84} (mm)	Mean size (mm)	Sorting (ϕ units)	Skew-ness	Mean of 10 largest clasts (mm)
Reach A								
ave.	19	22.3	292	698	188	-2.55	-0.492	1043
std. dev.		9.5	156	308	146	0.78	0.166	272
max.		38.0	776	1574	638	-3.91	-0.721	1517
min.		5.1	98	223	62	-1.36	-0.140	673
Reach B								
ave.	17	17.7	220	480	173	-1.82	-0.318	646
std. dev.		7.3	143	261	108	0.63	0.268	270
max.		27.9	653	989	536	-2.89	-0.675	1095
min.		6.9	96	182	48	-0.85	-0.041	267

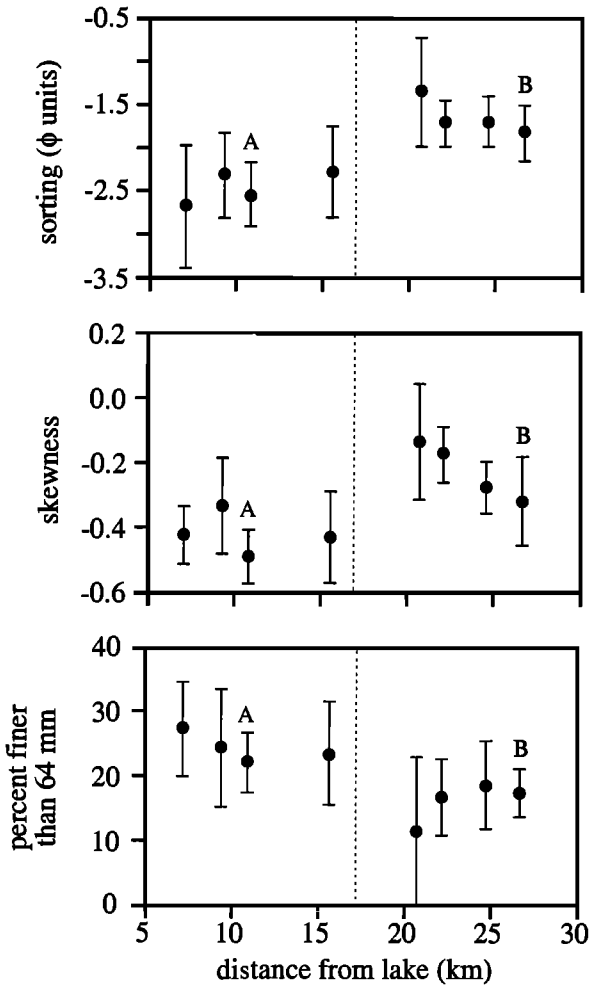

[1990] described multiple, linear, lobate cobble-boulder deposits produced by an extreme flood in a gravel-bed stream in Japan. These deposits are clast-supported, poorly sorted, reverse graded or massive, and become coarser in the downstream direction. The deposits were interpreted as being formed from a highly concentrated, deep bedload-flow process or a less dense, coarse-grained, hyperconcentrated-flow process. The deposits produced by the 1985 outburst flood along the upper 16 km of the flood route appear to be similar to those described by *Scott and Gravlee* [1968] and *Iseya et al.* [1990].

In flows approaching hyperconcentrated-flow conditions, turbulence is thought to be reduced because of the high sediment concentration, but remains an important sediment-support mechanism during transport, along with dispersive forces generated by grain-to-grain contact and buoyancy [*Bagnold*, 1954; *Scott and Gravlee*, 1968; *Smith*, 1986; *Iseya et al.*, 1990]. These sediment-support mechanisms cause the largest clasts to disperse to the surface during transport. Additionally, if deposition is rapid, the smaller particles are trapped between the larger particles [*Iseya et al*, 1990]. The poorly sorted nature and high percentage of fine-grained material at the surface of deposits along the upper 16 km of the 1985 outburst-flood route suggests that the sediment concentration profile was relatively uniform as turbulence and

Figure 9. Average reach values and 95 percent confidence intervals of sorting, skewness, and percentage of particles less than 64 mm in diameter at the eight reaches studied along the 1985 glacial-lake outburst flood route.

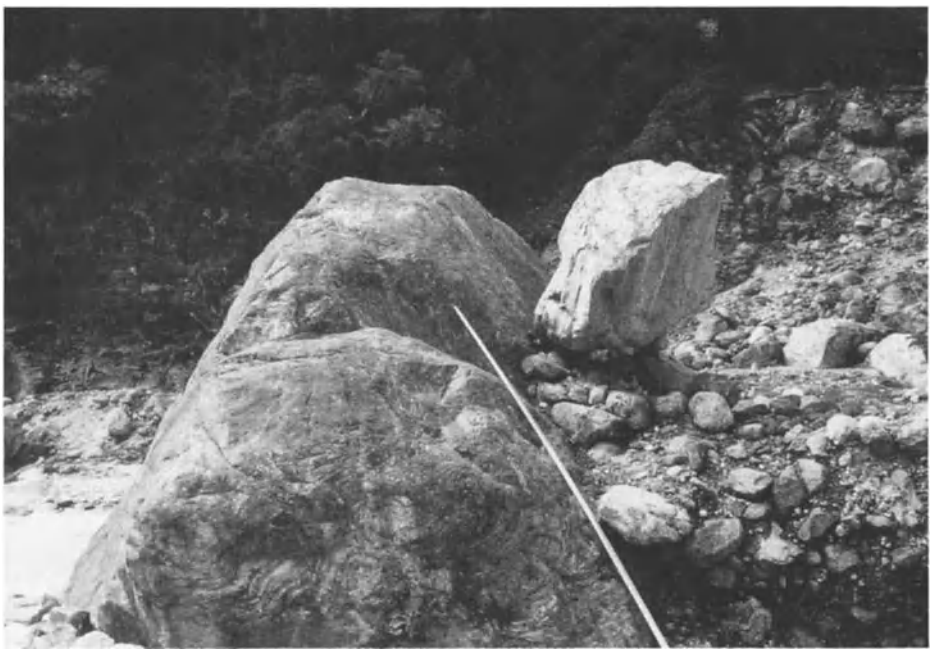

Figure 10. A boulder deposited 4.5 m above the channel bottom on the surface of a lower glacio-fluvial terrace. Perched boulders provide sedimentary evidence of intense turbulence or macroturbulence along the flood route.

dispersive forces transported cobbles and boulders above the bed just prior to deposition. The reverse grading displayed by the deposits along the upper 16 km of the outburst-flood route is additional evidence that dispersive pressures and buoyancy were lifting cobbles and boulders above the bed just prior to deposition (Figure 7).

In water floods with low sediment concentrations, turbulence is the principal sediment support-mechanism and particles are deposited individually through grain-by-grain tractive processes [*Smith*, 1986; *Costa*, 1988]. Extreme flows in high-gradient channels with irregular boundaries that transport low quantities of sediment are capable of generating large-scale turbulent conditions referred to as macroturbulence [*Matthes*, 1947; *Scott and Gravlee*, 1968; *Baker*, 1977, 1978, 1984; *Carling and Grodek*, 1994]. Macroturbulence is capable of entraining and transporting cobbles and boulders in suspension and depositing this material onto surfaces well above the channel bottom [*Krumbein*, 1942; *Matthes*, 1947; *Stewart and LaMarche*, 1967; *Scott and Gravlee*, 1968; *Baker*, 1977, 1978; 1984; *Carling*, 1987]. There is abundant evidence of macroturbulence occurring in the reaches below 16 km from the breached moraine; longitudinal bars (Figure 8) and perched boulders (Figure 10) were deposited on pre-flood surfaces three to five meters above the channel bottom. Thus, below 16 km from the breached moraine, the transport capacity of the flood waters was much greater than the sediment supply, probably resulting in macroturbulence to expend excess flow energy. In contrast, there was no sedimentary evidence of macroturbulence along the upper 16 km of the outburst-flood route. This suggests that the flood waters were close to their transport capacity and suppressed macroturbulence despite the high-energy gradients and irregular channel boundaries.

2.4. *Sediment Supply and Valley Bottom Aggradation or Degradation*

Deposition along the outburst-flood route was dependent upon sediment availability, not transport capacity. Along the upper 16 km of the outburst flood route, there is an abundance of glacial and glacio-fluvial sediment along the valley margins and valley bottom. Erosion of unconsolidated sediment along valley margins in narrow, steep reaches caused the flood waters to become loaded with coarse sediment and approach hyperconcentrated-flow conditions. Thus, along the upper segments of reach A, sediment transport was not supply limited and probably close to capacity. When the flood waters overtopped pre-outburst flood surfaces along the wider segments of reach A, deposition occurred on the pre-outburst flood surfaces. Valley bottom aggradation was spatially continuous and more

extensive along the depositional reaches of reach A when compared to reach B (Figures 5 and 6). The extensive deposition that occurred along reach A temporarily reduced the sediment concentration of the flood waters and increased its erosive abilities as the flood waters entered the narrow, steep lower segment of reach A (Figure 5). As a result, valley side slopes comprised of unconsolidated sediment were severely eroded by the flood waters along the lower segments of reach A (Figure 5). This spatial pattern of valley side slope erosion in narrow, steep valley reaches and deposition in wide, less steep valley segments was repeated along the upper 16 km of the outburst-flood routes because of the abundance of unconsolidated sediment along narrow, steep valley walls.

Between 15 and 16 km from the breached moraine, the sediment concentration of the outburst-flood was substantially reduced because of extensive deposition in a wider, less steep reach. Below 16 km, the sediment concentration of the flood waters remained low when the flow entered a steep, narrow, unglaciated bedrock gorge with limited sediment available for erosion and incorporation into the flood waters. Along reach B, sediment transport was supply limited, but local inputs of sediment from the chute channels eroded into pre-flood surfaces did occur and produced distinct deposits immediately downstream from the chute channels (Figure 6). Thus, vertical aggradation along the valley bottom of reach B was spatially discontinuous and strongly controlled by the erosion of sediment from the valley bottom immediately upstream.

Valley bottom degradation occurred only below 16 km from the breached moraine because the inferred reduced sediment concentration of the outburst flood waters likely enhanced the erosion of the pre-outburst flood surfaces when the flood waters overtopped these surfaces. In contrast, along the upper 16 km of the outburst-flood route there was no evidence of chute channels eroded into pre-outburst flood surfaces. This lack of erosion is attributed to the high sediment concentration of the flood waters that overtopped the pre-outburst flood surfaces, which prevented erosion of these surfaces.

3. FINE-GRAINED DEPOSITS

3.1. *Geomorphic Setting and Processes*

Resistant-boundary channels are often characterized by a repeating pattern of long, low velocity pooled reaches punctuated by short, abrupt drops through rapids and riffles. The rapids create the physical controls that govern the transport, sorting, and deposition of fine-grained sediments. Each fine-grained deposit has unique time scales of stability and motion for different particle-size classes. A classic example of an incised canyon is the Grand Canyon in Arizona, U.S.A. It is over 1500 m deep in places and the incision by the Colorado River has occurred over the past nine million years [*Breed,* 1974]. The Colorado River drops from an elevation of approximately 1000 m at the Utah-Arizona border to less than 300 m at the end of its 450 km course through the Grand Canyon. Approximately 90 percent of the elevation loss in the Grand Canyon occurs in the rapids, which only cover 10 percent of the horizontal distance [*Leopold,* 1969].

3.2. *Coarse-Grained Features: Rapids, Debris Fans, Cobble Bars*

Within the Grand Canyon, rapids are one of the physical controls for transport, sorting, and deposition of fine-grained sediments. After his 1869 journey down the Green and Colorado Rivers, John Wesley Powell [1875] suggested that mass movement processes from tributary streams and steep side-canyons periodically delivered large volumes of coarse sediment to the river, forming debris fans that locally obstruct the main channel. *Dolan et al.* [1978] showed the affinity of side canyon location for geologic structures, and *Webb et al.* [1989] found that reworking of debris fans by large floods supplies cobbles and gravel to the river, producing gravel-cobble bars and associated secondary rapids and riffles.

Debris fans and cobble bars in the river channel create flow constrictions, which create spatial variations in flow patterns and shear stress that result in sediment sorting and depositional processes along the channel margins. *Schmidt and Rubin* [1995] argued that this repeating pattern is a basic channel unit, a fan-eddy complex (Figure 11). The fundamental hydraulic controls of the fan-eddy complex consist of an upstream pool created by the damming effect of the constriction, a rapid that begins at the site of maximum constriction, and a channel expansion and plunge pool immediately downstream from the rapids.

3.3. *Fine-Grained Features: Channel Margin Sand Bars*

Flow accelerates through constricted channel cross sections at rapids [*Kieffer, 1985*], resulting in downstream scour holes in the main channel and flow separation where the channel widens [*Leopold,* 1969; *Howard and Dolan,* 1981; *Wilson,* 1986]. Between the point of flow separation and the point where flow reattaches to the bank is a zone of low velocity, recirculating flow [*Schmidt,* 1990]. Lateral flow separation also occurs along the upstream lobe of debris fans, creating low velocity zones and backwater pools with recirculating flow. Low velocities in these flow separation zones promote sand deposition from the suspended load [*Leopold,* 1969].

The repeating pattern of channel constrictions causes a corresponding pattern in the location, form, and large-scale

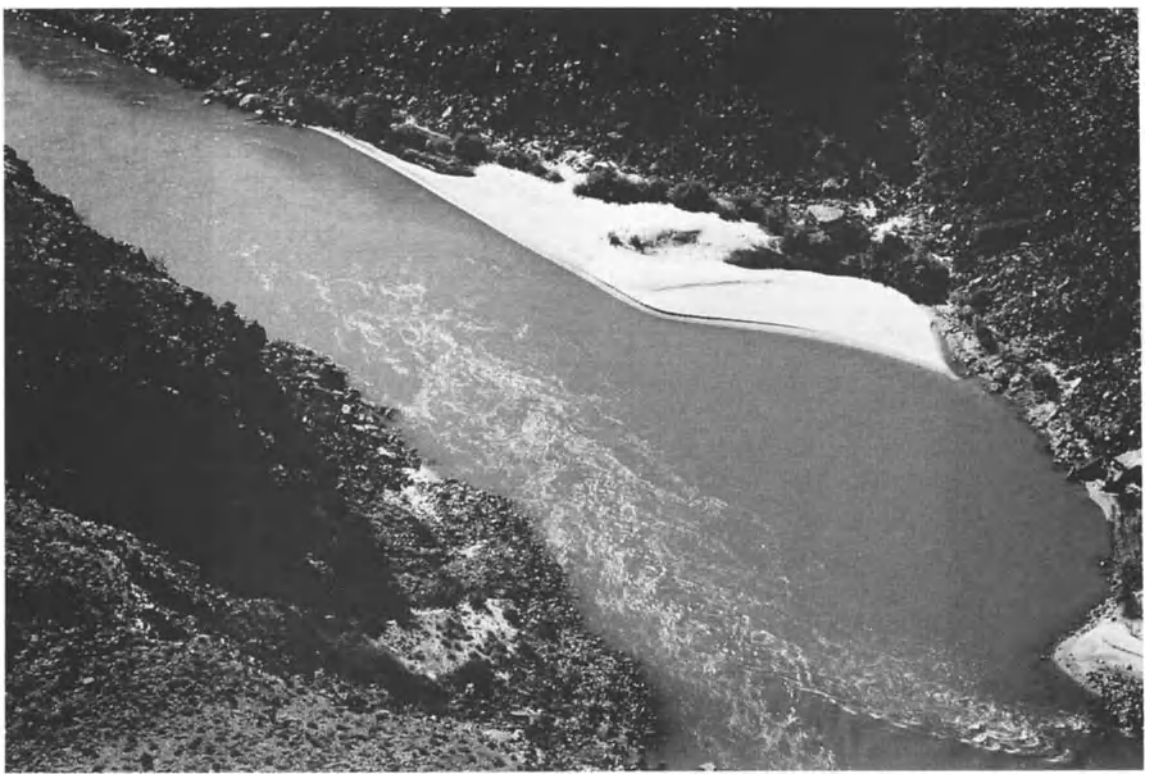

Figure 11. Oblique aerial photograph (taken in October 1991) showing incised channel, coarse debris-channel constriction, and associated fine-grained sand deposits. Flow is from the bottom to top of the photograph. Location is in the Grand Canyon, approximately 370 km downstream from Glen Canyon Dam.

characteristics of sand bars that form in channel expansions. Deposition of sand bars occurs where flow velocity is lowest; near the separation and reattachment points, and at the center of the eddy (Figure 12). *Schmidt* [1990] proposed the terms separation deposit, reattachment deposit, and eddy-center deposit for sand bars formed near the separation point, reattachment point, and center of the primary eddy, respectively. Separation bars mantle the downstream parts of channel constrictions. Reattachment bars begin at the point where low velocity flow reattaches to the bank and projects upstream in the form of spits. Eddy-center bars are located beneath the primary eddy recirculation cell. When observed at low flow, eddy-center bars and reattachment bars are actually one continuous deposit [*Schmidt,* 1990] and are referred to as eddy bars in this paper. Separation, reattachment, and eddy bars are sub-categories of what are often lumped together as channel margin bars, although the term channel-margin deposits is sometimes used to describe discontinuous narrow sand bodies along the banks. Eddy bars will be the focus of this section of this chapter because they are the largest of the fine-grained deposits found in incised river channels. Eddy bars account for up to 75 percent of the total sand stored along the banks of the Colorado River [*Schmidt and Rubin,* 1995].

3.3.1. *Site selection.* Two widely separated reaches of the Colorado River, U.S.A. (Figure 13) were selected to compare the processes and rates of deposition and erosion between a highly regulated river (unsteady flow on daily and hourly time scales) and a natural river (seasonally varying)(Table 3). One bar was located 50 km upstream from Moab, Utah, and the other was in the Grand Canyon, 303 km downstream from the Glen Canyon Dam. Both fan-eddy sand bar complexes have similar sizes and morphologic features. Channel widths are on the order of 80 to 100 m and the constriction/expansion ratios are approximately 0.5. These bars are both downstream from broad, low elevation debris fans that originate from short, steep, side-canyons. Fine-grained sand deposits occur on the lee side of the debris-fan channel constrictions. The Colorado River near Moab, which is close to the upstream site, is partially regulated by storage reservoirs in tributaries, but still maintains a fairly natural flow regime with a distinct annual flood cycle and high sediment load (Table 3). These

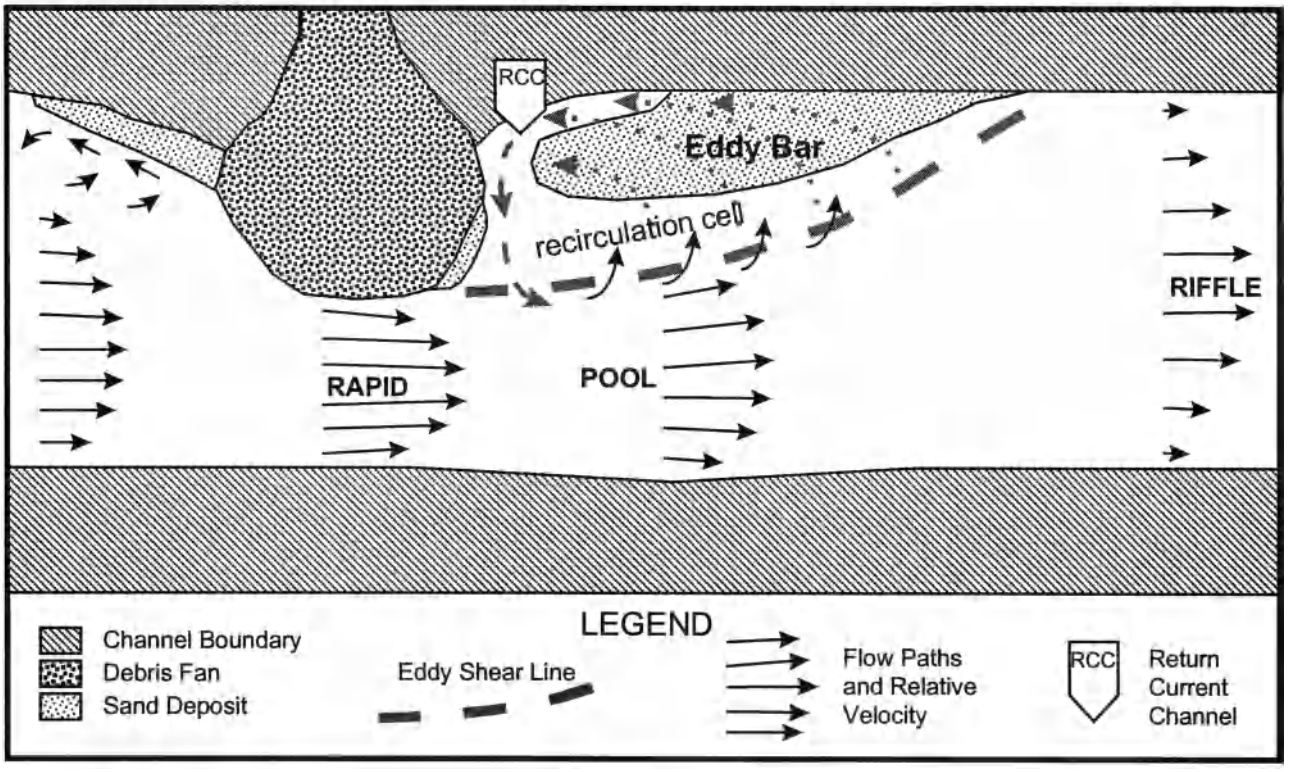

Figure 12. Schematic map showing typical channel margin sand deposits and features of lateral flow separation zones.

conditions satisfy the objective of comparing a naturally flowing river to the completely regulated river downstream from the Glen Canyon Dam.

3.3.2. *Sedimentology and bedforms associated with eddy bars.* Many investigators [e.g. *Howard and Dolan*, 1981; *Schmidt and Graf*, 1990; *Garrett et al.*, 1993; *Konieczki et al.*, 1997] have measured sediment caliber along the Colorado River from samples collected on the bed, in transport at gage sites, from tributary flows, and from sand bars. Sediment found on the channel bed and transported in suspension is typically fine to coarse sand with a median grain size of approximately 0.2 mm. The sand composing sand bars has similar grain-size distributions as that in transport at gaging stations [*Howard and Dolan*, 1981]. Finer sediment delivered to the channel from tributary flows is generally transported through the resistant-boundary channel, leaving little sedimentary evidence except for thin lenses of silt and clay locally deposited in stagnant backwater environments [*Stevens et al.*, 1995].

Internal sedimentary structures typically found within these eddy bars are ripple-drift cross-laminations and planar foresets. The sedimentary structures indicate that dunes and ripples within the recirculation zones migrate in a rotary pattern following observed patterns of recirculating flow [*Rubin et al.*, 1990]. Near reattachment points, ripples commonly resemble oscillation ripples in which the crests are aligned perpendicular to the bank due to fluctuations of the reattachment point position with discharge. Ripples climb steeply near reattachment points and at lower angles farther away.

3.4. *Evolution of Sand Bodies*

3.4.1. *Depositional processes.* In resistant-boundary channels, each depositional environment is unique, leading to a complex depositional history for each sand body. In order to describe the depositional processes of eddy bars, it is useful to first consider a flow recirculation zone devoid of sand and with steady flow in the main channel. Sand is suspended through the high velocity channel constrictions and where flow diverges at the downstream end of the constrictions sand is advected across the eddy shear line [*Nelson et al.*, 1994]. It can be observed that flow enters eddy recirculation cells primarily near the channel bottom and along the downstream end of the eddy shear zone. Flow exits eddy recirculation cells predominantly near the top of the

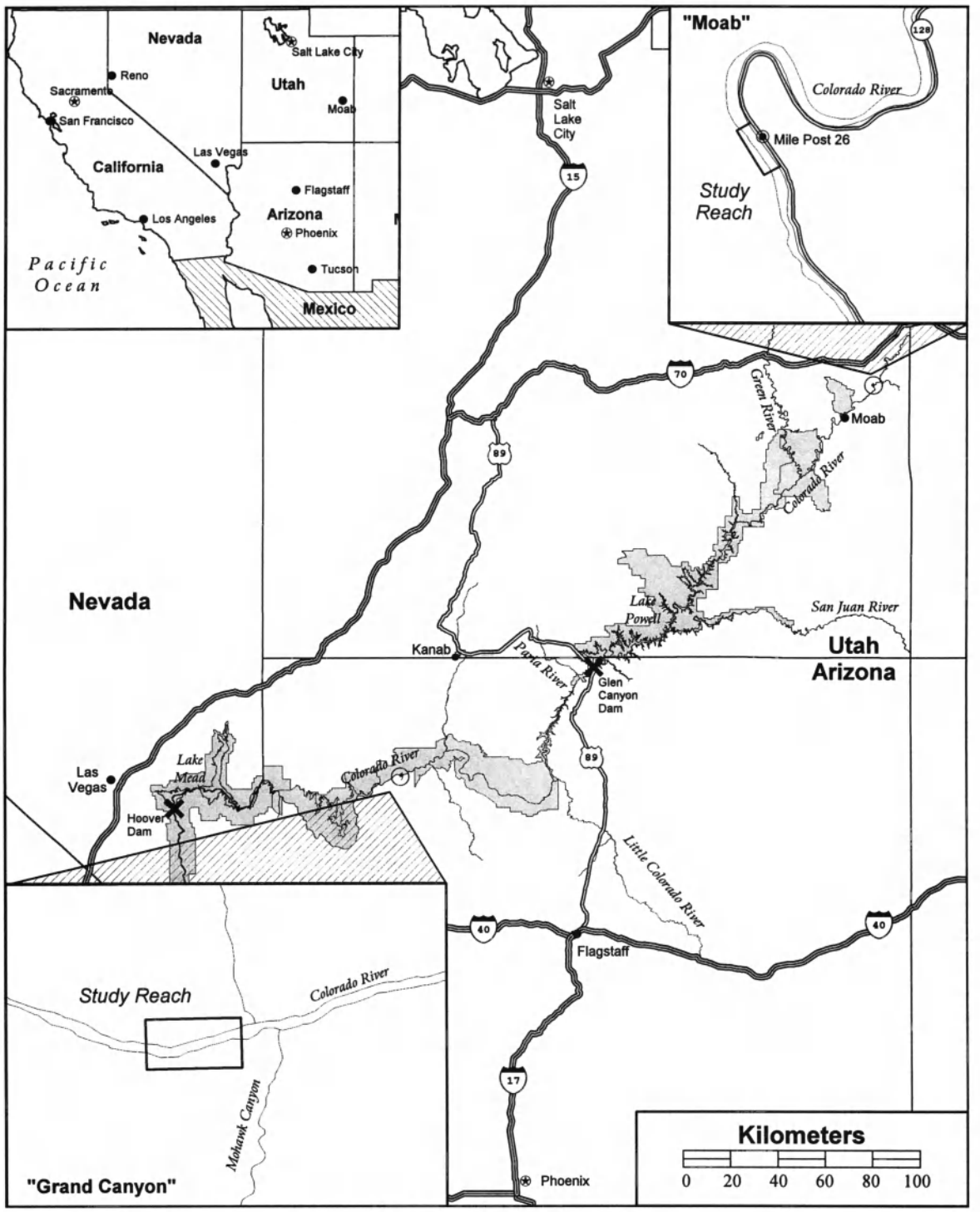

Figure 13. Location map showing study reaches upstream and downstream from the flow and sediment regulating Glen Canyon Dam. Shaded areas are National Park units.

Table 3. Summary of selected geologic and hydrologic attributes for two study reaches of the Colorado River.

Attribute	Regulated River - Grand Canyon	Near-Natural River - near Moab, UT
Elevation (above sea level)	521 m	1,242 m
Reference Stream Gage	Colorado River near Grand Canyon, AZ; Station # 09402500	Colorado River near Cisco, UT; Station # 09180500
Drainage Area	366,744 km^2	62,420 km^2
Discharge Data, Period:	1922 to present	1895 to present
peak flow (pre-dam)	3,600 m^3/s	2,176 m^3/s
peak flow (post-dam)	2,725 m^3/s	n/a
10-year flood (pre-dam)	2,460 m^3/s	1,784 m^3/s
10-year flood (post-dam)	1,130 m^3/s	n/a
mean annual flow (pre-dam)	480 m^3/s	209 m^3/s
mean annual flow (post-dam)	417 m^3/s	n/a
Sediment Discharge Data:	*at Lees Ferry*	1974-1984
mean annual load (pre-dam)	66 x 10^6 metric tons	9 x 10^6 metric tons
mean annual load (post-dam)	0 x 10^6 metric tons	n/a
	at Phantom Ranch	
mean annual load (post-dam)	10 x 10^6 metric tons (Andrews, 1991b)	n/a
Lithology at River Level	Cambrian - Bright Angel Shale	Jurassic - Entrada Sandstone
Hydraulic Control	debris fan constriction and downstream riffle	debris fan constriction/downstream riffle
Length of Study Reach	900 meters	450 meters

water column at the upstream end of the eddy. Sand quickly settles out of suspension in the low velocity recirculation cell (Figure 12). As a result, the sediment concentration of the flow exiting the recirculation cell is substantially reduced and this important process can usually be readily observed.

The first topographic indication of a new eddy bar is an elongate ridge just inside the eddy shear line, parallel to the main channel (Figure 14). As deposition continues, the ridge gradually assumes a dune-shaped profile with a steep foreshore face terminating at a crest, a lower angle platform terminating at a crest, and a slip face parallel to the channel boundary. The dune migrates from the shear line into the eddy toward the channel boundary as growth progresses. These processes continue at relatively high rates until the eddy bar begins to restrict flow in the recirculation cell, causing interactions between the deposit and local flow conditions.

3.4.2. *Flow and deposit interactions.* Deposition enlarges eddy bars until they reach a size and geometry such that sand is mobilized and transported across the bar at the rate it enters the recirculation cell. This equilibrium condition is a function of the depth and velocity of the flow, the geometry of the deposit, and the size and abundance of the incoming and deposited sediment.

Initially, the foreslopes of eddy bars have a small angle. As deposition progresses, the foreslope angle increases until a maximum stable angle is attained. This angle is in part due to the internal angle of friction of the sediment particles and local lift and drag forces. Sand samples taken from a Grand Canyon eddy bar in 1991 were tested and the angle of internal friction was 32° ± 2° [*Budhu and Gobin,* 1994]. If discharge is steady so that flow over the eddy bar is not interrupted, the upward component of flow over the eddy bar will allow the foreslope angle to increase beyond the internal angle of friction because upslope drag forces are exerted on the particles by the upward component of fluid flow. Because velocity increases with height due to decreasing cross sectional area of the flow as it approaches the foreslope crest, the upward component of flow increases and the slope angle should increase with height above the channel bed. For concave eddy bar foreslope angles measured on mature deposits in the Grand Canyon in 1993, the highest angle of 34° was measured near the crest [*Cluer,* 1997].

Eddy bars advance toward the main channel and impinge on the eddy shear zone as they evolve. The location of the foreslope toe is constrained by the eddy shear zone because turbulent downstream currents on the channel side of the eddy shear zone will erode the eddy foreslope. The maximum width of the eddy bar platform is determined by the distance between the foreslope and slipface, which both parallel the return current channel (Figure 14).

Eddy return current channels have their own processes which determine the ultimate location and shape of the dune slip face. Flow that crests the eddy bar encounters the resistant boundary of the channel at angles approximately perpendicular to the boundary. Consequently, the flow turns abruptly and changes from a broad shallow flow to a narrow deep flow, which increases in volume in the upstream direction. As the flow becomes channelized, turbulence increases and helical rotating flow results from flow shooting

off the bar crest and rolling under as it encounters the channel boundary. It can be readily observed that this spiral, rotating flow maintains a scoured channel and returns recirculating current to the main channel at the upstream end of the recirculating cell, just downstream from the separation point. At the eddy bar crest, sand particles are avalanched down the slope into the return current channel. Commonly, the angle of this slope exceeds the angle of repose because the upward spiraling flow paths directed along the avalanche slope provide upward directed drag force to the sand particles, similar to the process occurring on the eddy bar foreslope.

Under the simple conditions of steady flow and sediment concentration, eddy bars will attain an equilibrium form with dimensions relative to the geometry of the recirculation cell as described above. Such bars can be thought of as "mature eddy bars". Because these bars are the product of several interactions, it is expected that they are significantly affected by changes in flow, sediment transport, and channel characteristics. Some of these responses are discussed in the following section by considering the sites from regulated and naturally flowing reaches of the Colorado River.

3.5. *Stability of Eddy Bars*

3.5.1. *Minor eddy-bar adjustments.* Mature eddy bars respond quickly to changes in discharge because the cross section varies with discharge and the recirculation cells, unconstrained by a downstream channel constriction, elongate in direct proportion to discharge. *Rouse et al.* [1951] reported that unconstrained recirculation cells are longer at higher Froude numbers in flume experiments. *Schmidt* [1990], evaluating 13 sites in the Grand Canyon, found that the length of all recirculation cells increased in the downstream direction with increasing discharge. Little lengthening of the recirculation cell takes place in the upstream direction as discharge increases because the separation point remains stable. During high discharges, however, multiple recirculation cells sometimes form, producing multiple eddies with complexly bedded sand deposits and uneven topography.

As discharge recedes, recirculation cells shorten, bringing downstream current in contact with the downstream end of eddy deposits. Under these conditions, a zone of high boundary shear stress developes along the toe of the eddy bar foreslope, resulting in undercutting of the slope and localized slumping. Consequently, a vertical cut bank sometimes forms at the top of deposits during low flow periods. If discharge reduction is great, the reattachment point may migrate upstream the full length of the eddy bar. In such cases, the entire length of the eddy bar will slump and erode during low discharges. Adjustments of the foreslope erode a relatively small volume of the total sand body. The foreslope typically retreats only a few meters until it attains a slope stable with the new hydraulic conditions.

3.5.2. *Major eddy-bar adjustments.* Another style of eddy bar response is more dramatic. Fine-grained deposits are episodically evacuated from recirculation cells. This was first documented using repeat photography in 1990 in the Grand Canyon [*Cluer,* 1991] and then, further studied with water level and land tilt sensors in 1991-1993 by *Carpenter et al.* [1995], who concluded that eddy bars were rapidly eroded only during increases in discharge. This process is apparently common throughout the Grand Canyon [*Dexter et al.,* 1995], where eddy bars are commonly completely eroded in a few hours, and then grow back in a few weeks (Figure 15).

Similar eddy bar erosional events occur at the Moab study site in a more unregulated river environment [*Cluer,* 1997](Figure 16). At the Moab study site, eddy bar erosion took place over several days to a few weeks during increasing Spring floods, and new bars emerged as each annual flood receded. At both study sites, the pattern of erosion was along a semicircular arc, consistent with the shape of the flow recirculation cell, indicating that erosion took place within the recirculation cell. The repeated episodes of erosion and deposition suggest a natural deposition and erosion cycle for fine-grained deposits during a single flood that is difficult to detect or account for in river channel monitoring programs [*Cluer,* 1995]. For example, monitoring many of the same eddy bars in Grand Canyon, but using time scales ranging from one year to one century, *Howard and Dolan* [1981], *Schmidt and Graf* [1990], *Kaplinski et al.* [1994], and *Webb* [1996] described only minor size variations in the eddy bars. However, recent studies using bimonthly and daily time-step monitoring programs [*Beus and Avery,* 1991; *Dexter et al.*, 1995] documented major variation in sand bar sizes.

3.5.3. *Channel changes.* Just as evacuation of sand from eddy bars occurred during increases in flow, the adjacent river channels also underwent adjustments during flow increases. The channel at the Moab study site adjusted substantially in the pool area during the rising limb of the 1994 flood (Figure 17). Sand deposited in the pool since the last flood was scoured approximately two meters, but more importantly, the downstream part of the pool and pool exit slope were filled with approximately three meters of sand. These channel changes preceded the onset of eddy bar scour by about one week. At the Grand Canyon study site, similar channel changes were measured during a daily flow fluctuation by repeating hourly surveys (Figure 18). For example, between 4-5 PM on 31 August 1993, repeat surveys showed the development of lenses on the pool entry and exit slopes approximately two to three meters thick. However, these sedimentary lenses were short lived because the 6 PM survey showed a profile identical to the 4 PM profile.

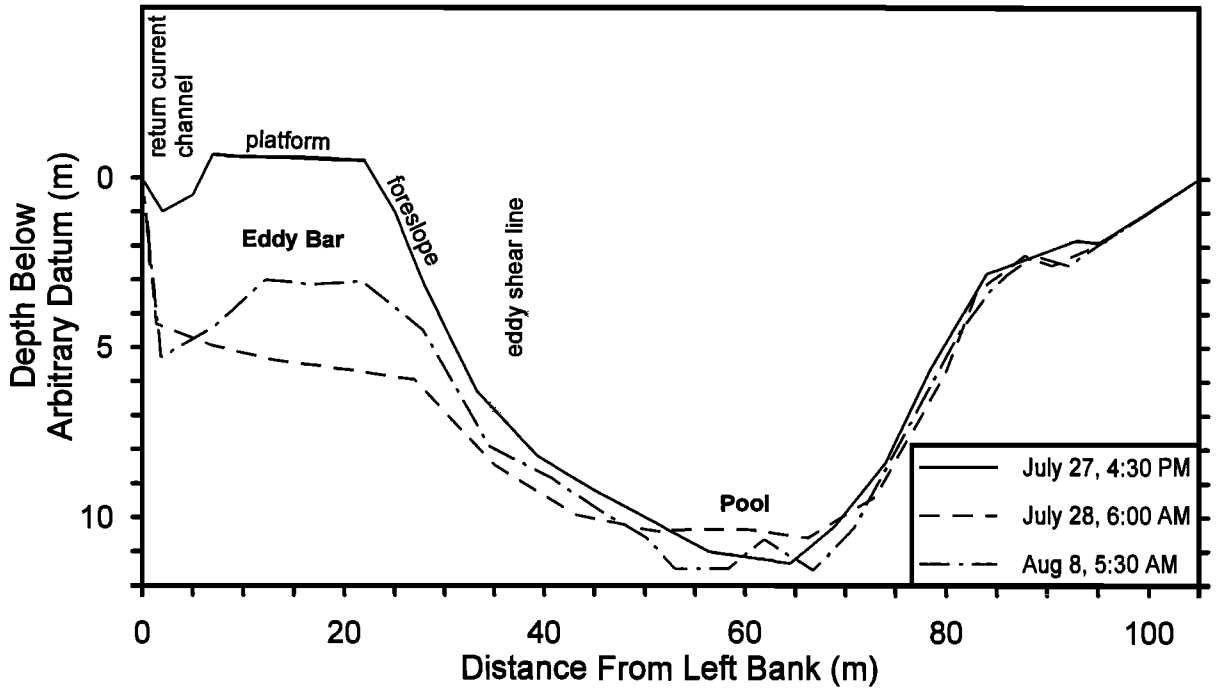

Figure 14. Cross sections of the channel and eddy bar at the Grand Canyon study site. Channel topography was measured in July and August of 1993, shortly before, shortly after, and several days after an eddy stripping event occurred.

An array of land tilt sensors installed in the Grand Canyon eddy bar showed that slope motion began within the foreslope of the bar coincident with pool filling. Within three hours the entire eddy bar, 12,000 m^3 of sand, was eroded from the eddy recirculation zone. This type of erosion has occurred during the rising limb of unsteady, fluctuating flows on multiple occasions and at multiple locations in the Grand Canyon [*Carpenter et al.,* 1995; *Dexter et al.,* 1995], during increasing discharge on the unregulated Colorado River near Moab, Utah [*Cluer,* 1997], and during steady, high discharge in the Grand Canyon [*Carpenter,* 1996; *Konieczki et al.,* 1997].

At the Moab site, the sediment transport rate on the rising limb is considerably greater than on the falling limb of any given flood (Figure 19). This loop rating effect is caused by sediment hysteresis, where greater supplies of sediment are available during the rising limb of a flood than on the descending limb. By examining the particle stability fields of numerous two-dimensional flow model runs, *Cluer* [1997] concluded that temporary pool sedimentation was the cause of eddy bar erosion events that occurred during the rising limb of frequent, small-magnitude floods in the Grand Canyon. Temporary pool sedimentation could be caused by sediment hysteresis, however, suspended sediment measurements have not been made at the frequency of the documented channel changes to test this hypothesis. We infer that the loop rating curve can have significant effects on local erosion and sedimentation patterns and that the range of the 'loop rating' effect may distinguish incised river channels (sediment limited) from alluvial river channels (capacity limited). We conclude that the short-term response and cut and fill histories of fine-grained deposits may be directly influenced by the effects of the 'loop rating' phenomenon.

3.6. *The Effect of Variations in Sediment Supply*

The frequency of episodic erosion events ranges from zero to ten or more per year for sand deposits in the Grand Canyon [*Cluer and Dexter,* 1994]. *Beus and Avery* [1991] and *Kaplinski et al.* [1994] also found that the distance downstream from the Little Colorado River sediment supply correlated to temporal variability in sand bar volumes. More recently, *Hoeting et al.* [1997] found a correlation between sediment delivery from the Little Colorado River and increased variance in sand bar size downstream. These monitoring studies reported that sand bars were more dynamic with increasing distance downstream. One factor required to make eddy deposits dynamic over short-time scales is available sediment that is mobilized by frequent, low-magnitude discharges.

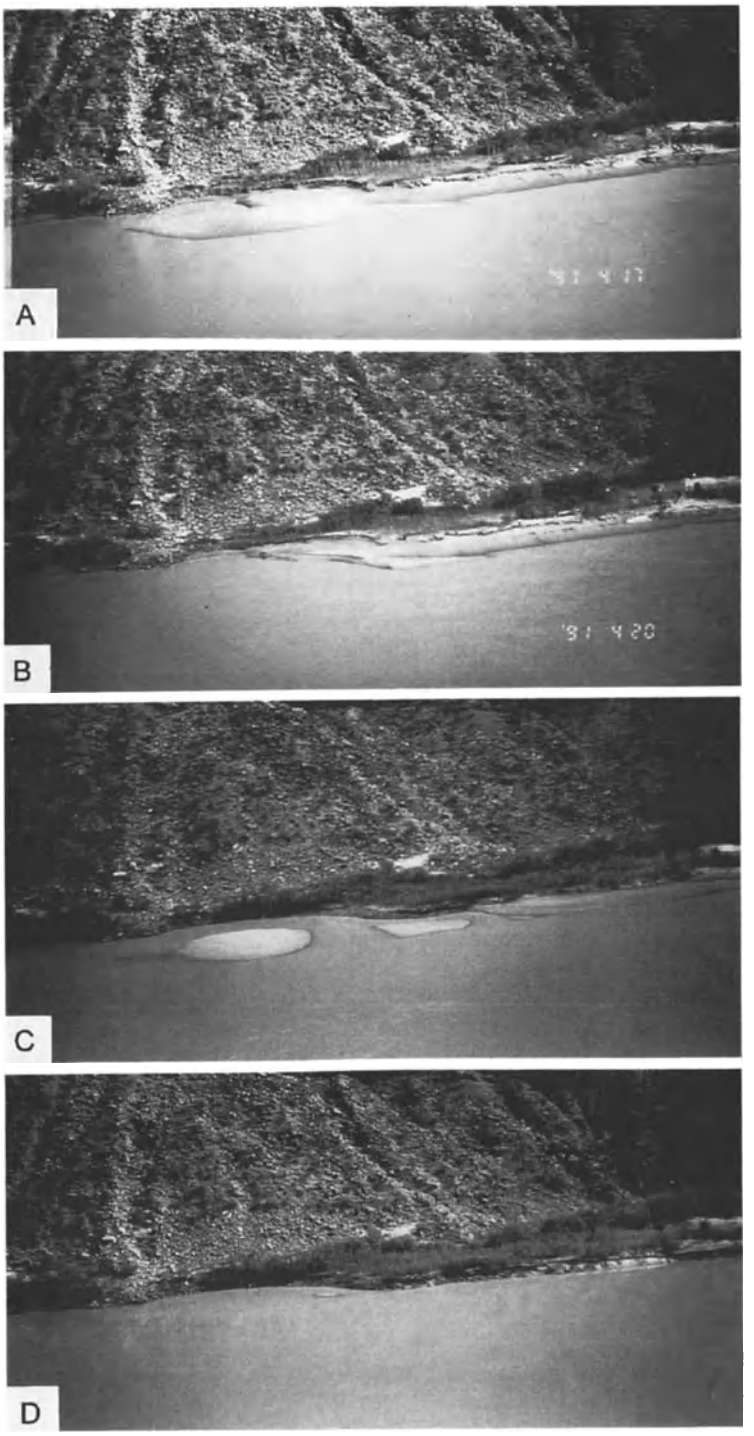

Figure 15. Selected daily time step photographs from the Grand Canyon study site taken in 1991 showing two typical eddy stripping events that occurred during daily flow fluctuations for peaking hydropower. Flow is from left to right with counterclockwise recirculating flow over the eddy bar. Widths of images are approximately 180 m. Photo A was taken on 17 April 1991, Photo B was taken on 20 April 1991, Photo C was taken on 1 September 1991, and Photo D was taken on 2 September 1991.

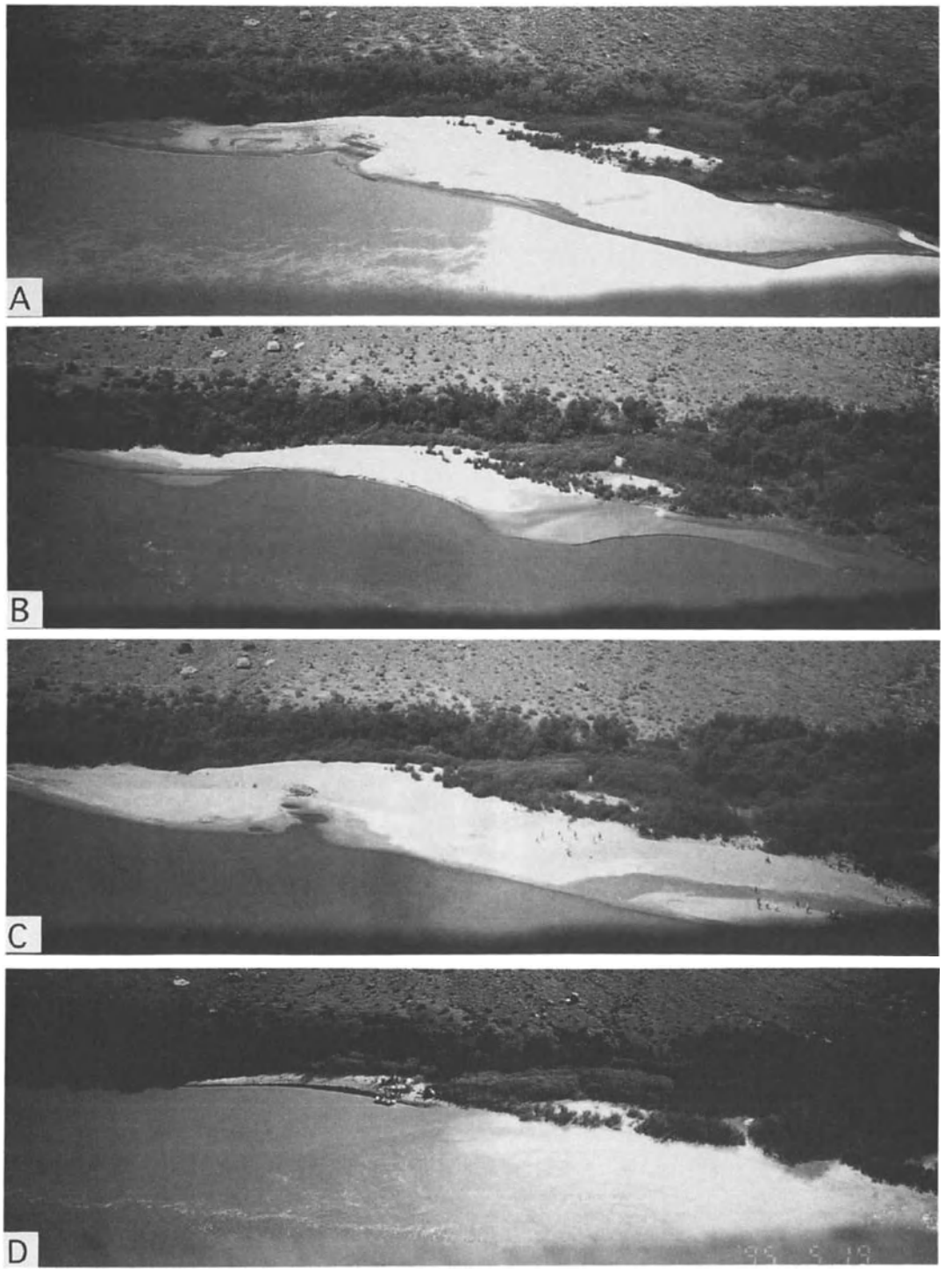

Figure 16. Selected daily time step photographs from the Moab study site taken in 1994-1995 showing two eddy stripping events. Flow is from right to left with clockwise recirculating flow on the right bank. Photo dates are: (A) 11 October 1993, showing large eddy bar that emerged as the 1993 flood receded, (B) 8 June 1994, showing scour during the rising limb of the 1994 flood, (C) 14 July 1994, showing a new eddy bar, and (D) 19 May 1995, showing scour during the rising limb of the 1995 flood.

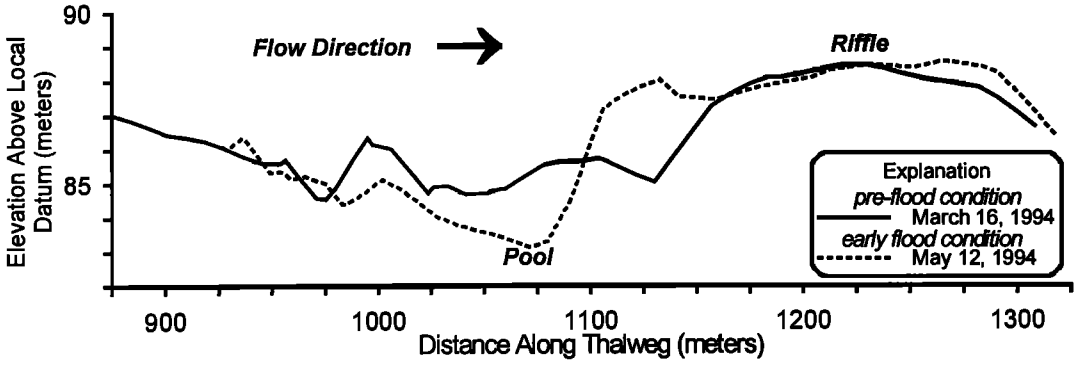

Figure 17. Naturally flowing river (Moab study site) channel profiles showing changes during the rising limb of the 1994 flood. The eddy bar is located adjacent to the pool on right side of channel.

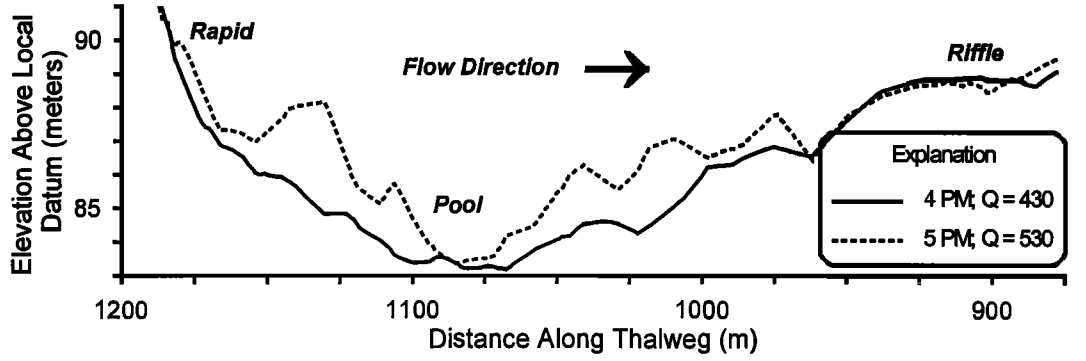

Figure 18. Grand Canyon channel profiles showing changes during the rising limb of the 31 August 1993 daily hydropower release. The eddy bar is located adjacent to the pool on the left side of channel. Discharge (Q) in legend is in m^3/s.

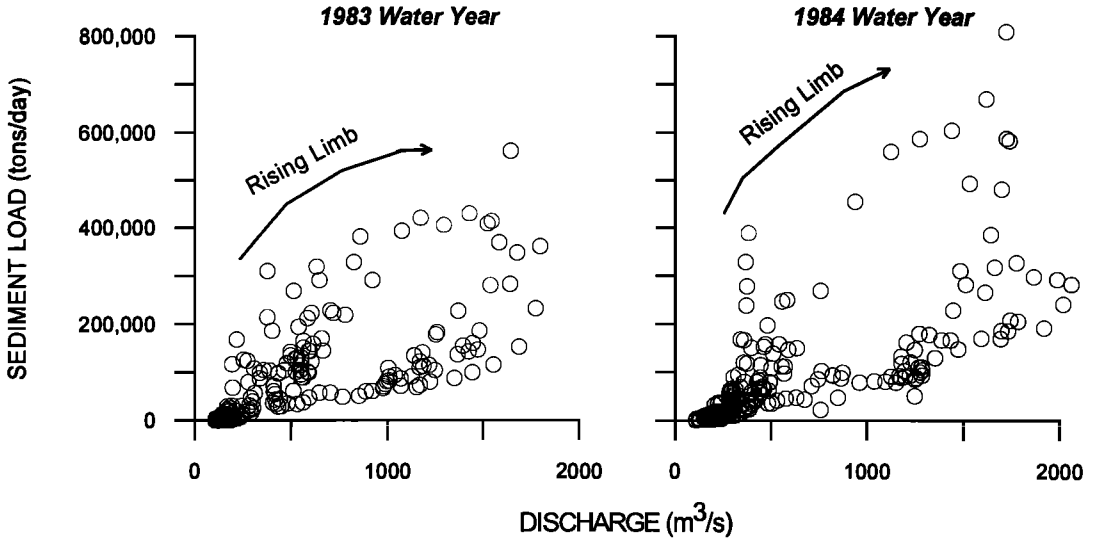

Figure 19. Examples of 'loop rating' curves from the relationship between discharge and suspended sediment load for last two years of sediment records at the Colorado River near the Moab study site.

Without mobile sediment in the channel, pool filling and erosion are limited, and scouring of eddy bars is unlikely. This remark is supported by the differing responses of Colorado River eddy bars downstream from Glen Canyon Dam in reaches where sediment availability differs markedly. In the reach directly downstream from the dam, the channel has been shown to be severely scoured and armored [*Pemberton,* 1976]. Nevertheless, this reach retains eddy bars that undergo only minor size adjustments over a wide range of discharges [*Kaplinski et al.,* 1994]. In contrast, an eddy bar 28 km downstream from Glen Canyon Dam was found to scour and fill immediately following large flows from the Paria River tributary [*Cluer and Dexter,* 1994]. Eddy bars downstream from the Little Colorado River behaved similarly following floods from that tributary in 1993 [*Kaplinski et al.,* 1994; *Wiele et al.,* 1996]. The lower Grand Canyon reach contains comparatively large volumes of sand-sized sediment in the river channel [*Randle and Pemberton,* 1987] and eddy bars in the lower Grand Canyon scour and fill on time scales driven by dam operations that frequently modulate discharge through ranges that locally scour and fill pools [*Cluer,* 1997].

4. CONCLUSIONS

The two case studies examined in this paper demonstrate the complex interactions between valley and channel geometry, flow hydraulics, flow magnitude and frequency, sediment size, and sediment supply in determining the spatial distribution, morphologic and sedimentologic characteristics, and longevity of deposits in resistant-boundary channels and valleys. We have demonstrated that the depositional patterns, processes, and mechanics along resistant-boundary channels are strongly influenced by sediment supply. The morphologic and sedimentologic characteristics of depositional macroforms produced by the 1985 glacial-lake outburst flood in Nepal reflect variations in flow processes and depositional mechanics as the sediment concentration of the flood waters changed. The sediment concentration of the flood waters varied because of the spatial discontinuity of sediment available to be entrained and deposited along the outburst-flood route.

Although most resistant-boundary channels are supply limited with respect to entrainment and transport of cobble- and boulder-sized particles during frequent, low to moderate flows, there is a dynamic cycle of erosion and deposition associated with sand deposits at frequent, low to moderate flows. Eddy sand bar deposits along the Colorado River in and near the Grand Canyon are an excellent example of how sediment supply drives this dynamic erosional and depositional cycle for a given flood. When the fine-grained sediment supply of a channel is reduced by a flow-regulation structure, the natural erosional and depositional cycle that occurs in pools and eddy bars is disrupted, causing the eddy bars to become stable. Conversely, when the sediment supply remains high, but the flow is fluctuated frequently, the natural erosion and deposition cycle is accelerated.

Acknowledgments. We wish to thank Paul Carling, Hugh Mills, and Jim O'Connor for reviewing an earlier version of this manuscript and providing helpful suggestions and comments that improved its content. Cenderelli would like also like to thank Ellen Wohl for many constructive discussions on the depositional processes associated with glacial-lake outburst floods in Nepal. Research by Cenderelli was supported by grants from the National Science Foundation (CMS-9320876) and the Geological Society of America. Research by Cluer on the Colorado River was funded by the U.S. Bureau of Reclamation and the U.S. National Park Service.

REFERENCES

Andrews, E.D., Sediment transport in the Colorado River Basin, in *Colorado River Ecology and Dam Management*, National Academy Press, 54-74, 1991b.

Bagnold, R.A., Experiments on a gravity-free dispersion of large solid spheres in a Newtonian fluid under shear, *Proc. Royal Soc., London, 225*, 49-63, 1954.

Baker, V.R., Stream channel response to floods with examples from central Texas, *Geol. Soc Am Bull, 88*, 1057-1071, 1977.

Baker, V.R., Large-scale erosional and depositional features of the Channeled Scabland, in *The Channeled Scabland*, edited by V.R. Baker and D. Nummedal, D., pp. 81-115, Nat. Aeronautics Space Adm., Washington D.C., 1978.

Baker, V.R., Flood sedimentation in bedrock fluvial systems, in *Sedimentology of Gravels and Conglomerates*, edited by E.H. Koster and R.J. Steel, pp. 87-98, Can. Soc. Pet. Geol., Mem. 10, 1984.

Baker, V.R., Flood erosion, in *Flood Geomorphology*, edited by V.R. Baker, R.C. Kochel, and P.C. Patton, pp. 81-95, John Wiley and Sons, New York, N.Y., 1988.

Baker, V.R., and R.C. Kochel, Flood sedimentation in bedrock fluvial systems, in *Flood Geomorphology*, edited by V.R. Baker, R.C. Kochel, and P.C. Patton, pp. 123-137, John Wiley and Sons, New York, N.Y., 1988.

Beus, S.S., and C.C. Avery, editors, The influences of variable discharge regimes on Colorado River sand bars below Glen Canyon Dam., U.S. Dept. Interior, Bureau of Reclamation Glen Canyon Environmental Studies Program report P3, Flagstaff, Arizona, 1991.

Breed, W.J., editor, *Geology of the Grand Canyon*, Museum of Northern Arizona, Flagstaff, Arizona, 1974.

Budhu, M., and R. Gobin, Instability of sandbars in Grand Canyon, *J. Hyd. Eng., 120*, 919-933, 1994.

Carling, P.A., Hydrodynamic interpretation of a boulder berm and associated debris-torrent deposits, *Geomorphology, 1*, 53-67, 1987.

Carling, P.A., Hydrodynamic models of boulder berm deposition, *Geomorphology, 2*, 319-340, 1989.

Carling, P.A., Flow-separation berms downstream of a hydraulic jump in a bedrock channel, *Geomorphology, 11*, 245-253, 1995.

Carling, P.A., and T. Grodek, Indirect estimation of ungauged peak discharges in a bedrock channel with reference to design discharge selection, *Hydrological Processes, 8*, 497-511, 1994.

Carpenter, M.C., Monitoring erosion and deposition using an array of load-cell scour sensors during the Spring 1996 controlled-flood experiment on the Colorado River in the Grand Canyon, Arizona, abst., *EOS, 77*, F271, 1996.

Carpenter, M.C., R.L. Carruth, J.B Fink, J.K. Boling, and B.L Cluer, Hydrogeology and deformation of sandbars in response to fluctuations in flow of the Colorado River in the Grand Canyon, Arizona, *Water-Res. Inves. Rept. 95-4010*, U.S. Geol. Surv., 1995.

Cenderelli, D.A., and E.E. Wohl, Hydraulics and geomorphic effects of the 1985 glacial-lake outburst flood in the Mount Everest region of Nepal, *Geol. Soc. Am., Abs. with Prog., 29*, 1997.

Cenderelli, D.A., and E.E. Wohl, Sedimentology and clast orientation of deposits produced by glacial-lake outburst floods in the Mount Everest region, Nepal, in *Geomorphological Hazards in High Mountain Areas*, edited by J. Kalvoda and C.L. Rosenfield, Kluwar Academic Publishers, Netherlands, 1-26. 1998.

Church, M., and Jones, D., 1982, Channel bars in gravel-bed rivers, in *Gravel-Bed Rivers*, edited by R.D. Hey, J.C. Bathurst, C.R. Thorne, pp. 291-324, John Wiley and Sons, London, UK, 1982.

Cluer, B. L., Catastrophic erosion events and rapid deposition of sandbars on the Colorado River, the Grand Canyon, Arizona, abst., *EOS, 72*, 223, 1991.

Cluer, B.L., Cyclic fluvial processes and bias in environmental monitoring, Colorado River in Grand Canyon, *J. Geol., 103*, 411-421, 1995.

Cluer, B.L., *Eddy Bar Responses To The Sediment Dynamics Of Pool-Riffle Environments*, Ph.D. diss., Colorado State University, 1997.

Cluer, B.L., and L.R. Dexter, Daily dynamics of Grand Canyon sandbars; monitoring with terrestrial photogrammetry, final report, U.S. Dept. Interior, National Park Service, Flagstaff, Arizona, 1994.

Davoran, A., and M.P. Mosley, Observations of bedload movement, bar development and sediment supply in the braided Ohau River, *Earth Surf. Proc. Landforms, 11*, 643-652, 1986.

de Jong, C., and P. Ergenzinger, The interrelations between mountain valley form and river-bed arrangement, in *River Geomorphology*, edited by E.J. Hickin, pp. 55-91, John Wiley and Sons, 1995.

Dexter, L.R., B.L. Cluer, and M.F. Manone, Using land based photogrammetry to monitor sandbar stability in Grand Canyon an a daily time scale, in Van Riper, C., III, editor, *Proceedings of the Second Biennial Conference of Research in Colorado Plateau National Parks*, Transactions and Proceedings Series, National Park Service, 1995.

Dietrich, W.E., and J.D. Smith, Bedload transport in a river meander, *Water Resour. Res., 20*, 1355-1380, 1984.

Dolan, R., A. Howard, and D. Trimble, Structural control of the rapids and pools of the Colorado River in Grand Canyon, *Science, 202*, 629-631, 1978.

Elfström, A., Large boulder deposits and catastrophic floods, *Geografiska Annaler, 69a*, 101-121, 1987.

Ely, L.L., and V.R. Baker, Reconstructing paleoflood hydrology with slackwater deposits, Verde River, Arizona, *Phys. Geog., 5*, 103-126, 1985.

Fahnestock, R.K., Morphology and hydrology of a glacial stream-White River, Mount Rainier Washington, *Professional Paper 422A*, 70 p. U.S. Geol. Surv., 1963.

Ferguson R.I., P.E. Ashmore, P.J. Ashworth, C. Paola, and K.L. Prestegaard, Measurements in a braided river chute and lobe; 1, Flow pattern, sediment transport, and channel change, *Water Resour. Res., 28*, 1877-1886, 1992.

Fushimi, H., K. Ikegami, and K. Higuchi, Nepal case study: Catastrophic floods, in *Techniques for Prediction of Runoff from Glacierized Areas*, edited by G.J. Young, pp. 125-130, Internat. Assoc. Hydrol. Sci., 149, 1985.

Garrett, W.B., E.K. Van De Vanter, and J.B. Graf, Streamflow and sediment-transport data, Colorado River and three tributaries in Grand Canyon, Arizona, 1983 and 1985-86, *Open-file Report 93-174*, U.S. Geol. Surv., 1993.

Hein, F.J., and R.G. Walker, Bar evolution and development of stratification in the gravelly, braided Kicking Horse River, British Columbia, *Can. J. of Earth Sciences, 14*, 562-570, 1977.

Hey, R.D., Design equations for mobile gravel-bed rivers, in *Gravel-Bed Rivers*, edited by R.D. Hey, J.C. Bathurst, and C.R. Thorne, C.R., pp. 553-574, John Wiley and Sons, 1982.

Hoeting, J.A., K. Varga, and B.L. Cluer, Predicting Colorado River sandbar size using Glen Canyon Dam release characteristics, final report, National Park Service, Flagstaff, Arizona, 1997.

Howard, A., and R. Dolan, Geomorphology of the Colorado River in the Grand Canyon, *J. Geol., 89*, 269-298, 1981.

Hydrologic Engineering Center, *HEC-RAS, River Analysis System, version 1.1*: U.S. Army Corps of Engineers, Davis, CA, 1995.

Iseya, F., H. Ikeda, H. Maita, and Y. Kodama, Fluvial deposits in a torrential gravel-bed stream by extreme sediment supply: Sedimentary structure and depositional mechanism, *Third International Workshop on Gravel-bed Rivers, Firenze, Italy*, 1990.

Ives, J.D., Glacial lake outburst floods and risk engineering in the Himalaya: A review of the Langmoche Disaster, Khumbu Himal, 4 August 1985: *International Centre for Integrated Mountain Development Occasional Paper No. 5*, 42 p., 1986.

Kaplinski, M.A., S.S. Beus, J.E. Hazel, and L. Kearsley, Monitoring the effects of interim flows from Glen Canyon Dam on sandbar dynamics and campsite size in the Colorado River corridor, Grand Canyon National Park, Arizona, draft final report, National Park Service, 1994.

Kieffer, S.W., The 1983 hydraulic jump in Crystal Rapid: Implications for river-running and geomorphic evolution in the Grand Canyon, *J. Geol., 93*, 385-406, 1985.

Knighton, D., *Fluvial Forms and Processes*, Edward Arnold, UK, 218 pp., 1984.

Kochel, R.C., V.R. Baker, and P.C. Patton, Paleohydrology of southwestern Texas, *Water Resour. Res., 18*, 1165-1183, 1982.

Konieczki, A.D., J.B. Graf, and M.C. Carpenter, Streamflow and sediment data collected to determine the effects of a controlled flood in March and April 1996 on the Colorado River between Lees Ferry and Diamond Creek, Arizona, *Open-file Report 97-224*, U.S. Geol. Surv., 1997.

Krumbein, W.C., Flood deposits of Arroyo Seco, Los Angeles County, California, *Geol. Soc. Am. Bull., 53*, 1355-1402, 1942.

Leopold, L.B., The rapids and pools-Grand Canyon, *Professional Paper 669-D*, U.S. Geol. Surv., 1969.

Leopold, L.B., and T. Maddock, The hydraulic geometry of stream

channels and some physiographic implications, *Professional Paper 282A*, 36 pp., U.S. Geol. Surv., 1953.

Martini, I.P., Gravelly flood deposits of Irvine Creek, Ontario, Canada, *Sedimentology, 24*, 603-622, 1977.

Matthes, G.H., Macroturbulence in natural stream flow, *Trans., Am. Geophys. Union, 28*, 255-265, 1947.

Mayewski, P.A., and P.A. Jeschke, Himalayan and trans-Himalayan glacier fluctuations since AD 1812, *Arctic and Alpine Res., 11*, 267-287, 1979.

Miller, A.J., Flood hydrology and geomorphic effectiveness in the central Appalachians, *Earth Surf. Proc. Landforms, 15*, 119-134, 1990

Miller, A.J., Valley morphology and boundary conditions influencing spatial patterns of flood flow, in *Natural and Anthropogenic Influences in Fluvial Geomorphology, The Wolman Volume*, edited by J.E. Costa, A.J. Miller, K.W. Potter, and P.R. Wilcock, pp. 57-81, Am. Geophys. Union, Monograph 89, 1995.

Miller, A.J., and D.J. Parkinson, Flood hydrology and geomorphic effects on river channels and floodplains: The flood of November 4-5, 1985, in the South Branch Potomac River Basin of West Virginia, in *Geomorphic studies of the storm and flood of November 3-5, 1985, in the upper Potomac and Cheat River Basins in West Virginia and Virginia*, edited by R.B. Jacobson, p. E1-E96, U.S. Geol. Surv. Bull. 1981, 1993.

Nanson, G.C., Episodes of vertical accretion and catastrophic stripping: A model of disequilibrium flood-plain development, *Geol. Soc. Am. Bull., 97*, 1467-1475, 1986.

Nelson, J.M., R.R. McDonald, and D.M. Rubin, Computational prediction of flow and sediment transport patterns in lateral separation eddies, abst., *EOS, 75*, 268, 1994.

O'Connor, J.E., Hydrology, hydraulics, and geomorphology of the Bonneville Flood, *Special Paper 274*, 83 pp., Geol. Soc. Am., 1993.

O'Connor, J.E., R.H. Webb, V.R. Baker, Paleohydrology of pool-and-riffle pattern development, Boulder Creek, Utah, *Geol. Soc. Am. Bull., 97*, 410-420, 1986.

Pemberton, E.L., Channel changes in the Colorado River below Glen Canyon Dam, in Proc. Third Interagency Sed. Conf., Water Resources Council, Sedimentation Committee, 5, 1976.

Powell, J.W., Exploration of the Colorado River of the West and its tributaries, U.S. Govt. Printing Office, Wash., D.C., 1875.

Randle, T.J., and E.L. Pemberton, Results and analysis of STARS modeling efforts of the Colorado River in Grand Canyon, Glen Canyon Environmental Studies technical report, Bureau of Reclamation, Salt Lake City, 1987.

Rouse, H., B.V. Bhoota, and E. Hsu, Design of channel expansions, *Trans. Am. Soc. Civil Eng., 116*, 347-363, 1951.

Rubin, D.M., J.C. Schmidt, and J.N. Moore, Origin, structure, and evolution of a reattachment bar, Colorado River, Grand Canyon, Arizona, *J. Sed. Pet., 60*, 982-991, 1990.

Schmidt, J.C., Recirculating flow and sedimentation in the Colorado River in Grand Canyon, Arizona, *J. Geol., 98*, 709-724, 1990.

Schmidt, J.C., and J.B. Graf, Aggradation and degradation of alluvial sand deposits, 1965 to 1986, Colorado River, Grand Canyon National Park, Arizona, *Professional Paper 1493*, 74 pp., U.S. Geol. Surv., 1990.

Schmidt, J.C., and D.M. Rubin, Regulated streamflow, fine-grained deposits, and effective discharge in canyons with abundant debris fans, in *Natural and Anthropogenic Influences in Fluvial Geomorphology, The Wolman Volume*, edited by J.E. Costa, A.J. Miller, K.W. Potter, and P.R. Wilcock, pp. 177-195, Am. Geophys. Union, Monograph 89, 1995.

Schumm, S.A., *The Fluvial System*, John Wiley and Sons, New York, 338 pp., 1977.

Schumm, S.A., and B.R. Winkley, The character of large alluvial rivers, in *The Variablility of Large Alluvial Rivers*, edited by S.A. Schumm, and B.R. Winkley, pp. 1-9, American Society of Civil Engineers, New York, NY, 1994.

Scott, K.M., and G.C. Gravlee, Flood surge on the Rubicon River, California-Hydrology, hydraulics and boulder transport, *Professional Paper 422-M*, 38 pp., U.S. Geol. Surv., 1968.

Shroba, R.R., P.W. Schmidt, E.J. Crosby, and W.R. Hansen, Storm and flood of July 31-August 1, 1976, in the Big Thompson River and Cache la Poudre River Basins, Larimer and Weld Counties, Colorado; Part B, Geologic and geomorphic effects in the Big Thompson Canyon Area, Larimer County, *Professional Paper 1115*, pp. 87-152, U.S. Geol. Surv., 1979.

Smith, G.A., Coarse-grained nonmarine volcaniclastic sediment: Terminology and depositional processes, *Geol. Soc. Am. Bull., 97*, 1-10, 1986.

Smith, N.D., Sedimentology and bar formation in the upper Kicking Horse River, a braided outwash stream, *J. Geol., 82*, 205-223, 1974.

Stevens, L.E., J.C. Schmidt, T.J. Ayers, and B.T. Brown, Geomorphic influences on fluvial marsh development along the dam-regulated Colorado River in the Grand Canyon, Arizona, *Ecol. Applications, 5*, 1995.

Stewart, J.H., and V.C. LaMarche, Erosion and deposition produced by the flood of December 1964 on Coffee Creek Trinity County, California, *Professional Paper 422K*, pp. 1-22, U.S. Geol. Surv., 1967.

Vuichard, D., Geological and petrographical investigations for the mountain hazards project, Khumbu Himal, Nepal, *Mtn. Res. Dev., 6*, 41-52, 1986.

Vuichard, D., and M. Zimmermann, M., The Langmoche flash-flood, Khumbu Himal, *Mtn. Res. Dev., 6*, 90-94, 1986.

Vuichard, D., and M. Zimmermann, The 1985 catastrophic drainage of a moraine-dammed lake, Khumbu Himal, Nepal: Cause and consequences, *Mtn. Res. Dev.*, 7, 91-110, 1987.

Webb, R.H., *Grand Canyon, A Century of Change*, University of Arizona Press, Tucson, Arizona, 1996.

Webb, R.H., P.T. Pringle, and G.R. Rink, Debris flows from tributaries of the Colorado River, Grand Canyon National Park, Arizona, *Professional Paper 1492*, U.S. Geol. Surv., 1989.

Wiele, S.M., J.B. Graf, and J.D. Smith, Sand deposition in the Colorado River in Grand Canyon from floods in the Little Colorado River, *Open-File Report*, U.S. Geol. Surv, 1996.

Wilson, R.P., Sonar patterns of Colorado riverbed, Grand Canyon, in Proc. Fourth Fed. Interagency Sed. Conf., Las Vegas, Subcommittee on Sedimentation, Interagency Advisory Committee on Water Data, pp. 5-133 to 5-142, 1986.

Wohl, E.E., Bedrock benches and boulder bars: Floods in the Burdekin Gorge of Australia, *Geol. Soc. Am., 104*, 770-778, 1992.

Zimmermann, M., M. Bichsel, and H. Kienholz, Mountain hazards mapping in the Khumbu Himal, Nepal, with Prototype Map, scale 1:50,000, *Mtn. Res. Dev., 6,* 29-40, 1986.

D. A. Cenderelli, Dept. of Geology, 202 Bevill Research Building, University of Alabama, Box 870338, Tuscaloosa, Alabama 35487.

B.L. Cluer, U.S. National Park Service, Water Resources Division, 1201 Oak Ridge Drive, Fort Collins, CO 80525

Bedrock Channel Morphology in Relation to Erosional Processes

Ellen E. Wohl

Department of Earth Resources, Colorado State University, Fort Collins, Colorado

Bedrock channel morphology reflects the interactions between erosive processes and the resistance of the channel substrate. The controls on these interactions change with spatial scale. Mineralogy, exposure age of the substrate, and local heterogeneities are particularly important in controlling substrate resistance at the micro scale (mm to cm). Substrate discontinuities created by bedding, joints, and lithologic contacts become progressively more important at the meso scale (cm to m), whereas regional structure and baselevel history may dominate substrate resistance at the macro scale (m to km). In a similar manner, turbulent fluctuations that create localized abrasion and cavitation are more important at the micro and meso scales, whereas longitudinal patterns of unit and total stream power exert a stronger influence on channel morphology at the macro scale. Most studies of bedrock channel morphology have described meso-scale erosional features. In the absence of direct measurements, investigators have inferred both the erosive processes that produced the observed features, and the controls on the location of the features. Fluvial erosion of bedrock may occur via; (1) corrosion, or chemical weathering and solution, (2) corrasion, or abrasion by sediment in transport along the channel, or (3) cavitation and other hydrodynamic forces associated with flow turbulence. Very few direct measurements of rate exist for any of these erosive processes. Bedrock channel morphologies may be divided into multiple or single flowpath channels, and subdivided on the basis of sinuosity, uniformity of bed gradient, and uniformity of erosion across a cross section. These categories may be used to infer dominant erosional processes and relative rates of erosion, but we cannot yet predict the occurrence of specific channel morphologies as a function of driving and resisting forces. In this context, the traditional assumption that substrate dominates bedrock channel morphology may be too restrictive.

INTRODUCTION

Using the definition of bedrock channels proposed in the introductory chapter of this volume, the presence of exposed bedrock along a channel implies only limited, localized deposition along the channel. Therefore, the morphology of many bedrock channels is dominated by erosional processes. The actual erosive processes operate at fairly small spatial scales, on the order of millimeters to meters, as a function of the chemical and physical mechanisms causing erosion. However, the channel forms that result from these processes may be considered at various spatial scales (Table 1). The controls that influence how erosive processes will interact with channel substrate to create channel morphology change with spatial scale. At the micro scale (mm to cm), heterogeneities in the form of intergranular or intercrystalline boundaries, bedding, foliation, and small fractures and joints, as well as primary mineral

Rivers Over Rock: Fluvial Processes in Bedrock Channels
Geophysical Monograph 107

Table 1. Scales of erosional features.

SCALE	EROSIONAL CHARACTERISTICS
Micro-scale (mm to cm)	Abrasion, flaking, or plucking of individual grains or small pieces of rock
Meso-scale (cm to m)	Selective erosion of portions of the channel boundaries across a cross-section or along a reach: produces potholes, longitudinal grooves, knickpoints, undulating walls, inner channel, pool-riffle or step-pool sequences
Macro-scale (m to km)	Reach- to basin-scale channel morphologies in planform (meandering, downstream alternations in width and gradient), and in gradient

composition, will determine porosity, permeability, and susceptibility to chemical weathering, abrasion, and hydrodynamic forces. The intact rock strength and resistance to erosion at this scale are most likely to be dominated by mineralogy and exposure age of the substance. Turbulent fluctuations that generate local cavitation and abrasion may be particularly important in micro-scale erosion.

At progressively larger spatial scales, substrate discontinuities in the form of bedding contacts, joints, and lithologic contacts play a greater role in localizing weathering and differential erosion. Differences in flow energy expenditure across and along the channel also influence erosional forms at the meso scale (cm to m). These differences are associated with turbulence resulting from variations and asymmetries in channel width, depth, and gradient. An initial weakness in the substrate or perturbation in the flow may create localized channel erosion that then continues through a self-enhancing feedback as the erosional feature further weakens the substrate or perturbs flow. This is the conceptual model commonly applied to potholes, for example: intersecting joints subject to more rapid chemical weathering promote formation of a depression that then traps more water even during low flow, promoting continued chemical weathering. Or, turbulent deflection of flow over an obstacle selectively abrades the bed, creating a depression that localizes a vortex which further abrades and deepens the depression. Differences in abrasion across and along the channel will also be governed partly by hydraulics, and partly by the quantity, grain-size distribution, and relative hardness of the sediment in transport.

At the macro scale (m to km), regional joint patterns, lithologic contacts, structural folding and faulting, tectonic regime/baselevel history, and longitudinal patterns of total and unit stream power may dominate the channel morphologies produced by erosive processes. The relative intensity of abrasion acting at the micro- and meso-scales, for example, may be influenced by macro-scale variations in gradient associated with tectonic uplift.

Studies of bedrock channels that have focused on the relations between erosive processes and channel form have generally considered one of two scales (Table 2). The majority of studies have focused on meso-scale erosional forms. These studies have been largely descriptive, although some investigators have performed experiments to measure erosive processes [*Alexander,* 1932; *Ängeby,* 1951; *Dzulynski and Walton,* 1963; *Dzulynski,* 1965; *Allen,* 1969, 1971, 1982; *Karcz,* 1970, 1973; *Shepherd and Schumm,* 1974; *Holland and Pickup,* 1976; *Gardner,* 1983; *Wohl and Ikeda,* 1997]. The initial approach to meso-scale erosional features, as exemplified by *Blank* [1958], was to describe a specific channel reach containing potholes or longitudinal grooves; to infer the erosive processes producing these features; and then to explain the location of the erosional features in terms of gradient, lithology, or other reach-length characteristics unique to that site. Another approach, developed largely by Baker [e.g. *Baker, 1973*], involved using paleostage indicators in conjunction with step-backwater hydraulic models to route a flood discharge along a channel reach. Modeled flood hydraulics were then related to specific erosional features such as pool-riffle sequences [e.g. *O'Connor et al.,* 1986; *Baker and Pickup,* 1987], to provide a more quantitative basis for inferring erosive processes.

Studies of meso-scale erosional features have been largely empirical and inferential almost by default. The majority of such erosional features have such a high threshold resistance to erosion that they are primarily shaped by the large discharges which can generate sufficient hydraulic force to overcome the threshold. Large discharges occur unpredictably, and it is difficult and dangerous to obtain direct measurements of hydraulic variables during such floods. We have therefore been confined to small-scale flume simulations, or to inferring process from form.

A second basic approach to erosive processes and channel form has focused on modeling macro-scale channel evolution. Models developed thus far have assumed that incision rate is predominantly a function of shear stress, stream power, or sediment scour, although there is general recognition that natural channels are eroded by a variety of processes [e.g. *Howard et al.,* 1994; *Rosenbloom and Anderson,* 1994; *Seidl et al.,* 1994]. Macro-scale studies tend to be more theoretical than meso-scale studies in the sense that the former assume a primary erosive process and a rate law (generally with erosion proportional to discharge), and then assess the accuracy of these assumptions by comparing model predictions to actual channel form as recorded by present longitudinal profile and by terraces. Macro-scale models of course devote much less attention than meso-scale studies to the actual mechanics of erosion, as these interact with substrate to produce specific channel forms. Macro-scale studies concentrate rather on

Table 2. Summary of selected studies of bedrock channel erosive processes and forms.

LOCATION	SUMMARY OF CONTENTS	REFERENCE
MESO-SCALE		
Description of morphology and inferred origin of features		
e. Canada	knickpoints (Niagara Falls)	Gilbert, 1895
various	potholes	Elston, 1917,1918
various	potholes, with experimental work	Alexander, 1932
various	potholes	Ives, 1948
Utah/Az.	potholes	Gregory, 1950
n. Sweden	potholes, with experimental work	Ängeby, 1951
Texas	potholes	Blank, 1958
e. Canada	knickpoints (Niagara Falls)	Philbrick, 1970
Spain	potholes	Lorenc and Saavedra, 1980
various	knickpoints	Young,1985
Japan	potholes	Sato et al., 1987a,b
e. Canada	various erosional forms - subglacial	Sharpe and Shaw, 1989
e. Canada	various erosional forms - subglacial	Kor et al., 1991
Indiana	knickpoints	Miller, 1991
se Australia	knickpoints	Bishop and Goldrick, 1992
e. Canada	various erosional forms	Tinkler, 1993
e. Canada	knickpoints, history of retreat (Niagara)	Tinkler et al., 1994
Virginia	potholes	Zen and Prestegaard, 1994
Israel	step-pool sequences	Grodek et al., 1994
w. Spain	potholes	Lorenc et al., 1994
Oregon	step-pool sequences	Duckson and Duckson, 1995
Modeled flood hydraulics used to infer origin of described features		
nw U.S.	various erosional features	Baker, 1973
sw U.S.	various erosional features	O'Connor et al., 1986
n Australia	various erosional features	Baker and Pickup, 1987
ne Australia	various erosional features	Wohl, 1992
California	pool-riffle sequences	Wohl et al., 1993
nw U.S.	various erosional features	O'Connor, 1993
nw U.S.	various erosional features	Rathburn, 1993
nw Australia	various erosional features	Wohl, 1993
Israel	various erosional features	Wohl et al., 1994
nw U.S.	various erosional features	Benito, 1997
Japan	various erosional features	Wohl and Ikeda, in press
MACRO-SCALE		
New Guinea	terraces and modeling long profiles	Chappell, 1974
Virginia	measurement of short-term incision rates	Howard and Kerby, 1983
Oregon	modeling long profiles	Seidl and Dietrich, 1992
California	terraces	Merritts et al., 1994
California	terraces and modeling long profiles	Rosenbloom and Anderson, 1994
Hawaii	modeling long profiles	Seidl et al., 1994

longitudinal profile as an indicator of the channel's ability to incise, or on channel network development.

Macro-scale approaches to channel form are described in detail in chapters 3, 9, 10, 11, and 14 of this volume, and the remainder of this chapter will focus on the micro- and mesoscales. We can begin by summarizing present knowledge of the actual erosive processes operating along bedrock channels. The alluvial veneer present along many bedrock channels may be shaped by the same erosive forces of clast entrainment and abrasion that operate along alluvial channels (see chapters 2 and 5). The bedrock substrate is eroded by processes of corrosion, corrasion, and cavitation.

Erosive Processes

Corrosion refers to chemical weathering and solution that may directly erode the bedrock, as in carbonate lithologies or, more commonly, may weaken the bedrock and render the substrate more susceptible to erosion by corrosion and cavitation [*Carling and Grodek*, 1994]. Very few estimates have been published of direct chemical weathering in channels. Most chemical erosion rates are averaged across a basin [*Summerfield and Hulton*, 1994], and thus incorporate groundwater and soil processes, or are obtained from rock faces exposed on hillslopes, buildings, or tombstones. Generalized estimates for drainage basins range from 0.005 mm yr^{-1} (shield provinces) to 0.2 mm yr^{-1} for carbonates and shales and 0.7 mm yr^{-1} for evaporites [*Lerman*, 1988]. In one of the few studies that quantified in-channel chemical erosion, *Smith et al.* [1995] measured rates of 0.022-0.200 mm yr^{-1} in carbonate terrains of eastern Australia.

Corrasion is abrasive weathering of bedrock by clasts moving along the channel as bedload or suspended load. Corrasion will be a function of: (i) the resistance of clasts in transport relative to the resistance of the bedrock substrate; (ii) the grain-size distribution and amount of sediment in transport, and (iii) the hydraulics of the flow, which determine the location, magnitude and frequency of sediment-bedrock abrasive contacts. Partly because it is very difficult to separate erosion caused by abrasion from erosion caused by other processes, and partly because rates of bedrock channel erosion are commonly slow relative to the duration of most field studies, there are few published rates of bedrock channel erosion caused solely by abrasion (see *Hancock et al.*, this volume). During one year, *Dick et al.* [1997] measured abrasion rates up to 3.9 mm yr^{-1} on shallow (1-3 cm) drill holes in the granite, schist, and gneiss of the Indus River, Pakistan. These rates were highly sensitive to localized flow conditions; longer-term erosion rates, obtained via cosmogenic radionuclide chronologies, were 0.25-0.48 mm yr^{-1}. The most rapid rates of abrasion probably occur during turbulent floods with large and fairly coarse suspended sediment loads, along channels of weakly resistant bedrock. Channels inferred to be dominated by corrasional erosion have numerous potholes, longitudinal grooves, knickpoints, and similar erosional features along the channel bed and walls.

Cavitation occurs when velocity fluctuations in a flow induce pressure fluctuations that cause the formation and implosion of vapor bubbles. The shock waves generated by implosion can weaken bedrock and pit the rock surface, a phenomenon common along the concrete spillways of dams [*Falvey*, 1982; *Kells and Smith*, 1991]. Cavitation may occur at flow separations induced by joints, bedding planes, or other surface irregularities in bedrock [*Barnes*, 1956]. Under sustained high flows, the erosive potential of this process can be phenomenal. During 1983, discharges up to 900 $m^3 s^{-1}$ through the spillway at Glen Canyon Dam on the Colorado River generated cavitation that within days eroded pools up to 10 m deep and 6 m long in a stairstep configuration down the 12.5-m-diameter concrete-lined spillway [*Eckley and Hinchliff*, 1986].

In addition to cavitation, other hydrodynamic forces in the flow may also cause erosion. Turbulence and lift forces contribute to the quarrying and plucking of jointed rocks [*Baker*, 1978], and this process may be especially important in eroding the beds of channels formed in thinly bedded and/or densely jointed sedimentary rocks. *Tinkler* [1993] describes blocks of sandstone 1.2 x 1.45 x 0. 11 m and 1.0 x 0.5 x 0.05 m being removed from the bed of Twenty Mile Creek, Ontario (293 km^2) during normal winter flows with a mean water depth of less than 0.4 m. A flood flow 2.7 m deep along the concrete-lined portion of Brush Creek, Kansas was able to quarry concrete slabs up to 5 x 4.6 x 0.2 m thick, and transport these slabs 50-300 m downstream [*Vaughn*, 1990]. *Wende* [in press] describes blocks with an average long axis of more than 4 m (and up to 13 m) plucked from a bed of jointed sandstone and deposited in imbricate boulder clusters along the Durack River, Australia during flood flows 10 m deep.

Remarkably little is known about the actual processes by which bedrock channels are eroded. Erosive processes are extremely difficult to measure directly because of the combination of relative inaccessibility (deep, turbulent flows; remote locations) and unpredictability (infrequent floods) that characterize erosion along bedrock channels. For a channel with resistant substrate, discernible bedrock erosion may be so slow and infrequent on a human time scale as to effectively preclude direct measurement. Quantitative experimental studies using cohesive silt or clay substrates in flumes have provided important insights, but more of these studies are needed, along with experiments using actual rock and coarse sediment to estimate abrasion rates. Multi-year detailed monitoring of erosion along channels in weak bedrock, as exemplified by the ongoing work of Tinkler on channels of the Niagara Escarpment (Ontario, Canada), would also be extremely useful. In the absence of such studies, we can only infer erosional processes from channel form and erosional rates from long-term averages based on good geochronologic control. These inferences yield scant information on the rate

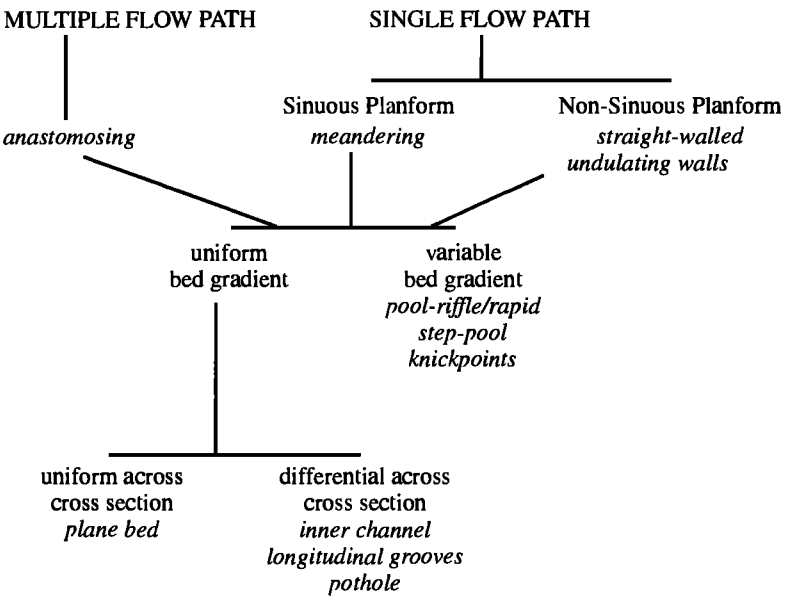

Figure 1. Typology of meso-scale bedrock channel morphologies.

of erosion during floods of varying magnitude, for example, and make it difficult to hypothesize potential erosional thresholds of channel form or stability.

CHANNEL MORPHOLOGIES

Multiple Flow-Path Channels

The majority of bedrock channels have single flow paths. However, multiple-flow path channels incised into bedrock have been described for several environments. These have been called both anastomosing channels and scabland topography or scablands. *Baker* [1973, 1978] described anastomosing complexes with individual channels of relatively low sinuosity in the Channeled Scabland of Washington. The Scabland topography was formed by catastrophic outburst floods from Glacial Lake Missoula. Baker attributed the anastomosis to the inability of preflood valleys to convey the tremendous discharges (approx. 21.3 x 10^6 $m^3 s^{-1}$) of the Missoula Flood without spilling over preflood divides into adjacent valleys. Regional-scale anastomosis was thus controlled by preflood topography. *Kale et al.* [1996] and *Gupta et al.* [in press] describe anastomosing channels along the Narmada River of India. They hypothesize that block or domal uplift of this portion of the Narmada basin steepened valley gradients so that floods along the channel could exploit linear weaknesses in the bedrock, leading to the establishment of multiple channels. *Kale and Shingade* [1987] describe the formation of multiple bedrock channels along the Indrayani River by coalescence of grooves and potholes along joints in basalt bedrock. The multiple channels of the Narmada River also provide a mechanism for channel widening in conjunction with incision, which *Simon* [1992] has identified as the most effective means of energy dissipation in a disturbed channel. Other examples of anastomosing channels have been described from the Katherine Gorge of northern Australia [*Baker and Pickup*, 1987], where a prominent channel constriction might be capable of hydraulically ponding floodwaters and diverting them across the adjacent upland (the scabland surface is approx. 20 m higher than the adjacent canyon floor); and from the Sabie River of eastern South Africa [*Van Niekerk et al.* 1995; *Heritage et al.*, in press; *Van Niekerk et al.*, in press].

The presence of active anastomosing channels along a bedrock drainage probably signals more rapid channel incision in the anastomosing reach than in the reaches up- and downstream. Anastomosis may result from insufficient channel capacity, localized uplift along the channel, and/or joint controlled weathering.

Single Flow-Path Channels

Single channels incised into bedrock may have diverse morphologies. Although no widely accepted classification exists for bedrock channel morphologies, they may be subdivided as in Figure 1. The subdivisions under single flow path focus on sinuosity and uniformity of reach gradient at the first level, and then on the uniformity of erosion across an individual cross section. One of the outstanding characteristics of bedrock channels is their downstream morphologic variability. The subdivisions proposed in Figure 1 are most appropriately applied at the reach-scale, where a reach is defined as being at least several times average channel width and having consistent channel morphology.

Figure 2. View upstream of pool-riffle sequence formed in bedrock and alluvium, Japan. Channel is approximately 20 m wide.

Figure 1 presents a descriptive classification in which the different categories do not necessarily belong to discrete, non-overlapping groups. A single bedrock channel may have any or all of the types of morphologies listed in Figure 1 occurring in longitudinal sequence. The placement of the distinction between multiple and single flow path at the top of the figure does not imply that the categories at the bottom of the figure cannot be associated with either or both. Rather, the figure is organized along a decreasing spatial scale from reach-length planform to variability at the scale of a single cross section.

Variable bed gradient. Bedrock channels with variable bed gradients are analogous to alluvial channels in that they have pool-riffle or step-pool bedforms resulting from differential expenditure of flow energy along the channel. These bedforms may be partly alluvial, as in channels with pools scoured to bedrock, and riffles or steps formed of coarse clasts or large woody debris (Figure 2) [*O'Connor et al.*, 1986; *Wohl*, 1992b; *Wohl et al.*, 1993; *Wohl and Grodek*, 1991]. The bedforms may also be formed entirely in bedrock as a result of differential scour of the bedrock [*Baker*, 1988; *Duckson and Duckson*, 1995] (Figure 3). The relatively few studies of pool-riffle and step-pool bedforms along bedrock channels suggest that: (1) weaknesses such as joints or bedding planes may localize pool scour [*Dolan et al.*, 1978] or influence step spacing [*Duckson and Duckson*, 1995]; (ii) only high magnitude flows are capable offering and maintaining these bedforms because of the high inertial resistance of the large clasts or intact bedrock constituting the bedforms [*Wohl*, 1992a]; and (iii) the spacing and magnitude of these bedforms may be greater than along alluvial channels because the high boundary resistance of bedrock channels facilitates adjustment to discharges of higher magnitude and lower frequency [*Roy and Abrahams*, 1980; *O'Connor et al.*, 1986; *Baker and Pickup*, 1987].

Because of the possibility of structural joints, bedding planes) control on the downstream spacing of bedrock pool-riffle or step-pool sequences, the role of hydraulic controls has often been downplayed. However, along at least some channels with mixed bedrock and alluvial bedforms, the characteristics of bedrock steps, riffles, and pools cannot be statistically distinguished from those of alluvial features [*Keller and Melhorn*, 1978; *Wohl and Grodek*, 1994]. This suggests that bedrock bedforms are affecting and responding to flow energy expenditure in a manner analogous to that of alluvial bedforms.

Recent studies of large canyon rivers in the western United States have provided insight into downstream variability in channel width and gradient associated with the formation of debris fans at tributary confluences. Arguments have been

Figure 3. Big Box Canyon, central Arizona. Channel formed in Precambrian quartzite, with step-pool sequence formed directly in bedrock.

made for a random spacing of these features as a function of downstream energy expenditure [*Leopold,* 1969; *Graf,* 1979], and for geologic (structural) controls on spacing [*Dolan et al.,* 1978]. The tributary fans constrict flow in the main channel, creating a distinctive suite of associated deposits, including fine-grained eddy and reattachment bars along the channel margins downstream from the constriction, and a "rock garden" of coarse clasts eroded from the constriction during high flows [*Kieffer,* 1985, 1987, 1989; *Webb et al.,* 1988; *Schmidt et al.,* 1993; *Cluer,* 1995]. As a result, the effect of lithology on channel morphology may be indirect even in a deeply incised bedrock canyon, particularly if the channel is formed on coarse sediment introduced by mass movements and tributaries [*Grams and Schmidt,* in press].

Bedrock channels may also have downstream variability in gradient as a result of knickpoints. Knickpoints may take the form of vertical or undercut waterfalls several meters in height (Figure 4), or they may be short, steep sections of channel more appropriately called knickzones. Cataract refers to a step-like succession of knickpoints. Knickpoints differ from bed-steps in that knickpoints: (1) are generally not regularly spaced along the channel, and do not have a spacing proportional to bed gradient; (ii) are commonly most well-developed in layered or jointed rocks, and (iii) are generally regarded as disequilibrium features that either migrate upstream, erode toward a lower angle, or otherwise change in form or location fairly quickly relative to the evolution of the stream channel.

Knickpoints may occur as rotating headcuts that tend to flatten as they migrate, or as stepped headcuts that retain nearly vertical faces as they migrate upstream [*Stein and Julien,* 1993]. Rotating headcuts characterize massive, homogeneous material, in which knickpoints may be created by baselevel fall. As flow approaches the lip of such a knickpoint, width decreases, but depth, velocity, and bottom shear stress increase [*Gardner,* 1983]. Consequently, an incising reach above the knickpoint lip increases in slope. Decrease in shear stress below the knickpoint lip facilitates a gradual decrease in slope with time, so that the knickpoint gradually flattens as it moves upstream.

The classic explanation for a process of knickpoint retreat in stepped headcuts was first proposed by *Gilbert* [1895]. This theory featured undercutting by erosion of less resistant strata due to turbulence and abrasion in the plunge pool, creating an increasingly unstable caprock that eventually failed. However, the plunge pool at Niagara Falls is not known to be undercut below the water *level* [*Tinkler, pers. comm.,* 1997], and the role of plunge pool erosion in knickpoint retreat remains unclear. Subsequent studies have described knickpoints for which pothole erosion at the lip is an important component of headward retreat [*Bishop and Goldrick;* 1992], and knickpoints buttressed outwards at the base, rather than undercut [*Young,* 1985]. Knickpoint distribution is influenced by joint frequency, lithologic layering, and the relations between strata dip and stream flow direction [*Miller,* 1991; *Wohl et al.,* 1994].

Knickpoints are the sites of the greatest concentration of energy dissipation along the course of a stream. Although waterfalls in tropical cratons have been interpreted as evidence that the stream is unable to incise through a resistant lithologic unit, such interpretations have been made without knowledge of rate of waterfall retreat [*Thomas,* 1974; *Faniran and Jeje,* 1983]. Most investigators have assumed that knickpoints retreat fairly rapidly, and have concentrated on the mechanisms and rates of knickpoint retreat. *Holland and Pickup* [1976] subdivided a knickpoint system into an aggraded reach upstream from each knickpoint, an oversteepened reach just above the knickpoint face, the knickpoint face, and an incising reach partially covered by moving sediment between successive knickpoints. Shear stress is highest just above and at the knickpoint face [*Gardner,* 1983]. Knickpoint retreat is proportional to discharge, and is a function of the balance

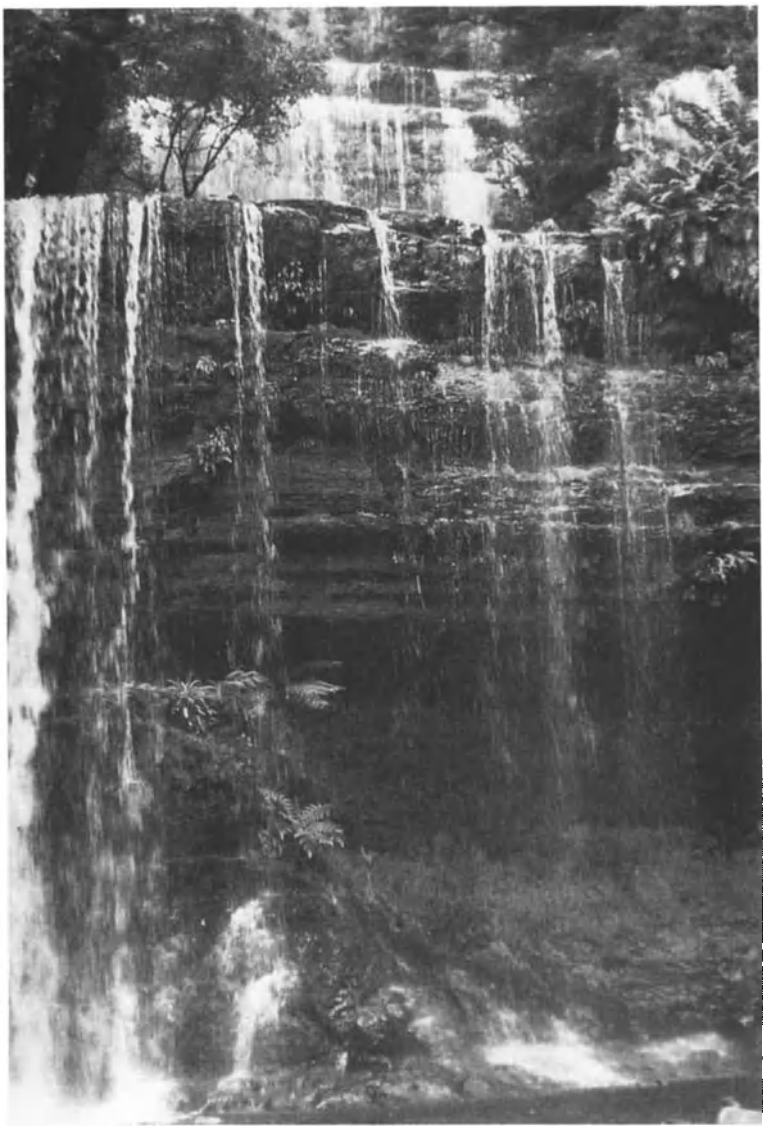

Figure 4. Vertical to slightly undercut knickpoint, Russell Falls, Tasmania, Australia.

between rate of downwearing on the oversteepened reach and rate of backwearing on the knickpoint face, and of knickpoint height [*Holland and Pickup,* 1976]. An arched planimetric shape stabilizes the forces of compression in the rocks until a notch breaks the shape of the arch, when the knickpoint retreats rapidly *Philbrick* [1970]. In a study of 72 knickpoints formed in Paleozoic sedimentary lithologies along the Niagara Escarpment of Canada, *Pyrce* [1995] found that as form width or knickpoint height increases, the curvature of the lip decreases. The greatest headward erosion at the middle of the lip (in planform) occurs with low knickpoint height relative to high width, and most of the erosion occurs through quarrying. *Seidl et al.* [1994, 1997] note that mantling of the channel by large, fairly immobile boulders may inhibit uniform incision, so that knickpoint propagation beneath the boulder pile is necessary for incision of bedrock to occur.

Very few actual measurements exist for rates of bedrock Knickpoint retreat. An exception is the well-dated Niagara Falls region. Radiocarbon ages of clam shells suggest that the 46 m high falls migrated at rates of 0.05-0.70 m yr^{-1} along the narrowed gorge section at Niagara Glen from 10500 to 5500 yr B.P., when upper Great Lakes water bypassed the site [*Tinkler et al.* 1994]. Prior to that interval, river discharge and recession rates were similar to those at present (1.57 m yr^{-1}), and similar rates resumed

after 5200 yr B.P. Seidl's work in Kauai [*Seidl et al.*, 1994, 1997] demonstrates that large boulders may remain in the channel below knickpoints for hundreds of thousands of years, suggesting waves of incision up the valley that take the form of knickpoint retreat at 40-100 cm/kyr. Despite such high rates of retreat for some knickpoints, there is now an increasing recognition that the maintenance of knickpoint *form* through headward retreat represents an equilibrium channel-bed form that may be maintained for centuries to millenia until profile adjustments to baselevel lowering can occur [*Holland and Pickup*, 1976; *Miller*, 1991; *Wohl et al.*, 1994].

Uniform bed gradient Bedrock channels with a uniform bed gradient may have the regular rectangular to trapezoidal cross-sectional form of a plane-bed channel (Figure 5). Few descriptions exist of bedrock plane-bed channels. These channels have uniform, relatively featureless beds along which erosion occurs by flaking of rock fragments, quarrying of blocks, and shallow abrasional features such as longitudinal grooves. This morphology characterizes fairly densely jointed or bedded soft rocks across which constant small-scale erosion can produce cross-sectionally and longitudinally even rates of channel incision.

Bedrock channels with a uniform bed gradient at the reach scale may also have differential erosion across the channel (Figure 1). Zones of enhanced erosion may take the form of longitudinal grooves (Figure 6); longitudinal or transverse scoops and troughs (Figure 7); potholes; or inner channels (Figure 8). Along with waterfalls, erosional bed features were one of the first aspects of bedrock channels to be studied in detail. Irregularities along an alluvial channel bed may be swiftly modified or removed as turbulent and shear forces reshape the mobile bed, or as sediment deposition buries the irregularity. The combination of greater turbulence, lower sediment supply, and greater boundary resistance along bedrock channels may facilitate the preservation of substrate irregularities and their enhancement into erosional features. Substrate irregularities may take the form of lithologic contacts between rocks of differing resistance to weathering and erosion; joints, fractures, or bedding planes; or differential weathering caused by heterogeneities in porosity, permeability, cementation, and rock structure. An initial irregularity on the channel substrate may perturb flow and sediment movement, initiating cavitation or turbulence which leads to differential erosion of the substrate in a self-enhancing feedback that eventually creates an erosional feature.

Examples of this process have been described by *Tinkler* [1993], who noted that even a small step in a channel bed may enhance the effect of low-velocity flows passing over it and thus enhance abrasion in areas immediately downstream. Incoming stream velocity v_i, is accelerated to velocity v_b, when passing over a step of height h:

$$v_b = (2gh + v_i^2)^{0.5} \quad (1)$$

Thus, 1 m s^{-1} flow over a 20-cm step is accelerated to 2.2 in m s^{-1}, for example. Smoothly abraded bedrock surfaces such as sichelwanne [*Kor et al.*, 1991], open spindles, or undercut downsteps, inhibit flow separation at low velocities and enable suction to keep thin sheets of water on the rock surface along the steep proximal slope of the erosional form. Flow accelerates on the proximal slope, and then breaks at a hydraulic jump in the distal furrow below. Accelerating sediment-laden water that maintains contact with the rock surface in this manner enhances bed abrasion, and the transition back to subcritical flow, which is induced by the bedform, helps to localize abrasion [*Tinkler*, 1993].

Experimental studies [*Dzulynski and Walton*, 1963; *Dzulynski*, 1965; *Karcz*, 1970, 1973] have demonstrated that varying ratios and substrate resistance produce regular progressions of erosional forms. *Allen* [1969], for example, observed longitudinal rectilinear grooves, then longitudinal meandering grooves, flute marks, and finally transverse erosional markings and shear wrinkles as velocity increased over a claybed. *Shepherd and Schumm* [1974] *and Wohl and Ikeda* [1997] observed a progression from parallel longitudinal grooves, to a broad, shallow inner channel with undulating walls, and finally to a progressively deeper and more sinuous inner channel as bed gradient increased. These experimental studies each used a cohesive but soft (silt or clay) substrate that responded readily to changes in flow regime. However, the results of the experiments imply that erosional forms present along the more resistant substrate of bedrock channels also may be used to infer at least relative hydraulic characteristics across the channel bed [*Allen*, 1982]. As a rule, these features occur along channel reaches with steady, rapid, sediment-charged flow and a channel geometry that accelerates flow through a constriction or a locally steeper gradient [*Maxson*, 1940; *Baker and Pickup*, 1987;*Wohl*, 1993].

Potholes also have an extensive literature going back to early field studies by *Elston* [1917, 1918], who classified these features into abrasive and solutional forms. *Alexander* [1932] subdivided abrasional potholes based on the angle of entry by water, and conducted experiments demonstrating feedbacks between pothole geometry and flow hydraulics [see also *Ängeby*, 1951]. Subsequent field descriptions of potholes include a wide range of lithologies, climates, and channel types (see Table 2). *Zen and Prestegaard* [1994] quantitatively related potholes to flow Reynolds number and proposed that potholes could be used to reconstruct hydraulic conditions. Quantitative estimates for rates of pothole erosion apparently do not exist, however, and it is likely that potholes in resistant substrate require hundreds to thousands of years to form. Potholes in less resistant bedrock, such as the sandstone along the Ukak River, Alaska described by *Dollenmayer et al.* [1997] may form rapidly. This channel is incising at least 4-10 cm/yr, and potholes up to 6 m in diameter and 5 m in depth have formed within 85 years.

Figure 5. (A) Torii Creek, Boso Peninsula, Japan. Channel formed in interbedded sandstone and mudstone, with a plane-bed morphology. Channel is approximately 4 m wide. (B) Shichiri River, Boso Peninsula, Japan. Plane-bed channel formed in interbedded sandstone and mudstone. Channel is approximately 20 m wide.

Figure 6. View downstream of parallel longitudinal grooves eroded into the sandstone bed of Piccaninny Creek, Australia.

Figure 7. Troughs eroded into welded rhyolitic tuff along the Burdekin River, Australia. Keys at right center for scale.

Figure 8. (A) View upstream of potholes eroded into the sandstone bed of Piccaninny Creek, Australia. (B) View upstream of inner channel with strongly undulating walls and bed formed by breaching of potholes, Peek-A-Boo Canyon, Utah. Field notebook at right for scale.

Most investigators have noted that potholes characteristically occur along constricted channel reaches of rapid flow. Many investigators have also hypothesized that the formation and subsequent breaching of potholes may be an important process in the formation of an inner channel [*Elston,* 1917; *Shepherd and Schumm,* 1974; *Wohl,* 1993; *Dollenmayer et al.* 1997]. Deep, narrow inner channels are present in particularly large bedrock channels such as the Columbia River [*Bretz,* 1924], the Colorado River [*Wilbur and Mead,* 1933], the Chang Jiang of China [*Baker,* 1988], and the Burdekin River of Australia [*Wohl,* 1992a], as well as along much smaller bedrock channels [*Tinkler,* 1971; *Wohl,* 1993]. Based on their experimental work, *Shepherd and Schumm* [1974] hypothesized that inner channels are formed by the large flow stresses generated during high discharges along steep bed gradients, an explanation supported by subsequent investigators [*Baker,* 1988; *Wohl,* 1992a; *Wohl and Ikeda,* 1997]. The presence of inner channels, which maximize shear stress and unit stream power for a given stage, may be the most efficient means for channels to incise into resistant substrate.

In general, the presence of differential erosion at the cross-sectional scale may imply that a bedrock channel is actively incising. Because of the resistant nature of most bedrock, relict erosional features may persist along a channel centuries to millennia after the conditions under which the forms were created have changed. Lack of chemical weathering or organic (lichen, moss) growth, and sharp, freshly abraded or polished surfaces indicate that erosional features are actively forming. *Shepherd and Schumm* [1974] noted that, subject to the constraints imposed by bedrock and structural variations, actively incising channels have more longitudinally regular scour patterns than stable channels, but there has been no quantification of this regularity.

Straight channels. Single channels incised into bedrock may also be subdivided on the basis of planform (Figure 1). Channels with a sinuosity less than 1.5 may have straight or undulating walls. Undulating walls have regular concavities and convexities that approximate a sine-generated curve, with undulations on each wall being out-of-phase relative to the opposite channel wall (Figure 9). Undulating walls are most characteristic of deep, narrow slot canyons, and occur along channels formed in every type of cohesive substrate from clay to volcanic ash to granite and gneiss; climatic environments from deserts to the wet tropics; and both active and quiet tectonic regions. In slot canyons, the channel walls form a much larger proportion of the channel boundary than does the channel bed, and "wallforms" are hypothesized to regulate and respond to flow energy expenditure in a manner analogous to bedforms [*Wohl,* 1994]. The presence of undulating walls typically indicates an actively incising channel that is incising headward via potholes and sinuous grooves or knickpoints. The undulations are preserved along a reach after the knickpoint has migrated upstream because the alternating

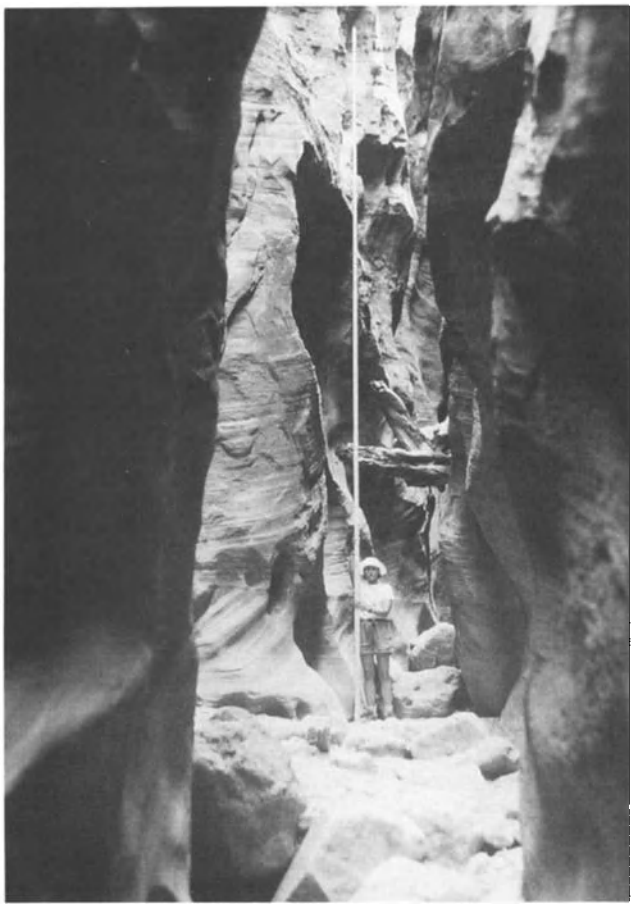

Figure 9. Wire Pass Canyon, southern Utah. Channel with undulating walls formed in Navajo Sandstone. Channel is approximately 3 m wide.

constrictions and expansions create a self-stabilizing flow pattern of critical flow through the constriction, with subcritical flow and flow separation along the margins of the expansion. This flow pattern in turn promotes differential velocity and sediment transport - and abrasion and hydrodynamic forces - along the constrictions and expansions [*Wohl et al.* in press].

Straight-walled bedrock channels also commonly exhibit periodic or aperiodic variability in channel width. One of the most ubiquitous characteristics of bedrock channels is a downstream alternation between relatively narrow, high gradient reaches and wider, lower gradient reaches that commonly have an alluvial veneer or fill. Depending on the size of the channel, this downstream alternation may occur at kilometers to tens of kilometers along channels such as the Bhote Kosi, Nepal [*Wohl et al.,* in press], the Snake River, Idaho [*O'Connor,* 1993], the South Branch Potomac River basin, West Virginia [*Miller and Parkinson,* 1993; *Miller,* 1995], or the Green River, Utah [*Grams and*

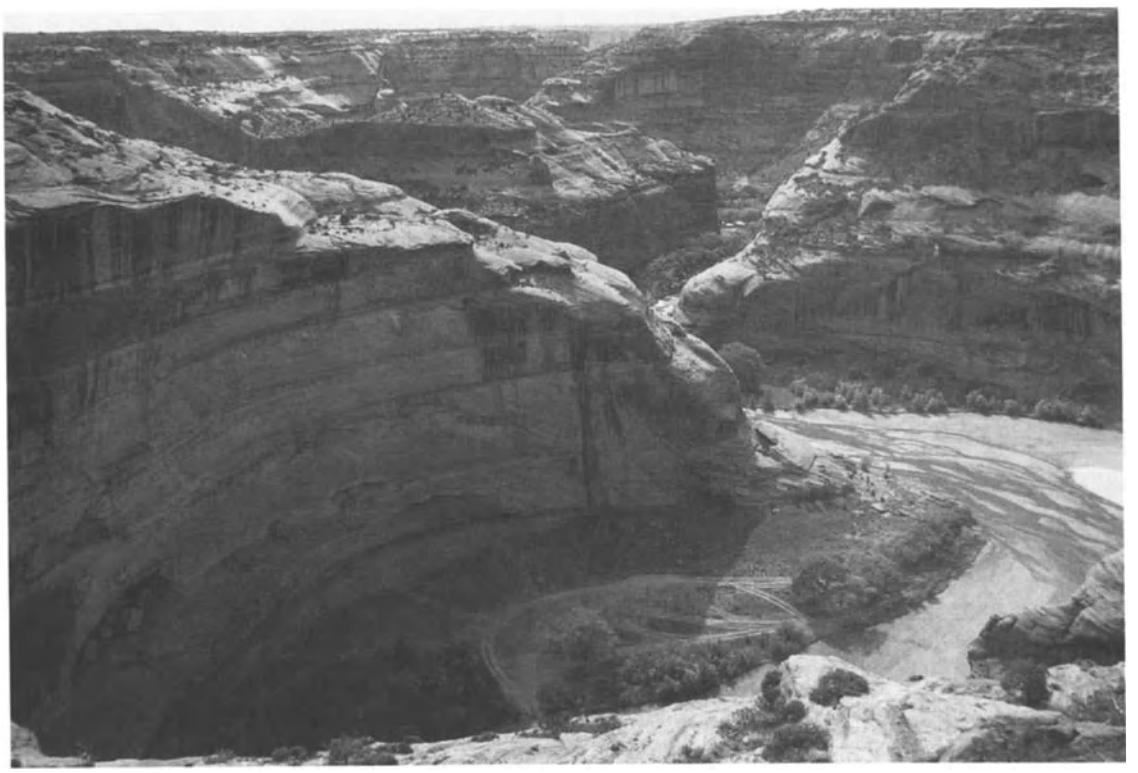

Figure 10. Meandering channel incised into sandstone, Canyon de Chelly, Arizona.

Schmidt, in press]; or at tens to hundreds of meters, as along Wire Pass Canyon, Utah [*Wohl et al.* in review], Piccaninny Creek, Australia [*Wohl,* 1993], or Big Thompson Canyon, Colorado [*Shroba et al.* 1979]. These downstream alternations may be partly controlled by underlying structural patterns. Joint patterns in granite, for example, tend to produce regularly stepped topography across which downstream alternations in valley width develop [*Twidale,* 1971]. The downstream alternations may partly be controlled by tributary debris fans, such as occur along the canyon rivers of the Colorado Plateau [*Webb et al.,* 1988]. However, structural patterns or tributary inputs are not necessary to create the downstream alternations; *Shepherd and Schumm* [1974] *and Wohl and Ikeda* [1997] noted a similar longitudinal pattern in experimental channels formed in homogeneous substrate.

Meandering channels. Single bedrock channels with sinuosity greater than 1.5 differ from meandering alluvial channels in some important respects. Flows effective in meander formation may have a much larger recurrence interval than those of meandering alluvial channels [*Tinkler,* 1971]. Both lateral and vertical differences in bedrock erodibility may strongly influence meander size and morphology, and inherited meander dimensions may be preserved along deeply incised channels, despite intervening changes in discharge and sediment regime (Figure 10). Several studies have concluded that resistant bedrock preserves a meandering pattern during channel incision, whereas softer bedrock has smaller meanders or a tendency toward reduced sinuosity with time [*Moore,* 1926; *Young,* 1978]. *Braun* [1983] noted that meanders incised into shaly bedrock of the Appalachian Valley and Ridge are generally 2 to 3 times the size (meander length and valley floor width) of meanders incised into massive carbonate bedrock, although channel slope and bedload sediment are similar. Working on the Colorado Plateau of the western U.S., *Harden* [1990] found that gradients of incised sinuous channels correlated significantly with bedrock type. Along some rivers, the channel was sinuous where it flowed against the bedrock dip and straight in reaches where flow was downdip. Symmetric bends were associated with resistant bedrock units, whereas ingrown forms developed in massive sandstone and highly erodible bedrock [*Harden,* 1990]. Experimental simulation of meander incision into bedrock has demonstrated that initial erosion is maximum at the inside of bends, and the channel incises vertically [*Shepherd,* 1972]. When scour decreases the gradient sufficiently to permit sediment deposition at the inside of bends, the site of maximum erosion shifts to the outer bank and lateral incision begins.

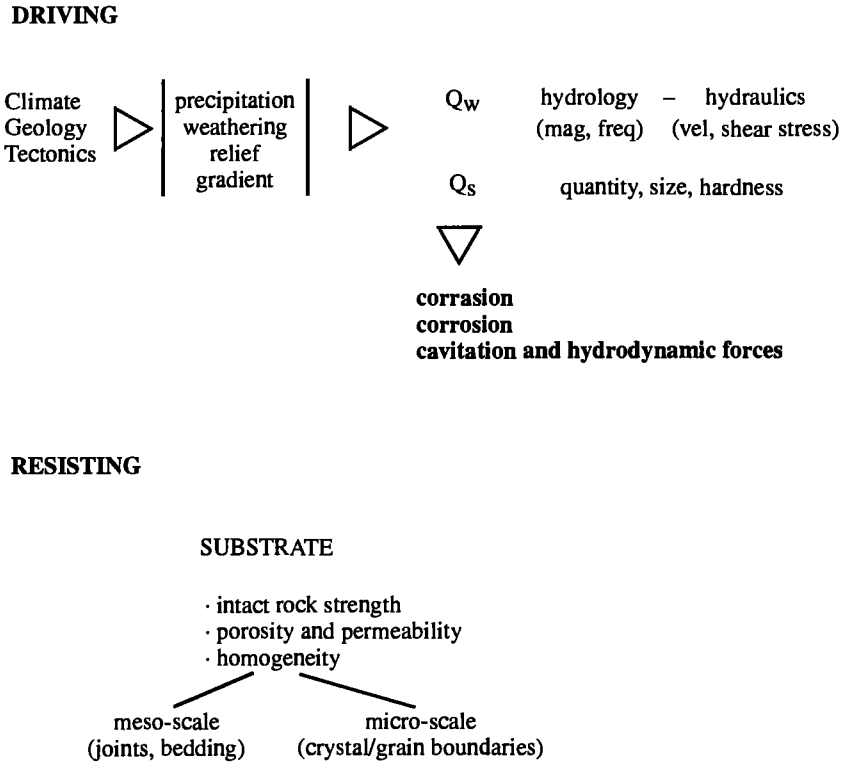

Figure 11. Variables influencing driving and resisting forces acting along bedrock channels.

CHANNEL GEOMETRY AS A REFLECTION OF EROSION

The controls on channel boundary (ir)regularity, width/depth ratio, planform, and gradient come under the two basic categories of substrate and hydraulics. The specific characteristics of these controls influence channel geometry at various spatial scales (e.g. micro scale variability in permeability to macro-scale regional joint patterns) and temporal scales (e.g. flood abrasion to low-flow corrosion). Meso-scale erosive processes and the resulting channel form appear to be dominated by hydraulic controls in some settings [e.g. *Wohl,* 1993, 1994], whereas substrate variability dominates channel form in other examples [e.g. *Miller,* 1991]. In most cases, we know too little about the forces acting along bedrock channels to precisely delineate the influences of individual controls.

Because most bedrock channel boundaries are very stable over the timespan of individual studies, most estimates of rates of bedrock channel incision are based on long-term averages (Table 1, chpt 1). These rates have a very large range (0.5-1000 cm kyr^{-1}) as a result of differences in basin area, discharge, gradient, substrate resistance, and tectonic regime. The few direct measurements of short-term incision rates are also quite variable (Table 2, chpt. 1) for the same reasons as the long-term rates, as well as the increased importance of recent flow history. Numerous investigators have suggested that high magnitude, low frequency floods are particularly important in shaping bedrock channels because of the high boundary resistance of these channels. If the majority of channel incision occurs during frequent floods, then short-term measurements of incision will be largely influenced by the (non)occurrence of such floods during the measurement period. Direct measurements of bedrock channel erosion during individual floods as well as during intervals between floods would be extremely useful.

CONCLUSIONS

At the most basic level, bedrock channel morphology reflects an adjustment between driving and resisting forces, which are controlled by the variables in Figure 11. Our ability to predict channel morphology as a function of controlling variables will thus be governed by our ability to quantify these driving and resisting forces. Both types of forces are dynamic in bedrock channels, varying both across space and as a function of time in response to rate of weathering, magnitude, frequency, and duration of flows, sediment supply to the channel, and so forth. The prevailing assumption has been that substrate dominates bedrock channel morphology. However, the description of morphological changes that seem to be independent of

substrate [e.g. *Wohl,* 1993], and the recurrence of various erosional patterns across a diversity of substrates, suggest that this assumption may be too restrictive. An alternative conceptual model is that bedrock channel morphologies occupy a continuum from the most homogeneous and least resistant substrates, which exhibit the fullest expression of flow structure [e.g. *Wohl,* 1993] to the most heterogeneous and resistant substrates, in which substrate strongly influences channel morphology [e.g. *Wohl et al.,* 1994; *Wohl and Ikeda,* in press]. Our ability to test these and other conceptual models of bedrock channel morphology in relation to erosional processes is limited by the paucity of quantitative data on either driving or resisting forces in bedrock channels. Studies of bedrock channels to date have either (i) described meso-scale erosional forms and inferred erosive processes and controlling variables, or (ii) tested the predictions of an assumed erosion rate law against actual channel longitudinal profiles. A few studies have quantified rates of corrosion, corrasion, or cavitation and hydrodynamic forces for either a specific flow or a longer-term average, but there are almost no datasets that permit direct comparison of flood erosion and erosion during base flow along a channel. Bedrock channel morphologies may be classified on the basis of multiple vs. single flow path, sinuosity, and uniformity of bed gradient and cross-sectional form. The subdivisions of this classification may be used to infer dominant erosional processes and relative rates of erosion, but it is imperative that we quantify the forces acting in bedrock channels before we can predict the occurrence of specific channel morphologies.

Acknowledgments. Critical reviews by Vishwas Kale and Andrew Miller substantially improved this chapter.

REFERENCES

Alexander, H. S., Pothole erosion, *J. Geol.*, 40, 305-337, 1932.

Allen, J. R. L., Erosional current marks of weakly cohesive mud beds, *J. Sed. Petrol.*, 39, 607-623, 1969.

Allen, J. R. L., Transverse erosional marks of mud and rock: their physical basis and geological significance, *Sed.Geol.*, 5(3/4), 167-370, 1971.

Allen, J. R., L., *Sedimentary structures, their character and physical basis*, 2, 663p, Elsevier Scientific Publishing, Amsterdam, 1982.

Ängeby, O., Pothole erosion in recent waterfalls, *Lund Studies in Geography, Series A, Phys.Geogr.* A 2, 1-34, 1951.

Baker, V., *Paleohydrology and sedimentology of Lake Missoula flooding in eastern Washington*, 79p, Geological Society of America Special Paper 144, 1973.

Baker, V. R., Large-scale erosional and depositional features of the Channeled Scabland, in *The Channeled Scabland*, edited by V. R. Baker and D. Nummedal, pp. 81-116, NASA, Washington D.C., 1978.

Baker, V. R., Flood erosion, in *Flood geomorphology*, edited by V. R. Baker, R. C. Kochel, and P. C. Patton, pp. 81-95, John Wiley and Sons, New York, 1988.

Baker, V. R. and G. Pickup, Flood geomorphology of the Katherine Gorge, Northern Territory, Australia, *Geol. Soc. Amer. Bull.*, 98, 635-646, 1987.

Barnes, H. L., Cavitation as a geological agent, *Amer. J. Sci.*, 254, 493-505, 1956.

Benito, G., Energy expenditure and geomorphic work of the cataclysmic Missoula flooding in the Columbia River Gorge, *Earth Surf. Proc. Land.*, 22, 457-472, 1997.

Bishop, P. and G. Goldrick, Morphology, processes and evolution of two waterfalls near Cowra, New South Wales, *Australian Geographer*, 23, 116-121, 1992.

Blank, H. R., Pothole grooves in the bed of the James River, Mason County, Texas, *Texas J. Sci.*, 10, 293-301, 1958.

Braun, D. D., Lithologic control of bedrock meander dimensions in the Appalachian Valley and Ridge Province, *Earth Surf. Proc. Land.*, 8, 223-237, 1983.

Bretz, J. H., The Dalles type of river channel, *J. Geol.*, 24, 129-149, 1924.

Carling, P. and T. Grodek, Indirect estimation of ungauged peak discharges in a bedrock channel with reference to design discharge criteria, *Hydrol. Proc.*, 8, 497-511, 1994.

Chappell, J., The geomorphology and evolution of small valleys in dated coral terraces, New Guinea, *J. Geol.*, 82, 795-812, 1974.

Cluer, B. L., Cyclic fluvial processes and bias in environmental monitoring, Colorado River in Grand Canyon, *J. Geol.*, 103, 411-421, 1995.

Dick, G. S., R. S. Anderson and K. X. Whipple, Fluvial bedrock erosion measurements, Indus River, Pakistan, reveal control by local flow conditions, *EOS, Transactions, American Geophys. Union*, 78(46), F299, 1997.

Dolan, R., A. D. Howard and D. Trimble, Structural control of the rapids and pools of the Colorado River in Grand Canyon, *Science*, 202, 629-631, 1978.

Dollenmayer, K. and K. X. Whipple, Rates and processes of bedrock channel incision along the upper Ukak River, Valley of Ten Thousand Smokes, AK, *EOS, Transactions of the American Geophys. Union*, 78(46), F299, 1997.

Duckson, D. W. &. L. J. D., Morphology of bedrock step pool systems, *Water Resour. Bull.*, 31(1), 43-51, 1995.

Dzulynski, S., New data on experimental production of sedimentary structures, *J. Sed. Petrol.*, 35, 196-212, 1965.

Dzulynski, S. and E. K. Walton, Experimental production of sole markings, *Trans. Edinb. Geol. Soc.*, 19, 279-305, 1963.

Eckley, M. S. and D. L. Hinchliff, Glen Canyon Dam's quick fix, *ASCE Civil Eng.*, 56, 46-48, 1986.

Elston, E. D., Potholes, their variety, origin, and significance (I), *Scientific Monthly*, 5, 554-567, 1917.

Elston, E. D., Potholes, their variety, origin, and significance (II), *Scientific Monthly*, 6, 37-53, 1918.

Falvey, H. T., Predicting cavitation in tunnel spillways, *Water Power and Dam Construction*, 34, 13-15, 1982.

Faniran, A. and L. K. Jeje, *Humid Tropical Geomorphology*, 414p, Longman, New York, 1983.

Gardner, T. W., Experimental study of knickpoint and longitudinal profile evolution in cohesive, homogeneous material, *Geol. Soc. Amer. Bull.*, 94, 664-672, 1983.

Gilbert, G. K., Niagara Falls and their History, *National Geographic Society Monograph*, 1(7), 203-236, 1895.

Graf, W. L., The impact of suburbanization on fluvial geomorphology, *Water Resour. Res.*, 11(14), 690-692, 1975.

Grams, P. E. and J. C. Schmidt, Geomorphology of the Green River in the eastern Uinta Mountains, Dinosaur National Monument, Colorado and Utah, in *Varieties of Fluvial Form*, edited by A. J. Miller and A. Gupta, pp. John Wiley and Sons, New York, 1998 in press.

Gregory, H. E., Geology and Geography of the Zion Park region, Utah and Arizona, *U.S. Geol. Surv. Prof. Pap.*, 2220, 200, 1950.

Grodek, T., M. Inbar and A. P. Schick, Step pool geometry and flow characteristics in low-sediment-storage channel beds, paper presented at Hydraulic Eng. 94, Buffalo, edited by G. V. Cotroneo and R. R. Rumer, ASCE, 819-823, 1994.

Gupta, A., V. S. Kale and S. N. Rajaguru, The Narmada River, India through space and time, in *Varieties of Fluvial Form*, edited by A. J. Miller and A. Gupta, John Wiley and Sons, New York, 1998 in press.

Harden, D. R., Controlling factors in the distribution and development of incised meanders in the central Colorado Plateau, *Geol. Soc. Amer. Bull.*, 102, 233-242, 1990.

Heritage, G. L., A. W. van Nierkerk and B. P. Moon, The geomorphology of the Sabie River, South Africa: an incised bedrock influenced channel, in *Varieties of Fluvial Form*, edited by A. J. Miller and A. Gupta, John Wiley and Sons, New York, 1998 in press.

Holland, W. N. and G. Pickup, Flume study of knickpoint development in stratified sediment, *Geol. Soc. Amer. Bull.*, 87, 76-82, 1976.

Howard, A. D., W. E. Dietrich and M. A. Seidl, Modeling fluvial erosion on regional to continental scales, *J. Geophys. Research*, 99(7), 13,971-13,986, 1994.

Howard, A. D. and G. Kerby, Channel changes in badlands, *Geol. Soc. Amer. Bull.*, 94(6), 739-752, 1983.

Ives, R. L., Plunge pools, potholes, and related features, *Rocks and Minerals*, 23, 3-10, 1948.

Kale, V. S., V. R. Baker and S. Mishra, Multi-channel patterns of bedrock rivers: an example from the central Narmada basin, India, *Catena*, 26, 85-98, 1996.

Kale, V. S. and B. S. Shingade, A morphological study of potholes of Indrayani Knick Point (Maharashtra), in *Explorations in the Tropics*, edited by V. S. Datya, J. N. Diddec, S. R. Jog, and C. J. Potil, pp. 206-214, Vol, Professor K.R. Dikshit Felicitation Volume, Professor K.R. Dikshit Felicitation Committee, Pune (India), 1987.

Karcz, I., Possible significance of transition flow patterns in interpretation of origin of some natural bedforms, *J. Geophys. Research*, 75, 2869-2873, 1970.

Karcz, I., Reflections on the origin of small-scale longitudinal streambed scours, in *Fluvial geomorphology*, edited by M. Morsisawa, pp. 149-173, Binghamton NY, 1973.

Keller, E. A. and W. N. Melhorn, Rhythmic spacing and origin of pools and riffles, *Geol. Soc. Amer. Bull.*, 89, 723-730, 1978.

Kells, J. A. and C. D. Smith, Reduction in cavitation on spillways by induced air entrainment, *Can. J. Civil Eng.*, 18, 358-377, 1991.

Kieffer, S. W., The 1983 hydraulic jump in Crystal Rapid: implications for river-running and geomorphic evolution in the Grand Canyon, *J. Geol.*, 93, 385-406, 1985.

Kieffer, S. W., The rapids and waves of the Colorado River, Grand Canyon, Arizona, U.S. Geol. Surv., Report 87-096, 97pp., 1987.

Kieffer, S. W., Geologic nozzles, *Rev. Geophys.*, 27, 3-38, 1989.

Kor, P. S. G., J. Shaw and D. R. Sharpe, Erosion of bedrock by subglacial meltwater, Georgian Bay, Ontario: a regional view, *Can. J. Earth Sci.*, 28, 623-642, 1991.

Lerman, A., Weathering rates and major transport processes: an introduction, in *Physical and chemical weathering in geochemical cycles*, edited by A. Lerman and M. Meybek, pp. 1-10, Kluwer Academic Publications, Dortrecht, 1988.

Leopold, L. B., The rapids and the pools - Grand Canyon, *U.S. Geol. Surv. Prof. Pap.*, 669-D, 131-145, 1969.

Lorenc, M. W., P. M. Barco and J. Saavedra, The evolution of potholes in granite bedrock, Western Spain, *Catena*, 22, 265-274, 1994.

Lorenc, M. W. and J. Saavedra, Remarks on the pothole erosion at the Tormes River (Salamance Province, Spain), *Acta Geologica Hispanica*, 15, 91-93, 1980.

Maxson, J. H., Fluting and faceting of rock fragments, *J. Geol.*, 48, 717-751, 1940.

Merritts, D. J., K. R. Vincent and E. E. Wohl, Long river profiles, tectonism, and eustasy: A guide to interpreting fluvial terraces., *J. Geophys. Res. (Special Issue on Tectonics and Topography)*, 99(B7), 14,031-14,050, 1994.

Miller, A. J., Valley morphology and boundary conditions influencing spatial patterns of flood flow, in *Natural and anthropogenic influences in fluvial geomorphology, The Wolman Volume*, edited by J. E. Costa, A. J. Miller, K. W. Potter, and P. R. Wilcock, pp. 57-81, Vol, 89, American Geophys. Union, 1995.

Miller, A. J. and D. J. Parkinson, Flood hydrology and geomorphic effects on river channels and floodplains: the flood of November 4-5, 1985, in the South Branch Potomac River basin of West Virginia, in *Geomorphic studies of the storm and flood of November 3-5, 1985, in the upper Potomac and Cheat River Basins in West Virginia and Virginia*, edited by R. B. Jacobson, pp. 1-96, U.S. Geol. Surv. Bull. E, Washington, 1993.

Miller, J. R., The influence of bedrock geology on knickpoint development and channel-bed degradation along downcutting streams in south-central Indiana, *J. Geol.*, 99, 591-605, 1991.

Moore, R. C., Origin of inclosed meanders on streams of the Colorado Plateau, *J. Geology*, 34, 29-57, 1926.

O'Connor, J. E., Hydrology, Hydraulics, and Geomorphology of the Bonneville Flood, *Geological Society of America Special Paper*, 274, 83, 1993.

O'Connor, J. E., R. H. Webb and V. R. Baker, Paleohydrology of pool-riffle pattern development: Boulder Creek, Utah, *Geol. Soc. Amer. Bull.*, 97, 410-420, 1986.

Philbrick, S. S., Horizontal configuration and the rate of erosion of Niagara Falls, *Geol. Soc. Amer. Bull.*, 81, 3723-3732, 1970.

Pyrce, R. S., A field investigation of planimetric knickpoint morphology from rock-bed sections of Niagara Escarpment fluvial systems, M.A., Wilfrid Laurier University, 1995.

Rathburn, S. L., Pleistocene cataclysmic flooding along the Big Lost River, east central Idaho, *Geomorphology*, 8, 305-319, 1993.

Rosenbloom, N. A. and R. S. Anderson, Hillslope and channel evolution in a marine terraced landscape, Santa Cruz, California, *J. Geophys. Research*, 99(B7), 14,013-14,029, 1994.

Roy, A. G. and A. D. Abrahams, Rhythmic spacing and origin of pools and riffles: discussion and reply, *Geol. Soc. Amer. Bull.*, 91, 248-250, 1980.

Sato, S., H. Matsuura and M. Miyazaki, Potholes in Shikoku, Japan, Parts I and II. Potholes and their hydrodynamics in the Kurokawa River, Ehime, *Memoirs of the Faculty of Education, Ehime University, Natural Sci.*, 7, 127-220, 1987.

Schmidt, J. C., Recirculating flow and sedimentation in the Colorado River in Grand Canyon, Arizona, *J. Geol.*, 98, 709-724, 1990.

Schmidt, J. C., D. M. Rubin and H. Ikeda, Flume simulation of recirculating flow and sedimentation, *Water Resour. Res.*, 29, 2925-2939, 1993.

Seidl, M. A. and W. E. Dietrich, The problem of channel erosion into bedrock, in *Functional Geomorphology*, edited by K.-H. Schmidt and J. d. Ploey, pp. 101-124, Vol, Catena Supplement 23, 1992.

Seidl, M. A., W. E. Dietrich and J. W. Kirchner, Longitudinal profile development into bedrock: an analysis of Hawaiian channels, *J. Geol.*, 102, 457-474, 1994.

Seidl, M. A., R. C. Finkel, M. W. Caffee, G. B. Hudson and W. E. Dietrich, Cosmogenic isotope analyses applied to river longitudinal profile evolution: problems and interpretations, *Earth Surf. Proc. Land.*, 22, 195-209, 1997.

Sharpe, D. R. and J. Shaw, Erosion of bedrock by subglacial meltwater, Cantley, Quebec, *Geol. Soc. Amer. Bull.*, 101, 1011-1020, 1989.

Shepherd, R. G., Incised River Meanders: evolution in simulated bedrock, *Science*, 178, 409-411, 1972.

Shepherd, R. G. and S. A. Schumm, Experimental study of river incision, *Geol. Soc. Amer. Bull.*, 85, 257-268, 1974.

Shroba, R. R., P. W. Schmidt, E. J. Crosby and W. R. Hansen, Storm and flood of July 31-August 1, 1976, in the Big Thompson River and Cache la Poudre River Basins, Larimer and Weld Counties, Colorado; Part B, Geologic and geomorphic effects in the Big Thompson Canyon area, Larimer County, *U.S. Geol. Surv. Prof. Pap.*, 1115, 87-152, 1979.

Simon, A., Energy, time and channel evolution in catastrophically disturbed fluvial systems, *Geomorphology*, 5, 345-372, 1992.

Smith, D. I., M. A. Greenaway, C Moses and A. P. Spate, Limestone weathering in eastern Australia. Part I Erosion Rates, *Earth Surf. Proc. Land.*, 20, 451-463, 1995.

Stein, O. R. and P. Y. Julien, Criterion delineating the mode of headcut migration, *J. Hydraulic Eng.*, 119, 37-50, 1993.

Summerfield, M. A. and P. J. Hulton, Natural controls of fluvial denudation rates in major world drainage basins, *J. Geophys. Research*, 99(B7), 13,871-13,881, 1994.

Thomas, M. F., Chapter 4: Denudation in tropical environments, in *Tropical geomorphology: a study of weathering and landform development in warm climates*, edited pp. 99-123, McMillan, London, 1974.

Tinkler, K. J., Active Valley Meanders in South-Central Texas and Their Wider Significance, *Geol. Soc. Amer. Bull.*, 82, 1783-1800, 1971.

Tinkler, K. J., Fluvially sculpted rock bedforms in Twenty Mile Creek, Niagara Peninsula, Ontario, *Can. J. Earth Sci.*, 30, 945-953, 1993.

Tinkler, K. J., J. W. Pengelly, W. G. Parkins and G. Asselin Postglacial recession of Niagara Falls in relation to the Great Lakes, *Quat. Res.*, 42, 20-29, 1994.

Twidale, C. R., *Structural Landforms*, 247p, The MIT Press, Cambridege, Massachusetts, 1971.

Van Niekerk, A. W., G. L. Heritage and B. P. Moon, River classification for management: the geomorphology of the Sabie River in the eastern Transvaal, *South African Geogr. J.*, 77, 68-76, 1995.

Van Niekerk, A. W., G. L. Heritage, J. L. Broadhurst and B. P. Moon, Bedrock anastomosing channel systems: morphology and dynamics in the Sabie River, Mpumalanga Province, South Africa, in *Varieties of Fluvial Form*, edited by A. J. Miller and A. Gupta, John Wiley and Sons, New York, 1998 in press.

Vaughn, D. M., Flood dynamics of a concrete-lined, urban stream in Kansas City, Missouri, *Earth Surf. Proc. Land.*, 15, 525-537, 1990.

Webb, R. H., P. T. Pringle, S. L. Reneau and G. R. Rink, Monument Creek debris flow, 1984: implications for formation of formation of rapids on the Colorado River in Grand Canyonn National Park, *Geology*, 16, 50-54, 1988.

Wende, R., Boulder bedforms in jointed-bedrock channels, in *Varieties of Fluvial Form*, edited by A. J. Miller and A. Gupta, John Wiley and Sons, New York, 1998 in press.

Wilbur, R. L. and E. Mead, *The construction of Hoover Dam*, U.S. Government Printing Office, Washington D.C., 1933.

Wohl, E. E., Bedrock benches and boulder bars: Floods in the Burdekin Gorge of Australia, *Geol. Soc. Amer. Bull.*, 104, 770-778, 1992.

Wohl, E. E., Gradient irregularity in the Herbert Gorge of northeastern Australia, *Earth Surf. Proc. Land.*, 17, 69-84, 1992.

Wohl, E. E., Bedrock channel incision along Picanniny Creek, Australia., *J. Geol.*, 101, 749-761, 1993.

Wohl, E. E., Energy expenditure in deep, narrow bedrock channels, paper presented at Annual Meeting, Geological Society of America, Abstracts with Program, 233-234, 1994.

Wohl, E. E., D. A. Cenderelli and M. Meija-Navarro, Geomorphic hazards from extreme floods in canyon rivers, in *The Schumm Volume*, edited by D.J. Anthony, M.D. Harvey, M.P. Mosley, and J.B. Laronne, Water Resources Publications, Littleton, Colorado, 1998 in press.

Wohl, E. E., N. Greenbaum, A. P. Schick and V. R. Baker, Controls on bedrock channel incision along Nahal Paran, Israel, *Earth Surf. Proc. Land.*, 19, 1-13, 1994.

Wohl, E. E. and T. Grodek, Channel bed-steps along Nahal Yael, Negev desert, Israel, *Geomorphology*, 9, 117-126, 1994.

Wohl, E. and H. Ikeda, Experimental simulation of channel incision into a cohesive substrate at varying gradients, *Geology*, 25, 295-298, 1997.

Wohl, E. E., D. M. Thompson and A. J. Miller, Canyons with undulating walls, *Geol. Soc. Amer. Bull.*, 1998 in press.

Wohl, E. E., K. R. Vincent and D. J. Merritts, Pool and riffle characteristics in relation to channel gradient, *Geomorphology*, 6, 69-84, 1993.

Wohl, E. E. and H. Ikeda, Patterns of bedrock channel erosion in the Bozo Peninsula, Japan, *J. Geol.*, 1998 in press.

Young, R. W., Geological and hydrological influences on the development of meandering valleys in the Shoalhaven catchment, southeastern New South Wales, *Erdkunde*, 32, 171-182, 1978.

Young, R. W., Waterfalls: form and process, *Zeitschrift für Geomorphologie*, Suppl. 55, 81-95, 1985.

Zen, E.-a. and K. L. Prestegaard, Possible hydraulic significance of two kinds of potholes: examples from the paleo-Potomac River, *Geology*, 22, 47-50, 1994.

E. Wohl, Department of Earth Resources, Colorado State University, Fort Collins, Colorado 80523, United States

The Role of Extreme Floods in Shaping Bedrock Channels

Victor R. Baker

Department of Hydrology and Water Resources The University of Arizona, Arizona

Vishwas S. Kale

Department of Geography, University of Poona, Pune ,India

Alluvial river channels adjust readily to formative discharges of moderate magnitude and frequency. Bedrock river channels present various thresholds to effective channel adjustment, such that only relatively rare, high-magnitude flood discharges contribute to shaping their morphologies. Very high values of power per unit area of bed, exceeding 10^2 Wm^{-2}, result in high-energy erosional processes, including cavitation and macroturbulent plucking. Although these processes are best exemplified in the Channeled Scabland and other late Pleistocene cataclysmic flood channels, they also can be achieved in modern bedrock gorges where very resistant rocks are acted upon by unusually large floods. Examples include the Katherine Gorge, northern Australia, and various gorges of the Narmada and Tapi Rivers in central India. Distinctive scabland-like morphologies occur, including wide, shallow bedrock surfaces with inner channels and narrow, deep gorges. As in alluvial rivers, there may be an adjustment to energy expenditure, but at a much higher level of energy associated with rare floods.

INTRODUCTION

How we understand the operation of river channels depends on the time scale over which we envision that operation [*Schumm and Lichty*, 1965]. This issue of time scale is especially important in distinguishing the response of stream channels to floods. Alluvial channels, with banks and beds composed of sedimentary particles relatively frequently in transport, are self-formed through the independent adjustment of the morphological variables comprising their hydraulic geometry [*Leopold and Maddock*, 1953; *Maddock*, 1976]. They are "authors of their own geometries" [*Leopold and Langbein*, 1962], and the latter are scribed by flows of moderate magnitude and frequency [*Wolman and Miller*, 1960; *Leopold et al.*, 1964]. Such channels may experience rare, high-magnitude events, but their morphology will tend to recover to the original dimensions at varying rates depending on the sequence of floods and other climatic-geomorphic factors [*Wolman and Gerson*, 1978].

Relatively common flows of moderate magnitude are both easy to monitor and easy to understand theoretically [*Baker*, 1988a]. Theoretical understanding is enhanced by abundant data on the prototype phenomenon to which the theory applies. Given the usual human monitoring time scales of 10 to 10^2 years, flood flows with annual exceedence probabilities of 1 to 10^{-1} are likely to certain to be sampled. With formative discharges of alluvial channels in this range, theory and empirical content can readily come into balance.

Rare, high-magnitude floods are capable of producing spectacular channel changes and movement of coarse sediments [*Baker*, 1977; *Gupta*, 1988]. Despite the intrinsic geomorphological interest, knowledge of such events remains scant. This is because the significant flows have annual exceedence probabilities less than 10^{-1}, typically 10^{-2} or 10^{-3}, but as small as 10^{-5} for cataclysms related to continental glaciation [e.g. *Baker*, 1996a]. Thus, the

Rivers Over Rock: Fluvial Processes in Bedrock Channels
Geophysical Monograph 107

reciprocals of the annual exceedence probabilities, with units of time in years, have values of 100 or more. Such events are unlikely to be monitored. Moreover, measurements of flow phenomena and sediment transport are lacking because of difficulties in accessing measurement sites during extreme events and because of the effects of suspended and floating debris on instrumentation. A result of the quantitative revolution in fluvial studies, therefore, has been a certain neglect of these geologically significant processes [*Baker*, 1988a]. The search for quantitative data favors attention to flows of lesser magnitude, generally for alluvial systems [see *Tinkler and Wohl*, this volume].

This paper will consider the less-studied high-energy processes that occur during extreme floods in highly resistant bedrock channel situations. Whereas, alluvial channel patterns can be systematically related to sediment types composing channel banks, to sediment loads, and to moderate flood characteristics [*Schumm*, 1977], the high thresholds for channel change in bedrock rivers [*Baker*, 1977] lead to a different spectrum of channel types and patterns [e.g. *Shepherd*, 1979; and *Wohl*, Chapter 6 of this volume]. Weathering and resistance characteristics of the bedrock induce certain channels to yield the highest energy expenditures of flow. For example, smooth bedrock meandering patterns can occur in softer lithologies. The meander pattern reduces energy expenditure and evens out the loss of power along the flow path. Because a high-magnitude flood cannot efficiently dissipate its energy at high angle bends, structurally controlled patterns can lead to manifestations of turbulent phenomena not usually observed in meandering systems. Energy expenditure is nonuniform along the longitudinal profile, and amazingly high expenditure can be achieved at especially resistant points.

CATACLYSMIC FLOOD EROSION

If the study of common, low magnitude flow processes fails to tell us much about the phenomena of interest in this paper, then an alternative is to study the most extreme cataclysmic flood phenomena known. This is possible because such floods leave lasting imprints on the landscape. The flood channels of Mars have preserved their morphologies for 10^8 to 10^9 years [*Baker*, 1982]. In the Channeled Scabland well-preserved flood morphologies date to the last glaciation [*Baker*, 1973]. The morphologies and processes of such areas can show what is possible in bedrock channels at process intensities that go unmeasured in modern rivers.

As noted by *Baker and Pickup* [1987], bedrock channels have the ability, "...to chronicle their own cataclysms." This is possible because a variety of high-water indicators are preserved that document flood paleostages [*Baker*, 1987; *O'Connor and Baker*, 1992]. Using an inverse form of scientific inference [*Baker*, 1996b] it is possible to calculate the paleohydraulic conditions prevailing during the floods responsible for emplacing the high-water indicators [*Baker*, 1973; *O'Connor and Baker*, 1992; *Baker et al.*, 1993].

Paleohydraulic studies have shown us properties of past high-energy floods (paleofloods) that can be compared to flow processes in modern rivers. Table 1 compares the hydraulic parameters for various cataclysmic paleofloods, including great Pleistocene ice-dammed lake bursts in the Altay Mountains of Siberia [*Baker et al.*, 1993] and the Lake Missoula region of the northwestern U.S. [*Baker* 1973; *O'Connor and Baker*, 1992]. Note that slopes (S) and flow depths (D) are much larger than for the modern Amazon River. Despite a large discharge (Q), the Amazon has flow velocities (V) and bed shear stresses (τ) that are comparable to those of much smaller alluvial rivers [*Baker and Kochel* 1988]. Particularly important is the rate of energy dissipation, or power, per unit area of streambed, which can be expressed

$$\omega = \gamma Q S / W = \tau V$$

where, W is bed width, Q is discharge, S is energy slope, γ is the specific weight of the transporting fluid, V is the mean flow velocity, and τ is the bed shear stress. The cataclysmic flood features of very deep, high-gradient flows are generated by power (ω) values many orders of magnitude larger than those produced in alluvial rivers [*Baker and Costa*, 1987]. Bedrock gorges of modern rivers, such as the Katherine Gorge of Australia, may experience high-energy conditions comparable to those in cataclysmic flood channels (Table 1).

The enormous flow velocities achieved in high-energy flood situations (Table 1) cause reduced absolute pressure in the flowing water, reaching the fluid pressure. Shock waves produced by collapse of the air bubbles which form in such situations are recognized as intense erosional events. Such cavitation erosion is inferred to be highly developed in cataclysmic flood flows [*Baker and Costa*, 1987; *O'Connor*, 1993].

Another fundamental hydraulic characteristic of very deep, high gradient flood flows is the development of secondary circulation, flow separation, and the birth and decay of vorticity around obstacles and along irregular boundaries. Such three-dimensional flow phenomena in rivers are termed collectively as *macroturbulence* [*Matthes*, 1947]. Conditions necessary for the generation of erosionally effective macroturbulence [*Matthes*, 1947] include the following: (1) a steep energy gradient, (2) a low ratio of actual sediment transported to potential sediment transport, and (3) an irregular, rough boundary capable of generating flow separation. Erosion results from the intense pressure and velocity gradients of vortices, which produce phenomenal lift forces that erode by plucking action [*Baker*, 1978a].

Table 1. Paleohydraulic parameters for bedrock and alluvial channelways, including cataclysmic flood channels - Chuja, Altay [*Baker et al.*, 1993] and Missoula Flood channels [*Baker*, 1973].

Flood Channel	Discharge Q	Width W	Depth D	Slope S	Velocity V	Bed Shear Stress, τ	Power per Unit Area, ω
	m^3s^{-1}	km	m		ms^{-1}	Nm^{-2}	Wm^{-2}
Chuja (Altay)	2×10^7	3	400	0.02	20-45	5×10^3 2×10^4	10^5-10^6
Rathdrum (Missoula)	2×10^7	6	175	0.01	25	1×10^4	2×10^5
Grand Coulee (Missoula)	5×10^6	1.7	100	0.01	30	1×10^4	3×10^5
Amazon River	3×10^5	2	60	1×10^{-5}	2	6	12
Katherine Gorge	6×10^3	0.05	45	3×10^{-3}	7.5	1.5×10^3	1×10^4

These processes generate a sequence of erosional forms on rock surfaces in bedrock stream channels. Initial channels have relatively smooth floors. These are marked by longitudinal grooves, which mimic the longitudinal vorticity of the streaming fluid. Deeper erosion creates irregular surfaces that generate flow separation and/or kolks. As erosive activity concentrates at these sites, the result is greater accentuation of the surface irregularities [see *Hancock et al.* this volume]. A critical threshold has to be crossed to achieve this change from longitudinal forms to the production of irregular potholes.

Experimental studies of fluvial erosion utilizing simulated bedrock [*Shepherd and Schumm*, 1974] indicate that a sequence of erosional bedforms may develop in bedrock as a function of time. First to appear in these experiments were the faint streaks of longitudinal lineations associated with potholes and transverse erosional ripples. The lineations then became enlarged into prominent longitudinal grooves. Eventually the grooves decreased in numbers, and finally one narrow, deep inner channel formed. In the layered basalt bedrock of the Channeled Scabland inner channels develop headwardly by the recession of subfluvial cataracts [*Baker*, 1978b]. Multiple horseshoe-shaped headcuts separate the inner channels from scabland surfaces marked by potholes and longitudinal grooves (Figure 1).

THE KATHERINE GORGE EXAMPLE

The Katherine Gorge is a 20-km long canyon developed in jointed, resistant sandstone. It is located in the north-central part of Australia (Figure 2), 32 km northeast of the town of Katherine, Northern Territory. The gorge is a slot-like chasm averaging 50 to 150 m wide and 40 to 60 m deep (Figure 3). Linear side canyons join the main gorge; these tributary mouths are ideal sites for slackwater sediment accumulation during rare, great flows (Figure 4).

The Katherine Gorge shows many morphological similarities to the Channeled Scabland. Inner channels are cut through broad surfaces of the very resistant quartzite bedrock (Figures 3 and 5). Locally, flood water even exceeds the capacity of the gorge, spilling across adjacent uplands (Figure 6). This latter phenomenon is a type of "overfitness" [*Dury*, 1964]. Overfitness is a characteristic of the Channeled Scabland in which flood flows exceed the capacity of stream valleys. Although such a condition would not persist long in an alluvial valley, the resistance of bedrock provides an opportunity to preserve overfit stream relationships.

EXAMPLES FROM CENTRAL INDIA

The Narmada and Tapi Rivers in central India (Figure 7) are situated in an environment typical of the monsoon tropics, with large floods during the summer monsoon season. Although the two rivers differ in basin size and morphology they have two hydro-geomorphic characteristics in common: high seasonal variability in the volume of flow and sediment load, and high-magnitude floods associated with monsoon depressions originating over Bay of Bengal [*Kale et al.*, 1994].

The Narmada and Tapi are characterized by both alluvial and bedrock channels. The morphological characteristics of the bedrock and alluvial reaches are strikingly different and reflect the control of lithology, gradient and flood processes. The bedrock reaches are characterized by rapids, waterfalls, scablands, inner channels and boulder berms. The

Figure 1. Pothole cataract in the Channeled Scabland of eastern Washington. Note the potholed scabland surface to the lower left. Cataclysmic flood flows came from the lower left and excavated the two alcoves (inner channels) by plucking erosion of the 120-m cliffs of basalt bedrock.

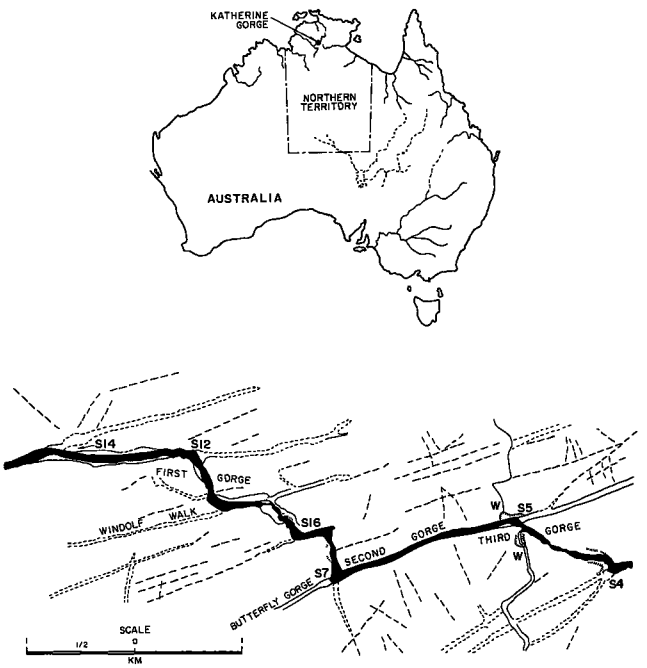

Figure 2. Location and sketch map of the Katherine Gorge, north-central Australia. Slackwater depositional sites are indicated by the "S" designation.

morphology of the bedrock channels suggest that the channels are largely adjusted to high flows [*Rajaguru et al.*, 1995]. Moreover, these high-magnitude floods recur relatively frequently [*Ely et al.*, 1996].

Wide, Shallow Bedrock Channels

Bedrock channels of the Narmada and Tapi are of two general types: (1) wide, shallow channels, and (2) narrow, deeply incised channels. The wide, shallow channels show scabland morphology, with erosional bedforms. At Mandla (Figure 8), Punghat, Dardi and Borkhedi the scablands are nearly 1-2 km wide, with well-developed inner channels (10-165 m wide and 5-15 m deep) and other erosional bedforms. In the Tapi River such shallow bedrock channels (200 to >500 m wide) occur upstream of the Bhainsadehi gorge (Figure 9). The channels are bounded by alluvial or low rocky banks. The average gradients of such reaches are

Figure 3. Aerial view of Katherine Gorge, looking upstream (east) near site S16 (Figure 2).

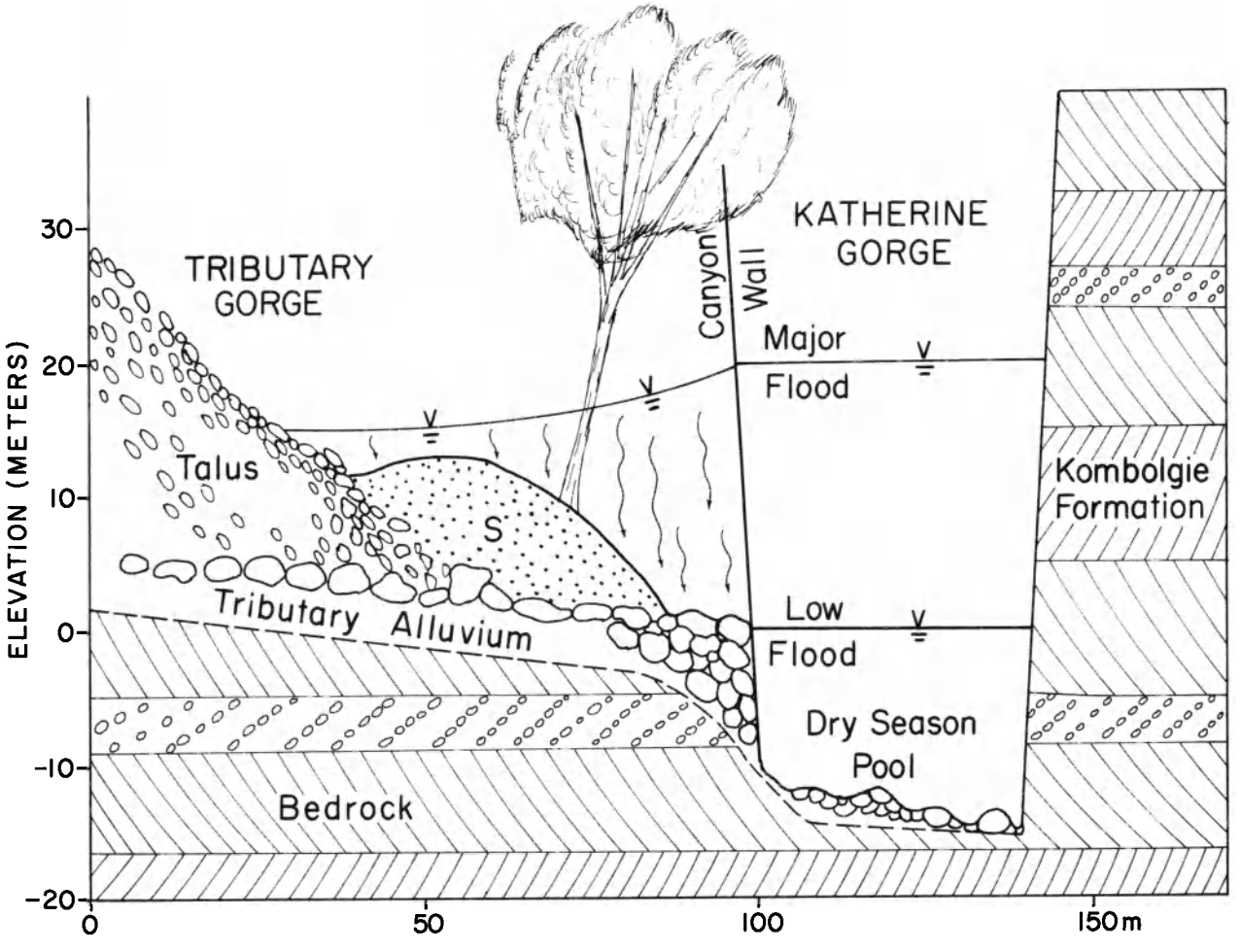

Figure 4. Mode of slackwater deposit emplacement by deep, high-magnitude floods in the narrow, deep canyon.

Figure 5. Floor of Katherine Gorge showing riffle area, a rock surface with fracture-bounded potholes. An inner channel is cut into this surface creating local maximization of power per unit area during extreme floods. See *Baker and Pickup* [1987].

low, and the channel bed surfaces are bare and devoid of sediments finer than cobbles. Potholes and other erosional bedforms are closely associated with major joints in bedrock (Figure 10). The exposed bedrock surfaces show evidence of flood erosion in the form of flute marks and polished surfaces (Figure 11). In general, the density and dimensions of the potholes are higher close to the waterfalls (head of the inner channels) and rapids, due to greater flow depths, and consequently greater flow velocity, unit stream power and shear stress. At Punghat the incision along the joints and weak zones (lineaments) in the underlying granite and gneissic rocks has given rise to multiple channels in bedrock [*Kale et al.*, 1996].

Wherever thickly bedded rocks, with high degree of jointing occur, slabs or blocks (0.5 to 2.0 m) are detached and deposited in areas of reduced flow velocity. Hence, isolated and scattered boulders are common across the scabland areas (Figure 9).

Narrow, Deep Bedrock Channels

The morphological characteristics of bedrock channels flowing through gorges are markedly different from the shallow channels in several respects. The confined narrow channels represent inner channels on a larger scale. The river channels are bounded on both sides by steep rocky cliffs, which form the banks during large monsoon floods (Figures 12 and 13). Consequently, during large floods the width/depth ratio rapidly decreases and the stream power per unit area reaches high values. Such channels are characterized by deep pools, rapids, narrow scabland areas and large boulder berms.

In the Punasa Gorge on the Narmada the flow depths during large floods can vary between 50 and 65 m. Consequently, the average power per unit area ranges between 200 and >900 W/m^2 [*Kale et al.*, 1994] (Table 2). In Bhainsadehi Gorge on Tapi the flow depth can vary between 5 and 17 m, and the unit stream power associated with a dam-failure flood was estimated to be about 600-900 W/m^2 (Table 2). On both the rivers, there are numerous rapids and waterfalls within the gorge sections, where the bed elevation drops rapidly by few meters giving an average slope of >0.02 (Figure 13). It is in these reaches that the bedrock erosion is most spectacular.

Velocity measurements for some gauging sites on Narmada indicate that even in the incised alluvial reaches

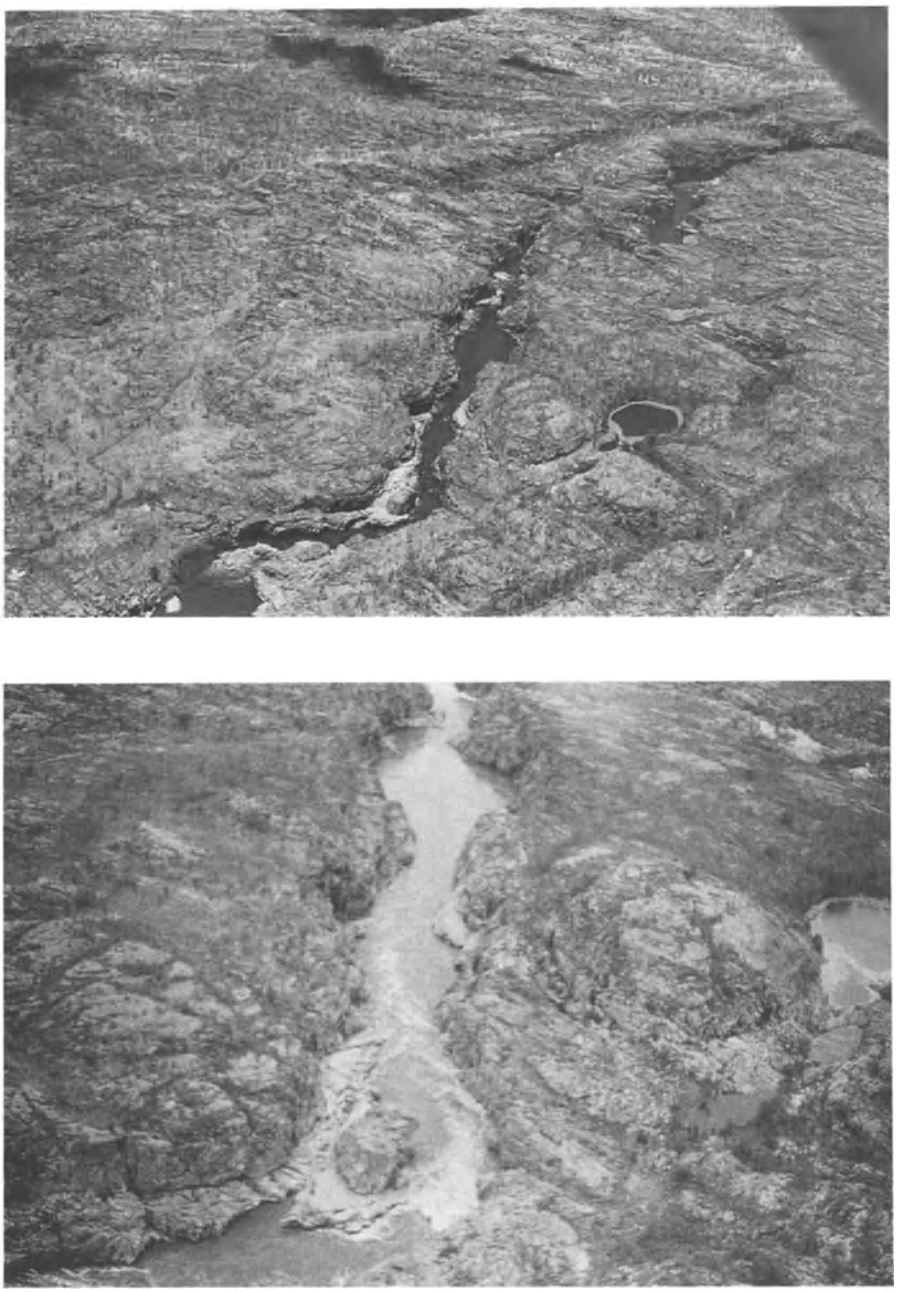

Figure 6. Inner channel development and high spillway channel in upper Katherine gorge. A. Dry season view with round pond (right center) in the spillway channel. Flow from lower left to upper right. B. Wet season view (February 1980) showing flow just filling inner channel at bottom center of picture.

the maximum velocities range between 4 and >7 m/s during large monsoon floods. Hydraulic modeling for the Punasa Gorge indicates that in the constricted and steep portions of the bedrock gorge the velocities can be as high as 10-15 m/s [*Kale et al.*, 1994]. Such flows are capable of eroding the bedrock and transporting cobbles and boulders. The high transportation capacity of the floods is indicated by large piles of 1 to 2 m imbricated boulders.

Due to the confined nature of the channels, depositional features occur wherever there is a marked reduction in the

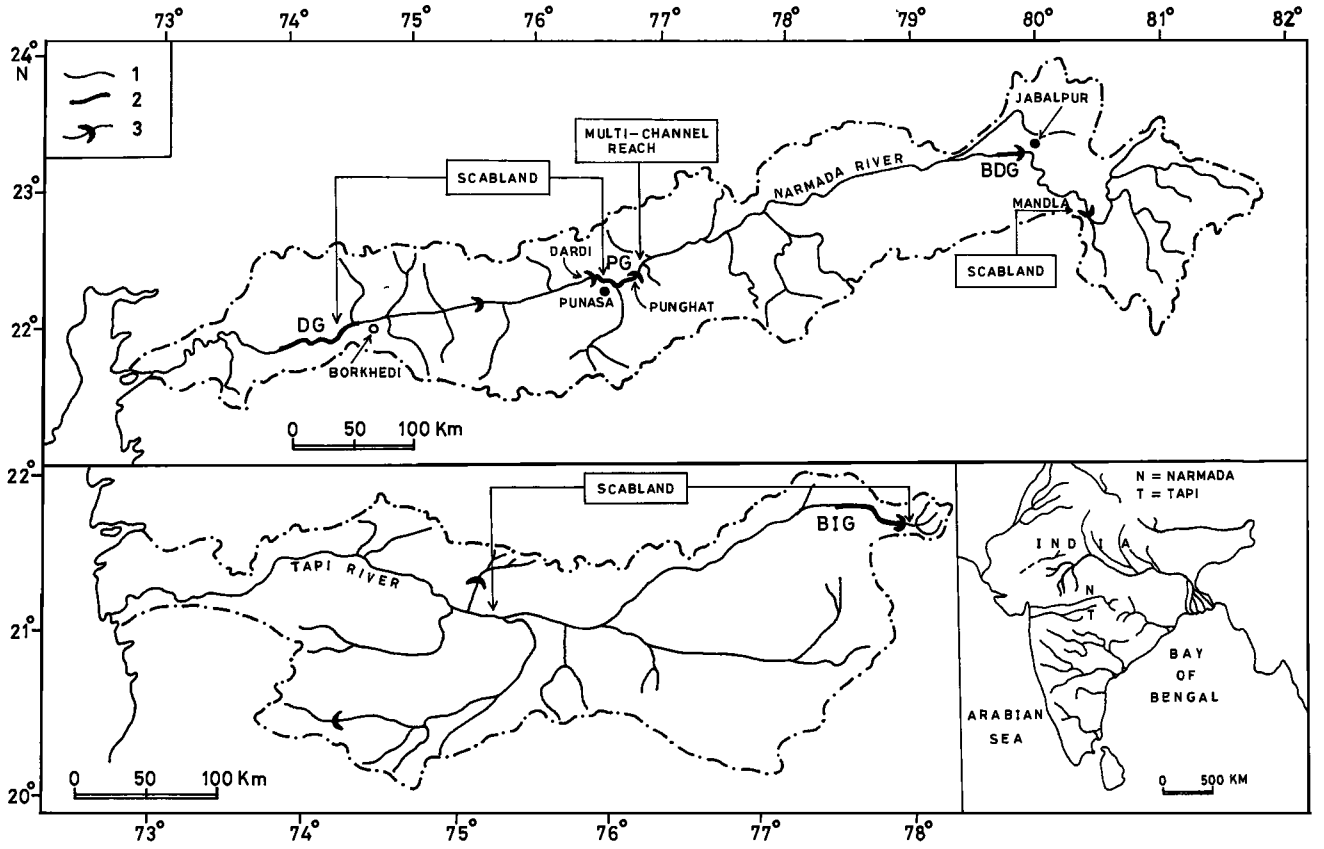

Figure 7. Location map, Narmada and Tapi Rivers, central India. Symbols (upper left) include (1) regional drainage, (2) bedrock study reaches, and (3) cataracts.

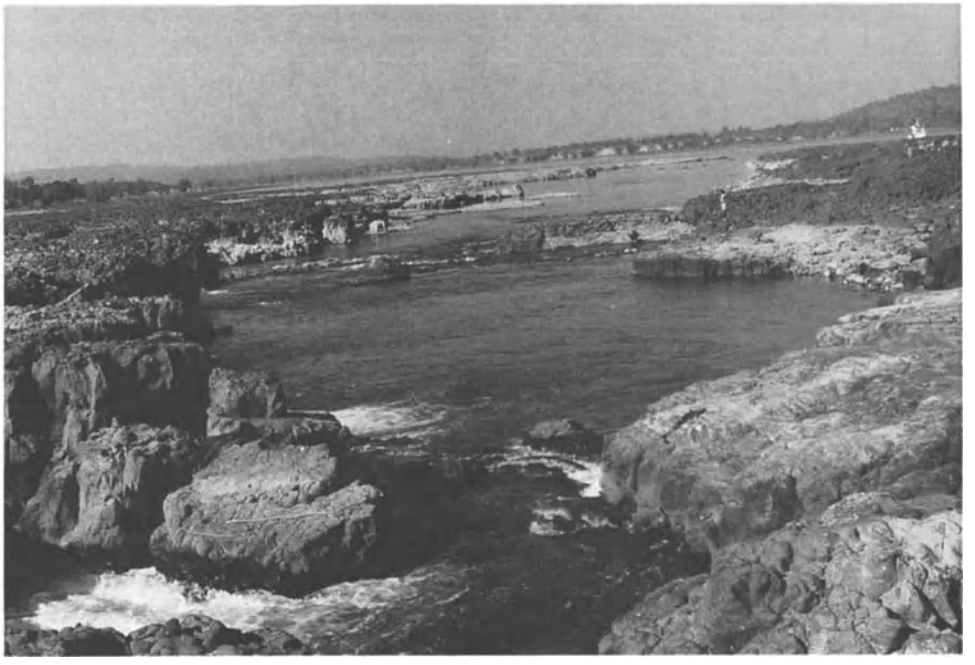

Figure 8. Inner channel cut into wide scabland at Mandla, Narmada River.

Figure 9. Wide, shallow scabland area with imbricated isolated boulder, upstream, of Bhainsadehi Gorge, Tapi River.

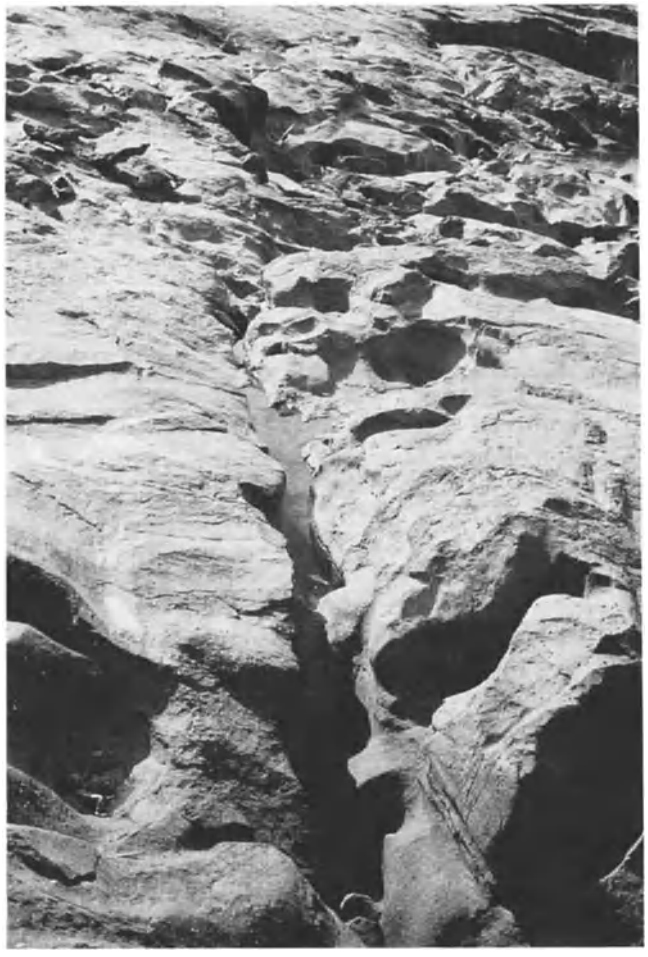

Figure 10. Control of potholes and grooves by a joint normal to flow direction, Tapi River, India.

Figure 11. Polished rock surfaces with flutes. Flow direction from upper right to lower left. Tapi River, India.

Figure 12. Punasa Gorge, Narmada River, showing narrow, deep bedrock cross section.

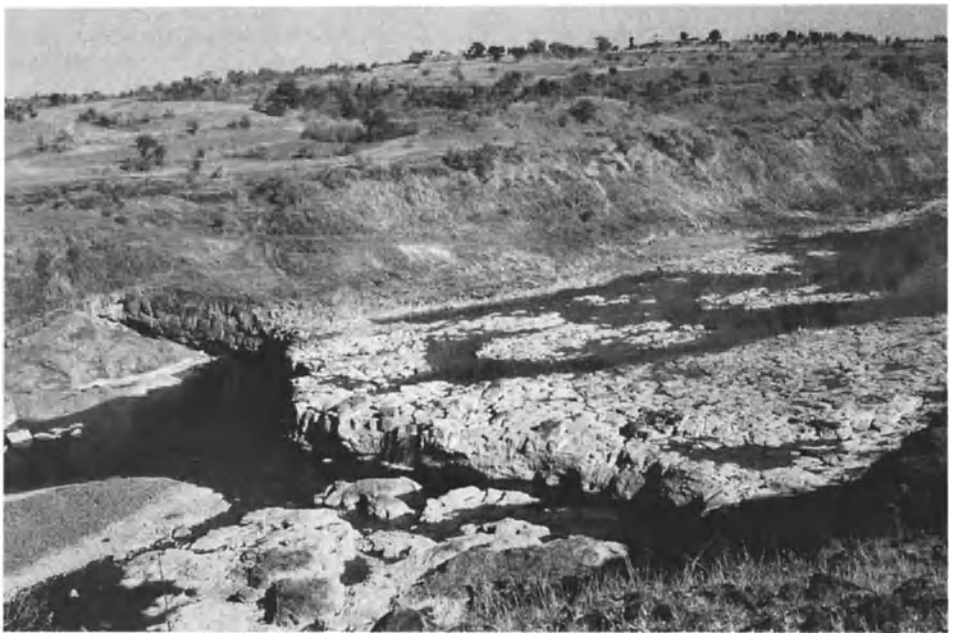

Figure 13. Bhainsadehi Gorge, Tapi River, showing a 4.5 m fall with plunge pool and potholes upstream of the lip zone. Compare to Figure 1.

Table 2. Paleohydraulic parameters for Indian river gorges (see text) estimated by hydraulic modeling of flood flows in the reaches.

River	Site	Discharge Q m^3s^{-1}	Width W m	Depth D m	Slope S	Power per Unit Area, ω Wm^{-2}
Narmada (Pools)	Punasa (Figure 12)	6×10^4	419	68	3×10^{-4}	421
Narmada (Rapids)	Punasa (Figure 12)	6×10^4	483	57	8×10^{-4}	948
Narmada (Multi-Channel)	Punghat	4.6×10^4	2750	13	1.2×10^{-3}	200
Narmada (Rapids)	Punghat	4.6×10^4	1900	10	3×10^{-2}	7118
Tapi (Gorge Head)	Dhanora	9.5×10^3	166	17	1.6×10^3	897
Tapi (Wide Gorge)	Guttigrab	1×10^4	205	15	1.3×10^3	621

Figure 14. Large boulder berm immediately downstream of the Bhainsadehi Gorge cataract (Figure 13). Erosional bed forms are visible in the foreground. Tapi River near Dhanora, India. Flow direction is from right to left.

flow velocity. Hence, large boulder berms are observed on the inner side of the bends or immediately downstream of waterfalls (Figure 14).

DISCUSSION AND CONCLUSIONS

Alluvial rivers conform to criteria of minimizing rates of work expenditure, whereby power per unit length of channel is made equal along the channel length and power per unit area of bed is made equal at all positions along the channel length [*Leopold and Langbein*, 1962; *Leopold et al.*, 1964]. The power per unit area for this equalization and minimization is in the range of 1 to 10 Wm^{-2} [*Baker and Costa*, 1987; *Baker and Kochel*, 1988] (Table 1).

Bedrock rivers with exceptionally resistant flow boundaries develop narrow, deep cross sections locally [*Baker*, 1988b], thereby increasing the power per unit area during extreme flows (Tables 1 and 2). Any adjustment seems to be to much higher levels of power expenditure, exceeding 10^2 or 10^3 Wm^{-2}, with the highest values characteristic of cataclysmic flood channels [*Benito*, 1997] (Table 1). There is some evidence that these channels are adjusting to an ideal Froude number condition near 1.0 [*O'Connor*, 1993], a condition also observed in alluvial channels when the slope is made to be unusually steep [*Grant*, 1997]. Further paleohydraulic work on bedrock channels will be needed to test this hypothesis.

Although this brief review of bedrock channel formation and maintenance by extreme floods presents but a few case studies from northern Australia and India, the general principles seem widely applicable. Current active work in many bedrock channel regions subject to extreme flooding, has and will do much to test these principles. Advances in our knowledge of extreme flood hydrology [e.g. *Benito*, 1997; *O'Connor*, 1993] are pointing the way to increased understanding.

Acknowledgments. We thank J. Harlen Bretz and George E. Neff for early inspiration to study the dynamics of cataclysmic flooding processes. Professor S.N. Rajaguru stimulated our interest in the bedrock rivers of India. A. Gupta and E. Wohl provided helpful review comments on the manuscript. This paper is Contribution Number 56 of the Arizona Laboratory for Paleohydrological and Hydroclimatological Analysis, The University of Arizona.

REFERENCES

Baker, V.R., Paleohydrology and sedimentology of Lake Missoula flooding in eastern Washington, *Geological Society of America Special Paper* 144, 1973.

Baker, V.R., Stream-channel response to floods with examples from central Texas, *Geol. Soc. Amer. Bull.*, 88, 1057-1071, 1977.

Baker, V.R., Paleohydraulics and hydrodynamics of scabland

floods, in *The Channeled Scabland*, edited by V.R. Baker and D. Nummedal, pp. 59-80, NASA Planetary Geology Program, Washington, D.C., 1978a.

Baker, V.R., Large-scale erosional and depositional features of the Channeled Scabland, in *The Channeled Scabland*, edited by V.R. Baker and D. Nummedal, pp. 81-116, NASA Planetary Geology Program, Washington, D.C., 1978b.

Baker, V.R., *The Channels of Mars*, University of Texas Press, Austin, 1982.

Baker, V.R., Paleoflood hydrology and extraordinary flood events, *J. Hydrol.*, 96, 79-99, 1987.

Baker, V.R., Cataclysmic processes in geomorphological systems, *Zeit.Geomorph.* 1988a.

Baker, V.R., Flood erosion, in *Flood Geomorphology*, edited by V.R. Baker, R.C. Kochel, and P.C. Patton, pp. 81-96, Wiley, N.Y., 1988b.

Baker, V.R., Megafloods and glaciation, in *Late Glacial and Postglacial Global Changes*, edited by I.P. Martini, pp. 98-108, Oxford University Press, Oxford, 1996a.

Baker, V.R., Discovering Earth's future in its past: Palaeohydrology and global environmental change, in *Global Continental Changes: The Context of Palaeohydrology*, edited by J. Branson, A.G. Brown, and K.J. Gregory, pp. 73-83, Geological Society Special Publ. 115, London, 1996b.

Baker, V.R., and Costa, J.E., Flood power, in *Catastrophic Flooding*, edited by L. Mayer and D. Nash, pp. 1-21, Allen and Unwin, Boston, 1987.

Baker, V.R., and Kochel, R.C., Flood sedimentation in bedrock fluvial systems, in *Flood Geomorphology*, edited by V.R. Baker, R.C. Kochel, and P.C. Patton, pp. 123-137, Wiley, N.Y., 1988.

Baker, V.R., and Pickup, G., Flood geomorphology of the Katherine Gorge, Northern Territory, Australia, *Geol. Soc. Amer. Bull.*, 98, 635-646, 1987.

Baker, V.R., Benito, G., and Rudoy, A.N., Paleohydrology of late Pleistocene superflooding, Altay Mountains, Siberia, *Science*, 259, 348-350, 1993.

Benito, G., Energy expenditure and geomorphic work of the cataclysmic Missoula flooding in the Columbia River Gorge, U.S.A., *Earth Surf. Proc.Land.*, 22, 457-472, 1997.

Dury, G.H., Principles of Underfit Streams, *U.S. Geol. Surv.Prof. Paper 452-A*, 1964.

Ely, L.L., Enzel, Y., Baker, V.R., and Kale, V.S., Paleoflood evidence of changes in the frequency of extreme floods on the Narmada River, Central India, *Geol. Soc. Amer. Bull.*, 108, 1134-1148, 1996.

Grant, G.E., Critical flow constrains flow hydraulics in mobile-bed streams, a new hypothesis, *Water Resour. Res.*, 33, 349-358, 1997.

Gupta, A., Large floods as geomorphic events in humid tropics, in *Flood Geomorphology*, edited by V.R. Baker, R.C. Kochel, and P.C. Patton, pp. 301-315, Wiley, N.Y., 1988.

Kale, V.S., Ely, L.L., Enzel, Y., and Baker, V.R., Geomorphic and hydrologic aspects of monsoon floods on the Narmada and Tapi Rivers in central India, *Geomorphology*, 10, 157-168, 1994.

Kale, V.S., Baker, V.R., and Mishra, S., Multichannel patterns of bedrock rivers: An example from the central Narmada basin, India, *Catena*, 26, 85-98, 1996.

Leopold, L.B.,and Langbein, W.B., The concept of entropy in landscape evolution, *U.S. Geol. Surve. Prof. Paper, 500-A*, 1962.

Leopold, L.B., and Maddock, T., III, The hydraulic geometry of stream channels and some physiographic implications, *U.S. Geological Survey Prof. Paper*, 252, 1-57,1953.

Leopold, L.B., Wolman, M.G., and Miller, J.P., *Fluvial Processes in Geomorphology*, Freeman, San Francisco, 1964.

Maddock, T. III, A Primer on flood plain dynamics, *Journal of Soil and Water Conservation*, 31, 44-47, 1976.

Matthes, G.H., Macroturbulence in natural stream flow, *Trans. Amer.Geophyis.Union*, 28, 255-262, 1947.

O'Connor, J.E., *Hydrology, Hydraulics, and Sediment Transport of Pleistocene Lake Bonneville Flooding on the Snake River, Idaho*, Geological Society of America Special Paper 274, 1993.

O'Connor, J.E., and Baker, V.R., Magnitudes and implications of peak discharges from Glacial Lake Missoula, *Geol. Soc. Amer. Bull.*, 104, 267-271, 1992.

Rajaguru, S.N., Gupta, A., Kale, V.S., Ganjoo, R.K., Ely, L.L., Enzel, Y., and Baker, V.R., Channel form and processes of the flood-dominated Narmada River, India, *Earth Surf. Proc. Land*, 20, 407-421, 1995.

Schumm, S.A., *The Fluvial System*, Wiley, N.Y., 1977.

Schumm, S.A., and Lichty, R.W., Time, space, and causality in geomorphology, *Amer. J. Sci.*, 263, 110-119, 1965.

Shepherd, R.G., River channel and sediment responses to bedrock lithology and stream capture, Sandy Creek drainage, central Texas, in *Adjustments of the Fluvial System*, edited by D.D. Rhodes and G.P. Williams, pp. 255-275, Kendall/Hunt, Iowa, 1979.

Shepherd, R.G., and Schumm, S.A., Experimental study of river incision, *Geol. Soc. Amer. Bull.*, 85, 257-268, 1974.

Wolman, M.G., and Gerson, R., Relative scales of time and effectiveness of climate in watershed geomorphology, *Earth Surface Processes*, 3, 189-208, 1978.

Wolman, M.G., and Miller, J.P., Magnitude and frequency of forces in geomorphic processes, *J. Geol.*, 68, 54-74, 1960.

Victor R. Baker, Department of Hydrology and Water Resources, The University of Arizona, Tucson, AZ 85721-0011 U.S.A.

Vishwas S. Kale, Department of Geography, University of Poona, Pune 411007 India

Recent Adjustments to the Long Profile of Cooksville Creek, an Urbanized Bedrock Channel in Mississauga, Ontario

Keith J. Tinkler

Department of Geography, Brock University, St Catharines, Ontario, Canada

John Parish

Parish Geomorphic, Georgetown, Ontario, Canada

Cooksville Creek (33 km^2) is based in weak Georgian Bay Formation shale and thin limestone and has been gradually urbanized by the City of Mississauga within the last thirty years. These conditions, together with a mean thalweg gradient of about 0.77%, have produced enhanced rates of channel bed erosion along much of the channel (the order of 2 centimetres per year), as revealed by installed engineering works, such as armour stone blocks and gabion baskets. Erosion rates below drop structures are up to an order of magnitude faster. A year-long monitoring program revealed that weather-ing of the shale bed by wetting and drying cycles was primarily responsible for fragmenting the shale to a size (a few centimeters on the long axis) which could be removed by frequent and moderate high flows with a magnitude much less than the Mean Annual Flood. Channel bed quarrying of shale and limestone slabs, and the transport of larger clasts and meter dimension armour stones toppled from channel structures, require flood flows with a recurrence interval of about the Mean Annual Flood. Such flows are characterized by critical or supercritical flow conditions along the thalweg, and with velocities typically in the range 4 to 6 meters per second, they are well able to quarry the bed, and transport clasts up to metre dimension in size.

INTRODUCTION

It is generally assumed that because of considerable resistance to erosion by bedrock, changes in the longitudinal profiles of bedrock streams can only be studied indirectly. However, if resistance is low, or erosive potential is high [*Hancock et al.*, this volume] there may be opportunities to evaluate change directly. Here we describe changes during the last thirty years in the long profile of Cooksville Creek at site, reach and basin scales, and evaluate the processes that cause them.

Our data are based on material obtained initially during an intensive study of Cooksville (December 1994 to April 1996) as part of an engineering contract financed jointly by the City of Mississauga and the Credit Valley Conservation Authority [*Totten Sims Hubicki et al.*, 1997]. The study was undertaken to understand the dynamics of fluvial activity in Cooksville Creek with particular emphasis on causes for the observed lowering of the shale bed with respect to engineering structures installed at known dates. It was hoped that the understanding obtained would "carry over" to a large number of very similar creeks in the Great Toronto vicinity, together with specific recommendations for management of such streams. The reaches used in the Cooksville Creek study have been kept under observation in

Rivers Over Rock: Fluvial Processes in Bedrock Channels
Geophysical Monograph 107

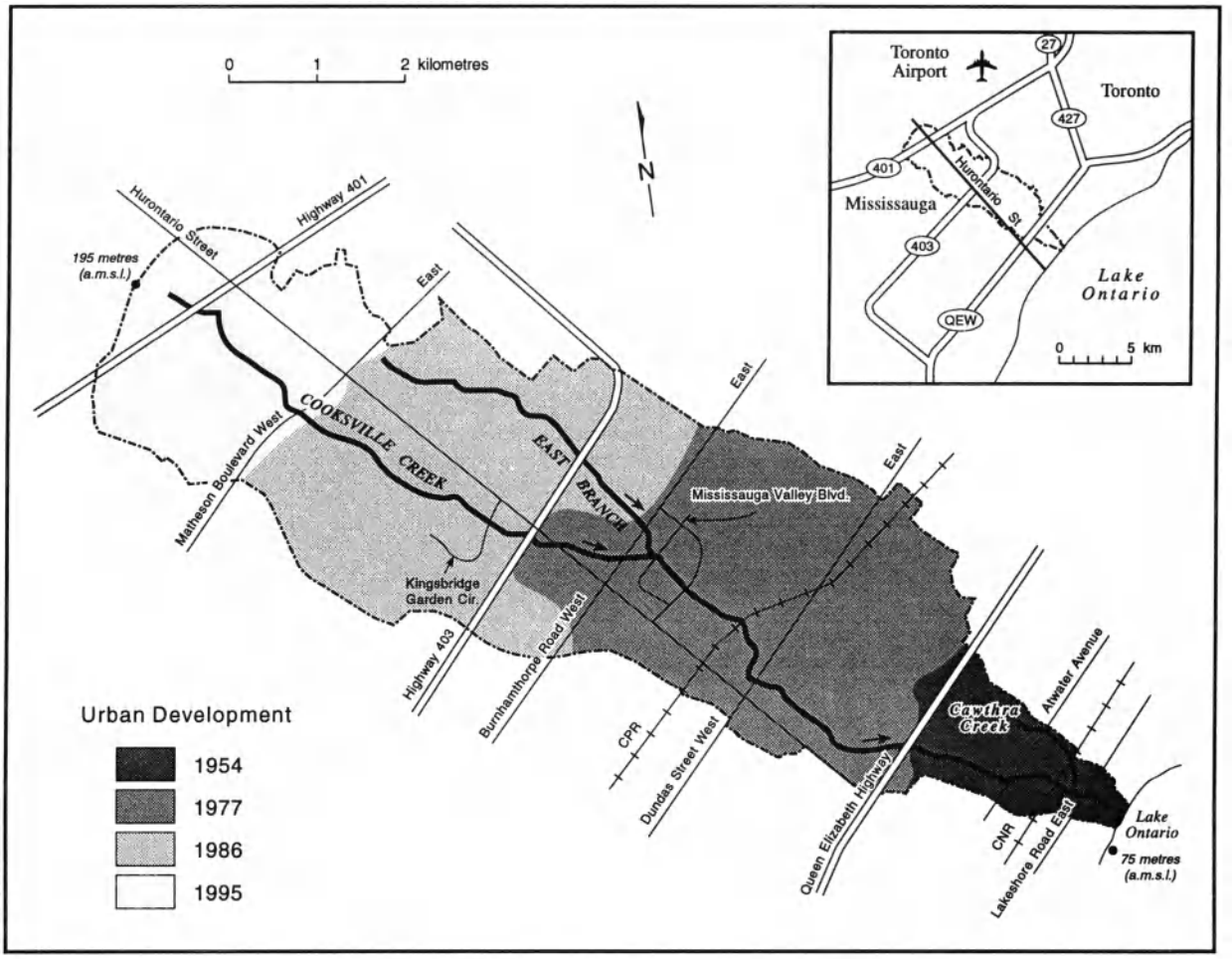

Figure 1. Base map reach locations, and the progress of urbanization in Cooksville Creek basin.

subsequent years in order to ensure that changes are not idiosyncratic to the contract study period.

The recent rate of bed erosion at Cooksville Creek has been remarkably high (~2 cm/yr), and incision and bed lowering has remained fairly consistent throughout the basin with the exception of headwater reaches which remain agricultural with limited downcutting, and one reach where there has been no vertical downcutting within the last few centuries. At the lake shore where the creek delivers sediment to Lake Ontario, water levels have been rising through postglacial time with a current rate of about 15 or 20 cm/century [*Tushingham*, 1992]. Therefore present incision cannot be attributed to a lowering of baselevel. We will compare present incision rates with estimates of postglacial incision rates for larger neighboring streams entering the northwest coastline of Lake Ontario, between Hamilton and Toronto, and with high rates known elsewhere from the literature.

Changes in peak discharge and the possible removal of bed armoring, both consequent upon changing land use, are assumed to be the primary control on the present erosion rate. Both act in association with steep basin and reach gradients, and friable rocks to produce critical and supercritical flow along the thalweg during floods which are close to a Mean Annual Flood frequency of about 2 years, and which are bankfull, about 1 to 1.5 m before overtopping channel structures installed in recent decades.

BACKGROUND

Watershed

The Cooksville Creek watershed is approximately 33 km^2, from north of the Highway 401 to the mouth at Lake Ontario (Figure 1). Is located entirely within the City of Mississauga, and is 90% urbanized. Agricultural headwater areas compose the remaining 10%, and land use is

residential (60%), industrial and commercial (25%), and 15% rural or open park land. The main channel is approximately 11 km in length and has a dimensionless slope of 0.0077, with local variations from 0.001 to 0.0192. It is 4th order with a bifurcation ratio of 3.31. Values for the more agricultural Halton region to the south average 3.28, and for another urban basin nearby, Sawmill Creek, they are 3.37. Drainage density is 1.34 km/km^2, a low figure when compared with neighboring agricultural basins of similar size. Using Provincial 1:10,000 maps, Fletcher's Creek which is further north and west in Brampton and which is 40% urban has a drainage density of 2.04 km/km^2, whereas more rural systems in Halton, specifically Black Creek and Silver Creek in Georgetown, have a drainage density of 2.72 km/km^2. However, the values for Cooksville Creek do not include the many storm drains which would certainly increase the values.

Bedrock and Quaternary Geology

The Cooksville drainage basin is underlain entirely by late Ordovician Georgian Bay Formation, a dark gray shale (density 1.8 to 2.2 g/cm^3) with interbeds of limestone (density 2.65 g/cm^3) [*Johnson et al.*, 1992] which is commonly exposed along the banks and bed of Cooksville Creek. The formation is up to 175 meters thick and extends below adjacent Lake Ontario. There is gentle regional dip of 12.1 m/km to the south-east, but within reaches bedding planes are essentially level. Rock characteristics are relatively consistent through the basin, with the proportion of shale being between 50 to 60%. The presence and thickness of the limestone interbeds is more variable: in the downstream areas interbeds are approximately 8 cm thick whereas upstream the thickness varies from from 3 cm to 12 cm, and interbeds are a slightly higher proportion of the total thickness. The limestone interbeds are more resistant and provide temporary stability in exposures. Downcutting of the channel occurs primarily as subjacent shale is eroded and removes the support of limestone blocks delimited by joints and bedding planes, and opened up by dissolution.

Overlying the Georgian Bay Formation are unconsolidated deposits from the Quaternary period, divided by the abandoned shoreline of glacial Lake Iroquois (Figure 2), a subtle bluff south of Central Parkway [*Karrow and Easton*, 1990]. North of the Iroquois shoreline is the Halton Till [*Karrow*, 1991], composed of silt and clay and whose thickness varies through the drainage basin from less than one meter to 4 meters. Immediately south of the Lake Iroquois shoreline, in the Cooksville Creek valley are beach deposits and gravel bars which increase in thickness towards the Iroquois shoreline. Limited reaches of Cooksville Creek are gravel-veneered bedrock in this area. The remainder of the basin is comprised of lacustrine deposits overlying the shale with a thickness ranging up to 3 meters [*Karrow*, 1991]. Similar conditions prevail in all basins draining to Lake Ontario between Hamilton and Toronto.

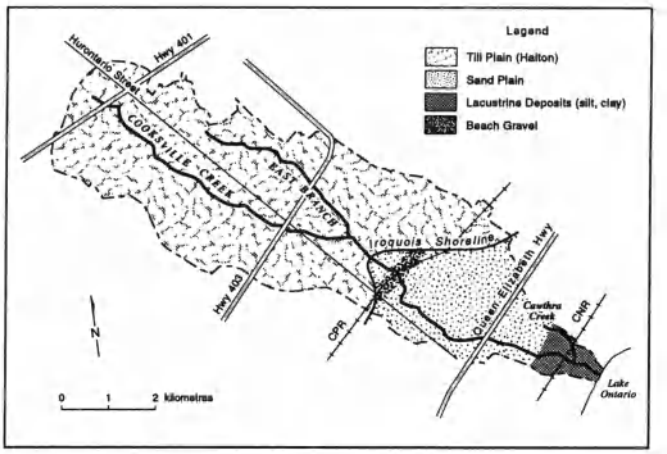

Figure 2. Surficial Quaternary geology.

Climate and Hydrology

The local climate of the drainage basin is slightly moderated from upstream (Pearson International Airport - 60 yr record) to downstream (Lakeview 28 yr record) due to the effects of Lake Ontario (which makes for milder temperatures). Although the total mean precipitation from the two stations is very similar [777 mm and 781 mm respectively, *Environment Canada*, 1993] there is noticeable variability in extreme point rainfall values. The extreme July rainfall at Pearson Airport was 118.5 mm on July 28, 1980 whereas only a few kilometers away at the Lakeview station the extreme July rainfall event was 59.7 mm on July 6, 1977. These intense convective events generate significant floods in upstream and pavemented parts of the basin and thus contribute to high peak flows.

The range of measured and simulated discharges for 2 year and 100 year flows were produced through OTTHYMO modeling as part of flood-line mapping study [*R.V. Anderson Ltd.*, 1996] and are summarized in Figure 3. Corresponding velocity measurements from a HEC-RAS version of the same model are tabulated in Table 1. The creek has not been gauged, although inconclusive efforts (foiled by vandalism) were made during the contract study to define the flow regime. However, review of previous studies, records of the City of Mississauga Engineering Department, and historic observations made by residents provided a relatively satisfactory indication of hydrological behavior.

The yearly hydrograph [*Glaves and Waylen*, 1997; *Irvine and Drake*, 1987; *Sangal and Kallio*, 1977] ought to follow the traditional shape for basins in Southern Ontario, with the peak flow occurring in the spring, and a secondary peak in the fall. However, Cooksville Creek, due to the urban setting, displays more variability. Baseflow is lower than normal due to low groundwater contribution. This is a

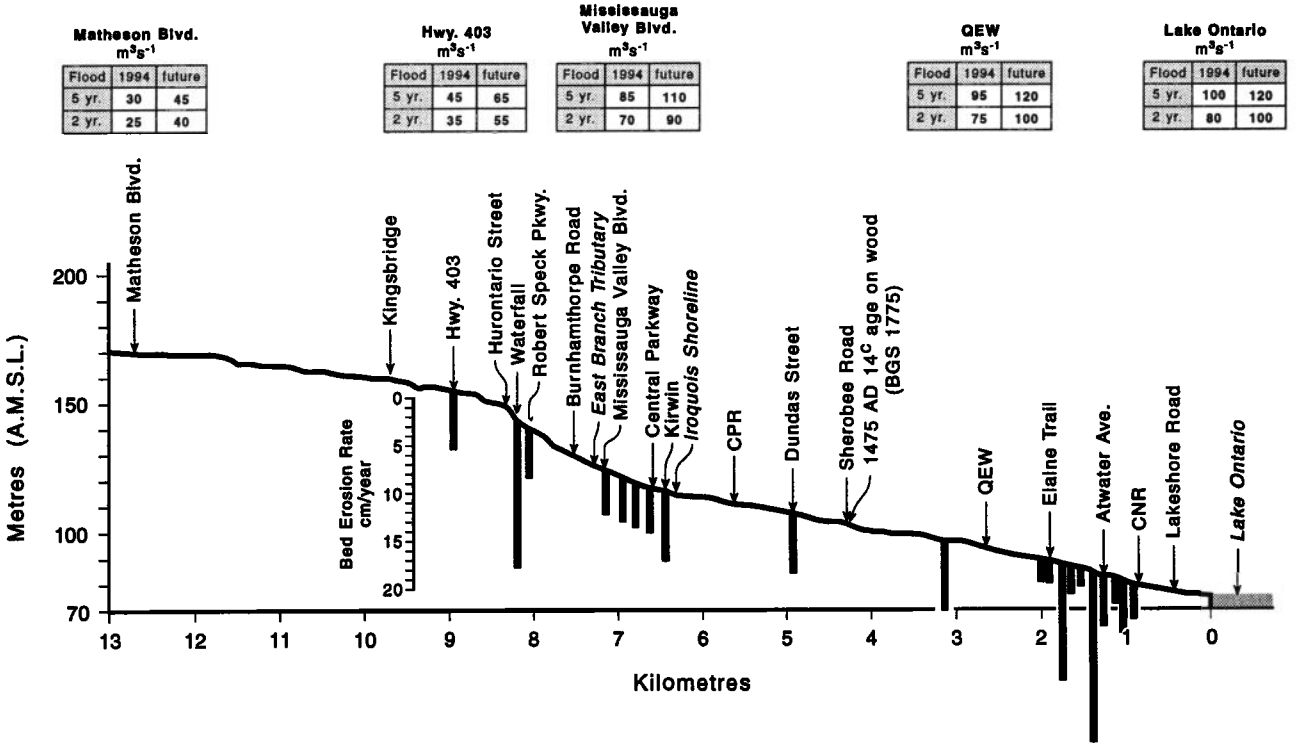

Figure 3. The long profile of Cooksville Creek, reach locations, incision rates, and expected magnitudes of flood flows.

product of the close proximity to bedrock and the high degree of channel lining and protective materials throughout the basin which combine to retard groundwater storage and contribution. During the winter and throughout the urbanized basin, snow is cleared and ablated. Therefore less snow is stored on the surface to be available for the spring meltout and this results in a more subdued spring hydrograph, compared to surrounding agricultural areas. The response of Cooksville Creek to all precipitation events, especially intense summer convective storms which dominate the hydrograph, is extremely fast and is characteristic of a flashy storm hydrograph. During an event on June 7, 1995, average flow velocity at Elaine Trail (see below) went from 0.114 m/s to 1.78 m/s in less than 5 minutes, with a corresponding discharges of 0.20 m^3/sec (low flow) and 9.30 m^3/sec (peak).

Flow Dynamics

It has been shown [*Tinkler*, 1997a] that by equating the condition for critical flow velocity along the thalweg to Manning's equation and solving for slope (s), that critical flow ensues at a slope defined by: $s = gn^2d^{-1/3}$, where g = gravity; n = Manning's n; d = flow depth in meters in the panel of interest. This is the standard criteria for "steep" channels [*Tinkler and Wohl*, Chapter 1, this volume; *Chow*, 1959]. For example, if flow depth is 1.5 m at mean annual flood (MAF) and the roughness value (on smooth shale) is 0.025, critical flow requires a slope greater than 0.0054, whereas the mean slope for the basin is 0.0077. Clearly, critical flow is possible throughout most of the basin, (Table 1). However, critical flow is independent of reach gradient [*Tinkler*, 1997a], once the minimum gradient needed is attained. The same figure for depth produces a mean velocity of 3.8 m/sec in critical flow. Because critical flow is self-adjusting in a reach even as stage rises [*Grant*, 1997; *Tinkler*, 1997a], it is frequently the reach flow condition along the thalweg, and because it represents maximum discharge for a given specific energy [*Henderson*, 1970], it is especially effective in sediment transport and in producing extremely high and localized basal shear stress.

Historical Perspective

An historical assessment of the watercourse and basin was performed through the review of aerial photos, and consultant's reports from the late 1970's and early 1980's. Numerous sets of aerial photos were available ranging from 1990 back to an undated set believed to be from the mid to early 1940's. For the historic assessment of channel form,

Table 1. Channel Attributes and Historic Change, by Reach

Reach	gradient as %	velocity range* (m/s)	Year	Channel Length (m)	sinuosity	Width (m)	Protection (m) both sides
$ Lake Ontario to	0.62	2.6 O	1954	1498	1.24	6.9	0
Atwater Avenue		3.7 C	1977	1318	1.09	15.2	367
		5.5 M	1986	1303	1.07	16.4	1521
			1990	1282	1.06	16.4	1591
$ Atwater Ave to QEW	0.75	4.1 O	1954	1684	1.24	6.5	0
		4.4 C	1977	1502	1.11	8.1	130
		6.0 M	1986	1482	1.09	10.0	1262
			1990	1480	1.08	10.1	1262
QEW to Dundas St.	0.53	4.4 C	1954	2302	1.14	5.1	16.4
		6.0 M	1977	2280	1.12	6.8	270
			1986	2244	1.09	7.3	1422
			1990	2236	1.09	9.6	1582
Dundas St. to	0.62	2.3 O	1954	1783	1.19	4.5	0
Central Parkway		3.1 C	1977	1696	1.13	4.6	259
		6.5 M	1986	1624	1.08	5.1	1120
			1990	1595	1.06	5.4	1120
$ Central Parkway to	1.40	2.5 O	1954	732	1.16	5.9	0
Mississauga Valley		4.0 C	1977	583	1.03	6.5	0
Boulevard		5.5 M	1986	543	1.03	6.9	950
			1990	526	1.02	6.9	950
Mississauga Valley	1.67	4.0 O	1954	689	1.10	1.1	0
Boulevard to Mutual Road		4.0 C	1977	650	1.09	2.2	0
Pedestrian bridge		6.0 M	1986	620	1.08	3.7	0
			1990	620	1.08	5.5	222
$ Mutual Road Pedestrian	1.92	2.4 O	1954	1050	1.08	4.9	0
Bridge to HWY. 403		3.1 C	1977	1036	1.07	5.4	0
		8.0 M	1986	1032	1.06	6.6	66
			1990	1032	1.06	6.6	148
$ Highway 403 to	0.47	1.2 O	1954	1394	1.22	6.2	0
Eglington, includes		3.1 C	1977	1285	1.12	6.3	0
Kingsbridge		5.0 M	1986	986	1.03	7.8	217
			1990	986	1.03	9.2	217
East Branch	0.87	3.1 C	1954	1241	1.06	1.0	0
		6.0 M	1977	1230	1.05	1.0	90
			1986	1220	1.04	4.1	90
			1990	1208	1.03	6.0	732

$ reach used and discussed in the text
* velocity code: O - observation, C - critical flow calculation from estimated MAF flood depth, M - modeled by HEC-RAS

aerial photos from 1954, 1977, 1986 and 1990 were selected and used to obtain morphometric measures such as channel length, width and sinuosity (Table 1). Data for reach gradient and bank protection are also provided.

Before extensive urbanization and development occurred, Cooksville Creek exhibited a limited meandering form usually associated with a channel in unconsolidated material and moderate slope [*Gregory and Walling*, 1973]. The drainage density of the basin in the 1950's was substantially higher than at present. Assessing channel stability in the 1950's is difficult because the creek in the lower areas exhibited numerous mid-channel bars and eroded areas, as a result of Hurricane Hazel (October 1954, estimated recurrence interval 100 years), and revealed by photos taken just afterwards. By 1977 Cooksville Creek had begun to be channelized and urbanization progressed upstream from Lake Ontario (Figure 1). In some instances localized erosion and sedimentation is evident downstream of developed areas as the creek responded to changing conditions.

Through the period of 1977 to 1990 channel width increased up to 60 % (typically from 6m to 10m) and the channel was straightened. Channel length decreased generally from 2% to 11%, with one reach seeing a change

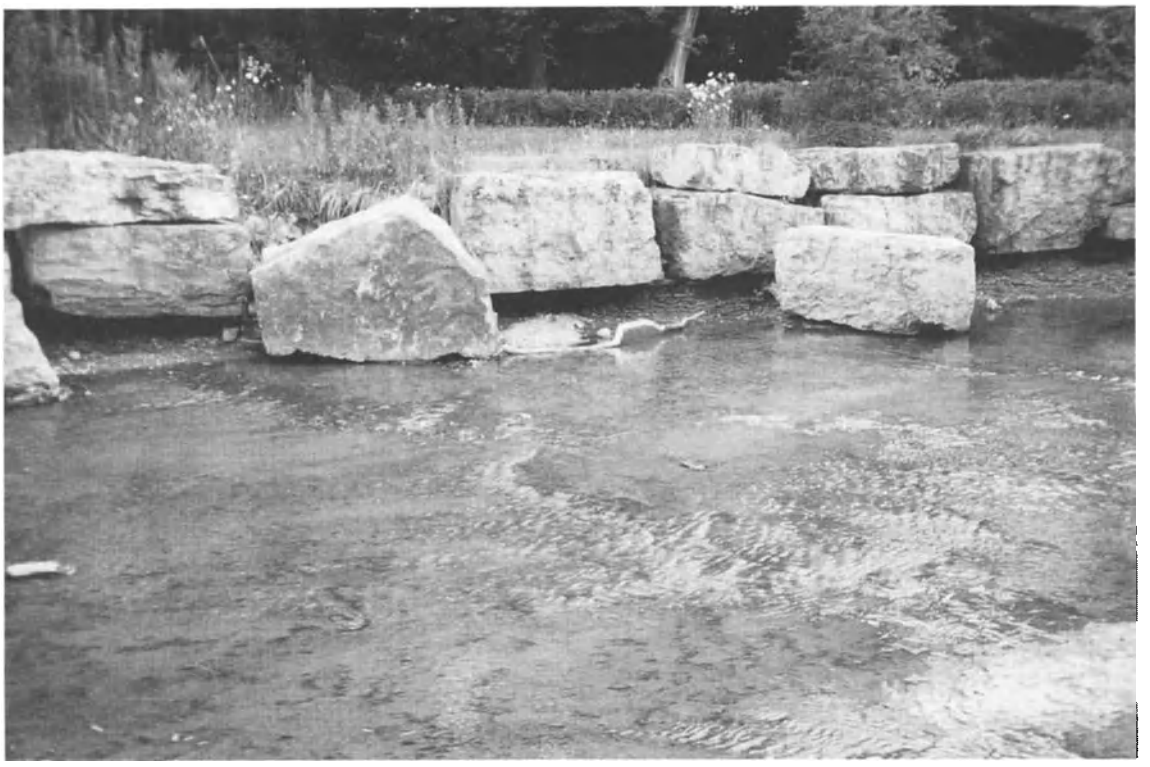

Figure 4. Undercut (45 cm), and toppled armour stone bank protection at Atwater Reach. Flow right to left. MAF flow depth is just over the armour stone, about 1.6 m. The stone on the right traveled 43 m to its present position (from site mapped in Figure 8) during the Opal event. Notice the flat bed to the stream rising only slightly at the channel margins under the blocks.

from 1285 m to 986 m or a loss of 30% (Table 1). The consequence for the channel is a correspondingly increased slope. As the basin was developed more channelization occurred because bank protection was thought to be necessary to reduce erosion from increased flows. Virtually zero bank protection in 1954 was still only 1116 m of channelization in 1977, but turned into 7820 m by 1990. Some of this involves both channel banks, and some of it just one side.

Methods

The field sites used in our evaluation were dictated by the concerns of the basin-scale Cooksville Rehabilitation Project, but cover the entire length of the basin (Figure 1). Reach sites chosen were, going upstream with distances from the lakeshore: Atwater Avenue (1.4 km), Elaine Trail pedestrian bridge (2 km), upstream and downstream of the Mississauga Valley Boulevard North bridge (6 km), Mutual Road pedestrian bridge to north of Robert Speck (6.75 to 7.25 km), and north of Kingsbridge Garden Circle (8.5 km). A number of other sites were inspected occasionally. The contractual study period was December 1994 to March 1996, but we have comparable photographs in several reaches dating back to June 1994, and carried forward to May 1998. The Atwater Reach, having been channelized early (1970s), and subject to substantial bank collapse and transport of meter dimension dolomite armour stones (Figure 4), was singled out for intensive study, especially with respect to coarse sediment transport and high-flow conditions.

A variety of techniques were employed to assess morphological change to the channel, and to characterize flow mechanics during high flows. Repeat photography of reaches during low stages was used to identify areas of change (Figure 5), and along armour stone walls uniquely distinctive patterns of blocks were very useful guides to location. For large clast sediment transport, the techniques included marking clasts with indelible markers - both on the clasts, and on adjacent armour stone walls, photographing, mapping and measuring large clasts resting on the bed or selected channel or plunge pool bars, and marking (indelible marker and spray paint) vertical lines on shale banks. At Kingsbridge a sediment trap caused by the design of the inflow to the culvert invert allowed us to trap an unknown fraction of clasts eroded from the bed upstream.

Figure 5. Looking upstream from immediately below the concrete end sill above Robert Speck Parkway. Top photograph: June 1994; middle photograph: October 1995, after Opal event; bottom photograph, May 1998. In the 16 months between the first two photographs (following installation in summer 1994) there has been: (i) the removal of the round "river" stones placed to stabilize the bed, (ii) the removal of the slabby apron of limestone interbeds (10 to 20 cm thick) on the left bank (top right in photographs), (iii) the development of undercutting below the dolostone armour stones (about one meter dimension on long axis) and below the endsill, and (iv) top left, middle photograph, displaced armour stones from weir. Water trickling through the end sill keeps the shale bed wet and leaves a small "apron" of wet shale (bottom photograph). Bottom photograph: high flows in March 1998 caused bank collapse of undermined armour stones.

Determination of flood stage peak flow depth was made by immediate post-flow assessment of wash lines of reeds and leaves. Velocity determination was by floats over measured reaches, wave length measurements of standing waves in critical flow, and the use of an electro-magnetic current meter. These methods were repeated whenever possible during different flow conditions (low flow, storms, post-high flow) in an effort to establish the types of flow regime. However, systematic flow measurements were not undertaken due to the extremely fast response of the system, and the dangerous conditions during flood peaks. A video taken from the road crossing at Camilla Avenue by Mr. Smania, of a flood peak on July 26th 1993 (a year before the study began) was also inspected, as were photographs taken by creekside residents of peak flow conditions during other floods in the basin (1989). From these, and records of the Mississauga City Engineering Department, we determined that in most reaches installed channel walls are just overtopped about every two years, that is to say roughly the mean annual flood (MAF) interval.

Postflood analysis was made of all significant flood events, and we were fortunate to be able to evaluate the results of a roughly two year event after the passage of Tropical Depression Opal (Opal event) on 5th/6th October 1995. Therefore, although it has not proved possible to obtain direct velocity measurements during such mean annual flood-type events, HEC-RAS modeling suggests *sectional mean* velocities of about 6 m/s through the Atwater reach (implying greater maximum velocities along the thalweg), and at relatively moderate flood stages a mean maximum surface velocity of 4.5 m/s has been measured over a 40 m reach in water no deeper than 40 to 50 cm in the Atwater reach. In the same reach water was nearly 2 meters deep during the Opal event - in critical flow the velocity would be 4.43 m/s for a depth of 2 m, and 4.2 m/s for a depth of 1.8 m.

Channel bed lowering was established by measuring the amount of undercut of installed armour stone walls and gabion baskets with respect to the known age of the engineering installations from City records (Table 2, Figure 3). The oldest such works are about 30 years old, the most recent are only 3 years old (as of summer 1997), and even in these cases significant lowering of the bed has been documented and is visible, both at drop structures (Figure 5a,b,c), and in reaches between drop structures (Figure 4). Throughout the basin the stream bed is essentially flat in cross-section (Figure 4), consequently rates measured along the base of installed structures represent lowering over the entire channel width and along substantial reaches.

OBSERVATIONS DURING THE STUDY PERIOD

Weathering - Preparation for Erosion

The channel bed is comprised of shale and limestone which are weathered for erosion by a variety of processes - solution/chemical; freeze-thaw (including anchor and shelf ice); physical displacement and hydraulic plucking by flowing water, and wetting and drying cycles.

The most effective weathering process within the channel is almost certainly wetting and drying cycles. Once exposed to the atmosphere, the coherent slabs of shale are observed to break down into smaller fragments. From rainfall records it is known that the average interval between significant rain events is about 3 days. Natural wetting and drying cycles, replicated in the laboratory using field samples, sprayed with water and air-dried, fragment the shale within 10 cycles. It was observed at several sites that large slabs of shale, quarried from the bed during high flood stages, disintegrated within a few months to a heap of shale fragments (centimeter dimensions) that could be, and were, removed by virtually any flood flow (Figure 6a,b) [*Magalhaes and Chau*, 1983]. In Cooksville Creek, the natural channel, subsequently channelized, became wider to accommodate increased discharges. The combination of a wide shale bed with low base flow and frequent higher flows is optimal for wetting and drying weathering. In comparison, in natural shale bedrock systems under primary forest, and to some extent even in agricultural areas at present, the channel characteristics - including localized gravel armoring - may be such that the bed is more constantly wet, thereby limiting weathering.

A less obvious process contributing to the form of the channel is chemical weathering. The action and significance of chemical weathering in the sub-surface is harder to evaluate, but it likely prepares shale for other processes, perhaps by partial loss of volume from solution of carbonates and salts. This process is gradual and the actual amount of material supplied to the sediment load is probably minimal, but if concentrated along planes of weakness it may be extremely important. This process likely plays a more significant role in the water quality of the creek by providing ions to the water. Systematic measurements of dissolved solids with a pocket TDS meter were made. However, the values measured were systematically much higher (sometimes over the meter limit of 2000 ppm) than for agricultural drainage basins in the region (140 to 600 ppm) and a pronounced winter peak suggests that natural values for ions are at present are masked by ions from urban sources including road salting. A laboratory analysis of water taken from three sites along the Creek on January 20th 1995 revealed pH of about 7.3, and chlorides at about 28% of the total dissolved load, with substantial fractions of magnesium and calcium (28% together), sulfate (11%) and sodium (19%). Suspended load averaged 30 mg/kg.

Ice acts on the channel through a variety of processes. Ice on the bank can literally pluck shale particles from the bank when it melts and falls. Perhaps most important. however, is the effect of channel icing: as flow levels drop in prolonged (up to several weeks) sub-zero temperatures after a mid-winter flood, supercooled channel water frazil ice freezes onto the bed as anchor ice [*Beltaos*, 1996] and marginal slack water freezes as shelf ice. As the active

Table 2. Estimated Downcutting Rates (also see Figure 3)

Location listed in order going upstream	Bank Protection	Construction Date	Measured* Downcutting (cm)	Estimated Downcutting Rate (cm/yr)
CNR to Atwater Ave.	Gabions	1977	66	3.6
Atwater Ave. Inlet	Gabions	1981	76	5.3
U/S Atwater Ave.	Armour Stone	1985	28	2.8
Storm Sewer Outlet	Armour Stone	1985	51	5.1
Sanitary Sewer Crossing	Concrete	1991	71	17.8
U/S Sanitary Sewer	Armour Stone	1991	8	2.0
Private Access Road	Concrete	1985	30	3.0
Outlet Concrete Channel	Armour Stone	1985	122	12.2
Elaine Trail	Armour Stone	1985	23	2.3
Pedestrian Crossing	Armour Stone	1985	25	2.5
Camilla Park	Armour Stone	1980	107	7.1
U/S Dundas St. E.	Concrete	1980	91	6.1
U/S Kirwin Avenue	Armour Stone	1980	107	7.1
Central Pkwy to Miss. VBN	Gabions	1978	76	4.6
U/S Robert Speck	Armour Stone	1994	5	5.1
Waterfall	Armour Stone	1993	30	15.2
Sanitary Sewer U/S Hwy. 403	Concrete	1985	61	6.1

Notes
* mean of between 10 (1 side) and 20 (2 sides) measurements along the reach

channel conduit constricts due to ice formation, and roughness increases, water overflows existing ice and freezes solid. Often the entire channel is covered with ice up to several decimeters deep. In a subsequent flood, flotation of ice acts in a variety of ways including plucking shale and rock from the bank or bed. When ice shells form around clasts resting on the bed [*Drake and McCann*, 1982], it increases dimensions slightly, but reduces the density of the particle substantially, which leads to transport at flow velocities significantly lower than normally required [*Carling and Tinkler*, this volume]. Ice can also transport particles on the bed through a pushing action. Larger blocks of ice floating during a high flow are driven into the creek bank, and the force of the impact dislodges bank material. Thus ice acts as a physical weathering process, but one which is also important in both erosion, particle entrainment and in transportation.

Despite appearances, bare rock exposed on the stream bed is rarely 'solid'. Tapping with a hammer usually produces a hollow sound. Attempts to take transects of readings across the bed with a Schmidt Concrete Hammer in the Atwater reach during lower flow stages in August 1995 produced a majority of readings which failed to register (<10 on the scale of 1 to 100). Figure 7 shows 28% of the bed eroded by thin flakes at the same location after the Opal event in October 1995. This indicates that surface and near-surface weathering has already parted potential clasts along underlying and hidden bedding planes, and of course along bounding joint planes. The extent to which this process is exacerbated by impact during passage of very coarse clasts is unknown, but is likely significant.

Spray painted lines on the shale on the dry channel banks in the Atwater reach were all removed (several times) during the one year study period (drawing with an indelible marker merely dislodges fragments). Because individual shale fragments are a several millimeters thick (Figure 6) and may be removed several times a year by competent flows, we have no difficulty in claiming that an estimate of 0 to 2 cm a year (zero to four shale pieces a year) is consistent with similar reachwise estimates of incision based on the amount of undercutting of the installed engineering works (Table 2).

It is worth emphasizing that "down time" hydrologically speaking, is not down time for the weathering processes affecting the channel bed, and so taking erodibility as an index, the amount of time between flow events, the relaxation time, may be expected to have a positive affect on the amount of erosion [*Wolman and Gerson*, 1978].

Fluid Flow Conditions

It is important to distinguish between the sectional mean velocities typically estimated by hydraulic procedures (OTTYMO; HEC-RAS) with the intent of establishing discharge, and estimates of mean maximum velocities through localized flow panels in the cross section corresponding to the thalweg [*Tinkler*, 1997a]. The latter velocities are important in determining the controls on bedrock processes such as hydraulic quarrying, and on near bed processes such as the entrainment and movement of very coarse sediment. Our focus has been on estimating mean maximum velocities in relatively narrow panels

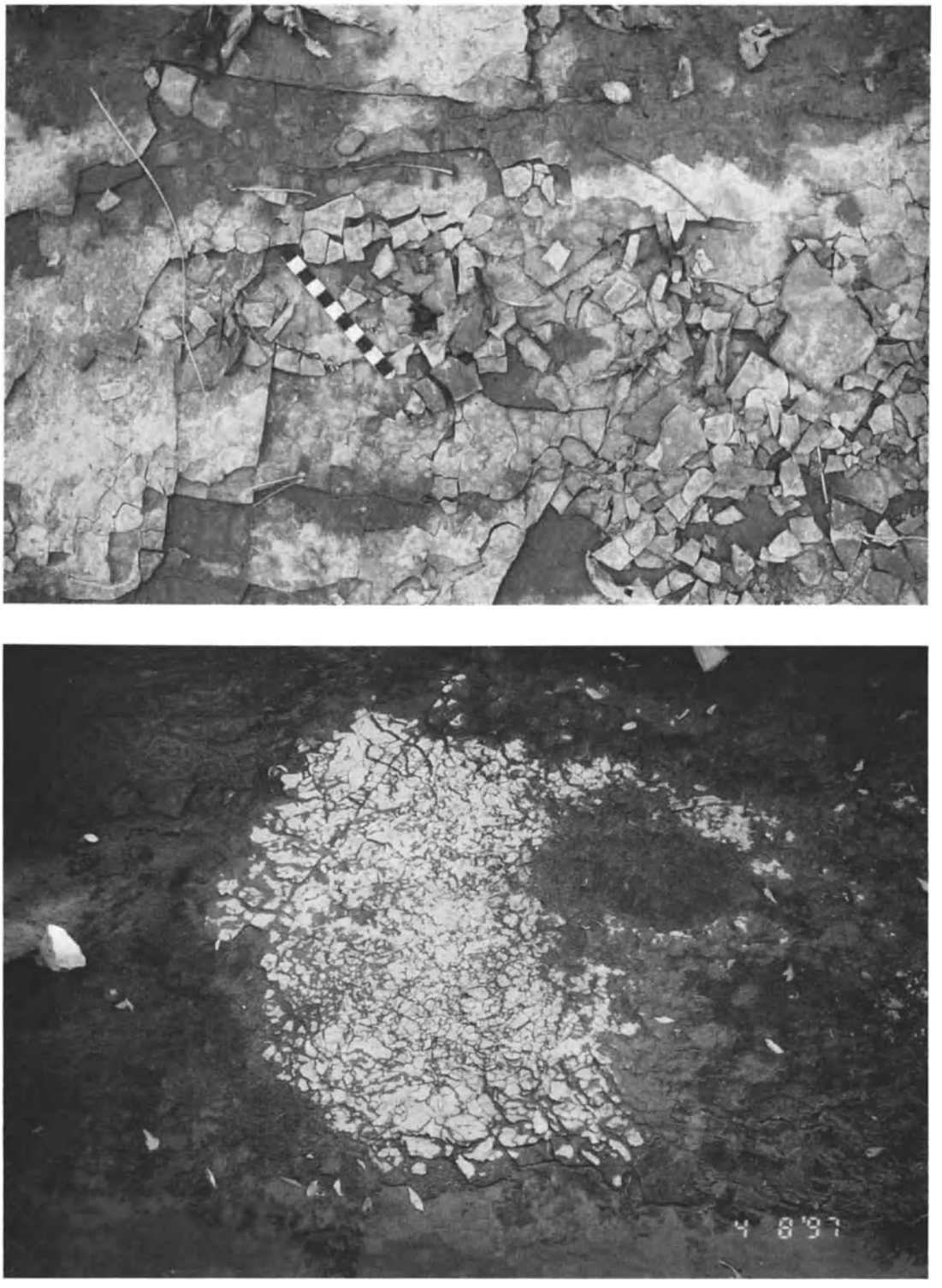

Figure 6. Upper photograph: loose shale fragments on channel margin in Atwater reach. Notice centimetre scale center left. Lower photograph: fracturing of the shale bed as the bed dries in summer - the dried (pale) portion is about 1 m^2.

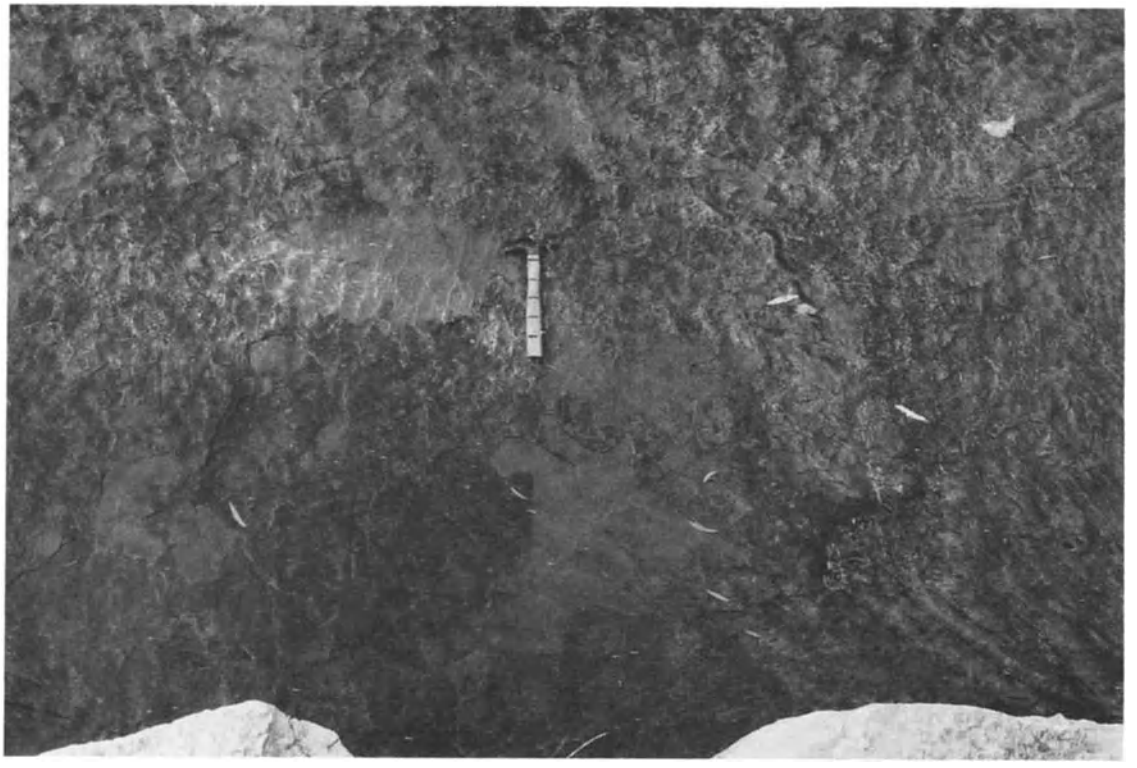

Figure 7. Scars of flakes eroded off the bed during the Opal event. About 28% of the bed was removed in the 3 m by 2 m section photographed, scar thickness estimated at 5 mm. Hammer about 30 cm, flow left to right.

(about a third to a half of the channel width) along the thalweg. Why this does not appear to produce a deep narrow channel, we will discuss later.

It is almost guarantied in alluvial systems that the flow regime is subcritical with a Froude number well below 1, indeed Froude numbers are rarely published. However, in a bedrock system the flow mode may be any of subcritical, critical and supercritical. Frequently two of these modes coexist in a cross-section, and along streamlines when a mixed flow regime is termed transcritical. This gives rise to a distinctive behavior for the system. It is a behavior that is efficient for sediment transport at quite low flood stages, and along strictly defined 'tracks' in the cross section. Steep smooth channels sometimes allow supercritical flow, a condition which may be checked by computing $Fr = v\sqrt{(gd)}$ where v is the measured mean stream or stream panel velocity, g is the gravitational acceleration, and d is the water depth along the flow panel of interest.

Critical flow in the channel center is probably a normal condition in steep channels [*Grant*, 1997; *Tinkler*, 1997a; *Tinkler*, 1997b]. The critical flow condition normally reveals itself as a series of distinct standing waves on the water surface. Critical flow maximizes discharge per unit cross-section and minimizes energy use relative to other possible flow states [*Henderson*, 1970]. A theory developed by *Kennedy* [1963] for standing waves over mobile beds also applies to standing waves over rigid beds, and from the theory, the mean velocity of water through the wave is given by $v = 1.25\sqrt{\lambda}$ where v is the mean velocity and λ is the measured wavelength between standing waves [*Tinkler*, 1997b]. Critical depth is defined as between 0.16λ to 0.24λ (the larger value in light that critical flow may ensue at Fr = 0.84, [*Middleton and Southard*, 1984].

Critical wave trains were observed at several locations in the Atwater reach on November 11th 1995, and through tens of meters of the reach above Robert Speck reach in January 1995. In both instances they occupied only about one third of the available channel width, and in both instances the flood stage observed was only about one third of bankfull depth. They have been observed frequently at even lower flow stages. A video of the July 26, 1993 flood (courtesy of Mr. Smania) observed at Camilla Road shows clearly standing waves in the center of the channel downstream of the bridge. An estimated water depth of about 2 m, gauged from marks on the retaining walls, yields a corresponding velocity would be 4.43 m/s.

It has been speculated that supercritical flow is rare or non-existent in natural channels [*Jarrett*, 1984; *Jarrett*,

1990; *Trieste*, 1992]. In supercritical flow, water flow is fast and shallow, and is therefore especially effective at sediment transport, and at the hydraulic quarrying of rock plates off the stream bed [*Reinius*, 1986]. In reality, while supercritical flow may be rare, it has been observed in Cooksville Creek for tens of meters downstream of drop structures above and below Robert Speck, below Mississauga Valley Boulevard, in the long steep reach before the sharp bend at Atwater. For example, on two occasions during moderate floods we have measured velocities using floats through a long reach of 40m at Atwater: once we obtained 3.61 m/s, and the other time 4.56 m/s. Water depths were estimated at 30 and 40 centimeters respectively, and the computed Froude numbers are 1.82 and 1.96. These are maximum values, adjusting surface velocity to cross-sectional mean velocity using a figure for alluvial streams of 0.80 [*Matthes*, 1956] would reduce the Froude numbers to 1.68 and 1.84. Lateral shock waves generated at channel margins by large clasts, or channel margin protuberances, confirmed that flow was supercritical.

The termination of supercritical flow is marked by hydraulic jumps as flow depth increases suddenly in the downstream direction, and water tries to flow upstream in accord with the immediate water surface slope. The downstream continuation below the jump may be either deep, slow flowing subcritical water (with bursting eddies originating on the bed below the jump), or as a series of standing critical waves [*Henderson*, 1970] called an undular hydraulic jump [*Chanson and Montes*, 1995] with eddies bursting at the sides.

Field observations show that when critical or supercritical flow exists in the channel center, marginal water is flowing sub-critically in slack waters, and sometimes as backwaters. Strong shear zones [eddy fences in canoeing parlance, *Kieffer*, 1985] exist between the two fluid states, and the sub-critical marginal water is often characterized by the rise of turbulent eddies generated close to the bed and revealed in surface water as apparent boils with concentric waves spreading from the burst point on the bed [*Leighly*, 1934; *Matthes*, 1947; *Kostachuk and Church*, 1993; *Lapointe*, 1993] and being carried downstream. Undoubtedly these structures entrain stream bed sediment and move it, on some occasions towards the stream margins where it is readily deposited in the slower moving water. When flood levels recede, the sedimentary evidence of this behaviour is longitudinal marginal bars characterized by imbricate cluster bedforms [*Martini*, 1977] with transverse axes aligned at roughly 45° to the channel direction and dipping towards the clear channel center. In the absence of a fine gravel fraction in the bed load, isolated cluster bedforms often serve to caricature such marginal bars. For example, after the Opal event, several large clasts of shale quarried from the bed were found resting nearly upright against the gabions below the downstep downstream of Mississauga Valley Boulevard - the largest had dimensions 1.80 m x 1.50 m x 0.08 m.

We summarise our discussion of velocity by saying that near-critical, critical and supercritical flow appears to be common at flood stages. Subcritical flow is rare along the thalweg, and is normally confined to channel margins. Estimates of velocity by reach, by direct observation and from HEC-RAS modeling are given in Table 1.

Sediment Transport

Our interest in sediment transport focused on the flow conditions needed to entrain the large clast component eroded from the stream bed and walls, and the large armour stones (meter dimensions) displaced from channel bank protection due to undercutting (Figure 4). Apart from the roughly cubical armour stone blocks, clast shapes are normally very slabby, with a *c* axis much smaller than *a* and *b* axes (Figure 8). In addition, we wished to know the typical response of channel bars to medium and MAF scale floods.

Within the study period we documented substantial change in coarse caliber sediment on bars in all the monitored reaches, Figure 9 is one example. The mean volumes (cm^3) of large clasts moved in selected reaches during medium and high flood stages at Cooksville Creek are shown in Table 3. The discharge with roughly a two-year flood frequency generated by the Opal event in October 1995 was capable of displacing meter-dimension dolostone armour stones from channel walls, and moving them up to 43 meters along the channel (Figure 4). At least ten similar armour stone blocks moved during the Opal event. Table 3 shows that the mean volume of armour stones remaining stable during the Opal event was slightly larger than those moving. A fuller discussion of large boulder movement in near-critical flow conditions is contained in *Carling and Tinkler* [this volume].

Sediment is moved efficiently through the system and sporadic marginal channel bars, and plunge pool bars act as transient storage elements in the system. In Cooksville Creek noticeable sediment bars are rarely more than 1 meter deep and rest on the channel bedrock. The Opal event effected considerable change on these bars, often scouring out sediment and revealing the underlying rock, for example in the reach above Lakeshore Road, in the reach leading from the sharp bend into Atwater/ Canterbury, downstream of the scour pool below the QEW, and in parts of the Robert Speck reach. At the latter, Table 3 (Robert Speck location) shows the mobility of 12 large clasts. Those marked "at threshold" displayed only slight shifts in position (<1m). The removed sediment passed down and through downstream bedrock reaches up to hundreds of meters long until it reached a bar that was building during the falling stage of the flood. Accumulation was substantial immediately downstream of the Atwater /Canterbury bridge where a bar added at least $20m^3$, and at least one marked particle (particle "N") traveled 250 m to reach its location on the top and distal end of this bar. Overbank sediment

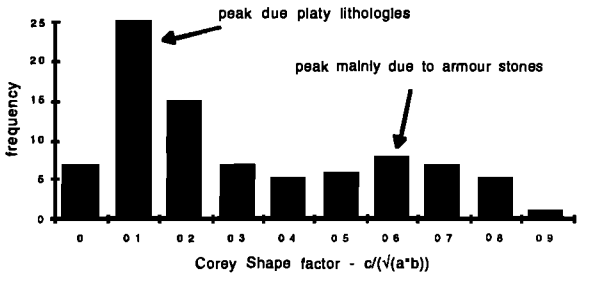

Figure 8. Corey-shape factors for large clasts marked in Cooksville Creek during the study of sediment transport.

storage is negligible. However, this bar has lost sediment in subsequent smaller flows.

In more moderate floods our data and observations suggest that smaller sediment is winnowed off the more substantial bars and is moved downstream to help rebuild and replenish bars destroyed during the larger flows. In the Atwater reach before the Opal event, the mean clast volume of large clasts leaving and arriving on the same bar is surprisingly close. Particle "N" subsequently moved 40 m off the bar to a position in center channel. It has now vanished downstream through a several hundred meter long reach of plane bedrock.

Coarse sediment transport is probably important in providing a supply of impacts to the bed, some of which fortuitously loosen partly weathered flakes on the bed by breaking them at their point of adherence. Examination of fresh flake scars usually reveals a freshly fractured joint plane bounding part of the scar. In the Atwater reach, armour stone blocks moved during the Opal event produced centimeter scale striae extending several meters and where they crossed flow facing edges, revealed evidence of pressure flaking (Figure 10). During the same event in the Robert Speck reach, a displaced armour stone from a weir produced in concrete, a 6 m striae about 2 cm wide and a few millimeters deep. Subsequently we have observed striae in the reach immediately downstream, produced by moving armour stones displaced from channel walls in flood flows in late March 1998.

Nevertheless, despite the very considerable movement of coarse sediment during the Opal event we did observe that in several locations (Robert Speck, Atwater) equally coarse sediment remained undisturbed in channel margin locations resting against the bottom of vertical armour stone. In the Robert Speck reach one large limestone slab has remained in imbricate position against the channel bank for over eighteen months despite the passage of substantial flows. We have made similar observations in the Atwater reach. We can infer therefore that exceptionally high velocities probably do not impinge on the base of the armour stone walls, and are not the primary cause of erosional undercutting in these locations. In addition, the imbricate position is one of stability in the face of flow [*Middleton and Southard*, 1984; *Hattingh and Illenberger*, 1995].

The effectiveness of sediment transport over plane bedrock means that the normal flow regime keeps substantial parts of the bed clear of loose sediment and ensures that during low to dry stages in the annual hydrograph the bed is open to the processes described earlier. Thus, in Cooksville Creek, stream bed and bank erosion is not primarily dependent on the existence or frequency of flow stages in excess of the MAF.

Morphology and Erosion of the Bed

A defining feature of Cooksville Creek is the steady and persistent downward erosion of the channel into the underlying shale. Figures 3, 4 and 5 show clearly the incision measurable from engineering works, both in reaches and at drop structures. Our intent was to observe the mode and scale of erosion without attempting an exact calibration in a short time period.

After medium to high flood stages there is clear evidence of the direct erosion of flakes off the bed of the stream. These are revealed as pale algae-free patches (Figure 7) which discolor within a few weeks to a few months with an algal "film". It takes longer for algal filaments to attach and become part of the algal matt. Because the removed flakes often leave evidence that they have been broken off along part of a joint, they may be dislodged by clast impact during sediment transport, as well as by hydraulic quarrying. In total, removal of the bed during an event averages from about 0.1% to 5 % of the bed, depending on the reach, and the flood magnitude. Typically, eroded flakes (Figure 7) are a few to a few tens of millimeters thick - to judge by the depth of the marginal walls of the flake along joints. Before the Opal event, transects in the Atwater reach, just upstream of Figure 7, revealed 2% of the bed flaked, probably due to March meltout flows, and about 1.5% of slightly less fresh, but still distinct, flakes probably due to the large January flow. After the Opal event they were very abundant in the Atwater reach. Figure 7 shows 28% of bed eroded, for which an estimated flake thickness was 5 mm generates a mean lowering of about 1.4 mm over 6 m^2. Clearly though, erosion is spatially episodic, and eroded flakes leave adjacent areas higher, more vulnerable to the next event, and provide enhanced access for weathering processes along discontinuities.

At knickpoints, repeat photography and mapping has revealed substantial and measurable change on all knickpoints monitored within a three years period, December 1994 to December 1997 (Figures 5, 11). The figures measured are difficult to convert systematically to either a lowering or recession rate, but they involve localised areas on the bed between one and several square meters, and with quarried slab thicknesses of 5 to 25 cm in channels 6 to 10 meters wide. During the Opal event at the Mutual Road site, a meter size dolostone armour block was

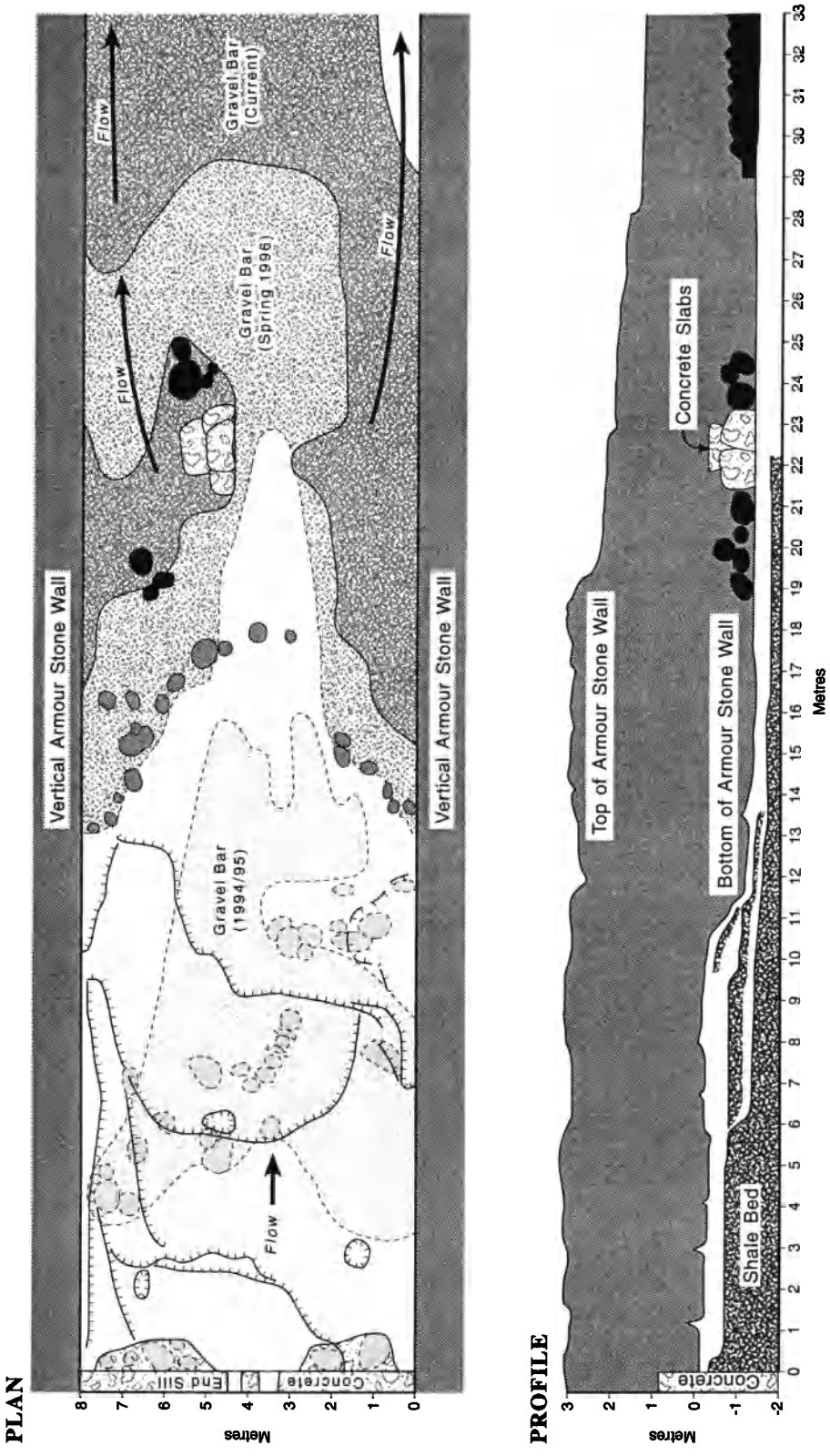

Figure 9. Map of the bed for 33 m below the concrete end sill at Mutual Road to show changes in the deposition of the gravel bars in a period of three years, and associated erosion off the bed in profile view. Since the diagram was drawn, the undercut block at 1.25 to 3 m has sagged to channel bed (cf Figure 5).

Table 3. Sediment Transport in Cooksville Creek

Location	mean clast volume cm^3	comment
Kingsbridge	3,520	moved into trap prior to January, 1995
	1,051	moved into trap between January 1 and July, 1995
	1,623	moved into trap during OPAL (October 5/6, 1995)
Robert Speck	98,207	stable through OPAL
	39,194	stable until OPAL - moved and found in Opal
	24,509	at threshold (< 1m movement) during OPAL
	22,370	moved and lost during OPAL
Atwater	240,000	marked and stable before OPAL
	70,000	arrived on marginal bars before OPAL
	68,000	marked on bars and moved before OPAL
	500,000	stable armour stones until OPAL
	528,635	armour stones moved during OPAL event

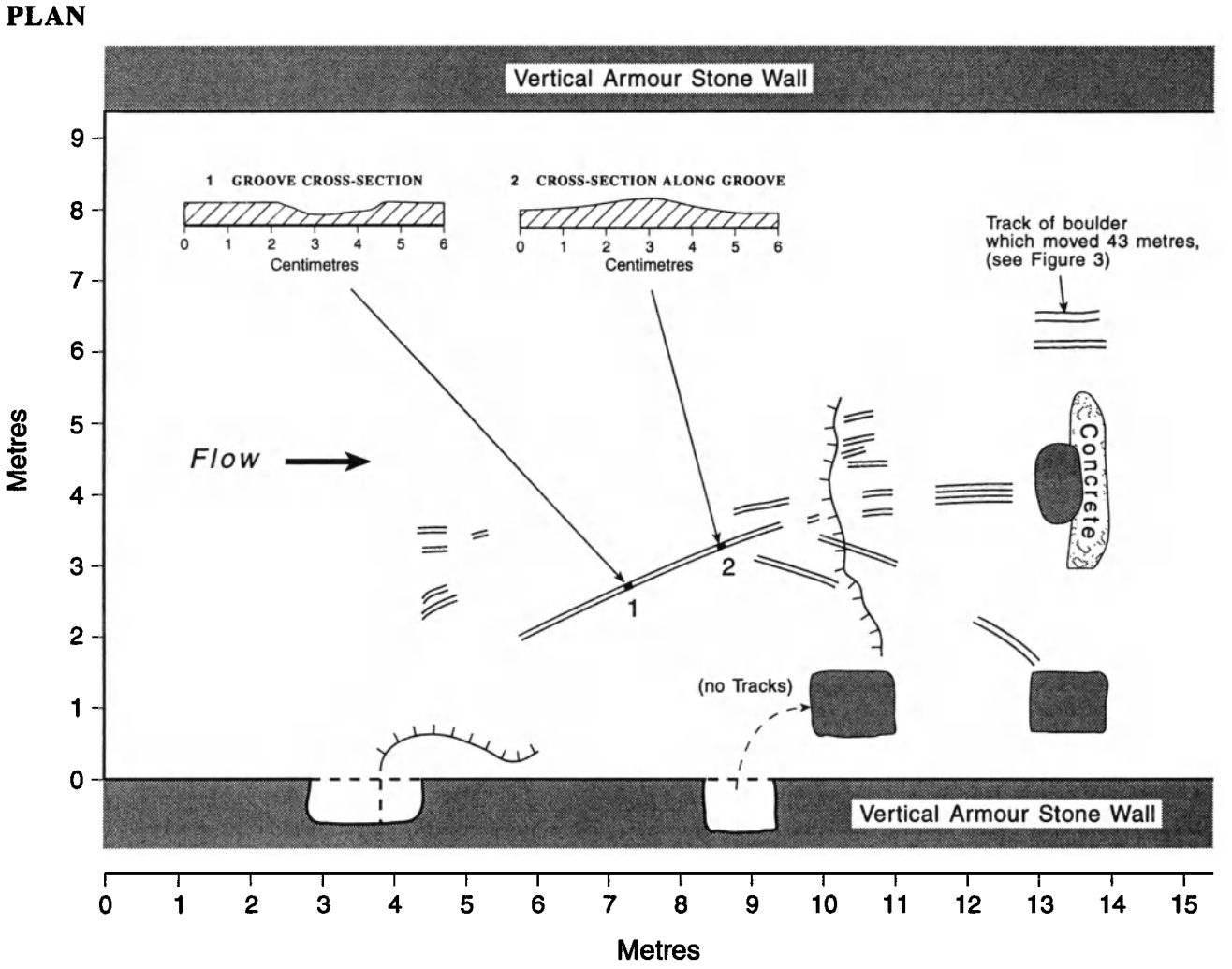

Figure 10. Map of striae on the shale bed (Atwater reach) caused by the passage of dolostone blocks falling off the retaining walls during the Opal event, and moving downstream.

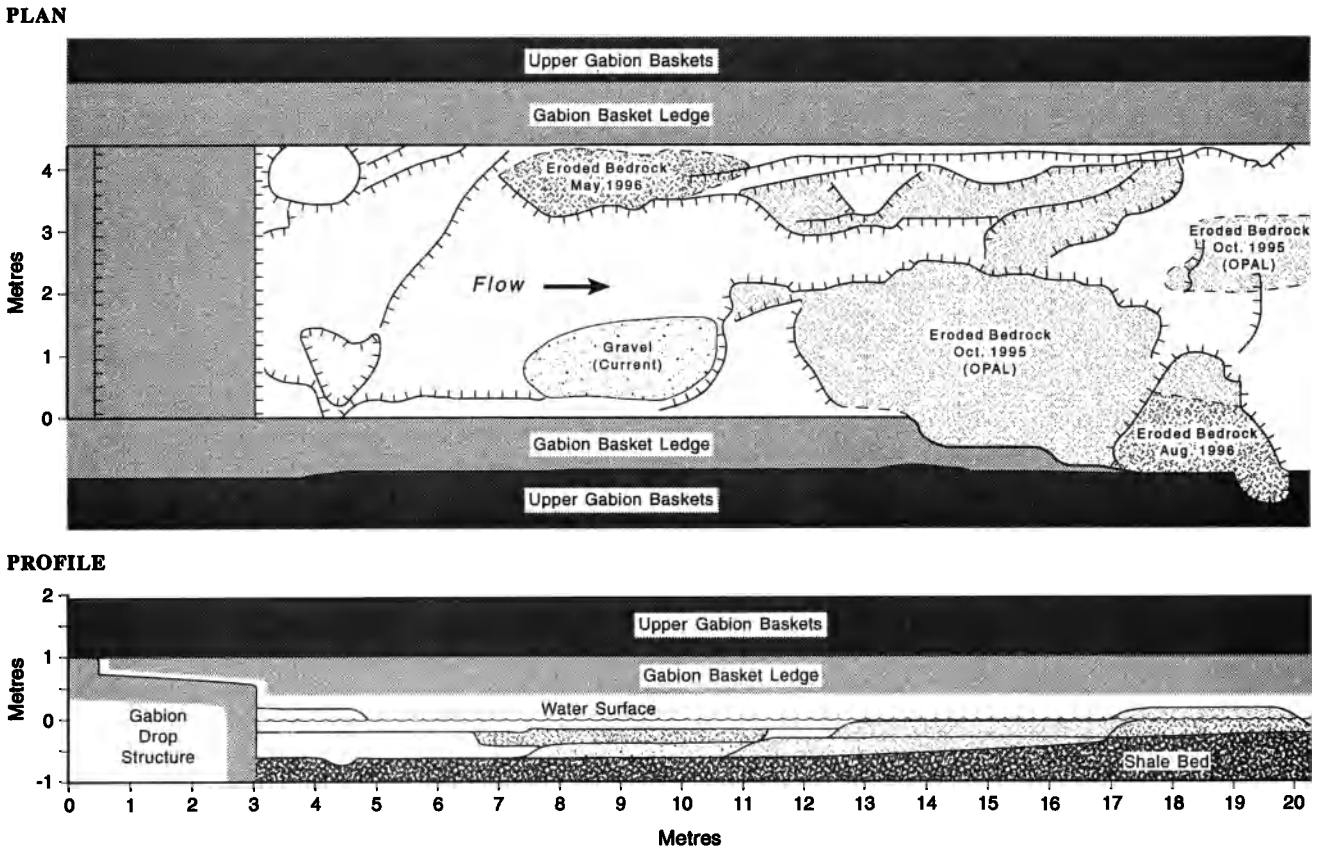

Figure 11. Map of change in plunge pool developed for 20 m below the gabion basket drop structure just downstream of Mississauga Road Boulevard. The Opal event effected considerable erosion of plates off the bed (order of 5 to 10 cm thick), and a subsequent flow of similar magnitude in 1996 removed the remaining pieces of the bed in the region of the rock bar at 18 m.

removed from one weir, and at all three weirs in the reach similar blocks were moved downstream within the concrete "plunge pool." Altogether, at all three weirs more than 50% of the armour stone protective blocks on the lips have been "eroded" into the plunge pool within a 4 year period.

We have depositional evidence of active quarrying below major downsteps, revealed as freshly imbricated slabs immediately downstream of plunge pools, e.g. below the Mutual Road end sill (compare change over one year on Figure 5, 11), below the gabion controlled drop structure just downstream of Mississauga Valley Boulevard (October 1995, slabs up to 0.1 m thick), at the scour pond below the QEW culvert (slabs to 0.25 m thick), and at a drop structure in the Atwater Reach. The channel bed below the gabion drop at Mississauga Valley Boulevard was mapped in August 1995 (Figure 11), because it was developing as a shallow (0.5 m) elongated (18 m) plunge pool in response to the drop. The channel bed was already uniformly lowered about 0.35 m below the base of the gabion baskets, with a pool below the drop about 40 cm deep. Pool morphology showed significant change after the Opal event (October 95), with freshly-quarried slabs resting against the gabion walls. Within the next year, subsequent smaller magnitude, but locally channel-filling events, eroded more rock slabs so that the channel became smooth in cross section where it was originally of a stepped character (Figure 10). The site is now effaced after restoration work on the entire reach in Winter 1998.

At the Kingsbridge Road site we measured all clasts trapped in a pool on the upstream side of a concrete weir and ramp leading under the road. It is an area above the main part of the urbanized basin, and underlain by a more flaggy lithology. Clasts trapped were deduced, from fresh scars seen on the channel bed, to originate within the 450 m of channel upstream with identical lithology. On the basis of total clast volume trapped and the exposed length and width (2 m) of the channel upstream, we estimate over the ten year period since the floodway was constructed, up to January 1995, mean lowering of 0.086 mm, for January to August 1995 (January and March flows) a total lowering

for two events of 0.030 mm, and for the single Opal Event in October 1995, a lowering of 0.034 mm. These are minimum estimates because some clasts pass the trap and are seen in scattered bars in the floodway tunnels below Kingsbridge Road. In fact, once the trap is full most clasts must pass over. Our allowance of 450 m x 2 m for the exposed stream bed as the source may be excessively high, but it produces a conservative estimate. In all, the rate could be almost an order of magnitude larger, but cannot be smaller.

The velocities involved in quarrying rock below drop structures may be roughly estimated. *Reinius* [1986], provides a formula for the threshold velocity, v_{thresh}, needed to quarry slabs. A formulation [*Rainer Wende,* personal communication] is:

$$v_{thresh} = \sqrt{(2g(\gamma_s-\gamma_w)/\gamma_w)\sqrt{(\beta/\phi)} \quad (1)$$

where γ_s and γ_w are the densities of the rock and immersing fluid (water) in g/cm^3, β is the rock slab thickness being quarried, ϕ is a lift coefficient which varies from 0.16 for vertical joints (difficult to quarry) to 0.45 (easy to quarry) for joints strongly inclined from the vertical, and g is the acceleration due to gravity.

Table 1 includes the minimum observed or estimated velocities in our reaches. As stage rises the maintenance and increase of an incoming velocity, v_i, from the additional acceleration at a drop structure with head h, given by $\sqrt{(v_i^2+2gh)}$ [*Tinkler*, 1993], provides ideal conditions for hydraulic quarrying. Table 4 shows the velocities needed to hydraulically quarry blocks off the bed following *Reinius* [1986]. In Table 4 only those entries underlined are not likely to occur in Cooksville during a flow with a MAF magnitude. Clearly slabs up to 25 cm can be quarried, and are indeed observed to be. Few naturally quarried units are thicker than that on the stream bed.

Measurable erosional wear of the bed. In a reach at Atwater we observed a 40 metres long trough, 60 cm wide at the top and 15 to 20 cm wide at the bottom, with an undulating bed 15 to 30 cm deep formed on the otherwise flat bed of the creek where it has already lowered 60 cm in 21 years. The feature is interpreted to be a pothole groove [*Blank*, 1958]. Natural clasts up to the dimension of the trough are regularly observed as a lag in parts of the trough, and trains of critical flow standing waves usually occupy the trough at low stages.

We have recently measured direct erosion of slots cut across the feature. The slot depth was approximately 2 to 3 mm deep (averaged from several measurements on each slot by micrometer) and of similar width. Two 40 cm long slots, 40 cm apart and transverse to flow, were cut in late August 1997. One was cut across the 'col' between two potholes about 60 to 80 cm apart, the other was cut through the base of the pothole. The slots extended onto the adjacent stream bed. In mid-May 1998 only 15 cm of the original 80 cm of slot remained. On the flanks, where the surface is irregular, it is assumed that the lowering was effected by removal of thin plates of rock. Within the trough itself, and its flanks, the smooth form and lack of any trace of the slots indicates it was achieved by smooth wear from the passage of water and sediment, and which lowered surrounding surfaces equally. Thus we have obtained a measure of direct erosional wear of about 0.4 cm/yr. This is roughly an order of magnitude less than that achieved by the removal of thin flakes of rocks in the same reach (Table 2).

Stability of the Profile in Some Localities

We have emphasized throughout the paper the active incision of the longitudinal profile. However, the estimated rates at Kingsbridge in the upper basin, even allowing for an order of magnitude under-estimation, are much lower than elsewhere. At one location (Sherobee Road) within the main part of the basin, where the stream still has a meandering trace and where the bed material is derived from the Iroquois shoreline and sediments, there are indications of zero incision in recent centuries. A sample of wood was extracted from within a gravel matrix in a natural stream bank exposure and below 1.5 meters of alluvium. The sample matrix was similar to modern lateral bar material and was resting on plane rock where the existing channel bed passed under the bank. A calibrated radiocarbon date of 1473 ± 70 AD (BGS-1775, corrected for fractionation) was obtained. Field indications are that the profile is stable in this region for several hundred meters up and downstream. Field exposures remain similar, and there have been no reported difficulties with installed structures.

Adjustment of the Channel

Given the high rates of channel lowering we have documented, in what ways does the channel morphology adjust, and with what hydraulic consequences? When Mean Annual Flood flow depths are between 1 to 2 m in depth, the lowering of the channel by between 30 and 50 cm represents a significant increase in channel capacity when, because of the fixed wall and bridge structures, channel width and longitudinal slope remain fixed. In a section 7 meters wide and initially 1.5 meters deep (similar to the Mississauga Boulevard reach), if an active width for critical flow is assumed to be 5 meters, then a 0.40 m increase in depth due to gradual erosion of the bed represents an increase in discharge capacity at bankfull from 40.6 m^3/s to 58.01 m^3/s - a 30 % increase.

Generally, channel lowering has been uniform across the width, except where master joints have been locally excavated. Although hydraulic forces are much stronger in the center channel location, the channel margins are more exposed frequently to wetting and drying cycles, and quite moderate stages rises can wash away shale fragments. In additional, despite active lowering of the channel, the total

Table 4. Entries are velocities in meters per second needed to quarry slabs with the given density and thickness

slab thickness	slab density					
meters	*1.8*	*2.0*	*2.2*	*2.4*	*2.6*	*2.8*
0.01	0.99	1.11	1.21	1.31	1.40	1.49
0.05	2.21	2.48	2.71	2.93	3.13	3.32
0.10	3.31	3.50	3.84	4.14	4.43	4.70
0.15	3.84	4.29	4.70	5.04	5.42	5.75
0.20	4.43	4.95	5.42	5.86	6.26	6.64
0.25	4.95	5.54	6.06	6.55	7.00	7.43
0.30	5.42	6.06	6.64	7.18	7.67*	8.14
0.35	5.86	6.55	7.18	7.75	8.29	8.79
0.30	6.26	7.00	7.67	8.29	8.86	9.39

* Entries underlined are the values not typically attained during flood flows in Cooksville Creek

proportion of the depth is still only a moderate fraction of the bankfull depth, and time has been too limited at most locations for much change in form.

Nevertheless, where lowering rates are more rapid, we have documented the excavation of a plunge pool in response to a drop structure at Mississauga Valley Boulevard (Figure 10). Elsewhere we have seen small scale wear on flow facing edges and small scour features, which must have developed in only a few years, given the general lowering rates. However, when lowering rates are rapid in weakly resistant rocks, dramatic sculpted forms are not expected [*Tinkler and Wohl*, this volume].

DISCUSSION

How typical is the Cooksville Creek case study of other recently developed urban drainage basins sited on bedrock? Very similar problems to those at Cooksville have been observed on many neighboring streams: Sawmill Creek, Loyalist, Shardawn Creek, and Tuck Creek. Cazenovia Creek in western New York State, cut into a Devonian Shale with similar geological properties to the Georgian Bay Formation, reveals 25 cm bed cm lowering relative to a retaining wall at the crossing with Highway 277 (no dates available, but twentieth century), and Twenty Mile Creek at the Highway 81 crossing in Niagara Peninsula similarly has cut down 35 cm through Queenston Shale, as revealed by armour stone bank protection installed a few decades ago. At the same location, the top of a terrace gravel has been dated by a contained mollusk to be 1285-1410 AD (TO-4686 640 ± 50, calendar calibrated), and implies incision (of one meter) of the present channel through Queenston Shale at a rate of about 1.54 mm/yr.

Vaughn [1990] summarizes the result of large-scale urban floods in Kansas City which offers illustrative parallels with observed effects in Cooksville Creek, albeit for more frequent floods. The Brush Creek basin (76 km^2) is about twice the size of Cooksville Creek and the main area reported upon is a 6.1 km concrete channel through the central Plaza district. The channel is 15 m wide and nearly 5 m deep with a longitudinal slope of between 0.0464 and 0.0635. In 1977, 1982, and 1986, flash floods caused extensive damage and in the last of these mean flow velocities of 5.8 m/s were estimated. Large concrete slabs 0.23 m thick used to construct the flood way were hydraulically quarried and transported several hundred meters. Shear stress values of 91-96 Nm^{-2} and stream power of 528-557 Wm^{-2} were estimated. Thus, given the difference in basin sizes, estimates in Cooksville of mean sectional velocities of 6 m/s and measured velocities in excess of 4 m/s are entirely comparable. Flow regime in Kansas was classified as supercritical (Froude = 1.16), and the reported mean flood depth of 2.74 m would yield at Froude = 1 a value of 5.18 m/s as a minimum estimate. Thus, flow regimes are comparable between the two systems. Likewise the quarried blocks (10-25 cm thick) from scour holes at Cooksville are not dissimilar. For Cooksville Creek with a flow depth of 1.6 m, a mean basin slope of 0.008, and a velocity of 4.5 m/s we can estimate shear stress of 126 Nm^{-2}, and power equal to 564 Wm^{-2}. As indicated in *Tinkler* [1997a] peak values of shear stress and power may be an order of magnitude larger under the distal faces of surface water waves. Shear stresses estimated by the HEC-RAS modeling generally range for 50 to 200 Nm^{-2} throughout the basin. Estimates of peak power in Wm^{-2} will be the stress values multiplied by the maximum velocities, whose range (5 to 8) is indicated in Table 1.

In Cooksville Creek, channel bed and bank erosion is an intrinsic part of a stream system based in a weak shale, with a steep gradient, and subject to a much flashier flow regime than before about 1970. Attempts to control bed erosion by brute force have been unsuccessful. As a basis of comparison for the erosion rate we have measured the total incision below the regional bedrock surface of some major valleys adjacent to Cooksville Creek below the regional surface (Table 5). They are based on total observed incision of substantial river systems below the level surface beveled by the Iroquois shoreline. It was abandoned about 13,000 calendar years ago. The variation of the erosion through time is unknown and was likely much higher in the initial stages of incision, but the values are consistent amongst themselves, and, with a recent estimate made at Twenty Mile Creek (see above). They are an order of magnitude smaller than those estimated for the last 30 years in Cooksville Creek. Elsewhere, *Dollenmayer et al.* [1997) and *Stock and Montgomery* [1996] have documented natural rates with comparable or even higher figures of about 4 to 13 cm/yr. However, *Righter* [1997] quotes a natural "high incision rate" in the range 2.3 to 2.5 mm/yr, that compares well with the rates we quote for the regional valley systems.

Table 5. Stream incision data between Hamilton and Oakville

Creek	rock type	road crossing location	incision * m	rate mm/yr
Bronte	Queenston	QEW	19	1.46
Bronte	Queenston	Upper Middle	28	2.15
Bronte	Queenston	Dundas Rd, Hwy. 5	32	2.42
Sixteen Mile	Queenston	Dundas Rd, Hwy. 5, s.e.	28	2.15
Sixteen Mile	Georgian Bay	Railway, s. of QEW	15	1.15

* All data were measured in the field from valley exposures of clean rock in the stream bed to the uppermost visible exposure on the valley wall cliff.

On the bright side (for municipal and hydraulic engineers), rapid incision (up to 2 to 3 cm/yr), acts to enlarge the channel, and stabilize and fix the channel location. Although some localized bank erosion will take place as the system attempts to re-establish a meandering thalweg, in most locations the rate at which this lateral migration takes place is not likely to cause immediate problems. All the factors - weak bed, steep gradient, high velocities and naturally platy clasts conspire to make the channel readily erodible.

Vertical banks, typical of most but not all of the engineering structures, are a mistake. Once undermined by shale erosion they are easily dislodged by overbank flow due the lack of a physical "tie" to back fill, or local "alluvium." The vertical bank provides a ready "drop" structure for water flowing between the armour stone (water was seen pouring from between armour stone during a smaller flood on November 11th 1995 in the Atwater reach). Debris lines made it clear that water overtopped the armour stone walls during the Opal flood, both at a drop structure above Robert Speck (and from which an armour stone on the weir was "popped" out), and at Atwater where 30 cm deep water flowed over the floodplain and back into the channel at right angles as a lateral waterfall. A stepped wall structure would act to baffle a clear drop, and it would provide a locus for deposition, and some protection for the underlying shale.

A number of important controlling factors are associated with erosion problems in the Creek, and are general elsewhere in the region, based on our experience.

1) We have clear documentation of velocities at all flood stages which are far in excess of those usually imagined or measured for fluvial (alluvial) systems. Although predicted by flow modeling exercises, they may not have been taken seriously for their ability to effect erosion and transport. High velocities make the system extraordinarily effective at hydraulic plucking below drop structures, and permits very coarse sediment transport.

2) The system has gradients which are very much steeper than those of alluvial systems, and which match the gradients in 'mountain' streams. These gradients are a primary control on generating high velocities, and the development of self-adjusting critical flow along the thalweg requires the dissipation of substantial amounts of energy by turbulence with adjacent water bodies. Some of this turbulence is applied to hydraulic quarrying of the bed and to very coarse sediment transport.

3) A weak, well and thinly-bedded geologic formation (Georgian Bay Formation) underlies the entire basin with a quasi-horizontal dip. The shales weather readily to small flakes and expose limestone interbeds that do not have dimensions sufficient to withstand transport during frequent high velocity events. Thus the channel bed remains mainly clear of sediment, with sediment stored in occasional longitudinal bars.

4) Progressive urbanization has increased peak flows (and associated velocities) and induced a much more flashy regime. The flashy regime and low base flows enhance the frequency of wetting and drying cycles, which quickly weaken shale exposed on the stream bed. Incision of the channel into underlying bedrock, which can substantially increase channel capacity, has been seen to be a problem because wall structures are undermined, even though the process also acts to stabilize channel location. The incision rate is about an order of magnitude faster than in neighboring non-urbanized basins, and is comparable to a recent high rate quoted by *Dollenmayer and Whipple* [1997], although their record is for a much stronger rock.

5) Everything we have documented about flow mechanics, sediment transport and erosion of the stream bed has been with respect to flood flows with frequency of 2 years or less, which lie at or below the MAF. Removal of weathered shale debris is effected by very moderate flood flows, and erosion and lowering is not dependent on catastrophic scale flows. However, flows close to MAF do tend to be responsible for toppling and moving armour stones off retaining walls, and along the channel bed.

Acknowledgment. This work benefited from numerous discussions with other members of the consulting team, namely Ray Tufgar, Chris Doherty, and Doug Jones who were

working on hydrological modeling, water quality and biology. The assistance provided by Allison McNeill, in the field and the office was greatly appreciated. The City of Mississauga and the Credit Valley Conservation supported this work, both financially and intellectually. Particular thanks are owed to Bob Levesque and Janice Teare at the City, and Hazel Breton and Bill deGeus from the Conservation Authority. Keith Tinkler thanks Brock University for research support, NSERC (Canada) for a Research Grant, Dr. M. Toda for the gift of a rock saw, and Loris Gasporotto for drawing the figures. Several residents provided helpful information on floods and especially we thank Mr. R. Smania for the loan of his video of the 1993 flood seen at Camilla Road. Incisive comments from Alexander Kirkbride, Kelin Whipple and David Harbor on an earlier draft are acknowledged with thanks.

REFERENCES

Beltaos, S., Editor, *River Ice Jams*, 390p, Highlands Ranch, Colorado, Water Resources Publications, LLC, 1996.

Blank, H. R., Pothole grooves in the bed of the James River, Mason County, Texas, *Texas Journal of Science*, 10, 293-301, 1958.

Chanson, H. and J. S. Montes, Characteristics of undular hydraulic jumps: experimental apparatus and flow patterns, *Journal of Hydraulic Engineering*, 121(2), 129-144, 1995.

Chow, V. T., *Open Channel Hydraulics*, 680p, McGraw-Hill, New York, 1959.

Dollenmayer, K. and K. X Whipple, Rates and processes of bedrock channel incision along the upper Ukak River, Valley of Ten Thousand Smokes, AK, *EOS, Transactions of the American Geophysical Union*, 78(46), F299, 1997.

Drake, J. J. and S. B. McCann, The movement of isolated boulders on tidal flats by ice floes, *Canadian Journal of Earth Sciences*, 19, 748-754, 1982.

Environment Canada, Canadian Climate Data Normals - 1961 to 1990, Government of Canada, Ottawa, 1993.

Glaves, R. and P. R. Waylen, Regional flood frequency analysis in Southern Ontario using L-moments, *The Canadian Geographer*, 41(2), 178-193, 1997.

Grant, G. E., Critical flow constrains flow hydraulics in mobile-bed streams: A new hypothesis, *Water Resources Research*, 33(2), 349-358, 1997.

Gregory, K. J. and D. E. Walling, *Drainage Basin Form and Process: a geomorphological approach*, 458p, Edward Arnold, London, 1973.

Hattingh, J. and W. K. Illenberger, Shape sorting of flood-transported synthetic clasts in a gravel bed river, *Sedimentary Geology*, 96, 181-190, 1995.

Henderson, F. M., *Open channel flow*, 522p, MacMillan, New York, 1970.

Irvine, K. N. and J. J. Drake, Spatial analysis of snow- and rain-generated highflows in southern Ontario, *The Canadian Geographer*, 31(2), 140-149, 1987.

Jarrett, R. D., Hydraulics of high-gradient streams, *Journal of Hydraulic Engineering*, 110, 1519-1539, 1984.

Jarrett, R. D., Paleohydrologic techniques used to define the spatial occurrence of floods, *Geomorphology*, 3, 181-195, 1990.

Johnson, M. D., D. K. Armstrong, B. V. Sanford, P. G. Telford and M. A. Rutka, Paleozoic and Mesozoic Geology of Ontario;, in *Geology of Ontario*, edited pp. 907-1010, Vol. 4 (part 2), Ontario Geological Survey, Toronto, 1992.

Karrow, P. F., Quaternary Geology of the Brampton Area, Ontario Geological Survey, 5819, 1991.

Karrow, P. F. and J. Easton, Quaternary Geology, Brampton area, by Preliminary Map 3171 ed., Ontario Geological Survey, Toronto, 1990.

Kennedy, J. F., The mechanics of dunes and antidunes in erodible-bed channels, *Journal of Fluid Mechanics*, 16(4), 521-544, 1963.

Kieffer, S. W., The 1983 hydraulic jump in Crystal Rapid: implications for river-running and geomorphic evolution in the Grand Canyon, *Journal of Geology*, 93, 385-406, 1985.

Kostachuk, R. A. and M. A. Church, Macroturbulence generated by dunes: Fraser River, Canada, *Sedimentary Geology*, 3, 179-183, 1993.

Lapointe, M. F., Monitoring alluvial sand suspension by eddy correlation, *Earth Surface Processes and Landforms*, 18(2), 157-175, 1993.

Leighly, J. B., Turbulence and the transportation of rock debris by streams, *Geographical Review*, 24, 453-464, 1934.

Magalhaes, L. and T. S. Chau, Initiation of motion conditions for shale sediments, *Canadian Journal of Civil Engineering*, 10, 549-554, 1983.

Martini, I. P., Gravelly flood deposits of Irvine Creek, Ontario, Canada, *Sedimentology*, 24, 603-622, 1977.

Matthes, G. H., Macroturbulence in natural stream flow, *EOS (Transactions of the American Geophysical Union)*, 28, 255-265, 1947.

Matthes, G. H., River surveys in unmapped territory, *American Society of Civil Engineers*, 121, 739-758, 1956.

Middleton, G. V. and J. B. Southard, *Mechanics of Sediment Movement*, 2nd ed., 401p, Society of Economic Paleontologists and Mineralogists, 1984.

R.V. Anderson Ltd., Cooksville Creek Flood-line mapping Study, City of Mississauga, 1996.

Reinius, E., Rock erosion, *Water Power and Dam Construction*, 38, 43-48, 1986.

Righter, K., High bedrock incision rates in the Atenguillo River Valley, Jalisco, Western Mexico, *Earth Surface Processes and Landforms*, 22, 337-343, 1997.

Sangal, B. and R. Kallio, Magnitude and frequency of floods in Southern Ontario, Ontario Ministry of the Environment, Technical Report Series 99, 1977.

Stock, J. D., D. R. Montgomery and N. P. Peterson, Extreme rates of bedrock river incision, Satsop River, Washington [Abstract], *EOS, Transactions of the American Geophysical Union*, 77(46), F252, 1996.

Tinkler, K. J., Fluvially sculpted rock bedforms in Twenty Mile Creek, Niagara Peninsula, Ontario, *Canadian Journal of Earth Sciences*, 30, 945-953, 1993.

Tinkler, K. J., Critical flow in rockbed streams with estimated values for Manning's *n*, *Geomorphology*, 20(1-2), 147-164, 1997a.

Tinkler, K. J., Indirect velocity measurement from standing waves in rockbed streams, *Journal of Hydraulic Engineering*, 123(10), 918-921, 1997b.

Totten Sims Hubicki et al., Cooksville Creek Rehabilitation Study, City of Mississauga and Credit Valley Conservation Authority, 1997.

Trieste, D. J., Evaluation of supercritical/subcritical flows in

high-gradient channels, *Journal of Hydraulic Engineering*, 118, 1107- 1118, 1992.

Tushingham, A. M., Postglacial Uplift Predictions and Historical Water levels of the Great Lakes, *Journal of Great Lakes Resources.*, 18(3), 440-455, 1992.

Vaughn, D.M., Flood dynamics of a concrete-lined, urban stream in Kansas City, Missouri, *Earth Surface Processes and Landforms*, *15*, 525-537, 1990.

Wolman, M. G. and R. Gerson, Relative scales of time and effectiveness of climate in watershed geomorphology, *Earth Surface Processes*, 3, 189-208, 1978.

Keith J. Tinkler, Department of Geography, Brock University, St. Catharines, Ontario L2S 3A1, Canada, ktinkler@spartan.ac.BrockU.ca

John Parish, Parish Geomorphic, 14 McIntyre Crescent, Georgetown, Ontario, L7G 1N3. jparish@aztec-net.com

Inland Propagation of Erosional Escarpments and River Profile Evolution Across the Southeast Australian Passive Continental Margin

Jeffrey K. Weissel

Lamont-Doherty Earth Observatory of Columbia University

Michele A. Seidl[1]

Department of Geological Sciences, Rutgers University

Denudation at passive continental margins occurs over time as erosional escarpments propagate inland, cutting through regions of elevated topography flanking ocean basins. Understanding the actual processes and time variability in propagation rates associated with the advance of escarpments across passive margins remains a largely unsolved problem for tectonic geomorphology. Here we report results from new analyses of detailed river longitudinal profiles and surface exposure age measurements using cosmogenic radionuclides from the New England Tableland portion of the southeast Australian passive margin. In that area, many plateau-draining tributaries of the Macleay River cascade into narrow gorges across large-scale river knickpoints that represent the tips of the leading edge of the inland-advancing escarpment. Previous river profile analyses showed most knickpoints to be the same distance, about 200 km, upstream from the mouth of the river, despite order-of-magnitude variations in the areas drained at the gorge heads. The implication is that all knickpoints have migrated upstream at a speed of about 2 km/Myr averaged over the ~100 Myr history of the margin. The new profile analyses confirm that, in general, distance upstream from the Macleay River mouth of the knickpoints is not related to area drained at the gorge head. We conclude that if sufficient fluvial transport power is available, the rate of upstream knickpoint migration is governed by slope failure mechanisms and the frequency of resulting mass wasting events on the steep rock slopes in the gorge head vicinity. In terms of the stream power model for channel incision, $z_t \propto A^{m'} S^n$ (where A is drainage area and S is channel gradient), the river profile analyses imply that the drainage area exponent $m' = 0$ (i.e., no dependence on drainage area so long as a threshold is met), and the slope exponent $n > 1$. Average erosion rates calculated from Be

[1]Presently at: The Pew Charitable Trusts, Philadelphia, PA

Rivers Over Rock: Fluvial Processes in Bedrock Channels
Geophysical Monograph 107

and Al radionuclide concentrations in samples collected across the knickpoint on Baker's Creek indicate that the plateau surface and the channel upstream of the gorge head – knickpoint are eroding slowly, ~5 m/Myr, whereas the channel at and downstream of the knickpoint is eroding much more rapidly, >100 m/Myr. The pattern of increasing erosion rates across the knickpoint in the downstream direction is consistent with the paradigm of inland escarpment retreat across passive continental margins.

1. INTRODUCTION

In common with many other passive margins, the eastern Australian continental margin features a seaward-facing erosional escarpment that demarcates a relatively undenuded inland plateau of subdued local relief from a dissected coastal zone of greater local relief but lower overall elevation [*Ollier*, 1982, 1985a, 1985b]. Based on the early work of *King* [1953] and *Ollier* [*op cit*], many workers now consider that the erosional development of passive margins is marked by the establishment of erosional escarpments at the time of continental rifting, and subsequently, by the inland propagation of these escarpments over time through the rock mass of uplifted rift flanks [*Gilchrist and Summerfield*, 1990; *Weissel*, 1990; *Summerfield*, 1991; *Gilchrist et al.*, 1994; *Tucker and Slingerland*, 1994; *Kooi and Beaumont*, 1994, 1996; *Seidl et al.*, 1996]. Long-term average propagation rates on the order of 1 km/Myr have been inferred at several passive margins by assuming that escarpment erosion began at the time of rifting, and that the seaward edge of the rift flank was originally located in close proximity to the present coastline [*King*, 1953; *Seidl et al.*, 1996; *Weissel*, 1990]. In this paper we analyze new river longitudinal profiles and short-term erosion rates estimated from cosmogenic radionuclides concentrations in exposed bedrock to develop a better understanding of the actual processes and time variability in rates associated with escarpment propagation across the eastern Australian margin.

1.1 Erosional Escarpment Forms

In map view, plateau-bounding escarpments generally exhibit two basic forms depending on the direction of surface water drainage on the plateau interior relative to the escarpment [*Schmidt*, 1987]. First, where surface water drainage is directed away from the escarpment on both the upland and coastal sides, the escarpment takes the form of embayments and promontories, such that its overall trend remains fairly straight as it evolves over time. We call this kind of escarpment the drainage divide type. Second, where upland streams flow towards the coast and cross the escarpment, the escarpment consists of dramatic, narrow gorges headed by large-scale river knickpoints which propagate up the plateau drainage system over time [*Schmidt*, 1987; *Weissel et al.*, 1995]. We call this second escarpment type the gorge head – knickpoint form.

Mass wasting on steep, bedrock hillslopes is characteristic of both types of escarpment. However, their fluvial environments are much different. The evolution of the gorge head – knickpoint escarpment type depends strongly on the magnitude of river discharge across the gorge head, as discussed later. Coupling (and feed-back) between river incision into bedrock and mass wasting on the immediately adjacent hillslopes distinguishes the knickpoint-headed gorge type from the drainage divide rim type of erosional escarpment [*Weissel and Seidl*, 1997].

Although both escarpment forms occur along passive margins [*Ollier*, 1982], observations and models for the development of these escarpments indicate a preference for the drainage divide escarpment form. However, the geometry of rifting, particularly upper versus lower plate margins [*Lister et al.*, 1992], along-strike segmentation of rifts [*Leeder and Gawthorpe*, 1987], the location and spatial concentration of extension achieved through surface faulting, as well as pre-existing topography [*Kooi and Beaumont*, 1996], are all factors that determine which type of escarpment will occur along a given segment of passive continental margin. Moreover, escarpment form might alternate between the gorge head – knickpoint and drainage divide – rim type over time at any particular location as the escarpment propagates through drainage basins on the upland surface, and because of regional flexural isostatic effects of erosion/sedimentation and thermal subsidence of the adjacent offshore oceanic lithosphere [*Seidl et al.*, 1996]. The gorge head - knickpoint escarpment type tends to form where a major drainage divide is located several tens to hundreds of kilometers inland, and the upland surface has a regional tilt towards the coast [*Weissel*, 1990; *Kooi and Beaumont*, 1996; *Seidl et al.*, 1996].

1.2 Australia's Southeastern Passive Continental Margin

Our work on gorge head – knickpoint erosional escarpments has focused on Australia's southeastern passive margin (Fig. 1) for several reasons. It has a well-known rifting and post-rift tectonic history [*Hayes and Ringis*, 1973; *Weissel and Hayes*, 1977], and characteristic passive margin topography, namely, an elevated upland surface bordered on its seaward side by one or other of the two erosional escarpment

forms [*Ollier*, 1982]. It is a good locale for studying the long-term course of denudation at passive margins because as *Young and McDougall* [1993] note, southeast Australia is remote from plate boundaries, implying that tectonic modification of topography since rifting is small at the local scale. Moreover, the dominance of humid subtropical to temperate climates during the margin's 100 Myr history means that the profound effect of Late Cenozoic climate change, particularly extensive glaciation, is largely absent in southeast Australia.

The work reported in this paper concerns the rates and processes associated with the inland propagation of the gorge head – knickpoint type of erosional escarpment at passive continental margins. The Macleay River system, which drains about 11,000 km^2 of the southeast Australian margin between the coast and the continental divide about 150 km inland (Fig. 1), is particularly important in this regard because many of its tributaries draining the New England Tableland cascade across large-scale river knickpoints into spectacular, narrow gorges as they flow to the main stream and the sea. Headwaters of the tributaries lie at elevations between 1000 m and 1300 m, and receive 800 to 1600 mm of precipitation annually, increasing west to east across the Tableland, mostly during summer, and predominantly as rainfall. The marked concentration of erosional activity in the gorge head vicinity allows us to investigate these features in great detail with efficient and economical field programs. Preliminary field work involving site photography took place in 1993 and 1995 in conjunction with NASA airborne radar and radar interferometry data acquisition over the escarpment in the New England region [*Weissel*, 1997]. A further visit was made in 1996 mainly to conduct reconnaissance sampling of granitic bedrock in and around the channel of Baker's Creek (E in Fig. 1) for exposure age dating using cosmogenic radionuclides, and to survey joint and fracture patterns in the vicinity of a few of the gorge heads (E, L, and M in Fig. 1).

In this paper we first briefly review the major results from our previous work on the knickpoint-headed gorges of the Macleay River system [*Seidl et al.*, 1996; *Weissel and Seidl*, 1997]. The main purposes of this paper, however, are to: 1) introduce new, detailed river longitudinal profiles for several streams crossing large-scale knickpoints, to discuss these profiles in terms of a stream power model for bedrock channel erosion and in terms of the basic processes involved in upstream migration of large-scale river knickpoints and escarpment propagation; and 2) report bedrock exposure ages and average erosion rates obtained from cosmogenic radionuclide measurements on the Baker's Creek samples, and to relate these results to the long term average escarpment propagation rates for this portion of the eastern Australian margin inferred from the upstream locations of the river knickpoints [*Seidl et al.*, 1996].

1.3 Summary of Previous Results

It is useful to regard the gorge head – knickpoints of the Macleay River system (Fig. 1) as tips on the "leading edge" of the escarpment advancing inland across the New England portion of the southeast Australian margin. Identifying the processes operating in the gorge head vicinity and determining the rate at which they act are crucial for understanding how the large-scale river knickpoints migrate upstream and therefore, how the escarpment propagates inland. Two main results from previous work on the Macleay River gorges [*Seidl et al.*, 1996; *Weissel and Seidl*, 1997] shed light on these questions.

First, most knickpoints on the plateau-draining streams of the Macleay River system are located the same distance, about 200 km, upstream from the mouth of the river, despite some differences in bedrock lithology, and more importantly, despite order-of-magnitude variations in the drainage areas presently upstream of the gorge heads (Fig. 2; *Seidl et al.* [1996]). Assuming river discharge to be proportional to drainage area, we can infer that the speeds at which the knickpoints have migrated up the individual streams do not appear to depend on discharge. We determine an average upstream propagation rate of about 2 km/Myr for the knickpoints, assuming they all originated at the mouth of the ancestral Macleay River at the time of formation of the Tasman Sea margin of eastern Australia about 85 - 100 Myr ago [*Hayes and Ringis*, 1973; *Weissel and Hayes*, 1977]. The average speed of headward migration of the Macleay River system knickpoints is very similar to the rate of headward advancement over the last 30 Myr of the knickpoint on the Shoalhaven River [*Nott et al.*, 1996], which which drains the Southern Tableland of New South Wales about 400 km farther south along the southeast Australian margin. The Baker's Creek sampling and analysis program was undertaken to determine whether the shorter-term exposure ages and average erosion rates obtained from cosmogenic radionuclide concentrations are consistent with the long term escarpment propagation rates inferred from the upstream locations of the river knickpoints.

Second, we found that bedrock strength discontinuities, imparted by joints and fractures, play an important role in the evolution of the headwalls and sidewalls of the gorges, and therefore in the upstream propagation of the knickpoints [*Weissel and Seidl*, 1997]. At issue here is the effect of jointing and fracturing on the strength of rock masses [*Terzaghi*, 1962; *de Freitas and Watters*, 1973; *Selby*, 1982, 1987]. The dip and orientation of bedrock discontinuities with respect to hillslope orientation and dip control the mode of slope failure and the geometry of resulting mass wasting events (Fig. 3; *Weissel and Seidl* [1997]).

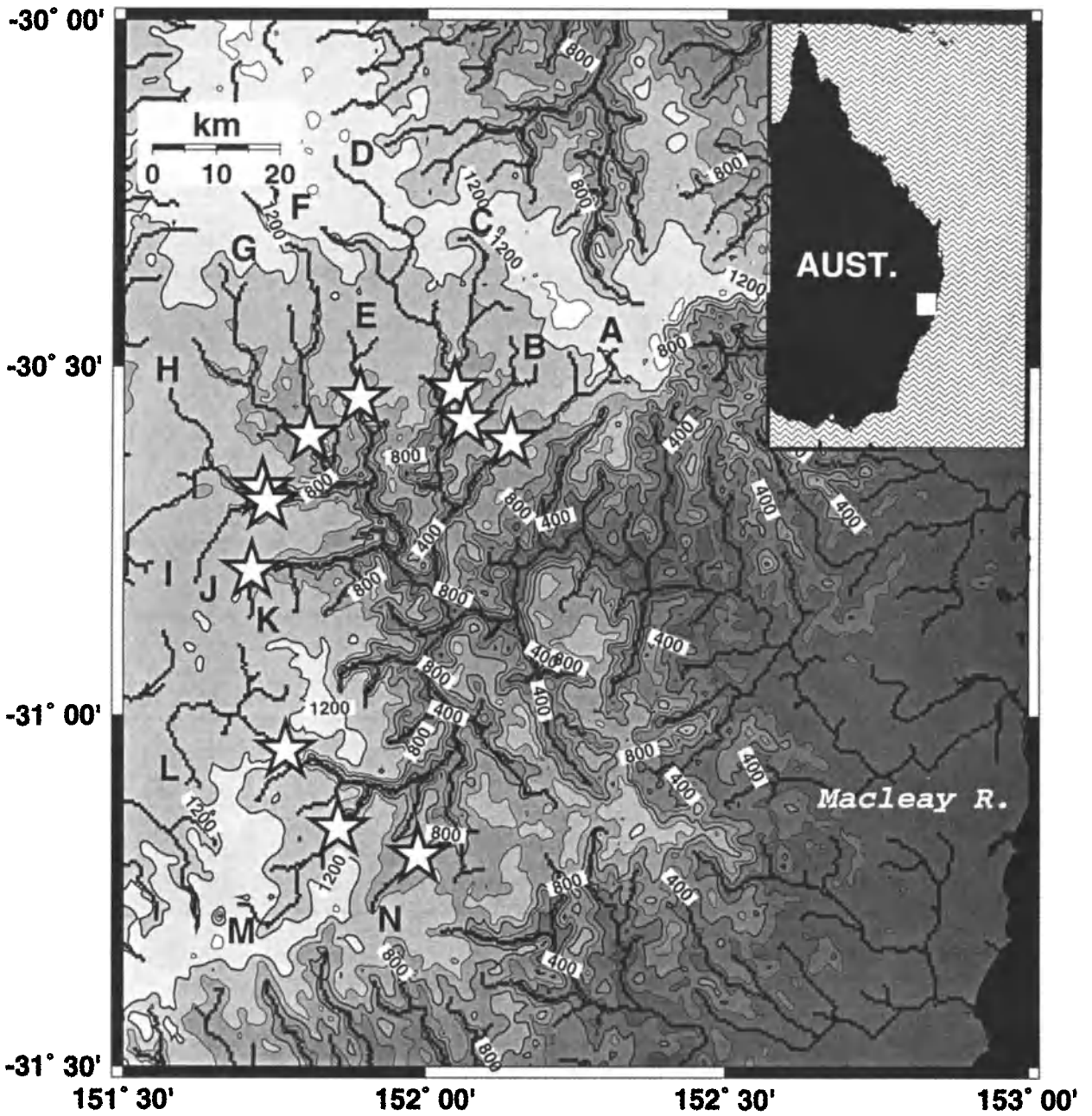

Figure 1. Generalized topographic map of New England region of southeast Australia (see inset map for location). Elevation is contoured at 200 m intervals, labeled every 400 m, and offshore areas (lower right) are black. Streams extracted from a 500 m gridded Digital Elevation Model [*Seidl et al.*, 1996] are shown in black. Large stars locate heads of gorges and stream-channel knickpoints that occur on plateau-draining tributaries of Macleay River, indicated by the black letters A – N.

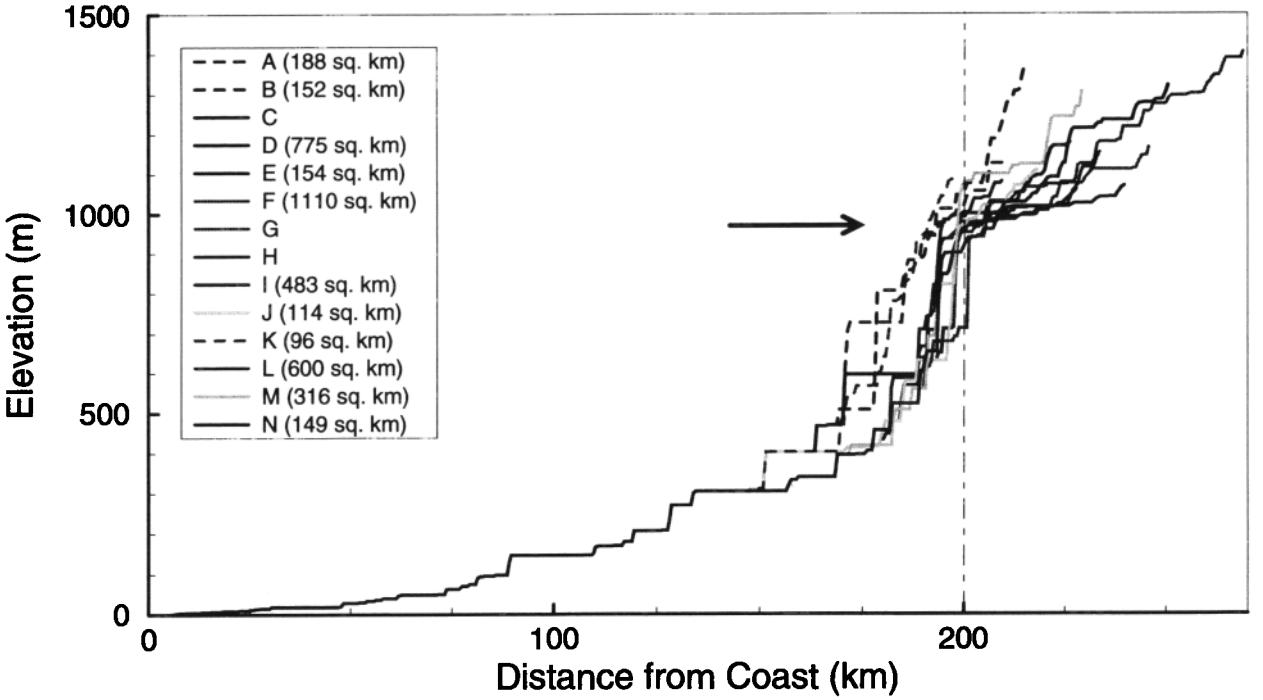

Figure 2. River longitudinal profiles for streams labeled A – N on Fig. 1, obtained from the 500 m DEM using the drainage extraction method of *Pratson and Ryan* [1996]. The horizontal arrow points to prominent knickpoints located about 200 km upstream from the Macleay River mouth. Inset gives upstream drainage areas for several gorge head – knickpoints.

The main conclusion from the previous work is that the pace of knickpoint propagation is regulated mainly by slope failure mechanisms and the frequency of resulting mass wasting events on steep rock slopes both at the gorge head and immediately downstream of the gorge head. Because this conclusion is likely to prove controversial, we explain our reasoning in some detail. It is well understood that the evolution of the gorges and, in particular, the upstream propagation of the gorge head – knickpoint requires coupling (and feedback) between fluvial and hillslope processes [*Seidl et al.*, 1996]. The observation that the large-scale knickpoints of the Macleay River system are all about the same distance upstream, regardless of drainage area upstream of the gorge heads (Fig. 2), suggests that peak discharge of plateau-draining streams across the gorge head exceeds a threshold sufficient to allow fluvial processes to accomplish the following: 1) Remove talus that accumulates at the foot of the knickpoint rock face to prevent buttressing, which would reduce the effective height of the knickpoint susceptible to further mass wasting and hence upstream propagation (perhaps eliminating it eventually), 2) allow the river downstream of the gorge head to incise its channel into bedrock, using both debris shed from the hillslopes and stream discharge, and 3) effect actual mass movement from the gorge sidewalls to the channel through continual removal of critical "toe" blocks at the base of the hillslopes [*Goodman and Bray*, 1977]. Basal slope erosion achieved by channel incision into bedrock destabilizes hillslopes by lengthening and steepening hillslopes adjacent to the channel, and provides space to accommodate the material shed from them (see also *Kelsey* [1988]). Our conclusion that hillslope processes, including rock slope failure mechanisms, are the rate-controlling processes for knickpoint propagation follows because the threshold condition for fluvial processes described above is met in the New England region of eastern Australia. In other words, if the magnitude of extreme rainfall events in the region was suddenly increased, we would expect no concomitant increase in the rate of knickpoint propagation. Because the knickpoints represent the leading edge of the escarpment, these hillslope processes also set the pace of escarpment advance across the New England section of the east Australian passive margin. Finally, the fluvial processes, and the role they play, distinguish the knickpoint-headed gorge form from the drainage divide rim form of erosional escarpment found on passive continental margins and elsewhere, and provide an explanation for their morphological and evolutionary differences.

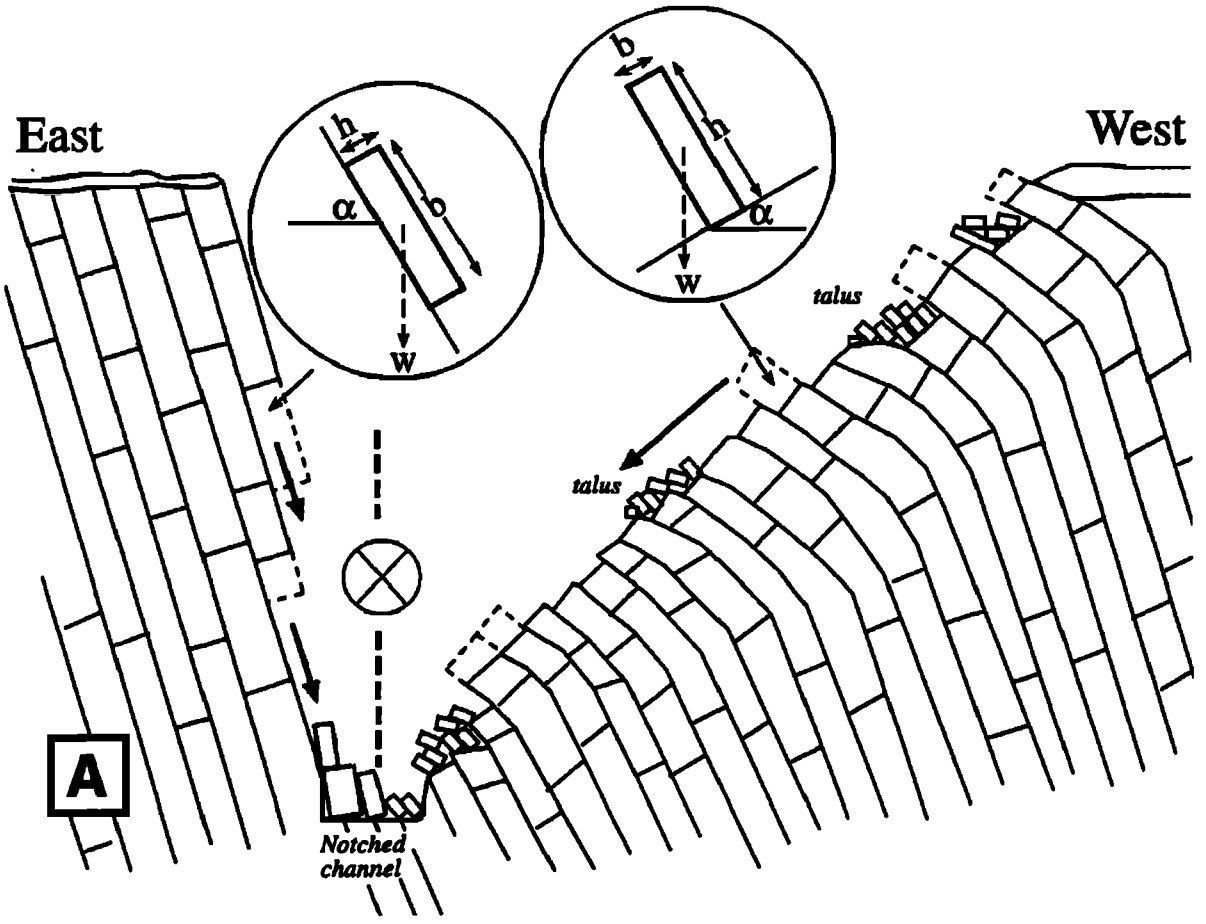

Figure 3. (A) Schematic cross section looking downstream along N-S reach below gorge head at Apsley River (L in Fig. 1). This is a broad interpretation of observed hillslope processes which indicates mass-wasting on west-facing slopes by sliding parallel to prominent jointing that dips steeply to west, and by block and column toppling on east-facing slopes [*Weissel and Seidl*, 1997]. Spacing of the dominant W-dipping joints has been increased for purposes of illustration. Circled insets show isolated blocks of weight w, base b and thickness h resting on potential sliding surfaces of dip α. (B) Field photograph looking downstream along a SW-trending reach about 1 km below the gorge head for comparison to the schematic cross section above. Note the striking asymmetry between steep west-facing slopes and more shallowly-dipping east-facing slopes covered by toppled debris. The stream channel, which is about 200 m below the Tableland surface at this location (Fig. 5), is "notched" into bedrock, indicating that rapid downcutting by fluvial action promotes mass wasting from the hillslopes.

2. RIVER LONGITUDINAL PROFILES AND MODELS FOR KNICKPOINT MIGRATION

2.1 Generating Stream Profiles

New stream profiles are used examine in more detail the earlier observation that most knickpoints on the Macleay River tributaries are situated similar distances ($\sim$ 200 km) upstream from the river mouth (Fig. 2). High-resolution profiles of several major tributary streams were generated in two ways: 1) hand digitization of stream bed elevations from 1:25,000 scale topographic maps, which are the most detailed currently available, and 2) extraction of drainage using the algorithms of *Pratson and Ryan* [1996] on a 20 m gridded DEM obtained from a stereo pair of SPOT multispectral imagery [*Seidl et al.*, 1996]. The two methods produce different results for the same stream channel. Figure 4 shows stream elevation versus distance for Baker's Creek (E in Fig. 1) using the two different methods. A close match between the smooth, topographic map-derived profile and the more jagged, SPOT DEM-derived profile is achieved if the SPOT-derived profile is uniformly reduced in height by 25 m. The elevation difference is not likely to be caused by different geodetic datums because ground

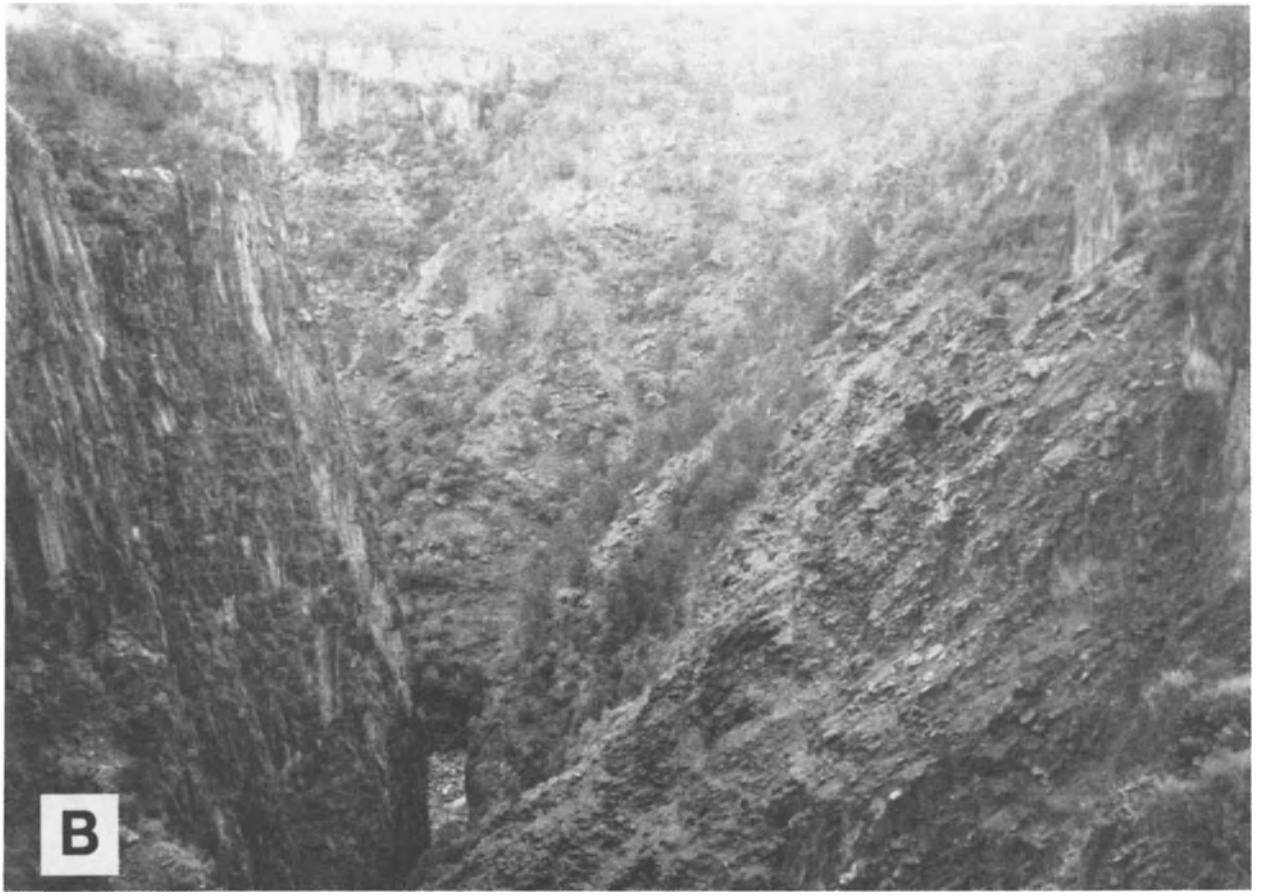

Figure 3. Continued.

control points from the topographic maps were used in the extraction of the DEM from the SPOT stereo pair. More likely the difference is attributable to the way the drainage extraction algorithm of *Pratson and Ryan* [1996] works. The drainage extraction strategy tacitly assumes that height errors in DEMs are all negative. A flooding algorithm is used to fill "pits" found along the drainage lines to ensure downstream continuity of drainage. The step-and-riser form of the SPOT DEM-derived profile in Figure 4 results from the pit-filling strategy. The net effect is to produce stream channel profiles with the positive height bias that we find when SPOT DEM-derived channel profiles are compared against profiles digitized from the topographic maps.

2.2 Knickpoint Migration and Upstream Drainage Area

The new stream profiles in Figure 5 are used to examine in more detail the relative upstream distances of the knickpoints in relation to the areas drained at the gorge head for the selected streams (see inset, Fig. 2). The top panel of Figure 5 shows stream elevation profiles for the Apsley and Tia Rivers (L and M, Fig. 1), both of which drain the southern part of the Tableland. The bottom panel of Figure 5 shows stream elevation profiles for Baker's Creek, Gara River, and Salisbury Waters (E, F, and I, respectively, Fig. 1), which are tributaries of the Macleay draining the New England Tableland from the north and west. The uppermost knickpoint on Apsley River appears to have migrated upstream almost twice as fast as the knickpoint on Tia River since the time the knickpoint was located at the confluence of these two streams (at about 15 km on the distance axis). The greater upstream distance of the Apsley knickpoint is consistent with the greater upstream contributing area for Apsley, if discharge across the gorge head plays a role in the rate of upstream migration of the knickpoint. On the other hand, the relation between relative distances upstream from confluences and upstream drainage area is not so clear for the streams in the lower panel of Figure 5. Here, the Gara River has by far the largest contributing area at its gorge head, yet its knickpoint has migrated a shorter distance upstream than the knickpoint on Baker's Creek, which has about one tenth the upstream drainage area (Fig. 2). The knickpoint on Salisbury Waters, which has less than one half the upstream drainage area of Gara River, has migrated about 10 km further upstream since

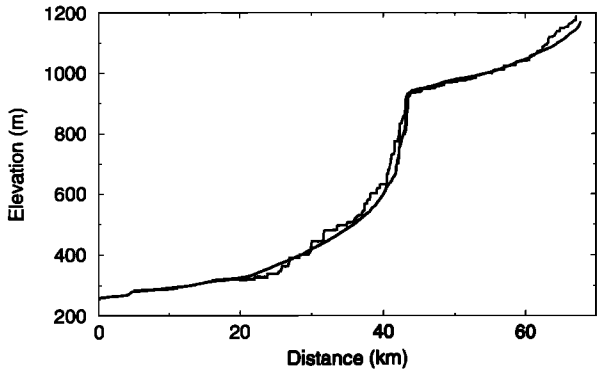

Figure 4. Comparison between river longitudinal profiles for Baker's Creek (E in Fig. 1) obtained from digitizing 1:25,000 scale topographic maps (solid line) and by drainage extraction [*Pratson and Ryan*, 1996] from a DEM obtained from a stereo pair of SPOT multispectral images (dotted line). The channel heights from the SPOT-derived DEM have been uniformly reduced by 25 m.

the time the knickpoint was situated at their confluence (at about 23 km on the distance axis).

The conclusion drawn from the relative distances upstream of the Macleay River system knickpoints revealed in the new, more detailed longitudinal river profiles remains the same as before [*Weissel and Seidl*, 1997]. To first order, the upstream distances appear unrelated to the areas drained at the gorge head. So long as sufficient fluvial transport power is available, the rate of upstream migration is governed by slope failure mechanisms and the frequency of resulting mass wasting events from the steep rock slopes at the gorge head and immediately downstream. Bedrock strength properties, imparted by jointing and fracturing, play an important role in slope failure mechanisms. As evidence, knickpoints on streams like Apsley and Salisbury Waters which have overall east-west trends, have migrated further upstream relative to tributaries with overall north-south trends (c.f. Fig. 5 and Fig. 1). This suggests a basic bedrock strength anisotropy favoring generally east-west oriented streams.

2.3 Knickpoint Migration and Stream Power Models

Even though we argued strongly above that hillslope processes, particularly mass-wasting, control the rate of headward migration of the large-scale knickpoints of the Macleay River system, we also stated that fluvial processes, particularly transport capacity and channel incision, were required to make knickpoint migration self-sustaining on long time scales. Many workers believe river incision into bedrock is governed by the river's local stream power, a physical concept describing the rate at which energy of the water flowing in the channel is made available for channel incision [*Seidl and Dietrich*, 1992; *Anderson*, 1994; *Howard et al.*, 1994; *Rosenbloom and Anderson*, 1994; *Tucker and Slingerland*, 1994; *Pazzaglia et al.*, 1998]. In this section we examine the conditions under which the stream power concept can be applied quantitatively to the headward migration of long-lived bedrock river knickpoints. We take the stream bed elevation profile of Baker's Creek (Fig. 6) as typical of bedrock river profiles for the Macleay tributaries. The gently curved grey line trending downstream from the plateau-level stream bed just above the knickpoint is taken to represent the former profile of the Tableland river before upstream propagation of the knickpoint. The former stream channel and its continuation upstream (Fig. 6) also denote the minimum height of the interfluves of the river valley.

We begin by defining a function $\mathcal{P}$, which we call "generalized" stream power/unit channel width:

$$\mathcal{P} \propto \frac{Q^p S^n}{w}, \qquad (1)$$

where Q is discharge, S is local channel gradient magnitude, and w is channel width, all of which are functions of distance along the channel. Stream power/unit channel width is ≥ 0 because Q, S, and w take only positive values (or zero, in the case of slope and discharge). In a strict definition of

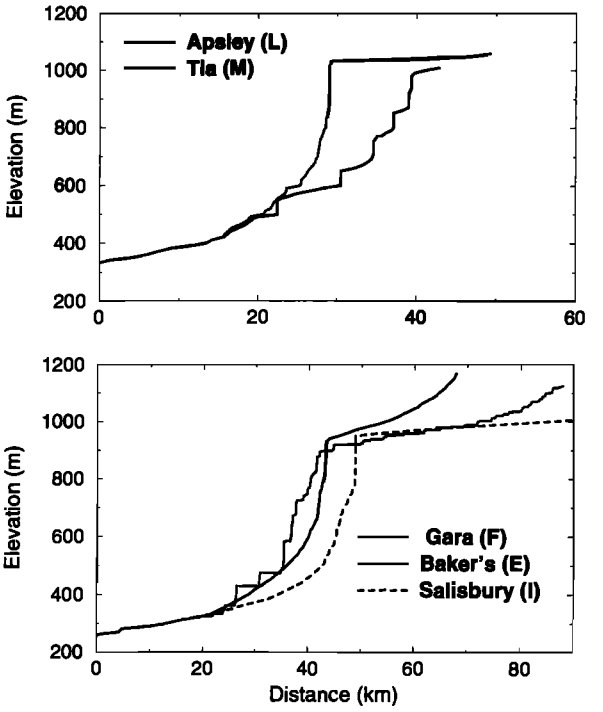

Figure 5. Detailed river longitudinal profiles for Macleay River tributaries draining the southern part of the New England Tableland (top panel), and for streams draining the north and west (bottom panel). The bracketed letters next to river names locate the streams on Fig. 1. All profiles were obtained by digitizing 1:25,000 scale topographic maps except the Gara River profile, which was extracted from the 20 m DEM derived from SPOT stereo imagery.

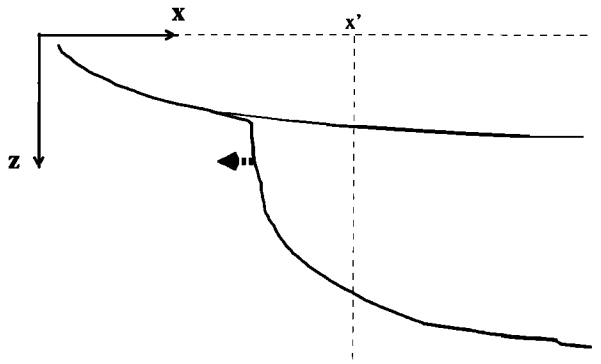

Figure 6. Schematic for the evaluation of stream power models for the migration of large-scale knickpoints up bedrock rivers. Solid line is present-day channel profile for Baker's Creek (Figs. 4 and 5). The grey curve tangential to the modern profile above the knickpoint represents the profile of the ancestral stream slowly and uniformly incising the plateau surface. Bold dashed arrow indicates direction of knickpoint propagation, and x' is a typical location downstream of the knickpoint.

stream power the exponents p and n are unity. However, in the more general case (1), these exponents may take other positive numbers or zero. Many simple models for erosion of bedrock channels have treated channel erosion rate as proportional to generalized stream power [*Seidl and Dietrich*, 1992; *Anderson*, 1994; *Howard*, 1994; *Howard et al.*, 1994]:

$$z_t \propto w(\mathcal{P} - \mathcal{P}_t),$$

where z_t stands for $\partial z(x, t)/\partial t$. The threshold value for stream power/unit width $\mathcal{P}_t$ is that required to transport all the sediment in the channel at a particular point [*Seidl and Dietrich*, 1992]. To simplify the following discussion, we set $\mathcal{P}_t = 0$. In many situations we can assume that discharge Q is related to upstream drainage area A as $Q \sim A^b$, so that the one-dimensional river channel erosion law becomes

$$z_t \propto A^{m'} S^n, \tag{2}$$

where the exponent m' is p/b.

We can rewrite (2) as

$$z_t \propto x^m |z_x|^n \tag{3}$$

by assuming that drainage area A is likely to vary as a power-law function of downstream distance x, although this does not simply imply that $m = 2m'$ [*Anderson*, 1994; *Seidl et al.*, 1994]. We also can drop the modulus sign on slope gradient in (3) in the $x - z$ coordinate frame used here (Fig. 6).

In the case of homogeneous bedrock, and slow, steady external base level lowering, erosion rate should become uniform throughout the drainage basin [*Howard et al.*, 1994], thus (3) implies

$$z_x \sim x^{-m/n}. \tag{4}$$

Under these conditions, channel gradient varies inversely with the distance x downstream, yielding a monotonically decreasing, concave up longitudinal river profile of the type envisaged for the plateau-surface stream before initiation of knickpoint retreat (Fig. 6). Also note that a log – log plot of channel slope versus downstream distance for the uniformly incising stream (4) will be a straight line whose slope depends on the ratio m/n.

Before proceeding further, we examine choices previous workers have made for the exponent m' for the drainage area term, m for the downstream distance term, and n for the channel slope gradient term, in stream power-based channel erosion laws (2) and (3). *Seidl and Dietrich* [1992] found that the ratio $m'/n \approx 1$ for rivers in California and Oregon by assuming equality of tributary and main stream incision rates at their junctions. In a later study of the fluvial dissection of Hawaiian volcanos, *Seidl et al.* [1994] found that areal variations in the amount of channel incision were consistent with $m' = n \approx 1$. *Howard et al.* [1994] solve (2) numerically for the case of a slowly and uniformly incising river (4) subject to large, instantaneous base level falls at discrete times. The model profiles essentially trace the evolution of upstream migrating knickpoints caused by the base level falls. Two sets of models were considered, one where $m' = n = 1$, called a stream power model by *Howard et al.* [1994], and another where $m' = 0.3$ and $n = 0.7$, referred to as a basal shear stress model for channel erosion (following *Howard and Kerby* [1983]). Both *Anderson* [1994] and *Seidl et al.* [1994] use $m < 2$ for stream channel erosion laws recast to depend on downstream distance x (3) instead of drainage area A (2).

Key properties of solutions to stream power-based models for channel form evolution can be readily inferred if we rearrange the terms in (3) slightly to give:

$$z_t \propto \left[x^m z_x^{n-1}\right] z_x. \tag{5}$$

The channel erosion equation is now in the form of a one-dimensional, first-order wave equation that is non-linear in general. Its solution $z(x, t)$ describes the evolution of an initial waveform $z(x, 0)$ as a function of position x and time t. The term in square brackets denotes the wave speed, which depends both on downstream distance and local channel gradient z_x.

Numerical solutions to (2) and (3) describing headward migration of knickpoints following sudden base-level lowering have been presented by *Howard et al.* [1994] and *Seidl et al.* [1994]. Our purpose here is to determine the values of exponents m and n in the stream power-based channel incision law (3) which give closest agreement with the inferred properties and behavior of the Macleay River system knickpoints. Instead of using numerical methods, however,

we show in the Appendix how to solve non-linear, first-order partial differential equations like (3) analytically and graphically by the method of characteristics. Results that provide insight into the knickpoint propagation problem are shown in Figure 7.

We use a gently inclined error function to represent an initial profile form containing a knickpoint (curves for time $t = 0$, Fig. 7). It is meant to portray the former profile of the Tableland river (grey curve, Fig. 6) with the addition of an elevation drop near its downstream end representing a fall to a new base level. Note, however, that we have no actual information on the original knickpoint shape. The choice of an inclined error function is somewhat arbitrary, but because it has a continuous distribution of slope gradients about a maximum slope value at the midpoint of the knickpoint, it provides a good way to demonstrate the dependence of propagation speed on slope gradient, following (5). We stress that because the stream power-based equation for channel incision (3) is, in general, non-linear, its solution depends heavily on the initial conditions. Figure 7 depicts three situations that are of special interest to the problem of knickpoint propagation.

1) $\boxed{n = 1}$ In this case (Fig. 7A), the governing equation (2) or (3) is linear and the speed of propagation depends only on downstream distance x (5). The propagation speed at any given position depends on the value of exponent m' or m, and knickpoints for a basal shear stress model ($m' = 0.3$) therefore migrate more slowly compared to those governed by the stream power model ($m' = 1$) in the models of *Howard et al.* [1994]. If $m' = m = 0$, we get the simplest solution $z(x, t) = z(x + ct)$, where the initial profile $z(x, 0)$ moves upstream in Figure 6 at a constant speed c [*Rosenbloom and Anderson*, 1994]. This situation corresponds to parallel recession of slopes model for erosion presented by *Hirano* [1968]. For any given $m > 0$, the positional dependence of propagation speed in (5) means that channel elements farthest downstream move at the highest rate. The effect is an overall steepening of the knickpoint with time as the downstream channel elements "catch up" with the upstream elements (Fig. 7A). The knickpoint steepening effect increases with the value of exponent m. It is clear then, that knickpoints on streams with smaller upstream drainage areas should move slower than those with larger upstream areas, and hence they would migrate a shorter distance upstream in a given length of time. Such behavior does not accord with observations presented in Figures 2 and 5 and discussed above, showing that knickpoints on the Macleay River system are all about the same distance upstream from the river mouth despite different upstream drainage areas. The only way out of this conflict is to imagine an unlikely situation where the drainage areas A_j and exponents m'_j in (2) were precisely adjusted for each stream j to give closely similar upstream distances for all knickpoints at the present time.

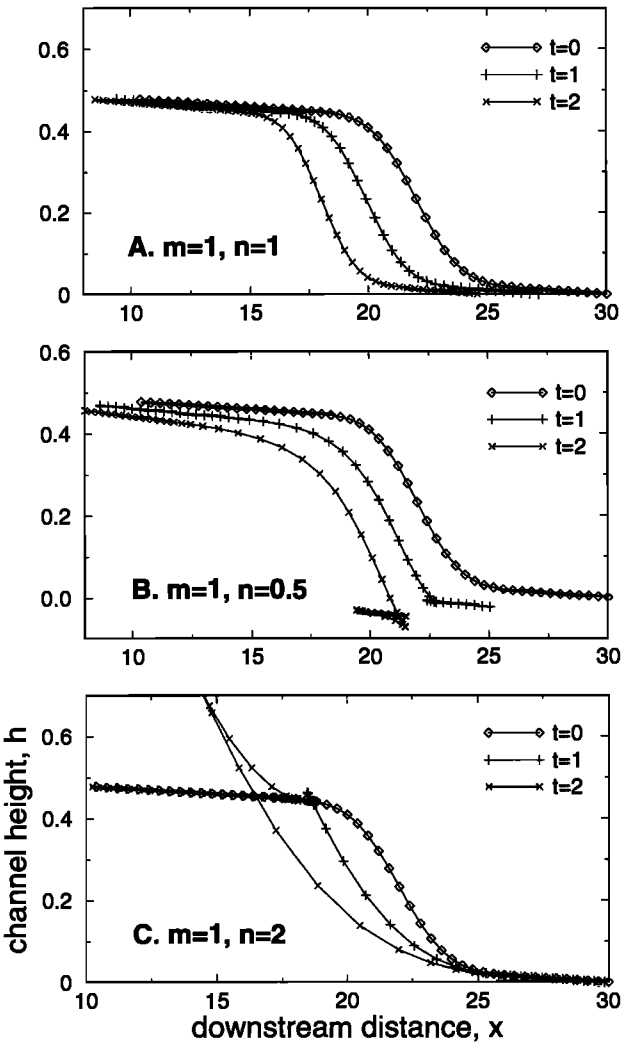

Figure 7. Solutions to the first order PDE, $h_t = -x^m h_x^n$, for stream channel height $h(x, t)$ at three times (t= 0, 1, and 2) obtained using the method of characteristics described in the Appendix. Compare resulting profiles with those in Figs. 5 and 6. In A, the governing equation is linear and also depends on downstream distance ($m = 1$, $n = 1$). In B, the equation is non-linear with $n < 1$. In C, the equation is non-linear with $n > 1$. Because of the non-linearity, shock conditions develop with time at the foot of the model knickpoint in B, and at the top of the knickpoint in C. If the resulting "bow ties" in the channel height profiles caused by the shocks are removed, leaving the maximum height in case B and the minimum height in case C, continuous single-valued stream profiles are obtained.

2) $\boxed{n < 1}$ Here (Fig. 7B), the governing equation (2) or (3) is non-linear. As well as a dependence on downstream distance x through the x^m term (3), propagation speed will also have an inverse relation with local channel gradient z_x. Segments of the channel with the lowest slope gradients will

therefore have the largest propagation speeds. In a given interval of time, the lower gradient portions of the knickpoint will propagate faster and hence travel further upstream. With time the shape of the upper portion of the migrating knickpoint becomes smeared out and diminished in overall gradient (Fig. 7B). A shock condition develops with time at the base of the knickpoint as the faster, lower gradient sections of channel below the knickpoint overtake the slower traveling, steeper gradient sections of the knickpoint (Fig. 7B). The shock condition makes the stream profile multi-valued, and the way shock conditions are handled is described in the caption to Figure 7. Thus, when $n < 1$ in the stream power-based channel incision model (2) or (3), the steepest slope gradients of the knickpoint will accumulate at its base. Figure 7B also highlights another feature of non-linear stream power models with $n < 1$. Channel heights actually decrease with time at a rate proportional to the slope gradient (see equation (20) in the Appendix).

3) $\boxed{n > 1}$ Now, because exponent $n - 1 > 0$ on the slope factor in the propagation speed term of (5), the steepest slope gradients of the initial river profile propagate fastest upstream, so that with time the high gradient portions of the knickpoint overtake the more slowly moving, lower gradient channel sections above the knickpoint. As before, shock conditions develop, but this time at the lip of the propagating knickpoint (Fig. 7C). Again, the shock treatment methods (caption, Fig. 7) can be applied to remove the height triplications to give continuous, single-valued stream profiles for any time t. Many years ago *Luke* [1972] showed that shocks develop in one-dimensional hillslope erosion models that have non-linear dependence of erosion rate on slope gradient with an exponent $n > 1$. A major feature of the knickpoints of the Macleay River system in southeast Australia is the sharp break in slope observed at the knickpoint lip (Figs. 2, 5, and 6). This feature of the river profiles is best matched in a simple stream power-based channel incision model like (2) or (3) if the value of the slope gradient exponent is high, i.e., $n > 1$.

It is worth reiterating that in the general case, where the channel incision model (2) or (3) is non-linear (i.e., $n \neq 1$), the solution is very sensitive to the chosen initial condition. For example, shock conditions do not develop in a non-linear model ($n = 2$) with a uniformly-sloping channel as an initial profile form [*Anderson*, 1994]. The reason is that propagation speed depends on slope, which in this case is constant, so all parts of the channel propagate at the same rate (so far as the slope term in (5) is concerned). The main reason for using the inclined error function as an initial profile of a stream with a large-scale knickpoint (curves for time $t = 0$ in Fig. 7) is to demonstrate that sharp breaks in slope can develop with time (at the top of the knickpoint for $n > 1$ and at the bottom for $n < 1$) from a stream profile that did not originally have sharp breaks in slope.

The only observation that appears to conflict with the final point of case 3) above is that channel gradients increase downstream starting a few hundred meters to a few kilometers above the sharp break in slope that defines the lip of the large-scale knickpoint (Fig. 5). These sections of the streams are bedrock channels and are often incised. Similar steepening upstream of knickpoints was found in flume laboratory experiments on knickpoint propagation by *Gardner* [1983]. The effect was attributed to hydraulic drawdown in water flow approaching the knickpoint, and the section of channel affected was called the drawdown reach [*Gardner*, 1983]. In terms of the simple model for channel incision discussed above, a value of the slope gradient exponent $n < 1$ (Fig. 7B) might be preferred.

However, we caution that a stream power-based model might not include the actual physical processes that give rise to the drawdown reach. It has been suggested to us (C.P. Stark, pers. comm., 1997) that the drawdown reach might instead result through recharge by surface water flowing in the upstream stream channel of groundwater that is discharged at the knickpoint rockface. In this view, flow rate in the channel decreases as the knickpoint is approached (because of surface water loss to groundwater), sediment carrying capacity is thereby decreased, and alluvial material is deposited upstream from the knickpoint. Severe storm events remobilize the upstream alluvial material scouring the reach above the knickpoint and incising the channel into bedrock. This explanation is in accord with the general observation that the steepened bedrock channel of the drawdown reach is separated from the stream below the knickpoint lip by a distinct break in slope (Fig. 5). We mention the problem of the drawdown reach as a suggestion for future work.

3. NEW COSMOGENIC SURFACE EXPOSURE AGE DATA

3.1 Sampling Strategy

We focused our sampling effort on one river within the Macleay River system, Baker's Creek (E in Fig. 1). The reconnaissance sampling and analysis program was undertaken to determine whether the shorter-term exposure ages and average erosion rates obtained from cosmogenic radionuclide concentrations are consistent with the long term escarpment propagation rates inferred from the upstream locations of the river knickpoints (Fig. 2). Baker's Creek is incised into the Hillgrove granite suite of late Carboniferous age [*Flood and Shaw*, 1977]. Upstream of the escarpment, the low gradient, bedrock-floored channel drains 154 km^2 of the low relief, upland plateau surface (Fig. 2). Strath terraces occur 1-3 m above the channel bed.

Where Baker's Creek flows across the escarpment, the channel takes the form of a large-scale, stepped knickpoint

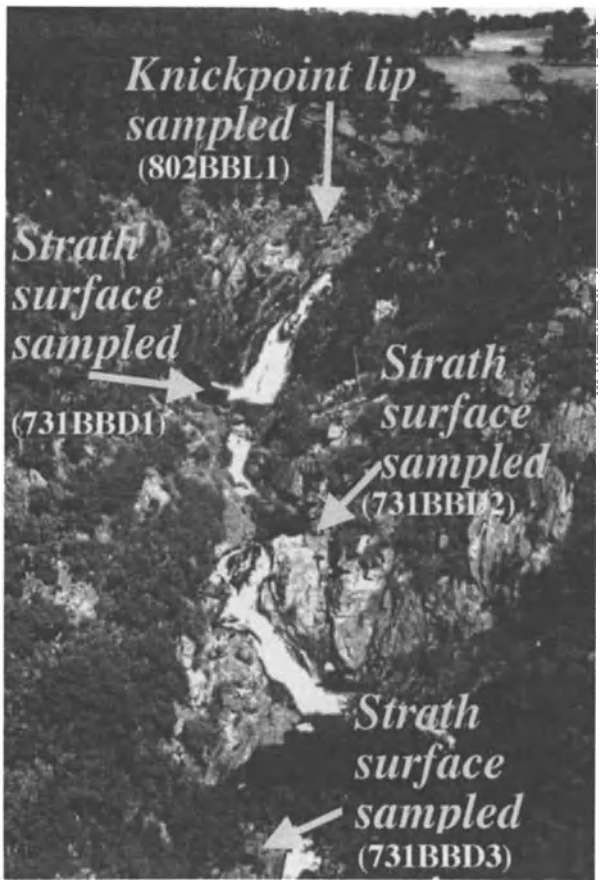

Figure 8. Field photograph taken in 1993 looking upstream toward the gorge head on Baker's Creek [*Seidl et al.*, 1996]. Locations of granitic bedrock samples and their sample numbers are shown. Measurements of ^{10}Be and ^{26}Al cosmogenic radionuclide concentrations in these samples are reported in Table 1.

(Figs. 5 and 8). Strath terraces are parallel to the channel and serve as links between the steps. Downstream from the knickpoint at the gorge head, the valley is deeply incised and strath terraces occur adjacent to the channel. These straths appear to be abandoned, and are infrequently covered in times of high discharge, as evidenced by their relatively clean surfaces. This landscape morphology is mirrored in other stream channels of the Macleay River system and is consistent with the general concept of inland escarpment propagation at passive continental margins [*King*, 1953; *Ollier*, 1985a, 1985b; *Weissel*, 1990; *Seidl et al.*, 1996], suggesting that exposure age data collected along Baker's Creek will have broad significance for the mode and rate of landscape evolution across the southeastern Australian margin.

Eight granitic bedrock surface samples were collected in a transect along Baker's Creek (Fig. 9). A hilltop bedrock exposure on the plateau surface was sampled. A strath surface located 100 m upstream of the knickpoint lip was also sampled. The rock here is very weathered and the surface has been abandoned. Both these upstream sites appear to be eroding in a slow, steady manner. Four samples were collected in the gorge head vicinity, including a sample from the knickpoint lip and samples from three straths (Fig. 8). Two strath surface samples were collected several kilometers downstream from the gorge head (Fig. 9).

3.2 Cosmogenic Isotope Analysis

Rock samples were crushed and quartz aliquots were extracted by magnetic separation and selective chemical dissolution [*Kohl and Nishiizumi*, 1992]. Be and Al samples were prepared by dissolving 20 g of quartz with 0.5 mg of Be

Figure 9. Samples for bedrock exposure age dating using cosmogenic radionuclides are located on a section scanned from a 1:25,000 scale aerial photograph of Baker's Creek taken in 1994. The photograph in Fig. 8 was taken in the direction of the arrow labeled "Gorgehead". Measurements of ^{10}Be and ^{26}Al cosmogenic radionuclide concentrations in these samples are reported in Table 1.

carrier. Total Al was measured by graphite furnace atomic adsorption spectrometry. Isotopic ratios were measured by accelerator mass spectrometry (AMS) at the Lawrence Livermore National Laboratory.

The concentration of cosmogenic isotopes in the upper layers of exposed rock surfaces is dependent upon several factors, including production rate of the nuclide, latitude, altitude, and topographic shielding of the surface samples. The ^{10}Be and ^{26}Al production rates in quartz were assumed to be 6 and 36.8 atoms/g/yr for sea level and high latitude, respectively [*Nishiizumi et al.*, 1989]. Production rates were corrected for latitude and altitude effects [*Lal*, 1991] and for the dip and shielding of the surface [*Nishiizumi et al.*, 1989].

Because the production of cosmogenically-produced nuclides decreases exponentially with depth, erosion of rock surfaces also affects nuclide concentration, such that the concentration N (in units of atoms/g) of a given cosmogenic isotope can be expressed

$$N = [P/(\lambda + \mu\epsilon)] \left(1 - e^{-(\lambda+\mu\epsilon)t}\right) \quad (6)$$

[*Lal*, 1991], where ϵ is erosion rate (cm/yr), P is the production rate of the isotope (atoms/g/yr), λ is the decay constant of the radionuclide (/yr), t is time (yr) since initial exposure to cosmic ray flux, and μ is absorption efficiency in the target material (/cm) given as the ratio of rock density (2.7 g/cm^3 assumed) to the cosmic ray attenuation length in quartz (assumed to be 145 g/cm^2 after *Brown et al.* [1992]).

After continuous long-term exposure to cosmic radiation, the isotopic concentration in the rock surface reaches an equilibrium state with respect to production and loss through radionuclide decay and denudation. If we can assume this equilibrium state, or saturation, has been reached, time can be eliminated from (6) and measured concentrations of cosmogenic isotopes can be used to calculate a steady state erosion rate, such that

$$\epsilon = 1/\mu \, [P/N - \lambda] \quad (7)$$

[*Lal*, 1991]. Conversely, if one assumes that erosion across a rock surface has been negligible, (6) can be used to calculate a minimum exposure age for the surface according to

$$t = -\frac{\ln [1 - (N\lambda/P)]}{\lambda} \quad (8)$$

[*Lal*, 1991].

3.3 Results

The results of the cosmogenic isotope analyses are presented in Table 1. Data are arranged with the furthest upstream and downstream samples at the top and bottom of the table, respectively. Ratios of ^{26}Al/^{27}Al and ^{10}Be/^{9}Be are reported, concentrations of ^{26}Al and ^{10}Be are noted, as are modeled vertical erosion rates calculated using (7). Minimum exposure ages, calculated using (8), are also presented, although we will base our discussion primarily on the modeled erosion rates. The slowest erosion rate is that calculated for the plateau surface (sample 806BBR1). There is good agreement between the Al-derived rate of 3.5 ± 0.7 m/Myr and the Be-derived rate of 4.4 ± 1.7 m/Myr for this sample. The upstream bedrock terrace (806BBU2) appears to be eroding at the slightly faster rate (Table 1). The Al and Be data measured for this bedrock strath yield similar denudation rates of 6.3 ± 1.3 m/Myr, based on the Al ratio, and 8.4 ± 1.8 m/Myr, based on the Be ratio. At the knickpoint lip (802BBL1) the average erosion rates modeled using the two isotopes are indistinguishable: 19.4 ± 3.9 m/Myr and 20.1 ± 6.3 m/Myr for the Al and Be data, respectively (Table 1). The erosion rates increase dramatically directly downstream of the knickpoint lip. The erosion rates calculated for strath surfaces occurring within the gorge head range from 51.8 ± 6.8 to 212.1 ± 83.0 m/Myr. The strath terraces located several kilometers downstream of the gorgehead are calculated to be eroding at similarly high rates ranging from < 50.8 to 155.1 ± 32.6 m/Myr.

Both ^{26}Al/^{27}Al and ^{10}Be/^{9}Be ratios were analyzed in the three upstream samples (Table 1). These upstream samples show good agreement between the erosion rates calculated using Be isotope ratios and those derived from Al isotopic ratios. All three upstream samples plot sufficiently close to the erosion island [*Lal*, 1991] to suggest a simple denudational history. ^{26}Al/^{27}Al ratios were measured in all of the five downstream samples, but ^{10}Be/^{9}Be ratios were measured in only three of the downstream samples. The Be data measured for the downstream samples have large uncertainties, primarily because of post-oxidation contamination with boron. Of the three samples in which both Al and Be were measured, two have low Al/Be ratios (731BBD1 and 809BBS1), implying that these surfaces have experienced a more complicated erosion history than have the upstream samples. The strath surface located just below the gorge head's third cataract plots close to the erosion island, but the uncertainty is large (Table 1).

3.4 Interpretation and Discussion

The pattern of increasing erosion rates in the downstream direction is consistent with our escarpment propagation model [*Seidl et al.*, 1996; *Weissel and Seidl*, 1997] and provide some of the first direct estimates of erosion rates occurring on passive margin escarpments. The very slow erosion rate calculated for the plateau surface, 3.5 to 4.4 m/Myr, is consistent with the antiquity of the upland plateau suggested by previous oxygen isotope [*Bird and Chivas*, 1993] and fission track [*Moore et al.*, 1986] studies. The slightly higher erosion rate calculated for the upstream strath surface suggests that the bedrock surfaces adjacent to the channel

Table 1. Cosmogenic Radionuclide Measurements from Baker's Creek, New South Wales

Sample Site & Number	Sample Weight (g)	$^{26}Al/^{27}Al$ Ratio, $^{10}Be/^{9}Be$ Ratio	^{26}Al Concentration, ^{10}Be Concentration (10^6 at/g SiO_2)	Average Erosion Rate (7) ^{26}Al, ^{10}Be (m/Myr)	Minimum Exposure Age (8) ^{26}Al, ^{10}Be (years)
UPSTREAM OF GORGEHEAD					
806BBR1 Plateau Surface	9.2	$1.53 \times 10^{-12} \pm 4.3 \times 10^{-14}$, $3.33 \times 10^{-13} \pm 6.5 \times 10^{-14}$	8.56 ± 0.48, 1.23 ± 0.48	3.53 ± 0.7, 4.38 ± 1.7	$1.5 \times 10^5 \pm 3.0 \times 10^4$, $1.2 \times 10^5 \pm 4.8 \times 10^4$
806BBU2 Strath Surface	17.2	$9.24 \times 10^{-13} \pm 2.9 \times 10^{-14}$, $3.33 \times 10^{-13} \pm 3.5 \times 10^{-14}$	4.75 ± 0.30, 0.65 ± 0.14	6.31 ± 1.3, 8.37 ± 1.8	$8.5 \times 10^4 \pm 1.6 \times 10^4$, $6.5 \times 10^4 \pm 1.4 \times 10^4$
802BBL1 Knickpoint Lip	25.8	$2.97 \times 10^{-13} \pm 1.3 \times 10^{-14}$, $1.99 \times 10^{-13} \pm 3.1 \times 10^{-14}$	1.71 ± 0.15, 0.27 ± 0.08	19.4 ± 3.9, 20.1 ± 6.3	$2.8 \times 10^4 \pm 5.6 \times 10^3$, $2.7 \times 10^4 \pm 8.6 \times 10^3$
GORGEHEAD					
731BBD1 Strath - below 1st cataract	17.7	$4.07 \times 10^{-14} \pm 8.6 \times 10^{-15}$, $< 4.03 \times 10^{-14}$	0.17 ± 0.07, <0.08	194.7 ± 82.3, < 67.3	$3.2 \times 10^3 \pm 1.3 \times 10^3$, $< 8.2 \times 10^3$
731BBD2 Strath - above 2nd cataract	21.0	$8.74 \times 10^{-14} \pm 5.7 \times 10^{-15}$, N/A	0.62 ± 0.08, N/A	51.8 ± 6.8, N/A	$1.1 \times 10^4 \pm 2.2 \times 10^3$, N/A
731BBD3 Strath - below 3rd cataract	15.6	$8.80 \times 10^{-14} \pm 7.9 \times 10^{-15}$, $1.18 \times 10^{-14} \pm 2.3 \times 10^{-14}$	0.35 ± 0.06, 0.03 ± 0.03	82.1 ± 14.8, 212.1 ± 83.0	$6.7 \times 10^3 \pm 1.2 \times 10^3$, $2.6 \times 10^3 \pm 1.0 \times 10^3$
DOWNSTREAM OF GORGEHEAD					
809BBS1 Strath	15.0	$1.14 \times 10^{-14} \pm 5.0 \times 10^{-15}$, $< 4.03 \times 10^{-14}$	0.29 ± 0.07, <0.09	100.9 ± 43.9, <50.8	$5.5 \times 10^3 \pm 2.6 \times 10^3$, $<1.0 \times 10^4$
729BBD2 Strath	24.9	$6.01 \times 10^{-14} \pm 6.3 \times 10^{-15}$, N/A	0.21 ± 0.04, N/A	155.1 ± 32.6, N/A	$3.2 \times 10^3 \pm 1.3 \times 10^3$, N/A

are eroding at a slightly higher rate and provides an upper limit on the rate of upstream bedrock channel incision of ~7 m/Myr. Erosion rates increase to ~20 m/Myr at the knickpoint lip, suggesting that the channel bed is being lowered twice as fast across the lip relative to the upstream strath and five times faster than the plateau surface.

Across the gorge head erosion rates increase dramatically, suggesting that most of the erosion is focussed in this area. We calculate that these erosion rates are on the order of ~100 m/Myr, twenty-five times faster than plateau surface erosion rates. This increase in downstream erosion rates is consistent with our knickpoint propagation model and implies that bedrock channel incision is occurring at a much faster pace across and directly downstream of the gorge head, relative to erosion rates upstream of the knickpoint. Our calculated rates are an order of magnitude lower than the inferred long term knickpoint propagation rate of ~2 km/Myr. However, it should be noted that our data constrain vertical downwearing rates.

Bedrock channel incision rates calculated for Baker's Creek can be compared with those estimated for channels in other areas. We would expect the Baker's Creek channel to be incising faster relative to channels draining towards the interior of Australia because of the spatial focus of erosion along the escarpment. *Young and McDougall* [1993] estimate channel erosion rates on the order of 5 m/Myr for inland-draining streams of southeastern Australia since Miocene time. These rates are based on well-dated lava flows and are roughly twenty times slower than the ~100 m/Myr erosion rates calculated along Baker's Creek. In contrast, we

would expect the ~100 m/Myr rate to be very slow compared to those incision rates calculated for the Indus River in the rapidly uplifting Himalayas. The ~10 km/Myr erosion rates calculated for the Indus River valley are indeed significantly faster [*Burbank et al.*, 1996].

The exposure histories inferred from the Al/Be data generally support the paradigm of inland escarpment retreat across passive continental margins. Field observations indicate frequent mass wasting events at the gorge head and along the steep hillslopes downstream of the gorge head. Several of the downstream samples have experienced complex denudation histories. That these surfaces have been subject to burial and re-exhumation is consistent with the degree of bedrock landsliding currently occurring on the very steep rockslopes in the vicinity of the gorge head. It is likely that these surfaces are covered by landslide debris periodically and then uncovered during high discharge events. In contrast, the upstream surfaces have experienced relatively simple denudation histories lacking intervening burial events. A simpler exposure history is consistent with the subdued relief and lower channel gradients found upstream of the gorge head (Fig. 5).

4. SUMMARY

In this study we have presented new, detailed river longitudinal profiles for several plateau-draining tributaries of the Macleay River that cross large-scale stream channel knickpoints (Figs. 5), in order to assess an earlier conclusion that the similarity in upstream distance of the knickpoints indicates that knickpoint migration rate is largely independent of the upstream area drained at the knickpoint [*Seidl et al.*, 1996]. The new profile analysis confirms this earlier conclusion. The main implication for the gorge head – knickpoint type of erosional escarpment is that, so long as sufficient fluvial transport power is present in the channel, the pace of inland propagation is mainly regulated by slope failure mechanisms and the frequency of resulting mass wasting events from the steep rock slopes at the gorge head and immediately downstream. This conclusion also has implications for modeling knickpoint migration using a simple one-dimensional stream power law for channel incision of the form $z_t \propto A^{m'} S^n$, where A is drainage area and S is channel gradient. The requirement that propagation rate is independent of upstream drainage area so long as a threshold is met would indicate that exponent $m' = 0$ in such models. In addition, the development and maintenance of a distinct break in slope at, and steep (sub-vertical) slope gradients below the knickpoint lip during headward migration indicates that the value of exponent $n > 1$.

Measurement of cosmogenic radionuclide concentrations in samples collected on a transect across the large-scale knickpoint on Baker's Creek has allowed, for the first time, direct determination of short-term, vertical erosion rates connected with knickpoint propagation and escarpment retreat. Average vertical erosion rates calculated from Be and Al radionuclide concentrations in the Baker's Creek samples (Table 1) indicate that the plateau surface and the channel upstream of the gorge head – knickpoint are eroding slowly, ~5 m/Myr, whereas the channel at and downstream of the knickpoint are eroding much more rapidly, >100 m/Myr. The pattern of increasing erosion rates across the knickpoint in the downstream direction is consistent with the concept of inland escarpment retreat across passive continental margins.

APPENDIX: SOLVING THE STREAM POWER EQUATION FOR CHANNEL INCISION BY THE METHOD OF CHARACTERISTICS

Given some initial stream profile $h(x, 0)$, we want to solve a one-dimensional, first-order, partial differential equation (PDE) of the form

$$h_t = -f(h_x, x), \tag{9}$$

where h_t is shorthand for $\partial h/\partial t$, etc. The solution of (9) gives channel height $h(x, t)$ as a function of upstream distance x and time t. Later we recast the solutions in the $x - z$ coordinate system used in Figure 6. Equation (9) indicates that channel incision is controlled by a very general function of channel slope gradient and position $f(h_x, x)$. *Luke* [1972] solved (9) for the erosion of one-dimensional hillslopes using the method of characteristics with some simple expressions of the form $f(h_x)$ (i.e., no x dependence). The intent here is to extend the work of *Luke* [1972] to cases where $f(h_x, x)$ includes a power-law function of downstream distance to account for stream discharge as in (3).

The method of characteristics is used for semi-analytical or graphical solution of first-order PDEs that are either linear, quasi-linear, or non-linear (as in the present case) [*Farlow*, 1982]. A characteristic is simply a curve in the $x - t$ plane along which some information or property of the initial profile propagates. Position, slope and height of the initial profile are the properties of most interest to us.

Following *Luke* [1972], we let $S(t)$ denote the value of slope h_x along some characteristic $x = X(t)$ in the $x - t$ plane:

$$S(t) = [h_x]_{x=X(t)} . \tag{10}$$

The square brackets and the subscript in (10) emphasize that the slope $S(t)$ is that measured along the characteristic. To find out how slope S changes with time we take the full, or material derivative, defined as

$$\frac{d}{dt}[\cdot] \equiv \left(\partial_t + \frac{dx}{dt}\partial_x\right)[\cdot] ,$$

along the characteristic path. Thus,

$$\frac{dS(t)}{dt} = [h_{xt}] + X'(t)\,[h_{xx}]\,, \tag{11}$$

where again, the square brackets denote evaluation along the characteristic. Differentiating (9) with respect to x, we get

$$h_{tx} = -\frac{\partial f(h_x, x)}{\partial h_x}\,h_{xx} - \frac{\partial f(h_x, x)}{\partial x}\,,$$

which, if evaluated along $x = X(t)$, becomes

$$[h_{xt}] = -\frac{\partial f\,(S(t), x)}{\partial S(t)}\,[h_{xx}] - \frac{\partial f\,(S(t), x)}{\partial x}\,. \tag{12}$$

Substituting (12) into (11) expresses the change of slope S with time along the characteristic as

$$S'(t) = [h_{xx}]\left(X'(t) - \frac{\partial f\,(S(t), x)}{\partial S(t)}\right) - \frac{\partial f\,(S(t), x)}{\partial x}. \tag{13}$$

Notice that if we choose

$$X'(t) = \frac{\partial f\,(S(t), x)}{\partial S(t)} \tag{14}$$

[*Luke*, 1972], the change of slope S with time along the characteristic becomes

$$S'(t) = -\frac{\partial f\,(S(t), x)}{\partial x}\,. \tag{15}$$

Further, the change of height $H(t)$ with time along the characteristic is given by the material derivative

$$\begin{aligned} H'(t) &= [h_x]\,X'(t) - f\,(S(t), x) \\ &= S(t)\,\frac{\partial f\,(S(t), x)}{\partial S(t)} - f\,(S(t), x)\,. \end{aligned} \tag{16}$$

We are particularly interested in solving equations for stream channel erosion of the form (c.f., equation (3)):

$$h_t = -x^m\,h_x^n\,. \tag{17}$$

Comparing (9) and (17), it is obvious that

$$f(S, x) = x^m\,S^n\,,$$

where, it should be noted, slope S and position x depend parametrically on time t along the characteristic. The equation for the characteristic (14) can now be written compactly as

$$X'(t) = n\,x^m\,S^{n-1}\,, \tag{18}$$

where, as expected, the term on the right is equivalent to the propagation speed term bracketed in (5). The rate of slope change from (15) becomes

$$S'(t) = -m\,x^{m-1}\,S^n\,, \tag{19}$$

and the rate of height change from (16) is now

$$H'(t) = (n-1)\,x^m\,S^n\,. \tag{20}$$

Thus, the change in position, slope gradient, and height along any characteristic starting from an initial height profile $h(x, 0)$, can be found from the set of ordinary differential equations (18) – (20). These equations depend upon exponents m and n, and for certain values of these exponents, solutions are relatively easy to obtain. When $n = 1$, for example, the original PDE (17) is linear and application of the method of characteristics to its solution for any $m \geq 0$ is straightforward [*Farlow*, 1982]. Note from (20), that height H remains constant along the characteristic in this case. For $m = 0$ and any $n \neq 1$ the governing PDE (17) is non-linear with a constant coefficient. As *Luke* [1972] pointed out, slope S in this case remains constant along the characteristic (19). From (18) the characteristics $x = X(t)$ are linear in the $x - t$ plane. Propagation rate increases with S for $n > 1$ and decreases with S for $n < 1$. By (20), height H also changes linearly with time t along the characteristic when $m = 0$, increasing with slope S for $n > 1$ and decreasing with S for $n < 1$. The most complicated expression for which (18) – (20) can be readily solved, is where $f(S, x) = x\,S^n$, i.e., for $m = 1$ and any $n > 0$. In this case, we first solve (19), and substitute the results into (18) and (20) in turn.

To relate solutions of the first order PDE (9) using the method of characteristics to the discussion in the body of the text on models for knickpoint propagation up bedrock river channels, we must transform the coordinate system used in solving (18) – (20) to that used in Figure 6. The transformation between the two coordinate systems is given by $z = h - h_d$ and $x' = x_d - x$, where x_d and h_d are the distance upstream to where the channel starts and the channel height at that location. In Figure 7 x_d is 22 distance units upstream from the midpoint of the knickpoint in the initial profile (curves for time $t = 0$).

Acknowledgments. This manuscript benefited from thorough reviews by Dorothy Merritts, Jonathon Nott, and an anonymous reviewer. This work was supported by National Aeronautics and Space Administration grant NAG5-2987, Office of Naval Research grant N00014-96-1-0027, and by a grant for field work from the National Geographic Society. We thank Niels Hovius, Neil Shubin, Colin Stark, and Rose Anne Weissel for help during the 1996 field season. Lamont-Doherty Earth Observatory contribution no. 5819.

REFERENCES

Anderson, R. S., Evolution of the Santa Cruz Mountains, California, through tectonic growth and geomorphic decay, *J. Geophys. Res.*, *99*, 20,161–20,179, 1994.

Bird, M. I., and A. R. Chivas, Geomorphic and palaeoclimatic implications of an oxygen-isotope chronology for Australian deeply weathered profiles, *Aust. J. of Earth Sci.*, *40*, 345–358, 1993.

Brown, E. T., E. J. Brook, G. M. Raisbeck, F. Yiou, and M. D. Kurz, Effective attenuation lengths of cosmic rays producing ^{10}Be and ^{26}Al in quartz: Implications for exposure dating, *Geophys. Res. Lett.*, *19*, 367–372, 1992.

Burbank, D. W., J. Leland, E. Fielding, R. S. Anderson, N. Brozovic, M. R. Reid, and C. Duncan, Bedrock incision, rock uplift and threshold hillslopes in the northwestern Himlayas, *Nature*, *379*, 505–510, 1996.

de Freitas, M. H., and R. J. Watters, Some field examples of toppling failure, *Géotechnique*, *23*, 495–514, 1973.

Farlow, S., *Partial Differential Equations for Scientists and Engineers*. John Wiley & Sons, New York, 1982.

Flood, R. H., and S. E. Shaw, Two "S-type" granite suites with low initial ^{87}Sr/^{86}Sr ratios from the New England batholith, Australia, *Contr. Mineral. & Petrol.*, *61*, 163–173, 1977.

Gardner, T. W., Experimental study of knickpoint and longitudinal profile evolution, *Geol. Soc. Amer. Bull.*, *94*, 664–672, 1983.

Gilchrist, A. R., and M. Summerfield, Differential denudation and flexural isostasy in the formation of rifted-margin upwarps, *Nature*, *346*, 739–742, 1990.

Gilchrist, A. R., H. Kooi, and C. Beaumont, Post-Gondwana geomorphic evolution of southwestern Africa: Implications for the controls on landscape development from observations and numerical experiments, *J. Geophys. Res.*, *99*, 739–742, 1994.

Goodman, N. M., and J. W. Bray, Toppling of rock slopes, in *Rock Engineering for Foundations and Slopes*, pp. 201–234, New York. Amer. Soc. of Civil Eng., 1977.

Hayes, D. E., and J. Ringis, Seafloor spreading in the Tasman Sea, *Nature*, *243*, 454–458, 1973.

Hirano, M., A mathematical model for slope development, *J. Geosciences, Osaka City Univ.*, *11*, 13–52, 1968.

Howard, A. D., A detachment-limited model of drainage basin evolution, *Water Resour. Res.*, *30*, 2261–2285, 1994.

Howard, A. D., and G. Kerby, Channel changes in badlands, *Geol. Soc. Amer. Bull.*, *94*, 739–752, 1983.

Howard, A. D., W. E. Dietrich, and M. A. Seidl, Modeling fluvial erosion on regional to continental scales, *J. Geophys. Res.*, *99*(B7), 13,971–13,986, 1994.

Kelsey, H. M., The formation of inner gorges, *Catena Suppl.*, *15*, 433–458, 1988.

King, L. C., Canons of landscape evolution, *Geol. Soc. Amer. Bull.*, *64*, 721–752, 1953.

Kohl, C. P., and K. Nishiizumi, Chemical isolation of quartz for measurement of in situ produced cosmogenic nuclides, *Geochim. Cosmochim. Acta*, *56*, 3583–3587, 1992.

Kooi, H., and C. Beaumont, Escarpment evolution on high-elevation rifted margins: Insights derived from a surface processes model that combines diffusion, advection, and reaction, *J. Geophys. Res.*, *99*, 12,191–12,209, 1994.

Kooi, H., and C. Beaumont, Large-scale geomorphology: Classical concepts reconciled and integrated with contemporary ideas via a surface process model, *J. Geophys. Res.*, *101*, 3361–3386, 1996.

Lal, D., Cosmic ray labeling of erosion surfaces: In situ nuclide production rates and erosion model, *Earth Planet. Sci. Lett.*, *104*, 424–439, 1991.

Leeder, M., and R. Gawthorpe, Sedimentary models for tilt-block/half-graben basins, in *Continental Extensional Tectonics*, edited by M. P. Coward, J. F. Dewey, and P. L. Hancock, pp. 139–152. Spec. Publ. Geol. Soc. Am., 28, 1987.

Lister, G. S., M. A. Etheridge, and P. A. Symonds, Detachment models for the formation of passive continental margins, *Tectonics*, *10*, 1938–1964, 1992.

Luke, J. C., Mathematical models for landscape evolution, *J. Geophys. Res.*, *77*, 2460–2464, 1972.

Moore, M. E., A. J. Gleadow, and J. F. Lovering, Thermal evolution of rifted continental margins: New evidence from fission tracks in basement apatites from southeastern Australia, *Earth Planet. Sci. Lett.*, *78*, 255–270, 1986.

Nishiizumi, K., E. L. Winterer, C. P. Kohl, J. Klein, R. Middleton, D. Lal, and J. R. Arnold, Cosmic ray production of ^{10}Be and ^{26}Al in quartz from glacially polished rocks, *J. Geophys. Res.*, *94*, 17,907–17,915, 1989.

Nott, J., R. Young, and I. McDougall, Wearing down, wearing back, and gorge extension in the long-term denudation of a highland mass: Quantitative evidence from the Shoalhaven catchment, Southeast Australia, *J. Geol.*, *104*, 224–232, 1996.

Ollier, C. D., The Great Escarpment of eastern Australia: Tectonic and geomorphic significance, *Jour. Geol. Soc. Aust.*, *29*, 13–23, 1982.

Ollier, C. D., Morphotectonics of continental margins with great escarpments, in *Tectonic Geomorphology, Binghamton Symposium in Geomorphology*, edited by M. Morisawa, and J. T. Hack, vol. 15, pp. 3–25. Allen and Unwin, Boston, 1985a.

Ollier, C. D., Morphotectonics of passive continental margins: Introduction, *Z. Geomorph., Suppl. Bd.*, *54*, 1–9, 1985b.

Pazzaglia, F. J., T. H. Gardner, and D. J. Merritts, Bedrock fluvial incision and longitudinal profile development over geologic time scales determined by fluvial terraces, in *Bedrock Channels*, edited by E. E. Wohl, and K. J. Tinkler. American Geophysical Union, Washington, D. C., (This volume), 1998.

Pratson, L. F., and W. B. F. Ryan, Automated drainage extraction in mapping the Monterey submarine drainage system, California margin, *Mar. Geophys. Res.*, *18*, 757–777, 1996.

Rosenbloom, N. A., and R. S. Anderson, Hillslope and channel evolution in a marine terraced landscape, Santa Cruz, California, *J. Geophys. Res.*, *99*, 14,013–14,029, 1994.

Schmidt, K., Factors influencing structural landform dynamics on the Colorado Plateaus and the necessity of calibrating theoretical models by empirical data, *Catena Suppl.*, *10*, 51–66, 1987.

Seidl, M. A., and W. E. Dietrich, The problem of channel erosion into bedrock, *Catena Suppl.*, *23*, 101–124, 1992.

Seidl, M. A., W. E. Dietrich, and J. W. Kirchner, Longitudinal profile development into bedrock: an analysis of Hawaiian channels, *J. Geol.*, *102*, 457–474, 1994.

Seidl, M. A., J. K. Weissel, and L. F. Pratson, Kinematics and pattern of escarpment retreat across the rifted continental margin of SE Australia, *Basin Res.*, *8*, 301–316, 1996.

Selby, M. J., Controls on the stability and inclinations of hillslopes formed on hard rock, *Earth Surf. Proc. Landf.*, *7*, 449–467, 1982.

Selby, M. J., Rock slopes, in *Slope Stability*, edited by M. G. Anderson, and K. S. Richards, pp. 475–504. John Wiley and Sons, New York, 1987.

Summerfield, M. A., *Global Geomorphology: An Introduction to the Study of Landforms*. Longman Scientific and Technical, London, 1991.

Terzaghi, K., Stability of steep slopes on hard unweathered rock, *Géotechnique*, *12*, 251–270, 1962.

Tucker, G. E., and R. L. Slingerland, Erosional dynamics, flexural isostasy, and long-lived escarpments: A numerical modeling study, *J. Geophys. Res.*, *99*, 12,229–12,243, 1994.

Weissel, J. K., Long-term erosional development of rifted continental margins: Toward a quantitative understanding, in *Pacific Rim Congress 90*, vol. III, pp. 63–70, Parkville (Vic.), Australia. Austr. Inst. Mining & Metall., 1990.

Weissel, J. K., Airborne radar investigation of escarpment erosion across the New England section of the southeast Australian continental margin, in *Significant results of the AIRSAR Australia 1993 mission, Proc. Int. Workshop on Radar Image Processing and Applications*, edited by A. K. Milne, pp. 62–65, Canberra, Australia. CSIRO, 1997.

Weissel, J. K., and D. E. Hayes, Evolution of the Tasman Sea reappraised, *Earth Planet. Sci. Lett.*, *36*, 77–84, 1977.

Weissel, J. K., and M. A. Seidl, Influence of rock strength properties on escarpment retreat across passive continental margins, *Geology*, *25*(7), 631–634, 1997.

Weissel, J. K., A. Malinverno, D. J. Harding, and G. D. Karner, Erosional development of the Ethiopian Plateau of northeast Africa from a fractal analysis of topography, in *Fractals in Petroleum Geology and Earth Processes*, edited by C. C. Barton, and P. La Pointe, pp. 127–142. Plenum Press, New York, 1995.

Young, R. W., and I. McDougall, Long-term landscape evolution: Early Miocene and modern rivers in southern New South Wales, *J. Geol.*, *101*, 35–49, 1993.

J. K. Weissel, Lamont-Doherty Earth Observatory of Columbia University, Palisades, NY 10964, USA (email: jeffw@lamont.ldeo.columbia.edu)

M. A. Seidl, Department of Geological Sciences, Rutgers University, New Brunswick, NJ, 08903, USA (email: seidl@rci.rutgers.edu)

Bedrock Fluvial Incision and Longitudinal Profile Development Over Geologic Time Scales Determined by Fluvial Terraces

Frank J. Pazzaglia

Department of Earth and Planetary Sciences, University of New Mexico, Albuquerque, NM

Thomas W. Gardner

Department of Geology, Trinity University, San Antonio, TX

Dorothy J. Merritts

Department of Geosciences, Franklin and Marshall College, Lancaster, PA

Fluvial terraces preserve the history of river incision into bedrock over geologic time scales. In this paper we use terraces and a comparison of terrace longitudinal profiles to stream longitudinal profiles to develop a conceptual model of bedrock fluvial incision in diverse geologic, tectonic, and climatic settings. The conceptual model highlights a distinction between bedrock stream behavior in settings of relatively high versus relatively low tectonic activity. This distinction arises from the fundamentally different ways in which runoff is generated in these respective tectonic settings and the positive feedbacks that exist between topography and climate. The model allows for qualitative predictions of long profile shape that can be directly compared to the longitudinal profiles predicted by the stream power law. Our approach has the advantage of helping understand the geologic (and climatic) constraints on the wide variations in k, m, and n revealed in recent applications of the stream power law. We reconcile diverse longitudinal profile shapes and long-term rates of bedrock fluvial incision by considering how a drainage basin generates fluvial discharge and whether that discharge can produce the necessary stream power distributed across a valley bottom such that the long profile can rapidly accommodate changes in base level, climate, and/or rates of rock uplift. We propose that in tectonically active settings (Type I basins), the entire drainage basin experiences uplift which, in turn, builds steep slopes and concomitant increases in orographic precipitation that effectively generate the high peak discharges and fluvial-system wide stream power necessary to create and maintain concave-up long profiles and rates of incision equal and opposite to rates of rock uplift. Measured stream power for one

INTRODUCTION

The longitudinal profile of a bedrock river is arguably the most outstanding expression of the dynamic feedback between rock uplift processes which construct topography

Rivers Over Rock: Fluvial Processes in Bedrock Channels
Geophysical Monograph 107

of these basins is highly correlated to the width of the channel and valley bottom which argues for a conservation of energy along the profile and the apportionment of stream power to vertical incision, lateral incision, and bedload transportation. The stream power used for lateral incision processes periodically widen the channel bottom during transient, hydrologically-driven changes in discharge and sediment load, producing fluvial terraces. In contrast, drainage basins in tectonically inactive settings (Type II) may not have a hydrology characterized by high peak discharges, particularly for those drainage basins which do not receive large, highly seasonal and/or highly-variable precipitation (Type IIa). Streams in the tectonically-inactive setting are more dependent on local changes in stream power, spatially restricted to knickpoints, that require long periods of time to propagate through the system. A change in down stream base level in these settings has a particularly profound impact on long profile shape, especially where the river crosses resistant rock-types. Type II basins located where climate favors highly seasonal and/or variable precipitation (Type IIb) retain minor rock-type controlled convexities on otherwise concave profiles.

and rock erosion processes which destroy topography. Fluvial terraces preserve a long-term history of paleo-long profiles that records the spatial and temporal changes in the fluvial incision of the landscape. The shapes of bedrock channel long profiles and their terraces provide useful information [*Ohmori*, 1991] regarding the manner in which streams distribute available power as they incise into the land mass which rises beneath them in three general stages [*Pinter and Brandon,* 1997]. In the constructive phase, rates of rock-uplift exceed those of erosion. Bedrock channels and their incision limit the rates of erosion during the constructive phase by creating relief and setting the boundary conditions for hillslope processes. With increasing development of high elevations and relief, rates of erosion dramatically increase as hillslopes reach their critical threshold of failure [*Carson,* 1970, 1971; *Burbank et al.,* 1996; *Hovius,* in press], a condition determined by rock mass strength [*Schmidt and Montgomery,* 1995] and hillslope hydrology [*Kirkby,* 1992, 1993]. Eventually, rates of erosion equal those of rock-uplift, denoting the steady state phase. Finally, decreasing rates or arrestment of rock-uplift results in the destructive stage where, rates of erosion exceed those of rock-uplift and isostatic adjustments and the overall elevation of the mountain range diminishes with time.

As rates of rock uplift and bedrock incision are fairly difficult to acquire, and are not commonly available for the same regions, it has been difficult to test conceptual models of mountain building and long profile evolution with actual data. Here, we provide three types of data that can be used to help understand changes in long profiles in diverse tectonic settings. First, we present data on rates of rock-uplift for different regions and corresponding rates of fluvial bedrock incision along stream channels in those regions. Second, we examine the shapes of the longitudinal profiles of those stream channels, as well as those of their ancestors, which are preserved in the fluvial terrace record. Lastly, we examine the discharge characteristics of our drainage basins to help elucidate important tectonic - climatic/hydrologic feedbacks or controls.

Many recent investigations of the dynamics of bedrock channel systems have focused on a model that links the rate of bedrock channel erosion to available stream power (based on shear stress), the latter of which is related to drainage area and stream gradient by a power-law function [*Howard and Kerby,* 1983]. This model commonly is referred to as the "stream power law" (see further discussion below). Other factors which affect rates of erosion include rock-type resistance, climate, soil thickness, and related hydrological factors that determine the rate of runoff from hillslopes to stream channels. These factors, which may be parameterized locally but typically show a wide variation regionally, are incorporated into the stream power law as the coefficients and exponents k, m and n. Recent analyses of the m/n ratio [e.g., *Anderson,* 1994; *Tucker,* 1996; *Sklar and Dietrich,* 1997; *Stock and Montgomery,* in press] and their roles in the stream power law indicate that this ratio and the distribution of stream power along a channel is reflected in the overall long profile shape.

Rather than trying to parameterize the stream power law, the data in this paper is far better suited to explaining diverse long profile shapes and rates of incision in terms of basin-scale processes and geologic characteristics. The hypothesis at the core of this approach is that a bedrock river

longitudinal profile is primarily shaped by the particular manner in which a drainage basin generates runoff. Drainage basins with rock-type, climatic, and/or rock-uplift characteristics that generate large discharges per unit area have long profiles typically devoid of large convexities. We demonstrate that these long profiles occur primarily in tectonically active regions, and to a lesser extent in the tectonically stable setting where precipitation is highly variable. In contrast, drainage basins with rock-type, climatic, and/or rock-uplift characteristics that generate small discharges per unit area more commonly exhibit profile convexities. We find that these long profiles occur primarily in tectonically stable regions, particularly in the presence of resistant rock-types and where there is little annual variation or seasonality in precipitation. Our approach has the advantage of helping understand the geologic (and climatic) constraints on the wide variations in k, m, and n revealed in recent applications of the stream power erosion law.

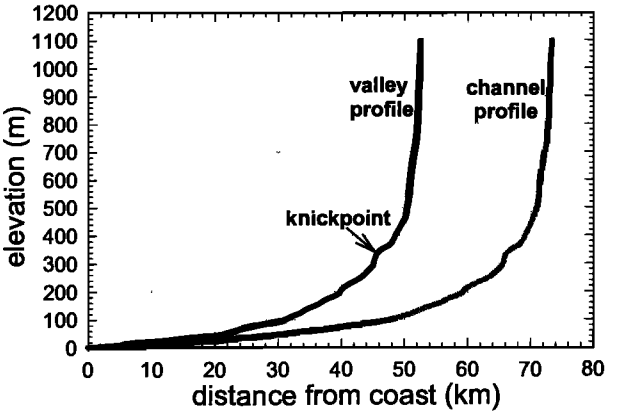

Figure 1. Examples of channel and valley-bottom longitudinal profiles for the Clearwater River, Olympic Mountains, Washington State. The valley-bottom profile is shorter than the channel profile because of channel sinuosity. Note locations of several prominent knickpoints.

FUNDAMENTAL CONTROLS ON INCISION OF BEDROCK STREAMS

Longitudinal Profile Evolution

The longitudinal profile (commonly shortened to "long profile") of a river is a simple plot of river length with respect to elevation above base level at the river's mouth. Two profiles are commonly considered: the longer, "channel" profile, where river length is measured along the channel thalweg, and the shorter, "valley-bottom" profile, where elevation of the valley bottom, typically denoted by the constructional top of a floodplain, is projected to a vertical plane oriented along the valley axis (Figure 1). The valley long profile represents a preferred frame of reference that lends itself well to comparisons between the valley bottom and fluvial terraces. This paper implicitly refers to valley-bottom long profiles in all subsequent discussion.

The progressive decrease in slope downstream, resulting in the characteristic concave-up shape of long profiles, reflects both the downstream increase in discharge and decrease in mean grain size [*Leopold et al.,* 1964] (Figure 2a). Concave-up long profiles commonly are associated with a river in the "graded" condition; however, the necessary and sufficient conditions for grade do not imply any characteristic longitudinal form [*Snow and Slingerland,* 1987; *c.f. Ohmori,* 1991; *Sinha and Parker,* 1996] and it will be important for our subsequent analyses to establish that long profiles of diverse shapes can be maintained over graded (10^5) time scales [*Schumm and Licthy,* 1965].

A graded river long profile is described as one where, for a given discharge, reach slopes are delicately adjusted so that they can effectively transport all of the sediment delivered from valley hillslopes [*Gilbert,* 1877; *Mackin,* 1948] (Figure 2a). A graded river is at capacity and neither aggrades nor incises [*Leopold and Bull,* 1979] with respect to a fixed datum [*Knox,* 1975]. Rather, it attains and maintains an individually unique shape [*Knox,* 1975] under steady, uniform boundary conditions, that is everywhere at its base level of erosion [*Bull,* 1991]. The concept of grade is crucial to our interpretation of bedrock fluvial incision; unfortunately, current understanding of the graded condition and the role it plays in terrace genesis is largely restricted to alluvial streams. The delicate adjustment of slope along a given reach of alluvial channel is a hydraulic geometry response [*Leopold and Maddock,* 1953] that generates the critical shear stress on the bed needed to transport bedload sediment [*Bull,* 1979]. Although not devoid of alluvium or predominantly alluvial reaches, bedrock stream channels are by definition under capacity, so reach slopes are not delicately adjusted primarily by the amount and caliber of sediment to be transported. Rather the slopes of individual bedrock channel reaches must be delicately adjusted to generate bed shear stresses necessary to maintain the rates of incision (1) equal and opposite to variable rates of rock-uplift acting on the channel bottom [*Pazzaglia and Gardner,* 1993], and to a lesser extent, (2) across rock-types of variable erodibility [*Gardner,* 1983; *Miller,* 1991; *Wohl et al.,* 1994], while still (3) transporting the given flux of sediment provided from valley hillslopes.

An important and dynamic feedback exists between the rock-uplift-governed rate of bedrock fluvial incision and hillslope sediment flux to the channel [*Sklar et al.,* 1996;

Sklar and Dietrich, 1997, *Slingerland et al.*, 1997; *Sklar and Dietrich*, this volume]. Incision rates are maximized by an optimum sediment flux not so large that the channel bed is insulated from abrasion and plucking processes, and is not so low such that channel bed erosion processes are negligible. Active tectonic settings may be preconditioned to quickly achieve a balance between rates of bedrock channel incision and incision-limiting processes of sediment delivery from hillslopes because gravitational potential energy is rapidly converted to kinetic energy and work in these landscapes. In contrast, bedrock streams in tectonically stable settings are not predisposed to rapidly achieve a similar balance because of the limited distribution of high relief or high relief localized near incising channels. The delicate adjustment between rates of rock uplift and channel incision dictates that a graded bedrock channel will, over graded spatial and temporal time scales, horizontally sweep out a valley bottom of variable width determined by local changes in rock-type erodibility and sediment load (Figure 2b). Thus, well-understood alluvial channel hydraulic geometry relations such as the dependence of channel width on the square root of bankfull discharge [*Leopold and Maddock*, 1953] do not necessarily hold for graded bedrock channels.

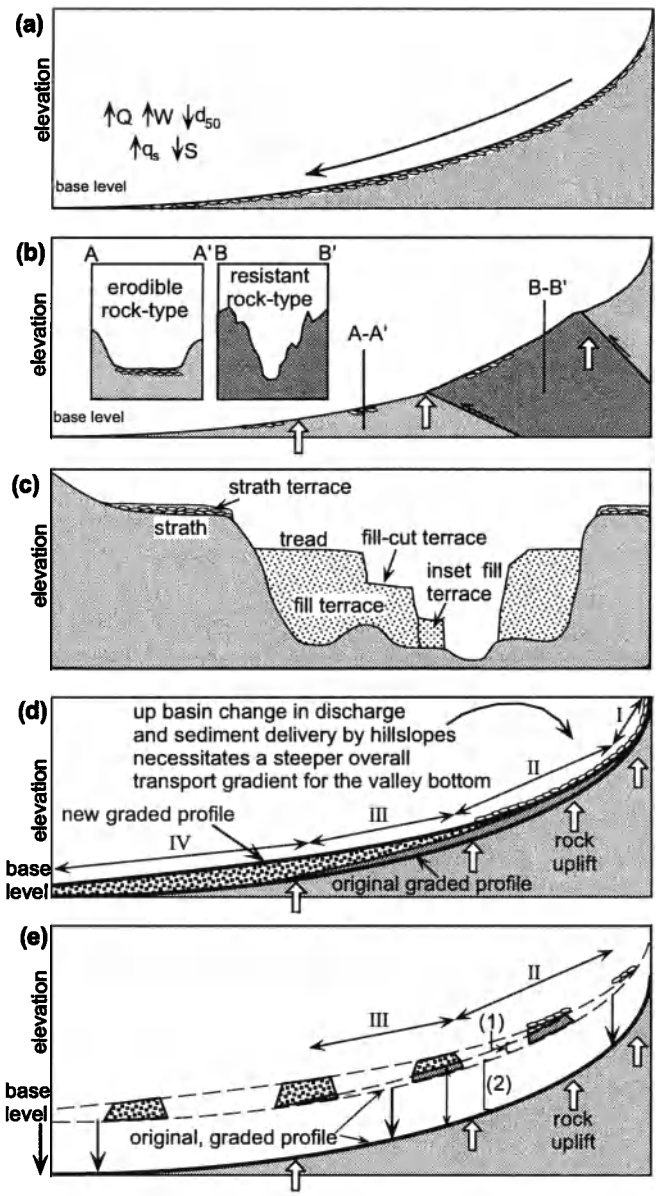

Figure 2. Concepts of bedrock channel graded profiles and terrace genesis (modified from Pazzaglia and Brandon, in prep). a) A graded profile for an alluvial stream [*Mackin*, 1948] develops the familiar concave-up longitudinal profile in part because discharge and slope are inversely proportional downstream. b) A similar graded profile shape can and does develop for bedrock streams; however, the reach slopes in this profile are delicately adjusted primarily to provide rates of incision equal and opposite to rates of rock-uplift through the channel (valley) bottom. Valley bottom widths respond to these rates of rock-uplift and incision and are adjusted locally to the amount of alluvium in the channel and variations in rock-type erodibility. c) A schematic valley cross section illustrating the major types of fluvial terraces [from *Bull*, 1991]. Straths are paleo-valley bottoms formed during former graded profile conditions. d) Temporal changes in overall graded profile concavity and reach-scale slope is dictated by changes in rates of rock uplift, down stream changes in base level, and/or upstream changes in basin-scale hydrology. This illustration considers an up basin increase in discharge and sediment load, and steady, uniform rates of rock uplift. Roman numerals refer to specific mechanisms operating along stream reaches during the hydrologic change where the long profile is not appreciably steepened (I), steepened primarily by a temporary slowing of the rate of vertical incision where the area between the new graded profile and original graded profile is "filled" by uplifted bedrock (II), steepened by a combination of reduced rates of vertical incision and valley aggradation (III), and steepened primarily by valley aggradation. e) Return of the "new" long profile to its "original" lower-gradient form during a subsequent interglacial portion of the glacial-interglacial climate cycle isolates a paleo-valley bottom (strath) in the valley wall. We assume here that alluvial valley fills can be rapidly incised as the streams reestablishes its "original" graded profile. Rock uplift passively carries the straths vertically where, if not removed by erosion, they are mapped as terraces. Note the thick dark arrows of identical length indicating the amount of fluvial incision. The vertical distance measured in the field between the strath and the current valley long profile (thin, dark, two-headed arrow) is a measure of (1) rock uplift during attainment of the "new" graded profile and (2) rock-uplift since the strath was preserved in the valley wall. The amount of incision attributed to (1) is restricted to zones II and III and should not be interpreted as a response to variable rates of rock uplift.

Fluvial Terrace Genesis

A river leaves a history of past long profiles in the form of fluvial terraces, preserved in the valley walls above the active valley bottom (Figure 2c). A fluvial terrace is a landform; the fluvial sands and gravels which constitute this landform are called terrace deposits. We define and use terrace deposits as allostratigraphic units, which are unconformity-bound, mappable stratigraphic units. The terrace deposit is bound at the base by an unconformity, typically cut into bedrock, called a strath. The terrace deposit top defines an unconformity with the surface called a tread. Fill terraces are formed by valley aggradation above a strath, followed by channel incision into the alluvium [*Bull,* 1991, *p. 8*]. In contrast, strath terraces are distinguished by a distinct strath basal unconformity, with thin overlying alluvial deposits. The cutting of a strath and deposition of the thin, overlying alluvial mantle occur simultaneously for a strath terrace (as long as that strath is not later reoccupied); however, a significant temporal difference (10^2 - 10^3 years) can exist between the strath and the tread of a fill terrace [*Weldon,* 1986]. This temporal difference represents the time during which the fill was deposited.

A bedrock river that has attained a graded long profile will laterally sweep out a valley bottom, whose width will be proportional to rock-type erodibility and rate of rock uplift. Narrow valley bottoms (Figure 2b, cross-section B-B') are favored by resistant rock-types and relatively rapid rates of vertical incision. In contrast, wide valley bottoms typically occur with erodible rock types (Figure 2b, cross-section A-A') and relatively slow rates of vertical incision. Paleo-valley bottoms, exposed by incision and fortuitously not removed by later lateral corrasion of the sweeping channel, may be preserved in the valley walls, resulting in unpaired [*Bull,* 1991, *p. 7*] strath terraces with little along-valley continuity [*Pazzaglia and Gardner,* 1993; *Merritts et al.,* 1994]. Basin-scale changes in fluvial system boundary conditions such as a down-basin base level fall [*Pazzaglia and Gardner,* 1994; *Merritts et al.,* 1994], hydrologic (climatic) effects [*Bull and Knuepfer,* 1987], and/or tectonics [*Merritts and Vincent,* 1989; *Willemin and Knuepfer,* 1994] usually compels a river to rapidly seek out a new, stable, graded configuration (Figure 2d), with the previous graded condition being preserved as commonly paired [*Bull,* 1991, *p. 8*] terraces that extend for significant distances along the river valley (Figure 2e).

Changes in discharge and sediment load are commonly occurring changes in fluvial system boundary conditions that introduce a transient response where the long profile transforms from an original graded condition to a new graded condition. For the glacial-interglacial climatic cycle changes illustrated in Figure 2d, consider that the "original" graded profile represents the interglacial portion of that cycle, while the "new" graded profile represents the late-glacial portion of the profile for a drainage basin in a tectonically active setting. Glacial-interglacial-like climate changes result in a stream initially adjusting its hydraulic geometry and channel patterns without adjusting the valley gradient [*Meyer et al.,* 1995]. In this way, valley bottoms (straths) are locally widened. Long profile gradients are adjusted as the stream attempts to accommodate and transport the increased sediment load only after all hydraulic geometry and channel pattern changes have been exhausted [*Schumm et al.,* 1987; *Harbor,* 1998]. The rate of fluvial bedrock incision is inversely proportional to increasing alluvial channel character because a channel at or above capacity will insulate the channel bed from erosive processes.

With these considerations in mind, we represent spatial variability in the fluvial system response by zones I through IV of Figure 2d. The channel is able to maintain a constant valley gradient and rate of incision in zone I where the valley gradient is very steep and the channel remains below capacity. Channel pattern changes may locally widen the valley bottom along this reach. An increasingly alluvial character in zone II initially widens the valley bottom, followed by a slowing in the rate of incision as the channel becomes increasing insulated. But the valley gradient is steep here and rock uplift quickly fills the accommodation space produced by the reduced rate of incision. The channel steepens beyond its original graded profile, increasing rates of incision and rapidly reaching a new graded mixed bedrock-alluvial valley bottom. As the valley gradient decreases downstream into zone III, rock uplift becomes less effective than alluviation at steepening the valley gradient. Vertical incision temporarily ceases as the channel falls below capacity. The elevation of the valley alluvial tread defines the new graded profile. The river continues as a pure alluvial stream through zone IV.

When a strath (paleo-valley bottom), independent of whether it underlies a fill or strath terrace, is preserved in the landscape (Figure 2e), it represents a datum with which to measure basin-scale rates of fluvial incision. Several studies have documented complex histories of strath cutting, reoccupation, and diachroneity [*reviewed in Bull,* 1991; *Merritts et al.,* 1994]. The important age for our purposes is when the channel incises below the strath, preserving it in the landscape (Figure 2e). The age of preservation closely follows the minimum age of the fluvial terrace deposits overlying the strath. We recognize that terrace treads themselves are diachronous, but in the most detailed study of dated terraces in a large basin [*Weldon,* 1986], the tread of a single terrace spanned no more than 9 k.y. We

will assume that the degree of diachroneity for a single terrace is small with respect to the time between major terraces. This assumption allows us to treat a terrace long profile essentially as a isochronous stratigraphic horizon from which magnitudes and rates of bedrock channel incision can be spatially reconstructed.

Stream Power Proportional Erosion Laws

Stream power (ω) is the time rate of conversion of potential gravitational energy into kinetic turbulent eddy energy by water flowing in the channel. Stream power is assumed to operate over a unit length of channel and is measured in watts (Nm/s) [*Bagnold,* 1960, 1966; *Kirkby,* 1971]:

$$\omega = \rho g Q S \qquad (1),$$

where ρ is the density of water (kg/m^3), g is the acceleration of gravity (m/s^2), Q is discharge (m^3/s), and S is local reach slope. The ability of a bedrock channel to incise its bed has been proposed to be proportional to the stream power per unit length raised to some power expended by the stream flow [*Howard and Kerby,* 1983; *Seidl and Dietrich,* 1992]:

$$-\frac{\partial z}{\partial t} = k(QS)^n \qquad (2),$$

where z is the incision of the channel below a datum, t is time, Q is discharge, S is the local reach slope, and k and n are empirically-parameterized constants. Discharge is commonly held to scale with basin area and equation 2 is recast into the more common form:

$$-\frac{\partial z}{\partial t} = kA^m S^n \qquad (3),$$

where m is also an empirically-parameterized constant. Constants m and n describe the incision processes and are typically taken to vary from 0.3 [*Howard and Kerby,* 1983; *Stock,* 1996] to 1.0 [*Seidl and Dietrich,* 1992, *Seidl et al.,* 1994] whereas k is a reflection of rock-type in the channel bottom and varies significantly over several orders of magnitude [*Stock,* 1996]. It should be noted that the incision law of equation 3 is a very general representation of bedrock stream behavior and can be used to interpret numerous fluvial behaviors [*L. Sklar,* personal communication]. For example, when discharge is proportional to drainage basin area and m/n = 1, the law predicts that incision is directly proportional to stream power per unit length. When channel width varies as a function of the square root of the discharge (alluvial streams only) and m/n = 0.5, equation 3 predicts that incision will be proportional to stream power per unit channel area. And when m/n = 4/7, equation 3 predicts that incision is proportional to average boundary shear stress [*Howard and Kerby,* 1983].

Previous studies which have investigated fluvial incision over geologic time scales in the context of a stream power incision law propose that there are three classes of bedrock channels: (1) those where basin area (discharge) plays an important role as incision increases downstream and the m/n ratio falls between 0.3 and 0.6; (2) those where basin area plays a negligible role in driving incision and the m/n ratio is less than 0.1; and (3) those where the stream power incision law is invalid because basin area is inversely proportional to incision as incision increases upstream [*Stock,* 1996; *Stock and Montgomery,* in press].

We wish to at least qualitatively evaluate the recent heightened interest in the stream power proportional rates of bedrock incision with our fluvial terrace data. For one of our investigated rivers, the Clearwater River in Washington State, a discharge - area functional relationship [*Wegmann,* unpublished data] has been developed by in-field measurements of flow at five surveyed cross sections:

$$Q = aA^b \qquad (4),$$

where Q is discharge (m^3/s), A is drainage area (km^2), and a and b are constants determined by a best fit regression. The data are best and most simply explained by a linear functional relationship (b=1) between discharge and area where a is 0.051 during base flow conditions and 2.24 during decadal-scale flood conditions.

A detailed one-dimensional profile of stream power distribution can be constructed with equation (1) by measuring long profile reach slope from topographic maps and determining discharge across that reach. This approach offers an alternative to locally parameterizing k, n, and m of equations 2 and 3 and is a more direct representation of the forces acting on the bed of the bedrock channel. When stream power is considered to act across the width of the channel, rather than per unit channel length, and Q is represented as the product of mean channel width, depth and velocity, it can be expressed as

$$\omega = \tau_0 \overline{U} \qquad (5),$$

where τ_0 is shear stress on the bed (N/m) and $\overline{U}$ is mean velocity (m/s).

It is a well known hydraulic geometry relationship of alluvial channels that mean channel width ($\overline{W}$) increases downstream as the square root of the discharge [*Leopold and Maddock,* 1953]:

$$\overline{W} = \sqrt{Q} \qquad (6).$$

Unfortunately, no simple functional relationship between discharge and channel width exists for bedrock channels or even mixed bedrock-alluvial channels. Furthermore, consideration of stream power across the width of the active channel only, while hydraulically valid, ignores the longer-term area affected by channel erosion processes represented by the valley bottom. We wish to capture the cumulative effect of instantaneous discharges over the temporal and spatial scales represented by the lateral carving out of a valley bottom and terrace genesis. This is most easily accomplished by normalizing measured values of instantaneous stream power (ω_n) using equations (1) and (4) to the ratio of valley bottom width (W_v) to width of the bankfull channel (W_c):

$$\omega_n = \omega / \left(\frac{W_v}{W_c} \right) \qquad (7).$$

The valley bottom width is the width of the active floodplain defined by the distinct topographic slope break between the flat floodplain and valley wall hillslopes. The normalized stream power retains units of Nm/s and should reflect the stream's long-term adjustment to rock-type, rates of rock uplift, and bedload transport expressed in terms of a proxy for instantaneous stream power. We envision the lateral corrasion of the valley bottom to proceed primarily by channel migration processes [*Crickmay,* 1960; *Yoxall,* 1969]. Brief occupation of the entire valley bottom by large magnitude flood events is not viewed as the dominant mechanism for valley bottom widening or lateral corrasion as shear stresses on the bed would be greatly diminished for flow outside of the main channel (see equation 5).

LONG PROFILES, TERRACES, AND INCISION RATES

Susquehanna River and related passive margin streams

The long profiles of streams that drain the U.S. Atlantic and Gulf passive margins (Figure 3, Table 1) provide useful comparisons for the influences of climate and rock-type for drainage basins of similar size that have experienced similar rock-uplift and base level (eustatic) changes through the late Cenozoic. Long profiles from four streams on the Atlantic margin, the Susquehanna, Potomac, Rappahannock, and James Rivers all show distinct convexities, especially along their downstream reaches where they traverse resistant rock-types in the vicinity of the Fall Zone (Figure 4a). In contrast, three drainage basins in Texas, the Colorado River, Rio Guadalupe, and Rio Nueces are decidedly concave, exhibiting only minor gradient convexity where they flow across the Balcones Escarpment which is supported by resistant rock-types in the upstream direction (Figure 4b). Miocene fluvial deposits preserved on the high-standing interfluves of the Fall Zone and Balcones Escarpment qualitatively indicate that all of these passive margin streams have experienced an increase in their downstream rates of fluvial incision during the late Cenozoic.

The largest river on the Atlantic slope, the Susquehanna River, drains some 62,000 km^2 of the Appalachian mountains and Piedmont (Table 1, Figure 3) and is the only drainage for which we have detailed long-term incision data. The Susquehanna river developed as the primary east-flowing drainage during Mesozoic rifting of the Atlantic margin [*Judson,* 1975]. Its post-rift evolution has been dominated by a relatively stable, passive margin tectonic setting, punctuated perhaps by four increases in rates of rock uplift by epeirogenic mechanisms [*Pazzaglia and Brandon,* 1996]. Basin-wide climate is humid-temperate with about 100 cm of annual precipitation, which probably is a reasonable representation of the long-term climate throughout the Cenozoic [*Barron,* 1989] with the exception of relatively cooler glacial and relatively warmer interglacial periods over the past ~2.5 Ma.

The river's headwaters rise at the continental divide on the Allegheny Plateau and feed a trunk stream which has impressive, incised bedrock reaches at Ridge and Valley water gaps. Between the Ridge and Valley and river mouth at the head of Chesapeake Bay, the valley bottom contains a nearly pure bedrock channel, 0.5 to 1 km wide, incised as much as a 250 m into high-grade, but pervasively fractured and jointed, metamorphic rocks of the Appalachian Piedmont. The bedrock channel rises abruptly from sea level onto the Fall Zone, a region of locally steep stream gradients where resistant rock-types of the Piedmont are flexed downward beneath the erodible rocks of the Coastal Plain [*Pazzaglia and Gardner,* 1994, 1998] (Figures 3, and 4a).

A steep valley gradient and overall long profile convexity are maintained along the lower 250 km of river stretching from the Fall Zone through the Ridge and Valley (Figure 4a). Observed processes of bedrock channel erosion in the convex reach are dominated by plucking and pothole coalescence and collapse. Potholes preferentially develop at the intersection of a NE-striking, steeply-dipping foliation

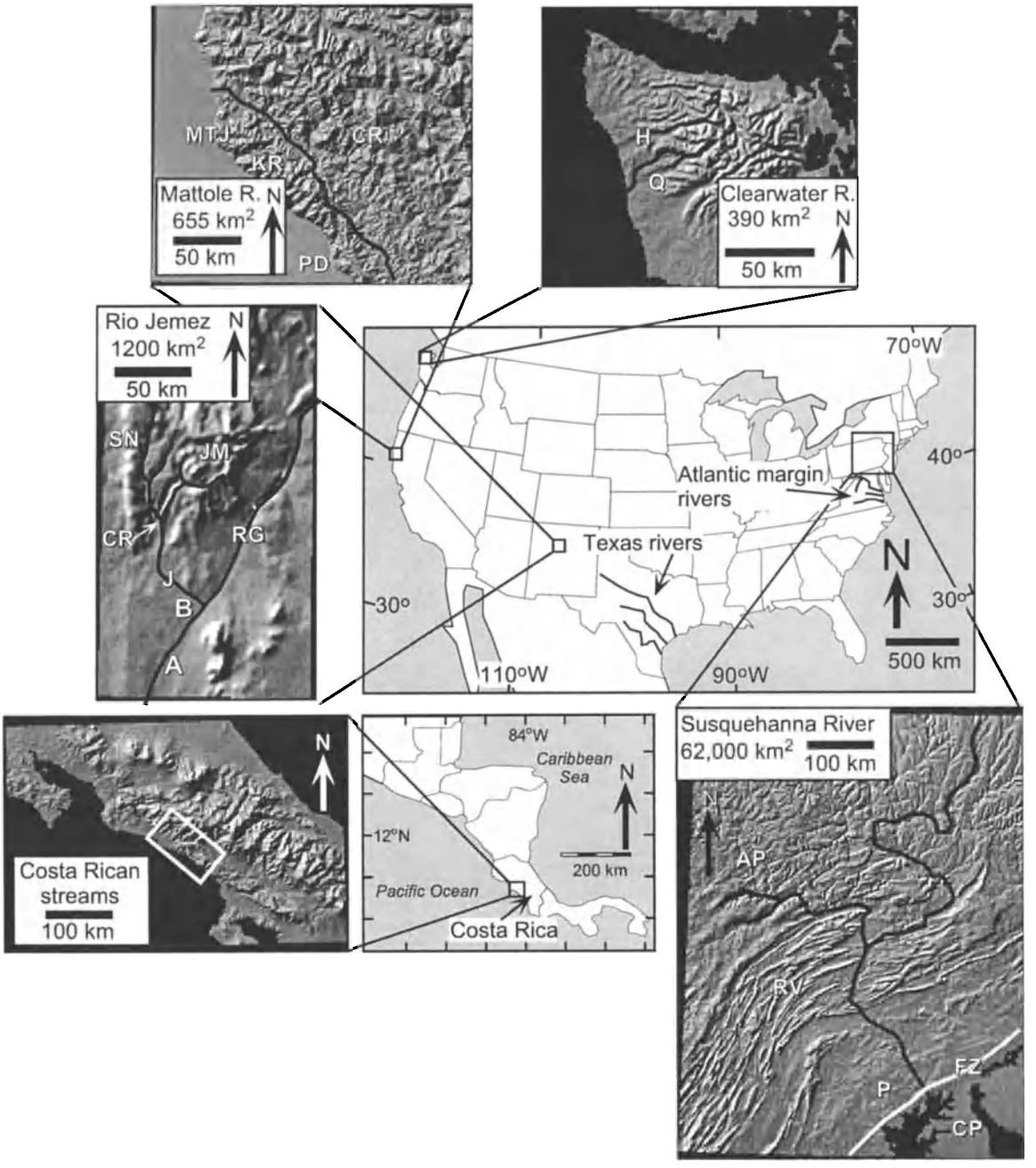

Figure 3. Location of rivers cited in this paper and their topographic settings. Abbreviations for inset maps: Susquehanna – FZ=Fall Zone, CP=Coastal Plain, P=Piedmont, RV=Ridge and Valley, AP=Allegheny Plateau; Rio Jemez – A=Albuquerque, CR=confluence reach, J=Rio Jemez, RG=Rio Grande, JM=Jemez Mountains B=Bernalillo, SN = Sierra Nacimiento; Mattole – KR=King Range, CR=Coast Range, MTJ=Mendocino Triple Junction, PD=Point Delgada; Clearwater – H=Hoh River basin, Q=Queets River basin. From north to south respectively, the Atlantic margin rivers shown are the Potomac, Rappahannock, and James. From north to south respectively, the Texas rivers shown are the Colorado, Guadalupe, and Nueces.

Table 1. Summary of drainage basin characteristics and rates of fluvial incision of bedrock channels.

River	Rock-type	Precip-itation (cm/yr) [a]	Drainage area (km^2)	Q / Q_p at mouth (m^3/s) [b]	Q / Q_p per unit area (m^3/s / km^2)	Rate of rock uplift [c] (m/ka)	Profile shape	Rate of chan-nel incision (m/ka)
Susquehanna			62,000	1025 / 9900	0.016 / 0.16		convex	
upstream	carb./schist	100				~ $1*10^{-2}$		$6*10^{-3}$
middle	schist/gneiss	100				~ $5*10^{-3}$		$1.2*10^{-2}$
downstream	schist/gneiss	100				< $5*10^{-3}$		$7*10^{-3}$
Jemez		20 - 30	1,200	2.25 / 51 [d]	0.002 / 0.04		straight to	
middle	sandstone					0.15 - 0.2	concave	0.17
Clearwater		150	390	- / 600	- / 1.54		concave	
upstream	sandstone					0.9		0.8
middle	siltstone					0.6		0.4
downstream	sandstone					0.1		0.1
Mattole		100	655	36 / 1100 [e]	0.05 / 1.68		straight to	
upstream	mixed sed.					~2 - 4	concave	0.7 - 1.8
downstream	mixed sed.					2 - 4		~2
Rio Aranjuez	volcanics	~200	210	- / -	- / -		strongly	
upstream						~0.5	concave	0.1
downstream						~0.5		0.7
Rio Barranca	volcanics	~250	470	- / -	- / -		strongly	
upstream						~1.5	concave	1.1
downstream						~1.5		0.5
Rio Narajno	forearc clas-tics	~350	270	- / -	- / -		strongly concave	
upstream						~2.5		0.5
downstream						~2.5		0.2
Texas Streams								
Colorado	carb./coastal Plain seds	variable ~ 75	109,885	84 / 673 [f]	0.0008/0.006	-	concave w/ knickpoint	-
Guadalupe	carb./coastal Plain seds	variable ~ 75	13,522	59 / 696 [f]	0.004 / 0.05[g]	-	concave	-
Nueces	carb./coastal Plain seds	variable ~ 75	43,340	22 / 605 [h]	0.0005/0.014	-	concave	-

Notes:

a = representative basin-wide average

b = mean annual discharge (mean of daily discharge records over entire period of record) and peak annual discharge (Q_p, annual peaks only) compiled from 1980-1997 gage data.

c = rates of rock uplift are inferred from geologic and modeling data other than fluvial incision including regional rates of rock ex-humation (fission track thermochronology), regional stratigraphic relationships, and geodynamic models.

d = more representative measure at Jemez Pueblo gage, not at mouth.

e = gage located at Petrolia, CA, 4 km upstream from mouth.

f = Q_p is storm-cell size-limited

g = The Rio Guadalupe has a huge subsurface drainage that far exceeds the surface divides. This subsurface drainage likely contrib-utes to the large peak discharge per unit area.

h = represents 1950-1980 data as 1980-1997 data is unavailable or incomplete.

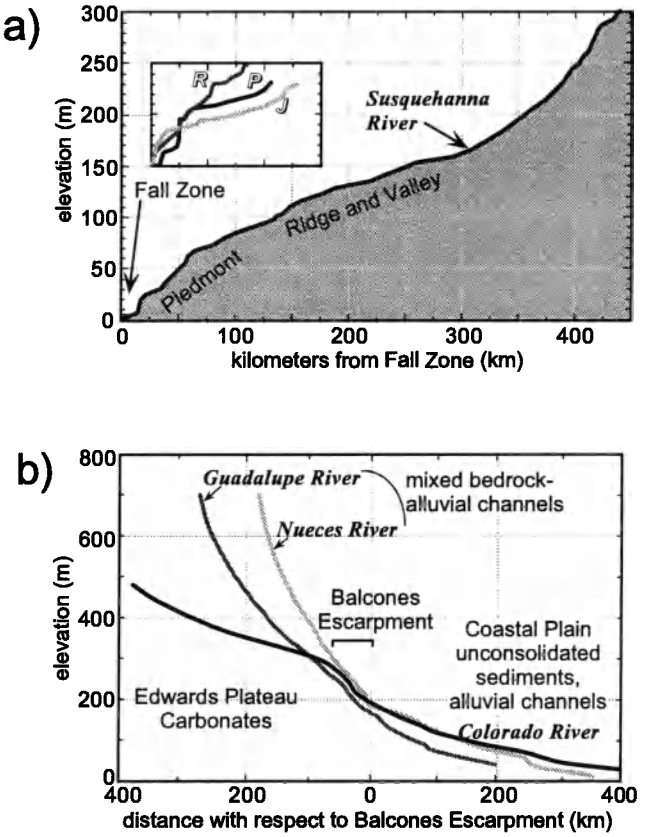

Figure 4. a) Longitudinal profile of the Susquehanna River (following the west branch; modified from *Pazzaglia and Gardner*, [1993]). Note the broad convexity stretched out over 250 km of the lower half of the profile and the very steep lower 60 km of the profile where the river crosses resistant rock-types of the Appalachian Piedmont. For comparison purposes, the lower 150 km of the Potomac (P), Rappahannock (R), and James (J) river profiles are plotted at the same scale in the inset box. b) Long profiles of three streams of variable size in central Texas that cross the Balcones Escarpment. Profiles have been adjusted to plot in terms of distance with respect to the Balcones Escarpment at San Antonio.

and NNW-striking joint set and bore into the bedrock at an inclined angle upstream [*Thompson,* 1990]. Potholes are well preserved along bedrock valley walls high above the active channel indicating the longevity of this bedrock channel erosion process.

The most spectacular geomorphic feature of the lower Susquehanna channel is the presence of six known channel "deeps" [*Mathews,* 1917]. First discovered during dam construction in the early 20th century, the deeps are separate, non-integrated, elongated, spoon-shaped excavations of the channel bottom confined to the eastern margin of the gorge. Walls of the deeps are intensely potholed and their floors locally reach up to 40 m below the current channel bottom, which is below sea level for deeps at or downstream of long profile km 40 (Figure 4a). The stream reach characterized by the deeps strongly resembles a scabland-like topography with numerous anastomosing bedrock channels and flat-topped, potholed bedrock islands [*Baker and Komar,* 1987].

Fluvial terraces of the lower Susquehanna River consist of strath remnants mantled with cobble and pebble lags. At least four late Cenozoic terraces have been identified, mapped, and correlated [*Pazzaglia and Gardner,* 1993]. Terrace ages, constrained by downstream petrographic correlation to well-dated Coastal Plain deposits [*Pazzaglia,* 1993], range from 15 m.y. for Tg1 to 2.5 m.y. for QTg (Figure 5a). Terraces are inferred to have been formed during periods of relative base level stability and valley-bottom widening, coincident with deposition of thick accumulations of fluvial gravel on the Fall Zone during downstream eustatic rise and highstands [*Pazzaglia and Gardner,* 1993]. Terraces have reconstructed long profiles that are steeper and more convex than the modern Susquehanna River channel, especially near the Fall Zone. Fluvial incision to make the Holtwood gorge since the middle Miocene (post Tg1) has been driven by long-term base level lowering, a combination of protracted post middle Miocene eustatic fall and flexural upwarping of the Piedmont [*Pazzaglia and Gardner,* 1994, 1998]. Average rates of fluvial incision, estimated from the terrace ages and elevations, range from approximately $7*10^{-3}$ m/ka at the river mouth, to $1.2*10^{-2}$ m/ka through Holtwood gorge, to $6*10^{-3}$ m/ka just downstream of Harrisburg (Figure 5b). Generally, rates of incision have accelerated through time, especially near the river mouth and in the Holtwood gorge area.

Rio Jemez

The Rio Jemez of north-central New Mexico rises in the Jemez Mountains and Sierra Nacimiento and flows south and southeast to its confluence with the Rio Grande at Bernalillo (Figures 3 and 6). The Jemez basin covers a total of 2690 km^2, but our study focuses on a reach near the confluence of the Rio Jemez and Rio Guadalupe, herein referred to as the confluence reach, (Figures 3 and 6), which drains approximately 1200 km^2. Basin climate varies as a function of elevation. Headwaters of the Rio Jemez, which lie above 2700 m, receive up to 80 cm of annual precipitation whereas elevations below 1650 m receive only about 30 cm. This climatic gradient results in a fluvial system with a perennial upper portion and ephemeral lower portion during dry years. The confluence reach lies in a structural saddle defined by the western margin of the Rio Grande rift between the Sierra Nacimiento uplift to the west and the

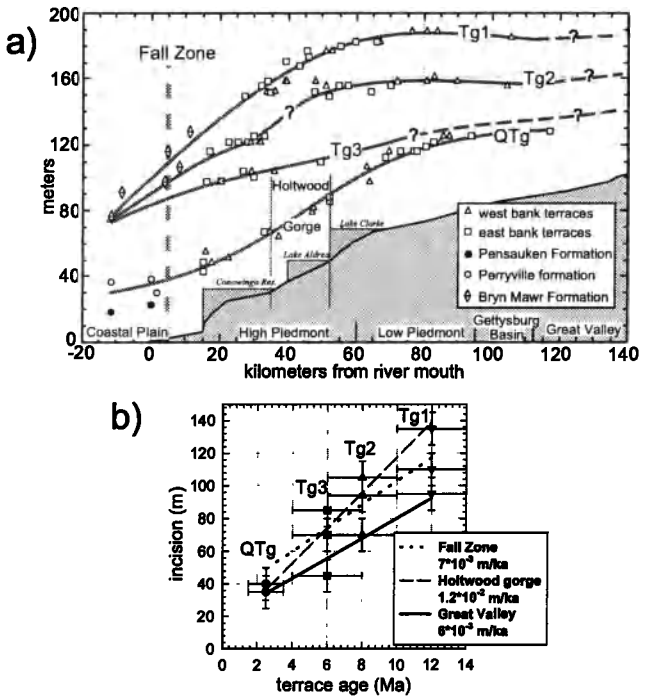

Figure 5. a) Long profile and terrace long profiles of the Susquehanna River below Harrisburg. Terrace ages are based on downstream petrographic elevation correlation to dated Fall Zone and Coastal Plain deposits. b) Incision and incision rates determined by terraces at three different localities along the lower reach of the Susquehanna River.

Jemez volcanic complex to the east. Recent exhumation of the Sierra Nacimiento mountain front [*Formento-Trigilio and Pazzaglia,* 1996, in press; *Pazzaglia and Kelley,* in press] and related volcanic plugs in the San Juan basin [*Hallett,* 1994; *Hallett et al.,* 1997] attest to late Cenozoic epeirogenic uplift of the Rio Jemez drainage. Although mapped [*Formento-Trigilio,* 1997; *Pazzaglia et al.,* 1998], active Quaternary faults represent a subordinate process in local rock uplift and do not play an important role in local or regional base level considerations for the Rio Jemez.

The overall concave long profile of the Rio Jemez noticeably straightens through the confluence reach and at least two distinct knickpoints (kp 1 and 2) are located where the river crosses mapped faults (Figure 6a). The confluence reach has a mixed alluvial - bedrock channel with well developed pools and riffles in the alluvial portions. Alluvium thickness in the valley bottom does not exceed 3 m and the channel bed is effectively scoured to bedrock during discharges which completely mobilize the alluvial bedload. Immediately downstream of the confluence reach, the valley bottom alluvium thickens significantly to about 30 m and the stream becomes alluvial in character. In the confluence reach, the valley bottom is approximately 0.5 km wide and incised into nearly horizontal beds of Permian sandstone, siltstone, and shale of variable erodibility. Valley walls begin at the valley bottom as relatively gentle slopes where underlain by the Permian sediments, but abruptly steepen to nearly vertical faces where the Quaternary Bandelier tuff acts as a caprock. Total valley depth from the top of the Bandelier Tuff to the valley bottom is approximately 300 m. Observed processes of bedrock channel erosion include plucking and slab-quarrying of resistant sandstones. Less resistant shales often underlie pools. The formation of potholes appears not to be an important mechanism in the erosion of the channel bed as compared to the Susquehanna River channel.

Four major fluvial terraces (Qt1 through Qt4) and river alluvium buried beneath the Bandelier Tuff (Qg) are well

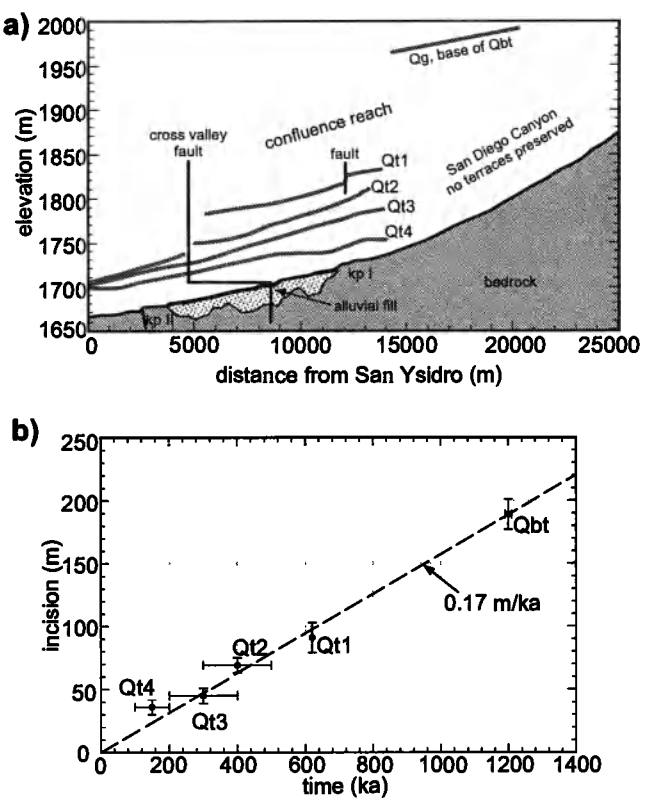

Figure 6. a) Rio Jemez and terrace long profiles along the confluence reach (modified from Formento-Trigilio and Pazzaglia, 1998). Note locations of knickpoints (kp) along the Rio Jemez long profile. b) Incision and rates of incision for the Rio Jemez determined by fluvial terraces at the head (upstream) portion of the confluence reach. Qbt = Bandelier Tuff. Best linear fit, long-term rate of incision is 0.17 m/ka.

preserved and mapped [*Rogers,* 1994, 1996; *Rogers and Smartt,* 1996; *Formento-Trigilio,* 1996; *Formento-Trigilio and Pazzaglia,* in press] through the confluence reach. The terraces have relatively smooth straths of low relief which are buried by up to 15 m of well stratified and sorted sandy gravel alluvium. The terrace deposits have a distinct coarse gravel base, overlain by a fine sandy middle, which in turn is overlain by a coarse gravelly top [*Rogers,* 1996; *Rogers and Smartt,* 1996]. Terrace long profiles generally are parallel to the modern valley profile (Figure 6a). Farther upstream where terraces are not preserved, the base of the 1.2 Ma Bandelier Tuff maintains a more or less constant vertical separation above the modern channel which argues for uniform rates of incision right up into the Rio Jemez headwaters.

Age control is well established for the Rio Jemez terraces. River gravels preserved beneath the 1.2 Ma Bandelier Tuff (Qg) demonstrate that a paleo-river valley bottom was buried by the welded tuff. The fine grained facies of Qt1 contains Lava Creek B (Yellowstone) ash dated at 0.602±0.004 Ma [*Gansecki et al.,* 1998]. Quartz sand grains embedded in travertine interbedded with Qt3 have been dated between 0.315 - 0.180 Ma by ESR (electron spin resonance) technique [S. Ikeda, University of Osaka, Japan, unpublished data]. The modern valley bottom floodplain has been dated in several locations using ^{14}C as late Holocene [*Formento-Trigilio,* 1997]. These numeric ages have been used to calibrate an amino acid racemization chronology for the remaining terrace deposits determined from fossil gastropods preserved in the terrace fine grained facies [*Rogers,* 1996; *Rogers and Smartt,* 1996]. A plot of terrace strath elevation above the modern valley bottom with respect to numeric or calibrated terrace age reveals a nearly linear rate of fluvial bedrock incision of 0.17 m/ka (Figure 6b). For comparative purposes, rates of regional exhumation based on stratigraphic reconstructions of the volume of rock removed from the Sierra Nacimiento front [*Formento-Trigilio and Pazzaglia,* in press] and fission track thermochronology [*Pazzaglia and Kelley,* in press] range from 0.15 to 0.2 m/ka.

Clearwater River

The Clearwater River is located on the western slope of the Olympic Mountains of Washington State, draining some 390 km^2 between the larger Hoh and Queets rivers (Figures 3 and 7). Basin elevations range from about 12 m at the river mouth to about 1130 m along its eastern divide. West flowing streams in the Olympic Mountains, including the Clearwater River, are incised into the leading edge of a subaerially exposed, and rapidly uplifting accretionary prism [*Brandon and Calderwood,* 1990; *Brandon and Vance,* 1992; *Brandon et al.,* 1998] which has peeled back forearc rocks and exposed the immature sedimentary rocks of the subduction complex. As a result, a rather homogeneous assemblage of medium to coarse grained sandstone of the Hoh Formation and related undifferentiated sedimentary rocks of the Western Olympic Lithic Assemblage underlies most of the basin [*Tabor and Cady,* 1978]. Lesser amounts of siltstone, mudstone, conglomerate, breccia, and basalt are also present. The Clearwater drainage is a somewhat unusual for the Olympic Peninsula in that it was not extensively glaciated in the Pleistocene [*c.f. Heusser,* 1974; *Rau,* 1973; *Thackray and Pazzaglia,* 1994]. The drainage receives approximately 200 cm of precipitation annually.

The Clearwater River is a mixed alluvial-bedrock stream. The river has a predominant alluvial character as it meanders through a 1 to 2 km-wide, low relief valley for its lower 30 km (Figure 7a). Nowhere has the alluvium been observed to be more than 2-3 m thick and alluvial reaches are interspersed with reaches where bedrock is exposed in the channel bottom. Average valley gradient along the alluvial reach is 0.0033 with a sinuosity (P) of 1.66. Meander loops exhibit abrupt angles consistent with a structural and/or rock-type control. From approximately long profile km 30 upstream to the divide, the valley gradient steepens to 0.0167, and the channel has a coincident drop in sinuosity to 1.15 as it flows primarily on bedrock (Figure 7a). Here, bedrock step-pools in 30 m wide valley bottoms predominate with lesser amounts of short alluvial reaches where the valley bottom tends to widen to approximately 100 m. Bedrock vs. alluvial reaches appear to be strongly influenced by rock-type. Relatively resistant sandstone beds are coincident with narrow valley bottoms and local gorges. Relatively erodible fractured and thinly bedded siltstones and shales commonly underlie wider valley bottoms. In both cases, the channel tends to be flat bottomed and noticeably lacking in potholes. Abrasion by a coarse bedload appears to be the primary process of channel erosion.

Overall, the Clearwater river exhibits a strongly concave longitudinal profile (Figure 7a) that follows an exponential function [*Ohmori,* 1991], with distinct knickpoints at profile kilometers 25, 40, and 46 (Figure 7a). A low, 2-km wide saddle separates the Clearwater drainage from the Hoh drainage at profile km 25. This low divide with the extensively glaciated Hoh valley has played an important role in the past as a point source and outlet via the lower Clearwater basin for glacio-fluvial outwash.

Fluvial terraces along the Clearwater River include six (Qt1 through Qt6) fill and strath terraces ranging from 1 to 120 meters above the modern valley bottom (Figure 7a). Paired fill terraces occur primarily along the lower reaches

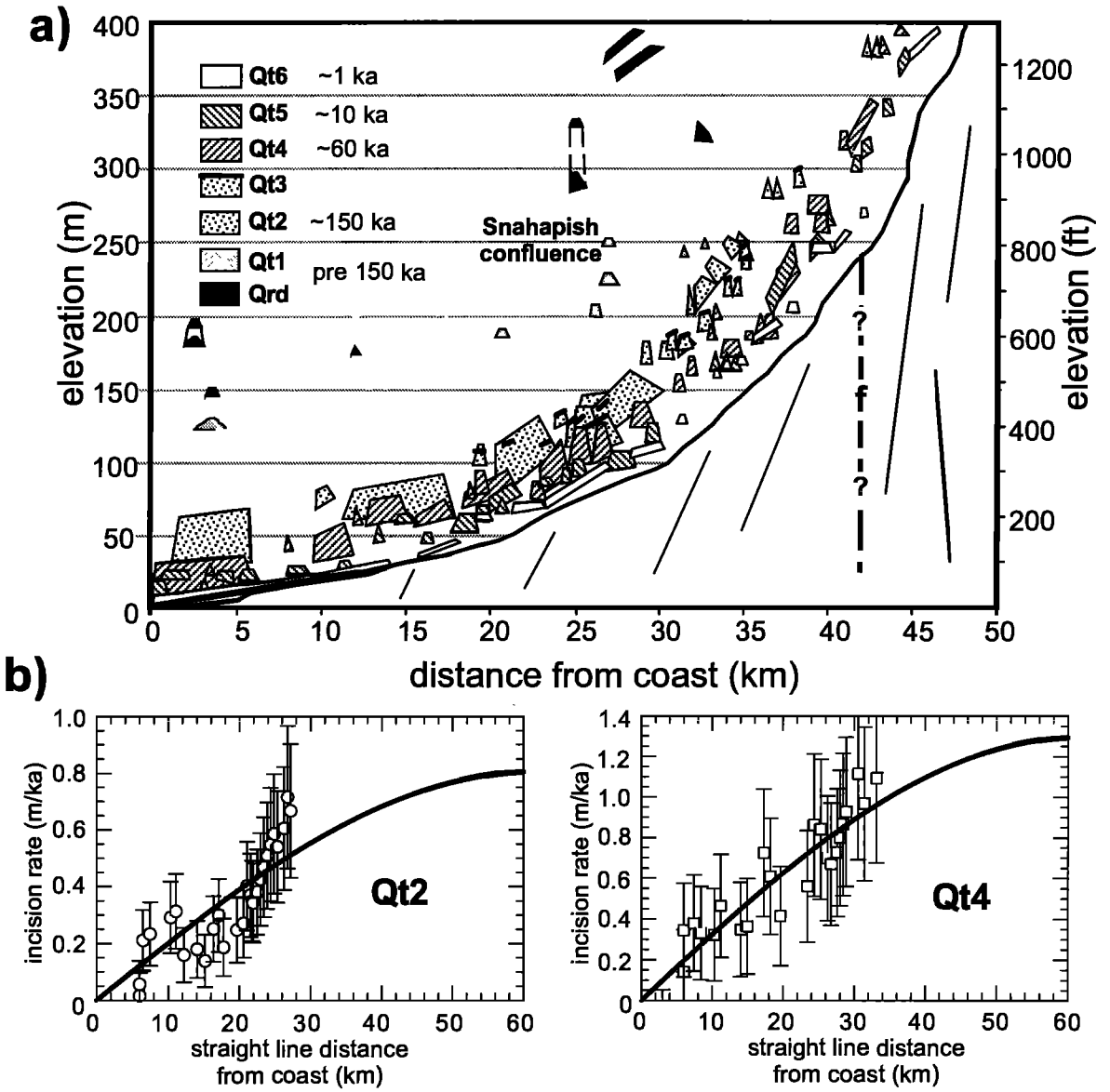

Figure 7. a) Clearwater River and terrace long profiles (modified from Pazzaglia and Brandon, [in prep.]). b) Rates of fluvial incision for the Clearwater River determined by terraces Qt2 and Qt4. Note the distribution in rates of incision varying from 0.1 m/ka at the coast (0 km) to ~1 m/ka 30 km towards the center of the Olympic peninsula (60 km). Incision rate curves depicted on both the Qt2 and Qt4 graph is a sine curve, the amplitude of which is constrained by the terrace incision rates. A sine curve fit to the data is used to capture the first-order, generally domal shape of rock uplift across the Olympic Peninsula.

of the Clearwater basin. These terraces have straths typically within 20 m (60 ft) of the present channel that are mantled with 5 - 40 m (20 - 120 ft) thick deposits of stratified sand and gravel. Locally, the fill terrace deposit buries paleotopography and valley side slopes adjacent to the strath. The upper Clearwater valley shows a strong contrast to the lower valley with strath terraces cut into both an inner, narrow, V-shaped gorge and outer, parabolic-shaped valley. Locally, pediment gravels and thin alluvial fan deposits mantle outer valley slopes and grade into the highest strath terraces which lie at the break in slope between the outer and inner valleys. In contrast to the lower portion of

the basin, upper basin strath terraces form flights of locally unpaired treads which step down to the modern stream.

Terrace ages (Figures 7a-7b) are constrained by limited radiocarbon numeric age data collected from the terrace deposits, and by physical correlation to dated glacio-fluvial and glacial deposits in adjacent basins and at the coast [*Crandell,* 1964, 1965; *Huesser,* 1964, 1972, 1973, 1974, 1978; *Florer,* 1972; *Easterbrook,* 1986; *Saunders et al.,* 1987; *Thackray and Pazzaglia,* 1994; *Thackray,* 1996] using relative weathering data [*Pazzaglia and Brandon,* unpublished data]. We use ages for Qt2 (approximately 150 ka) and Qt4 (approximately 60 ka) to calculate rates of incision. These terraces indicate rates of fluvial incision ranging from less than 0.1 m/ka along the lower, alluvial-dominated reach to about 1 m/ka in the upper, bedrock-dominated reach (Figure 7b).

Distribution of Stream Power along the Clearwater River. Measured discharge at five surveyed trunk-channel cross-sections in the Clearwater basin show a linear relationship (following from equation 4) between near base flow discharge (Q_{bf}) and basin area (A) of $Q_{bf} = 0.051A$. A well-preserved debris line resulting from a March 17th (St. Patrick's Day) flood of 1997 provided an opportunistic measure of the wetted perimeter during a decadal-scale flood. Discharge was estimated at the measured cross-sections with the Manning equation,

$$\overline{U} = \frac{1}{n} R^{2/3} S^{1/2} \qquad (8),$$

where n is Mannings roughness, parameterized as 0.06, R is hydraulic radius (m) and S is slope. As with the near base flow discharge, the decadal-scale discharge (Q_f) shows a linear relationship to basin area where $Q_f = 2.24A$. These linear relationships between discharge and drainage area are similar to those reported for instrumented Japanese Rivers [*Sugai,* 1993]. Using the discharge-area relationships, valley gradient determined from the long profile (Figure 8a) and equation 1, it is straight forward to calculate stream power per unit valley length for the Clearwater trunk stream.

Similarly, a normalized stream power per unit valley length (w_n) can be calculated from equation (7) using channel and valley widths (Figure 8b) obtained from in field surveys, topographic maps, and large-scale airphotos. The correlation between channel width and valley bottom width (Figure 8b) supports our assumption that the width of the valley bottom is a cumulative, long-term manifestation of the instantaneous stream power generated within the confines of the channel. Generally, the channel and valley bottom are wider in the predominantly alluvial reach of the Clearwater River.

We plot stream power per unit valley length for the Clearwater River using gradients determined by adjacent contours on a topographic map (Figure 8c, open circles) and gradients averaged over 1-km long valley reaches, also

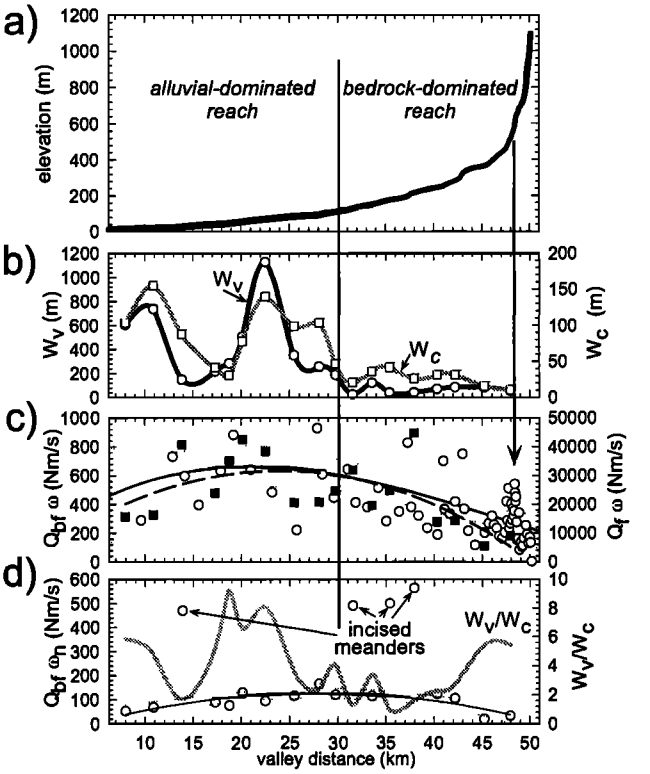

Figure 8. Distribution of stream power and stream power normalized to valley width for the Clearwater River. All stream power data generated from discharge-basin area and area-length curves (Wegmann, unpublished data) constructed for measured near-base flow discharge (Q_{bf}), and calculated decadal-scale flood discharge conditions (Q_f). a) Long profile of the Clearwater River for reference. b) Plots of the width of the valley bottom (W_V, solid black line and circle data points) and width of the bankfull channel (W_C solid gray line and square data points). c) Distribution of stream power based on the field-measured discharge-area relationship. The left axis scales stream power for near base flow discharge conditions. The right axis scales stream power for the decadal flood discharge conditions. Circle data points on the stream power graph represent a stream power value generated for stream reaches between adjacent contour lines on the 1:24,000 scale topographic maps. Square data points on the stream power graph represent values constructed from channel slopes averaged over 1 km-long reaches. The solid line is a second-order polynomial regression fit to the circle data points. Dotted lines are the 2-sigma error on the regression. The dashed line is a second-order polynomial regression fit to the square data points. Standard error in all plotted data falls within the width of the data point symbols. Arrow points out a "spike" in stream power attributed to a prominent knickpoint in long profile. d) The stream power values of square data points in (c) normalized by the valley width-channel width ratio. Note the four data outliers in this plot that correspond to known locations of resistant bedrock in the valley bottom.

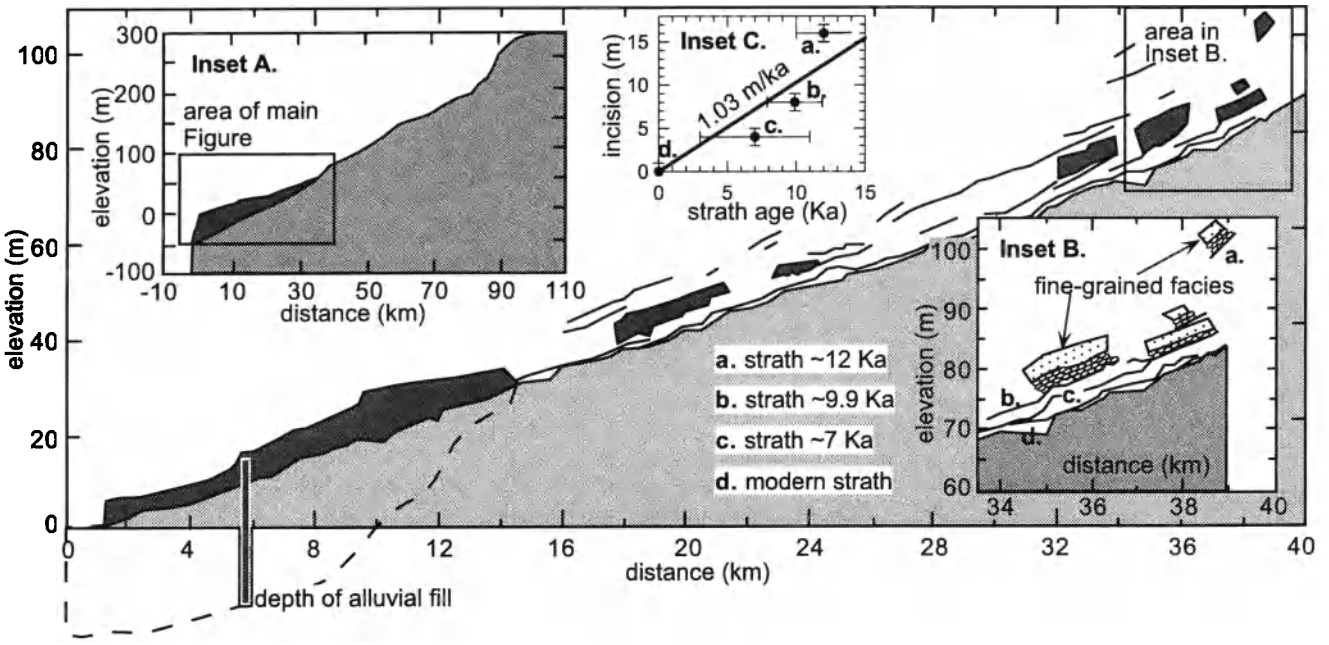

Figure 9. Mattole River and terrace long profiles (main figure). Inset A) Long profile of the Mattole River. Darkest shading indicates the thickness of alluvial fill in the lower Mattole valley. Inset B) Enlargement of the long profile and terrace long profiles between kilometer 34 and 40. Rates of incision for this reach are shown in Inset C.

determined from topographic map contours (Figure 8c, filled squares). Simple second-order polynomial curves fit to the two data sets both show that stream power is lowest both in the headwaters and near the river mouth, and reaches a maximum about two-thirds of the distance downstream from the basin headwaters (Figure 8c). The local variations in stream power of Figure 8c are significantly reduced to a near constant value of 100 Nm/s in Figure 8d where we plot the normalized stream power per unit valley length (w_n) for the square data of Figure 8c. Only four stream power data plot significantly above 100 Nm/s and these four data represent gorge-like stream reaches where the channel is an incised meander, locked into a resistant bedrock which has prevented lateral migration processes.

Mattole River

One of the larger fluvial systems in coastal northern California, the Mattole River drains 655 km^2 of the Coast Ranges (Figures 3 and 9) where climatic conditions are cool, temperate, and highly seasonal with mild and wet winters, and dry summers. Mean monthly temperatures vary less than 6°C throughout the year; mean annual temperatures are 12-14°C; and more than 90% of the mean annual precipitation of 100 cm occurs as rain resulting from regional maritime air masses during mild winters [*National Oceanic and Atmospheric Administration (NOAA),* 1985]. The sinuous Mattole River trunk stream originates less than 5 km from the coast near Point Delgada, flows inland and northwestward 80 km along the region of greatest uplift rates in the Mendocino triple junction (MTJ) region, and exits north of the rugged King Range, the westernmost of California's Coast Ranges (Figure 3). The MTJ marks the juncture of three lithospheric plates, the North American, Pacific, and Juan de Fuca (remnant of the Farallon). Pronounced relief (up to 1246 m), rapid uplift rates (2.5 - 3 m/ka) [*Merritts and Bull,* 1989; *Merritts et al.,* 1992; *Merritts,* 1996], and high seismicity are the result of complex interactions among the three plates joined at the northwestward-migrating triple junction.

The Mattole drains some of the youngest rocks within the accreted subduction-related Franciscan assemblage that formed within the convergent tectonic regime that existed prior to passage of the MTJ. The middle reach of the Mattole trunk stream flows along a broad shear zone that separates two northwest-oriented tectonostratigraphic units, the Coastal and King Range terranes [*Beutner et al.,* 1980; *McLaughlin et al.,* 1994]. As a consequence, the western part of the Mattole drainage basin drains the King Range terrane, whereas the eastern part drains the Coastal terrane. Predominant rock-types in the larger Coastal terrane (Late Cretaceous to late Eocene) are arkosic sandstone, siltstone,

and shale [*Bachman,* 1978; *McLaughlin et al.,* 1982; *Blake et al.,* 1985]. The younger King Range terrane (early Tertiary to middle Miocene) is lithologically similar to the Coastal terrane, and both units are highly sheared and folded, but the King Range rocks are more structurally intact.

Ongoing uplift of the coast at the mouth of the Mattole River is documented by emergent Pleistocene and Holocene marine terraces, as well as by the recent coseismic emergence of up to 1.4 m during the April 25, 1992, Cape Mendocino Ms 7.1 earthquake [*Merritts and Bull,* 1989; *Merritts et al.,* 1992; *Oppenheimer et al.,* 1993; *Merritts,* 1996]. In addition, Holocene and late Pleistocene marine platforms indicate that the coast along the entire length of the Mattole River has been subject to rapid surface uplift at rates of 2.5 - 3 m/ka (and locally up to 4 m/ka) over time periods of tens of thousands of years [*Merritts and Bull,* 1989; *Merritts,* 1996]. As the entire King Range terrane block, which extends inland to the Mattole trunk stream, has been uplifted during the Quaternary [*McLaughlin et al.,* 1982; *Dumitru,* 1991] and is at very high altitudes within 4-5 km of the coast, at least the western part of the Mattole Valley (which drains the King Range) and the trunk stream are presumed to have been subject to rapid rates of uplift during most of this time. Apatite fission track studies in the King Range and adjacent Coastal terranes indicate that Quaternary uplift and unroofing decrease in magnitude northeastward, from a local high in the King Range [*Dumitru,* 1991].

The longitudinal profile of the entire 80-km length of the Mattole River trunk stream (Figure 8, inset A) was obtained from 7.5 minute topographic maps, and a more detailed profile of the lower 40 km (Figure 8, main figure) was acquired through field surveying with a total geodetic station [*Merritts et al.,* 1994]. The long profile of the entire river indicates that the reach within longitudinal distances of zero and 60 km is composed of two linear segments that join at about 30 km.

Upstream of 30 km, the river has a gradient of 0.0032, but downstream of 30 km the gradient is only 0.0014, a decrease in gradient of about 55%. The active channel floor of the lower 30 km of the Mattole is alluvial, flowing atop a seaward thickening wedge of gravel that tapers to zero thickness upstream. The remainder of the stream has a mixed bedrock-alluvial channel, with increasing bedrock character in the uppermost 20 km. An estimate of the total thickness of the gravel wedge at the mouth, at km 5, is obtained from recent U.S. Geological Survey (USGS) drilling along the right bank of the channel. Bedrock was not encountered until a depth of at least 37 m, when a large mass of blue, argillaceous rock, identical to the local bedrock. was encountered [*T. Dunklin,* drill logger, personal communication, 1992, USGS Cape Mendocino Seismic Reflection Experiment; E. Criley project director]. At km 35, deep bedrock pools alternate with gravel riffles on the active channel floor, and the gravel veneer is less than several meters thick. However, the river's long profile in the bedrock reach from 30-60 km is nearly straight and projects downstream as the strath of the gravel wedge shown in Figure 8, inset A.

Prominent terrace treads are ubiquitous and nearly continuous along the lower 40 km of the Mattole River (Figure 8, main figure). Terraces and the active channel floor along the lower ~18 km of the river are composed of alluvium (cut and fill terraces). Occasional bedrock knobs are surrounded by alluvium, as at km 10 (elevation = 40 m). An estimate of the minimum thickness of the alluvium composing the elevated fill terrace at km 10 is available from multiple water-well logs which indicate that sand, gravel, and clay occur to a depth of at least 12 m. The upstream breaks in slope of the treads of prominent, near-horizontal fill terraces along the river at 3 and 12 km coincide with the inner edge altitudes of the two youngest marine terraces at the coast, 6.5 and 30 ka in age, respectively. The position of the 30-ka interstadial sea level highstand marine terrace is obtained from surveys along the coast 1 km south of the mouth of the Mattole. The position of the inner edge of the mid-Holocene marine platform, dated via a mussel shell attached to the platform (6163-6863 cal years B.P.), is from a survey 1 km north of the mouth [*Merritts,* 1996].

In an upstream direction from km 18, strath terraces along the valley walls and bedrock in the channel floor increase in frequency. These strath surfaces are distinct, can be followed for up to several km, and locally merge upstream, as at km 26, 32, and 37 (Figure 8, main figure). At all locations, straths are overlain by up to 1-2 m of coarse gravels, which in turn are overlain by up to 1-3 m of fine grained sands and silts. These terrace treads are shown also as fine lines in Figure 8, inset B. We wish to draw a distinction between these terrace treads which represent the capping of sediments on a strath surface, as opposed to those downstream that represent the surfaces of fill or cut terraces. The straths project into the modern channel bed between 18 and 38 km, forming a series of benches that emerge from the channel, one after the other, as one follows the river upstream. Although the strath surfaces are subparallel to one another, they are steeper than the modern channel bed downstream of 30 km, have the same gradient as the active Mattole channel does between 30 and 60 km, and do not merge with marine terraces at the river mouth.

Estimates of vertical incision are obtained from radiocarbon dated strath surfaces between km 34 and 36 [*Merritts et*

al., 1994] (Figure 8, inset B). Here, the modern bedrock channel floor is about 7 m below a strath surface overlain by gravel containing a log radiocarbon dated as 9,951 to 10,784 cal years B.P. Using this age as a minimum for the age of the strath, the maximum incision rate since about 10 ka is 0.7 m/k.y. (Figure 8, inset C). The next higher strath is 18 m above the present channel bed, and is overlain by gravel which in turn is overlain by overbank silts and clays containing charcoal with a radiocarbon date of 8,410 - 8,550 cal years B.P. Elsewhere along the river, overbank sediments have been as much as 3000 years younger than underlying gravels, the latter of which are more closely synchronous with the timing of strath cutting. If this strath is 12,000 years old, the vertical incision rate is about 1.5 m/ka (Figure 8, inset C). This strath must be older than the lower strath dated as about 10 ka, so using a minimum age of 10 ka yields a maximum incision rate of 1.8 m/ka. A linear fit to incision rate data for the region between river kilometer 34 and 38 based on four data straths is about 1.03 m/ka (Figure 8, inset C). In summary, incision rates for the past 12 k.y. on the predominantly bedrock reach range from 0.7 to 1.8 m/ka, or about 23-72% of the long-term average uplift rate measured at the river mouth by coastal marine terraces [*Merritts,* 1996].

Rios Aranjuez, Barranca and Naranjo

Southwest-flowing fluvial systems along the central Pacific coast of Costa Rica (Figure 3) drain a forearc with rapid, but spatially variable deformation rates and an active/extinct magmatic arc. Volcanism within the magmatic arc and deformation in the forearc are driven by northeastward-directed subduction of the Cocos plate at the Middle America Trench. Convergence is nearly orthogonal to the trench and approaches 10cm/yr along this sediment starved margin [*Gardner et al.,* 1987]. Deformation in the forearc is controlled by bathymetry on the subducting Cocos plate in the sense that broad, regionally distributed rock uplift can be related to the long wavelength roughness of the subducting Cocos Ridge [*Gardner et al.,* 1992; *Fisher et al.,* 1994; *Fisher et al.,* in press]. Average, regional rock uplift rates constrained by geodynamic modeling, parameterized from coastal marine terraces and Cocos Ridge bathymetry, varies from over 4 m/ka (maximum of 7 m/ka) astride the subducting Cocos Ridge to less than 1 m/ka 300 km to the northwest [*Gardner et al.,* 1992]. Locally, deformation in the forearc is controlled by a shorter wavelength sea floor roughness attributed to subducting seamount chains. Subduction of these seamounts has effectively segmented the forearc into discrete blocks with spatially variable rock uplift rates that range from less than 0.5 m/ka to over 3 m/ka across coast-orthogonal, segment bounding faults [*Fisher et al.,* in press]. These coast-orthogonal faults commonly control the position of trunk segments of major fluvial systems across the forearc [*Gardner et al.,* 1997]. Additionally, individual blocks in the forearc display measurable down-to-the-northwest rotation which has produced marked drainage basin asymmetries with numerous stream captures and diversions [*Gardner et al.,* 1997; *Fisher et al.,* in press].

Fluvial systems that drain the mountainous forearc and magmatic arc rise from sea level to several thousand meters elevation within distances of only 30-40 kilometers of the coast (Figure 3). Most have developed extensive fill and strath terraces that are dated by ^{14}C and $^{39}Ar/^{40}Ar$ of associated volcanic deposits. Terrace correlation is accomplished primarily through soil chronosequences and clast weathering rind thicknesses [*Drake,* 1989; *Gardner et al.,* 1992; *Marshall,* 1994; *Marshall et al.,* 1995; *Bullard,* 1995; *Fisher et al.,* in press]. Here, we report on three of these systems, the Rio Aranjuez, Rio Barranca and Rio Naranjo which occur along a 100 km stretch of the coast (Figure 3). These streams were selected for their limited variation in size, rock type, and basin precipitation, but range of rates of rock uplift (Table 1). Basin size ranges from 210 km^2 for Rio Aranjuez to 470 km^2 for Rio Barranca. Average annual precipitation varies from 250 cm/yr for both the Rio Aranjuez and Rio Barranca to 350 cm/yr for the Rio Naranjo. Precipitation is generally higher for all rivers in their mountainous headwaters, but is especially so for the Rio Naranjo. No discharge data is available. All three river systems head in the magmatic arc composed of resistant, predominantly andesitic extrusive rocks, although some intrusive rocks of predominantly dioritic composition are exposed in the Rio Naranjo headwaters. All rivers cross the forearc in their lower reaches. Forearc sediments are shelf/slope clastics and volcaniclastics and are generally much less resistant than the magmatic arc volcanics. Width of forearc transected by trunk segments decreases from 35 km for Rio Naranjo to 5-10 km for the Rio Barranca to less than 5 km for the Rio Aranjuez. All three rivers have channels directly on bedrock in their upper and middle reaches, but are alluvial downstream where they flow on late Quaternary alluvial, marine and estuary deposits near the coast.

Along this section of the Costa Rican coast, relative base level changes are strongly conditioned by both eustatic sea level variations and spatially variable rock uplift rates. All longitudinal profiles are strongly concave and all terraces diverge upstream from the modern profile (Figure 10). Terraces are inferred to have formed during times of relative downstream base level stability represented by sea level maxima or minima [*Marshall and Gardner,* in prep] as

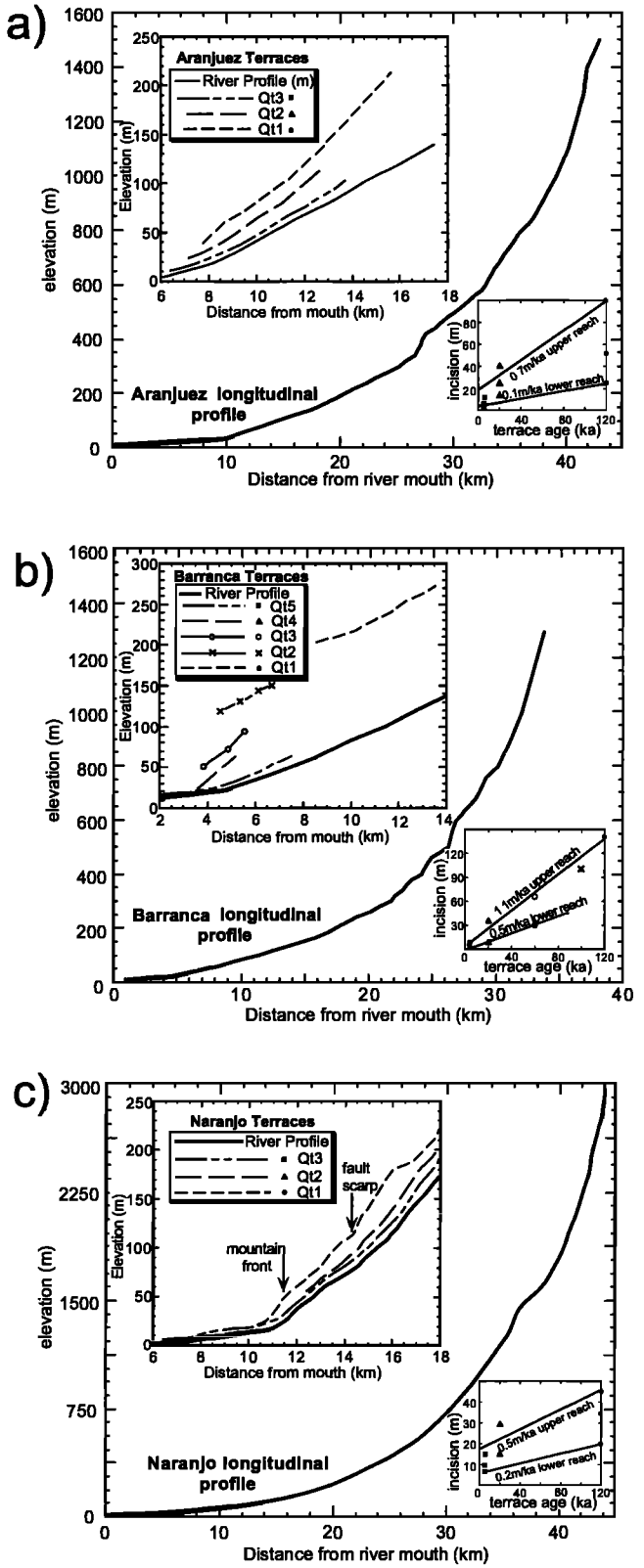

follows: Qt1, the most regionally extensive, aggradational terrace was assigned to oxygen isotope stage 5e (ca. 125 ka) [*Fisher et al.*, in press]; Qt2 (Rio Barranca) is thought to have formed during oxygen isotope stage 5c (ca. 100 ka) [*Marshall et al.*, in prep]; Qt3 (Rio Barranca) is correlated to oxygen isotope stage 3d (ca. 60 ka) [*Marshall and Gardner*, in prep]; Qt4 (Rio Barranca) and Qt2 (Rio Aranjuez and Naranjo) is correlated to the ~20 ka sea level minima and by a soil chronosequence correlation [*Marshall and Gardner*, in prep], to dated terraces further along the coast [*Gardner, et al*, 1992; *Bullard*, 1995]; and Qt5 (Rio Barranca) and Qt3 (Rio Aranjuez and Naranjo) are assigned to the post-6 ka Holocene marine bench along the coast [*Marshall and Gardner*, in prep].

The fluvial terraces indicate average incision rates that vary from 0.5 to 1.1 m/ka in the upper reaches of their limit of preservation, to 0.1 to 0.5 m/ka near the coast (Figure 10). Locally, maximum rates of incision do not approach the upper limits for rock uplift rates. For example, the estimated 2.5 m/ka rates of rock uplift along the lower course of the Rio Naranjo are far in excess of the maximum upstream incision rates of 0.5 m/ka determined by incision below the correlative fluvial terrace. Interestingly, where rock uplift rates are clearly in excess of incision rates, there is strong evidence of stream capture. Apparently, vertical incision of some fluvial systems is being defeated by rock-uplift, deflecting drainage basins off rapidly rising blocks in the forearc.

Summary of Long Profiles and Rates of Incision

We summarize the long-term rates of fluvial incision for the rivers presented above in the context of their respective diverse climatic, tectonic, and rock-type settings (Table 1). The streams with the highest rates of fluvial incision are located, not surprisingly, in tectonically active regions. More important than the rates themselves is how incision is distributed along a river profile. At least three incision rate distribution patters are evident: (1) incision that clearly increases towards the river headwaters, indicated by terraces that diverge upstream, suggestive of relatively higher rates of rock uplift near the headwaters (e.g. Clearwater River, Costa Rican streams); (2) incision that increases downstream, indicated by terraces that diverge downstream and

Figure 10. Longitudinal profiles with inset terrace profiles and incision rates for Costa Rican Rivers; a) Rio Aranjuez, b) Rio Barranca, and c) Rio Naranjo. Data for Rio Barranca are from Marshall et al., [in prep] and those for the Rio Naranjo are from *Drake* [1989]. See Figure 3 for location.

suggestive of downstream base level fall (e.g. Susquehanna River); and (3) incision that is more or less evenly distributed along the river profile, indicated by terraces that are parallel to the river profile and suggestive of epeirogenic, or spatially-uniform rates of rock uplift (e.g. Rio Jemez, Mattole River). Of particular interest to the distribution of incision rates is the fact that they do not appear to be significantly dependent upon available discharge. In this respect, the Susquehanna River has the largest (recorded) discharge of all the streams studied, but the slowest rates of incision and the most profound convexity in its river profile. In contrast, the Jemez River has been able to maintain incision into bedrock despite a relatively low discharge that does not increase appreciably downstream. Average, long-term rates of bedrock channel incision typically fall within about 70% of the measured or inferred rates of rock uplift with the notable exception of the Rio Naranjo. Nowhere except the Susquehanna basin are measured channel incision rates clearly equal to or in excess of rock uplift rates. Not coincidentally, the Susquehanna terraces show significantly different gradients with respect to the Susquehanna River longitudinal profile.

In the tectonically active settings represented by the Clearwater River, Mattole River, and Costa Rican streams, terraces are best preserved along a valley reach characterized by a relatively gentle and straight longitudinal profile (Figures 7, 9, and 10). These reaches are devoid of large knickpoints which tend to characterize the upper, steeper portions of these streams. Over the time span represented by the terraces, lateral incision conducive to the preservation of paleo-valley bottoms (terrace straths) has remained more or less spatially fixed. Preserved terraces for tens of kilometers within a valley, attest to a stream's ability to maintain a reach where lateral incision processes can and are maintained over geologic time spans.

DISCUSSION

The longitudinal profiles of the streams presented in this study contain useful information related to the spatial distribution of bedrock incision rates as well as to the probable geologic, hydrologic, and climatic conditions responsible for driving incision. We use our data to incorporate rock-uplift, climate, rock-type, channel bedload, and a consideration of how different drainage basins generate discharge in the development of a conceptual model for fluvial incision into bedrock.

Relative importance of rock-uplift and climate on long profile evolution

The rates of fluvial incision and long-term evolution of the long profile appears to be primarily a function of the tectonic setting; but the details in the long profile shape are determined by climate. For example, the convex profiles of the Susquehanna River and associated Atlantic margin streams are located in the most tectonically stable setting. Here the river profiles have a long-term history of adjusting their slope to very low rates ($< 1*10^{-3}$ m/ka) of flexural isostatic rock uplift. In this tectonic setting, changes in base level and/or rock-type have had the more profound impacts on the river profiles as illustrated by the distinct convexities that stretch for over 100 km through their lower reaches (Figures 4a and 5a). Protracted base level fall, driven by both eustatic drawdown and flexural isostatic uplift over the past 20 Ma, are driving the incision of these rivers. Paleo-long profiles of the river represented by the terraces track this base level fall by their divergence through the Piedmont reach (Figure 5a-5b). If we take the Atlantic margin stream long profiles to represent true, steady-state conditions, we would conclude that the stream power law would have to be parameterized by a low k value, balanced by steep slopes through the convex reaches. But the rates of incision determined by the terraces argue against a steady state profile, which would lead us to conclude that the non-steady state conditions result from a protracted increase in the rate of incision that is still working its way through the system. A problem with the latter interpretation that we will return to is that the non-steady state conditions would tend to persist, in this case, over 10^6 yr time spans.

The long profiles of Texas streams differ from those on the Atlantic margin in that they are broadly concave despite the overwhelming similarities in the tectonic setting and changes in rock-type (Figure 4b). A closer inspection reveals gentle convexities where the streams cross the Balcones Escarpment (analogous to the Fall Zone). One way to interpret the varying degree of profile convexity is to observe the relative climatic settings of the Atlantic and Gulf coast margins. The effectiveness of climate on fluvial systems is not separable from other variables which control process [*Wolman and Gerson,* 1978]. Streams in semi-arid climates, such as the Texas rivers may have relatively low mean annual discharges, but also are capable of generating high stream powers during infrequent, but large runoff events [*Baker,* 1977] (Table 1). Despite the dramatic differences in drainage basin size, the Texas rivers have very similar peak annual discharges suggesting that runoff is

primarily generated by highly-localized precipitation situated across the Balcones Escarpment in this specific case [*Baker,* 1977]. In both the Atlantic and Gulf coast cases, the tectonic setting and rock-type precondition a long profile to develop long-lasting profile convexities, but climate determines the degree to which those convex reaches are expressed. It is difficult to envision how the stream power law can capture the importance of highly localized runoff generation in the Texas stream basins because A^m does not correlate very well with peak annual discharge. The Texas streams may represent another class of streams, in addition to those already identified [*Stock,* 1996], where the stream power law cannot be applied.

The two streams studied with nearly-straight, slightly concave profiles also illustrate the trade-offs between tectonic setting and climate in determining profile shape. Both the Rio Jemez (Figure 6) and Mattole River (Figure 9) have had little trouble maintaining more or less spatially-uniform, linear rates of fluvial incision (0.17 m/ka for the Rio Jemez, and ~ 1 m/ka for the Mattole) which are very close to independently measured rates of rock uplift. Both the linear incision rates and their similarity to rates of rock uplift argues strongly that the long profiles of these rivers are at or near steady state. In the case of the Rio Jemez, we would argue that incision is dominated by the slope component of the stream power law ($m/n < 0.5$) because discharge in this semi-arid environment where precipitation is orographically controlled is the lowest of all streams we studied. The relatively larger discharges of the Mattole River still cannot produce strongly-concave long profiles because rates of rock uplift are an order of magnitude faster than those in the Jemez basin.

The remaining streams studied lie in very tectonically active settings and all show strongly concave long profiles. An apparent contradiction resides in a comparison of the profiles and discharge data of the Clearwater (Figure 7; Table 1) and Mattole (Figure 9; Table 1) rivers. Both streams have similar rock-type, climatic, and discharge characteristics, particularly when peak annual discharge is considered with respect to basin area. The differences in the long profiles therefore likely reside in the particular tectonic settings. The terrace data for these streams clearly indicate that unlike the Mattole River, incision increases upstream for the Clearwater River. The Clearwater River would fall into that category of streams in tectonically-active regions whose profiles cannot be predicted by the stream power law. Nevertheless, the incision rate data for two terraces (Figure 7b) and independent rock-exhumation data both argue strongly that the Clearwater profile is at or near steady state. The rivers in Costa Rica appear to mimic the Clearwater's behavior in having more rapid rates of incision in the headwaters than at their mouths (Figure 10). We interpret these similarities in long profile shape and long-term incision rates as an overriding dominance of tectonic setting on long profile evolution for these streams.

The preservation of terraces along bedrock rivers in very different tectonic settings indicates a commonality in the dominant bedrock channel processes governing incision. Regardless of the rate of rock-uplift, bedrock channels develop a reach where their valley bottoms can be sufficiently widened so that terraces are created and subsequently preserved in the valley walls. Close correspondence between the river long profile and terrace long profiles, and uniform, long-term rates of incision indicate that bedrock channels are capable of performing lateral incision and valley bottom widening without significantly changing the slope of the long profile or vertical incision rates. These are very important observations because they imply that significant divergence of terrace and river long profiles, and the resulting spatial variations in rates of vertical incision, are more indicative of temporal and spatial changes in the rate of rock uplift and/or base level. In essence, the bedrock long profile is capable of attaining a graded condition where the slopes are delicately adjusted to both transport bedload and maintain rates of vertical incision equal to rates of rock uplift. Graded bedrock long profiles, once established, are maintained over geologic time spans and represent a useful datum to which to compare variable rates of rock uplift. Even for cases where fluvial terrace genesis is favored by downstream base level stability, that is, the Costa Rican streams, lateral incision, and low profile gradients are necessary to create and preserve the terraces. In the face of rapid rock uplift, the Costa Rican streams have managed to vertically incise across a wide valley bottom so that accommodation space is present to preserve a fill terrace, created by a transient eustatic rise.

Importance of rock-type and the role of bedload

Details in the long profile shapes demonstrate the effect of rock-type erodibility in modulating the rates of fluvial incision. Profiles consistently exhibit steeper, more convex profiles where they cross resistant rock types. For example the broad convexities of the lower Susquehanna River and related Atlantic margin streams are largely coincident with resistant amphibolite-grade metamorphic rocks. The gentle convexities of the Texas stream profiles occur where the channels cross the resistant limestones of the Balcones Escarpment and flow out onto the soft Coastal Plain sediments. In contrast, the Clearwater and Mattole Rivers (Figures 7 and 9) do not have pronounced convexities despite the rapid rates of rock uplift. Both the Clearwater and Mattole Rivers are incising into relatively erodible, poorly-lithified sedimentary rock-types. Even where discharge,

does not increase appreciably downstream as in a semi-arid climatic setting such as the Rio Jemez (Figure 6), a straight long profile can be maintained across relatively erodible sedimentary rocks.

Rock-type can also play a role in the persistence of knickpoints over geologic time. Knickpoints obvious in the river long profile are not everywhere present in the terrace profiles, especially for the streams in tectonically active settings. In contrast, knickpoints in the long profiles of streams in the less-active settings are locally present in the terrace profiles. A steepened gradient in the Susquehanna River terrace Tg2 located above the modern channel knickpoint throughout the Holtwood gorge (Figure 5a) suggests survival of knickpoints in the tectonically-inactive setting over million-year time spans. Similar conclusions were reached for passive margin streams in eastern Australia whose Miocene long profiles are well-preserved by basalt flows [*Young and McDougall,* 1993].

The caliber and flux of bedload through the channel contributes to channel incision and reach slope. Where rates of rock uplift are high, the bedrock channel gradient is necessarily steep to accommodate both the rock uplift and transport the bedload. When even the relatively thin discontinuous alluvial cover of such a bedrock channel is removed, long profiles rapidly lower their gradients by incision [*Stock et al.,* 1996; *Montgomery et al.,* 1996] to accommodate the fact that they no longer have to use stream power to transport sediment.

The reverse of this argument is that there should be some optimum amount of bedload material acting as abrading tools in a river channel to maximize a river's ability to incise [*Sklar et al.,* 1996; *Sklar and Dietrich,* 1997; *Slingerland et al.,* 1997; *Sklar and Dietrich,* this volume]. Too much bedload as the river approaches its capacity insulates the bedrock from erosion, even where that bedrock might be a very erodible rock type. Such is the case for the Rio Jemez, where a late Pleistocene channel bedload armor and alluvial valley fill (Figure 6a) prevent the river from incising into the soft sedimentary rocks under the current hydrologic and discharge conditions. Too little bedload and the concomitant low flux of tools available for channel abrasion could result in low incision rates, as is observed for the lower Susquehanna River profile which is well under capacity. The combination of a small bedload and resistant rock-types likely both contribute to the profound convexity of that river's long profile.

Distribution of Basin-Scale Stream Power

Streams in active tectonic settings appear to have the ability to rapidly incise, maintain concave profiles and exhibit a strong component of lateral incision, periodically widening their valley bottoms and preserving terraces. Despite the large discharge and slow rates of rock uplift, the streams in the tectonically inactive setting, such as the Susquehanna River, have not been able to widen their valley bottoms over 10^6 yr time spans and instead find themselves incising a relatively narrow gorge along convex long profiles. We examine how a drainage basin in the tectonically active vs. tectonically inactive setting generates the stream power necessary to incise both laterally and vertically.

A hypothetical pure bedrock channel where the downstream increase in slope will be only inversely proportional to the downstream increase in discharge, that magically does not have to transport the very bedrock that it is eroding, and is underlain by a uniform rock-type, should have a constant, straight-line distribution of stream power along its profile (Figure 11a). Of course, rivers must transport the rock they erode as well as the sediment delivered from hillslopes, so schematic (Figure 11b) and real stream power distribution profiles (Figure 11c) show significant variations highly correlated to local changes in discharge, profile gradient, rock-type, and sediment in the channel. Nevertheless, to a first order, our calculation of stream power for the Clearwater River (Figures 8 and 11d) is not inconsistent with the hypothetical pure bedrock stream (Figure 11a). These data suggest that there may exist a fluvial tendency to minimize variance in stream power over the spatial scale representative of the entire basin.

The normalized stream power plots (Figures 8d and 11d) provide some insight into the processes that may control the minimization of stream power variance. The stream power per unit valley length tends to be relatively high (Figure 8c) where both the channel and valley bottoms are wide (Figure 8b), and relatively low (Figure 8c) where the channel and valley bottoms are narrow (Figure 8b). Because the stream power normalized to the valley width - channel width ratio returns essentially a constant value irrespective of location along the profile (Figures 8d and 11d), we are left to conclude that the valley bottom everywhere experiences essentially the same average shear stresses over geologic time scales. The Clearwater valley bottom, although highly variable in width (Figure 8b), has essentially the same potential to vertically lower (incise) its bed. In this way, a river can maintain a uniform rate of vertical incision everywhere along its profile; it just accomplishes the incision across valley bottoms of variable width.

Recall however that for streams like the Clearwater River, vertical incision is not uniformly spatially distributed being greater in the headwaters than near the mouth. In this case, we would argue that there must be some prioritization of how work is done along the profile. The headwaters portion has less sediment to transport so as long as the valley bottom can be narrowed to concentrate the stream power on

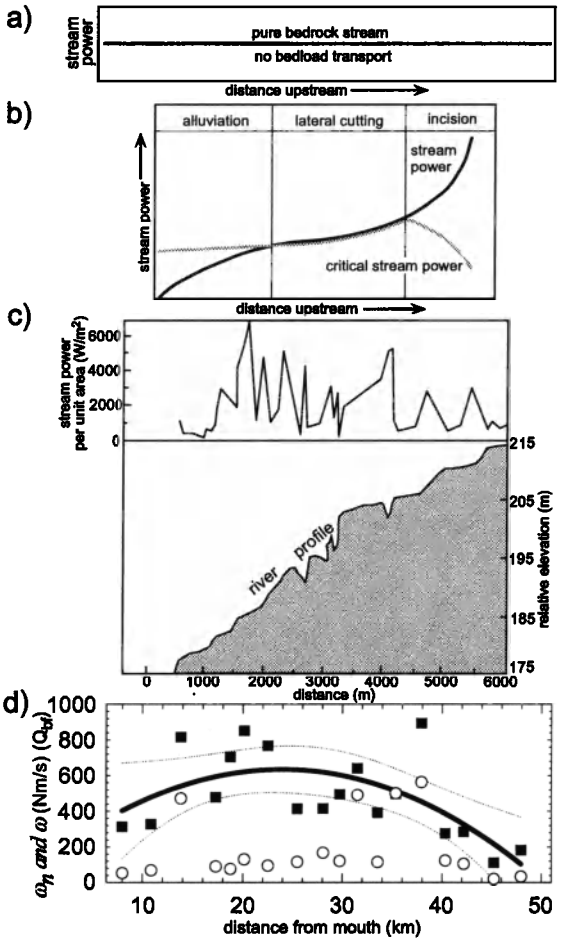

Figure 11. a) Stream power distribution for a hypothetical, pure bedrock stream with no bedload to transport. b) Schematic stream power distribution of *Bull* [1979] developed for ephemeral streams where discharge is only generated in the upper portion of the drainage basin. c) Model-calculated stream power (per unit area) distribution along Nahal Paran, Israel [*Wohl et al.*, 1994]. Stream power reflects a uniform discharge of 2500 m^3/s. d) Distribution of measured stream power (solid squares and polynomial regression) and valley width-channel width normalized stream power (open circles) along the Clearwater River. See Figure 8 for detailed discussion.

vertical incision processes, rather than lateral incision processes, higher rates of incision are attained and maintained. Conversely, the lower reaches of the river have more sediment which favors lateral incision processes and forces the stream to expend its stream power in the transport of that sediment. The valley bottom widens, and rates of vertical incision fall in the lower reaches.

This conservation of energy approach to understanding how stream power may be apportioned along a long profile has no real physical basis and clearly oversimplifies the system. Nevertheless, we are struck by the dramatic reduction in the variance in stream power along the profile when the valley width-channel width ratio is considered. Our assertion that there must be some prioritization of work expenditure is further supported by the four stream power data representative of valley reaches where the channel is known to be locked into a resistant rock-type [*Wegmann,* unpublished data] and precluded from any significant lateral migration process (Figure 8d). The normalized stream power value is high for these four locations because the valley width-channel width ratio is close to 1. Essentially, the valley widths and channel widths are the same. All of the available stream power is focussed across the narrowest valley bottom (= channel bottom) to maintain the necessary vertical incision rate across the resistant rock-type. If a conservation of energy condition did not exist, the stream should not have to so carefully adjust its valley bottom width to maintain variable rates of vertical incision. In these respects, we may have been fortunate to investigate the Clearwater River because the rock-type variations are relatively minimal with respect to most streams. The clear correlation between rock-type, stream power, and valley bottom width may not be so apparent in most fluvial systems.

Conceptual Model for Bedrock Incision Over Geologic Time Scales

Consideration of how a drainage basin generates stream power provides clues as to how long profiles in the tectonically-active setting can be concave-up and accompanied by fluvial terraces and convex-up and locally devoid of well-preserved terraces in the tectonically inactive setting. The manner in which an entire basin contributes to the stream power of the trunk channel is strongly dependent upon (1) basin hydrology, in particular the magnitude and frequency of bankfull discharge events [*Wolman and Miller,* 1960; *Baker,* 1977], which is related directly to rock-type controlled infiltration capacity [*Kelson and Wells,* 1989; *Ritter and Gardner,* 1993], and (2) the production and distribution of relief (high potential energy). For a given climate and precipitation, low-relief drainage basins underlain by rock-types that favor high infiltration capacities will not generate the peak discharges and stream power necessary to maximize fluvial incision (Figure 12a, 12c, and 12d). In contrast, high-relief drainage basins underlain by rock-types which primarily generate overland flow and high peak discharges during precipitation do produce the stream powers sufficient to maintain relatively high rates of bedrock incision (Figure 12b, 12c, and 12d).

We propose that in tectonically active and relatively moist settings, the entire drainage basin experiences uplift,

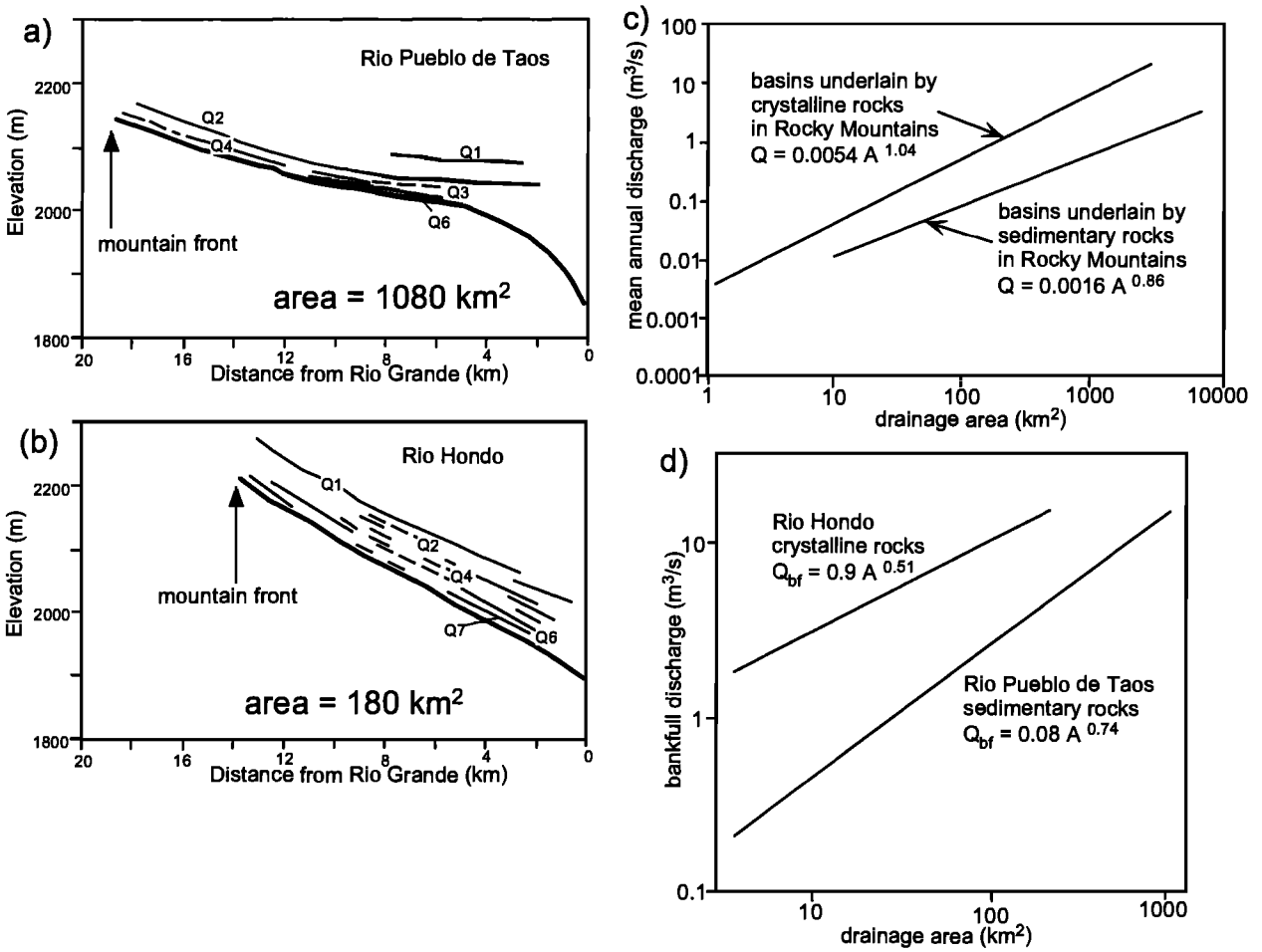

Figure 12. a) Long profiles and terrace profiles of the Rio Pueblo de Taos. b) Long profiles and terrace profiles of Rio Hondo. These adjacent streams have experienced the same down-stream base level fall of the Rio Grande. The smaller Rio Hondo has been able to maintain incision with that base level fall while the much larger Rio Pueblo de Taos has not. c) Basin area - mean annual discharge relationships for instrumented watersheds in the Rocky Mountains where n (number of basins) for basins underlain by crystalline rocks is 24; n for basins underlain by sedimentary rocks is 34. d) Calculated bankfull discharges from surveyed channel cross-sections as a function of basin area for the Rio Hondo (n=10) and Rio Pueblo de Taos (n=12). Despite the significant disparity in drainage basin size, the smaller Rio Hondo is able to generate greater bankfull discharge than the Rio Pueblo de Taos. Ability to generate discharge (and indirectly, stream power) is attributed to rock-type dependent basin hydrology. All figures and graphs modified from *Kelson and Wells* [1989].

high relief (high potential energy), and the concomitant increases in orographic precipitation that frequently generate the fluvial-system wide stream power necessary to create and maintain long profiles and rates of incision equal and opposite to rates of rock uplift (Figure 13a). These basins, categorized as Type I basins, have relatively high discharges per unit area (Table 1). The large percentage of exposed bedrock or bedrock very near the surface attributed to rapid rates of landsliding [*Hovius,* in press] limits infiltration rates resulting in high drainage densities and rapid peak discharges in the trunk channels. A positive feedback is established as basin-wide low infiltration rates favor rapid incision which undercuts hillslopes and ensures bedrock exposure by landsliding. Over graded time spans, upbasin hydrologic and sediment yield changes are manifest by alternately widening and narrowing of valley bottoms, producing fluvial terraces. In these respects, basins in tectonically-active settings tend to generate discharge and stream power analogous to the Rio Hondo [*Kelson and Wells,* 1989] (Figure 12b-12d). They are more likely to

a) Type I

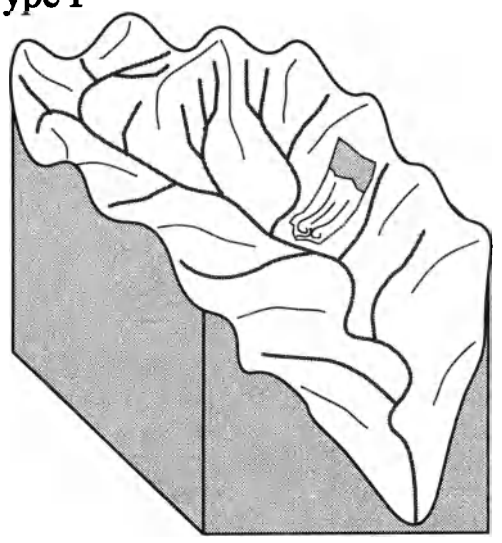

Active Tectonic Setting

- rapid rock-uplift
- orographic precipitation
- high percentage of exposed bedrock
- landslide-dominated hillslope processes
- low infiltration rates
- high drainage density
- generation of excess stream power

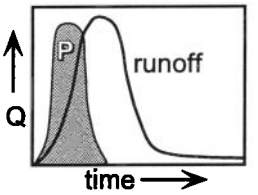

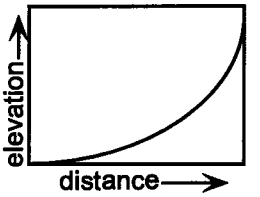

concave, graded long profiles that can incise at a rate equal to the rate of rock uplift

b) Type II

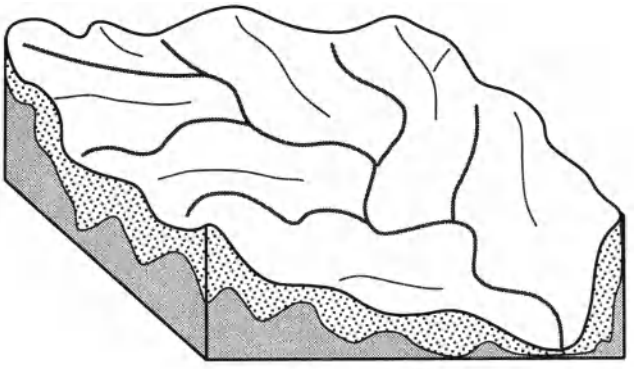

Tectonically Inactive Setting

- slow rock uplift
- low percentage of exposed bedrock
- thick regoliths/soils
- creep dominated hilllsope processes
- high infiltration rates
- low drainage density
- stream power limited
- sensitive to flash flood magnitude index

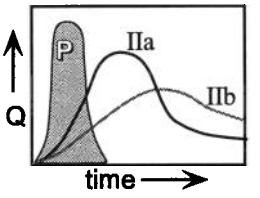

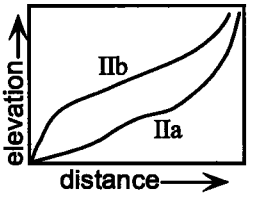

long profiles of variable shape, very sensitive to rock-type, climate and base level changes

c) Flash Flood Magnitude Index

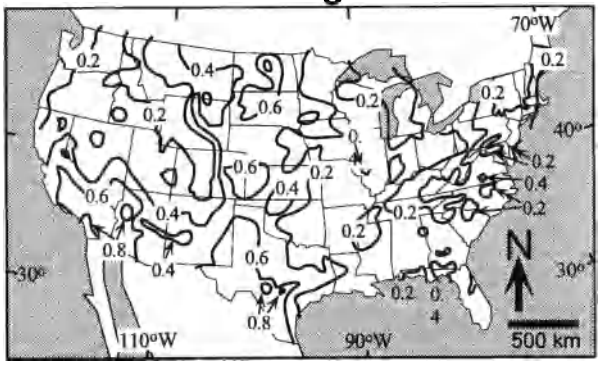

Figure 13. Summary of geomorphic, hydrologic, and long profile characteristics for a) tectonically active vs. b) tectonically inactive settings. P in the hydrographs indicates a unit precipitation event and varies for unit rock-type. c) Map of flash flood magnitude index (FFMI) is modified from *Baker* [1977]. Contoured FFMI values are the standard deviations of the logarithms of the annual flood peaks derived from stream gage data. Note the relatively high (0.8) values for central Texas, moderate values (0.4) for New Mexico, and relatively low (0.2) for both the east (passive) and west (active) coasts.

have concave long profiles with knickpoints restricted to rock-type, faults, or structural features.

In contrast, drainage basins in tectonically inactive and relatively moist settings, defined here as Type II basins (Figure 13b), tend to generate discharge more similar to the Rio Pueblo de Taos (Figure 12a-12d). A subset of the Type II basin, Type IIa is characterized by a large percentage of regolith and weathered bedrock that favors infiltration, lower drainage densities, and the resultant lower peak discharges to the trunk channels. Relatively low mean annual discharge and peak discharge per unit area (Table 1) in these streams less frequently generate high stream powers, manifest as a convex long profile in the case of the Susquehanna River, or a straight profile unable to incise through its own alluvium to the bedrock valley floor in the case of the Rio Jemez. Relatively tectonically inactive settings may be more dependent on local changes in stream power spatially restricted to knickpoints which require long periods of time (10^6 yrs) to propagate through the system. Down basin base level fall in these settings has a particular profound impact on the profile, producing convexities especially where the river crosses resistant rock-types. The initial fluvial response in these streams is to narrow their valley bottoms, followed by changes in the rate of vertical incision modulated by rock-type erodibility.

The Type IIb basins have similar drainage networks and hillslope hydrology, but are located in a climatic region characterized by highly seasonal and/or highly variable precipitation. A good quantitative measure of precipitation variability is the Flash Flood Magnitude Index (FFMI) [*Baker,* 1977] which is the standard deviation of the logarithms of annual flood peaks (Figure 13c). Some of the highest FFMI values for the conterminous United States are located astride the Balcones Escarpment in central Texas. Despite the low-standing topography, low relief, and relatively low mean annual discharge (Table 1), these streams experience highly variable, catastrophic discharges that concentrate geomorphic work over short time spans [*Baker,* 1977]. We interpret this characteristic of the Texas river basins as the overriding control on the concave long profile shapes in the tectonically stable setting. For comparison, the Atlantic margin and west coast river basins have some of the lowest FFMI values (Figure 13c). We are left to conclude that climate must play a subordinate role to tectonics in these settings for the respective observed long profiles.

CONCLUSIONS

Longitudinal profiles of bedrock streams are observed to have distinctly different shapes in different tectonic settings. Those shapes tend to be strongly concave, approaching the typical "graded" profile shape in tectonically active settings where rates of rock uplift are several meters per thousand years (Figure 13a), and convex, approaching the typical "non-graded" shape in tectonically inactive settings where rates of rock uplift are as slow as $5*10^{-3}$ m/ka (Figure 13b) and the climate can be characterized as generating low FFMI values (Figure 13c). We assert that there is nothing intrinsically important about the shape of the bedrock longitudinal profile that determines whether it is an equilibrium, graded profile [*Sinha and Parker,* 1996]. Rather, bedrock channel long profiles assume the shape needed in their attempt to attain rates of vertical incision equal to rates of rock uplift. Profiles that are strongly concave are distinguished from those that are straight or convex in that the former are generally able to generate the stream power necessary to keep up with rapid rates of rock uplift, while the latter do not have this ability. In fact, terrace genesis appears to be a ubiquitous process in the tectonically active setting attributed to the production of stream power in excess of what is actually needed to match the rate of rock uplift and bedload transport. Measured stream power along the long profile of the Clearwater River is highly correlated to the width of the channel and valley bottom. There appears to be a conservation of energy along the profile such that total stream power is both minimized and apportioned to vertical incision, lateral incision, and bedload transport processes. The stream power used for lateral incision processes periodically widen the channel bottom during transient, hydrologically-driven changes in discharge and sediment load, producing fluvial terraces. Absence of terraces in the tectonically active landscape is attributed not so much to their lack of formation, but rather to the problems of preserving such features in a rapidly eroding landscape. In contrast, streams in regions of relatively slow rates of rock uplift are stream power limited, resulting in profile convexities, relatively narrower valley bottoms, and less frequent terrace production and preservation.

We build a conceptual model where the tectonically-active drainage basin is thought to respond in a similar fashion to drainage basins known to produce high peak discharges and high mean annual discharge as a function of low infiltration rates in the basin headwaters [*Kelson and Wells,* 1989; *Ritter and Gardner,* 1993] (Figure 13a). These basins are capable of generating the stream power necessary not only to maintain vertical rates of incision equal to rates of rock uplift, but also the stream power needed for valley bottom widening and terrace production. Tectonically inactive basins are thought to respond in a fashion similar to drainage basins known to produce low peak discharges and low mean annual discharges as a function of high infiltration rates in the basin headwaters. These basins are stream power limited and more prone to having long profiles with straight or convex shapes (Figure 13b).

In the context of our proposed model for long profile evolution over geologic time scales we can provide some qualitative constraints on the validity and applicability of the stream power erosion law. Type I basins should favor increases in discharge downstream, except in arid climates where rainfall is orographically controlled, and rapidly attain and maintain a graded long profile consistent with a steady-state parameterization of the stream power law. The m/n ratio would nominally be 0.5 for profiles where discharge clearly increases downstream and less than 0.5 for drier settings. Terrace data indicate however that some Type I drainage basins are situated in tectonic settings where rates of rock uplift impose more rapid incision in the headwaters than at the river mouth. The stream power erosion law cannot be used to model bedrock fluvial incision for these long profiles. Furthermore, the importance of rock type on stream power variation along a long profile (Figure 8) shows qualitatively how k varies considerably for a single river. Our results are consistent with the wide ranging parameterization of k revealed in previous studies.

Type II basins typically will show an increase in discharge downstream and the terrace data are consistent with both linear and increasing rates of incision downstream. It remains unclear if profile convexities observed in these settings (Type IIa) reflect true graded profiles or non-steady-state profiles that require very long (10^6 yr) time spans to respond to a boundary condition change. Type IIb basins are particularly poorly-suited to an application of the stream power law because our data suggests that the profile shape is dominated by peak annual discharges caused by highly variable precipitation (the FFMI of Figure 13c). For these streams, the highly-localized precipitation events does not favor a correlation between discharge and drainage basin area, as required by the stream power law.

Acknowledgments. The authors wish to acknowledge the ideas and data shared by their students and co-workers including Don Fisher, Jeff Marshall, Mark Brandon, Merri Lisa Formento-Trigilio, and Karl Wegmann. The manuscript was significantly improved by careful and thoughtful reviews by Leonard Sklar, Jeffrey Weissel, and M. G. Wolman. This work was partially supported by NSF grant EAR-9736748 and the donors of The Petroleum Research Fund, administered by the American Chemical Society to Pazzaglia, NSF EAR-9214832 and EAR-9525517 to Gardner, and NSF EAR-8904785, EAR-8917116, EAR-9149176 and USGS NEHRP 1434-95-G-2544 to Merritts.

REFERENCES

Anderson, R.S., The growth and decay of the Santa Cruz Mountains, *J. Geophys. Res.*, 99, 20,161-20,180, 1994.

Bachman, S. B., A Cretaceous and early Tertiary subduction complex, Mendocino coast, northern California, in *Trench-forearc geology: Sedimentation and tectonics on modern and ancient plate margins*, edited by J. K. Leggett, pp. 401-418, Vol, 10, Geol. Society of London, London, 1978.

Bagnold, R. A., Sediment discharge and stream power: a preliminary announcement, *U. S. Geol. Surv. Bull.*, 421, 23, 1960.

Bagnold, R. A., An approach to the sediment discharge problem from general physics, *U. S. Geol. Surv. Prof. Pap.*, 422(I), 1966.

Baker, V. R., Stream-channel response to floods, with examples from central Texas, *Geol. Soc. Am. Bull.*, 88, 1057-1071, 1977.

Baker, V. R. and P. D. Komar, Cataclysmic flood processes and landforms, in *Geomorphic Systems of North America*, edited by W. L. Graf, pp. 423-443, Vol, Centennial Special Volume 2, Geol. Soc. Amer., Boulder, Colorado, 1987.

Barron, E. J., Climate variations and the Appalachians from the late Paleozoic to the present: results from model simulations, *Geomorphology*, 2, 99-118, 1989.

Beutner, E. C., R. J. McLaughlin, H. N. Ohlin and D. H. Sorg, Geologic Map of the King Range and Chemise Island Instant Study Areas, northern California, by Miscellaneous Field Studies Map MF-1196-A ed., Vol. U. S. Geol. Surv., Washington, 1980.

Blake, M. C., A. S. Jayko and R. J. McClaughlin, Tectonstratigraphic terranes of the northern Coast Ranges, California, in *Tectonstratigraphical terranes of the Circumpacific regions*, edited by D. G. Howell, pp. 159-171, Vol, 1, Circumpacific Council for Energy and Mineral Resources, 1985.

Brandon, M. T. and A. R. Calderwood, High-pressure metamorphism and uplift of the Olympic subduction complex, *Geology*, 18, 1252-1255, 1990.

Brandon, M. T. and J. A. Vance, Tectonic evolution of the Cenozoic Olympic subduction complex, Washington State, as deduced from fission track ages from detrital zircons, *Amer. J. Sci.*, 292, 565-636, 1992.

Brandon, M. T., M. K. Roden-Tice, and J. I. Garver, Late Cenozoic exhumation of the Cascadia accretionary wedge in the Olympic Mountains, northwest Washington State, *Geol. Soc. Am. Bull.*, 110, 1998 in press.

Bull, W. B., Threshold of critical power in streams, *Geol. Soc. Am. Bull.*, 90, 453-464, 1979.

Bull, W. B., *Geomorphic response to climatic change*, 326p, Oxford University Press, 1991.

Bull, W. L. and P. L. K. Knuepfer, Adjustments by the Charwell River, New Zealand, to uplift and climatic changes, *Geomorphology*, 1, 15-32, 1987.

Bullard, T. F., Neotectonics, Geomorphology, and Late Quat. Geology across a forearc region impacted by the subduction of the aseismic Cocos Ridge, Pacific Coast, Costa Rica, PhD, University of New Mexico, Albuquerque, 1995.

Burbank, D. W., J. Leland, E. Fielding, N. Brozovic, R. S. Anderson, M. R. Reid, and C. Duncan, Bedrock incision, rock uplift and threshold hillslopes in the northwestern Himalayas, *Nature*, 379(6565), 505-510, 1996.

Carson, M. A., The existence of threshold hillslopes in the denudation of the landscape, *Trans. Inst. Brit. Geogr.*, 49, 71-95, 1970.

Carson, M. A., An application of the concept of threshold slopes to the Laramie Mountains, Wyoming, in *Special Publication 3*

Slopes: Form and Process, edited by D. Brunsden, pp. 31-48, Institute of British Geographers, London, 1971.

Crandell, D. R., Pleistocene glaciations of the southwestern Olympic Peninsula, Washington, *U. S. Geol. Surv. Prof. Pap.*, 501(B), 135-139, 1964.

Crandell, D. R., The glacial history of western Washington and Oregon, in *The Quat. of the United States*, edited by H. E. Wright and D. G. Frey, pp. 341-353, Princeton University Press, New Jersey, 1965.

Crickmay, C. H., Lateral activity on a river of Northwestern Canada, *J. Geology*, 68, 337-391, 1960.

Drake, P. G., Quaternary Geology and Tectonic Geomorphology of the Coastal Piedmont and Range, Puerto Quepos Area, Costa Rica, MS, University of New Mexico, Albuquerque, 183p, 1989.

Dumitru, T., Major Quaternary uplift along the northernmost San Andreas fault, King Range, northwestern California, *Geology*, 19, 526-529, 1991.

Easterbrook, D. J., Stratigraphy and chronology of Quaternary deposits of the Puget lowland and Olympic Mountains of Washington and the Cascade Mountains of Washington and Oregon, in *Quaternary glaciations in the northern hemisphere*, edited by V. Sibrava, D. Q. Bowen, and G. M. Richmond, pp. 145-159, Vol, 5, Quat. Sci. Rev., 1986.

Fisher, D. M., T. W. Gardner, and J. J. Marshall, Kinematics associated with late Tertiary and Quaternary deformation in central Costa Rica: Western boundary of the Panama micro-plate, *Geology*, 22, 263-266, 1994.

Fisher, D. M., T. W. Gardner, J. S. Marshall, P. B. Sak and M. Protti, The effects of subducting seafloor roughness on forearc kinematics, Pacific coast, Costa Rica, *Geology*, in press 1998.

Florer, L. E., Quaternary paleoecology and stratigraphy of the sea cliffs, western Olympic Peninsula, Washington, *Quat. Res.*, 2, 202-216, 1972.

Formento-Trigilio, M. L., The tectonic geomorphology and long-term landscape evolution of the southern Sierra Nacimiento, northern New Mexico, MS, University of New Mexico, Albuquerque, 201 p, 1997.

Formento-Trigilio, M. L. and F. J. Pazzaglia, Quaternary stratigraphy, tectonic geomorphology, and long-term landscape evolution of the southern Sierra Nacimiento, by 47th annual field guidebook, 335-346 p, New Mexico Geol. Society, 1996.

Formento-Trigilio, M. L. and F. J. Pazzaglia, Tectonic geomorphology of Sierra Nacimiento; traditional and new techniques in assessing long-term landscape evolution of the southern Rocky Mountains, *J. Geol.*, in press 1998.

Gansecki, C. A., G. A. Mahooh, and M. McWilliams, New ages for the climactic eruptions at Yellowstone: Single crystal 40Ar/39Ar dating identifies contamination, *Geology*, 26, 343-346, 1998.

Gardner, T. W., Experimental study of knickpoint and longitudinal profile evolution in cohesive, homogeneous material, *Geol. Soc. Am. Bull.*, 94, 664-672, 1983.

Gardner, T. W., D. M. Fisher, J. S. Marshall and M. Protti, Effects of Subducting Seafloor Roughness on Drainage Basin Evolution and Morphology in the Forearc of Costa Rica, paper presented at 4th International Conference on Geomorphology, Bologna, Italy, 174, 1997.

Gardner, T. W., P. W. Hare, F. J. Pazzaglia and I. D. Sasowsky, Evolution of Drainage Systems Along a Convergent Plate margin, Pacific Coast, Costa Rica, in *Geomorphic Systems of North America*, edited by W. L. Graf, pp. 357-372, Vol, Decade of North American Geology, Centennial Volume 2, Geol. Society of America, Boulder, Colorado, 1987.

Gardner, T. W., D. Verdonck, N. M. Pinter, R. Slingerland, K. P. Furlong, T. F. Bullard, and S. G. Wells, Quaternary uplift astride the aseismic Cocos Ridge, Pacific coast of Costa Rica, *Geol. Soc. Am. Bull.*, 104, 219-232, 1992.

Gilbert, G. K., *Report on the Geology of the Henry Mountains*, Government Printing Office, Washington, DC., 1877.

Hallett, R. B., Volcanic geology, paleomagnetism, geochronology, and geochemistry of the Rio Puerco necks, west-central New Mexico, Ph.D, Socorro, New Mexico Institute of Mining and Technology, 340 p., 1994.

Hallett, R. B., P. R. Kyle and W. C. McIntosh, Paleomagnetic and $^{40}Ar/^{39}Ar$ age constraints on the chronologic evolution of the Rio Puerco volcanic necks and Mesa Prieta, west-central New Mexico: Implications for transition zone magmatism, *Geol. Soc. Am. Bull.*, 109, 95-106, 1997.

Harbor, D. J., Dynamic equilibrium between an active uplift and the Sevier River, Utah, *J. Geology*, 106, 184-194, 1998.

Heusser, C. J., Palynology of four bog sections from the western Olympic Peninsula, Washington, *Ecology*, 45, 23-40, 1964.

Heusser, C. J., Palynology and phytogeographical significance of a late Pleistocene refugium near Kalaloch, Washington, *Quat. Res.*, 2., 189-201, 1972.

Heusser, C. J., Environmental sequence following the Fraser advance of the Juan de Fuca lobe, Washington, *Quat. Res.*, 3, 284-306, 1973.

Heusser, C. J., Quaternary vegetation, climate, and glaciation of the Hoh River Valley, Washington, *Geol. Society of Amer. Bull.*, 85, 1547-1560, 1974.

Heusser, C. J., Palynology of Quaternary deposits of the lower Bogachiel River area, Olympic Peninsula, Washington, *Can. J. Earth Sci.*, 15, 1568-1578, 1978.

Howard, A. D. and G. Kerby, Channel changes in badlands, *Geol. Soc. Am. Bull.*, 94, 739-752, 1983.

Hovius, N., Macro scale process systems of mountain belt erosion, in *Geomorphology and Global Tectonics*, edited by M. A. Summerfield, pp. John Wiley and Sons, New York, in press 1998.

Judson, S., Evolution of Appalachian topography, in *Theories of landform development*, edited by W. N. Flemal and R.C. Melhorn, pp. 29-44., Vol, Proceedings of the 6th Geomorphology Symposium, Publications in Geomorphology, State University of New York, Binghamton, New York, 1975.

Kelson, K. and S. G. Wells, Geologic influences on fluvial hydrology and bedload transport in small mountainous watersheds, northern New Mexico, U.S.A., *Earth Surf. Proc. Landf.*, 14, 671-690, 1989.

Kirkby, M. J., Hillslope process-response models based on the continuity equation, in *Special Publication 3: Slope form and process*, edited by D. Brundsden, pp. 15-30, Institute of British Geographers, London, 1971.

Kirkby, M. J., An erosion-limited hillslope evolution model, in *Functional geomorphology; landform analysis and models*,

edited by K. H. Schmidt, pp. 157-187, Vol, Catena Suppl. 23, Springer-Verlag, 1992.

Kirkby, M. J., Long term interactions between networks and hillslopes, in *Channel Network Hydrology*, edited by K. Beven and M. J. Kirkby, pp. 225-293 John Wiley and Sons, Chichester, 1993.

Knox, J. C., Concept of the graded stream, in *Theories of Landform Development 6th Geomorphology Symposium*, edited by W. N. Melhorn and R. C. Flemal, pp. 169-198, State University of New York at Binghamton., Binghamton, 1975.

Leopold, L. B. and W. B. Bull, Base level, aggradation, and grade, *Proc. Amer. Phil. Soc.*, 123, 168-202, 1979.

Leopold, L. B. and T. Maddock, The hydraulic geometry of stream channels and some physiographic implications, *U. S. Geol. Surv. Prof. Pap.*, 282(A), 36, 1953.

Leopold, L. B., M. G. Wolman and J. P. Miller, *Fluvial processes in Geomorphology*, 522p, W.H. Freeman, San Francisco, 1964.

Mackin, J. H., Concept of the graded river, *Geol. Soc. Amer. Bull.*, 59(5), 463-511, 1948.

Marshall, J. S., Evolution of the Orotina debris fan, Pacific coast, Costa Rica: Late Cenozoic tectonism along the western boundary of the Panama microplate, paper presented at Annual Meeting Abstracts with Programs, Geol. Soc. Amer., A207, 1994.

Marshall, J. S., T. W. Gardner and D. M. Fisher, Active tectonics across the western Caribbean-Panama boundary and the subducting rough-smooth boundary, Pacific coast, Costa Rica, paper presented at Annual Meeting Abstracts with Program, Geol. Society of Amer., A124, 1995.

Mathews, E. B., Submerged "deeps" in the Susquehanna River, *Geol. Soc. Am. Bull.*, 28, 335-346, 1917.

McLaughlin, R. J., S. A. Kling, R. Z. Poore, K. McDougall and E. C. Beutner, Post-middle Miocene accretion of Franciscan Rocks, northwestern California, *Geol. Soc. Am. Bull.*, 93, 595-605, 1982.

McLaughlin, R. J., W. V. Sliter, N. O. Frederiksen, W. P. Harbert and D. S. McCulloch, Plate motions recorded in tectonostratigraphic terranes of the Franciscan Complex and evolution of the Mendocino triple junction, *U. S. Geol. Surv. Bull.*, B1997, 60, 1994.

Merritts, D. J., The Mendocino triple junction: Active faults, episodic coastal emergence, and rapid uplift, *J. Geophys. Res.*, 101(B3), 6051-6070, 1996.

Merritts, D. J. and K. R. Vincent, Geomorphic response of coastal streams to low, intermediate, and high rates of uplift, Mendocino, triple junction region, northern California, *Geol. Soc. Am. Bull.*, 101, 1373-1388, 1989.

Merritts, D. J. and W. B. Bull, Interpreting Quaternary uplift rates at the Mendocino triple junction, northern California, from uplifted marine terraces, *Geology*, 17, 1020-1024, 1989.

Merritts, D. J., T. B. Dunklin, K. R. Vincent, E. E. Wohl and W. B. Bull, Quaternary tectonics and topography, Mendocino triple junction, in *A look at the southern end of the Cascadia subduction zone and the Mendocino triple junction*, edited by R. M. Burke and G. A. Carver, pp. 119-169, Vol, Field Trip guidebook, Friends of the Pleistocene Guidebook, Arcata, Humbolt State University, 1992.

Meyer, G. A., S. G. Wells, and A. J. T. Jull, Fire and alluvial chronology in Yellowstone National Park: Climate and intrinsic controls on Holocene geomorphic processes, *Geol. Soc. Am. Bull.*, 107, 1211-1230, 1995.

Merritts, D. J., K. R. Vincent and E. E. Wohl, Long river profiles, tectonism, and eustasy: A guide to interpreting fluvial terraces., *J. Geophys. Res. (Special Issue on Tectonics and Topography)*, 99(B7), 14031-14050, 1994.

Miller, J. R., The influence of bedrock geology on knickpoint development and channel-bed degradation along downcutting streams in south-central Indiana, *J. Geol.*, 99, 591-605, 1991.

Montgomery, D. R., T. B. Abbe, J. M. Buffington, N. P. Peterson, K. M. Schmidt and Stock J. D., Distribution of bedrock and alluvial channels in forested mountain drainage areas, *Nature*, 381(June 13th), 587-589, 1996.

National Oceanic and Atmospheric Administration (NOAA), Local climatological data, in *Annual Summaries*, Environmental Data Service, National Climatic Center, Department of Commerce, Washington, D.C, 1985.

Ohmori, H., Change in the mathematical function type describing the longitudinal profile of a river through an evolutionary process, *J. Geol.*, 99, 97-110, 1991.

Oppenheimer, D. H., G. C. Beroza, G. A. Carver, L. Dengler, J. P. Eaton, L. Gee, F. I. Gonzalez, A. S. Jakyo, W. H. Li, L. M., M. Magee, G. A. Marshall, M. Murray, R. McPherson, B. Romanowicz, K. Satake, R. W. Simpson, P. G. Somerville, R. S. Stein, and D. Valentine, The Cape Mendocino, California earthquake sequence of April, 1992: Subduction at the triple junction, *Science*, 261, 433-438, 1993.

Pazzaglia, F. J., Stratigraphy, petrography, and correlation of late Cenozoic middle Atlantic Coastal Plain deposits: Implications for late-stage passive margin geologic evolution, *Geol. Soc. Am. Bull.*, 105, 1617-1634, 1993.

Pazzaglia, F. J. and M. T. Brandon, Macrogeomorphic evolution of the post-Triassic Appalachian Mountains determined by deconvolution of the offshore basin sedimentary record, *Basin Res..*, 8, 255-278, 1996.

Pazzaglia, F. J. and T. W. Gardner, Fluvial terraces of the lower Susquehanna River, *Geomorphology*, 8, 83-113, 1993.

Pazzaglia, F. J. and T. W. Gardner, Late Cenozoic flexural deformation of the middle U.S. Atlantic margin, *J. Geophys. Res.*, 99(B6), 12,143-12,157, 1994.

Pazzaglia, F. J. and T. W. Gardner, Late Cenozoic large-scale landscape evolution of the U.S. Atlantic passive margin, in *Geomorphology and Global Tectonics*, edited by M. Summerfield, pp. John Wiley and Sons, New York, 1998.

Pazzaglia, F. J. and S. A. Kelley, Large-scale geomorphology and fission-track thermochronology in topographic and exhumation reconstructions of the southern Rocky Mountains, in *Lithospheric evolution of the Rocky Mountains: Rocky Mountain Geology.*, edited by K. Karlstrom, pp. (in press 1998).

Pazzaglia, F. J., J. L. Pederson, G. A., D. Koning and C. Toya, Geologic map and report of the Jemez Pueblo quadrangle, New Mexico, by U.S. Geol. Surv. Open File Map 000,, 1998.

Pinter, N. and M. T. Brandon, How erosion builds mountains, *Scientific Amer.*, 276, 60-65, 1997.

Rau, W. W., Geology of the Washington coast between Point

Grenville and the Hoh River:, *Geology and Earth Resources Division Bull. (Washington Department of Natural Resources)*, 66, 58, 1973.

Ritter, J. B. and T. W. Gardner, Hydrologic evolution of drainage basins disturbed by surface mining, central Pennsylvania, *Geol. Soc. Am. Bull.*, 105, 101-115, 1993.

Rogers, J. B., Jemez River terraces: preliminary constraints on Quaternary incision, terraces, and breaching of the Valles caldera, Jemez Mountains, New Mexico, *New Mexico Geology*, 16, 58-59, 1994.

Rogers, J. B., The fluvial landscape evolution of San Diego Canyon, Jemez Mountains, New Mexico, M.S., University of New Mexico, Albuquerque, 123 p, 1996.

Rogers, J. B. and R. A. Smartt, Climatic influences on Quaternary alluvial stratigraphy and terrace formation in the Jemez River valley, New Mexico, in *The Jemez Mountains Region*, edited by F. Goff, B. S. Kues, L. D. McFadden, and J. N. Gardner, pp. 347-356, Forty-seventh annual field conference, New Mexico Geol. Society, 1996.

Saunders, I. R., J. J. Clague and M. C. Roberts, Deglaciation of the Chilliwack River valley, British Columbia, *Can. J. Earth Sci.*, 24, 915-923, 1987.

Schmidt, K. M. and D. R. Montgomery, Limits to relief, *Science*, 270, 617-620, 1995.

Schumm, S. A. and R. W. Lichty, Time, space, and causality in geomorphology, *Amer. J. Sci.*, 263, 110-119, 1965.

Schumm, S. A., M. P. Mosley, and W. E. Weaver, *Experimental Fluvial Geomorphology*, 413p. Wiley Interscience, New York, 1987.

Seidl, M. A. and W. E. Dietrich, The problem of channel erosion into bedrock, in *Functional Geomorphology*, edited by K. H. Schmidt and J. d. Ploey, pp. 101-124, Vol, Catena Supplement 23, 1992.

Seidl, M. A., W. E. Dietrich and J. W. Kirchner, Longitudinal profile development into bedrock: an analysis of Hawaiian channels, *J. Geol.*, 102, 457-474, 1994.

Sinha, S. K. and G. Parker, Causes of concavity in longitudinal profiles of rivers, *Water Resources Res.*, 32, 1417-1428, 1996.

Sklar, L., W. E. Dietrich, and A. D. Howard, The influence of sediment supply on river incision into bedrock: A theoretical investigation, *EOS Trans., AGU*, 77, 46, 251-252, 1996.

Sklar, L. and W. E. Dietrich, The influence of downstream variations in sediment supply and transport capacity on bedrock channel longitudinal profiles, *EOS Trans. AGU*, 78(F), 229, 1997.

Slingerland, R., S. D. Willet and H. L. Henessey, A new fluvial bedrock erosion model based on the work-energy principle [Abstract], *EOS Trans. AGU*, 78(F), 299-300, 1997.

Snow, R. S. and R. L. Slingerland, Mathematical modeling of graded river profiles, *J. Geol.*, 95, 15-33, 1987.

Stock, J. D., Can we predict the rate of bedrock river incision (using the stream power law)? M.S., University of Washington, Seattle, 57, 1996.

Stock, J. D. and D. R. Montgomery, Can we predict the rate of bedrock river incision using the stream power law?, *J. Geophys. Res.*, in press, 1998.

Stock, J. D., D. R. Montgomery and N. P. Peterson, Extreme rates of bedrock river incision, Satsop River, Washington [Abstract], *EOS Trans. AGU*, 77(46), F252, 1996.

Sugai, T., River terrace development by concurrent fluvial processes and climate changes, *Geomorphology*, 6, 243-252, 1993.

Tabor, R. W. and W. M. Cady, Geologic Map of the Olympic Peninsula, by I-994, 2 sheets ed., Vol. U.S. Geol. Surv. Map, Washington, 1978.

Thackray, G. D., Glaciation and neotectonic deformation on the western Olympic Peninsula, Washington, Ph.D., University of Washington, Seattle, 139 p., 1996.

Thackray, G. D. and F. J. Pazzaglia, Quaternary stratigraphy, tectonic geomorphology, and fluvial evolution of the western Olympic Peninsula, Washington, in *Geologic field trips in the Pacific Northwest Annual Meeting*, edited by D. A. Swanson and R. A. Haugerud, pp. 2A-1 - 2A-30, Geol. Society of Amer.., Washington, 1994.

Thompson, G. H., Geomorphology of the lower Susquehanna River gorge: Guidebook, in *Fifty-fifth Annual Field Conference of Pennsylvania Geologists, Lancaster County, Pennsylvania*, edited pp. 86-106, Pennsylvania Geol. Surv., Harrisburg, 1990.

Tucker, G. E., Predicting sediment flux from fold and thrust belts, *Basin Res.*, 8, 329-349, 1996.

Weldon, R. J., Late Cenozoic geology of Cajon Pass; implications for tectonics and sedimentation along the San Andreas fault, Ph.D, California Institute of Technology, 400 p. 1986.

Willemin, J. H. and P. L. K. Knuepfer, Kinematics of arc-continent collision in the eastern Central Range of Taiwan inferred from geomorphic analysis, *J. Geophys. Res.*, 99(B10), 20,267-20,280, 1994.

Wohl, E. E., N. Greenbaum, A. P. Schick and V. R. Baker, Controls on bedrock channel incision along Nahal Paran, Israel, *Earth Surface Processes and Landforms*, 19, 1-13, 1994.

Wolman, M. G. and J. P Miller, Magnitude and frequency of forces in geomorphic processes, *J. Geology* 68, 54-74, 1960.

Wolman, M. G. and R. Gerson, Relative scales of time and effectiveness of climate in watershed geomorphology, *Earth Surface Processes*, 3, 189-208, 1978.

Young, R. W. and I. McDougall, Long-term landscape evolution: Early Miocene and modern rivers in southern New South Wales, Australia, *J. Geol.*, 101, 35-49, 1993.

Yoxall, W. H., The relationship between falling base level and lateral erosion in experimental streams, *Geol. Soc. of Am. Bull.* 80, 1379-1384, 1969.

Gardner, T. W., Department of Geology, Trinity University, San Antonio, TX 78212, email: tgardner@trinity.edu.

Merritts, D. J., Department of Geosciences, Franklin and Marshall College, P.O. Box 3003, Lancaster, PA 17604, email: d_merritts@acad.fandm.edu.

Pazzaglia, F. J., Department of Earth and Planetary Sciences, University of New Mexico, Albuquerque, NM 87131-1116, email: fjp@unm.edu.

River Longitudinal Profiles and Bedrock Incision Models: Stream Power and the Influence of Sediment Supply

Leonard Sklar and William E. Dietrich

Department of Geology and Geophysics, University of California, Berkeley, California

The simplicity and apparent mechanistic basis of the stream power river incision law have led to its wide use in empirical and theoretical studies. Here we identify constraints on its calibration and application, and present a mechanistic theory for the effects of sediment supply on incision rates which spotlights additional limitations on the applicability of the stream power law. On channels steeper than about 20%, incision is probably dominated by episodic debris flows, and on sufficiently gentle slopes, sediment may bury the bedrock and prevent erosion. These two limits bound the application of the stream power law and strongly constrain the possible combination of parameters in the law. In order to avoid infinite slopes at the drainage divide in numerical models of river profiles using the stream power law it is commonly assumed that the first grid cell is unchanneled. We show, however, that the size of the grid may strongly influence the calculated equilibrium relief. Analysis of slope-drainage area relationships for a river network in a Northern California watershed using digital elevation data and review of data previously reported by *Hack* reveal that non-equilibrium profiles may produce well defined slope-area relationships (as expected in equilibrium channels), but large differences between tributaries may point to disequilibrium conditions. To explore the role of variations in sediment supply and transport capacity in bedrock incision we introduce a mechanistic model for abrasion of bedrock by saltating bedload. The model predicts that incision rates reach a maximum at intermediate levels of sediment supply and transport capacity. Incision rates decline away from the maximum with either decreasing supply (due to a shortage of tools) or increasing supply (due to gradual bed alluviation), and with either decreasing transport capacity (due to less energetic particle movement) or increasing transport capacity (due less frequent particle impacts per unit bed area). We use this model to predict longitudinal profiles under varying boundary conditions and sediment supply rates and find that even in actively downcutting rivers, the river slope needed to maintain incision may be only slightly greater than the slope required to transport the imposed load. Hence,

1. INTRODUCTION

River incision into bedrock, which drives landscape evolution and links topography to tectonics and climate, is a poorly understood process that is typically modeled as depending on the stream power expenditure of some unspecified flow recurrence [e.g. *Howard et al.*, 1994]. While a

Rivers Over Rock: Fluvial Processes in Bedrock Channels
Geophysical Monograph 107

the channel slope-drainage area relationships of rivers actively cutting through bedrock may predominately reflect the grain size and supply rate of sediment and only secondarily the influence of bedrock resistance to erosion.

stream power approach has the great appeal of simplicity, and to some degree appears testable with topographic data [*Howard and Kerby*, 1983; *Seidl and Dietrich*, 1992; *Seidl et al.*, 1994; *Stock and Montgomery*, in press], it obviously throws a blanket over a wide range of processes which may not comfortably fit into such a framework. As others have argued, these processes include not only abrasion by bedload and suspended load, but also erosion by plucking, cavitation, dissolution, periodic debris flows, and propagating knickpoints, all of which are unlikely to be characterized by some common stream power parameterization [*Howard et al.*, 1994]. Nonetheless, if the collective effect of these processes leads to river profiles that can be simulated by a simple stream power law, which, in turn, can be calibrated with river longitudinal profile analysis, then perhaps this law will suffice for modeling purposes.

Here we raise several issues about calibrating the stream power law and interpreting river profiles in light of this law. To do this, we review the derivation of the law and then explore limits to its application due to changes in processes and the influence of sediment supply. With the advent of widely available digital elevation data, the temptation is to use longitudinal profile analysis as evidence for, and calibration of, the stream power law by assuming approximately spatially uniform rates of erosion through the river profile. We show that care must be taken to avoid the effects of covariation of the coefficients and exponents in the fitted power law. Also, given that the erosion law should only apply to fluvial dominated erosion of channels and that the bedrock should be either exposed or not far from the surface, the possible combination of values of coefficients and exponents seems fairly constrained.

We illustrate the stream power analysis of longitudinal profiles with an example from a watershed in Northern California. Overall, we suggest that even in its simplest form, the stream power law may not be fully calibrated or validated from observations of longitudinal profiles and estimates of erosion rates, as it is difficult to confirm assumptions about initial conditions and long-term boundary conditions. More importantly, the basic idea of relating stream power to incision into bedrock may be seriously deficient in its specific neglect of the role of sediment size and supply.

Finally, we briefly review a new mechanistic model for river incision in which the abrasion by bedload is specifically treated [*Sklar et al.*, 1996]. Rather than provide a detailed accounting of this model, which will be presented elsewhere [*Sklar and Dietrich*, in press], we focus here on some implications of the model results for stream power-based longitudinal profile analysis. Our results suggest that in many actively downcutting cases, the shape of the profile may be more a reflection of the sediment load than it is an adjustment to an imposed lowering rate at its downstream boundary. Perhaps surprisingly, we are forced to conclude that the simple stream power hypothesis is difficult to validate, is limited to only a portion of the river network, and inadequately accounts for the effects of sediment.

2. STREAM POWER ANALYSIS OF RIVER LONGITUDINAL PROFILES

2.1. The Stream Power Bedrock Incision Rate Law

A simple and yet mechanistic approach to modeling river incision into bedrock is to propose that incision rate is proportional to stream power (Ω), the rate of energy expenditure by the flow [*Seidl and Dietrich*, 1992; *Howard et al.*, 1994]. Bedrock erosion rate (E), in units of volume eroded per channel bed area per time, can then be expressed as

$$E = \frac{K_p \Omega}{W} = \frac{K_p \rho_f g S Q_w}{W} \tag{1}$$

where S is channel slope, Q_w is a dominant discharge of unspecified recurrence interval, W is channel width, ρ_f is fluid density, g is gravitational acceleration, and K_p is a dimensional coefficient representing the efficiency of the incision process. Discharge is assumed to vary with drainage area (A)

$$Q_w = K_a A^r \tag{2}$$

and width is assumed to vary with discharge

$$W = K_w Q_w^{\ b} = K_w K_a^{\ b} A^{rb} \tag{3}$$

so that incision rate becomes a power function of area and slope

$$E = K_y A^{r(1-b)} S \tag{4}$$

where $K_y = K_p \rho_f g K_a^{\ 1-b} / K_w$.

Alternatively, incision rate can be assumed to be proportional to the average boundary shear stress [*Howard*, 1971a; *Howard and Kerby*, 1983], which as *Howard et al.* [1994] show in detail, can also be expressed in terms of area and slope

$$E = K_z A^{0.6r(1-b)} S^{0.7} \tag{5}$$

where $K_z = K_t \rho_f g (N_m K_a^{\ 1-b} / K_w K_p K_n)^{0.6}$, K_t represents rock erodibility, N_m is Manning's roughness coefficient and K_n

is a channel cross-section shape factor. In general, equations (4) and (5) suggest an incision rate law of the form

$$E = KA^mS^n \quad (6).$$

For convenience we will hereafter adopt the convention of referring to equation (6) as the 'stream power law' without implying any particular values for the exponents m and n, and without asserting it is an actual physical law.

The stream power law is appealing because it has a minimum number of parameters, is readily used in landscape modeling, and because it can be empirically calibrated from topographic data [*Howard and Kerby*, 1983; *Seidl and Dietrich*, 1992; *Seidl et al.*, 1994; *Stock and Montgomery*, in press]. But its simplicity comes at the price of obscuring the richness of the process mechanics. The exponent m, for example, incorporates hydrologic effects such as orographic gradients in mean precipitation, and the downstream rate of change in channel width, which for bedrock channels is not well understood. The coefficient K aggregates the influence of many factors, including channel geometry, hydraulic roughness, the magnitude-frequency relations implicit in the assumption of a dominant discharge, and rock resistance to erosion, which will vary with incision process, rock type, degree of weathering and tectonic history [e.g. *Augistinus*, 1991; *Selby*, 1980; *Suzuki*, 1982]. In addition to the factors specifically identified in the derivation of the stream power law, the value of K will also vary in space and time with shifts in the dominant incision mechanism, and with the quantity and size distribution of sediment supplied to the channel. Comparing values of K estimated from different rivers is further complicated by the fact that, because K is a dimensional coefficient, the magnitude and dimensions of K depend on the value of the exponent m.

To date only a handful of field studies have reported values for the exponents m and n. *Howard and Kerby* [1983] measured the spatial variation of erosion rates in an anthropogenic badlands in Virginia and found best fit values of m = 0.45 and n = 0.7, which are generally consistent with the assumption that bedrock incision rate is proportional to average boundary shear stress. Working in the Oregon Coast Ranges, *Seidl and Dietrich* [1992] compared the slope-area relationships at tributary junctions, where local incision rate and lithology were assumed to be constant, and obtained a ratio of m/n = 1.0, which is consistent with incision rate varying linearly with the stream power per unit channel length. Subsequent work in Hawaii, and analysis of data from Michigan reported in 1965 by *Hack* [*Seidl et al*, 1994], support a form of equation (6) with m and n = 1.0. Recently *Stock and Montgomery* [in press] attempted to calibrate equation (6) by numerically reconstructing incision into preserved paleo-surfaces by rivers in diverse tectonic and lithologic settings. They concluded that no single set of values for m or n applied to all rivers studied, and that differences in boundary conditions had a strong influence on the best fit parameters. They also recognized that estimates of K depended on the values assumed for the exponents m and n.

For topographically steady state longitudinal profiles in homogeneous lithology, if erosion is proportional to stream power per unit channel bed area, then there will be a uniform rate of stream power expenditure. Hence, in the context of river network theory, the often used assumption that river networks evolve towards a state of uniform energy expenditure [e.g. *Leopold and Langbein*, 1962; *Rodriquez-Iturbe and Rinaldo*, 1997] is equivalent to arguing that the networks evolve towards a spatially constant rate of incision. In this case, if discharge increases linearly with drainage area [r = 1 in equation (2)] while the width of the river bed increases as the 0.5 power of drainage area (as could be inferred from the general hydraulic geometry relationships of *Leopold and Maddock* [1953]), then m = 0.5 (if n = 1.0). These exponent values are used in the Optimal Channel Network theory of *Rodriquez-Iturbe* and his colleagues [i.e. *Rodriquez-Iturbe and Rinaldo*, 1997].

2.2. Applying the Stream Power Law to River Profiles

River longitudinal profiles can be used to infer the form of the incision rate law (i.e. the value of the exponent ratio m/n), at least in settings where incision rate and the factors which go into K can be assumed to be approximately spatially uniform. The stream power law [equation (6)] can be rearranged to solve for the dependence of channel slope on drainage area

$$S = K_sA^{-m/n} \quad (7)$$

where $K_s = (E/K)^{1/n}$, and the value of the ratio m/n can then be evaluated from the slope of a regression line in log-log space. With the advent of digital elevation models (DEMs) and the wide availability of digital topographic maps, this type of analysis offers the potential of a vastly increased data set.

Early quantitative studies of river longitudinal profiles [e.g. *Hack*, 1957; *Miller*, 1958; *Brush*, 1961] report values of the exponent in equation (7), which they call '*z*', ranging approximately from 0 to 1.0. These studies were not concerned with bedrock incision but rather with interpreting longitudinal profile form in terms of the size and durability of sediment supplied to the channel. Nonetheless, the occurrence of frequent bedrock outcrops suggests active incision in many of the streams they studied.

The ratio m/n strongly reflects river profile concavity. Larger values of m/n correspond to more concave profiles. Profile concavity also depends on the downstream rate of accumulation of drainage area

$$A = cx_d^f \quad (8)$$

where x_d is the distance downstream of the drainage divide, and the dimensional coefficient c and the exponent f are empirically determined. The exponent f describes the basin

shape, typically varying between 1.0 and 2.0 [e.g. *Brush*, 1961]. *Hack* [1957] proposed that basins tend toward a value of 1.67, although over large scales the value may be constrained to be close to 2.0 [*Montgomery and Dietrich*, 1992]. *Howard* [1971b] argued that greater values of m/n should correlate with wider basins (i.e. larger f) because more concave basins have a competitive advantage over less concave neighboring basins in eroding drainage divides.

Regression analysis of river slope against drainage area data can be used to estimate K_s and m/n in equation (7). Comparing values of K_s measured on different profiles, however, can be confounded by the inherent scale-dependent covariance of regression intercept with regression slope. In order to remove the dependence of K_s on m/n, equation (7) can be rewritten to obtain a non-dimensional coefficient by normalizing drainage area by a representative area (A_r) in the center of the range of area data

$$S = S_r\left(\frac{A}{A_r}\right)^{-m/n} \tag{9}$$

so that S_r is a representative slope [i.e. $S_r = S(A_r) = K_s A_r^{-m/n} = (E/K)^{1/n} A_r^{-m/n}$] which expresses the relative steepness of the profile. S_r can be used to check the assumption of uniformity in incision rate and lithology within a drainage basin by comparing S_r values obtained from individual subbasin profiles. This approach will be illustrated below.

Seidl and Dietrich [1992] showed that the ratio m/n can be estimated at tributary junctions, where, if the tributary joins the principal stream smoothly (i.e. without a waterfall), the assumption of similar incision rates and rock resistance for very different slopes and drainage areas is most reasonable. Setting equation (6) equal for both the tributary and principal channel, they obtained

$$m/n = \frac{\log(S_t/S_p)}{\log(A_p/A_t)} \tag{10}$$

where the subscripts t and p refer to tributary and principal streams respectively.

The longitudinal profile method of estimating m/n [equations (7) or (9)] has the advantage of yielding information about the controls on profile relief, as expressed in the ratio E/K, but requires that the assumption of spatial uniformity in E/K apply throughout the profile. The reverse is true of the tributary junction method [equation (10)], knowledge of E/K is exchanged for relaxing the assumption of basin-wide uniformity. Both methods should converge on the same value for m/n in an ideal, uniformly adjusted basin.

2.3. Modeling Equilibrium River Profiles

Here we look at equilibrium river longitudinal profiles to address two issues in modeling landscapes with the stream power law: 1) process constraints on the range of values of m/n and K where the stream power law might be appropriate, and 2) the sensitivity of model profile relief to the drainage area at the upstream channel boundary. We focus on equilibrium profiles because these constraints are more clearly illustrated, even though they apply to non-equilibrium conditions as well. The term 'equilibrium river profile' is used here to indicate a profile in which erosion rate is constant throughout the length of the river. This may happen in landscapes subject to long periods of steady uniform rock uplift in which the river incision rate matches the constant rock uplift rate. In this case, the profile boundary condition of uniform rock uplift is equivalent to a steady base level lowering.

The stream power law is generally intended to represent incision due to fluvial processes in bedrock dominated channels [*Howard et al.*, 1994]. Although the stream power law has no mathematical limit to how steep or gentle a channel slope can be, there is a finite range of slopes where fluvial processes, bedrock exposures, and active channel incision can be expected to occur. Figure 1 illustrates three major bounds to the application of the stream power erosion law.

An upper slope limit to the application of the stream power law may exist where channel incision occurs predominantly by debris flows [*Seidl and Dietrich*, 1992]. While we know of no theory for debris flow incision, empirically there is evidence that at least in some river systems there is a break in the slope-area relationship. Above a gradient of about 0.2, channel slopes have been found to be roughly straight, hence independent of drainage area [*Seidl and Dietrich*, 1992; *Montgomery and Foufoula-Georgiou*, 1993; *Dietrich and Montgomery*, in press]. On such slopes, field observations suggest that debris flows are the dominant sediment transporting agent [e.g. *Benda and Dunne*, 1997], and therefore are likely responsible for valley incision. In Figure 1, we have drawn a horizontal line at a slope of 0.2 to represent an upper bound on the applicability of the fluvial stream power erosion law.

This value of 0.2 is not meant to be precise. In fact, debris flows may dominate erosion on slopes well below this value, as low as 0.05 perhaps. Furthermore, on slopes steeper than about 0.08, the ratio of grain size to flow depth is greater than 1.0 for initial motion and conventional fluvial hydraulics do not apply [e.g. *Wiberg and Smith*, 1987]. Movement of coarse debris in these channels may be dominated by canyon-confined flood events [*Grant et al.*, 1990]. Hence, one can expect that the values of m/n and K may vary in this transition reach between lower gradient, clearly fluvial dominated conditions below about 5% up to the debris flow dominated steeper reaches.

The lower bound to the application of the stream power erosion law should be where the channel slope is sufficiently low such that the bed is chronically covered with sediment to a depth greater than the flood scour depth. This lower bound is not as yet defined, and may vary greatly with sediment supply. In Figure 1 we suggest a lower

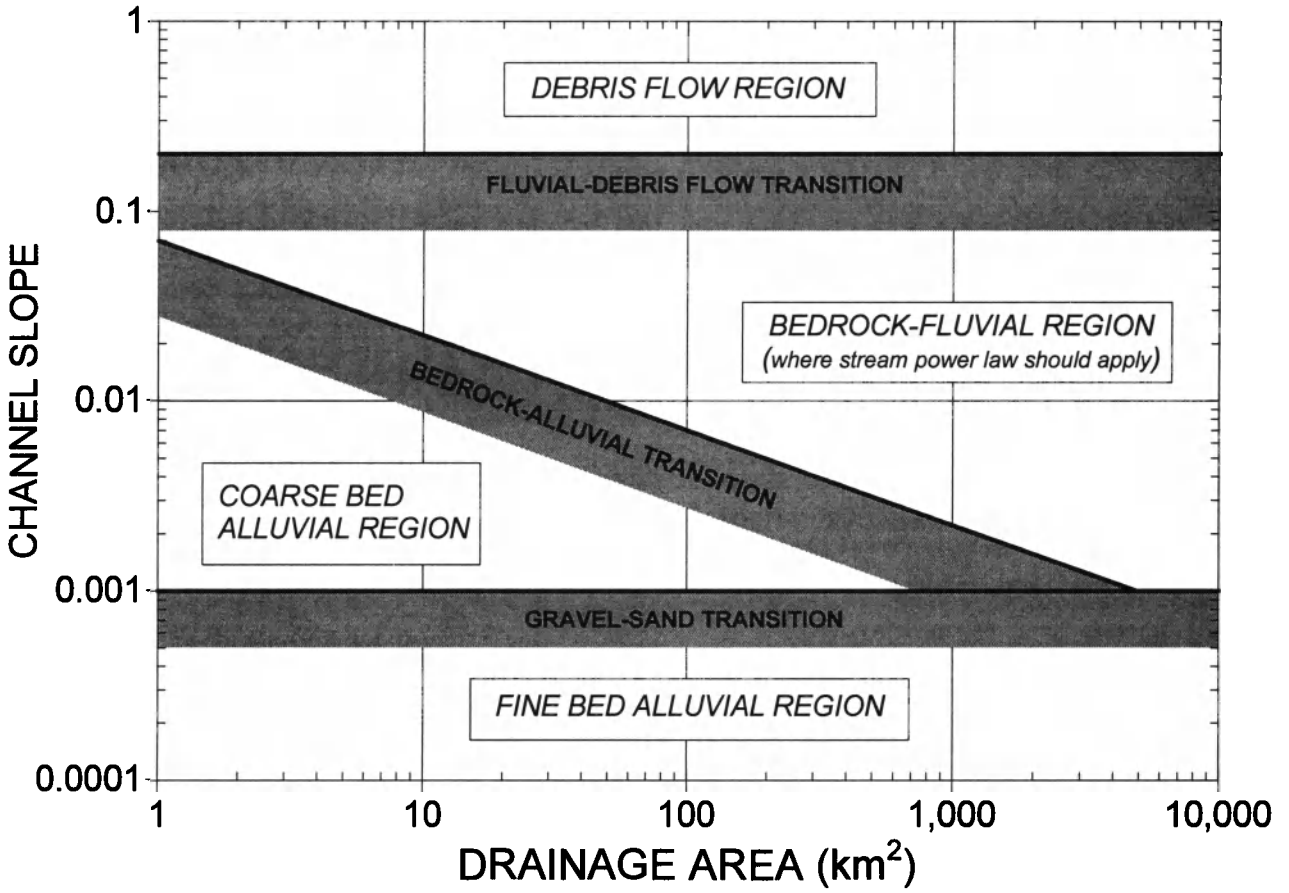

Figure 1. Illustration of constraints on slope-area region where bedrock incision by fluvial processes should occur, and thus where stream power law may apply. Suggested upper and lower slope bounds and width of process transition zones are approximate. Transition between coarse-bed alluvial and bedrock-bedded channels is estimated by $S = 0.07A^{-0.5}$ [*Montgomery et al.*, 1996], but will depend on grain size and sediment supply rate.

bound slope value of about 0.001, as commonly below this value rivers are sand-bedded and less likely to be actively cutting through rock, although we do not mean to suggest that sand-bedded rivers can not erode bedrock. Rarely are gravel bedded rivers found with slopes as low at 0.0001, as suggested by data reported by *Smith and Ferguson* [1995].

Between the upper and lower bounds shown in Figure 1 is a diagonal line which represents the threshold between bedrock and alluvium dominated channel beds. *Howard* [1980, 1987] has argued that the transition from alluvium to bedrock bedded channels is a fundamental threshold in the landscape, and occurs where sediment transport capacity exceeds sediment supply in the full range of grain sizes supplied to the channel. *Howard and Kerby* [1983] and *Montgomery et al.* [1996] have observed empirically that, for a given drainage area, there is a corresponding slope where the bedrock-alluvial transition occurs. As *Howard et al.* [1994] have shown, the minimum bedrock slope (S_m) can thus be expressed as a function of drainage area

$$S_m = K_m A^{-u} \tag{11}$$

where K_m and u depend on sediment supply and grain size. The bedrock-alluvium transition in Figure 1 is described by equation (11) with u = 0.5 and K_m = 0.07 km [*Montgomery et al.*, 1996]. Channels with a thin mantle of alluvium over bedrock, which might plot below the bedrock alluvial transition, can incise during scouring events or with shifting exposures of bedrock [e.g. *Howard and Kerby*, 1983]. Whether the stream power law applies to such channels depends on whether the slope is set by the requirement to transport the imposed sediment load or by the need to incise at the rate of rock uplift. This question will be addressed in more detail below.

Each suggested bound in Figure 1 should be considered a wide band as the process hand-offs implied here are not abrupt. If such bounds are roughly correct, they define a region in which a river longitudinal profile must exist if it is going to be fluvially dominated and able to erode its bed (referred to in Figure 1 as the bedrock-fluvial region).

Modeled equilibrium longitudinal profiles formed by stream power dominated processes, in which incision rate (E) and the coefficient K are spatially uniform, will plot as a straight line in Figure 1 and will extend from the upslope maximum gradient (and minimum drainage area) to the downslope minimum gradient (and maximum drainage area). Whether the entire profile lies within the fluvial-bedrock region will depend on the slope of the line (m/n), the intercept (K_s), and the size of the drainage area at the upstream and downstream boundaries of the profile. In other words, for a given channel length, basin shape, and drainage area at the upstream boundary, there is a limited range of combinations of m/n and K_s [and thus $(E/K)^{1/n}$] which will produce equilibrium profiles which fall entirely within the range of applicability of the stream power law. This can be explored analytically.

River profiles modeled with the stream power law must begin at an upstream boundary with an initial drainage area, because channel nodes with zero drainage area will not incise. Equation (8) can be modified so that

$$A = A_o + cx_h^f \tag{12}$$

where A_o is the area draining to the channel head and x_h is the distance downstream of the channel head. (Alternatively, A_o could be considered the area draining to the furthest upstream point along the profile where fluvial processes dominate.) The advantage of this approach is that no assumption is made about whether the values of c and f in equation (8) derived from the entire basin apply near the channel head [*Hack and Goodlett*, 1960]. Combining equations (7) and (12) we obtain

$$S(x_h) = \left(\frac{E}{K}\right)^{1/n}(A_o + cx_h^f)^{-m/n} = -\frac{dz}{dx_h} \tag{13}$$

where z is elevation. The elevation of any point along the profile is the integral of equation (13) from the channel outlet (x_h=L) to the point of interest

$$z(x_h) = \left(\frac{E}{K}\right)^{1/n}\int_{x_h}^{L}\left(A_o+cx^f\right)^{-m/n}dx \tag{14}$$

which must be integrated numerically unless f or m/n = 1. The profile relief is $z(x_h = 0)$, the elevation at the channel head.

From solutions to equation (14) we can construct Figure 2, which illustrates the constraints on m/n and $(E/K)^{1/n}$ by mapping the percentage of the total profile relief which has slope-area combinations in the 'bedrock-fluvial region' shown in Figure 1. Contours of equal percentages of profile relief are plotted for equilibrium profiles where L = 100 km, A_o = 1 km^2, f = 1.5 and c = 1 km$^{0.5}$. Figure 2 shows that for any choice of m/n between 0 and 2.0 there is only about an order of magnitude range of $(E/K)^{1/n}$ for which the stream power law is applicable for all or even the majority of the equilibrium profile relief. Thus, for steady state model profiles, a narrow range of possible values of K is effectively specified by the imposed erosion rate and ratio m/n. Note that even when most of the model profile length is within the bedrock fluvial range, much of the overall profile relief could occur in a small profile segment with channel slopes in the debris flow range.

Note that converting values of $(E/K)^{1/n}$ to S_r by normalizing the local drainage area by A_r (which would be about 5 km^2 in this case) would have the effect of removing the diagonal trend from the plot in Figure 2, but would not change the fundamental result. Note also that the particular values plotted can shift considerably for different choices of L, A_o, f and c so that data derived from basins where those parameters have other values cannot necessarily be plotted directly on Figure 2. Nevertheless, the plot illustrates that for the river profile to lie consistently below the debris flow threshold and above the threshold of alluvial burial (and cessation of incision), there is a only a narrow range of values of $(E/K)^{1/n}$ that are appropriate.

In the above example A_o was set to the relatively large value of 1 km^2 to reduce the sensitivity of the result to the size of the unchanneled area. As A_o gets smaller, the slope at the upstream boundary becomes correspondingly steeper, and the overall profile relief becomes greater. If the unchanneled area were allowed to go to an infinitely small value, the channel slope at the channel tip would approach vertical and consequently the relief would approach infinite. In models of landscape evolution, this result is avoided by one of two means, either a threshold area where channels begin is specified analytically (for example by solving for the area where the rate of erosion by hillslope processes equals that of fluvial incision [*Howard*, 1997]) or the minimum area is set to equal the size of one grid cell [*Tucker and Slingerland*, 1994]. If the drainage area at the upstream boundary is arbitrarily set to equal one grid cell, then the smaller the grid scale, the steeper the channel at the tip. As can be seen from equation (14) the sensitivity of profile relief to A_o depends on the ratio m/n. This is illustrated in Figure 3 where equilibrium profile relief as a function of A_o is plotted for a range of values of m/n, where E = 0.001 m/yr, n = 1.0, c, f and L are as in the previous example (Figure 2). K is fixed at 0.005, with dimensions depending on the value of m, which varies between 0.25 and 1.0. In this example, the sensitivity of profile relief to the choice of A_o increases with greater values of the ratio m/n.

It is beyond the scope of this paper to explore the sensitivity of profile relief to the full range of possible combinations

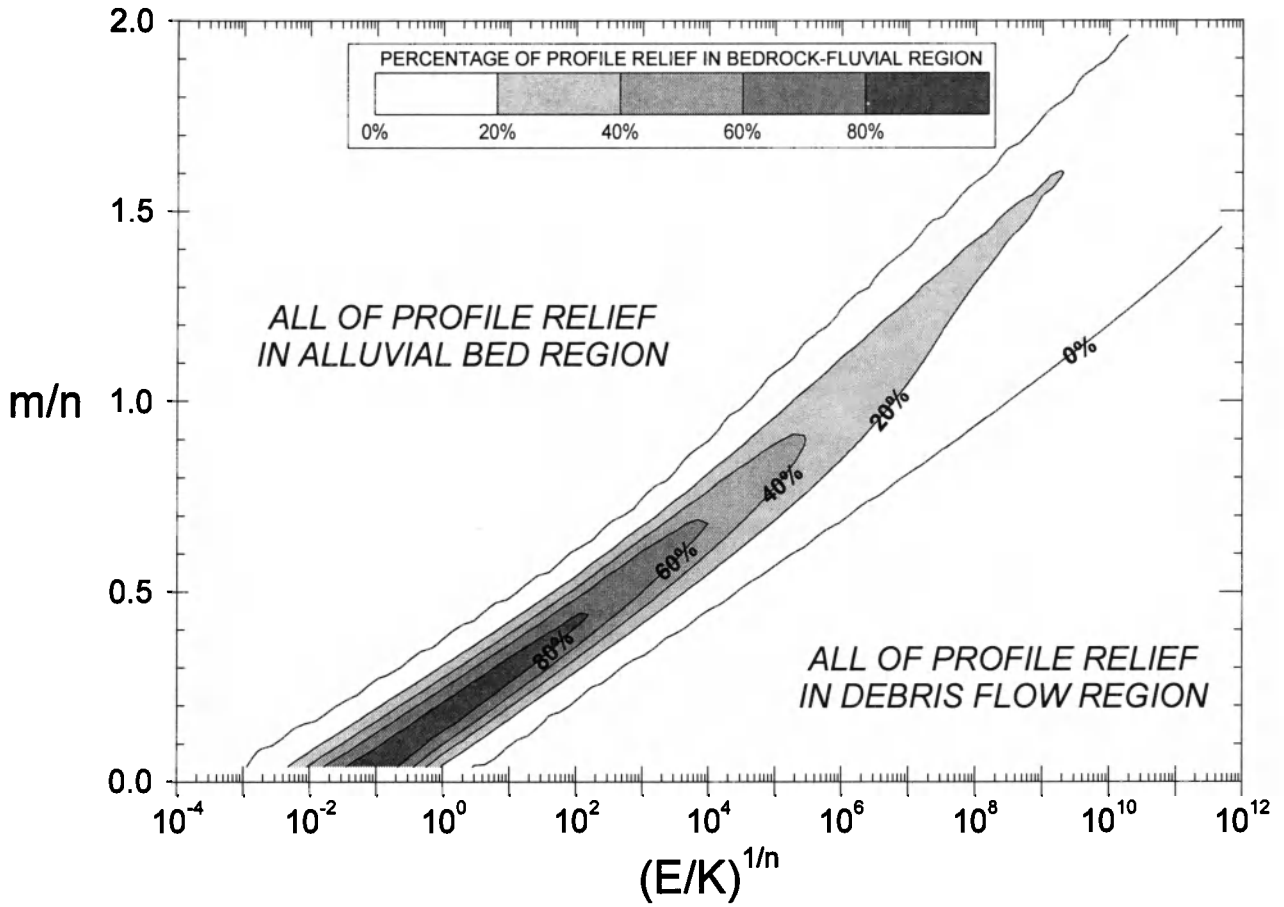

Figure 2. Contours of equal percentage of equilibrium profile relief within 'bedrock-fluvial' region (axis out of page) as a function of ratio of stream power exponents (m/n) and slope-area intercept [$K_s = (E/K)^{1/n}$]. Debris flow region and alluvial-bedded region correspond to those in Figure 1. Parameter values in text.

of the eight relevant parameters in equation (14). The question of how to treat the upstream boundary condition, however, serves to illustrate how even a simple incision rule such as the stream power law can invoke rather complex behavior in numerical modeling of landscape evolution. Thus, caution is called for when interpreting the results of modeling exercises where, for example, the stream power law is used to explain relief in terms of tectonics, lithology or climate.

3. PROFILE ANALYSIS OF THE UPPER NOYO RIVER BASIN, CALIFORNIA

In this section we explore how the parameters of the stream power bedrock incision rate law might be calibrated from analysis of a river network using data derived from digitized topographic maps. Consensus on the appropriate parameter values for use in river profile modeling has been hampered by the wide variation found in the small number of empirical studies to date [*Howard et al.*, 1994]. The recent availability of large digital topographic data sets offers the possibility that a global value of m/n may emerge from analysis of a sufficiently large set of river networks.

Stream power analysis of contemporary river profiles requires the assumption of an equilibrium profile form. Although the basin we examine here shows some evidence of disequilibrium conditions, it allows us to consider the role of the equilibrium assumption in the calibration of the stream power law by longitudinal profile analysis.

The upper Noyo River drains a 143 km^2 basin on the west side of the California Coast Ranges, entering the Pacific Ocean at Ft. Bragg, about 220 km northwest of San Francisco. The basin is underlain by mixed sandstones and shales of the Franciscan Formation [*Kilbourne*, 1986] and is located astride a complicated tectonic plate boundary.

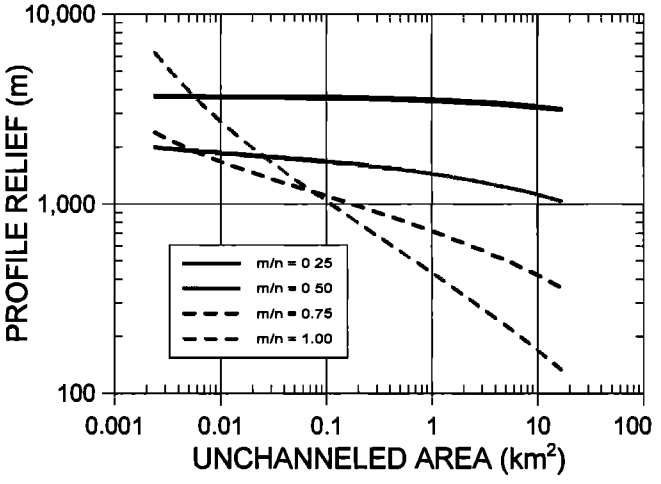

Figure 3. Sensitivity of equilibrium profile relief to choice of drainage area at the upstream boundary, for various values of the stream power exponent ratio m/n. Parameter values in text.

Based on flights of marine terraces near the Noyo, the average uplift rate during the Pleistocene has been estimated at about 0.3 mm/yr [*Merritts and Vincent*, 1989].

Figure 4 is a topographic map of the upper Noyo basin with 200 ft contours. The channel profile data are derived from USGS 40-ft-contour, 1:24,000 topographic maps. The channel network was hand digitized from the mapped blue lines and combined with a digital line graph of the topographic contours. Channel slopes are calculated between nodes where the channels cross contours or where tributaries connect to the main stem. The tributaries rarely meet the main stem at contour crossings, so the local slopes at junctions are calculated by interpolation and are the least accurate slope estimates. The drainage area for each channel node is calculated in a 10 m grid DEM overlay of the channel network.

Figure 5a is a plot of the channel slope-drainage area data for the seven principal streams of the upper Noyo River basin (no hillslope or small tributary elements are included). The most striking feature of this plot is the lack of areal dependence for channel elements with slopes greater than about 20%, nearly all of which have drainage areas of less than about 1 km^2. We interpret this as evidence of a shift to debris flow processes in steep, lower order channels. In the following analysis all channel elements steeper than 0.2 have been excluded.

Figure 5b shows the reduced slope-area data set relative to two empirical alluvial-bedrock threshold lines defined elsewhere [*Montgomery et al.*, 1996; *Stillwater Sciences*, unpublished data]. Field observations in the basin indicate that the channel bed is mostly mantled with alluvium, but that bedrock outcrops in the bed are common. Field observations also suggest that the site is currently receiving a relatively high coarse sediment load due to land use disturbance associated with intensive timber harvesting. Although we don't expect there to be a global value for the alluvium-bedrock threshold [*Howard et al.*, 1994], the data plot close to these lines and suggest that the upper part of the river network may tend to be more bedrock dominated than the lower part.

As a whole, a regression of the Noyo data shown in Figure 5a ($S < 0.2$) yields a value for m/n of 0.65, with an R squared of 0.75. Aggregating the data from the seven different profiles, however, ignores the physical fact that water and sediment take particular paths through the landscape; it is therefore more appropriate to look at the m/n values obtained for each profile individually. As listed in Table 1, profile-specific values for m/n range from 0.56 to 1.1, with a mean of about 0.75. Further limiting the analysis to channel elements which drain more than 1 km^2 (approximately where the break in the slope-area relationship occurs), does not significantly change the result.

Figures 6 and 7 illustrate the effect of non-dimensionalizing K_s to remove the artifactual influence of values of m/n. If we express drainage area in units of m^2, because the regression intercept lies far from the center of the data, the values of K_s range over more than four orders of magnitude (Table 1) and appear to depend on the value of m/n (Figure 6). Using equation (9), with $A_r = 3$ km^2, the strong covariance of K_s with m/n is removed; S_r shows no apparent relationship with m/n (Figure 7). The range of S_r is from 0.02 to 0.08 (Table 1). Note that using drainage area units of km^2 would move the intercept closer to the center of this particular data set, but for larger basins would still produce significant covariation between K_s and m/n.

The variation in estimated values for m/n between profiles could be due to several factors, including disequilibrium in incision rates and the effects of variable sediment supply. Inter-profile variation in the normalized intercept S_r can be interpreted as a measure of the differences between sub-basins in incision rate, rock resistance, or any of the other factors contributing to K. Significant spatial heterogeneity between sub-basins suggests non-uniformity within individual basins as well.

In order to avoid the assumption of network-wide constant erosion rates, we examine next just the slope-area relationships at the tributary junctions. Figure 8 is a plot of the ratios of channel slopes and drainage areas at tributary junctions along the seven principal streams of the Noyo basin. Channel elements with slopes greater than 20% have been excluded. A weak relationship is apparent ($R^2 = 0.36$), with an m/n value of about 0.34, roughly half the value estimated from the aggregated long profiles. Sorting the data by profile does not improve the result. The poor fit is explained by considering Figure 9 where the individual channel slopes and drainage areas for all channel elements making up the set of tributary junctions are plotted. The tributary channel slopes have no systematic dependence on drainage area. The m/n value estimated in Figure 8 is

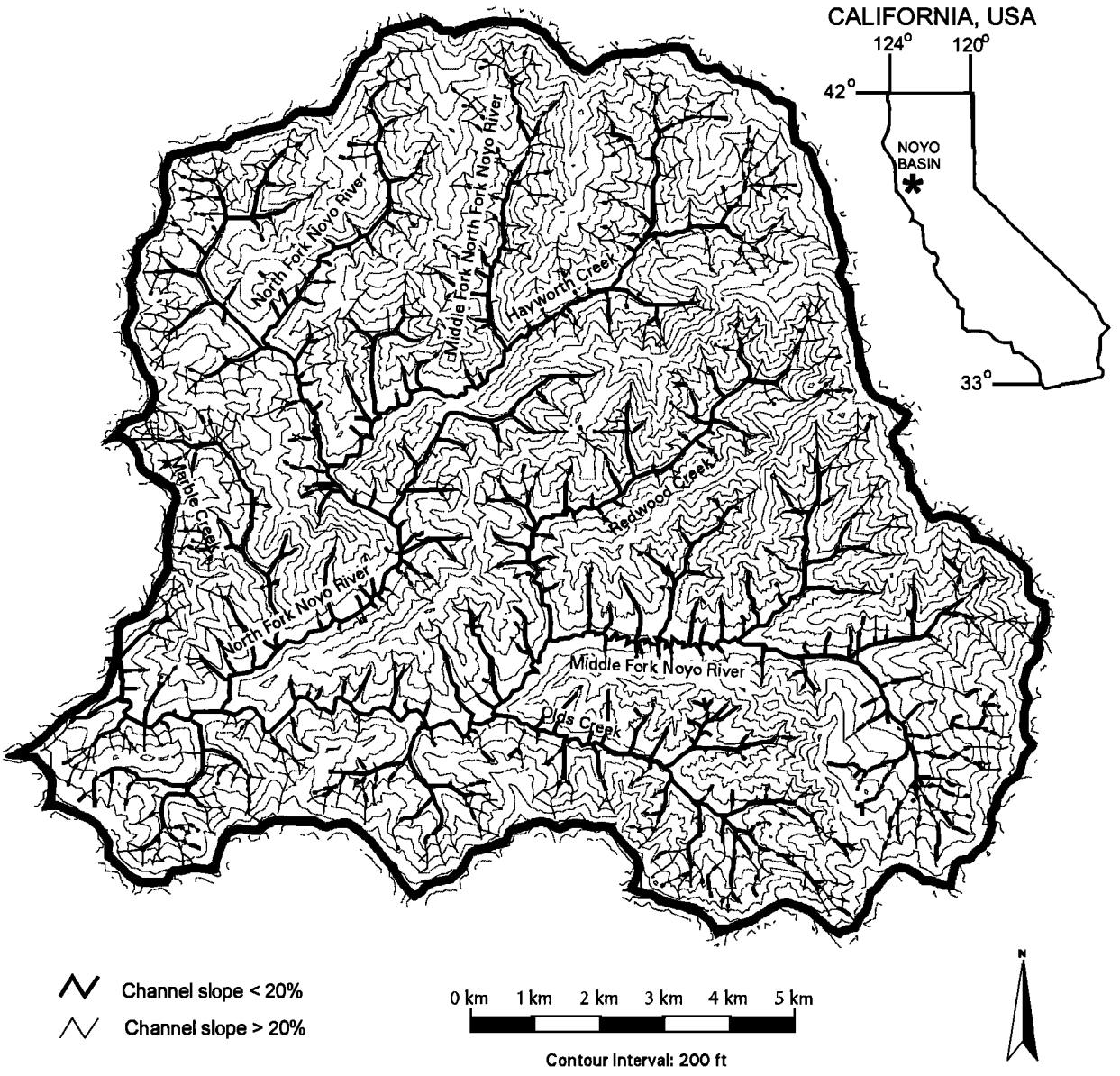

Figure 4. Topographic map of upper Noyo River basin, Mendocino County, California, with 200 ft. contour intervals. Channel segments with slopes > 20% are indicated by thin lines; those with slopes < 20% by thick lines. Seven principal streams discussed in the text are labeled.

roughly equivalent to the value obtained by fitting a line through all the data in Figure 5a.

The apparent lack of areal dependence in the channel slopes of the tributary streams may be a signal of a disequilibrium in incision pattern through the basin. The valley floor along the principal streams is wide and appears in many places to be underlain by bedrock, i.e. an active strath rather than a deep valley fill (Figure 4). We interpret this wide valley bottom as evidence for a period of arrested vertical incision which has allowed lateral incision and valley widening to occur along the principal streams. We note that tributaries draining areas smaller than about 1 km^2 generally do not have wide valley bottoms. It may be, therefore, that these smaller tributaries slopes are responding to rather complex dynamic boundary conditions associated with the widening of the valley bottoms.

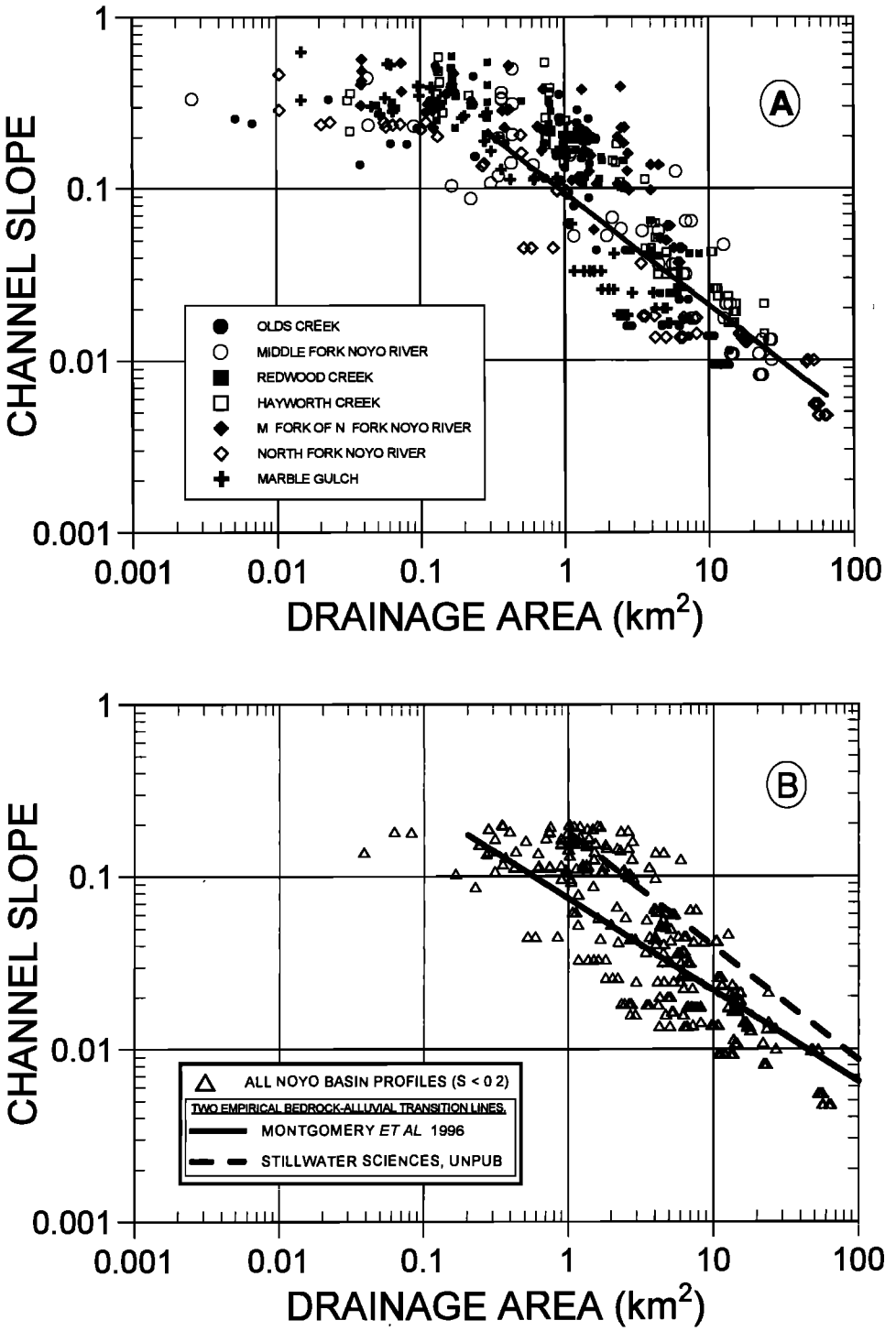

Figure 5. (A) Local channel slope and drainage area for seven profiles of the upper Noyo River basin. Plotted regression line, $S = 0.096A^{-0.65}$ ($R^2 = 0.75$), is for all channel elements with $S < 0.2$. (B) Comparison of upper Noyo basin channel slope and drainage area ($S < 0.2$) with empirical bedrock-alluvial transition threshold lines from *Montgomery et al.* [1996], and *Stillwater Sciences* [unpublished data].

TABLE 1. Summary of Longitudinal Profile Regression Results for the Upper Noyo River Basin.

Profile Name	m/n	K_s	R^2	S_r	Number of Data Points	Drainage Area (km^2)
Marble Gulch	0.89	15,000	0.84	0.024	36	5.4
North Fork Noyo River	0.56	130	0.90	0.030	70	64.7
Middle Fork North Fork Noyo River	0.65	1,500	0.58	0.087	36	6.3
Hayworth Creek	0.83	18,000	0.90	0.077	47	24.1
Redwood Creek	1.13	1,200,000	0.83	0.061	33	7.4
Middle Fork Noyo River	0.59	300	0.78	0.044	55	23.3
Olds Creek	0.67	810	0.73	0.036	44	13.7
Mean	0.76	180,000	0.80	0.051	46	21.0

K_s calculated with drainage area in units of m^2.
S_r calculated assuming $A_r = 3$ km^2.

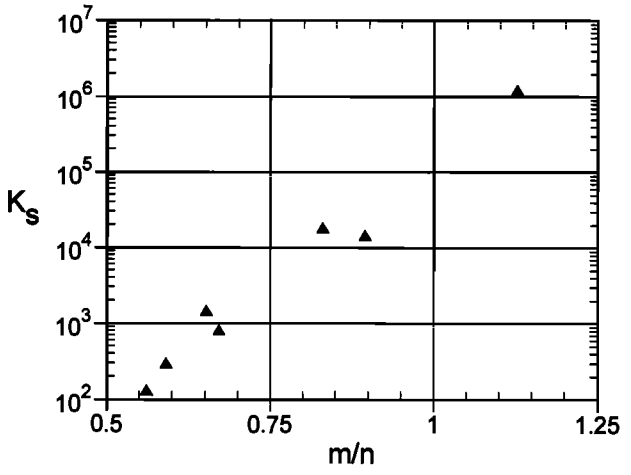

Figure 6. Covariation of regression intercept [$K_s = (E/K)^{1/n}$] with regression slope (m/n) for upper Noyo River basin profiles, K_s in units of $m^{2m/n}$.

The issue of disequilibrium between incision rate and relative base level lowering and its effects on the slope-area relationship may be more directly examined by exploring the data reported by *Hack* [1965] for rivers near Ontonagon, Michigan, which have incised following the post-glacial lowering of Lake Superior. Incision rates varied significantly with drainage area along these channels. *Seidl et al.* [1994] show that the erosion rate inferred by *Hack* from local valley depth can be linearly correlated with the product of drainage area and channel slope, suggesting that m and n = 1.0 in equation (6). This result, however, is not uniquely constrained by the data; a wide range of m and n values fit the data equally well. In fact, combinations of values of m and n which produce ratios of m/n >> 1.0 are consistent with the data, leading *Hack* to conclude that incision rate varied with drainage area independent of channel slope.

Although the Ontonagon channel profiles represent a clear case of disequilibrium, a reasonably well defined slope-area relationship exists in these data, as shown in Figure 10, suggesting a value of m/n of 0.33. This example shows that use of the equilibrium assumption in a slope-area analysis of longitudinal profiles to extract information about m, n and K may produce strong correlations, but lead to potentially incorrect evaluations of these parameters due to disequilibrium effects, which are often much more difficult to discern than in the Ontonagon region.

A confounding factor in slope-area analysis of river profiles is the undefined role in the stream power law of sediment supply and grain size. It may be that in the case of the upper Noyo basin, as suggested by Figure 5b and field observations, the lower reaches are predominantly alluvium mantled, limiting the rates of vertical incision. *Seidl et al.* [1994] have shown that stream power-based modeling of

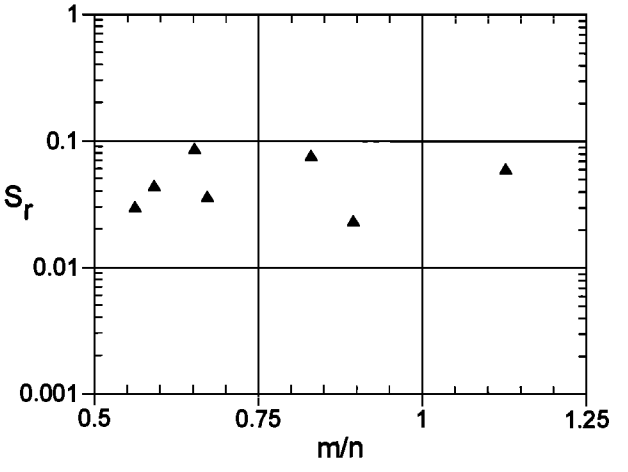

Figure 7. Non-dimensionalized regression intercept (S_r) and regression slope (m/n) for upper Noyo River basin profiles.

Hawaiian longitudinal profiles incorrectly predicts near zero slopes for the lower reaches. They argue that boulder deposition in these channels has inhibited channel incision and forced the channel gradients to be relatively steep (from 0.08 to 0.14). From examination of Appalachian streams where bedrock commonly occurs in the bed, *Hack* [1957] proposed that the slope-area relationship depends in part on the on median grain size of the bed material.

It is tempting to assume that the effects of variable sediment supply and grain size on bedrock incision rate can be submerged in the coefficient K. The complexities of sediment transport dynamics and their influence on both the mechanics of incision and the extent of exposure of bedrock in the channel bed, however, suggest that the role of sediment in bedrock incision is a critical unknown which confounds the use of the stream power law in interpreting river longitudinal profiles. In the next section, we specifically explore the role of sediment supply on bedrock incision rates and the development of equilibrium river profiles.

4. A COUPLED BEDLOAD TRANSPORT AND BEDROCK INCISION MODEL

4.1. Model Development

Gilbert [1877] was the first to propose that sediment supply should have a controlling influence on the rate of river incision into bedrock. He suggested that at low supply rates relative to transport capacity, increasing supply would increase the rate of abrasion, but that once the load became sufficiently great, particles would interact with each other to form mobile deposits which would cover portions of the bed and the incision rate would decrease. *Gilbert* [1877] hypothesized that there would be an optimum load, 'far within the transporting capacity' [p. 106] which would cause the most rapid incision. Hence, sediment supply should influence bedrock incision rates in two fundamental and opposing ways: 1) by providing tools to the flow to abrade the bed, and 2) by controlling the areal extent of bedrock exposed to the erosive forces of the flow.

Foley [1980] adapted *Bitter's* [1963a, 1963b] model for sandblast erosion to formulate an expression for bedrock incision rate as a function of sediment supply, but only addressed the "tools effect" half of Gilbert's hypothesis. Similarly, *Howard et al.* [1994] parameterized other ballistic erosion studies [*Head and Harr*, 1970; *Engle*, 1976] without accounting for progressive bed cover by increasing sediment load. The limiting effect of high sediment concentration on erosion rate has been demonstrated in engineering studies of slurry pipe wall wear [e.g. *de Bree et al.*, 1982; *Slingerland et al.*, 1997].

Here we briefly review a quasi-mechanistic model, which couples bedload sediment transport and abrasion of bedrock, to investigate the Gilbert hypothesis [*Sklar et al.*, 1996; *Sklar and Dietrich*, 1997]. The full development of the model will be reported elsewhere [*Sklar and Dietrich*, in press]. The model considers only erosion by saltating bedload, and neglects the potential for bedrock erosion by suspended load and other mechanisms such as plucking, cavitation and dissolution. We focus on abrasion because particle impacts arguably provide the avenue of most concentrated momentum transfer from the flow to the bed, and because all bedrock channels transport some sediment. We limit our analysis to saltating bedload because by definition bedload interacts more frequently with the bed than does the suspended load, and because saltation dynamics are reasonably well understood [e.g. *Wiberg and Smith*, 1985]. Here we provide an overview of the model and use it to explore the influence of variable sediment supply on longitudinal profile form in actively incising landscapes.

Bedrock erosion rate (E) is assumed to be proportional to the normal component of the flux of kinetic energy of bedload colliding with exposed bedrock in the channel bed in excess of that necessary to dislodge particles from the bedrock surface, i.e.

$$E = \left[\frac{\sin(\alpha)\rho_s\pi(u_s^2 + v_s^2) - \varepsilon_t}{\varepsilon_v}\right]\left[\frac{Q_s}{\rho_s\pi D^3 W\lambda}\right]\left[1 - \frac{Q_s}{Q_t}\right] \quad (15)$$

(i) (ii) (iii)

where D is a uniform grain size [m], u_s and w_s are horizontal and vertical sediment velocities on impact respectively [m/s], Q_s is mass flux of sediment supply [kg/s], Q_t is the sediment transport capacity [kg/s], W is channel width [m], λ is saltation length [m], α is the angle of particle impact, ρ_s is sediment density [kg/m^3], ε_v is the energy required to detach a unit volume of bedrock [J/m^3], and ε_t is a energy threshold which must be exceeded for detachment to occur [J]. Transport capacity is calculated by a Meyer-Peter and Muller-type bedload equation

$$Q_t = 8W\rho_s\left(\frac{(\rho_s - \rho_f)gD^3}{\rho_s}\right)^{0.5}(\tau^* - \tau_c^*)^{1.5} \quad (16)$$

where τ^* is a non-dimensional boundary shear stress

$$\tau^* = \frac{\rho_f RS}{(\rho_s - \rho_f)D} \quad (17)$$

τ_c^* is the value of τ^* at the threshold of particle motion, here set to 0.047, R is the hydraulic radius and S is the channel slope [*Raudkivi*, 1990]. The two energy terms in this model represent rock resistance to abrasion and are treated as free parameters as little is known about them.

Erosion rate is simply the product of three terms, labeled below equation (15): i) the volume of material removed per particle impact, which is a function of the impacting particle's kinetic energy (normal to the bed) above some threshold (ε_t); ii) the particle impact rate per unit area, which depends on total sediment flux per channel width, grain size,

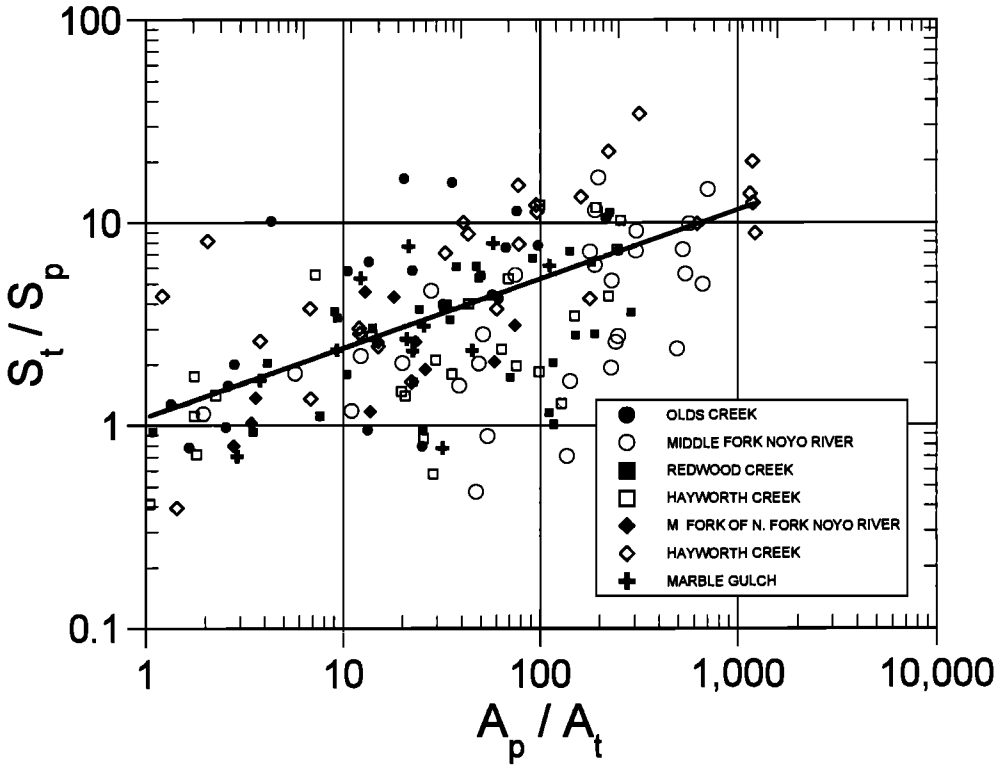

Figure 8. Ratios of tributary slope to principal slope and principal area to tributary area for stream junctions on seven upper Noyo River basin profiles. Plotted regression line is $S_t/S_p = 1.1(A_p/A_t)^{0.34}$ ($R^2 = 0.36$).

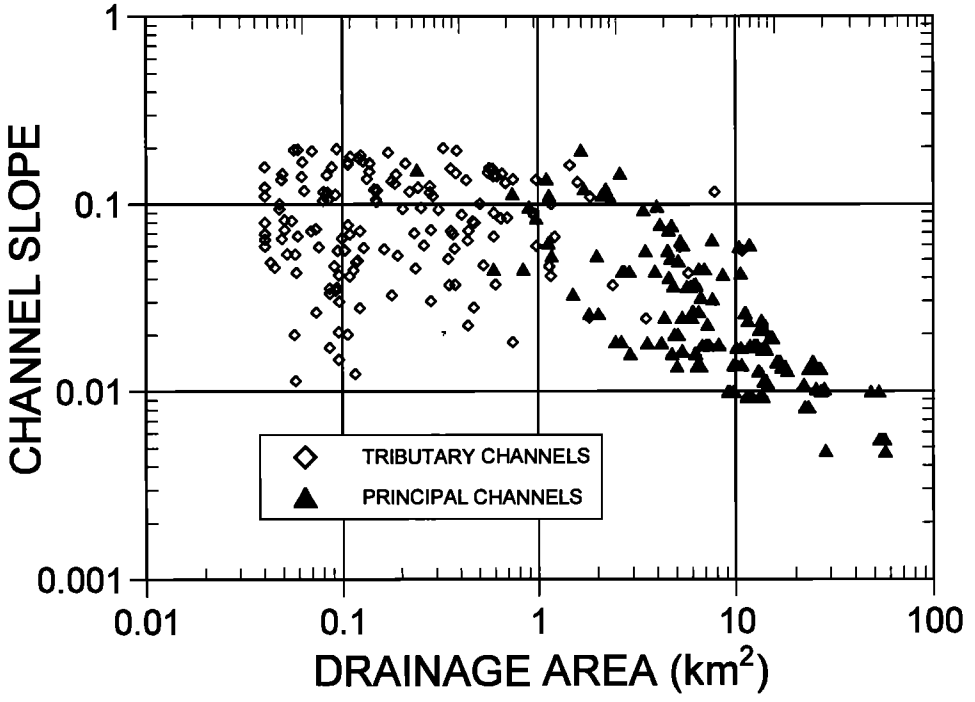

Figure 9. Local channel slope and drainage area for channel elements at tributary junctions for the streams plotted in Figure 8.

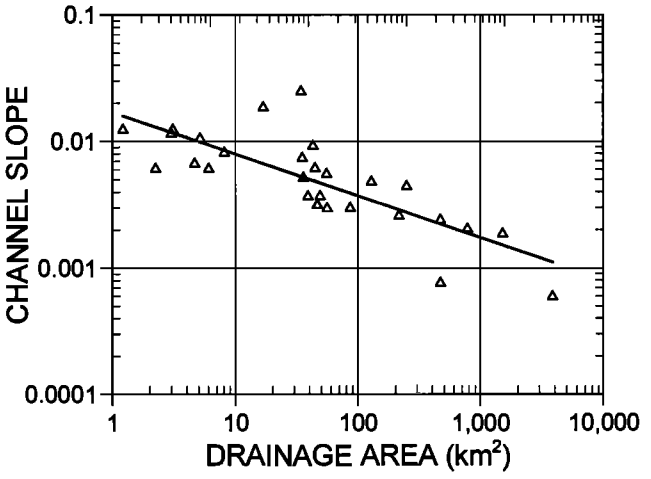

Figure 10. Channel slope and drainage area data for non-equilibrium profiles in Ontonagon, Michigan, as reported by *Hack* [1965]. Plotted regression line is $S = 1.7A^{-0.33}$ ($R^2 = 0.62$).

and the saltation hop length; and iii) the fraction of the channel bed composed of exposed bedrock, which is assumed to depend on the extent of excess transport capacity.

The calculation of bedrock erosion rate begins with the input variables of Q_s, D, W, S, discharge (Q_w), and a roughness coefficient (N_m), which are used to calculate the hydraulics which drive sediment transport. The channel cross-section is assumed to be rectangular and Manning's equation is used to calculate flow depth and thus hydraulic radius. Expressions for λ and u_s are taken from published studies of saltation trajectories [e.g. *Wiberg and Smith*, 1985] and are functions of excess shear stress (i.e. the ratio τ^*/τ_c^*). Vertical sediment velocity on impact is assumed to vary linearly between the fall velocity in still water [$w_s = f(D)$] and zero (corresponding to suspension), depending on the ratio of w_s to the shear velocity [$u^* = (gRS)^{0.5}$], such that $w_s = w_s$ when $w_s >> u^*$ and $w_s = 0$ when $w_s = u^*$. The model is not an attempt to realistically represent the complexity of particle motion and grain-to-grain interaction or the physics of bedrock fracture and detachment, but rather to capture mechanistically, with a minimum of free parameters, the gross effect of variations in sediment supply and transport capacity on bedrock abrasion rates.

Figure 11 illustrates the dependence of incision rate on sediment supply predicted by equation (15). For a fixed width, discharge and slope, incision rate increases with increasing sediment supply to a maximum. It then declines with further increases in sediment supply until incision is halted when the bed is fully covered. Note that the maximum incision rate itself increases with increasing slope, but then declines with further increases in slope. This effect results from the reduced frequency of particle impacts at high transport capacity due to increasing saltation hop length. In effect, the particles approach suspension and expend less energy per unit area, causing less wear. Hence, the model predicts two maxima: one associated with increases in sediment supply and the second associated with changes in the mode of transport with increasing excess shear stress.

The erosion law proposed in equation (15) can be fully portrayed for a fixed, uniform grain size by plotting bedrock incision rate as a function of two non-dimensional variables: the ratio of sediment supply to transport capacity (which is equivalent to the proportion of bed covered with sediment in this model), and the excess shear stress or transport stage (Figure 12). Note that the absolute values of the incision rate are arbitrary because they depend on the rock strength parameter (ε_v) in equation (15) which is a free parameter. The curves in Figure 11 are in effect vertical slices through the surface plotted in Figure 12, parallel to the vertical axis. Similar slices running parallel to the horizontal axis reveal, in effect, the second kind of maximum in erosion rate which results from the mode of transport shifting from bedload toward suspended load. Note that there is redundancy on the axes in that Q_t depends on excess shear stress to the 1.5 power in the Meyer-Peter and Muller bedload equation. The advantage of the non-dimensionalization of the sediment supply axis is that a unique solution is found for all reasonable combinations of channel slope, width and water discharge.

Dissecting the surface in Figure 12 by placing lines through the maximum erosion rate and parallel to the axes, creates four distinct quadrants. In the lower two quadrants (A and D), a 'tools effect' dominates. Increases in sediment supply accelerate incision due to more numerous particle collisions with the bed. In the upper two quadrants (B and C) a 'coverage effect' dominates. Here incision rate will increase if supply is reduced because of the increased fraction of bedrock exposed in the channel bed. On the other hand, in the two left quadrants (A and B), increases in sediment transport capacity, due to increases in either channel slope or discharge, result in more rapid incision as particle impacts become more energetic. Conversely, in the two right quadrants (C and D), increases in transport capacity reduce incision rate because the increase in particle energy is more than offset by the longer particle hop lengths and resulting reduction in frequency of particle impacts.

Note that bed coverage, or the extent of bedrock exposure, can be considered in either a spatial or a temporal sense. Spatially, a high fraction of channel bed covered with alluvium could, for example, be due to the presence of large bars which leave bedrock exposed only on the floor of deep pools. From a temporal perspective, the fraction of bed covered could be interpreted to represent the frequency of events which scour through a channel-spanning thin mantle of alluvium. Note also that the region of Figure 12 to the right of the transport maximum (quadrants C and D), where increases in slope or discharge have the effect of reducing incision rate by pushing the transport mode closer to suspension, the model predicts behavior opposite to that implied

by the stream power law. Such a situation may arise in channels carrying relatively fine grained bedload, perhaps due to rapid particle breakdown or to a low supply rate of coarse material.

4.2. Implications for Equilibrium Longitudinal Profiles

Below we report the results of four numerical experiments in which we explore the effects of rock uplift rate, sediment supply and grain size variation on equilibrium river longitudinal profiles (Table 2). In this one-dimensional model profile analysis, we use power function relationships to define the discharge dependence on drainage area, the channel bed width dependence on drainage area, and the drainage area dependence on distance from the upstream profile boundary [equations (2), (3) and (12), respectively]. We introduce bedload sediment to the profile as being proportional to drainage area,

$$Q_s = K_b A^p \tag{18}$$

in which K_b and p are free parameters [*Milliman and Syvitski*, 1992]. We assume that all the introduced bedload size material remains in bedload transport mode, i.e. there is no downstream loss to suspended load due to particle breakdown. In the case of downstream decreasing grain size, we use the Sternberg-like law

$$D = D_0 e^{-\phi x_s} \tag{19}$$

in which the representative grain size (D) decreases exponentially with distance downstream [*Krumbein*, 1937]. Although the grain size reduces downstream, in the case run here, we assume that the bedload fraction mass flux still follows the loading according to equation (18).

The drainage area to the channel head, A_0, is set at 1 km^2 to focus the model on the fluvial part of the profile (as suggested by the upper Noyo basin example). Mass of sediment in transport is conserved between channel elements but erosion rate and sediment supply are decoupled because supply is considered to be only the bedload fraction of the total mass removed from the basin and the material worn from the bed is assumed to leave as suspended or wash load.

Table 2 describes the four numerical experiments reported here and the corresponding parameters used to run the model. Figure 13 shows the results of Experiment 1 in which equilibrium profiles were determined for different rates of rock uplift (equivalent to the rate of downstream boundary lowering). These series of profiles lie along a trajectory across the bedrock erosion function surface shown in Figure 12, with each profile representing a single point in this field of relative sediment supply and excess shear stress. For the case of zero uplift, the longitudinal profile shown in Figure 13 is entirely controlled by the requirement to transport the imposed load. As the incision rate is increased, the resulting steady state profiles adjust by steepening, reducing the fraction of the bed covered. Uplift rates were varied through the range of values which could be accommodated by the erosion function surface plotted in Figure 12.

Figure 13 shows that as rock uplift rate (and thus incision rate at equilibrium) increases, only relatively minor increases in slope, above that needed to carry the load, are required to keep up with accelerating incision. Figure 14 shows how slope changes with distance along the profile for each incision rate. We found that we can collapse these results by plotting (Figure 15) the ratio of incision rate to maximum incision rate (the peak on the surface in Figure 12) against the dimensionless excess slope (S_e), defined here as the difference between the total slope (S) (i.e. that required to both transport the load and incise at the imposed rock uplift rate) and the alluvial slope (S_a) (i.e. that required only to transport the load), normalized by S.

$$S_e = \frac{S - S_a}{S} \tag{20}$$

In effect, the horizontal axis is the proportion of the total slope in the equilibrium longitudinal profile that results from the necessity to cut through the bedrock to maintain that equilibrium. It is zero where there is no incision, and for the particular parameters in this set of model runs, reaches a maximum of nearly 50% at the maximum incision rate. The relationship is an approximately logarithmic one in which progressively larger slope increases are needed to effect a similar increase in erosion rate. This occurs because as the alluvial bed cover is gradually removed by increasing excess transport capacity, the resulting increase in the fraction of particle impacts striking exposed bedrock, and the enhanced energy of particle impacts, is offset by a reduction in the frequency of particle impacts with the bed due to an increase in the saltation hop length.

The model result shown in Figure 15 suggests that bedrock incision rate varies with the slope in excess of that needed to carry the load. Therefore, even in rivers actively cutting through bedrock, the channel slope may be primarily controlled by the sediment supply rate rather than simply by the slope needed to cause channel incision as implicit in the stream power law. We cannot propose at this point that we can distinguish the supply effect from the incision necessity in evaluating real river profiles, but this model outcome clearly points out the need to consider such issues.

In Experiment 2, we explored how sediment supply might affect the slope-area relationship and, consequently, the parameterization of equations (6) and (7). A series of equilibrium profiles were generated by holding the imposed uplift rate constant at 1 mm/yr while varying the sediment supply coefficient (K_b), in effect changing the bedload fraction of the total load supplied to the channel. On the bedrock incision function surface shown Figure 12, this succession of runs with varying sediment supply all plot along a single contour line because the incision rate is uniform

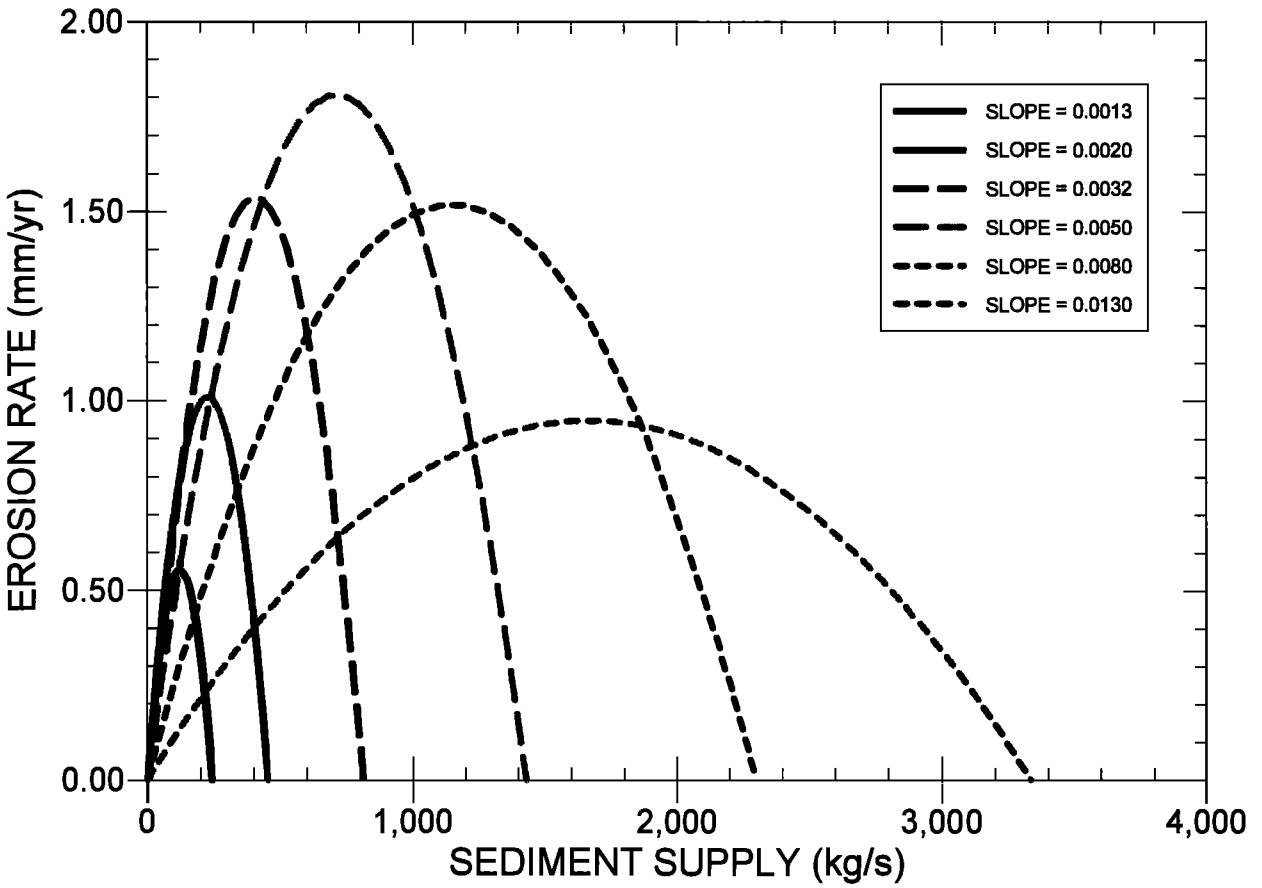

Figure 11. Bedrock erosion rate (E) as a function of sediment supply (Q_s) for various channel slopes as predicted by equation (15), with $Q_w = 100$ m^3/s, W = 26 m, D = 40 mm, and $N_m = 0.05$.

along the channel. Uniform incision rate is maintained with increasing supply through a trade-off between bed exposure and excess shear stress. This trade-off will vary depending on whether increases in sediment supply provide more tools for erosion, therefore allowing gentler slopes to accomplish the same rate of erosion, or tend to cover the bend, therefore requiring steeper slopes to increase the transport capacity and maintain some bedrock exposure.

For this case of varying supply while holding uplift constant, the resulting equilibrium profiles all have slope-area relationships with a constant m/n value of 0.44, but the intercept K_s increases with greater sediment supply. Because incision rate (E) is fixed, this is equivalent to a decrease in the coefficient K in equation (6), which is what we might expect as the supply increases and the bed is more frequently covered (Figure 16). Hence, the coefficient in the stream power law should depend on sediment supply, with K decreasing with greater sediment supply in the coverage effect dominated upper-left quadrant (B) of Figure 12, but increasing with greater sediment supply in the tools effect dominated lower-left quadrant (A).

In Experiment 3, we kept incision rate constant but specified a fixed downstream decrease in grain size, and again varied the sediment supply coefficient K_b as was done in Experiment 2 (Table 2). In this scenario, grain size declines from 120 mm to 40 mm through the profile, such that particle breakdown creates smaller bedload particles, with resulting lower critical shear stresses and greater relative mobility. All other parameters are held constant, in particular the supply exponent p in equation (18) which specifies the rate of downstream increase in the total mass flux of coarse sediment, in order to isolate the effect of downstream fining on profile concavity. Regressions of the resulting equilibrium channel slopes with drainage area reveal that m/n gradually decreases with increasing supply, from about 0.8 down to about 0.65 for this case of downstream decreasing grain size (Figure 17). This result differs from Experiment 2 and suggests that the combined effects of grain size and

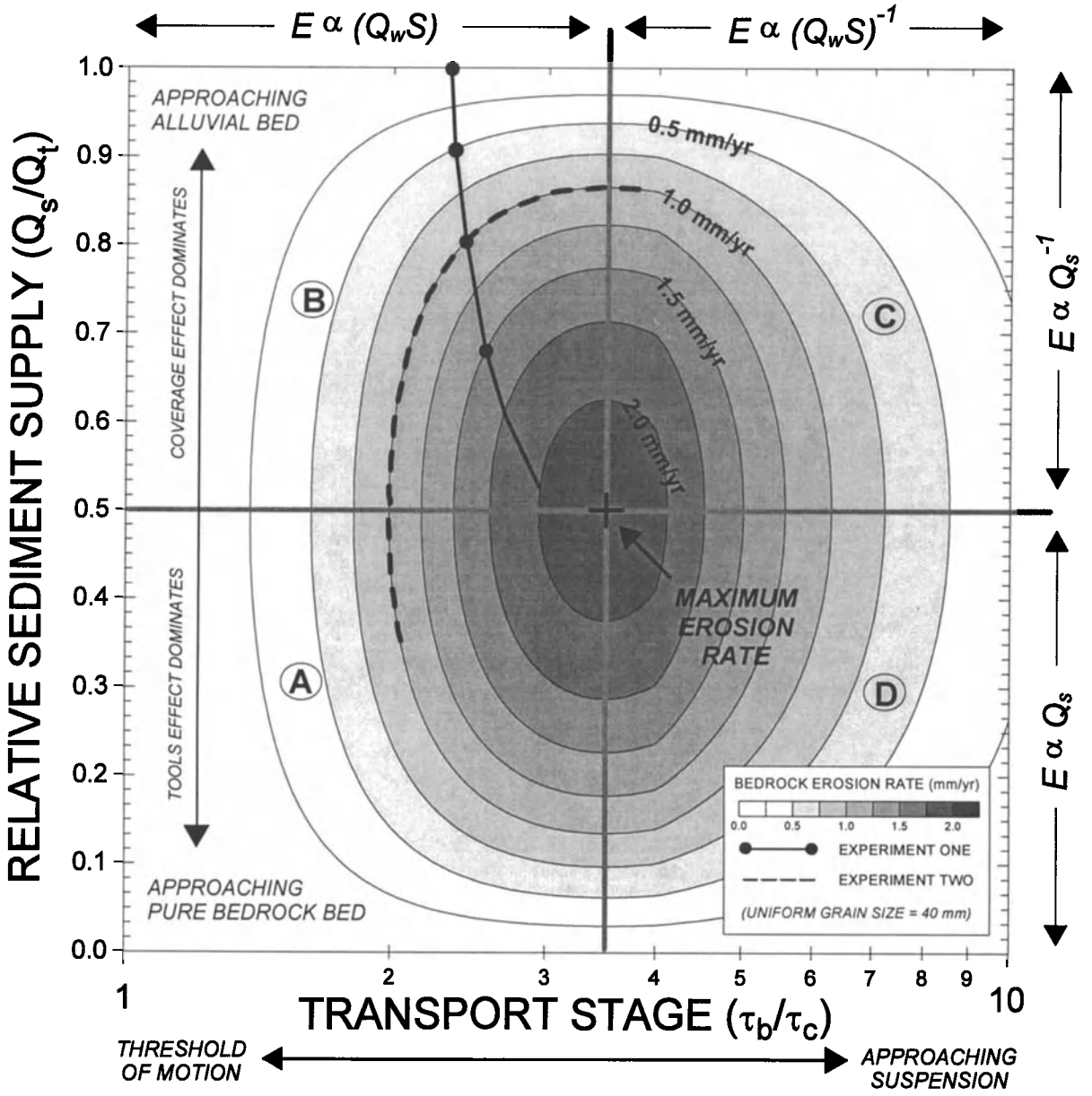

Figure 12. Bedrock incision rate (E) (contours, axis out of page) as a function of relative sediment supply (Q_s/Q_t) (assumed equal to fraction of bed covered by alluvium) and excess shear stress (τ_b/τ_c) as predicted by equation (15). This is a unique surface for a fixed uniform grain size of 40 mm, and for all reasonable combinations of slope, width and discharge. Erosion rate maximum occurs at intersection of lines of optimal bed coverage and optimal excess shear stress. Bed coverage varies from pure bedrock at bottom edge to fully alluvial at top edge; sediment transport mode shifts from threshold of particle motion at left edge to approaching suspension at right edge. Bedrock incision rate *increases* with increasing transport capacity in quadrants A and B, and with increasing sediment supply in quadrants A and D. Bedrock incision rate *decreases* with increasing transport capacity in quadrants C and D, and with increasing sediment supply in quadrants B and C. "Tools" refers to bedload particles responsible for abrading the bed. Experiment 1 values are plotted on surface as heavy solid line; Experiment 2 values are shown by the heavy dashed line. Note that transport stage is plotted on a logarithmic axis.

TABLE 2. Summary of Numerical Experiments

	EXPERIMENT 1	EXPERIMENT 2	EXPERIMENT 3	EXPERIMENT 4
UPLIFT RATE	Varied from 0 to 2.0 mm/yr	Held constant at 1.0 mm/yr	Held constant at 1.0 mm/yr	Held constant at 1.0 mm/yr
SEDIMENT SUPPLY RATE	Proportional to area ($p = 0.5$), $K_b = 6x10^5$ Tonnes/km-yr	Proportional to area ($p = 0.5$), K_b increased incrementally from 40% to 600% of value in experiment 1	Proportional to area ($p = 0.5$), K_b increased incrementally from 50% to 300% of value in experiment 1	Proportional to area ($p = 0.5$), $K_b = 6x10^5$ Tonnes/km-yr throughout profile
GRAIN SIZE	Uniform throughout profile ($\alpha = 0$; $D_o = 40$ mm)	Uniform throughout profile ($\alpha = 0$; $D_o = 40$ mm)	Declines downstream from 120 mm to 30 mm ($\alpha = 0.0275$; $D_o = 120$ mm)	Declines downstream from 120 mm to 60 mm; Tributary junction of equal area supplies 120 mm, mean = 90 mm then declines to 45 mm at outlet

Other parameters not varied:
Width ($b = 0.5$; $K_w = 3\ s^{0.5}\ m^{-0.5}$); Discharge ($r = 1.0$; $K_a = 1.0$ m/s); Area ($f = 1.5$; $c = 1.0\ km^{0.5}$; $A_o = 1\ km^2$); $N_m = 0.05$;

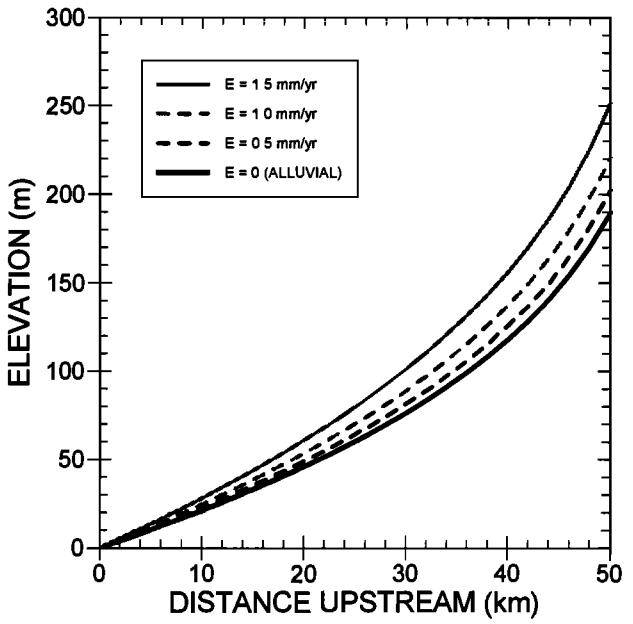

Figure 13. *Experiment 1:* Model equilibrium longitudinal profiles for varying rock uplift rates. Parameter values listed in Table 2.

sediment supply variation in rivers will be different from the sum of the individual effects. This synergy results from the trade-off of bed coverage and excess shear stress needed to maintain the equilibrium incision rate and transport the imposed load.

In Experiment 3, at low supply rates, there is a strong downstream gradient in bed coverage due to the downstream fining, with the largest fraction of the channel bed exposed in the upstream end of the profile. In the low supply case, profile concavity (expressed quantitatively by the ratio m/n) is dominated by the downstream fining effect, as greater particle mobility downstream allows less steep slopes. As sediment supply rate increases, the extent of bed exposure is reduced, first in the downstream portion of the profile and then increasing upstream, until at high supply rates the concavity is primarily produced by the slope adjustment required to keep enough of the bed exposed to

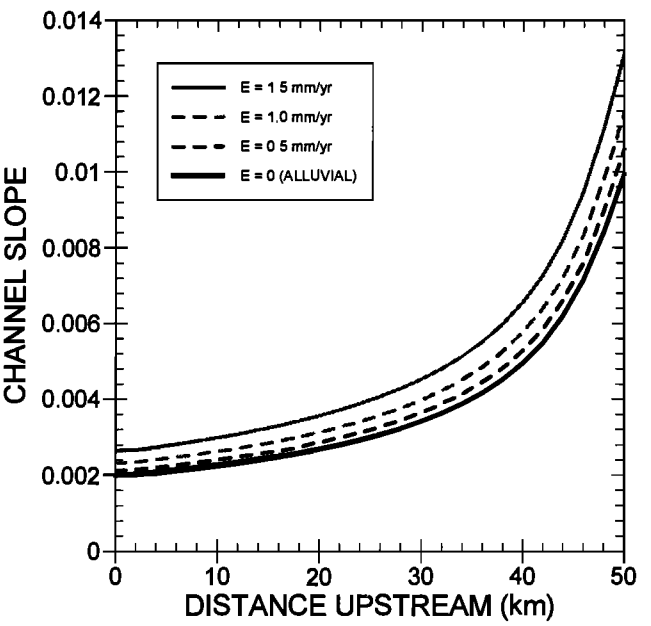

Figure 14. *Experiment 1:* Equilibrium profile slope variation with distance upstream for varying uplift rates.

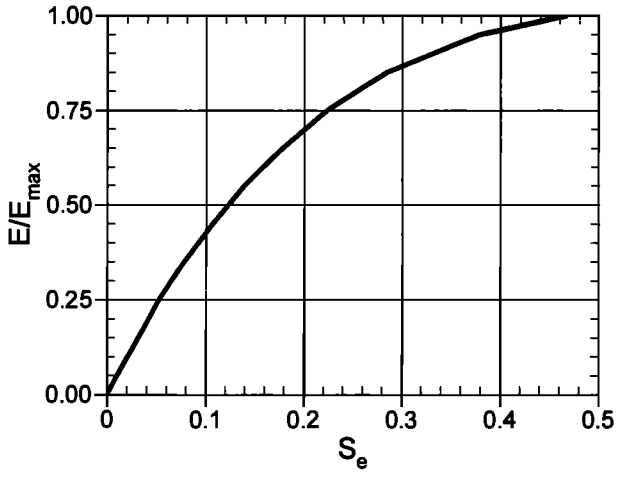

Figure 15. *Experiment 1:* Ratio of bedrock incision rate (E) to maximum possible bedrock incision rate (E_{max}) as a function of excess slope (S_e), the fraction of the total slope responsible for incision [equation (20)].

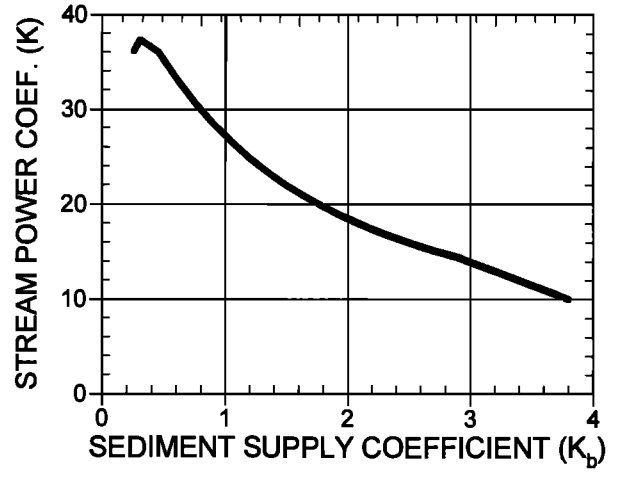

Figure 16. *Experiment 2:* Variation of stream power law coefficient (K) with changing sediment supply coefficient (K_b), all other parameters held constant (Table 2).

erode at the imposed uplift rate. In effect, the reduction in m/n values with increasing sediment supply rate reflects the shift from a tools-dominated to coverage-dominated regime.

The results of Experiments 2 and 3 suggest that the parameters m, n and K of the stream power law are complex functions of sediment supply and grain size. The wide variation in observed values of these parameters in field studies may be due in part to the role of sediment in controlling longitudinal profile form.

If the longitudinal profiles of rivers in actively incising terrain are strongly influenced by the quality and quantity of sediment supplied to the channel then we might expect to see this expressed at tributary junctions where abrupt changes in sediment supply characteristics can occur. For example, where a tributary draining a resistant lithology joins a main stem which primarily carries sediments of a weaker rock type, we might expect to see a significant coarsening of the bedload immediately downstream of the tributary junction. In Experiment 4, we model this effect by introducing sediment from a tributary equal in drainage area to the size of the main stem but which brings in larger (120 mm as compared to 60 mm on the main stem) and more resistant particles (Table 2). Figure 18 shows the equilibrium profile of a simulation of such a situation, in which a pronounced profile convexity occurs at the tributary junction.

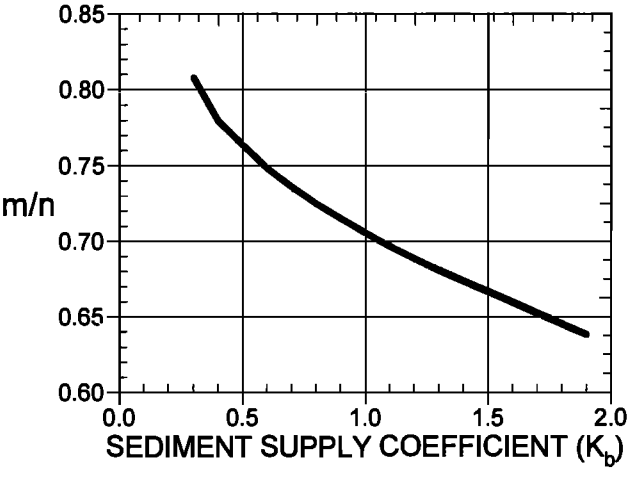

Figure 17. *Experiment 3:* Variation of ratio of stream power law exponents (m/n) with changing sediment supply coefficient (K_b), all other parameters held constant except grain size which decreases downstream (Table 2).

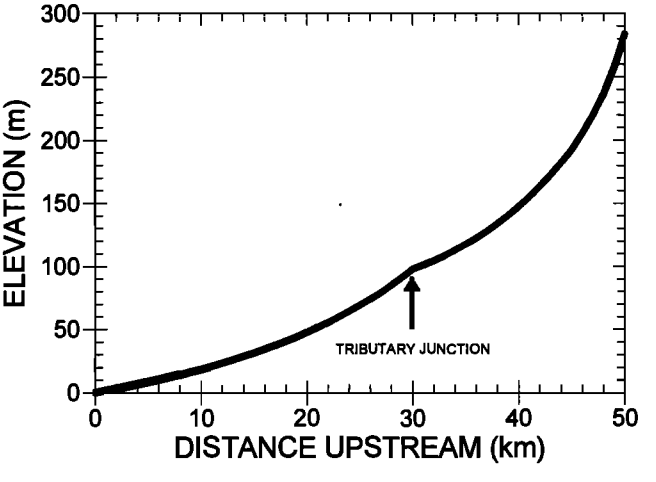

Figure 18. *Experiment 4:* Equilibrium longitudinal profile with tributary contributing coarse load. (See Table 2 for parameter values).

In this equilibrium profile, the incision rate is the same upstream and downstream of the junction, and although discharge has doubled below the junction (due to the discharge from the tributary), the equilibrium slope is steeper downstream as well because of the higher threshold of motion of the coarse material contributed to the bedload by the tributary channel. The role of coarse sediment supply from tributary junctions in creating profile convexities has been documented on the Colorado River [*Howard and Dolan*, 1981]. *Howard* [this volume] also describes a pronounced profile convexity at a major tributary junction on the South Fork Eel River. The results of experiment 4 illustrate the possibility that such convexities and other bedrock channel longitudinal profile features, commonly attributed to lithologic or tectonic discontinuities, may in fact occur as equilibrium forms, due to spatial variations in sediment supply.

5. DISCUSSION

While the stream power incision law is a simple physically-based expression for predicting the rate of channel incision into bedrock, our analysis suggests that it be used with considerable caution. This is because: 1) it appears to be difficult to calibrate, particularly by analysis of longitudinal profiles; 2) it should only apply to the fraction of the channel network where bedrock exposures and fluvial processes dominate; 3) model profiles generated with the stream power law have large and poorly understood sensitivities to choices of model parameters; and 4) its simple power law form may be inadequate to represent the first order effects of variations in sediment supply and grain size.

Analyses of channel slope-drainage area plots derived from longitudinal profiles offer the potential of a very large data set to use in attempting to calibrate the stream power law. The wide range, however, of measured values for the ratio m/n found in this analysis of the upper Noyo basin, and as found by others [e.g. *Hack*, 1957; *Miller*, 1958; *Brush*, 1961], suggests that we should not expect a global value to emerge from a larger data set. A major weakness of the profile analysis method is the assumption of a spatially uniform erosion rate. As illustrated by the Ontonagon data, a relatively strong slope-area correlation can occur even when the channel network is far from equilibrium. Given the large number of process variables lumped into the parameters of the stream power law, m/n and K_s values derived from slope-area plots may be of limited value in interpreting erosion rates or their controls.

Empirical slope-area plots can nonetheless be revealing. Lack of channel slope dependency on drainage area in the steeper part of the network may reveal a change in process from fluvial to debris flow dominated incision. The location of a reach above or below an empirical slope-area threshold between bedrock dominated and alluvium dominated channel beds may reveal whether it is currently actively cutting into rock, as well as show the effects of land use changes on rivers [*Montgomery et al.*, 1996]. Wide variation in m/n and K_s values within a watershed of uniform lithology may signal the effects of disequilibrium on the longitudinal profile. Analysis of tributary junctions may also reveal disequilibrium effects not evident in profile slope-area regressions.

The profile analysis of *Stock and Montgomery* [in press] did not require the assumption of uniform incision rates, but rather compared modern and dated paleo-profiles to estimate the local mean incision rate. They used a three parameter best-fit search procedure to attempt to assign values to m, n and K in equation (6) for 13 streams in California, Hawaii, Japan and Australia. They found large variations in best-fit values for all three parameters, which they concluded were due in part to the poorly constrained effects of variable boundary conditions. As *Seidl et al.* [1994] suggested for the Hawaiian case, propagating knickpoints and armoring of the bed with coarse debris strongly affect profile evolution and make stream power parameterization very uncertain. In order to compare estimated values of K, *Stock and Montgomery* [in press] assigned average values of m and n to sets of profiles, concluding that K varied strongly with rock type, and indirectly highlighting the inherent dependence of K on assumed values of m/n.

The limited data on m/n and K, and the unreliability of extracting these parameters from longitudinal profile analysis, means that at present, stream power-based equations for river incision used in landscape evolution models can not be independently calibrated. Consequently, these parameters must be selected to produce the desired results, such as the correct relief [e.g. *Tucker and Slingerland*, 1996]. As equation (14) illustrates, however, profile relief depends on as many as eight parameters. The complex sensitivity of model profile relief to different combinations of parameter values can be seen in our limited examination of variation in the area assumed to drain to the channel head.

Our analysis shows that profile relief and the maximum gradient of the channel will depend on what rule is used to define the upstream tip of the profile, which could simply be the model grid size. Landscape evolution models vary widely in how they treat this upstream boundary. Large scale models using grid sizes of 1 km^2 or more do not effectively distinguish between hillslopes and channels, and therefore extend the channels to the drainage divide [e.g. *Kooi and Beaumont*, 1994; *Tucker and Slingerland*, 1996]. Such models will consequently extend the stream power law well beyond where fluvial process dominate. The process 'hand-off' approach advocated by *Howard* [1994, 1997] and used by others [e.g. *Tucker and Slingerland*, 1997] imposes an upstream limit to the stream power-based incision. This limit is set by either an empirical threshold of channelization [*Montgomery and Dietrich*, 1992] or by calculating where hillslope sediment transport processes begin to dominate. While such approaches are more realistic, they still assume a stream power law applies to gradients where fluvial processes may not dominate.

The downstream portions of river profiles have also been inconsistently treated in landscape evolution models. In some cases the lower end of river profiles were allowed to approach near zero gradients, as will be predicted from a simple stream power incision law when sediment transport is ignored [e.g. *Anderson*, 1994]. Other models have specifically calculated sediment transport as well as bedrock incision and have assumed that alluvial reaches predominate where sediment supply exceeds transport capacity [e.g. *Howard*, 1994; *Tucker and Slingerland*, 1997]. Most such models assume that if the channel is bedrock dominated it erodes according to equation (6) and if it is alluvial then the channel does not cut into underlying bedrock.

In our coupled bedload transport-bedrock incision model we propose that the role of sediment in bedrock incision should not be thought of as a simple 'on-off' effect. *Howard and Kerby* [1983] have observed channel incision into bedrock even when the channel appeared alluvial. Moreover, the common occurrence of mixed bedrock-alluvial channels [*Howard*, this volume] suggests that this transition can in fact occur quite gradually. Our model suggests that there is a degree of partial bed alluviation which corresponds to a maximum incision rate, due to a trade off between the dual roles of sediment supply in providing scouring tools to the flow while covering and thus insulating underlying bedrock. We should emphasize that in the model, there are no bars or other alluvial features. Instead, bed coverage is the result of actively moving grains shielding other grains from striking the bed. It is assumed that the closer the sediment supply is to the transport capacity the more shielded the bed is and consequently fewer particles strike the exposed bedrock; erosion ceases when supply equals transport capacity [see term iii in equation (15)].

Although we assumed in constructing the model that bedrock erosion potential varied with the ratio of sediment supply to transport capacity, we did not assume that there would be a peak in the predicted erosion rate. This peak arises both from the coverage effect and from the calculated tendency for the transport mode to shift toward suspension at high excess shear stress. We also did not expect the finding that the equilibrium river slope may be dominated by the imposed sediment load and grain size, even while actively downcutting, rather than being set primarily by the slope required to incise at the rate of relative boundary lowering. Our model shows the effects to be additive, that is, there is an additional slope component beyond that needed to carry the load which is responsible for river incision. While this appears similar to the general incision model proposed by *Kooi and Beaumont* [1996], in which incision rate is linearly proportional to excess transport capacity, our model proposes that there is a maximum possible incision rate which occurs when the supply is about half the transport capacity.

This behavior is not readily accommodated by the stream power law and illustrates the potentially beneficial surprises which can come from building incision models from consideration of the detailed process mechanics. The predicted maximum possible incision rate, for a fixed grain size, no matter how energetic the flow (Figure 12), suggests that if boundary conditions effectively attempt to push a portion of the profile to incision rates beyond the maximum, other incision mechanisms will need to be invoked for the profile to keep pace. In the profile simulations, waterfalls form in this case, which remain fixed in place because there are no other incision processes modeled. This may be analogous to *Siedl et al.'s* [1994] analysis of profiles in Hawaii, in which they argued that bed armoring by coarse sediment resulted in formation of steep knickpoints which have swept upstream under the armor layer. As others have suggested [e.g. *Seidl et al.*, 1994; *Rosenbloom and Anderson*, 1994; *Howard et al.*, 1994; *Weissel and Seidl*, 1997], processes which may be responsible for knickpoint retreat, such as abrasion by suspended load, cavitation, sapping, and mechanical rock mass failure, may be essential to include in dynamic modeling of profile evolution.

6. CONCLUSIONS

Most landscape evolution models use a stream power or shear stress based theory to predict river incision into bedrock. Surprisingly little data exist to either support or offer calibration to this proposed law. Although the stream power incision law can be written as a function of three parameters (K, m, n), these parameters themselves are composed of several others which can vary in space and time. The few studies which have attempted to quantify the three parameters using field data on long term rates of channel incision have found it difficult to obtain unique values [e.g. *Stock and Montgomery*, in press].

Mechanistically, the stream power law with spatially constant parameters is unlikely to be appropriate for the entire river network of most landscapes. Slopes steeper than 5 to 8% have different hydraulic and sediment transport relationships relative to less steep slopes. Above these slopes, and likely by about 20%, fluvial processes give way to concentrated mass wasting processes, such as debris flows, which are unlikely to be well represented by a stream power law. The projection of the stream power law to steep slopes, and the choice of rule for assigning drainage area to the channel head, strongly affect relief calculation in landscape evolution models.

The role of sediment supply in channel incision does not fit comfortably into the stream power erosion hypothesis. The coupled bedload transport-bedrock incision model we propose here suggests a complex interaction of sediment supply and transport capacity, grain size, channel slope and incision rates. Specifically the model predicts, for a given bedrock erodibility, that erosion rate varies with sediment supply relative to transport capacity, excess shear stress and

grain size. Instead of a monotonic increase of bedrock incision rate with either excess shear stress or relative sediment supply, our model predicts a maximum incision rate at intermediate values of each. Higher sediment supply increasingly covers the bed with sediment and higher excess shear stress moves the transport mode toward suspension and less frequent bed contact; each of these effects reduces the potential bed erosion rates. The three parameters in the stream power law appear to be complex functions of sediment supply and grain size. This offers some explanation for the wide variability of these parameter values obtained from profile analysis.

There are several potentially fruitful directions that future work on river incision could go. Field studies that can capture the history of river incision over long spatial and temporal scales, for example through the use of cosmogenic radionuclide analysis [*Seidl et al.*, 1997], will provide crucial large scale constraints on incision theory. Field or laboratory studies focused on the erosional mechanisms and factors controlling rates of incision should lead to more physically-based models. Finally, physical modeling in which sediment supply, grain size, and channel erodibility are manipulated will allow the testing and development of mechanistic theories.

NOTATION

A drainage area
A_o drainage area at upstream boundary of profile
A_r representative profile drainage area
b exponent for change in channel width with discharge
c coef. for change in drainage area with profile distance
D grain size
D_o coef. for change in particle size with profile distance
E bedrock erosion rate
e base of natural logarithms
f exponent for change in drainage area with distance
g gravitational acceleration
K coefficient in stream power law
K_a coef. for change in discharge with drainage area
K_b coef. for change in sediment supply with area
K_n channel cross-section shape factor
K_p coef. for change in erosion rate with stream power
K_s slope-area regression intercept = $(E/K)^{1/n}$
K_w coef. for change in width with discharge
K_y consolidation coef. = $K_p\rho_f g K_a^{1-b}/K_w$
K_z consolidation coef. = $K_t\rho_f g(N_m K_a^{1-b}/K_w K_p K_n)^{0.6}$
K_m coef. for change in minimum bedrock slope with area
L profile length
m exponent on drainage area in stream power law
N_m Manning's 'n' roughness coefficient
n exponent on channel slope in stream power law
p exponent for change in sediment supply with area
Q_w discharge
Q_s sediment supply rate
Q_t sediment transport capacity
R hydraulic radius
r exponent for change in discharge with drainage area
S channel slope
S_a slope required to transport sediment load
S_e excess slope required to erode bedrock
S_m minimum channel slope for bedrock exposure
S_p principal channel slope
S_r representative profile slope
S_t tributary channel slope
u exponent for change in min. bedrock slope with area
u_s horizontal particle velocity
u^* shear velocity
W channel width
w_s vertical particle velocity
$\overline{w_s}$ particle fall velocity in still water
x_d distance from drainage divide
x_h distance from channel head
z elevation
α particle impact angle
ϕ exponent for change in particle size with distance
ε_v energy required to detach a unit volume of bedrock
ε_t energy threshold for bedrock detachment to occur
λ saltation hop length
Ω stream power per unit channel length
ρ_f fluid density
ρ_s sediment density
τ^* non-dimensional boundary shear stress
τ_c^* critical non-dimensional boundary shear stress

Acknowledgments. We wish to thank Alan Howard for many long debates and insightful papers that stimulated much of our analysis. Douglas Allen extracted the digital terrain data for the Noyo watershed, Martin Trso and Laurel Collins contributed insight about its river channels, and Rafael Real de Asua produced the topographic map. Jim Kirchner suggested non-dimensionalizing the slope-area regressions and Dino Bellugi provided programming support. We are grateful to Stillwater Sciences of Berkeley, California, for the use of unpublished data. Helpful comments on an earlier draft were provided by Amy Luers and Frank Pazzaglia. This work was supported by NSF EAR-9706082.

REFERENCES

Anderson, R. S., Evolution of the Santa Cruz Mountains, California, through tectonic growth and geomorphic decay, *J. Geophys. Res., 99, 20,161-20,179, 1994.*

Augistinus, P. C., Rock resistance to erosion: some further considerations, *Earth Surf. Proc Land., 16, 563-569, 1991.*

Benda, L. and T. Dunne, Stochastic forcing of sediment supply to channel networks from landsliding and debris flow, *Water Resour. Res. 33, 12, 2,849-2,863, 1997.*

Bitter, J. G. A., A study of erosion phenomena, part I, *Wear, 6, 5-21, 1963a.*

Bitter, J. G. A., A study of erosion phenomena, part II, *Wear, 6, 169-190, 1963b.*

Brush, L. M., Drainage basins, channels, and flow characteristics of selected streams in Central Pennsylvania, *U. S. Geol. Surv. Prof. Pap., 282-F, 1961.*

De Bree, S. E. M., W. F. Rosenbrand and A. W. J. de Gee, On the erosion resistance in water-sand mixtures of steels for application in slurry pipelines, *Proceedings of the 8th International Conference on the Hydraulic Transport of Solids in Pipes, Johannesburg, 1982.*

Dietrich, W. E. and D. R. Montgomery, Hillslopes, channels and landscape scale, in *Scale Dependence and Scale Invariance in Hydrology*, edited by G. Sposito, Cambridge University Press, in press.

Engle, P. A., *Impact Wear of Materials*, Elsevier, New York, N. Y., 1976.

Foley, M. G., Bedrock incision by streams, *Geol. Soc. of Am. Bull., Part II, 91, 2189-2213, 1980.*

Gilbert, G. K., Report of the geology of the Henry Mountains, Geographical and Geological Survey of the Rocky Mountain Region, Government Printing Office, Washington DC, 1877.

Grant, G. E., F. J. Swanson, and M. G. Wolman, Pattern and origin of stepped-bed morphology in high-gradient streams, Western Cascades, Oregon, *Geol. Soc. Am. Bull., 102, 340-352, 1990.*

Hack, J. T., Studies of longitudinal stream profiles in Virginia and Maryland, *U. S. Geol. Surv. Prof. Pap. 294-B, 1957.*

Hack, J. T., Postglacial drainage evolution and stream geometry in the Ontonagon area, Michigan, *U. S. Geol. Surv. Prof. Pap. P-0504-B, 1965.*

Hack, J. T. and J. C. Goodlett, Geomorphology and forest ecology of a mountain region in the central Appalachians, *U. S. Geol. Surv. Prof. Pap* . 347, 1960.

Head, W. J. and M. E. Harr, The development of a model to predict the erosion of materials by natural contaminants, *Wear, Vol. 15, 1-46, 1970.*

Howard, A. D., Problems in interpretation of simulation models of geologic processes, in *Quantitative Geomorphology, Some Aspects and Applications*, edited by M. Morisawa, pp. 61-82, 1971a.

Howard, A. D., Simulation model of stream capture, *Geol. Soc. Am. Bull., 82, 1355-1376, 1971b.*

Howard, A. D., Thresholds in river regimes, in *Thresholds in Geomorphology*, edited by D. R. Coates and J. D. Vitek, pp. 227-258, 1980.

Howard, A. D. and R. Dolan, , Geomorphology of the Colorado River in the Grand Canyon, *J. Geol., 89, 269-298, 1981.*

Howard, A. D. and G. Kerby, Channel changes in badlands, *Geol. Soc. Am. Bull., 94, 739-752, 1983.*

Howard, A. D., Modeling fluvial systems: rock, gravel and sand bed channels, in *River Channels*, edited by K. S. Richards, pp. 69-94, 1987.

Howard, A. D., A detachment-limited model of drainage basin evolution, *Water Resour. Res., 30, 7, 2261-2285, 1994.*

Howard, A. D., W. E. Dietrich and M. A. Seidl, Modeling fluvial erosion on regional to continental scales, *J. Geophys. Res., 99, 13,971-13,986, 1994.*

Howard, A. D., Badland morphology and evolution: Interpretation using a simulation model, *Earth Surf. Proc. and Landforms, 22, 3, 211-227, 1997.*

Kilbourne, R. T., Geology and slope stability of the Fort Bragg area, Mendocino County, California, *California Geology, 39, 3, 56-68, 1986.*

Kooi, H., and C. Beaumont, Escarpment evolution on high-elevated rifted margins - insights derived from a surface processes model that combines diffusion, advection and reaction, *J. Geophys. Res., 99, 12191-12209, 1994.*

Kooi, H., and C. Beaumont, Large-scale geomorphology: classical concepts reconciled and integrated with contemporary ideas via a surface processes model, *J. Geophys. Res., 101, 3361-3386, 1996.*

Krumbein, W. C., Sediments and exponential curves, *J. Geol., 45, 577-601, 1937.*

Leopold, L. B. and T. Maddock, The hydraulic geometry of streamchannels and some physiographic implications, *U. S. Geol. Surv. Prof. Pap., P-0252, 1953.*

Leopold, L. B. and W. B. Langbein, The concept of entropy in landscape evolution, *U. S. Geol. Surv. Prof. Pap., 282-D, 1962.*

Merritts, D. and K. R. Vincent, Geomorphic response of coastal streams to low, intermediate, and high rates of uplift, Mendocino triple junction region, Northern California, *Geol. Soc. Am. Bull., 101, 11, 1373-1388, 1989.*

Miller, J. P., High mountain streams: effects of geology on channel characteristics and bed material, *New Mexico State Bureau of Mines and Mineral Resources, Memoir 4, 1958.*

Milliman, J. D. and J. P. M. Syvitski, Geomorphic/tectonic control of sediment discharge to the ocean: the importance of small mountain rivers, *J. Geol., 100, 525-544, 1992.*

Montgomery, D. R. and W. E. Dietrich, Channel initiation and the problem of landscape scale, *Science, 255, 826-830, 1992.*

Montgomery, D. R. and E. Foufoula-Georgiou, Channel network source representation using digital elevation models, *Water Resour. Res., 29, 3925-3934, 1993.*

Montgomery, D. R., T. B. Abbe, J. M. Buffington, N. P. Peterson, K. M. Schmidt, and J. D. Stock, Distribution of bedrock and alluvial channels in forested mountain drainage basins, *Nature, 381, 13 June, 1996.*

Raudkivi, A. J., *Loose Boundary Hydraulics*, Pergamon Press, New York, N.Y., 1990.

Rodriquez-Iturbe, I. and A. Rinaldo, *Fractal River Basins: Chance and Self-organization.* Cambridge University Press, 1997.

Rosenbloom, N. A., and R. S. Anderson, Hillslope and channel evolution in a marine terraced landscape, Santa Cruz, California, *J. Geophys. Res., 99, 14,013-14,029, 1994.*

Seidl, M. A. and W. E. Dietrich, The problem of channel erosion in bedrock, in *Functional Geomorphology: Landform Analysis and Models*, edited by Schmidt, K. H. and J. de Ploey, Catena Supplement 23, 101-124, 1992.

Seidl, M. A., W. E. Dietrich, and J. W. Kirchner, Longitudinal profile development into bedrock: an analysis of Hawaiian channels, *J. Geol., 102, 457-474, 1994.*

Seidl, M. A., R. C. Finkel, M. W. Caffee, G. B. Hudson, and W. E. Dietrich, Cosmogenic isotope analysis applied to river longitudinal profile evolution: problems and interpretations, *Earth Surf. Proc. Land., 22, 195-209, 1997.*

Selby, M. J., A rock mass strength classification for geomorphic purposes: with tests from Antarctica and New Zealand, *Z. Geomorph. N. F., 24, 1, 31-51, 1980.*

Sklar, L., W. E. Dietrich and A. D. Howard, The influence of sediment supply on river incision into bedrock: a theoretical investigation, *EOS, Trans. AGU, 77, 46, F251, 1996.*

Sklar, L. and W. E. Dietrich, The influence of downstream variations in sediment supply and transport capacity on bedrock channel longitudinal profiles, *EOS, Trans. AGU, 78, 46, F299, 1997.*

Slingerland, R., D. D. Willet, and H. L. Hennessey, A new fluvial bedrock erosion model based on the work-energy principle, *EOS, Trans. AGU, 78, 46, F299, 1997.*

Smith, G. H. S. and R. I. Ferguson, The gravel-sand transition along river channels, *J. Sed. Res., A65, 2, 423-430, 1995.*

Stock, J. D., and D. R. Montgomery, Can we predict the rate of bedrock river incision using the stream power law?, *J. Geophys. Res., in press, 1998.*

Suzuki, T., Rate of lateral planation by Iwaki River, Japan, *Trans., Japanese Geomorph. Union, 3, 1, 1-24, 1982.*

Tucker, G. and R. Slingerland, Erosional dynamics, flexural isostasy, and long-lived escarpments: a numerical modeling study, *J. Geophys. Res., 99, 12,229-12,243, 1994.*

Tucker, G. and R. Slingerland, Predicting sediment flux from fold and thrust belts, *Basin Res., 8, 329-349, 1996.*

Tucker, G. and R. Slingerland, Drainage basin responses to climate change, *Water Resour. Res., 33, 8, 2031-2047, 1997.*

Weissel, J. K. and M. A. Seidl, Influence of rock strength properties on escarpment retreat across passive continental margins, *Geology, 25, 7, 631-634, 1997.*

Wiberg, P. L. and J. D. Smith, A theoretical model for saltating grains in water, *J. Geophys. Res., 90, C4, 7,341-7354, 1985.*

Wiberg, P. L., and J. D. Smith, Initial motion of coarse sediment in streams of high gradient, in *Erosion and Sedimentation in the Pacific Rim*, edited by R. L. Beschta, IAHS-AISH Publication 165, 299-308, 1987.

Leonard Sklar and William E. Dietrich, Department of Geology and Geophysics, University of California, Berkeley, CA 94720

Field Studies of Bedrock Channels

Keith Tinkler

Department of Geography, Brock University, St Catharines, Canada

Ellen Wohl

Department of Earth Resources, Colorado State University, Fort Collins, Colorado

A methodological focus on modern river processes in recent decades has directed attention away from large-scale landform development and commensurately long term timescales. Because the incision of bedrock channels lies at the core of the development of subaerial landscapes, field studies must be conducted over a variety of spatial and temporal scales. A renaissance of the historical approach to landscape development using new geochronologic techniques, coupled with flume and computational modeling of fluvial dynamics and landscape development, should serve to advance understanding of bedrock channels. Examples from Tinkler's work in Ontario exemplify some of the issues in field studies of bedrock channels.

INTRODUCTION

Research in fluvial geomorphology was affected by a pronounced change in emphasis during the 20th century. The foundation of fluvial geomorphology was created by 19th-century scientists who focused on large-scale landscape development over geological timescales. This perspective continued throughout the first half of the 20th century, but fell into disrepute after the Second World War for its failure to address both the specifics of landscape process [*Leighly*, 1940; *Strahler*, 1952], and the increasingly refined tectonic framework within which landscapes might have developed [*Chorley*, 1963; *Tinkler*, 1985]. Attempts to quantify measurable geomorphic processes lead to an increasing emphasis on process geomorphology, often at the expense of a geological perspective of landscape development. When *Leopold et al.* [1964] wrote the book which symbolized the then "new" approach to fluvial geomorphology, they began with a chapter entitled "The evolving landscape." They posed problems concerning the development of fluvial landscapes over geological time even though the focus of the "new" approach was characterized by others as "process" oriented. That introduction provided some comfort to those seeking to balance approaches to geomorphic research during the two decades of intensely detailed process work which followed, until in 1981 "*Earth Surface Processes*" saw fit to add "*and Landforms*" to the title. A consensus is now developing that process studies have failed to illuminate long-term landscape changes [*Church*, 1980]. But it is only recently, with problems posed by Quaternary landscapes, and the new geochronological tools available, that a better integration of the two poles of interest can be attempted [*Sugden et al.*, 1997].

Problems of interpreting bedrock channel development exemplify the need to integrate landscape and process approaches. One of the problems discussed in *Leopold et al.* [1964] is the deeply incised bedrock meanders of the North Branch of the Susquehanna River. Elsewhere in the book (p.313), the authors express their puzzlement at the process by which deeply incised meanders in bedrock come into being. It is no trivial problem and it neatly encapsulates the need to connect the micro-scale of process to the macroscale morphology and to extrapolate observable process over geological timescales so as to explain landforms we recognize. This issue has been raised again very recently [*Lane and Richards*, 1997; *Kochel and Miller*, 1997; *Spedding*, 1997; *Sugden et al.*, 1997]. Bedrock channels, in which piecemeal erosion integrates through geological time to yield, for example, large, deeply incised meanders, lie at the very center of this problem. It may seem self-evident

Rivers Over Rock: Fluvial Processes in Bedrock Channels
Geophysical Monograph 107

that field studies are central to geomorphology, but there are many ways in which the idea can be expressed, from basin-scale studies to work in a particular cross-section. Pressures in the work-place and on research budgets have placed many limitations on active and especially prolonged field work. In consequence, most research projects are directed towards very specific topics, which yield data within a limited time frame, a perspective which also derives from the "process" paradigm [*Lane and Richards*, 1997]. On its own, any such work may be consistent, but eventually the disparate threads need integrating across temporal and spatial scales, which for various reasons may not be accessible to direct investigation. *Sugden et al.* [1997] have even argued that the lack of prominence of the formerly popular historical approach to landscape interpretation has hindered understanding of landscape change on the broad front.

Field studies of bedrock channels have been conducted from both a landscape and a process perspective, but it is worthwhile enquiring whether we are approaching the type of problem typified by bedrock channels in an appropriate manner [*Spedding*, 1997]. Given the spatial and temporal expanse of the topic, it is also appropriate to ask how we should adapt to dealing with controls on channel development that may not be directly measurable. Should we be using the field to test the *instantiae crucis* of Francis Bacon; to point, with the *signpost*, the way to new directions or the next experiment? Should we use the field experience in a more holistic manner to generate the general problem from the specific field example [*Clayton*, 1970]? Should we be monitoring over long times scales because, as *Lane and Richards* [1997] point out, to identify "critical bifurcations during system evolution requires continual observation of a kind that is not common in process studies"? How are we to blend these approaches? Various investigators have answered these questions in different manners. In this chapter we briefly review the types of field studies that have been conducted in bedrock channels. We then use a detailed example of field approaches from Tinkler's research program on bedrock channels in Ontario, which is distinctive in that it is based on long-term monitoring at a few selected sites.

OVERVIEW OF FIELD STUDIES ON BEDROCK CHANNELS

The basic question which must be addressed in bedrock channel studies is quite straightforward in principle: how do bedrock channels form? Answering this question quickly becomes complicated. On the one hand is the very visible morphology of the bedrock channels and valleys, and on the other hand are the largely hidden interactions between the substrate forming the channel boundary and the highly turbulent hydraulics of flood flows which act to change the boundary. These interactions are augmented by weathering which acts to prepare the boundary for change, and sediment transport which acts to evacuate the sediment yielded by channel boundary change, and that supplied to the channel by the valley slopes.

Bedrock channels pose some unique challenges to field studies relative to other channel types. Because of large boundary resistance, changes in bedrock channel morphology are thought to occur infrequently during large floods. The occurrence of these floods is difficult to predict, and direct measurement of hydraulic processes during them may be dangerous in confined valleys with rapid, turbulent flow. Many studies of extraordinary floods are necessarily made *post hoc* [*Baker and Kale*, this volume]. As a result, many studies of bedrock channels emphasize the inference of process from form [*Wohl*, 1993, 1994; *Pyrce*, 1995], or the inference of controlling variables from correlations between morphology and substrate [*Braun*, 1983; *Harden*, 1990].

Commonly occurring channel morphologies such as potholes have been used to infer the presence of turbulent structures such as vortices [*Sharpe and Shaw*, 1989; *Lorenc et al.*, 1994; *Zen and Prestegaard*, 1994]. Form may also be related to process by means of hydraulic simulation models. Most studies to date have used a 1d model such as HEC-RAS [*Hydrologic Engineering Center*, 1995] to route a specified discharge through a surveyed channel geometry in order to relate variations in velocity, shear stress or unit stream power to specific erosional or depositional features [*O'Connor et al.*, 1986; *Baker and Pickup*, 1987; *Wohl*, 1992; *O'Connor*, 1993; *Cenderelli and Wohl*, 1998]. Two-dimensional models such as RMA2 or HIVEL2D are now being more commonly applied to bedrock channels [*Miller*, 1995, *Miller and Cluer*, this volume].

Estimating Flood Discharge

The discharge values used in hydraulic models may come from paleostage indicators or from systematic (gaged) discharge measurements. The primary limitation of systematic records of discharge is that they are far too short [*Baker and Kale*, this volume], especially in bedrock systems where often the appropriate timescale is geological in magnitude - from 10^3 to 10^7 years. Usually records are not long enough to detail climatic conditions during significant shifts in the climatic patterns, and they are rarely of sufficient length to document really extreme events. In Ontario, for example, a rapid extension of the stream discharge program *followed* the devastation caused by Hurricane Hazel in October 1954 in the Niagara and Toronto areas. There has been no comparable flow since. The Hurricane Hazel discharge is now used in Ontario, in conjunction with the 100 year flood, as a design criterion in floodplain mapping. Nevertheless, with care, estimates can be made about hydrologically extreme events, their rarity, and their relation to rainfall events [*Carling*, 1986; *Enzel et al.*, 1993; *Carling*, 1994; *Carling and Grodek*, 1994; *Enzel*, 1997].

Because of the deficiencies of short hydrological records, there have been a number of notable attempts to extend flood series records [*Baker and Kochel*, 1988; *Ely et al.*, 1993; *Kale et al.*, 1994; *Wohl et al.*, 1994a] by examining slackwater sediments, the deposits remaining from sediment-laden floodwaters left in backwaters and pondings. However, not all systems are suitable for preserving such a record [Figure 13 in *Kochel*, 1988], either because they do not have suitable locales for deposition; because the natural sediment load is too low; because of post-depositional disturbance [*Springer and Kite*, 1997]; or because the flood range is less extreme, and thus less liable to vertical differentiation in a flood sequence. Historical and botanical indicators [*Yanosky*, 1982, 1984; *Hupp*, 1988] have also been used to extend flood records [*Wohl and Enzel*, 1995].

A continual difficulty in extending flood series records is that even major floods for large basins are small on a global scale, and their relationship to globally significant climatic disturbances may be slight. A further difficulty is the bias towards large flows over long time scales. The impact of wetter periods on the frequency of other high, but not catastrophic, flows seems much harder to assess. Perhaps in the future a closer integration may be achieved by comparing known flood records with developing postglacial tree-ring and ice core chronologies to determine the extent to which there may be agreements and correlations for exceptional events. A recent paper [*Fuller et al.*, 1997] has been able to link aggradational episodes in northeastern Spain to ice core and marine oxygen isotope climate records. Something similar has been attempted from precipitates around the margins of waterfalls [*Nott and Price*, 1994]. There may be hope in re-constructing a paleo-environmental record from a regional tree ring record [*Cleaveland and Duvick*, 1992], to indicate periods of increased rainfall and potential flooding or even, for suitable lake basins, from lacustrine laminations [*Zolitschka*, 1998], or the record of rare inflows [*Enzel and Wells*, 1997].

However, large, intense rainfall events are not necessarily well-related to annual rainfall totals except perhaps in exceptionally arid regions, and it is dangerous to infer low magnitude flow frequencies from a record of high magnitude flows. Large magnitude flows attract attention, and are much easier to document, but they can distract attention from the fact that lower magnitude flows may be causing systematic change in the basin and on the channel boundary.

An additional difficulty associated with geological records of floods is that post-event assessments of exceptional flood flows are a poor substitute for seeing the real complexity of the flow in full flood. A particular problem with post-hoc assessment is that prior channel conditions are usually not known even in a rudimentary way for what is in effect a randomly chosen site. In the James River basin in Mason County, Texas, an interval of many decades between exceptional channel-clearing floods was occupied by gradual alluviation and maturing vegetation which considerably restricted the channel dimensions. *Baker* [1977] reports on a similar situation in the same region after an exceptional flood. However, accurately estimating the extent and nature of this prior alluviation in particular reaches is not always easy. In historical situations, such as the Scabland terrains of Washington [*Baker*, 1987], and the Snake River scablands [*O'Connor*, 1993], the state of the landscape prior to cataclysmic flooding can only be inferred.

Rates of Channel Change

One of the key questions in bedrock channel studies is that of rate of channel change. This is closely tied to flood magnitude and frequency. Geological chronologies of flooding may be based on soil development [*Costa*, 1974], 14C [*Baker, 1987*], 137Cs [*Ely et al.*, 1992], dendrochronological [*Webb et al.*, 1988], or TL [*Murray et al.*, 1992] dating of flood sediments.

Rate of channel change may also be estimated as an average from historic records. Historic photograph replication has been used to indirectly observe changes in bedrock channels of the southwestern United States during the late 19th to late 20th centuries [*Webb*, 1996]. In a modern context, *Tinkler and Parish* [this volume] use the date of installed engineering works and ongoing monitoring to assess recent erosion rates.

Bedrock channel incision and drainage network development over geologic timescales have been estimated from terrace sequences [*Pazzaglia and Gardner*, 1993, 1994; *Merritts et al.*, 1994]. In some erosional systems the existence of a tight chronological control for facets of the landscape enables an estimate of the rate of erosion [*Righter*, 1997; *Schumm and Chorley*, 1983; *Wohl et al.*, 1994b], which can range from long term to short term. Maximum estimates of time elapsed since incision began are provided by the age of the rocks, but these are usually excessive and not often useful. In many high latitudes, drainage systems have been initiated only since deglaciation, often from an initial surface of diamict, thus providing a *tabula rasa* for new stream development. The date of initiation is often derived indirectly from regional accounts of deglaciation. A frequent problem is whether previously excavated systems are partially re-occupied by post-glacial rivers [*Winchell*, 1888; *von Engeln*, 1931; *von Engeln*, 1961; *Tinkler*, 1994; *Tinkler et al.*, 1994]. In non-glaciated terrain the age of initiation of drainage systems may be difficult to determine, although rates for partial incisions may be easier to achieve. In other instances the filling of paleo-valleys with lava, an idea first developed in eighteenth-century France [*Ellenberger*, 1989], can provide valuable datelines [*Nott et al.*, 1996, *Righter, 1997*].

The dates of valley infills, cave infills and terraces can be used to gain insight into the erosional history of a valley system. Principal techniques include 14C [*Baker et al.*, 1985; *Tinkler et al.*, 1994], a range of thermo and optical

luminescence techniques [*Murray et al.*, 1992], magnetostratigraphy on cave sediments [*Sasowksy et al.*,, 1995; *Schmidt*, 1982], and precipitated carbonate dating using Uranium Disequilibrium Series [*Bartholomew and Mills*, 1991; *Granger and Kurchner*, 1997; *Mills and Wagner*, 1985]. Some of the newer approaches to surface crusts and varnishes using the accumulation rates of cosmogenic isotopes on scoured rock surfaces and isolated boulders [*Cerling et al.*, 1994] can help date events such as very large catastrophic floods or maximum ages for erosional surfaces [*Dethier et al.*, 1988; *Seidl et al.*, 1997].

In almost all cases, for a particular field problem there is often little choice about the appropriate technique, and in many others there is no choice at all, or even no applicable technique. At Niagara [*Tinkler et al.*, 1994], dating was achieved by 14C on molluscs preserved in gravels below a paleo-waterfall at Niagara Glen, but in smaller systems near Niagara such records are rare or non-existent. For one small remnant terrace on Twenty Mile Creek, an age on a mollusc extracted from the gravels (640 ± 50 yr BP, TO-4686, on a single *Stagnicola catascopium*) suggests that the terrace might be attributable to colonial interference with the basin regime. Other interesting elements in the complex gorge morphology cannot be dated with present methods.

A major complicating factor in estimating rates of channel change at the basin scale in most mid to high latitudes is the impact of Quaternary climatic change. This was first highlighted by *Dury* [1964a, 1965] for the case of large "valley" meanders which had a similar morphology to alluvial meanders. *Dury* described very large but, by late Holocene times, abandoned, incised meanders in bedrock. *Dury* [1964a] reported their existence across the entire north European plain from western Russia to the Atlantic seaboard and across the northern United States and Canada. The incised meanders seemed to correspond to a period of much more vigorous climate in the late- and early post-glacial period [*Dury*, 1964b], or alternatively they were fed extraneously by proglacial lakes. In general, the older valley meander form is isolated from the modern alluvial meanders by extensive flood plains and terraces and the dichotomy is clear. However, the possibility in Quaternary landscapes of repetitive re-occupation and continued development of paleoforms must always be borne in mind. The Channeled Scablands are now known to have been repeatedly flooded throughout the Quaternary [*Bretz*, 1923; *Bretz et al.*, 1956; *Baker*, 1978; *Waitt*, 1980, 1985; *McDonald and Busacca*, 1988]. Consequently the problem of how much erosion any one flood produces or might produce becomes vastly more complicated [*Benito*, 1997]. A similar comment may be made about the Lake Bonneville outburst flood [*O'Connor*, 1993] and the Big Lost River outburst flood [*Rathburn*, 1993].

More generally, in an erosional landscape it is extremely difficult to make the connection between the volumes of rock eroded out of a valley, and the responsible agencies. A conceptual difficulty is that we have typically tried to factor an environmental record into roughly homogeneous periods during which we believe the statistical properties of, say, streamflow or energy supply are constant. The landscape simply experiences an unending series of events with varying capacities to effect change, and in a bedrock system the period between significant events is as important in terms of prior weathering as the event is to removing a piece of weathered rock. Transitions between quasi-equilibria in the environment are of equal significance to the equilibria themselves, and the new dysfunction between morphology and process likely renders part of the landscape very susceptible to change, and other parts immune. In the end, our interest is in how potentially very variable rates of process add up to create morphology and effect sediment transport.

It is expected that different information will be gleaned at different scales of investigation and usually there will be a broad correspondence between spatial and temporal scales. It is normally taken for granted that basin size is easily evaluated for river systems, but the impact of river capture (the term is used generically to indicate all causes of basin size modification) must be considered for all systems, especially for basins whose continuous fluvial history extends through the Quaternary and into the Tertiary. In the absence of an ability to carry out large-scale basin experiments, river captures sometimes provide useful control cases for abrupt changes in basin size [*Shepherd*, 1979; *Foley*, 1980]. Using the standard power function relationships, because discharge typically scales with basin area with a power of less than 1 for larger basins, and because most hydraulic geometry parameters likewise scale to discharge with powers less than 1, quite substantial changes in basin area are needed to effect much detectable change in channel dimension. More subtle changes in discharge caused by a unilateral change in drainage basin magnitude may trigger systematic erosion or deposition until a new equilibrium channel form is established because of the highly nonlinear dependence of flow competence with respect to sediment transport as a function of velocity.

However, it cannot be assumed that an adjustment will be made, or that it will be made quickly. The Niagara River is overfit (with respect to discharge) in the Whirlpool Rapids Gorge section in the Niagara Gorge, as the modern river flows through an exhumed pre-Wisconsinan gorge element that is much smaller than the modern Upper Great Gorge cut in the same rock sequence [*Tinkler et al.*, 1994]. In this instance the adjustment has been made by creation of the rapids, and although the gorge walls are actively retreating, the process of gorge widening is very slow; in the 5,000

years since the gorge was exhumed no more than a few meters of recession have been effected. Despite estimated flows as high as 11 *m/s* [*Gilbert*, 1896] there is no evidence that the active channel has substantially enlarged itself in 5,000 years.

Direct Observations of Channel Change and Hydraulics

Rates of bedrock channel change, and the mechanics of hydraulic and sediment processes in bedrock channels, may also be extrapolated from direct, short-term observations. These observations may focus on erosion and deposition of alluvial deposits along bedrock channels, as in *Cluer's* work in the Grand Canyon [1995; *Cenderelli and Cluer*, this volume]. Direct observations may involve alteration of the bedrock channel boundaries [*Tinkler and Wohl*, this volume], as when rates of erosion are measured on newly-drilled holes or slots [*Toda*, 1994; *Hancock et al.*, this volume, *Tinkler and Parish*, this volume]. Direct observations may also focus on quantifying hydraulic variables. With the development of 3d doppler velocimeters that can be mounted on an inflatable raft [*Cluer*, 1997], or acoustic sensors mounted above the channel that can continuously monitor the water-surface [*Dick et al.*, 1997], it is becoming more feasible to measure the turbulent flow characteristics of bedrock channels using remote methods.

By definition, high gradient systems are very energetic. The methods developed for low gradient rivers, such as the equations of hydraulic geometry [*Leopold and Maddock*, 1953], are ill-adapted to high gradient systems. Flows in interesting reaches of even small bedrock systems in flood defy direct gaging, and a directly gauged velocity of 6.7 m/s (22 feet/s) in the Potomac River Gorge during the 1936 flood [reported in *Leopold et al.*, 1964, p.167] is an exception that proves the rule. They mention but do not cite 'known' velocities to 9 m/s (30 feet/s).

Distinctions can be made between hydrological and geomorphological approaches to river systems, with the former focusing on the water and mass (sediment) balance, the latter on morphological change and sediment transport in relation to channel morphology. Such differences are accentuated in a bedrock system because the key question is "how are erosion (morphological change) and the transport of large clasts effected?", rather than "what is the water and sediment balance in the basin?" This is not to say that the hydrological information is irrelevant, simply that it usually does not help answer the key questions about significant morphological change in bedrock systems. Part of the problem lies in the fact that governmental data collection programs for surface water are biased towards large low gradient rivers [*Clayton*, 1970; *Baker and Kale*, this volume] gauged at locations designed to provide satisfactory answers to questions about water and sediment budgets, but not about near-bed processes in extremely energetic environments and locations of active channel change. The question of discharge - with an intrinsic focus on the cross-section - is crucial to hydrology. It is less central to bedrock fluvial geomorphology, where the interest is on extreme conditions - shear stress, power, velocity - at selected points in the section.

Water-surface topography is diagnostic of flow once flow becomes nearly critical [*Henderson*, 1970]. Therefore, close examination of energetic high gradient systems can be expected to yield benefits once it has been established what can be observed, what can be measured and how it relates to processes on the bed. It should prove possible to map continuously the water-surface topography in space and time and determine how it changes with respect to stage. If water-surface topography can be tied to continuous recording instruments attached to the bed, real information gains can be expected. The disadvantages are the considerable expense and difficulties of installing recording systems, and the uncontrolled nature of flows. Instant results cannot be expected. The flows are so vigorous that special care is needed to protect instruments, and they may need to be self-logging if an adequately protected cable to the bank cannot be safely installed.

Near-bed shear velocities, v_*, are typically estimated from the equation $v_* = \sqrt{(gds)}$, where g is 9.81 m/s^2, d is depth in meters, and s is dimensionless slope. However, if this is applied with a value for reach slope, s, it may be seriously in error when the local water-surface slopes, on waves for example, may be one to two orders of magnitude larger. In bedrock streams it is quite easy to find water flowing at 1.5 to 2 m/s in thin (a few cm) sheets over smooth steep rock in the channel. Froude numbers can be in the range 2 to 4 and calculated roughness in the range 0.01 to 0.02. If such velocities are reached in free flow, clearly they are possible very close to the bed in deep flows wherever rock surfaces are smooth. Investigations have begun on velocity and velocity profiles over roughness elements in channels [*Bathurst*, 1996; *Wohl and Ikeda*, 1998].

Flow conditions which are unforeseen by standard inferential procedures based on post-flood assessments may be obvious when observed. Examples include the existence of critical and supercritical flow in many high gradient reaches. Critical flow typically develops within the body of the flow with the marginal parts remaining in subcritical flow [*Grant*, 1997; *Tinkler*, 1997b]. Even when allowances are made for small waves characteristic of the margins of rough water reaches, debris lines of reeds and twigs leave no evidence of the state of central channel flow. Even more misleading may be the trash lines associated with roll waves [see Chapter 1; *Hjalmarson and Phillips*, 1997] which may develop in steep broad shallow reaches (often

gravel-bedded) and then propagate downstream as travelling wave fronts (often described as "walls of water" by eye-witnesses) into different channel morphologies. Roll waves leave anomalously high trash lines, and may be so extreme that the channel between successive waves is almost dry [*Holmes*, 1936]. Trash lines caused by roll waves are therefore misleading both with regard to mean flood discharge and to peak velocities in parts of the channel. In-channel vegetation dam bursts and ice dams and jams [*Beltaos*, 1996] can all contribute to energetic traveling waves in the channel whose effects will confound standard analyses. *Fearnside* [1928] commented on the fact that his calculations seemed inadequate to account for the forces that seemed to be involved in moving boulders in a channel swept by a dam or cloudburst, and *Carling* [1986] made a similar remark. *Hjalmarson and Phillips* [1997] provided an explicit re-evaluation of flood evidence almost twenty years after the original event, which was made particularly to evaluate the possible presence and affect of roll waves, reported by eye-witnesses but neglected in analysis.

The imperative to monitor systems closely can be met by technology or by human labour and in the most useful implementation these would complement each other. Although they are often surrogate measures of the items of real interest, continuous gauge records of discharge, rainfall and temperature are examples of real-time monitoring. Noteworthy in this respect is the availability on line through the Internet (World Wide Web) of nearly all United States Geological Survey gaging stations, both with daily and historical flow data, and often with rainfall and temperature data. It can be expected that this initiative will grow, although in some instances (Canada) access is restricted and prohibitive in cost to isolated users. Similarly there are available on-line forecasts of weather systems for up to 10 days in advance. In principle such information allows a degree of contingency planning for the human complement in monitoring systems.

Remote sensing technologies hold some promise for surveillance of wilderness sites, although the tiny scale of the channels at the regional scale of typical coverage remains a problem. However, taking the term in its broadest sense, it may be possible to develop remote camera surveillance, triggered by visual cues of rapid change in the channel as stage rises. The same technology might trigger other recording devices to catch peak events, in a similar vein to tornado chasers! Thus at least photographic evidence of flow maxima might be obtained, although they must be matched to a thorough understanding of the transcritical flow patterns they are liable to reveal. Even normal air photographs of peak flows may reveal much. Very prominent wave forms may be seen in air and ground level photographs of the Tucson, Arizona flood in 1983 [*Kresan*, 1988; *Baker and Twidale*, 1991].

Almost all research work is conducted at spatio-temporal scales selected from within the broad range of space and time available. Often, but not always, the scale for a problem is chosen to suit the worker or the apparatus, or is dictated by the availability of suitable field data. Thus studies of bedrock channels may involve trying to determine the recession rate of an entire continental gorge system [*Derricourt*, 1976], or describing pinhead-sized sculpted forms [*Baker*, 1987]. In this context of trying to connect all the disparate elements, it is worth recalling *Spedding's* [1997] comment that we should restore the respectability of conceptual, qualitative methods and cease to apologize for the historical and interpretive character of our science [*Frodeman*, 1995].

A RESEARCH PROGRAM ON THE WORKINGS OF BEDROCK SYSTEMS

The intent of the research program outlined below is to explore and illuminate the workings of reach-scale processes on several bedrock river systems in southern Ontario, monitored over a period of years. Another system in the Isle of Man (UK) is monitored less frequently. Each system exhibits a different bedrock channel morphology and poses problems in connection with channel and valley development of a different spatial or temporal scale. In general, the work has progressed over the years from the observation of form to the examination of active processes. Figure 1 shows the location of the Ontario sites.

Niagara Peninsula

I began investigating bedrock channels with the view that it was important to observe the systems very closely for the interaction between the stream flows and the resultant impact on the channel boundary, and for the relationship between the channel and the valley walls. It was better to begin in ignorance and adapt to circumstances, rather than start with a specific pre-planned project which might fail. A number of obvious areas of interest were identified: the character of the flow regime through low flows to large floods; the impact of any flood on the bed in terms of erosion off the bed; sediment transport and deposition with special emphasis on large boulders [*Carling and Tinkler,* this volume]; and the relationship of the channel to the valley system, especially the removal of slope debris supplied to the channel.

Sites. Twenty Mile Creek (296 km^2) is gauged at Ball's Falls by Environment Canada a few hundred meters above the main reach chosen for investigation [*Tinkler*, 1993]. A nearly forty-year record is now available, and the gauge is now (in principle) accessible by modem. A stage gauge on a bridge abutment was calibrated to known stage and discharge on the official gauge. A complementary site chosen was Swayze Creek (6 km^2), which flows through Short Hills Provincial Park. Both sites (fig. 1) are within fifteen minutes driving of home and University, and require

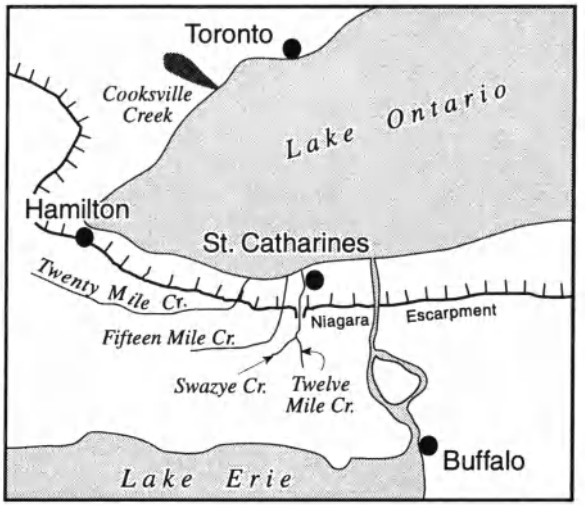

Figure 1. Location map of primary field sites (Tinkler) in southern Ontario.

only a few minutes of walking to access the reaches in question. This is relevant in terms of accessing flood peaks, which at Swayze Creek may last less than an hour. Other local localities of interest have been added as required, the primary one being Fifteen Mile Creek (30 km^2) [*Tinkler*, 1997c], which lies halfway between the first two and is used in a pothole sampling project for wash load. With different response times to major inputs (Twenty Mile Creek is about a half day to one day, Swayze Creek is about four to eight hours), it has proved possible to monitor peak flows in both these localities for the same event. Fifteen Mile Creek (which lies between the other two sites) is assessed for the frequency of high flow conditions, and the surface wave patterns over a series of potholes aligned with a flow junction [*Tinkler*, 1997c].

Cooksville Creek (33 km^2) in Mississauga (near Toronto) is also investigated [*Tinkler and Parish*, this volume]. This urbanized basin is farther from home. It has been difficult to monitor the flow regime adequately at peak flows, but clast movement was easier to map than is usually the case. The engineered dolomite armour stone walls made a good basis for marking large clast locations with indelible markers, and for locating the erosion of shale blocks off the bed of the channel. Fast recession and generally low base flows made it easy to work in the system at low flow.

Methods and findings. Base maps were prepared by trilateration. Distances are measured between stations placed to generate a triangular tesselation. The basic tesselation was drawn up accurately on paper and details were added by measured offsets. Individual boulders and prominent joints on the bed were marked (figure 2). In the often uneven terrain of the channel, this was found preferable to a plane table, and could be undertaken by a single individual. The scale for field maps produced was in the range 1:100 to 1:300. Vertical measurements were made with a graduated staff and a Suunto hand level, or by means of horizontally-levelled rod and a small graduated rod which passes through a hole in the rod to measure vertical offsets. I have found this instrument very useful for measuring small drops between pools in step/pool channels. Elevations of primary points are obtained by conventional levelling.

Survey stations, boulders, and other points of interest on the rock bed are usually marked with indelible black marker when the surface is dry (figure 3). Similar marks have also been made on cliffs to locate channel boulders (often from rockfalls), with the mark including the boulder name or number, and the offset from the channel wall. This has worked especially well on the engineered armour stone walls in Cooksville Creek. A horizontal scale of meters has also been marked along channel walls (Swayze and Twenty Mile Creek) to aid in the mapping of rock falls and deposited clasts during low flows, and for locating wave patterns and hydraulic jumps during high flow. The mark is made large enough to be visible from the opposite bank. Finally, marking has been used to identify every fracture-delineated unit along distinctive lithological units in the cliffs, with a view to determining removal rates from the cliff face. Distances marked have been about 8 to 12 m, with visible joints delimiting marked units every 5 to 40 cm.

Repeat photography has been used extensively to document channels, to record channel boundary conditions and flow patterns at various stages (figure 4), to identify boulders, and to compare reaches at low and high flow [see *Carling and Tinkler* this volume; *Tinkler and Parish*, this volume; *Tinkler and Wohl*, this volume]. Over more than five years, thousands of pictures have been taken (Twenty Mile Creek, Fifteen Mile Creek, Swayze Creek, Cooksville Creek), mainly with ISO 800 color film and as far as possible in flat light conditions (no direct sunlight) - often soon after local sunrise. Large boulders are photographed from several angles and marked on at least two sides when possible to aid in subsequent relocation. In a few instances boulders have been "placed" in the channel to be traced, and in others, the bed has been entirely cleared of debris prior to expected high flows. Clasts in rockfalls have been marked to study the dispersal downstream during subsequent flows.

With the two local creeks it proved possible to "catch" peak flows and to institute a program of velocity measurement through selected reaches. In addition to velocity measurement by float techniques, it was possible to map wave patterns on a prepared reach base map. It was also possible to assess velocity through bends using super-elevation [*Mears*, 1979; *Pierson*, 1985; *Mangelsdorf et al.*, 1990] from readings on reach stage gauges, and by measuring the wavelength of standing waves when flow was critical [*Tinkler*, 1997a,b].

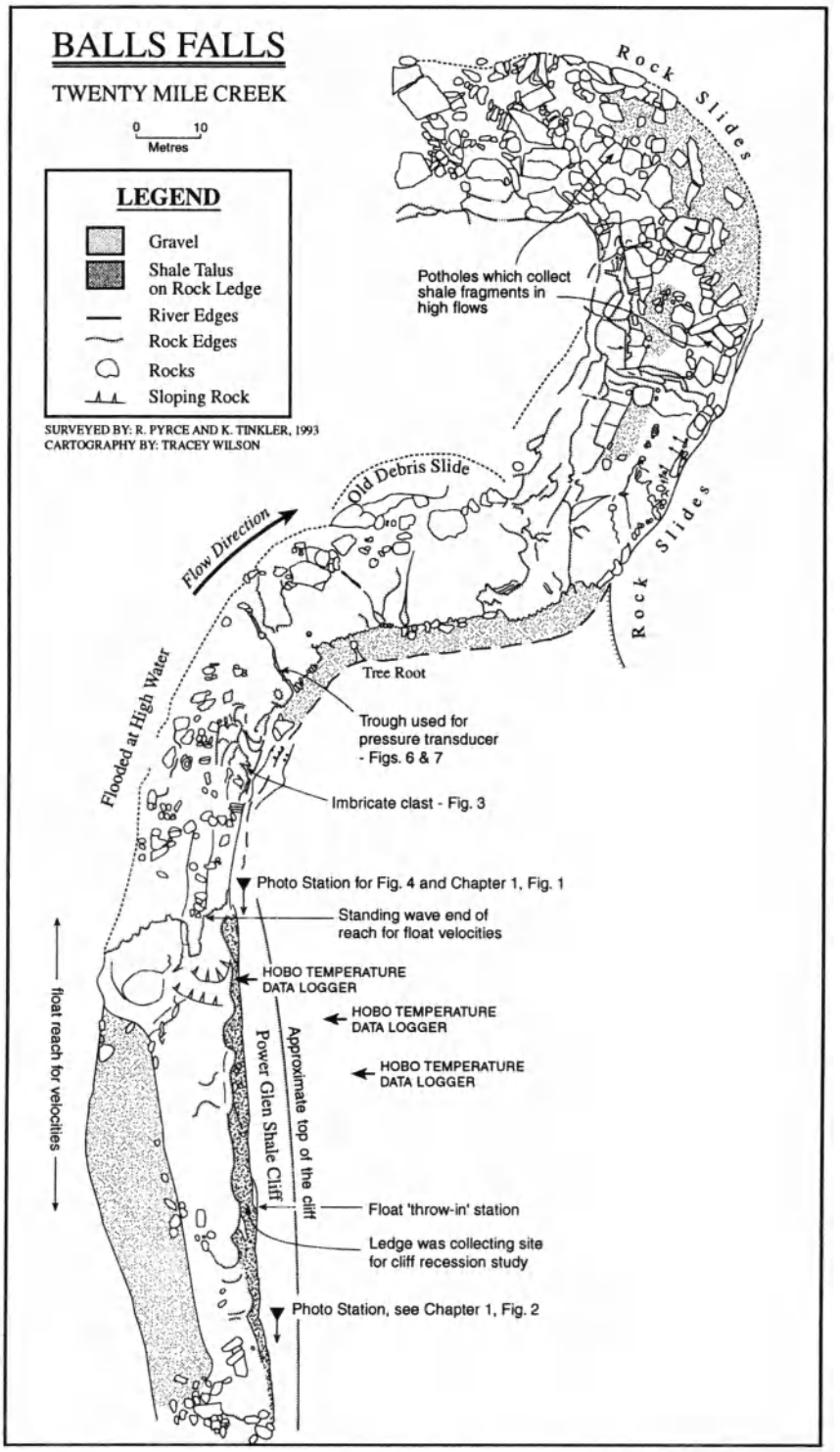

Figure 2. Basemap of bedrock reach at Balls Falls on Twenty Mile Creek, Ontario. The map was complied by trilateration, with details completed by offsets.

Figure 3. Clast marked with indelible marker moved from 25 meters up river and deposited in imbricate position at the channel margin. Looking upstream the clast is 1.8 metres long (across picture and transverse to flow), 55 cm wide and about 15 to 20 cm thick.

The use of floats seems primitive, but may be better adapted to the needs of steep river systems, and especially when the assessment of discharge is not required. In such systems, the crucial element to keeping the bedrock channel open is the transport of large clasts of boulder dimensions through what are "pooled" reaches at low flow. For this purpose, a longitudinal perspective is preferred by integrating velocity along the approximate thalweg streamline through a selected reach, rather than measuring velocity in the cross section. In an ideal world a truly three-dimensional view of velocity distribution through a reach would be preferred.

My practice is to use reaches of between 15 and 30 m normally marked at the downstream end by a prominent stationary wave or hydraulic jump (figures 2, 4, 5). Pieces of forest wood serve as floats and normally eleven measurements are taken to minimize the standard error on the mean. Measurements on floats which become trapped in marginal water, or for a long time in a breaking wave crest, are discarded. In very rough water, floats are frequently lost to view entirely and must be replaced, and in such circumstances I have also made adventitious use of logs already in transit in the flow.

In steep river systems there is usually a strong contrast between the thread of fast water along the thalweg, and the slack waters at the margins. Sometimes it is possible to take splits at intermediate points (usually passage though a standing wave or hydraulic jump, *Tinkler*, 1997b) in order to obtain a more complete view of velocity through an extended reach. There remains the question of the correction coefficient to apply to mean surface velocity in order to obtain mean velocity within the sampled streamlines. In deep subcritical flow with vertical floats, a figure of 0.8 is commonly used to convert streamline flow mean cross-section velocity [*Matthes*, 1956]. Appropriate values for critical or supercritical flow over smooth bedrock are not known. Critical flow is theoretically constant from top to bottom of the wave [*Henderson*, 1970], and *Tinkler* [1997b] found a distortion from mean velocity of between 2% and 6%, which implies a correction coefficient between 0.98 and 0.94. There is little information for supercritical flow. However, because velocities between 1.5 and 2 m/s can be recorded for flows a few centimeters deep over smooth rock surfaces [*Tinkler*, work in progress], it must be surmised that the correction coefficient may be closer to 1 than 0.8. *Carling* [1995] reported no distinction between theory and

Figure 4. Flood stage (130 cm) in the reach marked on Figure 2; the velocities in this reach with rising stage are recorded in Figure 5. Mean velocity in centre channel is 4.67 m/s, along the base of the cliff on the left, velocities are 2.7 m/s (about 2 m from the base, 4.2 m/s 4 m from the base). Along the near edge of the bar the velocity is 2.95 m/s and over the bar surface is 2.65 m/s. Notice the contrast in surface water patterns and topography over the bar on the right, compared to the main rockbed channel on the left.

reality when he used float (surface) velocities to represent mean velocities in supercritical flow.

Salt dilution gaging is a theoretical alternative to measure velocity, although sampling cross sections with different flow regimes in a wide vigorous river without a bridge may be a problem. For example, arrival times in channel center may differ markedly from those in marginal pools affected also by backwater effects. A salt dilution system is not manageable in a long rough reach by a solo worker. In flows which can be waded a velocity head meter gives useful results [*Vilm and Storey*, 1944]. A rod about 5 cm wide is placed in the water to provide a transverse obstruction. The vertical rise, h, of water on the rod, above the ambient flow elevation is measured. Mean velocity is calculated from $v = \sqrt{(2gh)}$ $(g = 9.81 m/s^2)$, and unit discharge, q, can be calculated from $q = 4.43d\sqrt{h}$, where d is depth (and which figure, therefore, in metric units, applies to a one meter width of channel).

In subsequent low flow periods it was possible to evaluate the impact of the peak flow on the bed, which included the removal of pieces from the bed, large boulder movement and sediment deposition. A primary finding is that bed erosion and large boulder transport is common in flows with recurrence interval (RI) on the order of 1 to 2. The amount of bed erosion in any particular flow is normally very limited (the order of 1 part in 1000 or less), but equally it is unusual for no erosion to be found in a reach 250 m long and 15 m wide [*Tinkler and Parish*, this volume]. In these bedrock streams of southern Ontario, exceptional flows are not required to effect morphological change.

On Twenty Mile Creek the existence of a large active shale cliff (80 m long by about 11 m high) abutting the channel at one location provided an opportunity to monitor the erosion rate of the cliff, and the efficiency of the stream in removing debris. At Swayze Creek rockfalls into the channel from 3 to 4 m high valley walls at two or three different locations provided a similar opportunity. At

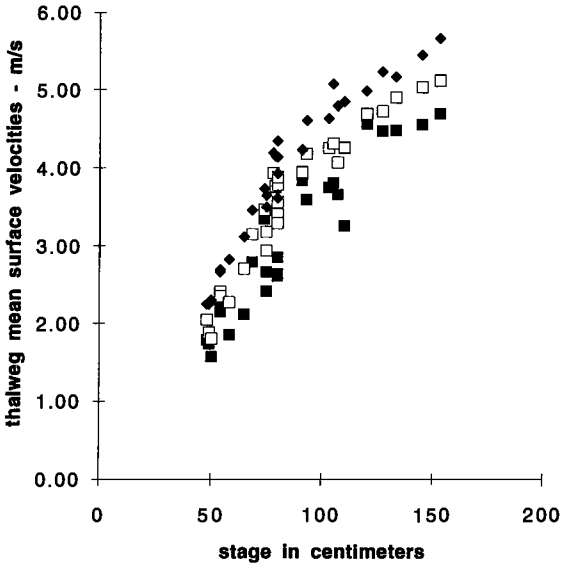

Figure 5. Mean water surface velocities through the 44 m reach below the Power Glen Reach as a function of stage. Stage is a good proxy for mean depth. At peak discharges, reducing surface velocities to 80% of measured values to estimate mean velocity still predicts Froude numbers in excess of 1 through this reach.

Twenty Mile Creek collections were undertaken every few days to sample the rock which had fallen onto slabs which had themselves fallen off the cliff. Surfaces were collected, swept clean, and left. Samples were dried in the lab and weighed, and many of them were sieved. Over 15 months nearly 600 kg of shale were collected. Collection strategies were designed to minimize human interference in a frequented scenic spot. Close monitoring of the cliff and the flows in the stream showed that floods with RI of 1 to 2 were capable of cleaning all debris from the cliff base, and that more moderate floods readily removed centimeter scale shale fragments. With care it also proved possible to get estimates of velocity along the marginal shelf during floods. At Swayze Creek small rockfalls were removed within a similar period. Nevertheless, maintaining the monitoring program, and processing the data, was draining on limited human resources.

Unexpected benefits

The most important lesson from the close observation of both creeks is that it was the unexpected and unplanned aspects which were particularly valuable. In particular, the close and frequent observation of flow up to and during moderate magnitude events allowed the recognition of the importance of critical and supercritical flow to the flow regime in general, and not just at peak flow [*Tinkler et al.*, 1994; *Tinkler*, 1997a,b]. For example, when using super-elevation to estimate mean velocity it is useful to know from direct observation that when flow is transcritical, the 'tilted' water surface affects only the accelerated portion of the flow which is contained by flanking zones of subcritical water. I have observed this for both supercritical flow at Swayze Creek, and critical flow at both Swayze Creek and Twenty Mile Creek. Thus estimates of the inner bend radius and observed active channel width can be adjusted to the edges of the accelerated flow for use in the equation, which improves its accuracy.

A chance observation of shale "sprinkle" onto a slab suggested the method used to monitor shale erosion, and hence sediment supply to the river, from the cliff. Similarly it also proved possible to clear out potholes in large boulders in the stream and then to collect the sediment which arrived as the result of a flood. This has enabled estimates to be made of the caliber of wash load in the stream, which would be impossible to sample in the reaches of interest when ambient velocities in the channel center can easily achieve 3 to 5 m/s.

More generally, it was seen that the rapid masking of the bed by mud on the waning stage [*Tinkler*, 1993] and algal blooms as the spring and summer progressed necessitated examination of the bed as soon as possible after a flood flow for signs of erosion. Close observation, especially after highflows, revealed striae from boulder movement (probably encased in icefloes) and localized and distinctive tracks of percussion marks on the bed which could sometimes be traced to an individual boulder. In most instances these tracks could no longer be discerned a few months after the event due to mud deposition and algal growth.

Observation every few days through several winters has shown that frozen bed conditions are normal annual events. Icing occurs in the recession stage of mid-winter meltout events, and is a positive feedback process requiring only several days to weeks of sub-zero temperatures to effect overall icing of the channel. Snowfall is not a necessary component. Ice adhering to clasts and bedrock can have an important effect on erosion and the transport capabilities of flow during meltout events [*Carling and Tinkler*, this volume] that tend to dominate the flood record and provide the peak flows.

Channel ice is most effective in causing bed erosion when weathering along joint and bedding planes is already well developed and anchor ice envelopes partly parted blocks on the bed. Subsequently buoyancy forces can act as stage rises to lever blocks off the bed. For this reason long time intervals between ice events on the bed need not be a hindrance to frozen bed conditions achieving significant erosion. At Twenty Mile Creek, a temperature logger (HOBO datalogger) in the north-facing cliff face one meter above the MAF floodline was originally installed for the shale collection project, but has since proved useful as a record of air temperatures at river level, as they affect icing conditions.

A pressure gauge (figure 6) installed in a bedrock trough (figure 7) in the channel center proved extremely useful in documenting short lived ice-drives (figure 8). The original intent was to use it as a stage gauge after correction for atmospheric pressure, and also to use it to document short term changes in water surface topography. However, the only safe location - a bedrock trough across the bed - tends to affect the location of the surface waves until very high flows. Nevertheless with a sampling interval set at 40 secs it was possible to detect water level rises and drops of up to half a meter occurring within two or three minutes during ice drives. Boulder movement described in *Carling and Tinkler* [this volume] took place one of these ice drives - probably the larger, second one. Such measurements are too short-term to be affected by air pressure changes and they were fortuitously validated by onshore observation of the same ice drives.

If locations could be found such that air pressure corrections could be easily made, the device which is sensitive to 1 cm changes in water depth, would have great utility in monitoring the fluctuation of the water surface, and eventually in enabling detailed maps of surface water topography to be produced.

Isle of Man sites

Frequent daily monitoring is not feasible at sites farther from my home. Indeed, in environments which are

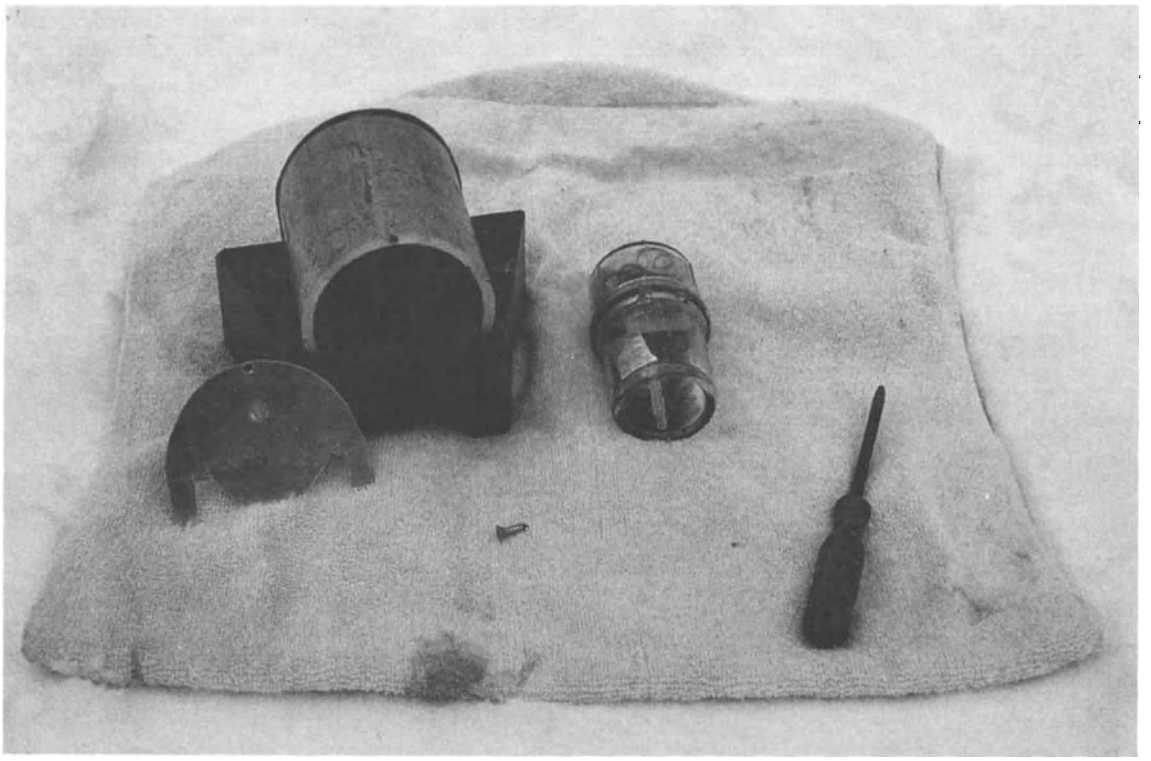

Figure 6. The waterproof bottle contains a 32K Stowaway logger and stand-alone pressure transducer for recording very short term changes in water level (see Figure 8). The pale tube just visible at the bottom of the bottle transmits water pressure though an oil-filled tube to the transducer. The housing is an aluminum pipe screwed to an 8 kg lead footing. Sampling time of 40 seconds optimizes the ability to capture short term water surface fluctuations, and the observer's ability to retrieve the gauge on the falling stage before it overwrites the record.

apparently less erosionally active on a year-by-year basis because the rocks are more resistant to low and medium magnitude flows, frequent monitoring would not be liable to yield immediate results. Thus sites the Isle of Man are inspected on an annual or semi-annual basis and estimated maximum flow data are collected from selected cross sections. Sediment is collected from sample sites at the same interval so that it is possible to sample with a frequency matching those of the standard rating curve. Flow monitoring is done on an 'as possible' basis and has only proved feasible in the Isle of Man to date when a prolonged visit during Fall 1997 enabled the lower portion of the flood frequency curve to be established. Observations during this visit indicate that nothing is effected in terms of bed erosion by moderately large flows approaching the Mean Annual Flood. Nevertheless, total postglacial incision of the channel is similar to that at Swayze Creek. I conclude that in the more resistant Manx Slate lithology of the Isle of Man sites, larger blocks are removed less frequently than at Swayze, with the commensurate observation that a much longer weathering time is available on the channel boundary to prepare blocks for removal.

The Isle of Man sites illuminate different aspects of bedrock channels, and together with Niagaran and Texan sites they have suggested one additional item of interest. That is: how do small first order bedrock channels operate efficiently? This is an important issue when sub-aerial weathering on slopes produces large blocks which may be the same order of magnitude as the channel width and depth.

CONCLUDING DISCUSSION

The field has primacy. It is the document we seek to read and to explain. It poses problems at all spatial and temporal scales, and it acts as the final, though enigmatic, arbiter on experiments performed and solutions proposed. It is enigmatic because we see what is there now, but in most cases we are ignorant of the initial state of the landscape, and we have gleaned limited information on the main stages in its evolution through geological time. We are still

Figure 7. Cross channel trough used as location to place pressure transducer. It was cleaned out for measurement, flow left to right, note the abraded lip on the distal side.

largely ignorant about how forces currently act to change the present condition, and our predictive abilities - in a hard quantitative sense - are abysmal.

The experimental method in field work is necessarily limited to the present and has been actively applied in recent decades. Its successes in articulating modern process have been confined for the most part to soft sediment systems undergoing rapid morphogenesis. In consequence it has been difficult to connect results in this area to slow morphogenesis in bedrock systems. We cannot for example, in the field, carry out experiments on a catastrophic or cataclysmic process scale, or upon geological time scales, which would enable an assesment of the importance of channel boundary weathering during "downtime". Likewise we are limited by the corresponding spatial scales of our experiments. For these reasons we must fall back on other methods as a means of evaluating hypotheses about slow change in the landscape, and these assessments must always be circumstantial.

The historical method seeks to determine the main stages of landscape evolution - to pin down the morphology at a point in time with some elucidation of the processes active at that time. It is currently undergoing a renaissance as a wide variety of geochronologic techniques are brought to bear upon different elements in the landscape. By re-vitaizing the importance of geologic timescales in viewing the mechanics of landscape change, we shall view bedrock channels, and theor corresponding drainage basins, from a viewpoint more compatible with their actual mechanisms of change.

Two areas in which progress can be expected to illuminate our field understanding of bedrock channels are flume and computer modelling of both landscape evolution and flow dynamics. Field sites lack controls which numerical modeling and the flume can supply. With a better understanding of highly turbulent situations in confined rocky spaces derived from the flume, we should be able to evaluate better what is happening in the field. In return the field can supply the examples of fixed boundaries of a bedrock channel that will enable replication in a flume [*Thompson and Wohl*, this volume], and also mathematical modelling if the appropriate algorithms are available [*Chanson and Montes*, 1995; *Howard*, this volume; *Meselhe et al.*, 1997; *Miller*, this volume, *Sklar and Dietrich*, this volume].

Lane and Richards [1997] have remarked that the controls possible in flume and computational work may lead to false impressions of order and rationality in our understanding of

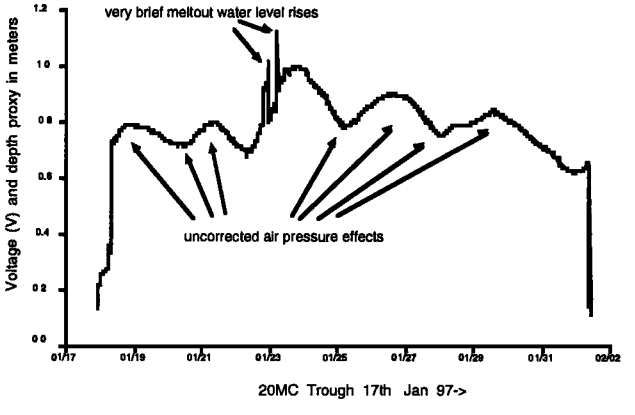

Figure 8. Water level record of meltout flood in February 1997. The two spikes in the record represent very short term water rises (a few minutes) as rising flood waters lifted an ice dome on an upstream plunge pool to generate an ice drive. Large boulder transport was effected in these drives, probably in the larger, second one [*Carling and Tinkler*, this volume].

real systems. Real world systems, they point out, depend very sensitively upon "morphological conditioning." By this they mean that very small elements in the topography, occurring at any point in time or space, may affect the future system trajectory. Even if valley-side rock slides, or ice and vegetation jams are predictable elements, a particular débris fan, ice or vegetation jam is unpredictable in detail and yet may be crucial in diverting flow to a new direction. Our increased realization of the sensitivity of non-linear systems to the system configuration focuses attention on the specifics as well as the generalities of landscape. In the end it brings us back to the field - rich in detail, replete with potential insight when properly read, complex and unpredictable in its behaviour.

Acknowledgements. Tinkler wishes to thank NSERC for a research grant, and Brock University for financial support over many years. Earlier drafts benefitted greatly from the comments of Alistair Kirkbride, Dan Cenderelli and Steve Kite.

REFERENCES

Baker, V. R., Stream-channel responses to floods, with examples from central Texas, *Geol. Soc. Amer. Bull.*, 88, 1057-1071, 1977.

Baker, V. R., Paleohydraulics and hydrodynamics of Scabland Floods, in *The Channeld Scabland*, edited by V. R. Baker and D. Nummedal, pp. 59-80, NASA, Washington, D.C., 1978.

Baker, V. R., Paleoflood hydrology and extraordinary flood events, *J. Hydr.*, 96, 79-99, 1987.

Baker, V. R. and G. Pickup, Flood geomorphology of the Katherine Gorge, Northern Territory, Australia, *Geol. Soc. Amer. Bull.*, 98, 635-646, 1987.

Baker, V. C., G. Pickup and H. A. Polach, Radiocarbon dating of flood events, Katherine Gorge, Northern Territory, Australia, *Geology*, 13, 344-347, 1985.

Baker, V. R., The Spokane Flood Debate and its legacy, in *Geomorphic Systems of North America*, edited by W. L. Graf, pp. 416-423, Vol, Centennial Special Volume 2, Geological Society of America, Boulder, 1987.

Baker, V. R. and R. C. Kochel, Flood sedimentation in bedrock fluvial systems, in *Flood Geomorphology*, edited by V. R. Baker, R. C. Kochel, and P. C. Patton, pp. 123-137, John Wiley & Sons, New York, 1988.

Baker, V. R. and C. R. Twidale, The re-enchantment of geomorphology, *Geomorphology*, 4, 73-100, 1991.

Bartholomew, M. J. and H. H. Mills, Old courses of the New River: Its late Cenozoic migration and bedrock control inferred from high-level stream gravels, southwestern Virginia, *Geol. Soc. Amer. Bull.*, 103, 73-81, 1991.

Bathurst, J. C., Field measurement of boulder flow drag, *J. Hydr. Eng.* 122(3), 167-169, 1996.

Beltaos, S., Editor, *River Ice Jams*, 390p, Highlands Ranch, Colorado, Water Resources Publications, LLC, 1996.

Benito, G., Energy expenditure and geomorphic work of the cataclysmic Missoula flooding in the Columbia River Gorge, *Earth Surf. Proc. Land.*, 22, 457-472, 1997.

Braun, D.D., Lithologic control of bedrock meander dimensions in the Appalachian Valley and Ridge Province, *Earth Surf. Proc. Land.*, 8, 223-237, 1983.

Bretz, J. H., The Channeled Scabland of the Columbia Plateau, *J. Geol.* , 31, 617-649, 1923.

Bretz, J. H., H. T. U. Smith and G. E. Neff, Channeled Scablands of eastern Washington: new data and interpretations, *Geol. Soc. Amer. Bull.*, 67, 957-1049, 1956.

Carling, P., Palaeohydraulic reconstruction of floods in upland UK bedrock streams: progress, problems and prospects, paper presented at Hydraulic Engineering 1994, Buffalo, edited by G. V. Cotroneo and R. R. Rumer, American Society of Civil Engineers, 860-864, 1994.

Carling, P. and T. Grodek, Indirect estimation of ungauged peak discharges in a bedrock channel with reference to design discharge criteria, *Hydr. Proc.*, 8, 497-511, 1994.

Carling, P. A., The Noon Hill flash floods July 13th,1983: Hydrological and Geomorphological aspects of a major formative event in an upland landscape., *Transactions of the Institute of British Geographers*, 11, 105-118, 1986.

Carling, P. A., Flow-separation berms downstream of a hydraulic jump in a bedrock channel, *Geomorphology*, 11, 245-253, 1995.

Cenderelli, D.A. and Wohl, E.E., Sedimentology and clast orientation of deposits produced by glacial-lake outburst floods in the Mount Everest region, Nepal, in *Geomorphological Hazards in High Mountain Areas*, edited by J. Kalvoda and C. L. Rosenfeld, pp. 1-26, Kluwer Academic Publishers, The Netherlands, 1998.

Cerling, T. E., R. J. Poreda and S. L. Rathburn, Cosmogenic 3He and 21Ne age of the Big Lost River flood, Snake River Plain, Idaho, *Geology*, 22(March), 227-230, 1994.

Chanson, H. and J. S. Montes, Characteristics of undular hydraulic jumps: experimental apparatus and flow patterns, *J. Hydr.Eng.*, 121(2), 129-144, 1995.

Chorley, R. J., Diastrophic background to twentieth-century geomorphological thought, *Geol. Soc. Amer. Bull.*, 74, 953-970, 1963.

Church, M., Records of recent geomorphological events, in *Timescales in Geomorphology*, edited by R. A. Cullingford, D. A. Davidson, and J. Lewin, pp. 13-30, John Wiley, New York, 1980.

Clayton, K. M., The problem of field evidence in geomorphology, in *Geographical essays in honour of K.C. Edwards*, edited by R. H. Osborne, F. A. Barnes, and J. C. Doornkamp, pp. 131-139, University of Nottingham, Nottingham, 1970.

Cleaveland, M. K. and D. N. Duvick, Iowa climate reconstructed from tree rings, 1640-1982, *Wat. Resour. Res.*, 28(10), 2607-15, 1982.

Cluer, B. L., Eddy bar responses to the sediment dynamics of pool-riffle environments, PhD dissertation, Colorado State University, Ft. Collins, Colorado, 128 p., 1997.

Costa, J. E., Stratigraphic, morphologic, and pedologic evidence of large floods in humid environments, *Geology*, 301-303, 1974.

Derricourt, R. M., Retrogression rate of the Victoria Falls and the Batoka Gorge, *Nature*, 264, 23-25, 1976.

Dethier, D. P., C. D. Harrington and Aldrich, M.J., Late Cenozoic rates of erosion in the western Espanola basin, New Mexico: evidence from geologic dating of erosion surfaces, *Geol. Soc. Amer. Bull.*, 100, 928-937, 1988.

Dick, G. S., R. S. Anderson and D. E. Sampson, Flash floods and channel evolution in the Blue Hills badlands, Caineville, Utah, *Abstracts with Programs, Geological Society of America*, 29(6), A-139, 1997.

Dury, G. H., Principles of Underfit Streams, *U.S. Geol. Surv. Prof. Pap.*, 452-A, 67, 1964a.

Dury, G. H., Subsurface explorations and chronology of underfit streams, *U.S. Geol. Surv. Prof. Pap.*, 452-B, 56, 1964b.

Dury, G. H., Theoretical Implications of Underfit Streams, *U.S. Geol. Surv. Prof. Pap.*, 452-C, 42, 1965.

Ellenberger, F., Les Méconnus: eighteenth century French pioneers of geomorphology, in *History of geomorphology: from Hutton to Hack*, edited by K. J. Tinkler, pp. 11-36, Unwin Hyman, Boston, 1989.

Ely, L. L., R. H. Webb, and Y. Enzel, Accuracy of post-bomb Cs-137 and C-14 in dating fluvial deposits, *Quat. Res.*, 38, 196-204, 1992.

Ely, L. L., Y. Enzel, V. R. Baker and D. R. Cayan, A 5000-year record of extreme floods and climate change in the southwestern United States, *Science*, 262, 410-412, 1993.

Enzel, Y., L. L. Ely, P. K. House, V. R. Baker and R. H. Webb, Paleoflood evidence for a natural upper bound to flood magnitudes in the Colorado River Basin, *Wat. Resour. Res.*, 29(7), 2287-2297, 1993.

Enzel, Y. and S. G. Wells, Extracting Holocene paleohydrology and paleoclimatology information from modern extreme flood events: An example from southern California, *Geomorphology*, 19, 203-226, 1997.

Fearnsides, W. G. a. W., W.H., A topographical study of the floodswept course of the Porth Llwyd above Dolgarrog, *Geographical Journal*, 72, 401-419, 1928.

Foley, M. G., Quaternary diversion and incision, Dearborn River, Montana, *Geol. Soc. Amer. Bull.*, 91(10), I 576-577 II 2189-2213, 1980.

Frodeman, R., Geological reasoning: Geology as an interpretative and historical science, *Geol. Soc. Amer. Bull.*, 107, 960-968, 1995.

Fuller, I., M. G. Macklin, J. Lewin, D. G. Passmore and A. G. Wintle, River response to high-frequency climate oscillations in southern Europe over the last 200 k.y., *Geology*, 26(3), 275-278, 1997.

Gilbert, G. K., Profile of the bed of the Niagara in its gorge, *American Geologist*, 18, 232, 1896.

Granger, D. E. and J. W. Kurchner, Quaternary downcutting rate of the New River, Virginia, measured from 26Al and 10Be, *J. Geol.*, 25(2), 107-110, 1997.

Grant, G. E., Critical flow constrains flow hydraulics in mobile-bed streams: A new hypothesis, *Wat. Resour. Res.*, 33(2), 349-358, 1997.

Harden, D.R., Controlling factors in the distribution and development of incised meanders in the central Colorado Plateau, *Geol. Soc. Amer. Bull.*, 102, 233-242, 1990.

Henderson, F. M., *Open channel flow*, 522p, MacMillan, New York, 1970.

Hjalmarson, H. W. and J. V. Phillips, Potential effect of translatory waves on estimation of peak flow, *J. Hydr. Eng.*, 123(6), 571-575, 1997.

Holmes, W. H., Travelling waves in steep channels, *Civil Engineering*, 6(7), 467-468, 1936.

Hupp, C. R., Plant ecological aspects of flood geomorphology and paleoflood history, in *Flood Geomorphology*, edited by V. R. Baker, R. C. Kochel, and P. C. Patton, pp. 335-356, John Wiley, New York, 1988.

Hydrologic Engineering Center, *HEC-RAS, River analysis system*, version 1.1., U.S. Army Corps of Engineers, Davis, California, 1995.

Kale, V. S., L. L. Ely, Y. Enzel and V. R. Baker, Geomorphic and hydrologic aspects of floods on the Narmada and Tapi rivers in central India, *Geomorphology*, 10, 157-168, 1994.

Kochel, R.C., Extending stream records with slackwater paleoflood hydrology - examples from west Texas, in *Flood Geomorphology*, edited by V.R. Baker, R.C. Kochel, and P.C. Patton, pp. 377-391, John Wiley & Sons, New York, 1988.

Kochel, R. C. and J. E. Miller, Geomorphic responses to short-term climatic change: an introduction, *Geomorphology*, 19, 171-173, 1997.

Kresan, P., The Tucson, Arizona, flood of October 1983, in *Flood Geomorphology*, edited by V. R. Baker, R. C. Kochel, and P. C. Patton, pp. 465-489, John Wiley & Sons, New York, 1988.

Lane, S. and K. S. Richards, Linking river channel form and process: time, space and causality revisited, *Earth Surf. Proc. Land.*, 22, 249-260, 1997.

Leighly, J. B., Walther Penck's contribution to geomorphology, *University of California Publications in Geography*, 6(1), 1-22, 1940.

Laing, D. and C. W. Stockton, Riparian dendrochronology: a method or determining flood histories of ungaged watersheds, Office of Water Resources Techonology, A-058-ARIZ, 1976.

Leopold, L. B. and T. Maddock, The hydraulic geometry of stream channels and some physiographic implications, *U.S. Geol. Surv. Prof. Pap.*, 282(A), 36, 1953.

Leopold, L. B., M. G. Wolman and J. P. Miller, *Fluvial processes in Geomorphology*, 522p, W.H. Freeman, San Francisco, 1964.

Lorenc, M. W., Barco, P. M., and Saavedra, J., The evolution of potholes in granite bedrock, W Spain, *Catena*, 22, 265-274, 1994.

Mangelsdorf, J., K. Scheurmann and F. H. Weiss, *River morphology: a guide for geologists and engineers*, Springer-Verlag, Berlin, 1990.

Matthes, G., River surveys in unmapped territory, *American Society of Civil Engineers*, 121, 739-758, 1956.

McDonald, E. V. and A. J. Busacca, Record of pre-late Wisconsinan giant floods in channeled scabland interpreted from loess deposits, *Geology*, 16, 728-731, 1988.

Mears, A. I., Flooding and sediment transport in a small alpine drainage basin in Colorado, *Geology*, 7, 53-57, 1979.

Merritts, D. J., K. R. Vincent, and E. E. Wohl, Long river profiles, tectonism, and eustasy: a guide to interpreting fluvial terraces, *J. Geophys. Res.*, 99(B7), 14,031-14,050, 1994.

Meselhe, E. A., F. Sotiropoulos and F. M. Holly, Numerical simulation of transcritical flow in open channel, *J. Hydr. Eng.*, 123(9), 774-783, 1997.

Miller, A. J., Valley morphology and boundary conditions influencing spatial patterns of flood flow, in *Natural and Anthropogenic Influences in Fluvial Geomorphology*, edited by J. E. Costa, A. J. Miller, K. W. Potter, and P. R. Wilcock, pp. 57-81, American Geophysical Union Press, Washington, D.C., 1995.

Mills, H. H. and J. R. Wagner, Long-term change in regime of

the New River indicated by vertical variation in extent and weathering intensity of alluvium, *J. Geol.* , 93, 131-142, 1985.

Murray, A., E. E. Wohl and J. East, Thermoluminescence and excess 226Ra decay dating of late Quaternary fluvial sands, East Alligator River, Australia, *Quat. Res.*, 37, 29-41, 1992.

Nott, J. and D. Price, Plunge pools and paleoprecipitation, *Geology*, 22, 1047-1050, 1994.

Nott, J., R. Young and I. McDougall, Wearing down, wearing back, and gorge extension in the long-term denudation of a highland mass: quantitative evidence from the Shoalhaven catchment, southeast Australia, *J. Geol.* , 104, 224-232, 1996.

O'Connor, J. E., Hydrology, Hydraulics, and Geomorphology of the Bonneville Flood, *Geological Society of America Special Paper*, 274, 83, 1993.

O'Connor, J.E., Webb, R.H. and Baker, V.R., Paleohydrology of pool-and-riffle pattern development, Boulder Creek, Utah, *Geol. Soc. Amer. Bull.*, 97, 410-420, 1986.

Pazzaglia, F. J. and Gardner, T. W., Fluvial terraces of the Susquehanna River, *Geomorphology*, 8, 83-113, 1993.

Pazzaglia, F. J. and Gardner, T. W., Late Cenozoic flexural deformation of the middle U.S. Atlantic margin, *J. Geophys. Res.* 99(B6), 12,143-12,157, 1994.

Pierson, T. C., Initiation and flow behavior of the 1980 Pine Creek and Muddy River lahars, Mount St Helens, Washington, *Geol. Soc. Amer. Bull.*, 96, 1056-1069, 1985.

Pyrce, R.S., *A field investigation of planimetric knickpoint morphology from rock-bed sections of Niagara Escarpment fluvial systems*. MA thesis, Wilfrid Laurier University, Canada, 119 p., 1995.

Rathburn, S. L., Pleistocene cataclysmic flooding along the Big Lost River, east central Idaho, *Geomorphology*, 8, 305-319, 1993.

Righter, K., High bedrock incision rates in the Atenguillo River Valley, Jalisco, Western Mexico, *Earth Surf. Proc. Land.*, 22, 337-343, 1997.

Sasowksy, I. R., W. B. White and V. A. Schmidt, Determination of stream-incision rate in the Appalachian plateaus by using cave-sediment magnetostratigraphy, *Geology*, 23(5), 415-418, 1995.

Schmidt, V. A., Magnetostratigraphy of sediments in Mammoth Cave, Kentucky, *Science*, 217, 827-829, 1982.

Schumm, S. A. and R. J. Chorley, Geomorphic controls on the Management of Nuclear Waste, US Regulatory Commission, Washington, DC, NUREG/CR-3276, 1983.

Seidl, M. A., R. C. Finkel, M. W. Caffee, G. B. Hudson and W. E. Dietrich, Cosmogenic isotope analyses applied to river longitudinal profile evolution: problems and interpretations, *Earth Surf. Proc. Land.*, 22, 195-209, 1997.

Sharpe, D. R. and Shaw, J., Erosion of bedrock by subglacial meltwater, Cantley, Quebec, *Geol. Soc. Amer. Bull.*, 101, 1011-1020, 1989.

Shepherd, R. G., River channel and sediment responses to bedrock lithology and stream capture, Sandy Creek Drainage, Central Texas, in *Adjustments of the fluvial system,*, edited by D. D. Rhodes and G. P. Williams, pp. 255-275, Kendall/Hunt, Dubuque, 1979.

Spedding, N., On growth and form in Geomorphology, *Earth Surf. Proc. Land.*, 22, 261-265, 1997.

Springer, G. S. and J. S. Kite, River-derived slackwater sediments in caves along Cheat River, West Virginia, *Geomorphology*, 18, 91-100, 1997.

Strahler, A. N., The dynamic basis of geomorphology, *Geol. Soc. Amer. Bull.*, 63, 923-938, 1952.

Sugden, D. E., M. A. Summerfiled and T. P. Burt, Editorial: Linking short-term geomorphic processes to landscape evolution, *Earth Surf. Proc. Land.*, 22, 193-194, 1997.

Tinkler, K. J., *A Short History of Geomorphology*, 1st ed, 317p, Croom Helm, London, 1985.

Tinkler, K. J., Fluvially sculpted rock bedforms in Twenty Mile Creek, Niagara Peninsula, Ontario, *Canadian J. Earth Sciences*, 30, 945-953, 1993.

Tinkler, K. J., Entre Lacs: a Postglacial Peninsula Physiography, in *Niagara's Changing Landscapes*, edited by H. J. Gayler, pp. 13-51, Carleton University Press, Ottawa-Canada, 1994.

Tinkler, K. J., Critical flow in rockbed streams with estimated values for Manning's *"n"*, *Geomorphology*, 20(1-2), 147-164, 1997a.

Tinkler, K. J., Indirect velocity measurement from standing waves in rockbed streams, *J. Hydr. Eng.* 123(10), 918-921, 1997b.

Tinkler, K. J., Rockbed wear at a flow convergence zone in Fifteen Mile Creek, Niagara Peninsula, Ontario, *J. Geol.* , 105(2), 263-274, 1997c.

Tinkler, K. J., J. W. Pengelly, W. G. Parkins and G. Asselin, Postglacial recession of Niagara Falls in relation to the Great Lakes, *Quat. Res.*, 42, 20-29, 1994.

Toda, M., Bedrock channel erosion on the Upper Obitsu, Boso Peninsula: a field experiment on the influence of a fissure on erosion, *Geographical Review of Japan*, 67A(1), 14-25, 1994.

Vilm, H. H. and H. C. Storey, Velocity head rod calibrated for measuring stream flow, *Civil Engineering*, 14, 475-476, 1944.

von Engeln, O. D., A Preglacial or Interglacial Gorge near Seneca Lake, New York, *New York State Museum Bulletin*, (286), 127-131, 1931.

von Engeln, O. D., *The Finger Lakes Region: its origin and nature*, 156p, Cornell University Press, Ithaca: New York, 1961.

Waitt, R. B., About forty last-glacial Lake Missoula jökulhlaups through southern Washington, *J. Geol.* , 88, 653-679, 1980.

Waitt, R. B., Case for periodic, colossal jökulhlaups from Pleistocene glacial Lake Missoula, *Geol. Soc. Amer. Bull.*, 96, 1271-1286, 1985.

Webb, R.H., J.E. O'Connor, and V.R. Baker, Paleohydrologic reconstruction of flood frequency on the Escalante River, south-central Utah, in *Flood Geomorphology*, edited by V.R. Baker, R.C. Kochel, and P.C. Pattob, pp. 403-420, John Wiley & Sons, New York, 1988.

Webb, R. H., *Grand Canyon, a Century of Change*, The University of Arizona Press, Tucson, 290 p., 1996.

Winchell, N. H., The recession of the Falls of St Anthony, *Geological Survey of Minnesota, Final Report*, II, 313, 1888.

Wohl, E. E., Bedrock benches and boulder bars: floods in the Burdekin Gorge of Australia, *Geol. Soc. Amer. Bull.*, 104, 770-778, 1992.

Wohl, E. E., Bedrock channel incision along Piccaninny Creek, Australia, *J. Geol.* , 101, 749-761, 1993.

Wohl, E. E., Energy expenditure in deep, narrow bedrock canyons, *Abstracts with Programs, Geological Society of America*, 26(7), A-233-234, 1994.

Wohl, E. E. and Y. Enzel, Data for palaeohydrology, in *Global Continental Palaeohydrology*, edited by K. J. Gregory, L. Starkel and V. R. Baker, pp. 23-59, John Wiley, Chichester, 1995.

Wohl, E. E., S. J. Fuertsch and V. R. Baker, Sedimentary records of late Holocene floods along the Fitzroy and Margaret Rivers, Western Australia, *Aust. J. Earth Sci.*, 41, 273-280, 1994a.

Wohl, E. E., N. Greenbaum, A. P. Schick and V. R. Baker, Controls on bedrock channel incision along Nahal Paran, Israel, *Earth Surf. Proc. Land.*, 19, 1-13, 1994b.

Wohl, E. E. and H. Ikeda, The effect of roughness configurations on velocity profiles in an artificial channel, *Earth Surf. Proc. Land.*, 23, 159-169, 1998.

Yanosky, T. M., Hydrologic inferences from ring widths of flood-damaged trees, Potomac River, Maryland, *Environ. Geol.* , 4, 43-52, 1982.

Yanosky, T. M., Documentation of high summer flows on the Potomac River from the wood anatomy of ash trees, *Water Resources Bulletin*, 20(2), 241-250, 1984.

Zen, E. and K. L. Prestegaard, Possible hydraulic significance of two kinds of potholes: examples from the paleo-Potomac River, *Geology*, 22, 47-50, 1994.

Zolitschka, B., A 14,000 year sediment yield record from western Germany based on annually laminated lake sediments, *Geomorphology*, 22, 1-17, 1998.

K. J. Tinkler, Department of Geography, Brock University, St Catharines, Ontario L2S 3A1, Canada, ktinkler@spartan.ac.brockU.ca

E. Wohl, Department of Earth Resources, Colorado State University, Fort Collins, Colorado 80523, United States.

Flume Experimentation and Simulation of Bedrock Channel Processes

Douglas Thompson

Department of Physics, Astronomy and Geophysics, Connecticut College, New London, Connecticut

Ellen Wohl

Department of Earth Resources, Colorado State University, Fort Collins, Colorado

Flume experiments can provide cost effective, physically manageable miniature representations of complex bedrock channels. The inherent change in scale in such experiments requires a corresponding change in the scale of the forces represented in the flume system. Three modeling approaches have been developed that either ignore the scaling effects, utilize the change in scaled forces, or assume similarity of process between scales. An understanding of the nonlinear influence of a change in scale on all the forces involved is important to correctly analyze model results. Similarly, proper design and operation of flume experiments requires knowledge of the fundamental components of flume systems. Entrance and exit regions of the flume are used to provide good experimental conditions in the measurement region of the flume where data are collected. To insure reproducibility, large-scale turbulence must be removed in the head of the flume and velocity profiles must become fully developed in the entrance region. Water-surface slope and flow acceleration effects from downstream water-depth control must also be isolated in the exit region. Statistical design and development of representative channel substrate also influence model results in these systems. With proper experimental design, flumes may be used to investigate bedrock channel hydraulics, sediment-transport relations, and morphologic evolution. In particular, researchers have successfully used flume experiments to demonstrate the importance of turbulence and substrate characteristics in bedrock channel evolution. Turbulence often operates in a self perpetuating fashion, can erode bedrock walls with clear water and increase the mobility of sediment particles. Bedrock substrate influences channel evolution by offering varying resistance to erosion, controlling the location or type of incision and modifying the local influence of turbulence. An increased usage of scaled flume models may help to clarify the remaining uncertainties involving turbulence, channel substrate and bedrock channel evolution.

INTRODUCTION

Rivers Over Rock: Fluvial Processes in Bedrock Channels
Geophysical Monograph 107

The direct study of bedrock channel processes in natural channels is extremely difficult because much of the change

along these resistant channels occurs during high magnitude, low frequency flows. The recurrence interval between such flows is very long relative to the time-spans of most research projects, and conditions within the channel commonly make direct measurement hazardous or impossible. Consequently, many investigators must rely on indirect study using flume experiments, computerized simulations, or the inference of process from form. Each of these indirect approaches has it's own limitations and strengths. The primary limitation of flume experimentation is scaling. In order to obtain realistically scaled results, researchers must strike a compromise between a perfect full-size representation of the fluvial system and a smaller physically and financially manageable experiment. Fortunately, a well-designed flume experiment can be used to shrink the physical and temporal scales of complex natural systems, and still provide realistic results. Flume experimentation also allows for some control of the driving and resisting forces with an associated simplification of channel response and result analysis. Consequently, researchers often rely on flume experiments to provide data for systems that would be difficult to study in a natural, uncontrolled state.

As reviewed by *Mosley and Zimpfer* [1978], flume experiments have several advantages relative to the study of natural channels:

- They permit identification, isolation, manipulation, and precise measurement under controlled conditions of processes and variables.
- They facilitate study of channel evolution and of equilibrium versus non-equilibrium systems.
- They permit study of varying boundary and initial conditions.

However, flume experiments also have several disadvantages:

- Flumes are expensive to build, time and labor intensive to operate, and require operating and storage space
- Initial and boundary conditions in the model may be dissimilar to those in natural channels and may influence model behavior.
- Materials and processes in the model may be dissimilar to those in nature (e.g. constant operation of model processes versus episodic natural processes), and there may be no obvious means of relating model behavior (e.g. rate of evolution) to that of natural systems.
- The study of limited processes or independent variables may mask interactions that occur in natural channels.
- There is usually a trade-off between precision of measurement and accuracy of representation as model size decreases.

To fully understand the limitations associated with flume experimentation, it is necessary to understand the problems that arise with a change in the scale or characteristics of a physical channel system. Although flume experimentation does have its inherent risks, it provides the best means for obtaining physical measurements of moving fluids in dangerous or inaccessible situations. The flume can also be used to reduce the time required to observe a representative long-term evolutionary process. Both changes in scale are particularly useful when simulating bedrock channels.

1. SCALING ISSUES

A change in physical scale inherently creates a change in the relative strength of forces acting within the experimental channel. Interestingly, a specified reduction in physical scale does not result in an equal reduction in dynamic and kinematic scales. Although computational methods have been developed to scale forces within a flume, it is impossible to create a perfectly rescaled representation of all the forces acting within the fluvial system. For example, the hydraulics in a bedrock flume experiment might be a function of the Reynolds number (turbulent versus laminar flow), and the Froude number (supercritical versus subcritical flow). Unfortunately, it is physically impossible to create a flume system with a rescaled geometry that maintains the same balance of inertial, viscous and gravity forces. Hence, it is impossible to have both Froude and Reynolds numbers identical in the model and prototype. To counter this tendency, researchers must predict channel dynamics and incorporate adjustments in the experimental design and analysis. Scientists have selected three approaches to handle these scaling problems: the unscaled model, the scaled model and the analog model.

1.1. Unscaled Models

An unscaled model may be useful to demonstrate a channel process or evolutionary principle, but it cannot provide truly predictive data that address specific changes in channel dimensions, fluid forces or sediment-transport rates. In addition, the greater the change in physical scale or physical characteristics, the greater will be the uncertainty associated with the flume results. Because these models do not consider nonlinear changes in forces, unscaled physical models should primarily be used to provide qualitative data. Despite these drawbacks, unscaled models continue to provide limited amounts of quantitative data. For example, the well know channel meandering experiment, using the common stream table, produces realistic planimetric patterns and sinuosity values. However, this

type of experiment tends to be the exception rather than the rule. Therefore, scientists often rely on dimensional analysis to scale forces within a flume system to provide better control on quantitative results, or they change model characteristics in a controlled manner in order to modify the various forces operating in the fluvial system.

1.2. Scaled Models

Scaled models provide the best means for obtaining quantitative data on specific processes or events. However, in order to obtain these types of specific results, scaled models require more planning and a greater number of initial assumptions. For example, a scaled model can be used to measure realistically scaled velocities assuming that the major driving forces in the model have been correctly identified. The obvious trick is to determine which forces are important for a given situation. Typically, based on experience or intuition, the dominant forces in the fluid are selected a priori and used to represent the scaled processes operating in the natural system. In this procedure, dimensional analysis is used to provide dimensionless numbers for use in a dynamic similitude calculation. Simply stated, the important driving variables are used to produce scale invariant numbers for use in comparisons between the natural channel (prototype) and flume (model). The most commonly used dimensionless variables are the Reynolds number and Froude number. With this technique, a properly scaled flume experiment can provide detailed qualitative and quantitative data. Unfortunately, omission of an important force will undermine the usefulness of the flume results, but this omission may not become apparent during the course of the research. Consequently, all scaled flume experiments reflect a delicate balance between previously defined methodologies and scientific intuition.

1.3. Analog Models

The majority of flume experiments designed to simulate bedrock channel processes have been analog models. An analog model may reproduce some important aspect of the form and function of a natural phenomenon, but the forces, materials, and processes may be dissimilar to those in natural systems [*Schumm et al.*, 1987]. For bedrock channel simulation, the resistance of channel substrate is often altered to account for differences in channel forces and temporal scales. For example, the resistance of the flume substrate is usually lowered to help provide erosion with the smaller shear stresses in the smaller flume channel. Ideally, the channel evolutionary process will follow similar complex progressions and produce comparable resultant landforms. Conversely, the scientist may conduct an experiment with a redesigned fluvial system in order to reduce or eliminate forces resulting from secondary processes. For example, a simplification of flow and boundary conditions may be useful for investigating dominant secondary flow patterns related to large-scale changes in channel morphology [*Schmidt et al,*, 1993]. In this manner, the uncertainties related to sediment transport, bursting flow phenomenon and unsteady flow conditions can be removed from the experimental results. Another common approach is to eliminate interactions between the channel banks and bed by using a non-erodible, immobile flume wall [*Parker and Wilcock, 1993*]. In both cases, the scientist can obtain useful qualitative and quantitative data but must be careful to examine the uncertainties resulting from changes in force magnitude and process. It is also quite possible that complex interactions drive many of the observed processes, and these interactions may be lost with certain experimental designs. Unfortunately, in an attempt to simplify the problem, we may disrupt or diminish the dominant processes we seek to explain [*Mosley and Zimpfer*, 1978].

2. FLUME DESIGN AND OPERATION

Complete design of a flume requires knowledge of many flume characteristics and procedures beyond the scope of this chapter. A more complete explanation of flume design can be found in *Williams* [1971] and a more complete description of the use of flume experiments in fluvial geomorphology is included in *Schumm et al.* [1987]. Most flumes also have unique dimensions and personal quirks that require a certain familiarity in order to completely design a flume experiment. However, all properly designed flumes incorporate standard components and operating procedures that are designed to provide suitable experimental conditions. Many of the physical attributes of a flume are used to suppress artificial turbulence generated by pumping action and pipe inflow conditions. Most flumes also have an optimal design range for discharge and water depth. Researchers should plan flume experiments with the flume components and limitations in mind to insure good experimental results.

Generally, larger flumes are capable of producing more realistic field conditions [*Williams*, 1971]. As flume size decreases, complications from channel walls [*Williams*, 1970] and inappropriate approach conditions begin to affect the quality of results [*Williams*, 1971]. For example, an experiment with 0.2 m deep water and 1 m/s mean velocities will require a length of over 6 m just to achieve an equilibrium logarithmic velocity profile. As a general rule of thumb, the width of the flume should be at least 4

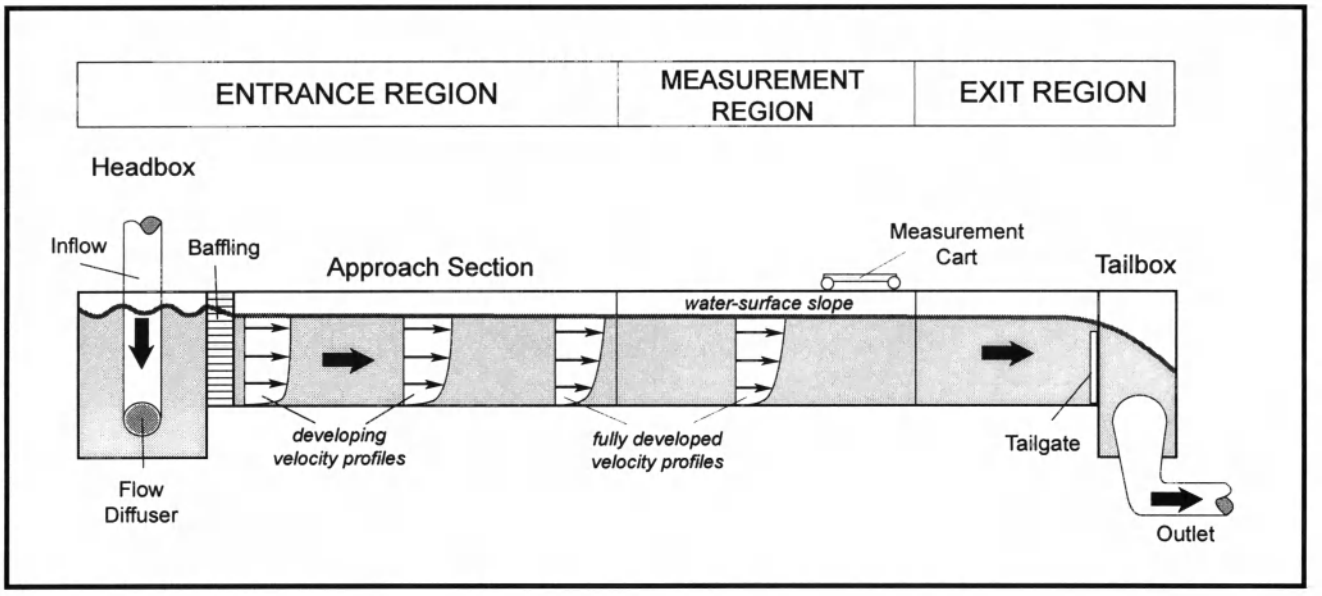

Figure 1. Typical design and fundamental components of experimental flumes. The size and design approach of different regions within the flume will vary from flume to flume.

times the water depth [*Williams*, 1971], with an optimal total flume length of over 30 m. Smaller flumes will require reductions in discharge levels with careful attention to the hydraulic conditions within the flume. Therefore, the ability to create a hydraulically simplified environment will depend on the flume dimensions, flume attributes and operating conditions.

2.1. Flume Components

Most important flume components are used to reduce variability (turbulence) in the experimental channel and produce realistic hydraulic conditions. Since large-scale turbulence generation occurs in almost every natural channel in the world, it may seem inappropriate to suppress turbulence in the flume system. However, the goal of many flume features is to suppress artificial turbulence generated by pumping action and pipe inflow. Consequently, the dominant hydraulic pattern or processes observed in the flume can be attributed to an influence of the physical channel attributes.

To design an experiment, a flume can be logically subdivided into three main sections: the entrance region, the measurement region, and the exit region (Figure 1). Since the goal of all flume experimentation is collection of measurements or data, the measurement region is clearly the most important section of the flume. Conversely, the only function of the entrance region is to provide stable hydraulic conditions for the measurement region. Similarly, the exit region is used to provide the desired depth and water-profile conditions in the measurement region. If accurate quantification of processes is an important component of a flume experiment, careful attention should be paid to conditions in the entrance and exit regions. With some simpler experiments, only the measurement section will be of interest. In either case, realization of the hydraulic conditions in different sections of the flume will aid in analysis of the experimental results.

Entrance Region. In order to provide hydraulic approach conditions that mimic natural velocity profiles, it is first necessary to eliminate dominant velocities or large-scale turbulence generated by the inflow conditions at the head of the flume. Then the flow must be given an adequate downstream distance to develop a representative velocity profile. For example, the discharge to the flume will usually be supplied by a pump or gravity fed pipe with a much small diameter than the flume width. The difference in cross-sectional area implies that the mean velocities in the pipe will be higher than mean velocities in the flume. Therefore, to prevent a fire hose-type situation, it is necessary to reduce pipe flow velocities at the head of the flume. A flume headbox, flow diffuser, and baffling are all used in an attempt to reduce these velocities and provide a uniform velocity profile at the head of the flume channel. Then a long approach section is used to insure that a fully turbulent velocity profile is developed that reflects the flume experimental conditions, rather than the conditions within the inflow pipe.

The flume headbox is a section used to help reduce incoming mean velocities by creating a larger cross-sectional area of flow. The headbox is usually a large rectangular box located at the immediate upstream end of the flume. In order to provide adequate kinematic energy dissipation, *Williams* [1971] recommends a headbox length of two channel widths with a headbox width at least as wide as the flume channel. The floor of the headbox section should also be depressed relative to the flume bed to further increase cross-sectional areas of flow. When used in conjunction with a flow diffuser and baffling, the headbox section can completely remove large-scale turbulence and coherent structures entering the flume.

The flow diffuser is simply designed to provide a larger cross-sectional area of flow as the incoming discharge exits the inflow pipe within the headbox section. By definition, the increase in cross-sectional area will reduce incoming mean velocities. A popular flow diffuser design uses a T-junction at the end of the inflow pipe with a series of slots along the bottom of the T cross-members (Figure 2). Well-designed flow diffusers will direct incoming velocities in a range of directions especially towards the bed of the headbox. The ensuing chaotic flow patterns will help to further dissipate kinetic energy. Simply stated, the flow diffuser splits the incoming discharge into several segments lowering velocities and generating turbulence. Subsequently, small-scale turbulence generation and dissipation within the headbox section is used to help create a quieter, slower moving body of water entering the flume.

Although the flow diffuser and headbox section can create more homogeneous flow conditions, it is still necessary to run the discharge through a series of baffles or vanes in order to eliminate any large-scale eddies. The baffling can range in complexity from a simple set of screens or an elaborate array of elongated tubes organized in a honeycomb network. The first example might be used in an evolution study where general trends or processes are of primary interest. The more involved baffling would be required if detailed velocity measurements or turbulence characterizations were planned. In either case, the purpose of the baffling is to force flow to enter the flume in a predominantly downstream direction. After exiting the baffling, flow entering the approach section of the flume should have a fairly uniform velocity profile with little or no lateral velocity components. Once again, the level of detail desired in velocity characterization will determine the sophistication of the baffling needed for a particular experiment. As *Williams* [1971] emphasizes, it is worthwhile devoting attention to baffling in order to provide better initial conditions to the flume.

The last portion of the entrance region of the flume is the approach section. As most geomorphologists realize, the well-known logarithmic or S-shaped velocity profiles take some time to develop. Since the water in the flume is in constant downstream motion, time here equates to distance along the flume. Therefore, at a short distance along the flume, velocity conditions in the column of water will still be in a developing state. In order to ensure repeatable experiments, flume experiments must be conducted at a sufficient distance downstream from the baffling to ensure that the velocity profiles are fully developed. The distance increases with depth, velocity and over smooth boundaries. For example, a 3-m long entrance section would be required for a 10 cm depth of flow with a 1 m/s mean velocity [*Williams*, 1971]. A full description of this type of boundary layer development is contained within most fluid mechanics textbooks [*Tritton*, 1987; *Roberson and Crowe*, 1997]. Obviously, the hydraulic conditions of the flow could affect experimental results. For example, velocity profiles collected in the approach and measurements sections will have distinctly different shapes regardless of the particular experimental conditions. The bed of the approach section should also contain a similar bed structure or sediment distribution as the measurement section to insure the developed velocity profile is appropriate for the measurement section. If both conditions are fulfilled, velocity measurements can be collected anywhere within the measurement region without concern for the exact distance to the head of the flume. Ultimately, an entrance region and approach section of the flume can be used to remove artificial turbulence and generate velocity profiles entering the measurement region that best replicate natural stream conditions.

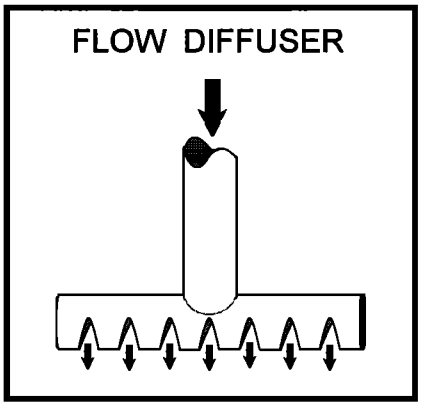

Figure 2. A T-shaped flow diffuser commonly found in the headbox section of flumes.

Measurement Region. The measurement region of the flume is where all the work takes place. In this area, fully turbulent flow conditions should already exist, so we can feel comfortable collecting data anywhere along this

region. The exact dimensions of the measurement region will be determined by the flume selected and will depend on the specifics of the experimental design. As a general rule, *Williams* [1971] suggests that the length of the measurement region should increase with water depth, and should be represented by a ratio of 1:75 to 1:100 of water depth to measurement region length. Other restrictions will depend on the physical system modeled, the type of data desired and the size of the flume used.

In order to collect data, most flumes will use a measurement cart. The cart can help for measurement access in larger flumes, and will serve as a reference datum for accurate elevation measurements. To further improve precision and accuracy of elevation measurements, a point gauge can be used in conjunction with a measurement cart to provide millimeter-scale precision. Additional equipment needs will depend on the experiment conducted and the level of precision desired.

Exit Region. Under most experimental conditions, the flow regime in the flume will be characterized by subcritical flow conditions. A gravity wave will move upstream under this hydraulic regime. Under these conditions, a change in the physical dimensions of the channel at the downstream end of the flume will create an effect on depth that propagates in the upstream direction. The hydraulics principles behind this water-surface slope effect are described in most introductory fluid mechanics books [*Roberson and Crowe*, 1997, *Young et al.*, 1997]. In order to manipulate the depth of flow in subcritical flow conditions, a downstream control is utilized. Therefore, in most flume experiments an exit region is used to help maintain the desired depth of flow in the measurement region.

Depending on the flume used, downstream depth control for subcritical flow conditions can be accomplished with two standard approaches. One approach uses a funnel type arrangement at the end of the flume or a continuous curved channel with no water storage capacity in the flume. The depth of water in the flume is controlled by the volume of water added to the system prior to startup. The advantage of this type of system is continuous maintenance of subcritical flow conditions throughout the length of the flume and the lack of channel-bed obstructions. A simpler approach for adjusting water depth in the flume uses tailgates in a dam type arrangement at the end of the flume. The depth of water is simply a function of the water discharge and height of the flume tailgate. With this arrangement, a series of boards can be used to incrementally adjust the depth of water. Alternatively, a hinged plate can be used to provide a more continuous selection of water depths. Although the tailgate approach is much simpler than the funnel approach, the tailgate provides a physical barrier to sediment movement, and also creates some undesirable hydraulic conditions. In particular, the water plunging over the tailgate will achieve a supercritical flow regime. Downstream depth control will usually produce a slight drawdown near the end of the flume that will propagate upstream. This condition is described by the M2 water-surface profile [*Roberson and Crowe*, 1997]. An adequate distance will need to be maintained from the water-surface drawdown to insure velocity profiles in the measurement section are not affected by flow acceleration. This distance will vary from 1 m for 0.5 m wide and 0.5 m deep flow over the tailgate to 6 m for deeper and wider flows [*Williams*, 1971].

In the event that a flume experiment is conducted under primarily supercritical flow conditions, the exit section becomes less important. As long as water is effectively removed and/or channeled to the pump system, the exit section will not effect results. To control water depths in these conditions, an upstream control will need to be utilized. Usually a sluice gate provides the depth control desired for these types of flow conditions.

2.1. Slope and Discharge Control

Slope control entails both determination of flume-bed and water-surface gradient. Selection of flume-bed gradient is usually achieved by tilting the entire flume apparatus. Often, one end of the flume pivots while large jacks are used to raise and lower the opposite end of the flume. A desired channel-bed slope can be achieved by changing the total drop over the fixed flume length. In other situations with non-tilting flumes, the channel substrate may be graded to provide a desired slope. In both of these cases, the initial slope is a prescribed condition for the experiment and can be viewed as a control variable for evolutionary process and form. Conversely, many evolution experiments will want sufficient substrate depth to allow alteration of channel-bed slopes with time. For example, knickpoint migration investigations will need an adequate depth of channel substrate to insure that the flume-bed does not act as a local base-level. In either situation, flume-bed slope will need to be monitored in combination with water-surface slope to provide good experimental conditions.

Water-surface slopes are controlled through a combination of factors. The slope of the flume-bed has an effect on the normal depth of water and the slope of the water surface. For example, experiments conducted with steady, uniform flow conditions will have a channel-bed slope that is equal to the water-surface slope. Conversely, the tailgate may be used to change water-surface slopes by creating backwater or drawdown effects and non-uniform flow. The

discharge level can also influence water-surface slopes if non-uniform flow conditions exist. The combination of high tailgate positions and low discharge levels will tend to produce water-surface slopes that are lower than flume-bed slopes. Conversely, a low or absent tailgate will create a drawdown effect that will propagate upstream creating higher water-surface slopes relative to flume-bed slopes. For most experimental situations, equality of flume-bed and water-surface slopes will be desirable to insure steady, uniform flow conditions in the measurement region of the flume. To achieve the desired water-surface slope, the scientist usually conducts an iterative adjustment sequence among flume-bed slope, tailgate height and discharge level. Eventually, a proper balance of conditions can produce the water-surface slope of interest.

Most experiments will require control of water discharge and may require control of sediment discharge to the flume. Control of both conditions will depend on the type of flume used for the research. Flumes can generally be divided into one of two categories: Recirculating and non-recirculating flumes. Recirculating flumes can be easier to run and control, but require more difficult initial design criteria. Non-recirculating flumes are simple to understand and cheap to build, but are more difficult to run [*Williams*, 1971]. Some of theses difficulties are related to the possible variation in discharge conditions resulting from changes in the supply reservoir. Sediment will also need to be continuously supplied to the head of the flume if sediment transport is to be maintained. Once again, the type of flume used will depend on the goals of the experiment.

Most recirculating flumes use an electric pump and a closed hydraulic system to provide continuous discharge within the flume. In these systems, the pump supplies a designated flow rate to the entrance region, water flows through the flume, leaves the exit region and eventually returns to the pump. Discharge control can be achieved through an electrical controller manipulating pump revolutions and flow rate, or a series of bypass lines can be used to change the flow rate with a constant pumping volume. In many cases, sediment transported from the flume can be redirected into the entrance region of the flume to achieve continuity of sediment. For long-term evolution studies this type of system may have some advantages, especially in alluvial channels. Unfortunately, with recirculating flumes the initial sediment distribution conditions can have an influence on the final bedload distribution if temporary storage along the channel-bed is common [*Parker and Wilcock*, 1993]. Other recirculating flumes circulate only water and trap sediments in a settling tank. These systems may have problems with fine sediments that do not settle rapidly and with high sediment-transport rates. However, recirculating flumes are often easier to run [*Williams*, 1971]. Discharge can be easily manipulated with electric pumps and sediment can often be recirculated with the water. Unfortunately, recirculating flumes involve difficult engineering challenges to deal with large sediment sizes and volumes, and have higher maintenance costs related to pump operation and wear.

Non-recirculating flumes use a large supply of water to provide a single pass of flow through the flume, like most natural channels. These systems are easy to design, cheap to maintain, but require a good water supply source. Water is supplied by a reservoir or natural channel, flows through the flume system and discharges to another natural channel or reservoir. Flow rate is usually metered with a series of gate values or diversion intakes to vary the discharge in the flume. The water supply must by large enough to provide constant head, or unsteady flow conditions will persist in the flume. Like the water, sediments exiting the flume are permanently carried out of the experimental system. Therefore, non-recirculating flumes require a constant source of sediment to the approach section in order to maintain continuity of sediment. Unfortunately, reliable, constant-rate sediment feeds are difficult to design and operate. Conveyor belt system may be ideal for short-duration experiments with sand or gravel. But generally speaking, a vibrating sediment feed system is preferable to other designs because of the larger volume of sediment that can be introduced [*Williams*, 1970]. However, most of these systems have problems with cohesive sediments, and are usually only used to supply sand to the system [*Schumm et al.*, 1987]. One advantage of sediment feed systems relates to equilibrium bedload conditions with mixed sediment sizes [*Parker and Wilcock*, 1993]. Channel-bed evolution and the resulting bedload distribution tends to be independent of initial conditions with sediment feeds, but can be strongly influenced by channel-bed sediment distributions in recirculating flumes because of the possibility of partial transport [*Parker and Wilcock*, 1993]. Sediment feed systems may also provide a better representation of bedrock systems because, unlike many alluvial systems, bedrock channel tend to respond to an imposed bedload distribution and supply.

2.3. Flume Scaling

For all scaled flume experiments, careful consideration of scaling issues will be required. Even for unscaled and analog models, some recognition of the scaling problems in a given experiment may help clarify results. In either case, the concept of similitude, or similarity of variables, is used to provide comparisons between the model and prototype. All scaling calculations begin with the physical scale of the model and then determine corresponding dynamic

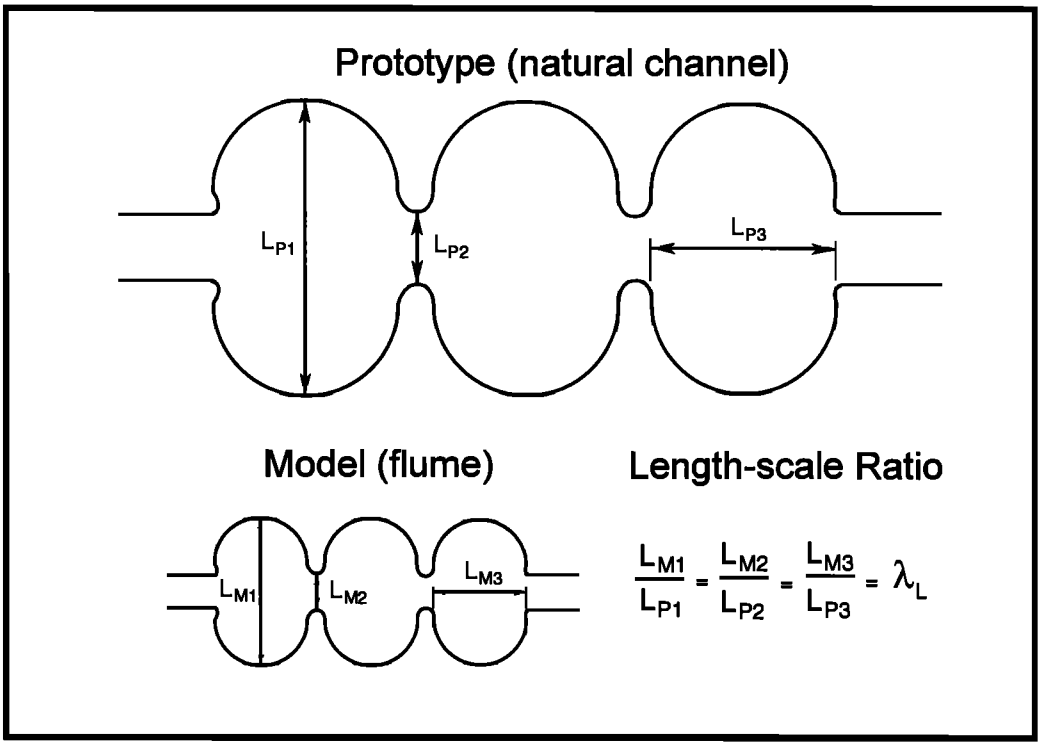

Figure 3. Use of geometric similitude and calculation of the length-scale ratio for flume experimentation.

and kinematic scaling relations. Ultimately, a proportional representation of all the key variables involved in the experiment can be determined.

Geometric Similitude. The easiest scaling principle involves a change in the physical size of the channel of interest. The simplest and most common approach is to reduce channel dimensions based on a constant ratio or percentage (Figure 3). For a natural channel with a width of 100 m, a $1/100^{th}$-scale flume model would have a corresponding width of 1 m. Likewise, all remaining length scales would be reduced to 1 percent of the original length. Close adherence to this approach will produce a perfect miniaturized version of the natural channel of interest, creating a condition of geometric similitude. The change in scale is often referenced by the length-scale ratio:

$$\lambda L = l_m/l_p \qquad (1)$$

where λL is the length-scale ratio (dimensionless), and l_m and l_p are reference length measurements in the model and prototype, respectively (same units). The length-scale ratio is then used to scale dynamic variables in the miniature channel. The length-scale ratio is usually determined by the dimensions of the flume available for the research. In most cases, the width or length of the flume is the constraining factor, and is used to determine the constant length-scale ratio. In certain circumstances, it may be desirable to have a variable length-scale ratio. In these cases, vertical distortion is often introduced in order to avoid problems associated with laminar flow development or surface tension.

Kinematic and Dynamic Similitude. Like length-scale ratio based rescaling, kinematic and dynamic similitude calculations can be performed to insure a similarity of kinematic variables (for example, velocity and discharge) and dynamic variables (for example, force and power). This scaling technique relies on a balance of dominant forces represented by dimensionless numbers, usually the Froude number and Reynolds number. The Froude number is often depicted as the ratio of the inertial force to the gravity force:

$$Fr = V/(g\,L)^{0.5} \qquad (2)$$

where Fr is the Froude number (dimensionless), V is velocity (m/s), g is the acceleration due to gravity (m/s^2), and L is a representative length scale (m). The Reynolds number is usually depicted as the ratio of the inertial force to the viscous force:

$$Re = V L \rho / \mu \quad (3)$$

where Re is the Reynolds number (dimensionless), ρ is the fluid density (kg/m^3), and μ is dynamic viscosity (N·s/m^2). In shallow flows with moderate gradients the Froude number would be important. Conversely, viscous forces and the Reynolds number may begin to dominate in systems with slow moving water or areas in close proximity to physical channel boundaries. Many other dimensionless variables exist and can be used for similitude analysis. These variables and the process of dimensionless analysis are covered in most introductory fluid mechanics texts [*Tritton*, 1987; *Roberson and Crowe*, 1997]. The basic similitude procedure assumes that a flume experiment with geometric similitude and dynamic similitude will also exhibit kinematic similitude. That is to say, a miniature channel with a rescaled force balance should exhibit a perfectly scaled field of velocity magnitudes and directions.

In order to scale kinematic and dynamic variables, the dominant dimensionless variable is set equal in the model and prototype. The Froude number will be the appropriate dimensionless variable for most bedrock flume simulations, and can be used to produce the same ratio of inertial to gravity forces in the flume and natural channels. The length-scale ratio is then used to determine the ratio of other variables of interest (Table 1). For example, a 1/100-scale model will only require a discharge of 1/10,000 in order to achieve equality of Froude numbers. Conversely, a Reynolds number based 1/100 scale model would still require a discharge of 1/100 in order to maintain a constant Reynolds number value. The various scale ratios listed in Table 1 can then be used to calculate expected prototype values based on measured flume data. For example, based on the Froude number, a measured flume velocity of 1 m/s in a 1/100 scale model should equate to a velocity of 10 m/s in the natural channel. This general scaling procedure can be used to predict a range of conditions in the natural system.

As most people probably recognize, gravity, inertial and viscous forces are all important in bedrock channel evolution. We typically have high-gradient channels with locally accelerating flows (represented by moderate and high Froude numbers) and highly turbulent flows (represented by high Reynolds numbers). Since we cannot equate both the Froude numbers and Reynolds numbers, we usually equate Froude numbers and perform a check to insure turbulent forces are dominating over laminar forces in both the flume and natural systems. As long as the Reynolds number indicates that the flow in the flume is fully turbulent, inequality of model and prototype Reynolds numbers should not undermine the quality of experimental results [*Carling*, 1995; *Roberson and Crowe*; 1997]. Conversely, Reynolds number based similitude with unequal Froude numbers will usually produce unrepresentative data. Before applying either approach, researchers should analyze the driving forces in their experiment to insure that the dimensionless number selected is the appropriate scaling variable.

Table 1. Scale ratios as a function of the length-scale ratio for Froude number and Reynolds number based similitude calculations.

			Proportion of Length-scale Ratio	
Variable	Symbol		Froude Number[a]	Reynolds Number[b]
Length	λ_L	=	λ_L	λ_L
Mass*	λ_M	=	λ_L	λ_L
Time	λ_T	=	$\lambda_L^{0.5}$	λ_L^{2}
Velocity	λ_V	=	$\lambda_L^{0.5}$	λ_L^{-1}
Discharge	λ_Q	=	$\lambda_L^{2.5}$	λ_L
Shear Stress	$\lambda_{\tau o}$	=	λ_L	λ_L
Force	λ_F	=	λ_L	$\lambda_L^{?}$
Power	λ_Ω	=	$\lambda_L^{3.5}$	$\lambda_L^{?}$

[a] Assuming constant density (same fluid).
[b] Assuming constant density and kinematic viscosity (same fluid).

Temporal Scaling. Many bedrock channel research projects involve an investigation of sediment transport or bedrock erosion over long time-spans. Fortunately, flume experiments can be used to reduce evolutionary time-scales. Therefore, flume research offers one of the best means to investigate long-term evolutionary change in bedrock channels. The trick, once again, lies in the ability to use dynamic similitude to alter the relative importance of the driving variables in an experiment. As Table 1 shows, a Froude number based dynamic scaling will yield a time-ratio scale, λ_T, equal to $\lambda_L^{0.5}$. For a 1/100-scale model, this will reduce the relative time of erosion from 10 years to 1 year. Considering the extreme time periods involved in bedrock channel evolution, dynamic scaling alone cannot solve the temporal problems we face. However, temporal scaling can be used in conjunction with a change in substrate to achieve an experiment of acceptable duration.

Sediment Scaling Problems. For most bedrock channel experiments, sediment will be needed to produce erosion of competent bed material [*Schumm et al.*, 1987]. Unfortunately, mobile sediments represent a unique scaling problem. It is a fairly uncomplicated matter to reduce all

length scales in a prototype to produce a constant-ratio, scaled model. The question that immediately becomes apparent is, what should we do with sediment sizes? A simple ratio-based approach would require reduction in the entire grain-size distribution in relation to the prototype-model ratio. However, the famous erosion curves by *Hjulstrom* [1935] clearly show a nonlinear relation between entrainment velocity and particle size. *Schumm et al.* [1984] also underline the importance of cohesive forces in many fluvial landforms. Therefore, a linear scaling technique will tend to skew sediment transport results and could affect landform development. For example, in a sediment-transport experiment we can lower the boundary shear stress values or manipulate a dimensionless transport parameter to reflect a reduction in channel size, but we cannot alter the cohesive forces that become increasingly important with smaller particle sizes. A reduction from sand-sized particles in a natural system to clay-sized particles in a flume will not reduce the necessary entrainment thresholds. As a result, the particle-size distribution of mobile sediments in the prototype will shift in a nonlinear fashion in the model, producing a unique sediment-size distribution curve. Although some techniques have been developed to limit this problem [*Schumm et al.*, 1987; *Carling*, 1989], it is impossible to uniformly replicate all sediment dynamics in a flume system.

One method to scale sediment transport in the model is to adjust the viscosity or density of the transporting medium. The most obvious impact of these changes is a modification of the Reynolds number. For example, water may be cooled to its maximum kinematic viscosity allowing a reduction in physical scale without a similar reduction in the Reynolds number. Another common method involves manipulating the density of material in motion. With a careful reduction in the density of flume sediments, realistic sediment transport rates are achievable. However, there are some potential dangers to avoid. Common sense would dictate that a reduction in the specific gravity of sediments to a value of less than 1.0 would result in floating particles. Although this may seem self-evident, some researchers have failed to recognize this problem a priori. Surprisingly, specific gravity values slightly in excess of 1.0 may also be subject to errors. With these low-density materials, surface tension forces may begin to influence or dominate particle force balances. Since the surface tension force is generally not recognized as a dominant force in bedload sediment transport, specific gravity values very close to 1.0 should be avoided in most cases. Common low specific gravity materials used for flume experimentation include granulated coal [*Carling*, 1989], Haydite, an industrial material with a specific gravity of 1.85 [*Schumm et al.*, 1987], and a variety of other synthetic materials.

3. EXPERIMENTAL DESIGN

3.1. Simulation of Bedrock Substrate

Any material used to simulate a bedrock channel substrate must satisfy at least two criteria: (1) the material must be sufficiently cohesive to resist grain-by-grain erosion in a manner analogous to bedrock, and (2) the material must be sufficiently erodible under the conditions of the flume experiment to exhibit measurable change during the time-span of the experiment. A variety of materials have been used to achieve these criteria, but investigators have not attempted to dynamically scale the material such that the flume substrate has an erosional resistance proportional to the hydraulic and abrasive forces of the flow. Materials used to simulate bedrock are generally composed of sand mixed with clay, concrete, or plaster-of-Paris to provide cohesion. A criterion commonly used is that the substrate not be erodible by clear water flows [e.g. *Shepherd and Schumm*, 1974; *Wohl and Ikeda*, 1997], although most of the early studies of erosional bedforms [e.g. *Dzulynski*, 1965; *Allen*, 1969] used clay mixtures that did erode under clear water flows. Very few investigators have designed experiments to determine the effect of heterogeneities on substrate erosion, the exceptions being *Holland and Pickup's* [1976] stratified bed, and *Toda's* [1993, 1994] work on fissures.

3.2. Statistical Design of Flume Experiments.

For many flume experiments, proper design will include some statistical considerations. Because flumes allow for careful control of variables, reproducibility of results is possible [*Schumm et al.*, 1987]. Therefore, statistical reproduction of results can be used to test significance or provide confidence intervals for important relations. For example, a study designed to determine the effect of discharge and substrate on the rate of channel incision will benefit from a statistical test of significance for the driving variables. This significance test will often simply require the development of a regression equation relating control variables to the observed responses. These statistical tests usually assume a random sampling strategy. Unfortunately, it is impossible to conduct truly random sampling strategies in many flume experiments because of the predictable spatial variation of most hydraulic variables. For example, velocity increases in a predictable manner from the bed of a channel to the water-surface and from the channel banks to the middle of the channel. Therefore, random measurements collected near the bed or banks should display a systematic tendency to record lower point velocities than velocities collected higher in the water

column or in the middle of the channel. Unfortunately, in order to utilize most statistics we have little choice but to ignore these failures of normality and assume that a random sampling of velocities in the same location would be normally distributed. In this manner, we can take advantage of many of the tests for significance used to support scientific conclusions.

Few flume experiments contain the repetitions needed to utilize the variety of univariate significance tests available. In many cases, the type of data collected or the nature of the experiment excludes the possibility of experimental repetition. However, there are other situations that could benefit from repetition with similar initial conditions and controls. For example, a difference in resultant landforms attributable to a change in channel substrate may be a random influence or an indication of a change in the dominant evolutionary processes. Recreation of the same landforms in subsequent flume runs would allow for statistical support for a change in the evolutionary outcome. Although replication involves additional time and expense, expanded use of this technique could improve reliability of flume results.

Many flume experiments are used to predict the response of a system to a specific perturbation. If a large number of independent variables is needed, the number of measurement repetitions required for t-tests may prove unrealistic. Because of the continuous nature of many geomorphic variables, regression analysis will provide a more logical tool for data evaluation. A flume experiment designed to provide predictive data will need a controlled modification of the important driving variables in order to develop regression relations. If too many variables are altered simultaneously it may be difficult or impossible to identify a true link between the independent and dependent variables. Ideally, these types of flume experiments should be completed with a change in only one variable for each flume run. The degree of change in the dependent variable can then be directly related to the modification in the independent variable to provide a predictive equation. Unfortunately, in most flume experiments it is almost impossible to vary a single independent variable. For example, a change in discharge inherently involves a change in depth and velocity. Once again, regression analysis offers the best technique for dealing with this type of data problem. Each independent variable can be included in an equation designed to predict the dependent variable response. The resultant multiple regression equations should be used only if the independent variables are statistically significant and the equation has a high R-square value. Regression equations with statistically significant independent variables and low R-square values can be used to identify a direct relation between the driving and response variables, but have poor predictive reliability. Conversely, a lack of significance with high R-square values may simply indicate low variability in the response variable. In either case, the completion of additional flume runs may improve the quality of the regression equation. Reduction of artificial turbulence in the flume can also help to unmask true effects of the driving variables.

Many processes may respond to a range of variables and interactions between variables. Because scientists do not always know the importance of each independent variable, it would be advantageous to conduct flume experiments that would identify important independent variables. Unfortunately, experiments designed for regression analysis would require numerous flume runs for each variable involved, and the number of flume runs grows exponentially if you want to consider interactions between variables. For example, a study designed to evaluate the influence of channel-bed slope on sediment transport would also need to consider the bedforms produced, changes in mean velocity or discharge, and the change in water depth or water-surface slope. Since some of the independent variables of interest may not prove significant, this level of time and expense may not be justified.

Fortunately, factorial experiments can be used to evaluate individual driving variables and interaction between these controls. For example, a four-way factorial experiment can be used to determine the influence of four separate variables and interactions between these variables with only 16 flume runs. The trick is to vary each variable at only two levels, and conduct flume runs with each possible combination of factors. For example, *Thompson* [unpublished data] altered pool depth, pool length, pool exit-slope gradient and constriction width, each at two levels, to determine the most important controls on velocities in pool systems. Although no true experimental replication is performed, an analysis of variance test can be used to predict the relative importance of each variable. Unfortunately, the lack of true repetition prevents characterization of measurement and sampling errors. The interactions between any two variables can also be evaluated without any replication. In addition, a separate analysis of variance test can be conducted for each response variable measured. Although this type of experiment does not provide much detail on the influence of each variable, it does provide a first step in identifying important variables for future study.

3.3. Effects of Flume Characteristics on Experimental Results

Flume results are only useful if the results collected represent general trends as opposed to the specific

characteristics of the experimental flume. Luckily, most data collected does transfer readily among flumes. However, the flume walls do have a strong influence on hydraulics and sediment transport within flume systems [*Williams*, 1970]. Recognition of the potential interactions between flume walls and results can aid in designing proper experiments.

The width of a flume can have a large influence on the results [*Williams*, 1970]. Flumes are generally rectangular, with steep vertical walls. Hence, boundary layer effects from the walls of the flume are generally more influential than in alluvial channels. Narrow flumes tend to have greater boundary resistance and correspondingly higher energy slopes [*Williams*, 1970]. As the width of a flume decreases, the affect of the flume walls on water-surface slope, energy slope, shear stress, sediment transport and bedform development becomes more pronounced [*Williams*, 1970]. *Williams* [1970] suggests that flume wall effects are potential problems with flumes less than 0.6 m (2 feet) wide. Side-wall correction factors have been developed to account for the increased boundary resistance in these narrower flume experiments [*Williams*, 1970]. However, for most bedrock channel simulations the vertical flume walls are less of a concern because of the low width-to-depth ratios common in canyon type environments. In fact, the hydraulic influence of high, immobile channel banks are probably well represented in the typical flume. Therefore, bedrock channels can be more accurately physically scaled and exemplified than many alluvial systems.

4. FLUME EXPERIMENTATION OF BEDROCK CHANNELS

4.1. Hydraulics

Turbulence and secondary-flow experiments. Investigators have recognized the importance of turbulent forces in shaping natural channels for at least half a century [e.g. *Matthes*, 1947], but there has been little quantification of how these forces shape bedrock channels. A huge body of civil engineering literature describes experiments designed to quantify turbulent flow [*Clifford and French*, 1993] as it affects velocity distribution [*Keulegan*, 1938; *Odgaard*, 1984; *Tominaga and Nezu*, 1991; *Robert et al.*, 1992], bed scour [*Wen et al.*, 1993], eddy development [*Tamai et al.*, 1986], flow separation and reattachment [*Abbott and Kline*, 1962; *Driver and Seegmiller*, 1985], formation of vortices [*Tani*, 1962], bursts and sweeps [*Bogard and Tiederman*, 1986], bedform development [*Kennedy*, 1963; *Karcz and Kersey*, 1980; *Nelson et al.*, 1995] and, ultimately, channel boundary erosion. However, investigators have not yet developed a general predictive equation for secondary flow in artificial channels [*Cantwell*, 1981], and the situation is infinitely more complex in irregular natural channels [*Clifford et al.*, 1992].

Most experiments have been designed to measure flow characteristics (turbulence, velocity distribution, shear stress) produced by either (1) a discrete obstacle or channel irregularity, such as a bridge pier or a downward step, or (2) a specified boundary roughness. These results may be indirectly applied to bedrock channels if the hydraulic effects of a given channel feature can be quantitatively related to mean velocity. *Tinkler* [1993], for example, used a formula relating incoming stream velocity to height of a downstep to calculate flow acceleration produced by the step at various discharges. However, few investigators have attempted to directly relate turbulent forces to erosion of natural cohesive substrates.

An exception comes from the work of Annandale and his colleagues, who have developed an erodibility index for materials ranging from cohesionless granular soil to massive bedrock [*Wittler et al.*, 1993; *Annandale*, 1995]. The index is based on mass strength, particle size, discontinuity or interparticle bond shear strength, and relative ground structure, and combines basic principles of hydraulics with engineering geology classifications of material strength. *Annandale* [1995] correlated rate of energy dissipation of flow and erodibility using 137 field observations of dam spillway performance, and demonstrated the presence of erosion for various cohesive substrates exposed to clear-water flows. The definition of this threshold should facilitate scaling of flume experiments using a cohesive substrate other than bedrock.

Along the same lines, despite the recognized importance of pools in creating channel-bed scour, very little work has been attempted to relate the geometry of pool systems to channel hydraulics and scour. However, *Thompson* [unpublished data] has shown that both the longitudinal and cross-sectional dimensions of a pool system can effect the hydraulic conditions in high-gradient pool systems. In these flume experiment, a physical constriction created a jet of high velocity entering a pool, and a recirculating eddy along the channel margin. An upstream sloping portion of the pool channel-bed, the pool exit-slope, affected the size and strength of the recirculating eddy system. In turn, the recirculating eddy system helped to control the size and strength of jet formation in the pool upstream of the pool exit-slope. The adjustments in jet strength can scour the pool system and change pool geometry. The resulting change in pool exit-slope geometry will create a feedback influence on channel hydraulics and jet strength. This type of complex hydraulic

feedback has only recently been investigated with flume studies [*Carling*, 1989], but may drive many of the evolutionary processes in bedrock channels.

Cavitation experiments. The civil engineering literature includes numerous studies on flow hydraulics along resistant-boundary channels. Cavitation in particular has received much attention because of the potential for damage to reservoir spillways. The conditions which create cavitation along concrete-lined channels also exist in bedrock channels, where cavitation may be an important erosive process during extreme flows [*Baker*, 1978].

Cavitation represents the formation and collapse of vapor bubbles in a fluid stream. Bubble formation is caused by a local reduction in absolute pressure to the vapor pressure of the fluid (usually caused by an increase in local velocity). Bubble collapse is caused by a subsequent pressure increase. Powerful shock waves initiated by the collapse may rapidly erode even very resistant substrate (Figure 4). Natural channel-bed roughness promotes flow separation, bubble formation, and cavitation [*Barnes*, 1956]. Although measurements of cavitation erosion have not been published for natural channels, published values for floods along reservoir spillways include scour holes 10.6 m deep in sandstone produced during 900 m^3/s flows from Glen Canyon Dam [*Eckley and Hinchliff*, 1986], and holes 34 m long, 19 m wide, and 11 m deep in the concrete lining of the Hoover Dam spillway after 4 months of operation [*Falvey*, 1982].

The conditions producing cavitation can be mathematically predicted for both natural [*Baker*, 1978] and artificial [*Falvey*, 1982; *Young*, 1989] channels. Laboratory experiments involving cavitation have focused on how flow velocity, channel irregularity (up- or down-step), or obstacle shape influence bubble formation and collapse [*Young*, 1989]. Experimentation has also demonstrated that air entrainment may substantially reduce cavitation by mitigating the high-pressure effects of the cavitation bubble collapse [*Mason*, 1989; *Kells and Smith*, 1991]. Natural air entrainment is primarily a surface condition that may not be effective in reducing cavitation at the bed [*Kells and Smith*, 1991]. Laboratory experiments have focused on the resistance of artificial materials such as concrete and steel to cavitation, and almost nothing is known about the resistance of various lithologies to cavitation.

4.2. Sediment Transport

Extensive literature describes flume experiments on sediment entrainment and transport and bedforms in sand-bed and, to a lesser extent, gravel-bed channels [*Schumm et al.*, 1987]. This discussion will focus on studies designed to replicate processes and bedforms characteristic of bedrock channels. Bedrock channels may contain deposits ranging from fine-grained slackwater sediments through very coarse-grained boulder berms, and any experimental study of sediment processes and bedforms may apply to the alluvial veneer commonly present along bedrock channels (Chapter 5, this volume). The unique aspect of bedrock channels that is particularly difficult to replicate experimentally is the extreme turbulence that may carry even very coarse sediments in suspension [*Baker and Kochel*, 1988].

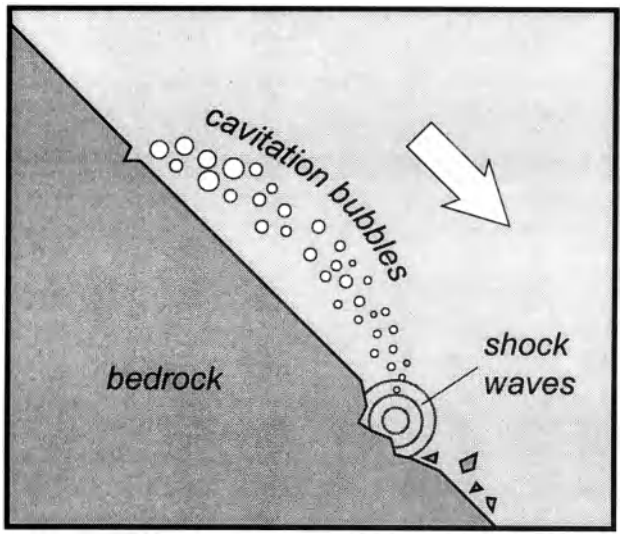

Figure 4. Generation of cavitation and subsequent downstream erosion along bedrock surface with a slight irregularity.

Kochel and Ritter [1987] experimentally produced slackwater sedimentation along a bedrock channel (simulated by cement) in order to assess the influences of variable flood hydrographs and channel geometries on the deposition process. Using a main channel that had 20 tributaries entering at various junction angles and gradients, they conducted four runs at varying discharge and main channel slope. Maximum backflooding and slackwater sedimentation occurred at junction angles between 50° and 130°, at lower main channel gradients, and at higher discharges.

Carling [1989] used Froude-scaled models with Lytag and coal clasts to simulate deposition of longitudinal boulder berms. The berms formed at low Froude numbers ($F < 1.5$) as a result of deposition of individual bedload clasts and the formation of transverse bars in the shear flow zone at the edge of flow separation associated with a channel expansion. Berm development was constrained by hydraulics, rather than sediment supply. Subsequent

experiments demonstrated (1) that various bar facies may be caused by spatial and temporal variability in the local flow structure during rapid deposition of sand and gravel downstream from a negative step [*Carling and Glaister*, 1987], (2) that differing facies assemblages may be generated as subsequent bars prograde over immobile bars deposited earlier, reflecting hydrodynamic rather than sediment-supply controls [*Carling*, 1990], and (3) that lateral gravel berms associated with hydraulic jumps in bedrock channels may be used to estimate flow regime because the angle subtended by the berm crestline with respect to a regular bankline is related to the Froude number of the flow that created the berm [*Carling*, 1995].

Schmidt et al. [1993] conducted flume simulations to reproduce sedimentation patterns created within lateral separation eddies of the Grand Canyon. A reattachment deposit was formed in the recirculating-eddy system and grew in the upstream direction. Sediment trapping efficient of the recirculating eddy varied from 37% with an empty eddy system to 24% with an eddy partially filled with sediments. The characteristics of the eddy deposits were directly related to the location of eddy reattachment. *Schmidt et al.* [1993] concluded that eddy reattachment length was primarily a function of jet characteristics and channel topography downstream of the pool.

Longitudinal and transverse boulder bars commonly form in the coarse alluvium that partially mantles many bedrock channels. Some of the earliest flume experiments involving coarse bar deposition were conducted by *Leopold and Wolman* [1957]. They hypothesized that some local condition facilitated initial deposition of the coarsest particles moving along a channel. A bar could then form by successive deposition downstream from these coarse particles. Flume experiments with a poorly sorted medium sand supported this hypothesis. *Ashmore* [1982] noted similar processes during bar formation in a sand-bed experimental channel, and emphasized downstream fining along the bar as a result of deposition at the avalanche face created by particles moving along the bar crest.

In a series of flume experiments with sand and gravel substrates, Ikeda and Iseya demonstrated how grain-size distribution affects mobility and transport mode [*Ikeda*, 1984; *Ikeda and Iseya*, 1986, 1988; *Iseya and Ikeda*, 1987; *Iseya et al.*, 1990; *Lisle et al.*, 1991], with mixtures of coarse and fine particles with fines dominant moving more readily than uniform fines. When the coarse clast fraction exceeds a critical mixture ratio, transport changes from mainly suspension mode to traction mode with an associated change in bedform type. *Iseya et al.* [1990] also demonstrated that longitudinal boulder bars might be formed by uneven transport of bedload in lobe-shaped waves.

Step-pool bedforms occur along high-gradient channels formed in both alluvium and bedrock. *Whittaker and Jaeggi* [1982] ran clear water over poorly sorted gravel, and initially observed regularly spaced antidunes. As the bed degraded, larger particles anchored some of the antidunes and the bed became armored, fixing the steps in place. *Whittaker* [1987] used a succession of discrete weirs placed first at 0.5m intervals down the channel, and then at 0.25m intervals during subsequent tests. The pools between the steps were filled with gravel, and pool scour depth was measured as a function of flow rate, slope, and sediment-transport rate. Instabilities developed in the sediment-transport rate and in the flow despite constant inputs, suggesting that waves of sediment move through step-pool systems. *Grant and Mizuyama* [1991] used an initially even gravel bed under a range of slope, discharge, and sediment discharge conditions to create alluvial steps. Steps formed at near critical to supercritical flow conditions, close to but not exceeding the entrainment thresholds for the largest particles, and step spacing correlated with the antidune wavelength. *Abrahams et al.* [1995] used fixed steps filled with mobile gravel to demonstrate that step-pools evolve toward a condition of maximum flow resistance. Although bedrock step-pool systems have been described [*Wohl and Grodek*, 1994; *Duckson and Duckson*, 1995], flume experiments have not yet been undertaken to determine the controls (e.g. cavitation, sediment transport, joints in substrate) on step formation in a cohesive channel substrate.

These flume experiments have demonstrated how turbulent forces and flow transitions influence patterns of sediment movement along cohesive-boundary channels. By directly observing the relation between process and form in the flume, investigators have been able to infer flood hydraulics from slackwater and boulder deposits preserved along natural channels.

4.3. Channel Incision and Morphology

Knickpoints. *Holland and Pickup* [1976] used horizontally stratified units of unconsolidated sand and cohesive sand-and-plaster mix to create stepped knickpoints that were maintained as they moved upstream. Erosion rates were lower for models with stratification than for those in homogeneous material. Working with cohesive, homogeneous material, *Gardner* [1983] found that knickpoints created by baselevel drop were rapidly destroyed through knickpoint replacement and subsequent inclination. This suggests that knickpoints do not undergo retreat in homogeneous bedrock except in cases of extensive and pervasive bedrock jointing. *Clemence* [1988] used a wind tunnel with Styrofoam particles and slabs to

determine that fracture spacing was the most significant control on knickpoint erosion in stratified materials. *Stein and Julien* [1993] used loamy sand with an initially vertical headcut to define an erosional time-scale ratio of headcut migration that is a function of the Froude number and of the aspect ratio of drop height to normal flow depth. Stepped headcuts form when this ratio exceeds 1, whereas rotating headcuts form when the ratio is less than 1.

Other erosional features. Some of the earliest experimental work utilizing a cohesive substrate employed plaster-of-Paris, silt, or clay and clear water flows to create erosional sedimentary structures [e.g. *Dzulynski and Walton*, 1963]. Investigators were able to observe secondary flow features associated with specific types of erosional structures [*Dzulynski*, 1965], and to classify these structures with respect to velocity or flow regime [*Allen*, 1969, 1971, 1982; *Karcz*, 1970, 1973]. Both geologists [e.g. *Komar*, 1985] and civil engineers [e.g. *Blaisdell et al.*, 1981] have conducted experiments designed to predict bed scour around fixed obstacles.

The lack of accurate data on the mechanics of pothole erosion led *Alexander* [1932] to undertake a series of experiments to determine the effect of (1) angle and location of the entering water jet, and (2) geometry of the pothole on turbulent flow patterns and abrasion by grinders. *Ängeby* [1951] also experimentally measured secondary flow structures in potholes. *Toda* [1993] and *Toda and Sunamura* [1993] have conducted related studies, creating transverse slits 2 to 25 mm wide in a cohesive bed of sand and cement. They noted characteristic vortices that changed when the step height attained a critical value. *Toda* [1994] then repeated the experiment by cutting slits into natural sandstone and mudstone channels.

These studies focused on small-scale or isolated erosional features. *Shepherd* [1972] and *Shepherd and Schumm* [1974] used a cohesive mixture of sand and kaolinite to simulate channel incision. They noted an erosional sequence following an increase of slope at constant water and sediment discharges: potholes and longitudinal lineations, longitudinal grooves, and finally a deep, narrow inner channel. They also simulated bedrock meander incision and found that the nature of incised meanders (predominantly lateral vs. vertical incision) depends on the amount of sediment load entrained by the flow. *Gardner's* [1975] simulation of meander incision using a kaolinite-sand mixture indicated that meander geometry varied in relation to bedrock slope, orogenic movement, thickness of alluvial cover, and sediment load. *Wohl and Ikeda* [1997] conducted experiments similar to those of *Shepherd and Schumm* [1974], and demonstrated a progression with increasing bed gradient from a broad, shallow channel, to longitudinal grooves, and finally an inner channel with undulating bed and walls.

Despite the lack of dynamic scaling in these channel erosion flume experiments, investigators have been able to isolate the effect of a single change, such as increasing discharge or gradient, on erosional patterns. This data has provided important insights into the evolution of bedrock channel morphology. In addition, the appearance of similar erosional features at scales ranging from centimeters to kilometers in natural bedrock channels (e.g. regular downstream alternations in valley-bottom width) suggests that the small-scale flume features produced during flume experiments may be scale invariant.

5. SUGGESTIONS FOR FUTURE EXPERIMENTAL WORK

Despite extensive flume simulation of river channel processes [*Schumm et al.*, 1987], very few flume experiments have focused specifically on processes along bedrock channels. The experiments conducted thus far, by facilitating the isolation and manipulation of variables, and the direct observation and measurement of processes, have provided valuable insight into hydraulics, sediment entrainment, transport, and deposition, and channel erosion. As experimentation continues, these analog models are likely to be replaced by scale models [e.g. *Carling*, 1995] in order to better understand the ratios between driving and resisting forces in bedrock channels. The lists below provide a preliminary inventory of problems that could be addressed using flume experiments; the possibilities are endless.

5.1. Hydraulics

Several topics related to hydraulic patterns and influences of bedrock channels can be addressed. The following list contains some suggests for research:

- Hydraulic relations as a function of at-a-station and longitudinal geometry.
- Feedbacks between hydraulics and channel geometry; to date, studies of channel incision have not included detailed characterization of flow patterns.
- Conditions conducive to cavitation and the erosional impact of cavitation relative to abrasion.
- Effect of cavitation on varying bed substrates.
- Distribution of flow energy along alternating bedrock-alluvial channel reaches.

5.2. Sediment Transport

Sediment transport issues continue to be one of the primary areas for research. The following topics would provide strong avenues for research:

- Relation between alluvial cover and bedrock channel incision; when is the cover protective, and when does it become abrasive.
- Influence of sediment supply on the rate and pattern of incision.
- Characterization of sediment sorting patterns and sediment storage sites along bedrock channels.
- Prediction of sediment-transport rates with low width-to-depth ratios.

5.3. Channel Morphology and Incision

Much of the basic research in bedrock channels will focus on evolution and maintenance of the forms of these unique channels. Some promising topics related to bedrock channel evolution are listed below:

- Conditions under which step-pool and pool-riffle bedforms are formed in bedrock.
- Effect of substrate heterogeneities (dipping strata, joints, etc) on morphology.
- Determine "stability field" (Q, Q_s, gradient, substrate) for various bedrock channel morphologies, such as inner channel, step-pool, pool-riffle, undulating walls.
- Influence of self-perpetuating channel forms in bedrock channel incision

CONCLUSIONS

Flume models alone cannot reveal all the processes operating in bedrock channels because of limitations in reproducing truly representative hydraulic forces and substrates in the flume. However, flume experiments can provide a great deal of insight into bedrock channels, revealing previously unsuspected processes, similarity of form between scales, and a glimpse of long-term evolutionary trends. Therefore, the continued and expanded use of flume simulations to supplement direct field observations is recommended in the study of bedrock channels.

REFERENCES

Abbott, D.E. and S.J. Kline, Experimental investigation of subsonic turbulent flow over single and double backward facing steps, *Jour. Basic Eng., 84*, 317-325, 1962.

Abrahams, A.D., G. Li, and J.F. Atkinson, Step-pool streams: adjustment to maximum flow resistance, *Water Resources Res., 31*, 2593-2602, 1995.

Alexander, H.S., Pothole erosion, *Jour. of Geol., 40*, 305-337, 1932.

Allen, J.R.L., Erosional current marks of weakly cohesive mud beds, *Jour. of Sed. Petrology, 39*, 607-623, 1969.

Allen, J.R.L., Transverse erosional marks of mud and rock: their physical basis and geological significance, *Sed. Geol., 5*, 167-385, 1971.

Allen, J.R.L., *Sedimentary structures, their character and physical basis*, vol. 2. Elsevier Scientific Publishing Co., Amsterdam, 663 pp., 1982.

Ängeby, O., Pothole erosion in recent waterfalls, *Lund Studies in Geog., Series A Phys. Geog., 2*, 1-34, 1951.

Annandale, G.W., Erodibility, *Jour. of Hydraulic Res., 33*, 471-494, 1995.

Ashmore, P.E., Laboratory modeling of gravel braided stream morphology, *Earth Surface Processes and Landforms, 7*, 201-225, 1982.

Baker, V.R., Paleohydraulics and hydrodynamics of Scabland floods, in *The Channeled Scabland*, edited by V.R. Baker and D. Nummedal, pp. 59-79,. NASA, Washington, D.C., 1978.

Baker, V.R. and R.C. Kochel, Flood sedimentation in bedrock fluvial systems, in *Flood Geomorphology*, edited by V.R. Baker, R.C. Kochel and P.C. Patton, pp. 123-137, John Wiley and sons, NY, 1988.

Barnes, H.L., Cavitation as a geological agent, *Am. Jour. of Science, 254*, 493-505, 1956.

Blaisdell, F.W., C.L. Anderson, and G.G. Hebaus, Ultimate dimension of local scour, *ASCE Jour. of Hydraulics Div., 107*, 327-337, 1981.

Bogard, D.G. and W.G. Tiederman, Burst detection with single-point velocity measurements, *Jour. of Fluid Mechanics, 162*, 389-413, 1986.

Cantwell, B.J., Organized motion in turbulent flow, *Annual Rev. of Fluid Mechanics, 13*, 457-515, 1981.

Carling, P.A., Hydrodynamic models of boulder berm deposition, *Geomorphology, 2*, 319-340, 1989.

Carling, P.A., Particle over-passing on depth-limited gravel bars, *Sedimentology, 37*, 345-355, 1990.

Carling, P.A., Flow-separation berms downstream of a hydraulic jump in a bedrock channel, *Geomorphology, 11*, 245-253, 1995.

Carling, P.A. and M.S. Glaister, Rapid deposition of sand and gravel mixtures downstream of a negative step: the role of matrix-infilling and particle-overpassing in the process of bar-front accretion, *Jour. of the Geol. Soc., London, 144*, 543-551, 1987.

Clemence, K.T., Influence of stratigraphy and structure on knickpoint erosion, *Bull. of the Ass. of Eng. Geol., XXV*, 11-15, 1988.

Clifford, N.J. and J.R. French, Monitoring and modeling turbulent flow: historical and contemporary perspectives, in *Turbulence: perspectives on flow and sediment transport,*

edited by N.J. Clifford, J.R. French, and J. Hardisty, pp. 1-34, John Wiley and Sons, Chichester, 1993.

Clifford, N.J., A. Robert, and K.S. Richards, Estimation of flow resistance in gravel-bedded rivers: a physical explanation of the multiplier of roughness length, *Earth Surface Processes and Landforms, 17*, 111-126, 1992.

Driver, D.M. and H.L. Seegmiller, Features of a reattaching turbulent shear layer in divergent channel flow, *AIAA Jour., 23*, 163-171, 1985.

Duckson, D.W., Jr. and L.J. Duckson, Morphology of bedrock step pool systems, *Water Resources Bull., 31*, 43-51, 1995.

Dzulynski, S. and E.K. Walton, Experimental production of sole markings, *Transactions, Edinburgh Geological Society, 19*, 279-305, 1963.

Eckley, M.S. and D.L. Hinchliff, Glen Canyon Dam's quick fix, *ASCE Civil Eng., 56*, 46-48, 1986.

Falvey, H.T., Predicting cavitation in tunnel spillways, *Water Power and Dam Construction, 34*, 13-15, 1982.

Gardner, T.W., The history of part of the Colorado River and its tributaries: an experimental study, *Four Corners Geological Society Guidebook, 8th Field Conf., Canyonlands, Utah*, pp. 87-95, 1975.

Gardner, T.W., Experimental study of knickpoint and longitudinal profile evolution in cohesive, homogeneous material, *Geol. Soc. of Am. Bull., 94*, 664-672, 1983.

Grant, G.E. and T. Mizuyama, Origin of step-pool sequences in high gradient streams: a flume experiment, *in Proc. of Japan-U.S. workshop on snow avalanche, landslide, debris flow prediction and control*, pp. 523-532, 1991.

Hjulstrom, F., Studies of the morphological activity of rivers as illustrated by the River Fryis, *Bull. of the Geol. Institute. Univ. of Uppasala, 25*, 221-527, 1935.

Holland, W.N. and G. Pickup, Flume study of knickpoint development in stratified sediment, *Geol. Soc. of Am. Bull., 87*, 76-82, 1976.

Ikeda, H., Flume experiments on the causes of superior mobility of sediment mixtures, *Annual Report, Institute of Geoscience, Univ. of Tsukuba (Japan), no. 10*, pp. 53-56, 1984.

Ikeda, H. and F. Iseya, Thresholds in the mobility of sediment mixtures, in *International Geomorphology, Part I*, edited by V. Gardiner, pp. 561-570, Wiley and Sons, Chichester, 1986.

Ikeda, H. and F. Iseya, Experimental study of heterogeneous sediment transport, *Env. Res. Center Papers, Univ. of Tsukuba (Japan), no. 12*, 50 pp, 1988.

Iseya, F. and H. Ikeda, Pulsations in bedload transport rates induced by a longitudinal sediment sorting: a flume study using sand and gravel mixtures, *Geografiska Annaler, 69A*, 15-27, 1987.

Iseya, F., H. Ikeda, H. Maita, and Y. Kodama, Fluvial deposits in a torrential gravel-bed stream by extreme sediment supply: sedimentary structure and depositional mechanism, *Third International Workshop on Gravel-Bed Rivers, Firenze, Italy, 24-28 Sep. 1990*, pp. 1-24, 1990.

Karcz, I., Possible significance of transition flow patterns in interpretation of origin of some natural bedforms, *Jour. of Geophysical Res., 75*, 2869-2873, 1970.

Karcz, I., Reflections on the origin of source small-scale longitudinal streambed scours, in *Fluvial Geomorphology*, edited by M. Morisawa, pp. 149-173, Binghamton, New York, 1973.

Karcz, I. and D. Kersey, Experimental study of free-surface flow instability and bedforms in shallow flows, *Sed. Geol., 27*, 263-300, 1980.

Kells, J.A. and C.D. Smith, Reduction of cavitation on spillways by induced air entrainment, *Canadian Jour. of Civil Eng., 18*, 358-377, 1991.

Kennedy, J.F., The mechanics of dunes and antidunes in erodible-bed channels, *Jour. of Fluid Mechanics, 16*, 521-546, 1963.

Keulegan, G.H., Laws of turbulent flow in open channels, *Jour. of Research of the National Bureau of Standards, 21*, 707-741, 1938.

Kochel, R.C. and D.F. Ritter, Implications of flume experiments on the interpretation of slackwater deposit paleoflood sediments, in *Regional Flood Frequency Analysis*, edited by V.J. Singh, pp. 365-384, D. Reidel, Boston, 1987.

Komar, P.D., Experiments and analyses of the formation of the Martian outflow channels, in *Reports of planetary geology and geophysics program - 1984*, edited by H.E. Holt and T.R. Watters, pp. 322-324, NASA Technical Memorandum, 87563, 1985.

Leopold, L.B. and M.G. Wolman, River channel patterns: braided, meandering, and straight, *U.S.G.S. Prof. Paper 282-B*, pp. 39-73, 1957.

Lisle, T.E., H. Ikeda, and F. Iseya, Formation of stationary alternate bars in a steep channel with mixed-size sediment: a flume experiment, *Earth Surface Processes and Landforms, 16*, 463-469, 1991.

Mason, P.J., Effect of air entrainment on plunge pool scour, *ASCE Jour. of Hydraulic Eng., 115*, 385-399, 1989.

Matthes, G.H., Macroturbulence in natural stream flow, *Transactions, Am. Geophysical Union, 28*, 255-265, 1947.

Mosley, M.P. and G.L. Zimpfer, Hardware models in geomorphology, *Progress in Phys. Geog., 2*, 438-461, 1978.

Nelson, J.M., R.L. Shreve, S.R. McLean, and T.G. Drake, Role of near-bed turbulence structure in bed load transport and bed form mechanics, *Water Resources Res., 31*, 2071-2086, 1995.

Odgaard, A.J., Shear-induced secondary currents in channel flows, *ASCE Jour. of Hydraulic Eng., 110*, 996-1004, 1984.

Parker, G., and P.R. Wilcock, Sediment feed and recirculating flumes: Fundamental differences, *Jour. of Hydraulic Eng., 119*, 1192-1204, 1993.

Roberson, J.A., and C.T. Crowe, *Engineering Fluid Mechanics*, John Wiley and Sons, New York, 689 pp., 1997.

Robert, A.R., A.G. Roy, and B. de Serres, Changes in velocity profiles at roughness transitions in coarse-grained channels, *Sedimentology, 39*, 725-735, 1992.

Schmidt, J.C., D.M. Rubin, and H. Ikeda, Flume simulation of recirculating flow and sedimentation, *Jour. of Geol., 29*, 2925-2939, 1993.

Schumm, S.A., The shape of alluvial channels in relation to sediment type, *U.S.G.S. Prof. Paper 352-B*, pp. 17-30, 1960.

Schumm, S.A., M.P. Mosley, and W.E. Weaver, *Experimental fluvial geomorphology*, John Wiley and Sons, New York, 413 pp., 1987.

Shepherd, R.G., Incised river meanders: evolution in simulated bedrock, *Science, 178*, 409-411, 1972.

Shepherd, R.G. and S.A. Schumm, Experimental study of river incision, *Geol. Soc. of Am. Bull., 85*, 257-268, 1974.

Stein, O.R. and P.Y. Julien, Criterion delineating the mode of headcut migration, *ASCE Jour. of Hydraulic Eng., 119*, 37-50, 1993.

Tamai, N., T. Asaeda, and H. Ikeda, Study on generation of periodical large surface eddies in a composite channel flow, *Water Resources Res., 22*, 1129-1138, 1986.

Tani, I., Production of longitudinal vortices in the boundary layer along a concave wall, *Jour. of Geophysical Res., 67*, 3075-3080, 1962.

Thornton, E.G. and L.S. Romer, Comparison of hydraulic and numerical tidal models, *Symposium on Modeling Techniques, ASCE*, New York, pp. 1311-1328, 1975.

Tinkler, K.J., Fluvially sculpted rock bedforms in Twenty Mile Creek, Niagara Peninsula, Ontario, *Canadian Jour. of Earth Sciences 30*, 945-953, 1993.

Toda, M., An experimental study on the influence of a fissure on bedrock channel erosion, *Geog. Rev. of Japan, 66A*, 336-337, 1993.

Toda, M., Bedrock channel erosion on the upper Obitsu, Boso Peninsula: a field experiment on the influence of a fissure on erosion, *Geog. Rev. of Japan, 67A*, 24-25, 1994.

Toda, M. and T. Sunamura, A model for erosion at the fissure in bedrock by running water: a laboratory approach, *Annual Report of the Institute of Geoscience, Univ. of Tsukuba (Japan) 19*, 19-22, 1993.

Tominaga, A. and I. Nezu, Turbulent structure in compound open-channel flows, *ASCE Jour. of Hydraulic Eng., 117*, 21-41, 1991.

Tritton, D.J., *Physical Fluid Dynamics*, Oxford University Press, New York, 519 pp., 1987.

Wen, F., D. Seymour, , and H.W. Shen, The separated flow around a circular bridge pier, in *Hydraulic Engineering '93, vol. 1*, edited by H.W. Shen, S.T. Su, and F. Wen, pp. 905-910, ASCE, 1993.

Whittaker, J.G. and M.N.R. Jaeggi, Origin of step-pool systems in mountain streams, *ASCE Jour. of Hydraulics Div., 108*, 758-773, 1982.

Williams, G.P., Flume Width and Water Depth Effects in Sediment-Transport Experiments, *U.S.G.S. Prof. Paper 562-H*, 37 pp., 1970.

Williams, G.P., Aids in Designing Laboratory Flumes, *U.S.G.S. Open-file Report*, 294 pp., 1971.

Wittler, R., B. Mefford, G. Annandale, , S. Abt, and J. Ruff, Dam foundation erosion: pre-test report, *Dam Safety: Overtopping Dam Foundation Erosion and Embankment Dam Breaching Parameters*. San Francisco, CA, Oct. 28, 1993, 47 pp., 1993.

Wohl, E.E. and T. Grodek, Channel bed-steps along Nahal Yael, Negev desert, Israel, *Geomorphology, 9*, 117-126, 1994.

Wohl, E.E. and H. Ikeda, Experimental simulation of channel incision into a cohesive substrate at varying gradients, *Geology, 25*, 295-298, 1997.

Young, D.F., B.R. Munson, and T.H. Okiishi, *A Brief Introduction to Fluid Mechanics*, John Wiley and Sons, New York, 492 pp., 1997.

Young, F.R., *Cavitation*, McGraw-Hill, London, 418 pp., 1989.

D.M. Thompson, Department of Physics and Astronomy, Connecticut College, 270 Mohegan Avenue, Campus Box 5585, New London, CT 06320

E.E. Wohl, Department of Earth Resources, Colorado State University, Fort Collins, CO 80523

Long Profile Development of Bedrock Channels: Interaction of Weathering, Mass Wasting, Bed Erosion, and Sediment Transport

Alan D. Howard

Department of Environmental Sciences, University of Virginia, Charlottesville, Virginia

Erosion of bedrock channels seldom involves solely hydraulic processes such as plucking, abrasion, and solution. Weathering, mass wasting and burial by sediment cover modulate the rate of bedrock erosion. In headwater channels weathering generally must reduce rock strength to the point that entrainment may occur by hydraulic processes or rapid mass wasting. Simple quantitative models are introduced that demonstrate how erosion rates can depend upon both weathering rate and stress applied by moving fluids and debris. Rockfalls and avalanches can trigger additional failures in partially weathered bedrock on lower parts of alpine bedrock slopes before they would fail solely by weathering; this generates an economy of scale that results in development of spur and gully landforms. Streambed weathering also enhances bed erosion by water and debris flow in headwater bedrock channels within moderate relief landscapes. In large bedrock channels erosion rates are controlled both directly and indirectly by the throughflowing sediment. Abrasion by bedload and suspended load is often the dominant process. The rock beds of many streams are mantled partially or shallowly by alluvium. Two primary issues are unresolved about long-term evolution of these mixed bedrock-alluvial channels: 1) how and when the bedrock is eroded and 2) whether the gradient is determined by the necessity to transport the alluvium or to erode the bed. A semi-quantitative model suggests that bed erosion occurs due to exposure during extreme floods, at the base of migrating bedforms, and during periods of low sediment influx. Erosion rates in rapidly downcutting bedrock channel reaches are often regulated by influx of boulders that partially or wholly mantle the bed. These locally contributed boulders are primarily derived from steepening of sideslopes and tributaries due to the rapid incision.

INTRODUCTION

Present understanding of the processes and evolution of bedrock channels lags significantly behind that for alluvial channels. Little is known about the distribution of bedrock channels, process models are primitive and incomplete, quantitative field measurements are rare and difficult to make, and the erosional history evolution of such channels is largely uncertain. This lack of quantitative characterization of erosional processes in bedrock channels is unfortunate, because such channels are widespread in high-relief terrain and the pace of long-term erosion and the overall relief is often governed by channel bed erodibility [e.g. *Burbank et al.,* 1996]. Realistic modeling of the interactions between tectonic deformation, landform development and erosion, and sedimentation processes will require better characterization of bedrock channel erosion. The same is true for prediction of the effects of short term climatic and land use changes upon channel morphology and sediment transport.

Rivers Over Rock: Fluvial Processes in Bedrock Channels
Geophysical Monograph 107

This paper explores three related topics. The first relates to the difficulty in making *a-priori* predictions about the distribution of channel types due to the interplay of controlling factors. The second issue is that erosion of bedrock channels seldom can be characterized solely as a relationship between applied fluid force and the rate of channel bed incision. Rather, erosion most often involves interplay between weathering, mass-wasting, sediment transport and fluid motion. This interplay is particularly important for the common mixed bedrock-alluvial channels that constitute the third topic.

These issues are first explored for headwater channels in which weathering, mass-wasting, and fluvial erosion interact. Further downstream in the stream network, weathering becomes less important, but bed erosion still involves the interaction of sediment transport, local mass wasting, and hydraulics.

HEADWATER BEDROCK CHANNELS

Channels and hollows forming the headward tips of the drainage network are commonly bedrock floored, at least episodically. These low-order channels differ from large bedrock streams in that the erosional process involves a mixture of weathering and rapid mass wasting in addition to fluvial erosion. Furthermore, because of the convergent topography of headwater hollows, colluvial infilling competes with erosion [e.g., *Dietrich and Dunne,* 1978; *Dietrich et al.,* 1982; *Montgomery and Dietrich,* 1994; *Dietrich et al.,* 1995]. Because the mixture of processes varies between landscapes, few generalizations are possible.

The simplest headwater bedrock channels occur when the main concentrative erosional process is fluvial erosion rather than rapid mass movement. In order to sustain a topographic hollow the long-term fluvial erosion along the hollow axis must be sufficient to erode colluvial infilling from superjacent slopes as well as the bedrock in the channel bed. In *Howard's* [1994a] drainage basin model, it is envisioned that during each simulation timestep runoff first erodes colluvial infilling and then the underlying bedrock. On convex and straight hillslopes, however, the colluvial flux is sufficient to prevent permanent channel development, although ephemeral rills may occur. In badland landscapes, the cycles of colluvial infilling and fluvial scour may follow simple seasonal patterns (Figure 1), with attendant growth and retreat of the fluvial network [*Schumm,* 1956; *Howard and Kerby,* 1983]. More typically, epicycles of infilling and scour may occur over much longer timescales [e.g., *Hack and Goodlett,* 1960; *Dietrich and Dunne,* 1978; *Reneau et al.,* 1989].

Interaction of Weathering and Fluvial Scour

The mechanism of fluvial erosion in headwater bedrock channels has received little study. *Howard and Kerby* [1983] and *Howard* [1994a] proposed that the rate of bedrock erosion is proportional to the shear stress exerted by runoff, with an implicit assumption that the bedrock can be directly scoured by runoff. In badland landscapes developed on weak sediments or saprolite, this assumption may be appropriate. *Howard and Kerby* [1983] showed that the spatial pattern of erosion rates in badlands on Coastal Plain sediments in Virginia is consistent with erosion being proportional to the shear stress exerted by runoff. In most other rock types, however, the bedrock must be partially weathered prior to fluvial erosion. *Howard* [1994b] presented a conceptual model of how weathering and detachment might interact in headwater channels. Assume that the flow characteristically removes weathered layers of thickness δd (e.g., weathered shale chips or exfoliation sheets) and that the weathering at that depth decreases the shearing resistance C at a negative exponential rate from the initial cohesion C_i to a minimum value C_f

$$C = C_f + (C_i - C_f)\, e^{-\lambda \delta t}, \qquad (1)$$

where δt is the elapsed time since weathering has begun and λ is a characteristic weathering rate that might depend upon wetting duration, bedrock or regolith permeability, and the substrate physico-chemical properties. Detachment of the weathered layer occurs when $\tau \geq C$, which occurs after a time

$$\delta t = \frac{1}{\lambda} \ln\left[\frac{(C_i - C_f)}{(\tau - C_f)}\right]. \qquad (2)$$

Assuming that weathering begins anew when a layer is stripped by the flow and that τ_e is the effective shear stress, then the average erosion rate would be given by

$$\frac{\partial z}{\partial t} = -\frac{\partial d}{\delta t} = -\delta d \lambda \Big/ \ln\left[\frac{(C_i - C_f)}{(\tau_e - C_f)}\right]. \qquad (3)$$

Although (3) suggests that the rate of erosion would increase with layer thickness, δd, the intrinsic weathering rate should decrease with depth beneath the surface. For example, if

$$\lambda \propto \frac{1}{\delta d^k}, \qquad (4)$$

Figure 1. Exposed shale bedrock in badlands in an abandoned claypit, Shenandoah Valley near Vesuvius, Virginia. Sunlight glints on shale surface. Badland slopes are underlain by a thin weathered shale regolith. Picture taken in early fall. Mass wasting from adjacent slopes mantles the bedrock floor during the winter season.

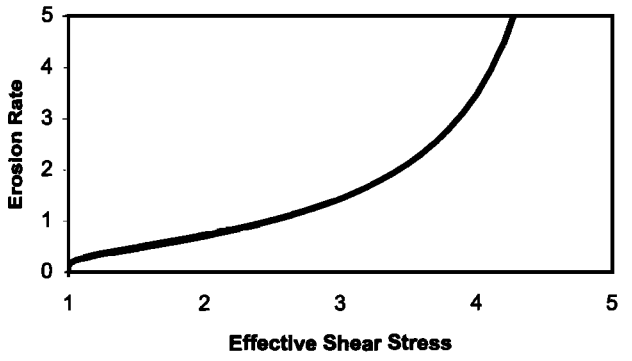

Figure 2. Relationship between effective shear stress and long-term erosion rate in a model of combined weathering and shear stress detachment in headwater channels. For this diagram C_f=5, C_f=1, and λ=1.

then the erosion rate decreases with layer thickness for $k>1$.

If $\tau_e < C_f$ no erosion occurs; if $\tau_e > C_f$ there is a minimum erosion rate of about $0.2\delta d\lambda$, and as τ_e approaches (or exceeds) C_i the erosion rate becomes infinite (Figure 2). For the more interesting case of $C_i > \tau_e > C_f$ the erosion rate increases with τ_e, and nearly linearly so if $C_i >> \tau_e > C_f$. Although this model is simplistic (for example, it does not account for gravitational stresses on the weathered material) and lacks supporting field or laboratory measurements, it shows how erosion in headwater bedrock channels can involve interaction between weathering and fluvial detachment.

The potential weathering rate of bedrock exposed in headwater channels may be greater or less than that for bedrock on adjacent slopes (either exposed or with a regolith cover). Flow in such channels is likely to be ephemeral, so that if the rock is susceptible to physical weathering by wetting and drying or freeze-thaw, weathering potential may be high [*Stock et al.*, 1996]. On the other hand, if the weathering on slopes is primarily chemical, the lack of a soil cover and the prevalence of exfiltrating flow may restrict the weathering potential of bedrock exposed in channels.

Erosion by Debris Flows and Avalanches

In high-relief landscapes bedrock erosion in headwater channels may primarily occur by energetic mass movement. In mountainous areas of the Appalachian Mountains (Figure 3, Figure 4) and in the Pacific Coast Ranges, debris flows episodically flush accumulated colluvium from hollows. Some progress has been made to develop quantitative models of such slope failures [e.g., *Montgomery and Dietrich*, 1994; *Dietrich et al.*, 1995; *Benda and Dunne*, 1997a]. On the other hand, little attention has been directed towards the role of debris flows eroding the underlying bedrock. In intervals between debris flows colluvium refills the hollows. In most cases the unweathered bedrock is sufficiently massive that debris flows would be ineffective in deepening hollows and low-order channels without accompanying weathering, suggesting that weathering and scour by debris flows interact much as scour and weathering in the channels discussed above. The relative roles of weathering by physical processes when bedrock is exposed following debris flows versus chemical weathering beneath colluvium is uncertain, and may vary in different rock types and climates. Some evidence suggests a different erosion rate law characterizes debris-flow dominated headwater bedrock channels than downstream fluvial channels, because there is a kink in the area-gradient relationship such that debris flow channels are less concave than fluvial channels [*Seidl and Dietrich*, 1992; *Montgomery and Foufoula-Georgiou*, 1993].

On mountainous slopes debris avalanches and rockfalls may also be a concentrative process, eroding steep bedrock chutes on headwall slopes. Examples include arctic and alpine mountain slopes (Figure 5) [*Matthes*, 1938; *Blackwelder*, 1942; *Rapp*, 1960a,b; *Akerman*, 1984; *Rudberg*, 1986, *Luckman*, 1977, 1978], canyon walls on Mars (Figure 6) [*Sharp and Malin*, 1975; *Blasius et al.*, 1977; *Lucchitta*, 1978], and the pali landscapes of tropical mountains (Figure 7). The main distinction between these and the mountain slopes discussed above is that energetic mass movement occurs over the whole landscape and not just the hollows. In arctic and alpine terrain dry rockfalls, debris avalanches, and snow avalanches appear to be capable of rock erosion [*Matthes*, 1938; *Blackwelder*, 1942; *Rapp*, 1960a,b; *Peev*, 1966; *Gardiner*, 1970, 1983; *Luckman*, 1977, 1978; *Hewitt*, 1972; *Corner*, 1980; *O'Loughlin and Pearce*, 1982, *Ackroyd*, 1987].

Again, weathering and erosion by rapid mass wasting probably interact to erode headwall chutes. The upper slopes of such landscapes are organized into steep, primitive basins ('spur-and-gully' topography) with divides at the scarp crest and along the crests of spurs extending down the slope (Figures 5 and 6). Topographic profiles from the divides at scarp or spur crests are concave, with the upper portions being very steep (45-90°) and bedrock floored, giving way abruptly downslope to talus at the angle of repose (30-45°, depending upon talus angularity and grain size range). Two classes of models might explain the development of these basin forms. One possibility is that stress-strain-failure relationships in near surface rocks coupled with topography, spatially variable rock resistance or fracture patterns, and surface-directed weathering processes might develop spur and gully forms independent of direct involvement of mass-wasting processes. Although not specifically applied to spur-and-gully forms, a number of investigators have proffered such arguments for development of crenellated forms of alpine relief [*Whalley*, 1984, and references

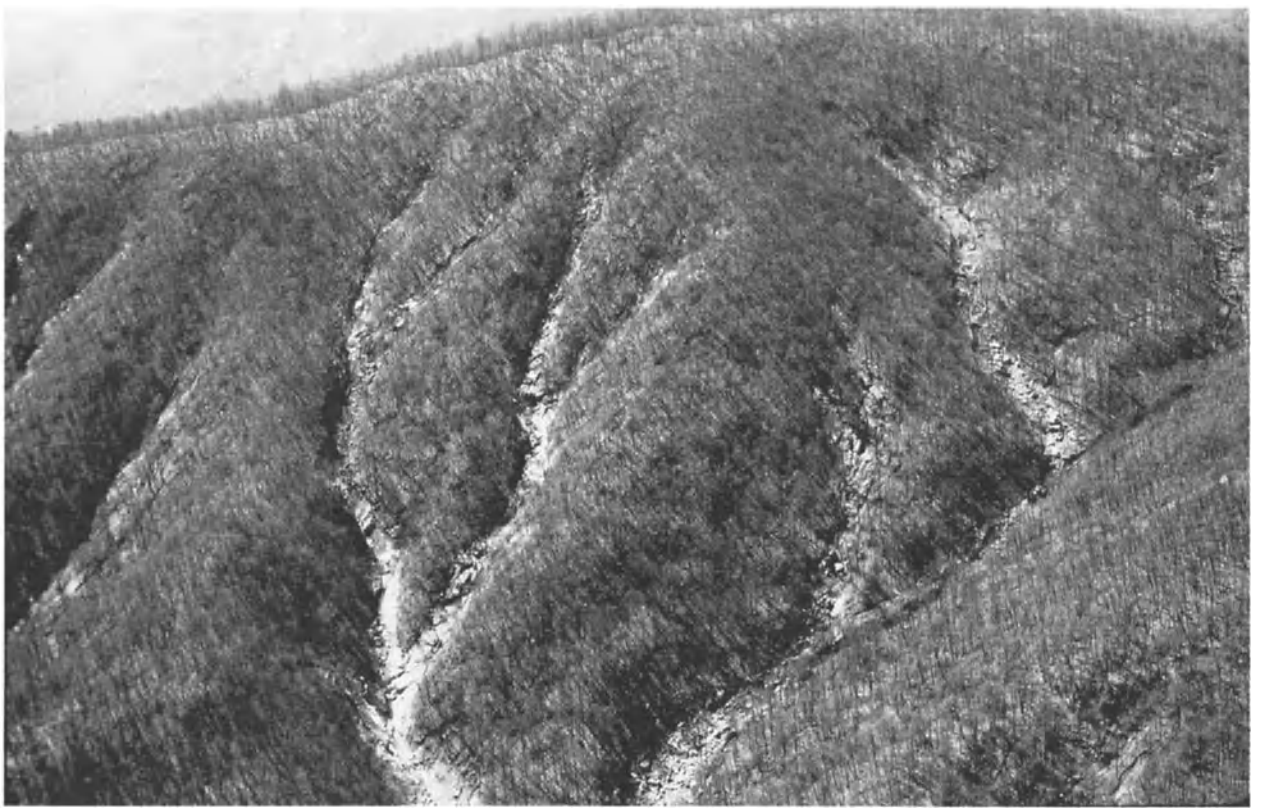

Figure 3. Avalanche scars in hollows on Kirtley Mountain, Madison County, Virginia resulting from more than 600 mm of rain in 8 hours in June, 1995. As opposed to the landscapes of Figures 5 and 6, debris avalanche scour is primarily limited to the hollows and low order channels.

therein]. The above-cited studies suggest, however, that the rockfall and avalanche processes are erosive, such that the basins develop due to economy of scale in the erosive processes similar to that responsible for creation of fluvial drainage basins, although structural influences complicate the resulting pattern.

Howard [1990] modeled the development of a mountain slope in profile from a combination of weathering and erosion and deposition by rapid mass movement. In this model, the basic driving process is assumed to be physical weathering (e.g., frost wedging, progressive failure, etc.) extending inwards from the rock surface. Rock shearing is modeled by Coulomb failure with a linear relationship between maximum shearing strength, τ_f, and normal stress, σ_f, on the failure plane:

$$\tau_f = c + \sigma_f \tan \Phi , \qquad (5)$$

where c is cohesion and Φ is the angle of internal friction. Weathering slowly reduces cohesion through a characteristic thickness, d, of the exposed rock while Φ remains constant:

$$c = c_0 e^{-\alpha(t-t_0)} , \qquad (6)$$

where c_0 is the initial cohesion at time t_0 and α is a characteristic rate of weathering. This temporal change in cohesion differs from (1) in that the cohesion eventually drops to zero. The cohesion in this case is envisioned to be due to coherent bedrock between fractures, the extent of which diminishes as physical weathering extends and connects fractures. Individual failures are assumed thin ($d<<H$, the overall relief) so that a potential failure plane parallel to an infinite slope can be assumed. Under these conditions failure occurs if:

$$1 \geq \frac{c + \rho g d \cos\theta \tan \Phi}{\rho g d \sin\theta + \tau_s} , \qquad (7)$$

Figure 4. Debris avalanche scar in Nelson County, Virginia resulting from more than 600 mm. of precipitation in a few hours in August, 1969. Most of the colluvial cover was stripped, exposing bedrock that had undergone varying degrees of saprolitic weathering.

Figure 5. Steep bedrock slopes in the Alaska Range, Alaska eroded into spur-and-gully forms by avalanching from exposed bedrock and scree accumulation at the slope base. Note the crudely dendritic avalanche chutes eroded into the bedrock exposures. The initial steep relief was created by glacial erosion of the slope base.

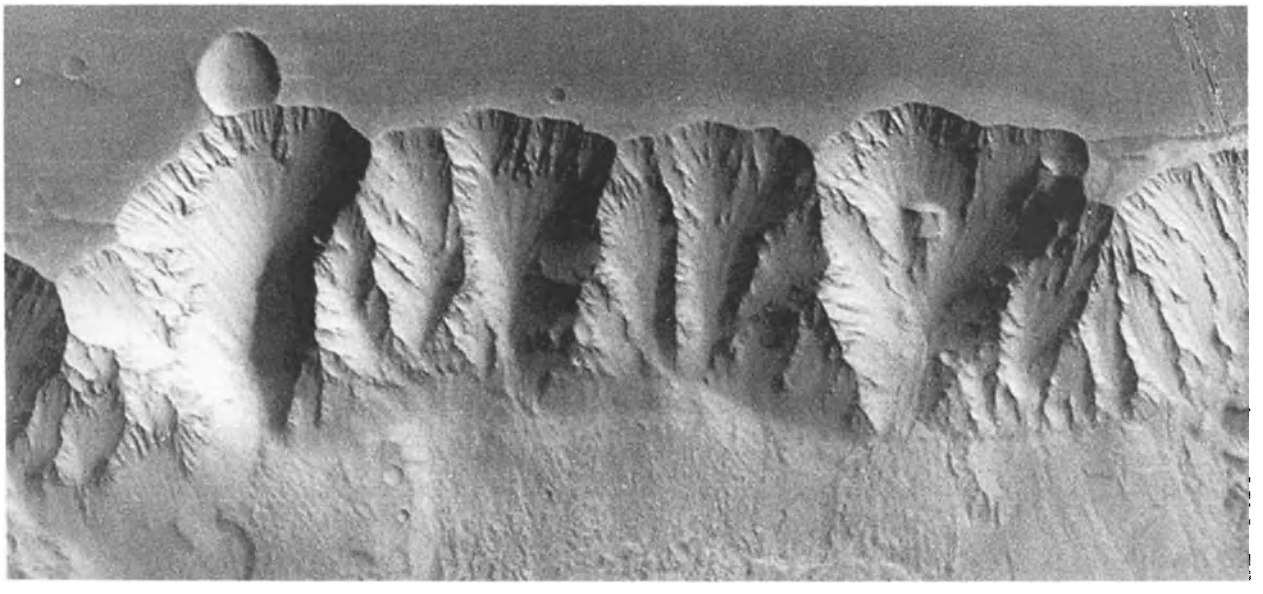

Figure 6. Spur and gully landforms dissecting the north wall of Ophir Chasma, Mars. The image is approximately 60 km across. The drop from the flat upland at the top of the picture to the base of the scarp is approximately 1.6 km. The bottom of the chasma is partially mantled by debris from large landslides, which have helped to create the large alcoves. Subsequent to the landslides, weathering and mass wasting have created the spur and gully terrain (part of Viking image 911A12).

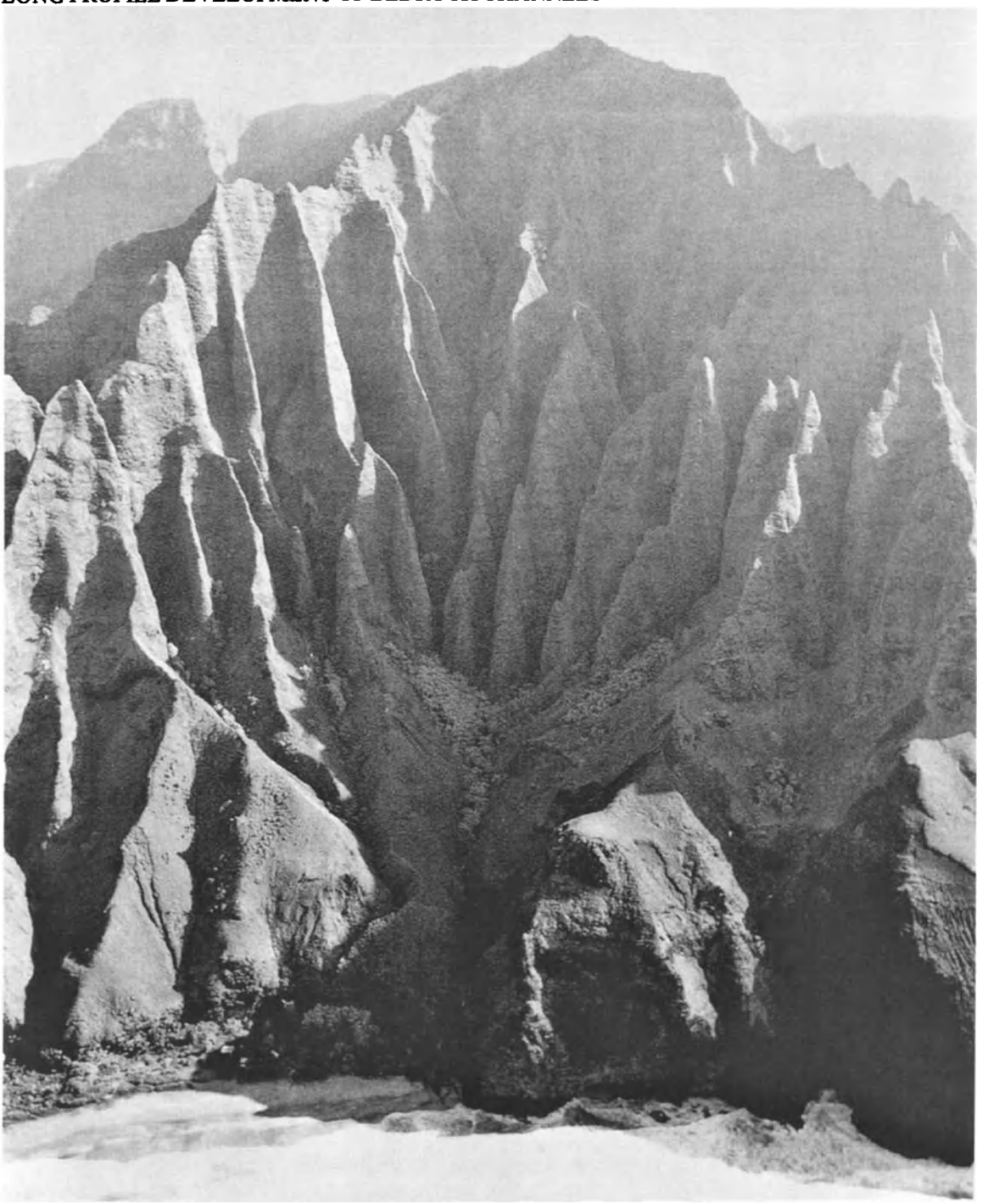

Figure 7. Steep landscape along the Napali Coast, Kauai Island, Hawaii. Note the nearly vertical slopes with knife-edged divides and steep chutes.

where θ is the local slope gradient and τ_s is a surface shear exerted by mass-wasting debris shed from higher on the slope. If a section of scarp becomes unstable due to decreasing cohesion, c, the debris shed from the slope is routed downslope. Models of snow and rock avalanche motion [*Perla et al.*, 1980; *Dent and Lang*, 1980, 1983; *Martinelli et al.*, 1980; *Pariseau*, 1980; *Lang and Dent*, 1982; *McClung and Schaerer*, 1983; *Schiewiller and*

Hunter, 1983; *Cannon and Savage,* 1988; *McEwen and Malin,* 1990] suggest the following form for flow resistance:

$$\tau_r = \rho g d \cos\theta \tan\mu + \rho C_1 V^2 , \qquad (8)$$

where μ is a coefficient of sliding friction, V is mean velocity, and C_t is a coefficient of "turbulent" friction. A theoretical basis for C_t is not firmly established and may represent air drag, internal frictional dissipation, and "plowing" of surface material [*Perla et al.,* 1980]. Some models [*Perla et al.,* 1980; *Martinelli et al.,* 1980; *McEwen and Malin,* 1990] suggest an additional "laminar" frictional term proportional to velocity. Empirical estimates in snow avalanching suggest $\tan\mu \approx 0.27$ and $\xi \equiv g/C_t \approx 1500$ m/s^2 [*Perla et al.,* 1980; *Dent and Lang,* 1980; *Martinelli,* 1980; *Buser and Frutiger,* 1980; *McClung and Schaerer,* 1983]. In rock avalanches, air drag at the avalanche surface is generally unimportant so that shear at the avalanche-bedrock interface, τ_s, is equated with flow resistance, τ_r. Change in flow momentum equals the difference between downslope gravitational force and flow resistance, such that:

$$\frac{\partial(\rho d V)}{\partial t} = \rho g d \sin\theta - \rho g d \cos\theta \tan\mu - \rho C_t V^2 . \quad (9)$$

For simplicity, the avalanche thickness is assumed to equal that of the failed layer and both avalanche depth and density are assumed to remain constant during motion. Because

$$\frac{\partial V}{\partial t} = \frac{\partial V}{\partial s}\frac{ds}{dt} = V\frac{\partial V}{\partial s} = \frac{1}{2}\frac{\partial V^2}{\partial s}, \qquad (10)$$

where s is distance along the flow path, then

$$\frac{\partial V^2}{\partial s} = 2g\left(\sin\theta - \tan\mu\cos\theta - \frac{V^2}{\xi d}\right). \qquad (11)$$

Eroded material is deposited where V decreases to zero, generally on the talus slope.

The above assumptions are incorporated into a profile (2-D) finite-difference simulation model. Initial conditions (Figure 8) are a mountain front, or scarp, of height H=5000 m extending above a flat valley floor with constant initial gradient θ_0=70°, and randomly assigned values of c_0 (values are assumed to be lognormally distributed with a specified mean and variance). This scaling was selected to model spur-and-gully development on the 2-10 km high structural scarps of Valles Marineris on Mars (Figure 6). The values of c_0 are chosen to assure initial slope stability (values of simulation parameters are given in the figure caption for Figure 8). A vertical, rather than the normal horizontal grid (100 m increments), is utilized because of the steep gradients, so that the rate of horizontal retreat of the slope is modeled. Erosion is directed perpendicular to the surface, so that the horizontal erosion rate, $\partial x/\partial t$, equals the normally-directed erosion rate, $\partial n/\partial t$, divided by the sine of the slope angle. The simulation model progressed through iterations, with weathering gradually reducing the strength of the surface layer as indicated above. Once an avalanche occurs on a given segment of slope, flow of that plug of material is routed downslope and the factor of safety is determined for each slope segment traversed by the flow. In general, the value of τ_s is sufficiently large that a number of downslope segments also fail. Debris from the additional failed segments is also routed downslope (for simplicity it is assumed that each plug moves independently, although observations suggest an almost simultaneous movement of all portions of the slope involved in an individual avalanche). Once the surface skin of thickness d is removed from the slope, weathering of the underlying layer begins, with a value for c_0 assigned randomly as discussed above. In the simulations, provision is made for lack of flow contact and weathering exposure in overhangs. Furthermore, only the component of flow momentum in the direction of the continuing flow is assumed to be preserved when the avalanche changes direction, e.g.,

$$V_d^2 = V_u^2 \cos^2\Psi , \qquad (12)$$

where V_d is the flow velocity below a bend of angle ψ, and V_u is the flow velocity entering the bend.

One simulation was run in which there was no instability due to surface stress (τ_s=0). In this case (Figure 8A), the valley wall retreats by parallel motion while the foot of the slope is covered by a growing talus mound, and the bedrock-talus contact develops the convex upward profile that is characteristic of scarps undergoing cliff retreat and talus accumulation [*Lehmann,* 1933; *Bakker and Le Heux,* 1952; *Scheidegger,* 1991, pp. 130-134]. The slightly irregular profile of the retreating upper slope is due to the random assignment of values of initial cohesion, c_0. Under these conditions, there is no enhanced downslope erosion and spur-and-gully topography would be unlikely to form in the 3-D case.

In a second simulation (Figure 8B) instability due to surface stress by moving debris was permitted, with τ_s=τ_r. The important feature of this case is the valley wall steepening through time due to greater chances for instability at the base of the slope due to weight of the avalanche block plus the V^2 dependence of τ_s. That is, for a

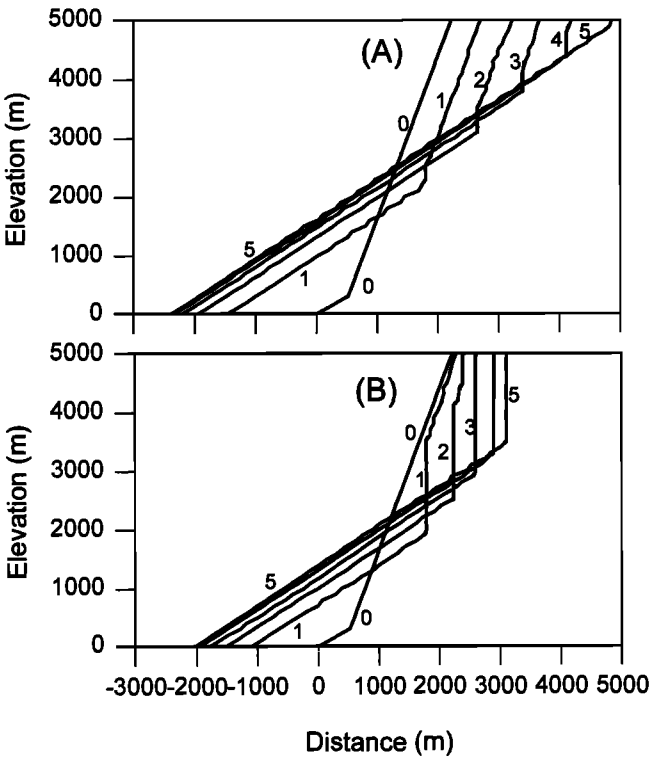

Figure 8. Profile models of slope erosion by the combined effects of weathering and avalanche scour with scree accumulation at the slope base. Numbers indicate successive profiles. (a) Erosion by weathering only. (b) Combined erosion by weathering and avalanche detachment. Note that the bedrock profile steepens. Parameters for the simulation are d=10 m, g=3.9 m s^{-2} (appropriate for Mars), c_0=6.125×10^5 kg m^{-1} s^{-2}, and ρ=2500 kg m^{-3}. For rock Φ=45° and for talus Φ=35°. For avalanche motion on rock ξ=500 m^2 s^{-1} and μ=15°, and on talus ξ= 10 m^2 s^{-1} and μ=30°. The weathering time units are arbitrary, with α in (1) being 0.03 with time measured in iterations, and the simulation is continued over 500,000 iterations.

constant gradient, the potential rate of bedrock erosion increases with distance downslope. This is an advective process having an economy of scale that is analogous to development of channels by fluvial erosion (e.g., *Howard* [1994a]), and can result in development and deepening of flow chutes. In three dimensions, the scale economy would be magnified by the potential for avalanche flow convergence into established chutes. Full simulation of chute development would require an areal model with a surface-conforming grid to permit treatment of vertical or overhanging slopes.

The pinnacled slopes of the Hawaiian Napali Coast (Figure 7) are probably eroded primarily by debris avalanches. *Wentworth* [1943] and *White* [1949] describe the 'tipping bucket' cycle of weathering and rapid mass wasting that characterize steep mountain slopes on Hawaii. The rapid basal erosion by streams and the greater mobility of debris avalanches in the wet environment preclude much scree accumulation at the foot of the slopes.

In steep landscapes with vegetated, regolith-covered slopes, episodic landslides in hollows trigger wet debris flows that travel through the headwater tips of the channel network [e.g., *Dietrich and Dunne,* 1978; *Montgomery and Dietrich,* 1994; *Dietrich et al.,* 1995; *Benda and Dunne,* 1997a]. The bedrock flooring these debris flow channels is eroded by a combination of weathering and debris flow detachment in a manner similar to the mountain slopes described above [*Seidl and Dietrich,* 1992; *Montgomery and Foufoula-Georgiou,* 1993]. The wet debris flows that occur in such channels have a wide range of composition and water content, so that no single model of rheology and motion can cover all cases. A variety of rheology models have been utilized, including Coulomb friction (the first term in (8)), empirical velocity-dependent friction (the second term in (8)), grain flow mechanics [*Takahashi,* 1991; *Savage and Hutter,* 1991], Bingham fluids [*Johnson,* 1970; *Whipple,* 1997], and non-linear fluids (e.g., *Chen* [1988]). Flow routing methods include Eulerian center-of-mass routing (as in the avalanche model presented above), kinematic wave routing [*Weir,* 1982; *Hunt,* 1994; *Huang and Garcia,* 1997], and Lagrangian routing [e.g., *Iverson,* 1997b, *Hungr,* 1995, *Rickenmann and Koch,* 1997]. A promising approach is outlined by *Iverson* [1997a,b], which combines Lagrangian routing with depth-averaged equations, a Coulomb rheology incorporating effects of pore water pressure on reducing effective normal stresses on the bed, and Rankine earth pressure theory (active stresses in extending parts of the flow and passive stresses in the compressional region at the front of the flow).

Headwater Channels: Conclusions

Modeling of erosion by debris flows in headwater channels requires rate laws for bedrock weathering and debris flow detachment in addition to flow routing models. Such erosion models are, unfortunately, only in a speculative state of development, as illustrated in the previous discussion. Systematic field observations will be required to elucidate erosion mechanisms and rates.

In summary, the rate of erosion of headwater bedrock channels is controlled by interplay between scour by water and debris flows, infilling by colluvium, and weathering processes. Because erosion by runoff or debris flow/avalanche strips partially weathered bedrock from slopes before they would fail by a combination of weathering and gravity alone, these energetic flows are concentrative erosional agents that create hollows and low-order channels.

DOWNSTREAM BEDROCK CHANNELS

The discussion in this section focuses on larger bedrock and mixed bedrock-alluvial channels in which weathering processes and scour by debris flows are quantitatively subordinate to fluvial erosion. Several important issues are discussed: 1) What factors determine whether channels are bedrock, wholly alluvial, or a mixture; 2) What processes are responsible for erosion of bedrock channel beds; and 3) Can erosion rates in bedrock channels be quantitatively modeled?

The Distribution of Bedrock Channels

Bedrock channels, which lack an appreciable cover of alluvium, occur when stream flow has excess transporting capacity, compared to supply rate, for all size ranges supplied from upstream and from local slope erosion. Channel incision into bedrock occurs when the supply of sediment to the channel cannot keep it continuously mantled with an alluvial cover, usually due either to steep gradients or to meager sediment supply. Thus, bedrock channels are favored by one or more of the following factors: high relative relief, high uplift rates and steep slopes, rapid local upwarping or faulting, resistant bedrock, and low sediment yields. Because of scouring and plucking that occur during high flow stages, channels with a thin alluvial cover can erode the underlying bedrock while maintaining an alluvial cover during low flow conditions [*Howard and Kerby*, 1983]. The bedrock erosional capacity of alluvial channels is limited, so that if downstream erosion rates exceed this capacity, local gradients steepen and bedrock becomes exposed [*Merritts and Vincent,* 1989]. This may occur in particularly resistant rock, as a result of differential uplift along a river profile, or as a result of relative land-sea elevation changes (such as the Fall Line in the Appalachian Mid-Atlantic region [*Reed*, 1981; *Hack*, 1982]).

Despite these general tendencies, attempts at *a-priori* prediction of the nature of the channel bed (bedrock, gravel, sand) based solely upon basin relief and channel gradient are likely to be erroneous, as is illustrated by the following simple analysis. Consider a reach in a river system that is subject to a constant rate of base level lowering at its lower end. If the channel is wholly alluvial, the rate of bed lowering is governed by the divergence of sediment transport:

$$\frac{\partial z}{\partial t} = -\frac{\partial q_s}{\partial x}, \qquad (13)$$

where q_s is the volumetric rate of sediment transport and x is the downstream direction. Figure 9 shows how the gradient of an alluvial channel changes as the rate of lowering of the lower end of the reach is varied (a typical bedload transport

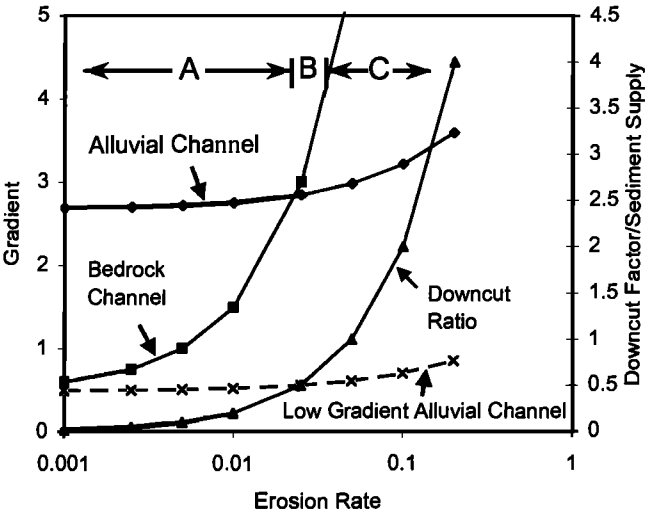

Figure 9. Relationship between channel gradient and erosion rate for bedrock and alluvial channels. The "Downcut Ratio" for an alluvial channel is defined as $(E\ L) / q_s$, where E is the erosion rate, L is the stream reach length, and q_s is the volumetric rate of bedload supply from upstream. In region 'A' the required alluvial channel gradient is much greater than for a bedrock channel, in region 'B' the gradients are commensurate, and in 'C' the required bedrock gradient is much greater than for an alluvial channel. The dashed curve shows alluvial channel gradients for a basin with a meager bedload supply; such a river system would be bedrock throughout. The gradient and erosion rate scales are arbitrary.

formula is assumed, see *Howard* [1994a, p. 2265-6]). The rate of supply of alluvium from upstream is taken to be fixed and independent of short-term or reach-length variations in main channel erosion rate. If the rate of bed lowering is close to zero (left side of Figure 9) the channel gradient is simply that required to transport sediment supplied from upstream. As the rate of erosion increases, the gradient must steepen to transport both sediment supplied from upstream and that from local bed lowering. Until the rate of erosion reaches very high values the bed steepening is very modest, which is why it is often assumed that channel gradients are in equilibrium with sediment supply from upstream and unaffected by erosion rate [*Mackin*, 1948]. On the other hand, if bedrock channel erosion rates depend upon shear stress or stream power (see analysis below), channel gradients must steepen appreciably to accommodate greater rates of downcutting (Figure 9 and (20)). For this analysis, the assumption is made that the gradient required for erosion of a bare bedrock channel at low rates of downcutting is less than that required to transport sediment supplied from upstream. As a result, the curves for required gradient for alluvial and bedrock channels should cross at a critical

erosion rate, such that for low rates of erosion gradient control by sediment transport should dominate and for high rates the bedrock erosion should be controlling. For low rates of erosion (Region A in Figure 9) the required gradient for bedrock erosion is much lower than that for sediment transport. Bedrock erosion during infrequent intervals of deep scour of the alluvial bed might suffice to keep pace with base level lowering, and the bed would be alluvial. For high rates of erosion (Region C in Figure 9), the steep required gradient would discourage deposition of bed sediment, even during waning flow stages, producing the commonly observed steep, "clean" bedrock channels. Only in a narrow range of erosion rates (Region B) would required gradients for bedrock erosion and alluvial transport be commensurate. For such reaches a partial alluvial mantling might be expected -- the mixed alluvial-bedrock channels discussed below. This simple analysis thus suggests that, within a basin of uniform sediment yield, steep channel gradients should be associated with bedrock channels, whereas low-gradient channels should favor alluvial beds.

These expectations for channel bed type are often invalid. The South Fork Eel River (Figure 10a) has a high-gradient canyon reach that is mantled with coarse boulders (Figure 11) whereas a low gradient reach upstream is largely exposed bedrock (Figure 12). The steep canyon reaches of the Colorado River expose bedrock only in deep scour holes and rapids are floored by boulders contributed by side-canyon debris flows [*Howard and Dolan,* 1981; *Howard et al.,* 1994; *Grams and Schmidt,* 1997]. Finally, a short, steep canyon reach of the Maury River in Virginia (Figures 10b and 13) is largely mantled by boulders. The common thread for these examples, considered more fully below, is the importance of locally contributed coarse debris.

The central Coastal Ranges of Oregon near Coos Bay have been subject to uplift rates of about 0.1 mm/yr, producing steep relief. Steep headwater tributaries are bedrock-floored. However, stream profiles are strongly concave, and the low-gradient downstream reaches of rivers such as the Smith River and the Umpqua River might be expected to be alluvial, whereas they generally remain bedrock-floored. This is probably because the ease of weathering and comminution of the Tyee Sandstone bedrock produces little gravel bedload, and the sand is transported largely in suspension (although some caution is in order because lumbering earlier in the century may have removed large woody debris and sediment from channels due to 'splash damming' – large short-lived floods produced by creation and intentional breaching of temporary dams). Thus the alluvial channel gradients required for the range of local erosion rates appears to be lower than that for bedrock erosion (e.g., the dashed line in Figure 9). Coastal ranges to the north and south of this region in more indurated bedrock support steeper gravel rivers. These examples illustrate the need to consider the properties of sediment supplied from slope erosion, both regionally and locally, in addition to relief and uplift rate as determinants of channel gradient and bed type.

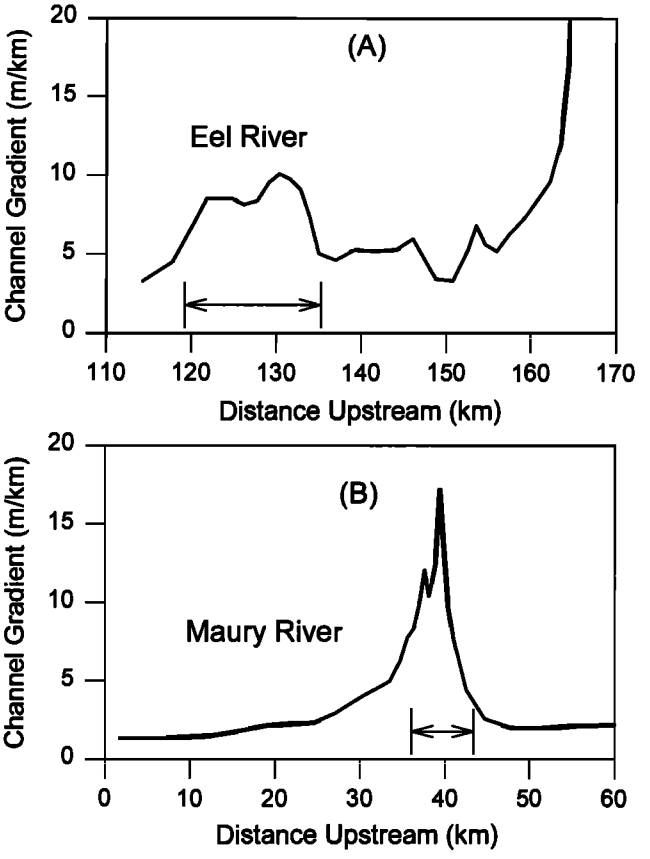

Figure 10. Channel gradient of (a) the South Fork Eel River, California and (b) the Maury River, Virginia. Distances measured from the mouth of the Eel River, but from an arbitrary datum for the Maury River. Segments marked with arrows are canyon sections.

Finally, the above analysis suggests that few channels should exhibit beds transitional between full alluvial and bare bedrock. The discussion of mixed bedrock-alluvial channels below demonstrates that this expectation is also incorrect.

Quantifying Erosional Processes in Downstream Bedrock Channels

In streams with bedrock beds, the critical concern is the rate of bed erosion. Erosion may occur by several mechanisms, including hydraulic plucking [*Miller,* 1991; *Wende,* 1997; *Whipple et al.,* 1997; *Dollenmayer and Whipple,* 1997], cavitation [*Barnes,* 1956; *Matthes,* 1947),

abrasion by sediment [*King,* 1927; *Alexander,* 1932; *Maxson and Campbell,* 1935; *Maxson,* 1940; *Foley,* 1980; *Sharpe and Shaw,* 1989; *Howard et al.,* 1994; *Slingerland et al.,* 1997; *Ellis et al.,* 1997; *Whipple et al.,* 1997; *Tinkler,* 1997; Sklar and Dietrich, 1996,1998], solution [*King,* 1927], and weathering [*Stock et al.,* 1996]. General reviews are given by *Baker* [1978], *Baker and Pickup* [1987], *Baker* [1988], *Tinkler and Wohl* [1998], *Dick et al.,* [1998], and *Wohl* [1998]. The relative importance of these processes depends upon rock type, channel hydraulics, water chemistry, sediment type and load, and climate. Thus there is no simple, universal law of bed erosion, and due to the general slowness of bed erosion in resistant rocks, few process observations have been made.

Modeling of erosion in bedrock channels to date has primarily been based upon the assumption that erosion rate $\partial z/\partial t$ is a function of some measure of flow intensity, ϑ:

$$\frac{\partial z}{\partial t} = - K_t \left(\vartheta - \vartheta_c\right)^{\zeta} , \qquad (14)$$

where ϑ_c is a critical flow intensity that must be exceeded for erosion to occur, K_t is an erodibility that depends upon bedrock properties, and ζ is an exponent (most models have assumed that ζ is unity). The most common assumed measures of flow intensity are the bed shear stress, τ, and the stream power per unit area of channel bed, $\omega = \tau V$, where V is mean flow velocity. Simple equations of continuity, flow resistance, and downstream hydraulic geometry are usually also assumed [e.g. *Howard,* 1994a].

$$\tau = \gamma R S , \qquad (15)$$

$$V = K_n R^{2/3} S^{1/2} / N , \qquad (16)$$

$$Q = K_p R W V , \qquad (17)$$

$$Q = K_a A^e , \qquad (18)$$

$$W = K_w Q^b , \qquad (19)$$

where γ is the unit weight of water, R is hydraulic radius, S is channel gradient, V is mean velocity, N is Manning's resistance coefficient, Q is an effective discharge, A is drainage area, and K_n, K_p, K_a, K_w are coefficients. The coefficients and exponents are generally assumed temporally and spatially invariant. These, when substituted into (14) allow the erosion rate to be expressed as a function of drainage area and local gradient:

$$\frac{\partial z}{\partial t} = - K_t \left(K_z A^g S^h - \vartheta_c\right)^{\zeta} , \qquad (20)$$

where the various coefficients are incorporated into K_z. The exponents have the values $g=0.6e(1-b)$ and $h=0.7$ for $\vartheta=\tau$, whereas $g=e(1-b)$ and $h=1.0$ for $\vartheta=\omega$.

Several approaches can be used to estimate the values of the coefficients in (20) from field data. All of these assume $\vartheta_c=0$, so that three parameters $K_\zeta=K_t K_z^\zeta$, $m=b\zeta$, and $n=h\zeta$ must be estimated. The most direct approach is to collect data on net channel bed erosion over a known period of time for a range of values for contributing drainage area and channel gradient, ideally for a single bedrock type. *Howard and Kerby* [1983] estimated K_ζ, m, and n by regression analysis of 10 years of erosion in badland channels in Coastal Plain sediments in Virginia, finding m=0.45 and n= 0.7, consistent with linear dependency of erosion rate upon shear stress. Similar methods have been used for larger channels in more indurated bedrock, with varying results. *Seidl et al.* [1994] found $m=n=1$ for channels incised into a volcanic shield on the island of Kauai. *Stock and Montgomery* [1998] analyze erosion data from several different rivers with known prior profiles and find a considerable variation in estimates of K_ζ, as might be expected for differences in rock type and climate. The estimated values of m and n also varied widely, however, with m ranging from 0 to 0.5 and n from 0 to 2. This might reflect variations in bedrock erosion processes amongst locations, but parameter estimation may also compromised by 1) limited ranges of drainage area and gradient in the target streams, 2) downstream variations in lithology, 3) uncertainties in estimation of the initial profile, 4) presence of alluvial reaches along the stream profile (erosion rates will be lower where a protective alluvial cover is present), and 5) uncertain or irregular relationship between discharge and contributing area (18). Even where insufficient information on erosional history is available to estimate all parameters, it is sometimes possible to estimate the ratio of m to n. *Seidl and Dietrich* [1992] reasoned that tributaries and mainstem streams should be lowering at the same rate near their junctions, so that measurements of A and S in both streams allows calculation of m/n. Similarly, if geologic evidence suggests that a drainage basin has been undergoing a constant long-term erosion rate (that is, the topography is in steady state), then the ratio of m/n can be estimated by regressing channel gradient on drainage area:

$$S = -\left(\frac{\partial z}{\partial t} \Big/ K_r\right)^{1/n} A^{m/n} . \qquad (21)$$

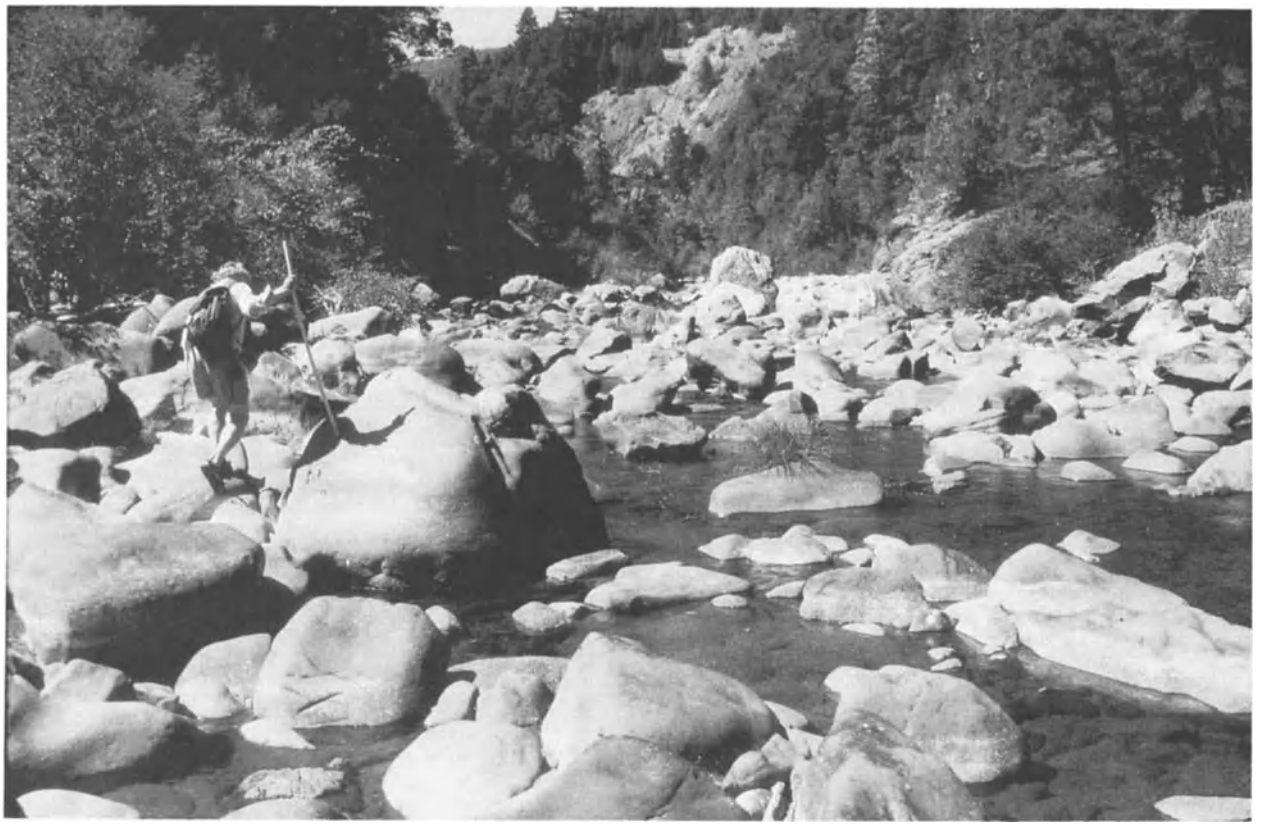

Figure 11. Channel bed of the South Fork Eel River at about km. 131 in Figure 10a. The bed is dominated by boulders derived by mass wasting from canyon walls, the channel bed, and local tributaries. Bedrock exposures occur locally in scour holes. The sandstone boulders are strongly rounded and fluted by suspended load abrasion except for the tops of the largest monoliths.

The assumption of a simple bedrock erosion rate law, such as (20), has been motivated by the desire to model long term landscape evolution in a variety of geologic and climatologic settings. It is uncertain at present how reasonable these assumptions will turn out to be as the study of bedrock channels progresses. It is probable that, even if such equations remain viable, no universal values of the exponents m and n will emerge because of a wide diversity of processes eroding bedrock channels.

The gradient of some bedrock channels may be determined by the threshold of detachment, ϑ_c, in (20). In thin-bedded or well-fractured bedrock, hydraulic plucking may dominate bedrock erosion, such that there is a well defined flow intensity ϑ_c for plucking. Erosion would progress rapidly until gradients dropped such that only the largest floods could detach bedrock slabs. From (20) the gradient would be:

$$S \approx \left(\frac{\vartheta_c}{K_z A^g} \right)^{1/h} . \tag{22}$$

This situation would have a close analogy to threshold gravel bed channels [*Howard,* 1980; *Howard et al.,* 1994]. Operation of a bedrock channel system close to threshold conditions would also occur if the exponent ζ in (20) were greater than unity, because gradient would be only a slight function of erosion rate.

The temptation to use simplified models of bedrock erosion such as (14) and (20) is great given the paucity of

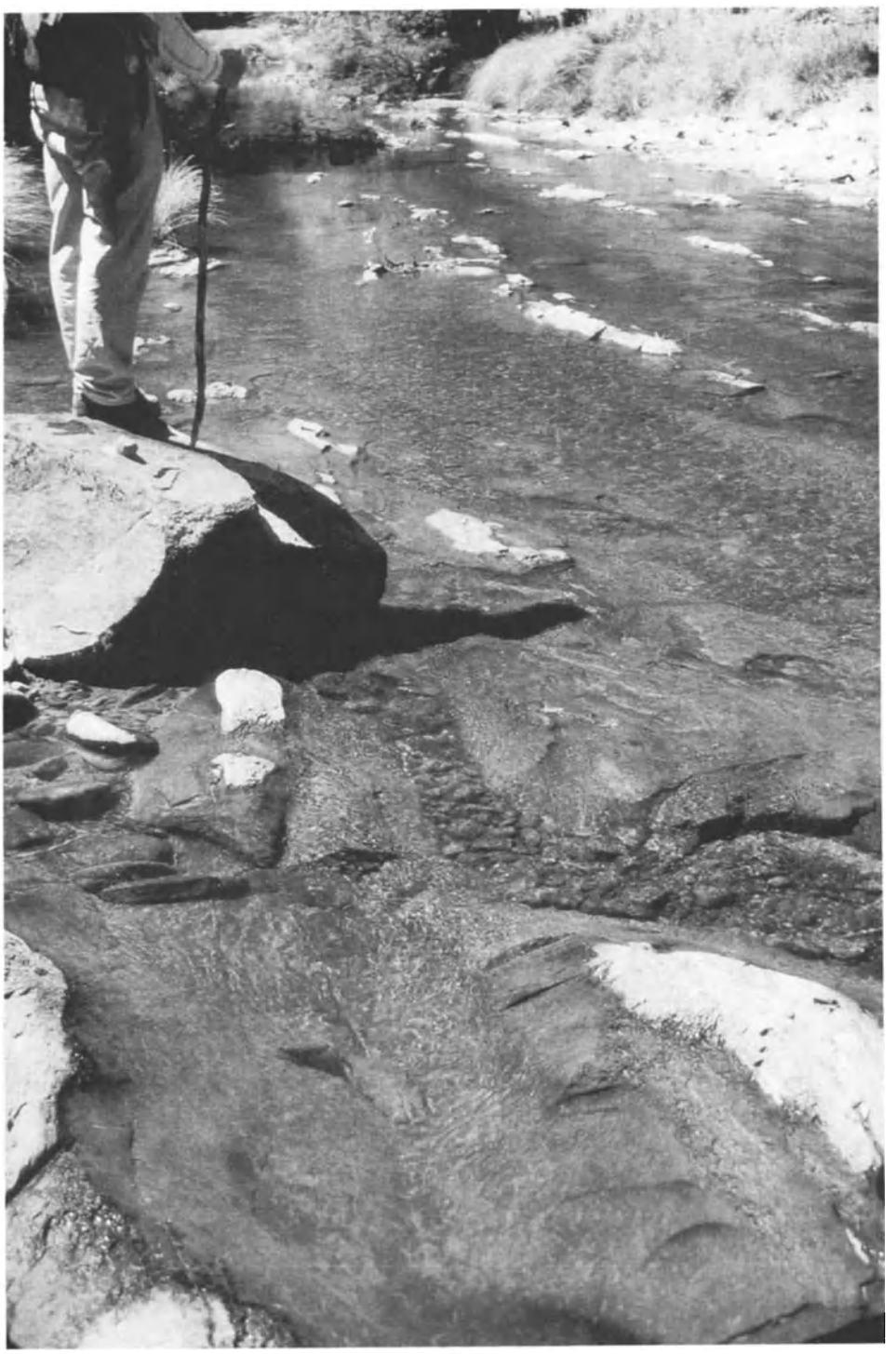

Figure 12. Channel bed of the South Fork Eel River at about km. 142 in Figure 10a. The bed is predominantly exposed sandstone, with thin gravel mantling in some of the low points.

Figure 13. The Maury River in the Goshen Pass (approximately km. 40 in Figure 10b). The bed is dominated by large blocks of Tuscarora Sandstone delivered by mass-wasting from adjacent canyon slopes. Bedrock ledges are exposed in the rapids in the upper left of the picture and locally elsewhere in deeper portions of the channel.

quantitative observations and the need for erosional rate laws in regional models of uplift, denudation, and sedimentation. The multiplicity of processes involved in bedrock channel erosion suggests caution. Some of this variability can be accounted for in appropriate choices of intrinsic bedrock erodibility (K_r in (14)). The most glaring omission in (14) is the lack of explicit treatment of the role of sediment load in bed erosion. Several new models incorporate abrasion explicitly [*Sklar et al.*, 1996; *Sklar and Dietrich*, 1998; *Slingerland et al.*, 1997; *Ellis et al.*, 1997; *Dick et al.*, 1998]. If sediment load is low and sediment contributions are areally uniform, abrasion rate laws may converge to a form similar to (14) or (20).

Mixed Bedrock-Alluvial Channels

A surprising number of streambeds expose bedrock locally during normal low flows (say 5% to 60% of total bed area) while elsewhere the alluvial cover is no more than 2-3 meters thick – these are the mixed bedrock-alluvial channels discussed here (simplified to mixed channels for this discussion) [*Miller*, 1991; *Seidl and Dietrich*, 1992; *Wohl*, 1992, 1993, *Howard et al.* 1994]. As pointed out by *Brush* [1961] and *Howard et al.* [1994], many of the streams in the Appalachian Mountain region could be so classified. Flume experiments of erosion of weak "bedrock" by through-flowing sediment commonly exhibit alternation of bedrock exposures in narrow sections and alluvium mantle in divergent flow [*Wohl and Ikeda*, 1997]. The simple but flawed analysis considered above (Figure 9) suggested that such mixed channels should be uncommon.

What, then explains the frequent occurrence of mixed channels? *Howard et al.*, [1994] propose two scenarios of temporal change that could result in (geologically) short-term coexistence of alluvial and bedrock channels. The first case occurs when alteration in sediment load and discharge occasioned by climatic or land use change causes the channel to undergo transition between bedrock and alluvial cover (in either direction). A mixed channel might persist for some time during the transition. The second case occurs

when sudden drop of baselevel causes dissection of a former alluvial channel system. Most of the subsequent erosion occurs by migration of a steep bedrock knickpoint. Channel sections well upstream from the knickpoint experience modest steepening and incision, however, as observed in experiments by *Gardner* [1983] and simulations by *Howard et al.*, [1994]. These sections upstream from the knickpoint might be mixed bed.

A reliance on evolutionary scenarios to explain the widespread occurrence of mixed channels seems *ad hoc*. The remainder of this discussion will focus on the possibility that such channels are either an equilibrium form or one adjusted to short-term oscillations in sediment supply. If mixed channels are temporally persistent as the river system downcuts, then the most crucial question is how bedrock erosion can occur when the bedrock is largely mantled. *Gilbert* [1880] suggested that the most important mechanism of bed erosion in bedrock channels is scour by sediment in transport. When the quantity of bedload is small, erosion rate should be proportional to the quantity of sediment in transport. But Gilbert pointed out than when the rate of sediment supply is large, grains interfere with each other and begin to mask the bed, so that the rate of erosion reaches a maximum and presumably goes to zero as the bed becomes 100% covered by alluvium. This inhibition of abrasion by large sediment load has been observed in studies of industrial slurry transport. Recent models of abrasional bedrock erosion by *Sklar et al.* [1996], *Sklar and Dietrich* [1998] and *Slingerland et al.* [1997] highlight the non-linear relationship between abrasion rates and quantity of sediment in transport. Not only is there reduced abrasion during high transport rates, but a rapid and sudden transition from exposed bedrock to nearly complete alluvial cover is favored by higher frictional dissipation in grain-to-grain collisions on the bed than in grain-to-bedrock collisions [*Howard*, 1980].

Several circumstances can explain the widespread occurrence and temporal persistence of mixed channels. One case is where the bedrock exposures are particularly resistant requiring the development of local rapids or falls for erosion to keep pace with the overall rate of stream lowering. The short knickpoints described by *Miller* [1991] in sedimentary rock may be an example, where development of knickpoints permits quarrying or undermining of resistant beds. However, irregular alternating bedrock and alluvial sections are often found even when the bedrock is massive and apparently homogeneous [*Wohl*, 1992, 1993].

A second possible mechanism permitting or requiring mixed channels is bedrock erosion primarily through migration of local knickpoints or waterfalls separating alluvial reaches. Because an alluvial cover inhibits bedrock corrosion and weathering, erosion of bedrock might only occur in steep sections where high flow velocities maintain a largely sediment-free bed. In order to maintain a stable, migrating knickpoint, the potential erosion rate of the bed for a given channel gradient must be greater at the base of the knickpoint that at the crest. Otherwise, the knickpoint will gradually disappear by diffusional flattening, as is implicit in bedrock erosional models such as (14). Two mechanisms can produce concentrated basal attack. One is exposure of weak units or bedding planes at the base of the knickpoint, permitting undermining, as in the streams in sedimentary sequences described by *Miller* [1991] and the famous Niagara Falls. The other is development of locally supercritical flow over the crest of the knickpoint, which accelerates bedload particles and induces high turbulence at a hydraulic jump at the base of the knickpoint. The presumably stable and migrating knickpoints described by *Seidl and Dietrich* [1992], *Wohl* [1992, 1993], and *Dick et al.* [1997] may be examples. The height of knickpoints can be determined by bed thickness in sedimentary rocks. Knickpoints developed by rapid base level lowering of a master stream are influenced by the depth of downcutting. In addition, knickpoints might be a stable feature of a relatively constant rate of downcutting in mixed channel systems, even in homogeneous bedrock. The height of such knickpoints might be conditioned by the spatial scale required by the flow to develop a supercritical transition-hydraulic jump pair or, possibly, an integrated vortex system. Characteristic of knickpoints in many cases is a downstream transition from broad longitudinal grooves on a nearly flat exposed bed to incised inner channel [*Wohl*, 1992, 1993]. If hydraulic controls determine the height, ΔZ, of knickpoints, then, if a master stream is eroding at a rate $E = -\partial z/\partial t$, a knickpoint on a tributary will form after a time $\Delta T = E\Delta Z$. Assuming that knickpoints migrate upstream with a constant velocity, $V_k = \partial x/\partial t$, the linear density of knickpoints on the tributary, $n/\Delta X$, will equal $E/(V_k\ \Delta Z)$. For sufficiently high rates of base level lowering, all alluvial cover will be stripped, and a totally bedrock reach will occur.

The remaining scenarios for mixed channels involve temporal alternation of exposed and mantled bedrock. Migrating bedforms such as dunes, bars, and sediment waves may provide local exposure of bedrock that permits continuing erosion. Spatial consistency of bed erosion rates would be enforced by gradual lagging of bedrock scour and eventual bedrock exposure in bed areas that would otherwise favor relatively permanent alluvial cover. In headwater channels in forested watersheds large woody debris serves to trap sediment [*Keller et al.*, 1995; *Montgomery et al.*, 1995; *Abbe and Montgomery*, 1996; *Montgomery and Buffington*, 1997], and in some cases creates short, temporary alluvial reaches in otherwise bedrock channel [*Montgomery et al.*, 1996].

The final explanation for mixed channels involves episodic sediment delivery to the channel system. In many high-relief areas, sediment is contributed primarily by debris flows during intense precipitation events whose recurrence interval is multi-decadal to millennial [e.g., *Williams and*

Guy, 1973; *Dietrich and Dunne,* 1978; *Dietrich et al.,* 1982; *Benda,* 1990; *Benda and Dunne,* 1997a]. The interaction of sediment supply and bedrock erosion in this case will be illustrated by a simple spreadsheet-based conceptual model in which all sediment delivered to the valley bottom occurs by infrequent debris flows associated with large floods. Relative to the overall simulation timescale these delivery events are essentially instantaneous. In between events, this sediment is reworked by moderate floods, causing bed abrasion. The moderate floods are represented as a continuum process, implying that they are very frequent compared to intervals between the debris flow delivery events. For the purposes of discussion only, the dependency of bedrock corrasion by these moderate floods upon the thickness of sediment cover will be modeled by the relationship:

$$\frac{\partial z}{\partial t} = -K_e T_s \left[1 - e^{-\eta\left(T_c - T_s\right)}\right], \qquad (23)$$

where the coefficient K_e depends upon bedrock and sediment mechanical properties as well as flow intensity, T_s is the average thickness of sediment cover over the bedrock, T_c is a critical alluvial thickness beyond which $\partial z/\partial t = 0$, and η is sufficiently large that the exponential term becomes important only when T_s approaches T_c. This is a humped relationship going to zero at both T_c and T_s. The sediment thickness, T_s, is averaged over the whole bed (or valley bottom), including exposed bedrock and bar deposits. The model implies that the bed sediment load during moderate floods is derived from the valley bottom deposits and is therefore an increasing function of T_s. Sediment delivery by debris flows occurs during rare, high-intensity events (Figure 14a). Between these rare storms are the numerous moderate floods (not explicitly shown in Figure 14a). These moderate floods gradually entrain, transport, and comminute the sediment introduced by the major floods, so that the average sediment cover diminishes exponentially between high-intensity storms (Figure 14b). This stochastic modeling of sediment supply, gradual removal, and episodic bed exposure is similar to *Benda and Dunne* [1997b]. Channel aggradation following large storms and gradual removal by smaller storms has been noted in many streams [e.g., *Benda,* 1990; *Madej and Ozaki,* 1996]. The rate of bedrock scour by moderate floods is assumed to follow (23), with T_c=0.2 (all units in Figure 14 are arbitrary). Consequently, the rate of bedrock erosion is limited by both too great a sediment mantling ($T_s \geq T_c$) and too little sediment supply (T_s=0)(Figure 14c). In addition, the major sediment-producing floods are assumed to have high scour potential, at least up to the point that they bury the bed (T_c is assumed to be 0.4 for these large floods, reflecting greater scour potential of major floods). Note that the last major flood occurs so soon after the previous flood that the bed is still sediment-covered, resulting in no additional bed erosion.

This last scenario differs from the climatic-change explanation for mixed channels in that no systematic environmental change is envisioned. All of the "steady-state" explanations for mixed channels suggest that bedrock is episodically exposed. This permits bedrock erosion despite a sediment thickness that, if spread over the bed and averaged through time, might be thick enough to prevent bed erosion. The episodic exposure can result from exposure in the troughs of migrating bedforms, in migrating knickpoints, or as a result of episodic addition and removal of sediment from the channel bed and valley floor (Figure 14). Channels with such episodic exposure are operating in region (B) as well as the portion of region (A) close to region (B) in Figure 9.

Gradient Control in Mixed Channels

For long-term erosional modeling it is important to be able to predict the relationship between channel gradient and erosion rate. In alluvial channels the use of equation (13) plus a bedload transport formula will allow prediction of channel gradient if the size distribution and rate of sediment influx can be estimated. For pure bedrock channels a process approach such as (14) may be appropriate for predicting long profile evolution. However, in mixed channels it is not clear whether the gradient is determined primarily by divergence of sediment transport or by the necessity for bed erosion. The actual gradient may even be greater than for a pure bedrock or alluvial channel because of the necessity to accomplish both bed scour and transport [*Howard and Kerby,* 1983]. The issue is further complicated by the feedback between rate of incision and the quantity and size of sediment supplied.

Kodama and Nakamura [1996] discuss one such feedback. In a canyon section of the Ojika River, local additions of nearly immobile coarse boulders from tributaries is associated with steepening of the mainstem gradient. Flume experiments [*Kodama and Nakamura* 1996] show that steeper gradients are required to transport the same amount of bedload through boulder-strewn reaches than through boulder-free reaches. If bedrock erosion were primarily related to the quantity of bedload in transport, steeper gradients would be required in bouldery reaches to assure continuity of sediment transport and equality in bed erosion rates as in boulder-free reaches. The presence of boulders does not necessarily reduce bed erosion rates, however, because obstructions on the bed increase turbulent intensity and may create systematic vorticity that can locally enhance bed scour by suspended load [*Sharpe and Shaw,* 1989; *Tinkler,* 1997].

When rates of bedrock river incision are high, negative feedback in the form of increased sediment delivery can

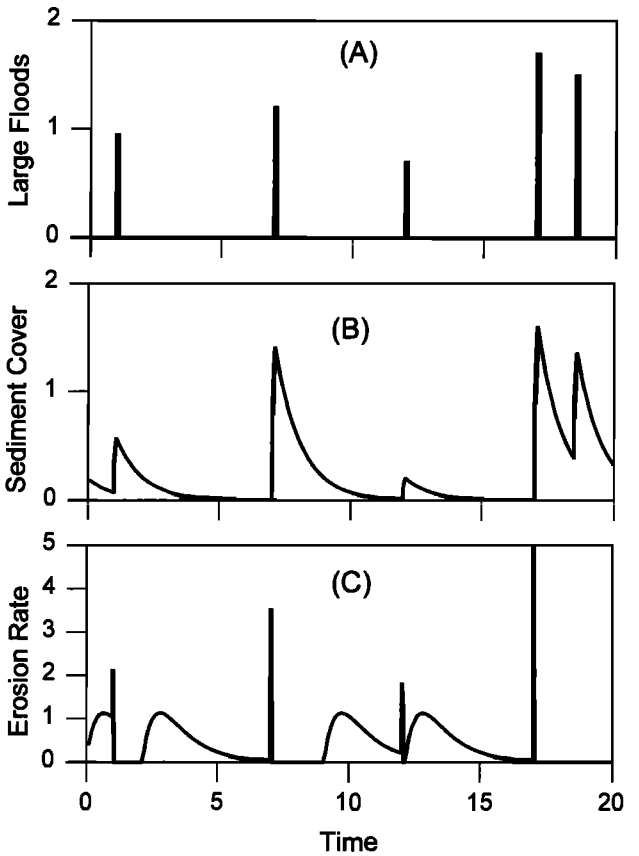

Figure 14. Conceptual model of episodic sediment supply, sediment cover, and erosion of bedrock channel bed. Scales are arbitrary. See text for explanation.

limit the rate of incision and even control the channel gradient. Although long-continued rapid incision results in generation of steep relief throughout the drainage basin, and thus high sediment loads, the immediate effect of accelerated incision is to cause canyon reaches with steep slopes and steep tributaries. This in turn triggers delivery of coarse boulders that may partially or wholly mantle the channel bed. This *locally contributed* debris often controls gradient and more severely limits incision rates than *through-flowing* alluvium derived from the entire drainage basin [*Howard and Dolan,* 1981; *Seidl and Dietrich,* 1992]. The Ojika River, cited above, appears to be an example. A classic example is the Colorado River in the Grand Canyon. As discussed by *Howard and Dolan* [1981], *Kieffer* [1985, 1990], *Webb et al.* [1989], and *Howard et al.* [1994], debris flows from canyon walls delivered through short, steep tributaries create fan-like deposits containing large boulders that are reworked into the steep rapids that account for most of the elevation fall through the Grand Canyon. A similar control of channel gradient by debris-flow fans occurs in other canyon reaches of the Colorado River and its tributaries [*Grams and Schmidt,* 1997]. The continued production of coarse debris from canyon walls has been sufficient to balance the weathering and comminution of boulders in the debris fans such that the Colorado River within the canyon has downcut very little during the Pleistocene, at least in the western portion [*Lucchitta,* 1990]. The overall gradient of the river is controlled by the long-term balance between rate of debris flow delivery and rate of reworking of the debris fans by the Colorado River.

Another example is the canyon reach of the Maury River at Goshen Pass, Virginia, where the river cuts through the resistant Tuscarora sandstone. Above and well below the canyon reach the alluvial bed is coarse gravel, but in the canyon mass-wasted sandstone monoliths 2-5 m in diameter cover 20 to 100 percent of the bed (Figure 13). The gradient of the river steepens dramatically through this reach (Figure 10b). It remains an open question whether the gradient is controlled primarily by the necessity to erode the bedrock or by the need to transport and comminute the locally contributed alluvium. This influx of coarse sediment affects the channel gradient for about 10 km downstream from the canyon. The degree of bedrock exposure in this reach may have varied throughout the Quaternary due to climate changes, particularly as they affect mass wasting from the canyon walls.

A final example is the South Fork Eel River, California (Figure 10a). Between kilometers 74 and 85 the river has an atypically steep gradient and high relief, steep slopes adjacent to the channel. The steep reach has originated by an uncertain combination of higher bedrock resistance or rapid incision due to tectonic deformation or stream capture. A largely bedrock-floored channel with patches of fine gravel is present above the canyon (Figure 12). This bedrock reach probably undergoes episodic burial by sediment contributed by debris flows from tributaries during major floods [*W.E. Dietrich,* personal communication] and is probably an exemplar of the time varying rates of bedrock erosion shown in Figure 14. At present, bed erosion may be limited by the small quantity of bedload (the last major flood occurred in 1964). In the canyon reach erosion is limited by the opposite circumstance – a nearly complete cover of boulders derived from superjacent slopes and steep tributaries (Figure 11). Steep relief generated by earlier rapid incision has permitted rapid mass wasting and avalanche delivery of boulders to the valley bottom, largely burying the channel bed. These boulders exhibit the streamlined upstream faces, sharp downstream-pointed edges and concave potholing on the downstream faces that indicate that suspended load abrasion rather than impacts with other large boulders dominates their comminution. Abrasion by relative movement of bed particles without net transport (abrasion-in-place) may also occur

[*Schumm and Stevens,* 1973]. Deep scour pools downstream from constrictions and large bar forms indicate that all but the largest boulders can be moved locally by the largest floods, but it is uncertain whether there has been sufficient supply of boulders to force the overall gradient to a threshold condition.

DISCUSSION

Erosion of bedrock channels seldom involves just hydraulic detachment. In headwater channels some weathering must precede erosion, and rapid mass wasting is often the mechanism for mobilizing weathered bedrock. In larger channels a variable mix of hydraulic plucking, cavitation, abrasion by bedload and suspended load, and weathering is involved. Consequently there can never be a rate law representing a single process of bedrock channel erosion that applies universally [*Seidl and Dietrich*, 1992; *Howard et al.*, 1994]. Nonetheless, predictive models must be developed for various classes of dominant processes; this and other papers in this volume present initial analyses for certain types of bedrock channels. A number of unresolved and complicating issues remain unaddressed in these models, however.

One of these issues is how rock beds are eroded when an appreciable sediment cover is present. The simplest hypothesis assumes that erosion ceases when a single grain thickness is present over bedrock or if sediment transport reaches capacity. However, bedform migration, episodic scour and fill, and alluvial bed suspension during extreme floods may permit long-term erosion even with an appreciable bed cover under normal conditions. Perhaps gradual reductions in predicted erosion rate as sediment cover increases (e.g., (20)) might suffice in erosion models.

Modeling of long-term profile development in bedrock channels must account for the sediment flux through the channel. This is true not only because abrasion by bedload and sediment load may be the dominant erosional process, but also because locally contributed coarse sediment often partially or wholly mantles the bedrock channel, reducing erosion rates. Long-term rates of bedrock channel erosion are often regulated by delivery of coarse boulders to the valley bottom due to steep relief created by past rapid incision. Because these boulders must be comminuted in place before further transport by processes similar to those eroding the bedrock proper, channels partially or totally mantled by locally contributed coarse sediment can be viewed as a special type of bedrock channel.

The timescale over which bedrock channels have eroded is much longer than that for alluvial channel grading. Therefore, present processes and bed characteristics are not necessarily representative of those pertaining during development of the channel profile. In mixed alluvial-bedrock channels the fractional coverage by alluvium may vary temporally. Inheritance of channel profiles, valley form, and slope and channel sediment from different past climates may be important. Most erosion may occur during extreme floods that have not occurred during the period of observation. Most rivers have been severely modified by recent land-use changes: deforestation leading to increased sediment delivery by mass wasting or overland flow, diminishment of large woody debris in channels, elimination of beavers, gravel mining, construction of flood levees, channelization, inter alia. In extreme cases, the "natural" morphology of the channel may be unknowable.

Despite these difficulties, field investigations, laboratory experiments, and theoretical model development will gradually improve our understanding of the evolution of bedrock channels.

Acknowledgements. This work is supported by a grant from the National Aeronautics and Space Administration Planetary Geology and Geophysics Program. Many of the concepts discussed here have been developed through collaboration with William Dietrich, Leonard Sklar, and Michelle Seidl, and Dietrich's comments on the draft version of this paper led to considerable improvements.

REFERENCES

Abbe, T.B. and D.R. Montgomery, Large woody debris jams, channel hydraulics and habitat formation in large rivers, *Regulated Rivers: Res. Managm , 12,* 201-221, 1996.

Ackroyd, P. Erosion by snow avalanche and implications for geomorphic stability, Torlesse Range, New Zealand, *Arctic and Alpine Res., 19,* 65-80, 1987.

Akerman, H.J, Notes on talus morphology and processes in Spitsbergen, *Geografiska Annaler 66A*, 267-284, 1984.

Alexander, H.S., Pothole erosion, *J. Geol.*, 40, 305-337, 1932.

Baker, V.R., Large-scale erosional and depositional features of the Channeled Scabland, in *The Channeled Scabland*, edited by Baker, V.R. and D. Nummedal, National Aeronautics and Space Administration, Washington, D.C., 81-116, 1978.

Baker, V.R., Flood erosion, *in Flood Geomorphology,* edited by V.R.Baker, R.C. Kochel and P.C. Patton, John Wiley & Sons, New York, 87-98, 1988.

Baker, V. R., and G. Pickup, Flood geomorphology of the Katherine Gorge, Northern Territory, Australia., *Geol. Soc. Amer. Bull.*, 98, 635-646, 1987.

Bakker, J.P. and Le Heux, J.W.N., A remarkable new geomorphological law, *Koninklijke Nederlandsche Academie van Wetenschappen, B55*, 399-410 and 554-571, 1952.

Barnes, H.L., Cavitation as a geological agent, *Am. J. Sci., 254,* 493-505, 1956.

Benda, L., The influence of debris flows on channels and valley floors in the Oregon Coast Ranges, U.S.A., *Earth Surf. Processes. Landforms, 15,* 457-64, 1990.

Benda, L., and T. Dunne, Stochastic forcing of sediment supply to channel networks from landsliding and debris flow, *Water Resourc. Res., 33,* 2849-2863, 1997a.

Benda, L., and T. Dunne, Stochastic forcing of sediment routing

and storage in channel networks, *Water Resourc. Res., 33,* 2865-2880, 1997b.

Blackwelder, E., The process of mountain sculpture by rolling debris. *J. Geomorph., 4,* 324-328, 1942.

Blasius, K.R., J.A. Cutts, J.E. Guest and H. Masursky, Geology of the Valles Marineris: first analysis of imaging from Viking 1 orbiter primary Mission. *J. Geophys. Res., 82,* 4067-4091, 1977.

Brush, L.M., Jr., Drainage basins, channels and flow characteristics of selected streams in Central Pennsylvania, *U.S. Geol. Survey Prof. Pap. 282-F,* 181 pp., 1961.

Burbank, D.W., Leland, J., Fielding, E., Anderson, R.S., Brozovic, N., Reid, M.R., and Duncan, C., Bedrock incision, rock uplift and threshold hillslopes in the northwestern Himalayas, *Nature, 379,* 505-510, 1996

Buser, O. and H. Frutiger, Observed maximum run-out distance of snow avalanches and the determination of the friction coefficients mu and epsilon. *J. Glaciology, 94,* 121-130, 1980.

Cannon, S.H. and W.Z. Savage, A mass-change model for the estimation of debris-flow runout. *J. Geol., 96,* 221-227, 1988.

Chen, C-L., Generalized viscoplastic modeling of debris flow, *J. Hydraul. Engr.,* 114, 237-258, 1988.

Corner, C.D., Avalanche impact landforms in Troms, north Norway, *Geografiska Annaler, 62A,* 1-10, 1980.

Dent, J.D., and T.E. Lang, Modeling of snow flow, *J. Glaciol., 26,* 131-140, 1980.

Dent, J.D., and T.E. Lang, A biviscous modified Bingham model of snow avalanche motion. *Ann. Glaciol., 4,* 42-46, 1983.

Dick, G.S., Anderson, R.S., and D.E. Sampson, Flash floods and channel evolution in the Blue Hills badlands, Caineville, Utah [Abstract], *Geol. Soc. Amer. Abstr. Progr., 29(7),* A-139, 1997.

Dietrich, W.E., and T. Dunne, Sediment budget for a small catchment in mountainous terrain, *Z. Geomorphol. Suppl.,* 29, 191-206, 1978.

Dietrich, W.E., T. Dunne, N. Humphrey, and L. Reid, Construction of sediment budgets for drainage basins, *Gen. Tech. Rep. PNW-141,* U.S. Forest Serv., WHERE pp. 5-23, 1982.

Dietrich, W.E., Reiss, R., Shu, M-L., and D.R. Montgomery, A process-based model for colluvial soil depth and shallow landsliding using digital elevation data, *Hydrol. Proc., 9,* 383-400, 1995.

Dollenmayer, K, and K.X. Whipple, Rates and processes of bedrock channel incision along the upper Ukak River, Valley of Ten Thousand Smokes, AK [Abstract], *EOS, Trans. Am. Geophys. Union, 78(46),* F299, 1997.

Ellis, M., Cai, X., and R.S. Anderson, Graded longitudinal river profiles by coupled bedrock incision and bedload sediment transport [Abstract], *EOS, Trans. Am. Geophys. Union, 78(46),* F299, 1997.

Foley, M., Bed-rock incision by streams, *Geol. Soc. Am. Bull., Part II, 91,* 2189-2213, 1980.

Gardiner, J., Geomorphic significance of avalanches in the Lake Louise area, Alberta, Canada. *Arctic and Alpine Res., 2,* 135-144, 1970.

Gardiner, J., Observations on erosion by wet snow avalanches, Mount Rae area, Alberta, Canada. *Arctic and Alpine Res., 15,* 271-274, 1983.

Gardner, T.W., Experimental study of knickpoint development and longitudinal profile evolution in cohesive, homogeneous material, *Geol. Soc. Am. Bull., 94,* 664-672, 1983.

Grams, P.E. and J.C. Schmidt, Indirect lithologic control on channel form of the Green River in the Eastern Uinta Mountains, Colorado and Utah [Abstract], *EOS, Trans. Am. Geophys. Union, 78(46),* F299, 1997.

Hack, J.T., Physiographic divisions and differential uplift in the Piedmont and Blue Ridge, *U.S. Geol. Surv. Prof. Pap. 1265,* 48 pp., 1982.

Hack, J.T. and J.C. Goodlette, Geomorphology and forest ecology of a mountain region in the central Appalachians, *US Geol. Surv. Prof. Paper 347,* 66 p, 1960.

Hancock, G., Anderson, R.S. and K.X Whipple, Beyond power: bedrock river incision process and form, *this volume,* 1998.

Hewitt, K., The mountain environment and geomorphic processes, *in Mountain Geomorphology,* edited by H.O. Slaymaker & H.J. McPherson, 17-34, Tantalus Press, Vancouver, 17-34, 1972.

Howard, A.D., Thresholds in river regimes, in *Thresholds in Geomorphology,* edited by D.R. Coates and J.D. Vitek, pp. 227-258, Allen and Unwin, Winchester, Mass., 1980.

Howard, A.D., Preliminary model of processes forming spur-and-gully terrain [Abstract], in *Reports of Planetary Geology and Geophysics Program--1989,* NASA Tech. Memo. TM 4210, 345-347, 1990.

Howard, A.D., A detachment-limited model of drainage basin evolution, *Water Resour. Res.,* 30, 2261-2285, 1994a.

Howard, A.D., Badlands, in *Geomorphology of Desert Environments,* edited by A. Abrahams and A Parsons, pp. 213-242, Chapman and Hall, London, 1994b.

Howard, A.D., and R. Dolan, Geomorphology of the Colorado River in the Grand Canyon, *J. Geol., 89,* 269-298, 1981.

Howard, A.D., Dietrich, W.E., and M.A. Seidl, Modeling fluvial erosion on regional to continental scales, *J. Geophys. Res.,* 99, 13,971-13,986, 1994.

Howard, A.D., and G. Kerby, Channel changes in badlands, *Geol. Soc. Am. Bull. 94,* 739-752, 1983.

Huang, X, and Garcia, M.H., Asymptotic solution for Bingham debris flows, in *Debris-Flow Hazards Mitigation: Mechanics, Prediction, and Assessment,* edited by C-L. Chen, Am. Soc. Civil Engineers, New York, 560-575, 1997.

Hungr, O., A model for the runout analysis of rapid flow slides, debris flows, and avalanches, *Canadian Geotech. J., 32,* 610-623, 1995.

Hunt, B, Newtonian fluid mechanics treatment of debris flows and avalanches, *J. Hydraul. Engr., 120,* 1350-1363, 1994.

Iverson, R.M., The physics of debris flows, *Rev. Geophys., 35,* 245-296, 1997a.

Iverson, R.M., Hydraulic modeling of unsteady debris-flow surges with solid-fluid interactions, in *Debris-Flow Hazards Mitigation: Mechanics, Prediction, and Assessment,* edited by C-L. Chen, Am. Soc. Civil Engineers, New York, 550-560, 1997b.

Johnson, A.M, *Physical Processes in Geology,* Freeman, Cooper & Co., San Francisco, 577 p., 1970.

Keller, E.A., Macdonald, A., Tally, T., and N.J. Merrit, Effects of large orgainic debris on channel morphology and sediment storage in selected tributaries of Redwood Creek, Northwestern California, *U.S. Geol. Survey Prof. Paper 1454-P,* P1-P29, 1995.

Kieffer, S.W., Hydraulic jump in Crystal Rapid: Implications for river-running and geomorphic evolution in the Grand Canyon, *J. Geol. 93,* 385-406, 1985.

Kieffer, S.W., Hydraulics and geomorphology of the Colorado

River in the Grand Canyon, in *Grand Canyon Geology*, edited by S.S. Beus and M. Morales, Oxford Univ. Press, New York, 333-383, 1990.

King, P.B., Corrosion and corrasion on Barton Creek, Austin, Texas, *J. Geol.*, 35, 631-638, 1927.

Kodama, Y. and K. Nakamura, An effect of large boulders on forming a longitudinal profile of bedrock channel, [Abstract], Bedrock Channels Conference, Pingaree Park, CO., 1996.

Lang, T.E., and J.D. Dent, Review of surface friction, surface resistance, and flow of snow. *Rev. Geophys. Space Phys., 20*, 21-37, 1982.

Lehmann, O., Morphologishe Theorie der Vervitterung von Steinschlag Wandern, *Vierteljahrschrift der Naturforschende Gesellschaft in Zurich, 87*, 83-126, 1933.

Lucchitta, B.K, Morphology of chasma walls, Mars, *J. Res., U.S. Geol. Survey 6*, 651-662, 1978.

Lucchitta, I., History of the Grand Canyon of the Colorado River in Arizona, in *Grand Canyon Geology*, edited by S.S. Beus and M. Morales, Oxford Univ. Press, New York, 311-332, 1990.

Luckman, B.H., The geomorphic activity of snow avalanches. *Geografiska Annaler 59A*, 31-48, 1977.

Luckman, B.H., Geomorphic work of snow avalanches in the Canadian Rocky Mountains, *Arctic and Alpine Research 10*, 261-276, 1978.

Mackin, J.H., Concept of the graded river, *Geol. Soc. Am. Bull., 101*, 1373-1388, 1948.

Madej, M.A., and Ozaki, V., Channel response to sediment wave propagation and movement, Redwood Creek, California, USA, *Earth Surf. Proc. Landf., 21*, 911-927, 1996.

Martinelli, M. Jr., Lang, T.E., and A.I. Mears, Calculations of avalanche friction coefficients from field data. *J. Glaciology, 26*, 109-119, 1980.

Matthes, F.E., Avalanche sculpture in the Sierra Nevada of California, *Int. Assoc. Sci. Hydrol. Bull., 23*, 631-637, 1938.

Matthes, G.H., Macroturbulence in natural stream flow, *Trans. Am. Geophys. Union*, 28, 255-262, 1947.

Maxson, J.H., Fluting and faceting of rock fragments, *J. Geol.*, 48, 717-751, 1940.

Maxson, J.H., and I. Campbell, Stream fluting and stream erosion, *J. Geol.*, 43, 729-744, 1935.

McClung, D.M. and P.A. Schaerer, Determination of avalanche dynamics friction coefficients from measured speeds, *Annals Glaciol., 4*, 170-173, 1983.

McEwen, A.S. and M.C. Malin, Dynamics of Mount St. Helens' 1980 pyroclastic flows, rockslide-avalanche, lahars, and blast, *J. Volcanol. Geothermal Res., 37*, 205, 1989.

Merritts, D., and K.R. Vincent, Geomorphic response of coastal streams to low, intermediate, and high rates of uplift, Mendocino triple junction region, northern California, *Geol. Soc. Am. Bull., 101*, 1373-88, 1989.

Miller, J.R., The influence of bedrock geology on knickpoint development and channel-bed degradation along downcutting streams in south-central Indiana, *J. Geol., 99*, 591-605, 1991.

Montgomery, D.R. and J.M. Buffington, Channel-reach morphology in mountain drainage basins, *Geol. Soc. Amer. Bull., 109*, 596-611, 1997.

Montgomery, D.R., Buffington, J.M., Smith, R.D., Schmidt, K.M., and G. Pess, Pool spacing in forest channels, *Water Resourc. Res., 31*, 1097-1105, 1995.

Montgomery, D.R., Abbe, T.B., Buffington, J.M., Peterson, N.P., Schmidt, K.M., and Stock, J.D., 1996, Distribution of bedrock and alluvial channels in forested mountain drainage basins, *Nature, 381*, 587-589, 1996.

Montgomery, D.R., and W.E. Dietrich, A physically based model for the topographic control on shallow landsliding, *Water Resourc. Res., 30*, 1153-1171, 1994.

Montgomery, D.R., and E. Foufoula-Georgiou, Channel network source representation using digital elevation models, *Water Resourc. Res.*, 29, 3925-3934, 1993.

O'Loughlin, C.L. and A.J. Pearce, Erosional processes in the mountains, in *Landforms of New Zealand*, edited by J.M. Soons and M.J. Selby, Longman Paul Ltd, Auckland, 67-79,1982.

Pariseau, W.G., A simple mechanical model for rockslides and avalanches, *Engin. Geol.*, 16, 111-123,1980.

Peev, C.D., Geomorphic activity of snow avalanches, *Int. Assoc. Sci. Hydrol. Publ., 69*, 357-368, 1966.

Perla, R., Cheng, TT., and D.M. McClung. A two-parameter model of snow-avalanche motion, *J. Glaciology, 26*, 197-207, 1980.

Rapp, A., Recent development of maintain slopes in Karkevagge and surroundings, northern Scandinavia, *Geografiska Annaler, 42*, 73-200, 1960a.

Rapp, A., Talus slopes and mountain walls at Templefjorden, Spitzbergen, *Norsk Polarinstitutt Scrifter, 119*, 96 pp, 1960b.

Reed, J.C., Jr., Disequilibrium profile of the Potomac River near Washington, D.C.--A result of lowered base level or Quaternary tectonics along the fall line?, *Geology, 9*, 445-450, 1981.

Reneau, S.L., Dietrich, W.E., Rubin, M., Donahue, D.J., and Jull, A.J.T., Analysis of hillslope erosion rates using dated colluvial deposits, *J. Geol.*, 97, 45-63, 1989.

Rickenmann, D., and Koch, T., Comparison of debris flow modelling approaches, in *Debris-Flow Hazards Mitigation: Mechanics, Prediction, and Assessment*, edited by C-L. Chen, Am. Soc. Civil Engineers, New York, 576- 585, 1997.

Rudberg, S., Present-day geomorphological processes in Prins Oscars Land, Svalvard, *Geografiska Annaler, 68A*, 41-63, 1986.

Savage, S.B., and Hutter, K., The dynamics of avalanches of granular materials from initiation to runout. Part I: Analysis, *Acta Mechanica, 86*, 201-223, 1991.

Scheidegger, A.E., *Theoretical geomorphology* (3rd Ed.), Springer Verlag, Berlin, 434pp., 1991.

Schumm, S.A., Evolution of drainage systems and slopes in badlands at Perth Amboy, New Jersey, *Geol. Soc. America Bull, 67*, 597-646, 1956.

Schumm, S.A., and Stevens, M.A., Abrasion in place: A mechanism for rounding and size reduction of coarse sediments in rivers, *Geology, 1*, 37-40, 1973.

Schiewiller, and K. Hunter 1983, Avalanche dynamics. Review of experiments and theoretical models of flow and powder-snow avalanches, *J. Glaciology, 29*, 283-285, 1983.

Seidl, M.A., and W.E. Dietrich, The problem of channel erosion into bedrock, *Catena Suppl. 23*, 101-124, 1992.

Seidl, M.A., W.E. Dietrich, and J.W. Kirchner, Longitudinal profile development into bedrock: An analysis of Hawaiian channels, *J. Geol, 102*, 457-474, 1994.

Sharp, R.P., and M.C. Malin, Channels on Mars, *Geol. Soc. America Bull., 86*, 593-609,1975.

Sharpe, D.R. and J. Shaw, Erosion of bedrock by subglacial meltwater, Cantley, Quebec., *Geol. Soc. Amer. Bull.*, 101, 1011-1020, 1989.

Shepherd, R.G., and S.A. Schumm, Experimental study of river incision, *Geol. Soc. Amer. Bull., 85*, 257-268, 1974.

Sklar, L., Dietrich, W.E., and Howard, A.D., The influence of

sediment supply on river incision into bedrock: a theoretical investigation [Abstract], *EOS, Trans. Am. Geophys. Union, 78(46)*, 251, 1996.

Sklar, L., and Dietrich, W.E., Bedrock channel evolution and sediment supply effects under varying boundary conditions, *this volume*, 1998.

Slingerland, R., Willet, D.D., and H.L. Hennessey, A new fluvial bedrock erosion model based on the work-energy principle [Abstract], *EOS, Trans. Am. Geophys. Union, 78(46)*, F299, 1997.

Stock, J.D., Montgomery, D.R., and N.P. Peterson, Extreme rates of bedrock river incision, Satsop River, Washington [Abstract], *EOS, Trans. Am. Geophys. Union, 77(46)*, F252, 1996.

Stock, J.D. and D.R. Montgomery, Can we predict the rate of bedrock river incision (using the stream power law)?, *Water Resources Research, in press.*

Takahashi, T., *Debris Flow*, Balkema, Rotterdam, 165pp.,1991.

Tinkler, K.J., Rockbed wear at a flow convergence zone in Fifteen Mile Creek, Niagara Peninsula, Ontario, *J. Geol., 105*, 163-274, 1997.

Tinkler, K.J. and E. Wohl, A primer on bedrock channels, *this volume*, 1998.

Webb, R.H., P.T. Pringle, and G.R. Rink, Debris flows from the tributaries of the Colorado River, Grand Canyon National Park, Arizona, *U.S. Geol. Surv. Prof. Pap. 1492*, 39 pp., 1989.

Weir, G.J., 1982, Kinematic wave theory for Ruapehu lahars., *New Zealand J. Sci.*, 25, 197-203, 1982.

Wende, R., Aspects of the fluvial geomorphology of the Eastern Kimberley Plateau, Western Australia, Ph.D. Dissertation, Univ. of Wollongong, 278 pp., 1997.

Wentworth, C.K., Soil avalanches on Oahu, Hawaii, *Geol. Soc. America Bull., 54*, 53-64, 1943.

Whalley, W.B.,, In: *Slope Instability*, Brunsden, D. and Prior, D.B., (Eds.), John Wiley & Sons, Chichester, 217-256, 1984.

Whipple, K.X, Open-channel flow of Bingham fluids: Applications in debris-flow research, *J. Geol., 105*, 243-262, 1997.

Whipple, K.X, Anderson, R.S., and G.S. Dick, Processes of river incision into bedrock, constraints from observations of channel bed and bank morphology [Abstract], *EOS, Trans. Am. Geophys. Union, 78(46)*, F298, 1997.

White, S.E., Processes of erosion on steep slopes of Oahu, Hawaii, *Am. J. Sci., 247*, 168-186, discussion, *248*, 511-514, 1949.

Williams, G.P. and H.P. Guy, 1973, Erosional and depositional aspects of Hurricane Camille in Virginia, 1969, *U.S. Geol. Survey Prof. Paper 804*, 80pp, 1973.

Wohl, E.E., Gradient irregularity in the Herbert Gorge of northeastern Australia, *Earth Surf. Processes Landforms, 17*, 69-84, 1992.

Wohl, E.E., Bedrock channel incision along Piccaninny Creek, Australia, *J. Geol., 101*, 749-761, 1993.

Wohl, E.E., Bedrock channel morphology in relation to erosional processes, *this volume*, 1998.

Wohl, E.E., and H. Ikeda, Experimental simulation of channel incision into a cohesive substrate at varying gradients, *Geology., 25*, 295-298, 1997.

Alan D. Howard, Department of Environmental Sciences, University of Virginia, Charlottesville, Virginia 22903

SUBJECT INDEX